

Evaluation of Recycled Concrete Aggregate Performance in Structural Concrete

by

Liam Butler

A thesis
presented to the University of Waterloo
in fulfillment of the
thesis requirement for the degree of
Doctor of Philosophy
in
Civil Engineering

Waterloo, Ontario, Canada, 2012

© Liam Butler 2012

Author's Declaration

I hereby declare that I am the sole author of this thesis. This is a true copy of the thesis, including any required final revisions, as accepted by my examiners.

I understand that my thesis may be made electronically available to the public.

Signature

Abstract

Sustainable resource management and development have been at the forefront of important issues concerning the construction industry for the past several years. Specifically, the use of sustainable building materials and the reuse and recycling of previously used building materials is gaining acceptance and becoming common place in many areas. As one of the most commonly used building materials in the world, concrete, composed of aggregate, sand, cement and water, can be recycled and reused in a variety of applications.

Using crushed concrete as fill and subgrade material under roads, sidewalks and foundations has been the most common of these applications. However, research has been ongoing over the past 50 years in many countries including Germany, Canada, Japan, the United States, China, and Australia investigating the use of crushed concrete from demolished old concrete structures to fully or partially replace the virgin aggregate used to produce new concrete for use in building and pavement applications. Producing concrete using recycled concrete aggregates (RCAs) has several advantages, namely, the burden placed on non-renewable aggregate resources may be significantly decreased, the service life and capacity of landfill and waste management facilities can be extended, and the carbon dioxide emissions and traffic congestion associated with the transport of virgin aggregates from remote sites can be reduced.

This research is directed at benchmarking typical RCA sources for usage in structural concrete and investigating the inter-relationships between aggregate properties, concrete properties and the bond properties between reinforcing steel and RCA concrete.

The experimental program focused on four main areas: aggregate properties testing, development of concrete mixture proportions, concrete fresh and hardened properties testing, and beam-end bond testing. Four coarse aggregate sources were investigated including one virgin or natural aggregate (NA) source, and three RCA sources. Two RCA sources were derived from the crushing of decommissioned building and pavement structures (RCA-1 and RCA-2) while the third source was derived from the crushing of returned ready-mix concrete (RCA-3). A variety of typical and non-typical aggregate tests were performed to provide a basis for correlation with fresh and hardened concrete properties results.

A total of 24 concrete mixtures were developed and divided into three separate categories, 1) control, 2) direct replacement, and 3) strength-based mixtures. The control mixtures were proportioned to achieve compressive strengths of 30, 40, 50 and 60MPa with slump values between 75 and 125 mm and served as a basis for comparison with the RCA concrete mixtures. The direct replacement mixtures were developed to investigate the effect that fully replacing (i.e., 100% replacement by volume) virgin coarse aggregate with RCA has on the fresh and hardened properties of the resulting concrete. The strength-based mixtures were developed to investigate the influence of aggregate properties on reinforcement bond in concrete having the same compressive strength. In addition, two separate experimental phases were carried out which had varying compressive strength ranges, different RCA sources, and different suppliers of the same type GU cement. Concrete properties such as slump, compressive strength, splitting tensile strength, modulus of elasticity, Poisson's ratio, linear coefficient of thermal expansion (LCTE), modulus of rupture and fracture energy were all measured. In total, 48 beam-end

specimens were tested that incorporated three bonded lengths (125, 375, and 450 mm) and four concrete compressive strengths (30, 40, 50 and 60 MPa).

Based on the results of the aggregate testing it was found that concrete incorporating pre-soaked (i.e., fully saturated) RCA as a 100% replacement for natural aggregate had slump values between 21% and 75%, compressive strengths between 81% and 122%, splitting tensile strengths between 78% and 109%, modulus of elasticity values between 81% and 98%, LCTE values in the same range, flexural strengths between 85% and 136%, and fracture energies between 68% and 118%, of the equivalent control (natural aggregate) concrete mixture.

Overall, reductions in bond strength between natural aggregate and RCA concrete ranged between 3 and 21%. The strength of coarse aggregate as quantified by the aggregate crushing value (ACV) was found to be the most significant aggregate property for influencing bond strength. A regression model (based on the beam-end specimens test results) was developed to extrapolate the experimental development lengths as a function of $f'_c{}^{1/4}$ and ACV. Theoretical development lengths for RCA concrete were up to 9% longer than for an equivalent natural aggregate concrete.

A detailed flowchart of the various inter-relationships between aggregate properties, concrete properties and reinforced concrete bond properties was compiled based on the results of this research.

A comprehensive guideline for use of RCA in concrete was developed based on the findings of this research. It includes a systematic decision tree approach for assessing whether a particular RCA source can be categorized into one of three performance classes. The range of allowable applications of a concrete which incorporates the RCA source as replacement of natural coarse aggregate will depend on the RCA performance class.

Acknowledgements

I would like to extend my sincerest thanks to my supervisors Dr. J.S. West and Dr. S.L. Tighe from the Civil and Environmental Engineering Department at the University of Waterloo, for their guidance, advice and encouragement throughout these past years of research.

I would also like to thank the many other individuals who had a direct hand in helping with my research. Namely, the Civil Engineering Department lab technicians, Richard Morrison, Doug Hirst, Jodi Norris, Ken Bowman, Rob Sluban, Mark Sobon and Terry Ridgeway. Day to day and month to month dilemmas and technical problems were made much easier with the help of these dedicated and talented individuals.

Appreciation is also extended to the Cement Association of Canada, the Greater Toronto Airports Authority, Dufferin Construction, Steed and Evans Construction, St. Mary's Cement, Lafarge, Dufferin Aggregates, Holcim, and the National Sciences and Engineering Research Council (NSERC) for the supply of research materials and funding for this project.

I would like to thank the dedicated individuals at the University of Waterloo Engineering Machine Shop for their high level of professionalism and technical skills in the fabrication of various testing components used throughout this research. In addition, I very much appreciate the assistance from the individuals at the Centre for Pavement and Transportation Technology for all their help and support throughout this project.

Finally, to my fellow students and colleagues at the University of Waterloo who extended their time and effort during my project whether it involved shovelling, sieving, casting, design checking, batching, or just helping to keep things in perspective, I would like to thank you all, this work would not have been possible without you.

Dedicated to my family and friends
and to all those who strive to live their life in balance

Table of Contents

Author’s Declaration	iii
Abstract.....	v
Acknowledgements	ix
Dedication	xi
List of Tables	xxiv
List of Figures.....	xxviii
Chapter 1: Introduction	1
1.1 Background	1
1.1.1 The State of the Aggregate Resource.....	1
1.1.2 The State of the Concrete Industry	2
1.1.3 Construction and Demolition Waste.....	2
1.1.4 RCA as an Alternative Coarse Aggregate Source in Concrete.....	3
1.1.5 Current use of RCA Concrete in Structural Applications.....	3
1.2 Significance of RCA Research.....	5
1.3 Important Terms and Definitions	6
1.4 Thesis Organization	6
Chapter 2: Literature Review.....	9
2.1 General	9
2.2 Recycled Concrete Aggregates (RCAs).....	9
2.2.1 RCA Production Process.....	9
2.2.2 Quantitative and Qualitative Aggregate Classification.....	10
2.2.3 Grading	13
2.2.4 Absorption and Surface Moisture	13
2.2.5 Bulk Density	16
2.2.6 Abrasion Resistance.....	16
2.2.7 Aggregate Crushing Strength.....	17
2.2.8 Adhered Mortar Content	18
2.2.9 Recycled Concrete Aggregate Preparation for use in Concrete.....	20

2.2.10	National and International Standards and Guidelines for use of RCAs.....	20
	2.2.10.1 <i>Canadian Standards Association (CSA)</i>	20
	2.2.10.2 <i>American Concrete Institute (ACI)</i>	20
	2.2.10.3 <i>European Guidelines (RILEM)</i>	20
	2.2.10.4 <i>German Institute for Standardization</i>	21
	2.2.10.5 <i>Japanese Industrial Standard</i>	21
2.3	Properties of RCA Concrete	22
2.3.1	RCA Concrete Mixture Proportioning and Production	22
2.3.2	Workability	24
2.3.3	Wet Unit Weight and Air Content	24
2.3.4	Interfacial Transition Zone (ITZ).....	24
2.3.5	Compressive Strength	26
2.3.6	Tensile Strength	27
2.3.7	Flexural Strength.....	28
2.3.8	Linear Coefficient of Thermal Expansion	29
2.3.9	Modulus of Elasticity and Poisson’s Ratio	29
2.3.10	Fracture Energy.....	31
	2.3.10.1 <i>Fracture Energy of NA Concrete</i>	31
	2.3.10.2 <i>Fracture Energy of RCA Concrete</i>	35
2.3.11	Bond Behaviour with Reinforcing Steel	36
2.4	Bond of Reinforcement in Concrete	38
2.4.1	Overview	38
2.4.2	Mechanics of Bond	38
	2.4.2.1 <i>Failure Mechanism</i>	38
	2.4.2.2 <i>Derivation of Bond Forces</i>	40
	2.4.2.3 <i>Bond-Slip Response</i>	41
2.4.3	Factors Affecting Bond.....	42
	2.4.3.1 <i>Cover and Bar Spacing</i>	42
	2.4.3.2 <i>Transverse Reinforcement</i>	42
	2.4.3.3 <i>Bonded or Spliced Length</i>	42
	2.4.3.4 <i>Bar Size</i>	42
	2.4.3.5 <i>Compressive Strength</i>	42
	2.4.3.6 <i>Tensile Strength and Fracture Energy</i>	43

2.4.3.7	<i>Slump and Workability</i>	43
2.4.3.8	<i>Aggregate Type</i>	43
2.4.4	Tests Specimens for Determining Bond Strength.....	44
2.4.4.1	<i>Pullout Specimen</i>	44
2.4.4.2	<i>Beam-End Specimen</i>	44
2.4.4.3	<i>Beam Anchorage and Splice Specimens</i>	45
2.4.5	Bond Models and Equations	46
2.4.5.1	<i>Orangun, Jirsa and Breen (1977)</i>	46
2.4.5.2	<i>ACI Committee 408 (2003)</i>	47
2.4.6	Design Code Provisions for Development Length	49
2.4.6.1	<i>CSA A23.3-04</i>	49
2.4.6.2	<i>ACI 318-09</i>	50
2.4.6.3	<i>CEB-FIP Model Code 1990</i>	51
2.5	Identification of Research Gaps	53
Chapter 3: Research Objectives and Experimental Program		55
Chapter 4: Aggregate Testing Procedures, Results and Discussion		59
4.1	Overview	59
4.2	Aggregate Sources and Preparation	59
4.3	Aggregate Physical Classification and Grading.....	60
4.3.1	Physical classification.....	60
4.3.2	Grading	64
4.4	Aggregate Testing Procedures	66
4.4.1	Adhered Mortar Content of Recycled Concrete Aggregates	66
4.4.1.1	<i>Nitric Acid Dissolution Method</i>	67
4.4.1.2	<i>Freeze-Thaw Method</i>	69
4.4.1.3	<i>Thermal Expansion Method</i>	70
4.4.2	Density and Absorption of Fine and Coarse Aggregates.....	71
4.4.3	Rate of Absorption of Coarse Aggregates	73
4.4.4	Moisture Content and Adhered Surface Moisture of Pre-Soaked Coarse Aggregates	74
4.4.5	Absorption of Original Aggregates and Adhered Mortar	75
4.4.6	Abrasion Resistance.....	75

4.4.7	Aggregate Crushing Value (ACV).....	76
4.5	Discussion and Analysis of Results	78
4.5.1	Adhered Mortar Content of Recycled Concrete Aggregates	78
	4.5.1.1 Nitric-Acid Dissolution.....	78
	4.5.1.2 Freeze-Thaw Method.....	80
	4.5.1.3 Thermal Expansion Method.....	81
4.5.2	Density and Absorption of Fine and Coarse Aggregates.....	84
4.5.3	Rate of Absorption of Coarse Aggregates	85
4.5.4	Moisture Content and Adhered Surface Moisture of Pre-Soaked Aggregates ...	87
4.5.5	Absorption of Original Aggregates and Adhered Mortar	88
4.5.6	Abrasion Resistance.....	89
4.5.7	Aggregate Crushing Value (ACV).....	91
	4.5.7.1 Response of Confined Bulk Aggregate to Crushing.....	94
4.5.8	Relationship between Aggregate Properties	98
4.6	Conclusions.....	102
Chapter 5: Development of Concrete Mixture Proportions		105
5.1	Overview of Mixture Proportion Types and Phases	105
5.1.1	Control Mixtures.....	105
5.1.2	Direct Replacement Mixtures	105
5.1.3	Strength-Based Mixtures	106
5.1.4	Mixture Proportion Phases and Summary	106
5.2	Mixing Procedure, Aggregate Preparation and Curing Program	108
5.2.1	Absolute Volume Method of Mixture Proportioning	108
5.2.2	Mixing Procedure and Batching Methods	110
	5.2.2.1 Mixing Procedure	110
	5.2.2.2 Batching Method A	111
	5.2.2.3 Batching Method B	111
	5.2.2.4 Batching Method C	111
5.2.3	Aggregate Preparation and Controlling the Actual Water-Cement Ratio	112
5.2.4	Curing Program.....	115
5.3	Control Concrete Mixture Proportions.....	115
5.4	Direct Replacement Concrete Mixture Proportions.....	116

5.5	Strength-Based Concrete Mixture Proportions	117
5.6	Summary of Mixture Proportions and Applications	119
Chapter 6: Concrete Properties Testing Procedures.....		121
6.1	Overview	121
6.2	Testing Procedures	121
6.2.1	Workability	121
6.2.2	Measurement of Hardened Density	122
6.2.3	Compressive Strength	123
6.2.4	Splitting Tensile Strength	125
6.2.5	Linear Coefficient of Thermal Expansion	126
6.2.6	Static Modulus of Elasticity and Poisson's Ratio	128
6.2.7	Fracture Energy and Modulus of Rupture	130
6.3	Summary	135
Chapter 7: Evaluation of Direct Replacement Mixture Test Results		137
7.1	Overview	137
7.2	Failure Modes of RCA Concrete.....	137
7.3	Phase 1 Direct Replacement Mixtures (30 and 50MPa).....	139
7.3.1	Workability	140
7.3.2	Compressive Strength Results	141
	7.3.2.1 <i>Statistical Significance of Compressive Strength Results</i>	144
	7.3.2.2 <i>Failure Mechanism and Effect of RCA Properties on Compressive Strength</i>	144
7.3.3	Conclusions from Phase 1 Mixtures	148
7.4	Phase 2 Direct Replacement Mixtures (40 and 60MPa).....	149
7.4.1	Workability and Hardened Density Results.....	149
	7.4.1.1 <i>Workability</i>	149
	7.4.1.2 <i>Hardened Density</i>	150
7.4.2	Compressive Strength Results	153
	7.4.2.1 <i>Statistical Significance of Compressive Strength Results</i>	155
	7.4.2.2 <i>Failure Mechanism and Effect of RCA Properties on Compressive Strength</i>	156
7.4.3	Splitting Tensile Strength Results.....	159
	7.4.3.1 <i>Statistical Significance of Splitting Tensile Strength Results</i>	161

7.4.3.2	<i>Failure Mechanism and Effect of RCA Properties on Splitting Tensile Strength</i>	162
7.4.4	Linear Coefficient of Thermal Expansion Results.....	163
7.4.5	Modulus of Elasticity and Poisson’s Ratio Results	165
7.4.5.1	<i>Statistical Significance of Modulus of Elasticity Results</i>	167
7.4.5.2	<i>Effect of RCA Properties on Modulus of Elasticity</i>	168
7.4.5.3	<i>Poisson’s Ratio Test Results</i>	172
7.4.6	Conclusions from Phase 2 Mixtures	172
7.5	Overall Conclusions	174
Chapter 8:	Evaluation of Strength-Based Mixture Test Results	177
8.1	Overview	177
8.2	Phase 1 Strength-Based Mixtures (30 and 50 MPa)	178
8.2.1	Workability	178
8.2.2	Compressive Strength Results	179
8.2.3	Splitting Tensile Strength Results.....	180
8.2.4	Modulus of Rupture Results	183
8.2.5	Fracture Energy Results	186
8.2.5.1	<i>Load-Deflection Response of Phase 1 Fracture Energy Specimens</i>	188
8.2.5.2	<i>Examination of Fracture Surfaces</i>	192
8.2.6	Conclusions from Phase 1 Mixtures	195
8.3	Phase 2 Strength-Based Mixtures (40 and 60 MPa)	196
8.3.1	Workability and Hardened Density Results.....	196
8.3.1.1	<i>Workability</i>	196
8.3.1.2	<i>Hardened Density</i>	197
8.3.2	Compressive Strength Results	198
8.3.3	Splitting Tensile Strength Results.....	199
8.3.3.1	<i>Statistical Significance of Tensile Strength Results</i>	202
8.3.3.2	<i>Comparison of Strength-Based and Direct Replacement Mixture Results</i>	203
8.3.4	Linear Coefficient of Thermal Expansion Results.....	204
8.3.4.1	<i>Comparison of Strength-Based and Direct Replacement Mixtures Results</i>	206
8.3.5	Modulus of Elasticity and Poisson’s Ratio Results	207

8.3.5.1	<i>Comparison of Strength-Based and Direct Replacement Mixtures Results</i>	210
8.3.5.2	<i>Poisson's Ratio Test Results</i>	211
8.3.6	Modulus of Rupture Results	213
8.3.7	Fracture Energy Results	215
8.3.7.1	<i>Load-Deflection Response of Phase 2 Fracture Energy Specimens</i>	218
8.3.7.2	<i>Examination of Fracture Surfaces of the Fracture Energy and Modulus of Rupture Specimens</i>	223
8.3.8	Conclusions from Phase 2 Mixtures	226
8.4	Evaluation of Combined Results from Phases 1 and 2	227
8.4.1	Effect of Aggregate Properties on Splitting Tensile Strength	227
8.4.2	Effect of Aggregate Strength on Modulus of Rupture	229
8.4.3	Overall Evaluation of the Fracture Energy of RCA Concrete	231
8.5	Effect of Natural Aggregate Replacement with RCA on Mixture Proportions	232
8.6	Overall Conclusions	235
Chapter 9: Bond Testing and Evaluation of Beam-End Specimens		239
9.1	Overview	239
9.2	Experimental Program	239
9.2.1	Pilot Study	240
9.2.2	Phase 1 Beam-End Batching	240
9.2.3	Phase 2 Beam-End Batching	242
9.3	Test Frame Design	244
9.4	Design and Construction of Beam-End Specimens	247
9.5	Test Setup and Procedure	249
9.6	Evaluation of Bond-Slip Response of Phase 1 (30 and 50 MPa) Specimens	250
9.6.1	Summary and Discussion of Test Results	251
9.6.1.1	<i>Bond-Slip Response and Failure Mechanism of Beam-End Specimens</i>	254
9.6.2	Effect of Aggregate Crushing Value on Bond Behaviour	261
9.6.3	Effect of Aggregate Abrasion Resistance on Bond Behaviour	262
9.6.4	Effect of Compressive Strength on Bond Behaviour	264
9.6.5	Effect of Splitting Tensile Strength on Bond Behaviour	265
9.6.6	Effect of Modulus of Rupture on Bond Behaviour	266
9.6.7	Effect of Fracture Energy on Bond Behaviour	268

9.6.8	Dissection and Forensic Analysis of Beam-Ends	269
	9.6.8.1 Specimen BE-NAC-30-375A	271
	9.6.8.2 Specimen BE-NAC-50-375A	272
	9.6.8.3 Specimen BE-RAC1-30-375A	274
	9.6.8.4 Specimen BE-RAC2-30-125B	276
	9.6.8.5 Specimen BE-RAC2-50-375A	277
	9.6.8.6 Summary and Conclusions from Phase 1 Dissections and Forensic Analysis	279
9.6.9	Conclusions from Phase 1 Bond Testing	280
9.7	Evaluation of Bond-Slip Response of Phase 2 (40 and 60 MPa) Specimens	281
9.7.1	Summary and Discussion of Test Results	282
	9.7.1.1 Bond-Slip Response and Failure Mechanism of Beam-End Specimens	285
9.7.2	Effect of Aggregate Crushing Value on Bond Behaviour	289
9.7.3	Effect of Aggregate Abrasion Resistance on Bond Behaviour	290
9.7.4	Effect of Concrete Hardened Density on Bond Behaviour	292
9.7.5	Effect of Compressive Strength on Bond Behaviour	294
9.7.6	Effect of Splitting Tensile Strength on Bond Behaviour	295
9.7.7	Effect of Modulus of Rupture on Bond Behaviour	296
9.7.8	Effect of Fracture Energy on Bond Behaviour	298
9.7.9	Dissection and Forensic Analysis of Beam-Ends	300
	9.7.9.1 Specimen BE-NAC-40-450A	300
	9.7.9.2 Specimen BE-NAC-40-450B	302
	9.7.9.3 Specimen BE-RAC1-40-125A	304
	9.7.9.4 Specimen BE-RAC1-40-125B	306
	9.7.9.5 Specimen BE-RAC3-40-125A	308
	9.7.9.6 Specimen BE-RAC3-40-125B	309
	9.7.9.7 Summary and Conclusions from Phase 2 Dissections and Forensic Analysis	311
9.7.10	Conclusions from Phase 2 Bond Testing	312
9.8	Overall Evaluation of the Effect of Aggregate and Concrete Properties on Bond Strength	314
9.8.1	Effect of Bonded Length on Bond Strength	315
9.8.2	Effect of Aggregate Strength on Bond Strength	316

9.8.3	Effect of Compressive Strength on Bond Strength.....	317
9.8.4	Effect of Splitting Tensile Strength on Bond Strength	318
9.8.5	Effect of Modulus of Rupture on Bond Strength.....	319
9.8.6	Effect of Fracture Energy on Bond Strength	320
9.8.7	Statistical Summary of Factors Affecting Bond Strength.....	321
9.9	Predictive Experimental Bond Equations for RCA Concrete	324
9.9.1	Predicted Development Lengths Based on Regression Model C Developed from Experimental Results	329
9.10	Overall Conclusions	332
Chapter 10: Guidelines for Use of RCA in Structural Concrete.....		335
10.1	Overview	335
10.2	Guideline Formulation and Methodology	335
10.3	Recycled Concrete Aggregate Selection Guideline	335
10.3.1	The Original Concrete Structure(s), Demolition, and Crushing.....	336
10.3.2	RCA Selection Decision Tree.....	337
	<i>10.3.2.1 CSA A23.1 Requirements for Coarse Aggregates for use in Concrete</i>	<i>337</i>
10.3.3	Proposed RCA Performance Classes	341
	<i>10.3.3.1 Justification for RCA Performance Class Limits.....</i>	<i>343</i>
10.3.4	RCA Concrete Mixture Proportioning Guidelines	344
10.3.5	Performance Requirements of RCA Structural Concrete	346
10.3.6	Recommended Durability Testing for RCA Concrete.....	348
10.3.7	Recommended References.....	348
Chapter 11: Conclusions, Contributions and Recommendations for Future Work		349
11.1	Overview	349
11.2	Conclusions.....	349
11.2.1	Recycled Concrete Aggregate Properties	349
11.2.2	RCA Concrete Mechanical Properties and Mixture Proportioning	351
11.2.2	Bond Performance of RCA Concrete	354
11.3	Contributions.....	356
11.4	Recommendations for Future Work.....	357
11.4.1	RCA Property Testing.....	357
11.4.2	RCA Concrete Mixture Proportions	357

11.4.3	RCA Concrete Properties.....	357
11.4.4	Bond Performance of RCA Concrete	357
References		359
Appendix A: Trial Concrete Mixture Proportions		375
A.1	NAC-30 Mixtures (Phase 1).....	375
A.2	NAC-50 Mixtures (Phase 1).....	375
A.3	RAC1-30 Mixtures (Phase 1).....	376
A.4	RAC1-50 Mixtures (Phase 1).....	376
A.5	RAC2-30 Mixtures (Phase 1).....	377
A.6	RAC2-50 Mixtures (Phase 1).....	377
A.7	NAC-40 Mixtures (Phase 2).....	377
A.8	NAC-60 Mixtures (Phase 2).....	378
A.9	RAC1-40 Mixtures (Phase 2).....	378
A.10	RAC1-60 Mixtures (Phase 2).....	378
A.11	RAC2-40 Mixtures (Phase 2).....	379
A.12	RAC2-60 Mixtures (Phase 2).....	379
A.13	RAC3-40 Mixtures (Phase 2).....	379
A.14	RAC3-60 Mixtures (Phase 2).....	380
Appendix B: Sample Statistical Calculations		381
B.1	Multiple Comparisons of Means using the Least Significant Difference Method	381
Appendix C: Beam-End Test Frame Design Overview		383
C.1	Design Concept and Parameters	383
C.2	Structural Models and SAP 2000 Analysis.....	384
C.3	Stiffness-Based Displacement Criteria	390
C.4	Component #1 Design – Left Strut	390
C.5	Component #2 Design – Right Strut	392
C.6	Component #3 Design – C-Channels.....	394
C.7	Component #4 Design – Reaction Block	394
C.8	Component #5 Design – Support Beam.....	397
C.9	Miscellaneous Design Items	397
C.9.1	Bearing resistance of concrete	397

C.9.2	Shear resistance of beam-end specimen	397
C.9.3	Development length calculations	397
C.9.4	Right strut and reaction block adjustable spacers/bearing pads.....	397
C.9.5	Pre-stressed Coupler Assembly	398
C.10	Design Drawings.....	398
Appendix D: Bond-Slip Response Curves and Crack Patterns for Beam-End Specimens		409

List of Tables

Table 2.1 Gradation requirements for coarse aggregates for use in structural concrete, sidewalks, curb and gutter (MTO, 2004)	13
Table 2.2 Summary of findings from previous researchers on absorption of coarse RCA	15
Table 2.3 Summary from previous researchers on bulk relative density of coarse RCA.....	16
Table 2.4 Summary from previous researchers on abrasion resistance of coarse RCA	17
Table 2.5 Summary from previous researchers on aggregate crushing value of coarse RCA.....	18
Table 2.6 Summary from previous researchers on adhered mortar content of coarse RCA	19
Table 2.7 German standards on use of RCA in concrete (DIN, 2002)	21
Table 2.8 Japanese standards on use of high-quality RCA in concrete (JIS, 2011)	22
Table 2.9 Summary of findings from previous researchers on compressive strength of RCA Concrete.....	26
Table 2.10 Summary of findings from previous researchers on tensile strength of RCA Concrete	28
Table 2.11 Summary of findings from previous researchers on flexural strength of RCA Concrete	29
Table 2.12 Summary of findings from previous researchers on bond strength of RCA concrete with reinforcing steel	37
Table 4.1 Particle shape classification using BS 812 Part 1: 1975 (adapted from Neville, 1997)	61
Table 4.2 Surface texture of aggregates using BS 812 Part 1: 1975 (adapted from Neville, 1997)	61
Table 4.3 Aggregate particle shape and surface texture classifications and descriptions for natural aggregate, RCA-1, RCA-2 and RCA-3	62
Table 4.4 Fine aggregate gradation requirements.....	65
Table 4.5 OPSS 1002 Gradation requirements for coarse aggregates for use in structural concrete	65
Table 4.6 Aggregate gradations as used for nitric acid dissolution testing	68
Table 4.7 Adhered mortar content* – Nitric acid dissolution method	79

Table 4.8 Adhered mortar content* – Freeze-thaw method	81
Table 4.9 Adhered mortar content – Thermal treatment method.....	81
Table 4.10 Fine aggregate properties.....	84
Table 4.11 Coarse aggregate densities and absorption capacities	84
Table 4.12 Statistical moisture analysis of pre-soaked coarse aggregates.....	87
Table 4.13 Absorption of the RCA original aggregates and adhered mortar	88
Table 4.14 Micro-Deval abrasion loss percentages for each coarse aggregate type	89
Table 4.15 Aggregate crushing value results.....	93
Table 4.16 ACV secant bulk moduli and maximum strain values	96
Table 5.1 Summary of all mixture proportions and associated naming conventions	107
Table 5.2 Pre-soaking time required for aggregates to reach SSD.....	113
Table 5.3 Coarse aggregate pre-treatment methods.....	114
Table 5.4 Phase 1 (30 and 50MPa) control concrete mixture proportions	116
Table 5.5 Phase 2 (40 and 60MPa) control concrete mixture proportions	116
Table 5.6 Phase 1 (30 and 50MPa) direct replacement concrete mixture proportions.....	117
Table 5.7 Phase 2 (40 and 60MPa) direct replacement concrete mixture proportions.....	117
Table 5.8 Phase 1 (30 and 50MPa) strength-based concrete mixture proportions	118
Table 5.9 Phase 2 (40 and 60MPa) strength-based concrete mixture proportions	119
Table 6.1 Summary of the various fracture energy test procedures	131
Table 7.1 Summary of nominal compressive strengths and failure modes (Phase 1 control and direct replacement mixtures)	145
Table 7.2 Summary of nominal compressive strengths and failure modes (Phase 2 control and direct replacement mixtures)	156
Table 7.3 Splitting tensile results, statistics and failure modes for Phase 2 direct replacement mixtures	162
Table 7.4 Linear coefficient of thermal expansion test results (Phase 2 control and direct replacement mixtures)	164

Table 7.5 Modulus of elasticity results and statistics for Phase 2 direct replacement mixtures.	168
Table 7.6 Poisson’s ratio test results (Phase 2 control and direct replacement mixtures)	172
Table 8.1 Fracture energy test results (Phase 1 strength-based mixtures)	187
Table 8.2 Splitting tensile results, statistics and failure modes for Phase 2 strength-based mixtures	202
Table 8.3 Statistical comparison of the mean splitting tensile strength values between the RCA concrete direct replacement and RCA concrete strength-based mixtures	204
Table 8.4 Linear coefficient of thermal expansion test results (Phase 2 control and strength-based mixtures)	205
Table 8.5 Statistical comparison of the mean LCTE values between the RCA concrete direct replacement and RCA concrete strength-based mixtures	206
Table 8.6 Statistical comparison of the mean $E_c/f_c^{1/2}$ values between the direct replacement and strength-based mixtures	210
Table 8.7 Poisson’s ratio test results (Phase 2 control and strength-based mixtures)	211
Table 8.8 Statistical comparison of the mean Poisson’s ratio values between the direct replacement and strength-based mixtures	212
Table 8.9 Fracture energy test results (Phase 2 control and strength-based mixtures)	216
Table 8.10 Summary of fracture energy test results statistics (Combined Phase 1 and 2)	231
Table 8.11 Summary of fracture energy data for NA concrete specimens reported by other researchers	232
Table 9.1 Pilot study beam-end test results	240
Table 9.2 Phase 1 Beam-end testing control variables	241
Table 9.3 Phase 1 Beam-end specimen identification and test matrix	242
Table 9.4 Phase 2 beam-end specimen control variables	243
Table 9.5 Phase 2 beam-end identification and test matrix	244
Table 9.6 Material properties for 25M reinforcing steel test bar (Obtained from mill certificates courtesy of reinforcing supplier)	247
Table 9.7 Phase 1 beam-end bond strength test data (30 and 50 MPa; NAC, RAC1 and RAC2)	252

Table 9.8 Phase 2 beam-end bond-slip response test data	283
Table 9.9 Statistical summary of aggregate and concrete properties affecting bond strength ...	323
Table 9.10 Summary of developed regression models and their associated parameters	326
Table 9.11 Summary of theoretical development lengths calculated based on regression model C and calculated development lengths based on CSA A23.3 and ACI 318 code equations	330
Table 10.1 Grading requirements for coarse aggregates (adapted from CSA A23.1, 2009)	339
Table 10.2 Limits for deleterious substances* (Part a) and physical properties (Part b) of coarse aggregates (adapted from CSA, 2009)	339
Table 10.3 Selection chart for determining whether a particular RCA or blended RCA source is a performance class A2, B or C.....	342
Table 10.4 Pre-wetting procedures for RCA prior to batching in concrete	345
Table 10.5 Selection chart for determining whether a particular Class A2 RCA source may be suitable for use in reinforced concrete structures	346
Table 10.6 Additional references for RCA and RCA concrete	348
Table C.1 Design loads summary based on SAP 2000 analysis of structural models.....	390

List of Figures

Figure 1.1 Aggregate reserves located within 75 km of the Greater Toronto Area (GTA) (Adapted from MNR, 2010)	2
Figure 1.2 J-Cube Capital Mall, Singapore (IES, 2011).....	4
Figure 1.3 Enterprise Park at Stapleton, Denver, United States (Etkin-Johnson, 2012)	5
Figure 2.1 Production process for recycled concrete aggregates (ACI 555, 2001)	10
Figure 2.2 Various moisture states of aggregates (adapted from Neville, 1997)	14
Figure 2.3 Interfacial transition zone in RCA concrete (Note: Adhered mortar + original aggregate = recycled concrete aggregate)	25
Figure 2.4 Stress-deformation curve for additional deformation within the fracture process zone (RILEM, 1985)	32
Figure 2.5 RILEM notched beam specimen and corresponding load-deflection curve for measuring the fracture energy of concrete (RILEM, 1985)	34
Figure 2.6 Bond transfer mechanisms for a reinforcing bar embedded in concrete (adapted from ACI 408, 2003)	39
Figure 2.7 Change in bond force due to change in moment in a beam (ACI 408, 2003).....	40
Figure 2.8 Typical bond-slip response curve.....	41
Figure 2.9 Typical bond pullout specimen	44
Figure 2.10 Beam-end test specimen	45
Figure 2.11 Typical beam anchorage specimen (ACI 408, 2003)	45
Figure 2.12 Typical beam-splice specimen	46
Figure 2.13 University of Texas beam (adapted from Ferguson, 1973).....	46
Figure 3.1 Experimental program staging, mixture proportion summary and corresponding research objectives.....	57
Figure 4.1 RCA-2 various gradations	60
Figure 4.2 Deleterious materials present within RCA-2.....	64
Figure 4.3 Fine aggregate gradation	65

Figure 4.4 Particle size distributions for the natural aggregate, RCA-1, RCA-2 and RCA-3	66
Figure 4.5 RCA-1 old adhered mortar and original aggregates	66
Figure 4.6 Heating of RCA in nitric acid bath	68
Figure 4.7 Muffle furnace for use with the thermal expansion test	71
Figure 4.8 Aggregate crushing value test apparatus	76
Figure 4.9 Aggregate crushing value test in progress	78
Figure 4.10 RCA samples after nitric acid dissolution	79
Figure 4.11 RCA samples after freeze-thaw test (size fractions from left to right: 4.75 mm, 9.5 mm, 16.0 mm, 19.0 mm)	80
Figure 4.12 RCA-1 original aggregates after thermal treatment (separate size fractions)	82
Figure 4.13 RCA-2 original aggregates after thermal treatment (separate size fractions)	82
Figure 4.14 RCA-3 original aggregates after thermal treatment (separate size fractions)	83
Figure 4.15 Moisture absorption over time for natural aggregate	85
Figure 4.16 Moisture absorption over time for RCA-1	85
Figure 4.17 Moisture absorption over time for RCA-2	86
Figure 4.18 Moisture absorption over time for RCA-3	86
Figure 4.19 Natural aggregate and RCA-1 samples before and after micro-deval abrasion testing	90
Figure 4.20 RCA-1 and RCA-3 samples before and after micro-deval abrasion testing	91
Figure 4.21 Crushed RCA-1 and cylinder mould after aggregate crushing value test	92
Figure 4.22 Loose crushed aggregate samples after aggregate crushing value test.....	92
Figure 4.23 Pre- and post-crushing behaviour of ACV test samples.....	94
Figure 4.24 Stress-strain response of rodded aggregate during ACV testing.....	95
Figure 4.25 Relation between average secant modulus of bulk aggregate and aggregate crushing value.....	97
Figure 4.26 Relation between maximum average axial strain and aggregate crushing value	97

Figure 4.27 Relationship between the bulk density of aggregate squared and the average secant modulus of elasticity of bulk aggregate.....	98
Figure 4.28 Relationship between oven dry bulk density and absorption of coarse aggregate	99
Figure 4.29 Relationship between oven dry bulk density and aggregate crushing value\.....	99
Figure 4.30 Relationship between absorption and aggregate crushing value.....	100
Figure 4.31 Relationship between aggregate crushing value and micro-deval abrasion resistance	101
Figure 4.32 Relationships between aggregate properties	101
Figure 5.1 Range of concrete pan mixers used for batching.....	112
Figure 5.2 Aggregate hopper systems and pre-wetting of coarse aggregates in hoppers as per batching methods B and C.....	112
Figure 5.3 Summary of mixture proportion types and applications	120
Figure 6.1 Slump cone apparatus and measurement.....	122
Figure 6.2 Cylindrical specimen used for measurement of density of hardened concrete	122
Figure 6.3 Compressive strength tester and three-cylinder concrete end grinder.....	124
Figure 6.4 Sketches of types of fracture of cylindrical concrete cylinders loaded under uniaxial compression (excerpted from CSA A23.2-9C, 2009)	124
Figure 6.5 Aligning apparatus and bearing strips used to position splitting tensile strength specimens.....	125
Figure 6.6 Specimen test setup and instrumentation for measurement of the coefficient of thermal expansion of concrete	127
Figure 6.7 Specimen test setup and instrumentation for measurement of the coefficient of thermal expansion of concrete	127
Figure 6.8 Modulus of elasticity and Poisson`s ratio test setup and compressometer-extensometer	129
Figure 6.9 Stress-strain response and calculation of the static modulus of elasticity and Poisson`s ratio of concrete in uniaxial compression.....	129
Figure 6.10 Single-edge notched double cantilevered (SENDC) fracture energy specimen.....	132
Figure 6.11 Fracture energy SENDC specimen test setup and instrumentation.....	132

Figure 6.12 Underside of fracture energy test specimen and clip gauge setup.....	133
Figure 6.13 Side view of fracture energy test specimen and LVDT for midspan displacement measurement	134
Figure 6.14 Load vs. displacement plot for calculation of fracture energy of concrete using single-notched double-cantilevered specimen.....	134
Figure 7.1 Failure modes of RCA concrete	138
Figure 7.2 Slump values for Phase 1 direct replacement mixtures.....	140
Figure 7.3 Relationship between slump and adhered surface moisture of aggregate particle (Phase 1 direct replacement mixtures).....	141
Figure 7.4 Early (7 day) compressive strength test results and statistics for Phase 1 direct replacement mixtures.....	142
Figure 7.5 Nominal (28 day) compressive strength test results and statistics for Phase 1 direct replacement mixtures.....	142
Figure 7.6 Early compressive strength normalized to 28 day strength for Phase 1 direct replacement mixtures.....	143
Figure 7.7 Fracture surfaces of the Phase 1 30 MPa direct replacement compressive strength specimens.....	145
Figure 7.8 Fracture surfaces of the Phase 1 50 MPa direct replacement compressive strength specimens.....	146
Figure 7.9 Relationship between adhered surface moisture of aggregate particle and compressive strength (Phase 1 direct replacement mixtures).....	147
Figure 7.10 Slump values for Phase 2 direct replacement mixtures.....	149
Figure 7.11 Relationship between slump and adhered surface moisture of aggregate particle (Phase 2 direct replacement mixtures).....	150
Figure 7.12 Hardened density results for the phase 2 direct replacement mixtures	151
Figure 7.13 Relationship between aggregate bulk density and concrete hardened density (Phase 2 direct replacement mixtures)	152
Figure 7.14 Relationship between aggregate crushing value and concrete hardened density (Phase 2 direct replacement mixtures).....	152
Figure 7.15 Early (7 day) compressive strength results and statistics for Phase 2 direct replacement mixtures.....	153

Figure 7.16 Nominal (28 day) compressive strength results and statistics for Phase 2 direct replacement mixtures.....	154
Figure 7.17 Early compressive strength normalized to 28 day strength for Phase 2 direct replacement mixtures.....	155
Figure 7.18 Fracture surfaces of the Phase 2 40 MPa direct replacement compressive strength specimens.....	157
Figure 7.19 Fracture surfaces of the phase 2 60 MPa direct replacement compressive strength specimens.....	158
Figure 7.20 Splitting tensile strength results and least significant difference (LSD) limits	159
Figure 7.21 Relationship between compressive strength and splitting tensile strength (Phase 2 direct replacement mixtures)	161
Figure 7.22 Fracture surfaces of the phase 2 40 MPa direct replacement splitting tensile strength specimens.....	162
Figure 7.23 Fracture surfaces of the phase 2 60 MPa direct replacement splitting tensile strength specimens.....	163
Figure 7.24 Linear coefficient of thermal expansion test results (Phase 2 direct replacement mixtures).....	164
Figure 7.25 Relationship between LCTE, water-cement ratio and aggregate density (Phase 2 direct replacement mixtures)	165
Figure 7.26 Modulus of elasticity results (Phase 2 direct replacement mixtures)	166
Figure 7.27 Modulus of elasticity results normalized with respect to $f'_c{}^{1/2}$ (Phase 2 direct replacement specimens).....	167
Figure 7.28 Modulus of elasticity results normalized with respect to $f'_c{}^{1/2}$ and hardened density	169
Figure 7.29 Relationship between modulus of elasticity and concrete hardened density	170
Figure 7.30 Relationship between coarse aggregate bulk density and modulus of elasticity of concrete (Phase 2 direct replacement mixtures)	170
Figure 7.31 Relationship between modulus of elasticity of concrete and modulus of elasticity of bulk aggregate (Phase 2 direct replacement mixtures).....	171
Figure 8.1 Overview of strength-based mixtures properties and motivation for testing	177
Figure 8.2 Slump values for Phase 1 strength-based mixtures	179

Figure 8.3 Nominal (28 day) compressive strength test results (Phase 1 strength-based mixtures)	180
Figure 8.4 Splitting tensile strength results (Phase 1 strength-based mixtures)	181
Figure 8.5 Normalized splitting tensile strength results (Phase 1 strength-based mixtures)	182
Figure 8.6 Relationship between $f_{ct}/f_c^{1/2}$ and aggregate crushing value (Phase 1 strength-based mixtures)	183
Figure 8.7 Modulus of rupture (flexural strength) results (Phase 1 strength-based mixtures)	184
Figure 8.8 Normalized modulus of rupture (flexural strength) test results (Phase 1 strength-based mixtures)	185
Figure 8.9 Relationship between aggregate crushing value and $f_r/f_c^{1/2}$ (Phase 1 control and strength-based mixtures)	185
Figure 8.10 Load vs. midspan deflection for NAC-30 fracture energy specimens (Phase 1)	189
Figure 8.11 Load vs. midspan deflection for RAC1-30 fracture energy specimens (Phase 1)	189
Figure 8.12 Load vs. midspan deflection for RAC2-30 fracture energy specimens (Phase 1)	190
Figure 8.13 Load vs. midspan deflection for NAC-50 fracture energy specimens (Phase 1)	190
Figure 8.14 Load vs. midspan deflection for RAC1-50 fracture energy specimens (Phase 1)	191
Figure 8.15 Load vs. midspan deflection for RAC2-50 fracture energy specimens (Phase 1)	191
Figure 8.16 Fracture zones of fracture energy prisms (Phase 1 30 MPa specimens)	193
Figure 8.17 Fracture zones of fracture energy prisms (Phase 1 50 MPa specimens)	194
Figure 8.18 Slump values for Phase 2 strength-based mixtures	197
Figure 8.19 Hardened density results for the Phase 2 strength-based mixtures	198
Figure 8.20 Nominal (28 day) compressive strength results (Phase 2 strength-based mixtures)	199
Figure 8.21 Splitting tensile strength results (Phase 2 strength-based mixtures)	200
Figure 8.22 Normalized splitting tensile strength values (Phase 2 control and strength-based mixtures)	201
Figure 8.23 Relationship between aggregate crushing value and $f_{ct}/f_c^{1/2}$ (Phase 2 control and strength-based mixtures)	201
Figure 8.24 Relationship between concrete hardened density and splitting tensile strength (Phase	

2 control and strength-based mixtures)	203
Figure 8.25 Linear coefficient of thermal expansion results (Phase 2 strength-based mixtures)	205
Figure 8.26 Modulus of elasticity results.....	208
Figure 8.27 Modulus of elasticity results normalized with respect to $f'_c{}^{1/2}$	208
Figure 8.28 Modulus of elasticity results normalized with respect to $f'_c{}^{1/2}$ and hardened density (Phase 2 strength-based mixtures).....	209
Figure 8.29 Relationship between modulus of elasticity of concrete and average secant modulus of elasticity of bulk aggregate	209
Figure 8.30 Modulus of rupture (flexural strength) results (Phase 2 control and strength-based mixtures).....	214
Figure 8.31 Normalized Modulus of rupture (flexural strength) results (Phase 2 control and strength-based mixtures).....	214
Figure 8.32 Relationship between aggregate crushing value and modulus of rupture (Phase 2 control and strength-based mixtures)	215
Figure 8.33 Relationship between aggregate strength (ACV) and fracture energy	217
Figure 8.34 Load vs. midspan deflection for 40 MPa NA concrete fracture energy specimens (Phase 2)	219
Figure 8.35 Load vs. midspan deflection for 60 MPa NA concrete fracture energy specimens (Phase 2)	219
Figure 8.36 Load vs. midspan deflection for 40 MPa RCA-1 concrete fracture energy specimens (Phase 2)	220
Figure 8.37 Load vs. midspan deflection for 60 MPa RCA-1 concrete fracture energy specimens (Phase 2)	220
Figure 8.38 Load vs. midspan deflection for 40 MPa RCA-2 concrete fracture energy specimens (Phase 2)	221
Figure 8.39 Load vs. midspan deflection for 60 MPa RCA-2 concrete fracture energy specimens (Phase 2)	221
Figure 8.40 Load vs. midspan deflection for 40 MPa RCA-3 concrete fracture energy specimens (Phase 2)	222
Figure 8.41 Load vs. midspan deflection for 60 MPa RCA-3 concrete fracture energy specimens (Phase 2)	222

Figure 8.42 Fracture zones of fracture energy prisms (Phase 2 40 MPa specimens)	224
Figure 8.43 Fracture zones of fracture energy prisms (Phase 2 60 MPa specimens)	225
Figure 8.44 Relationship between splitting tensile strength normalized to compressive strength and aggregate crushing value	228
Figure 8.45 Relationship between splitting tensile strength normalized to compressive strength and coarse aggregate volume in concrete	228
Figure 8.46 Modulus of rupture test results (Combined Phase 1 and 2 control and strength-based mixtures)	229
Figure 8.47 Relationship between aggregate crushing value and $f_r/f_c^{1/2}$ (Combined Phase 1 and 2 results)	230
Figure 8.48 Water and cement demands for the Phase 2 40MPa strength-based mixtures	233
Figure 8.49 Water and cement demands for the Phase 2 60MPa strength-based mixtures	234
Figure 8.50 Overview of relationships between various aggregate and concrete properties.....	237
Figure 9.1 Beam-end test frame apparatus as per ASTM A944-05.....	245
Figure 9.2 Modified, vertically oriented beam-end test frame apparatus	245
Figure 9.3 Beam-end structural idealization	246
Figure 9.4 Beam-end specimen cross-section dimensions and reinforcement layout	247
Figure 9.5 Typical beam-end formwork casting beds and reinforcement	248
Figure 9.6 Beam-end casting and curing techniques	249
Figure 9.7 Beam-end loaded-end and free-end LVDT mounting setup	250
Figure 9.8 Summary charts of bond strength normalized to $f_c^{1/2}$ (Phase 1)	253
Figure 9.9 Typical observed stress fields and cracking of beam-end specimens	255
Figure 9.10 Typical splitting failure for beam-end specimens (BE-RAC2-50-375B).....	256
Figure 9.11 Typical bond-slip response of beam-end specimen (BE-RAC3-40-450B).....	257
Figure 9.12 Comparison of bond-slip responses for 30 MPa Phase 1 beam-end specimens.....	259
Figure 9.13 Comparison of bond-slip responses for 50 MPa Phase 1 beam-end specimens.....	260
Figure 9.14 Relationship between average bond strength and aggregate crushing value (Phase 1	

specimens)	261
Figure 9.15 Relationship between average bond strength and abrasion resistance (Phase 1 specimens)	263
Figure 9.16 Relationship between average bond strength and compressive strength (Phase 1 beam-end specimens)	264
Figure 9.17 Relationship between average bond strength and splitting tensile strength (Phase 1 specimens)	266
Figure 9.18 Relationship between average bond strength and $f_r/f_c^{1/2}$ (Phase 1 specimens).....	267
Figure 9.19 Relationship between average bond strength and fracture energy (Phase 1 specimens)	269
Figure 9.20 Schematic of the beam-end dissection procedure	270
Figure 9.21 Modes of bond failure (adapted from CEB-FIP, 2000).....	270
Figure 9.22 Main anchorage zone and splitting crack pattern (dissected BE-NAC-30-375A) ..	271
Figure 9.23 Main failure planes through concrete cover (dissected BE-NAC-30-375A)	272
Figure 9.24 Main test bar, measured bonded length, and concrete rib indentations (dissected BE-NAC-30-375A)	272
Figure 9.25 Main anchorage zone and splitting crack pattern (dissected BE-NAC-50-375A) ..	273
Figure 9.26 Main failure planes through concrete cover (dissected BE-NAC-50-375A)	273
Figure 9.27 Main test bar, measured bonded length, and crushing of concrete rib indentations (dissected BE-NAC-50-375A)	274
Figure 9.28 Main anchorage zone and splitting crack pattern (dissected BE-RAC1-30-375A)	275
Figure 9.29 Main failure planes through concrete cover (dissected BE-RAC1-30-375A).....	275
Figure 9.30 Main test bar, measured bonded length, and adhered concrete (dissected BE-RAC1-30-375A).....	276
Figure 9.31 Main anchorage zone and splitting crack pattern (dissected BE-RAC2-30-125B).	276
Figure 9.32 Main failure planes through concrete cover (dissected BE-RAC2-30-125B).....	277
Figure 9.33 Main test bar, measured bonded length and adhered concrete (dissected BE-RAC2-30-125B).....	277
Figure 9.34 Main anchorage zone and splitting crack pattern of (dissected BE-RAC2-50-375A)	

.....	278
Figure 9.35 Main failure planes through concrete cover (dissected BE-RAC2-50-375A).....	278
Figure 9.36 Main test bar, measured bonded length and adhered concrete (dissected BE-RAC2-50-375A).....	279
Figure 9.37 Evidence of crushing of concrete rib indentations (dissected BE-RAC2-50-375A)	279
Figure 9.38 Summary charts of average bond strength normalized to $f_c^{1/2}$ (Phase 2).....	284
Figure 9.39 Comparison of bond-slip responses for 40 MPa Phase 2 beam-end specimens.....	287
Figure 9.40 Comparison of bond-slip responses for 60 MPa Phase 2 beam-end specimens.....	288
Figure 9.41 Relationship between average bond strength and aggregate crushing value (Phase 2 specimens)	290
Figure 9.42 Relationship between average bond strength and abrasion resistance (Phase 2 specimens)	291
Figure 9.43 Relationship between average bond strength and concrete hardened density (Phase 2 specimens)	293
Figure 9.44 Relationship between average bond strength and compressive strength (Phase 2 beam-end specimens)	294
Figure 9.45 Relationship between average bond strength and splitting tensile strength (Phase 2 specimens)	296
Figure 9.46 Relationship between average bond strength and modulus of rupture (Phase 2 specimens)	297
Figure 9.47 Relationship between fracture energy and average bond strength (Phase 2 specimens)	299
Figure 9.48 Main anchorage zone and splitting crack pattern (dissected BE-NAC-40-450A) ..	301
Figure 9.49 Main failure planes through concrete cover (dissected BE-NAC-40-450A)	301
Figure 9.50 Main test bar, measured bonded length, and evidence of slip (dissected BE-NAC-40-450A).....	302
Figure 9.51 Main anchorage zone and splitting crack pattern (dissected BE-NAC-40-450A) ..	303
Figure 9.52 Main failure planes through concrete cover (dissected BE-NAC-40-450A)	303
Figure 9.53 Main test bar, measured bonded length, and adhered concrete (dissected BE-NAC-40-450B).....	304

Figure 9.54 Main anchorage zone and splitting crack pattern (dissected BE-RAC1-40-125A)	304
Figure 9.55 Main failure planes through concrete cover (dissected BE-RAC1-40-125A).....	305
Figure 9.56 Main test bar, measured bonded length, and adhered concrete (dissected BE-RAC1-40-125A).....	305
Figure 9.57 Main anchorage zone and splitting crack pattern (dissected BE-RAC1-40-125B).	306
Figure 9.58 Main failure planes through concrete cover (dissected BE-RAC1-40-125B).....	307
Figure 9.59 Main test bar, measured bonded length, and evidence of slip (dissected BE-RAC1-40-125B).....	307
Figure 9.60 Main anchorage zone and splitting crack pattern (dissected BE-RAC3-40-125A)	308
Figure 9.61 Main failure planes through concrete cover (dissected BE-RAC3-40-125A).....	309
Figure 9.62 Main test bar, measured bonded length, and adhered concrete (dissected BE-RAC3-40-125A).....	309
Figure 9.63 Main anchorage zone and splitting crack pattern (dissected BE-RAC3-40-125B).	310
Figure 9.64 Main failure planes through concrete cover (dissected BE-RAC3-40-125B).....	310
Figure 9.65 Main test bar, measured bonded length, and adhered concrete (dissected BE-RAC3-40-125B).....	311
Figure 9.66 Relationship between bonded length and maximum bond force (Combined results of Phase 1 and 2).....	315
Figure 9.67 Relationship between aggregate strength (ACV) and $T_b/f_c^{1/4}$ (Combined Phase 1 and 2 results)	316
Figure 9.68 Relationship between maximum bond force and $f_c^{1/2}$ (Combined results of Phase 1 and 2).....	317
Figure 9.69 Relationship between maximum bond force and $f_c^{1/4}$ (Combined results of Phase 1 and 2).....	318
Figure 9.70 Relationship between $T_b/f_c^{1/4}$ and $f_{ct}/f_c^{1/2}$ (Combined results of Phase 1 and 2)....	318
Figure 9.71 Relationship between $T_b/f_c^{1/4}$ and $f_r/f_c^{1/2}$ (Combined results of Phase 1 and 2).....	320
Figure 9.72 Relationship between $T_b/f_c^{1/4}$ and fracture energy, $G_{f,1mm}$ (Combined results of Phase 1 and 2).....	321
Figure 9.73 Experimental bond force, T_b normalized with respect to $f_c^{1/4}$ versus predicted normalized bond force, based on ACI 408 equation (Equation 9.2)	325

Figure 9.74 Experimental bond force, T_b versus predicted maximum bond force, based on regression Model A (Equation 9.4)	327
Figure 9.75 Experimental bond force, T_b normalized with respect to $f_c'^{1/4}$ versus predicted normalized experimental bond force, based on regression Model B (Equation 9.5)	327
Figure 9.76 Experimental bond force, T_b normalized with respect to $f_c'^{1/4}$ versus predicted normalized experimental bond force, based on regression Model C (Equation 9.6)	328
Figure 9.77 Concrete compressive strength versus development lengths predicted by CSA A23.304 code equation and equation 9.7 (Model C).....	331
Figure 9.78 Relationship between aggregate, concrete, and concrete-steel bond properties	334
Figure 10.1 Process for determining whether a particular RCA source can be used as a coarse aggregate in structural concrete applications.....	340
Figure 10.2 Process for assessing the performance of RCA concrete mixture proportions	347
Figure C.1 Beam-end test frame schematic and component layout.....	384
Figure C.2 SAP 2000 structural models and applied design loads	389
Figure D.1 Bond-slip response and crack pattern for BE-NAC-30-125A.....	410
Figure D.2 Bond-slip response and crack pattern for BE-NAC-30-125B	410
Figure D.3 Bond-slip response and crack pattern for BE-NAC-30-375A.....	411
Figure D.4 Bond-slip response and crack pattern for BE-NAC-30-375B	411
Figure D.5 Bond-slip response and crack pattern for BE-NAC-50-125A.....	412
Figure D.6 Bond-slip response and crack pattern for BE-NAC-50-125B	412
Figure D.7 Bond-slip response and crack pattern for BE-NAC-50-375A.....	413
Figure D.8 Bond-slip response and crack pattern for BE-NAC-50-375B	413
Figure D.9 Bond-slip response and crack pattern for BE-RAC1-30-125A	414
Figure D.10 Bond-slip response and crack pattern for BE-RAC1-30-125B	414
Figure D.11 Bond-slip response and crack pattern for BE-RAC1-30-375A.....	415
Figure D.12 Bond-slip response and crack pattern for BE-RAC1-30-375B	415

Figure D.13 Bond-slip response and crack pattern for BE-RAC1-50-125A	416
Figure D.14 Bond-slip response and crack pattern for BE-RAC1-50-125B	416
Figure D.15 Bond-slip response and crack pattern for BE-RAC1-50-375A	417
Figure D.16 Bond-slip response and crack pattern for BE-RAC1-50-375B	417
Figure D.17 Bond-slip response and crack pattern for BE-RAC2-30-125A	418
Figure D.18 Bond-slip response and crack pattern for BE-RAC2-30-125B	418
Figure D.19 Bond-slip response and crack pattern for BE-RAC2-30-375A	419
Figure D.20 Bond-slip response and crack pattern for BE-RAC2-30-375B	419
Figure D.21 Bond-slip response and crack pattern for BE-RAC2-50-125A	420
Figure D.22 Bond-slip response and crack pattern for BE-RAC2-50-125B	420
Figure D.23 Bond-slip response and crack pattern for BE-RAC2-50-375A	421
Figure D.24 Bond-slip response and crack pattern for BE-RAC2-50-375B	421
Figure D.25 Bond-slip response and crack pattern for BE-NAC-40-125A	422
Figure D.26 Bond-slip response and crack pattern for BE-NAC-40-125B	422
Figure D.27 Bond-slip response and crack pattern for BE-NAC-40-450A	423
Figure D.28 Bond-slip response and crack pattern for BE-NAC-40-450B	423
Figure D.29 Bond-slip response and crack pattern for BE-NAC-60-125A	424
Figure D.30 Bond-slip response and crack pattern for BE-NAC-60-125B	424
Figure D.31 Bond-slip response and crack pattern for BE-NAC-60-450A	425
Figure D.32 Bond-slip response and crack pattern for BE-NAC-60-450B	425
Figure D.33 Bond-slip response and crack pattern for BE-RAC1-40-125A	426
Figure D.34 Bond-slip response and crack pattern for BE-RAC1-40-125B	426
Figure D.35 Bond-slip response and crack pattern for BE-RAC1-40-450A	427
Figure D.36 Bond-slip response and crack pattern for BE-RAC1-40-450B	427
Figure D.37 Bond-slip response and crack pattern for BE-RAC1-60-125A	428

Figure D.38 Bond-slip response and crack pattern for BE-RAC1-60-125B	428
Figure D.39 Bond-slip response and crack pattern for BE-RAC1-60-450A	429
Figure D.40 Bond-slip response and crack pattern for BE-RAC1-60-450B	429
Figure D.41 Bond-slip response and crack pattern for BE-RAC3-40-125A	430
Figure D.42 Bond-slip response and crack pattern for BE-RAC3-40-125B	430
Figure D.43 Bond-slip response and crack pattern for BE-RAC3-40-450A	431
Figure D.44 Bond-slip response and crack pattern for BE-RAC3-40-450B	431
Figure D.45 Bond-slip response and crack pattern for BE-RAC3-60-125A	432
Figure D.46 Bond-slip response and crack pattern for BE-RAC3-60-125B	432
Figure D.47 Bond-slip response and crack pattern for BE-RAC3-60-450A	433
Figure D.48 Bond-slip response and crack pattern for BE-RAC3-60-450B	433

Chapter 1: Introduction

1.1 Background

1.1.1 The State of the Aggregate Resource

Between 2000 and 2009, approximately 179 million tonnes per year, on average, of aggregate were used in Ontario. The construction of roads, buildings, sewers and water mains accounts for approximately 75% of this total. Specifically, of all the aggregate used in construction related activities, approximately 28% were used in the production of ready-mixed concrete and other concrete products (MNR, 2010).

Even though Ontario is abundant with natural rock and aggregate deposits, the costs of shipping the supply to an area where there is sufficient demand (i.e., in Southern Ontario) is the central issue. The transportation costs are estimated to comprise approximately 60% of the total cost of aggregate. Therefore, the economic value of an aggregate source is based as much on its proximity to its final destination as the quantity and quality of the deposit itself (MNR, 2010). In addition to the financial costs associated with transporting aggregates long distances, significant environmental impacts such as increased greenhouse gas emissions make the aggregate production cycle less sustainable. Approximately 85% of total aggregate production in Ontario takes place in Southern Ontario where the demand for aggregates and aggregate-derived products is the highest. Figure 1.1 provides a summary of the total aggregate reserves in Ontario along with high quality reserves within 75 km of the Greater Toronto Area. High quality aggregate reserves refer to aggregate that is suitable for use in concrete and asphalt applications.

In terms of future aggregate consumption, it is project that 186 million tonnes of aggregate per year on average will be used in Ontario in the next 20 years. Note that this consumption includes the demands of all areas of Ontario and aggregate types of varying quality. For the Greater Toronto Area, consumption of aggregate (both of low and high quality) over the next 20 years is expected to be 61 million tonnes per year, on average (MNR 2010). Based on the projected consumption in the Greater Toronto Area, the aggregate industry may face a shortage of high-quality aggregate reserves within close proximity. Alternative and/or supplemental sources of

aggregates will therefore need to be considered to ensure an adequate long-term supply for the construction industry.

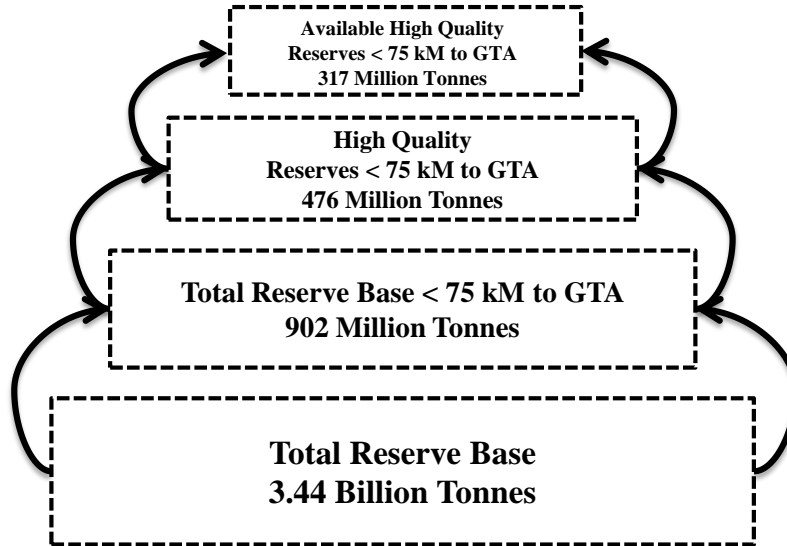


Figure 1.1 Aggregate reserves located within 75 km of the Greater Toronto Area (GTA) (Adapted from MNR, 2010)

1.1.2 The State of the Concrete Industry

In 2008, the Canadian concrete and cement industry combined contributed over \$3.2 billion to the gross domestic product, and in total, 28.1 million cubic metres of concrete were used in construction projects (CAC, 2008). Concrete is produced by combining cement, gravel, sand and water. The gravel and sand represent the coarse and fine aggregates, respectively and make up 60% to 75% of the total concrete volume (Kosmatka et al., 2002). Due to the high percentage of aggregate used in concrete, the sufficient production of high quality aggregate sources is essential to sustaining the concrete industry.

1.1.3 Construction and Demolition Waste

In Canada, approximately 11 million tonnes of landfill waste per year can be attributed to construction activities alone, of which 21% is from concrete rubble (CAC, 2009). In comparison, there is close to 100 million tonnes of demolished concrete produced annually in the United States and European countries combined (Masood et al., 2002).

1.1.4 RCA as an Alternative Coarse Aggregate Source in Concrete

The construction industry will have two options for dealing with the pending shortage of locally-available high-quality aggregate: accepting the added increase in transportation costs incurred by importing aggregate from other sources or, finding supplementary sources of aggregate that are readily available. Recycled concrete aggregate (RCA), produced by crushing concrete from demolished concrete structures may potentially serve as a new supplementary source. This secondary source of aggregate may be a viable solution for alleviating the aggregate supply shortage and will also assist in diverting considerable amounts of construction waste from landfills. As noted by Rao et al. (2007), there are several barriers that have affected the widespread use and promotion of RCA for use as coarse aggregate in new concrete (herein referred to as RCA concrete). These include: lack of concrete recycling facilities located in proximity to areas of construction demand, absence of appropriate concrete recycling processes that optimize RCA production and categorization, lack of awareness by the construction industry of the potential uses of RCAs and their associated properties, lack of government support to provide incentives for usage of these materials, and lack of standards to properly regulate the use of RCAs as a supplement for natural aggregates.

The properties of RCA concrete can vary widely due to the various sources and quality of the RCAs. As a result, the use of such materials in structural applications has been limited mainly to experimental and research work. However, some countries like China have begun to use RCA concrete on a very limited scale. Approximately 14 million tonnes of construction and demolition waste are generated in Hong Kong annually, but as of October 2003, only 22,700 m³ of RCA concrete was being used in structural applications (Rao et al., 2007). In other countries such as England, approximately 220 million tonnes of aggregates were used in 2001 of which 25% were recycled materials (Rao et al., 2007). The European Union produced approximately 180 million tonnes of construction and demolition waste annually of which 28% was reported to be recycled in the late 1990s (Rao et al., 2007). By comparison, in Ontario in 2007, 7% of the total aggregates used came from recycled or recovered materials (MNR, 2010).

1.1.5 Current use of RCA Concrete in Structural Applications

A limited number of research studies have investigated using RCA concrete in reinforced or

structural concrete applications. These studies have mainly involved the testing of high strength RCA concrete (Ajdukiewicz and Kliszczewicz, 2002); the shear strength of RCA concrete (Gonzalez-Fonteboa and Martinez-Abella, 2007, Fathifazl, 2008) and the bond strength of RCA concrete with reinforcing steel (Fathifazl, 2008, Choi and Kang, 2008, Xiao and Falkner, 2007). However, there are very few case studies of actual structures built utilizing RCA concrete to fully or partially replace NA concrete.

The new J-Cube Capital Mall in Singapore (completed in 2011) is an example of the use of RCA concrete in a structural application. Built on the site of the demolished Jurong Entertainment Center, the new mall utilized the reclaimed concrete as aggregate in 50% of the new concrete structural elements that comprise the superstructure (IES, 2011). Figure 1.2 illustrates artist renderings of the 200,000 ft² mall.

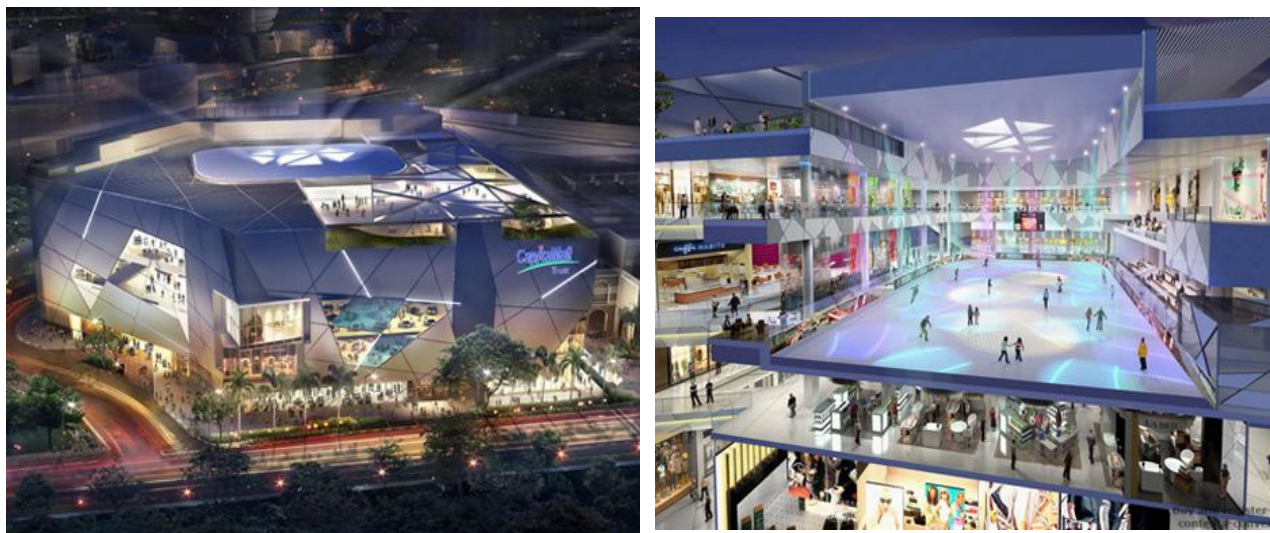


Figure 1.2 J-Cube Capital Mall, Singapore (IES, 2011)

A case study from North America was the demolition of the former Stapleton Airport in Denver, Colorado in which 2.1 million kilograms (2100 tonnes) of recycled concrete were utilized from old runway, office and warehouse structures in the construction of the new Enterprise Park at Stapleton (see Figure 1.3). In total, 4300 m³ of recycled concrete incorporating approximately 1400 tonnes of RCA was used in the construction of the tilt-up wall panels, making it the largest application of recycled concrete in a tilt-up application (CMRA, 2012).



Figure 1.3 Enterprise Park at Stapleton, Denver, United States (Etkin-Johnson, 2012)

1.2 Significance of RCA Research

Although there have been numerous studies on the use of RCA as a replacement for natural aggregate in concrete, there is still hesitation by the Canadian construction industry to use these materials. In part, this is due to the reluctance from owners, engineers, and concrete suppliers to assume the risk associated with guaranteeing the quality of a material for which there is still limited technical and in-place field data. The research presented in this thesis will provide concrete researchers, suppliers, engineers, developers, and contractors with new information on:

- Basic and advanced RCA properties and how they are related to one another,
- Basic and advanced mechanical properties of RCA concrete and how they differ from those of natural aggregate (NA) concrete,
- Mixture proportioning considerations for RCA concrete and the effect of RCA properties on cement and water demand,
- Bond performance of reinforced RCA concrete members including the effect of particular RCA properties on structural design criteria such as development length, and
- Classifying and selecting a particular RCA source for a specified application.

Based on the review of the current state-of-the-art of RCA concrete research, an identification of research gaps in the area of structural RCA concrete along with the specific objectives of this research will be presented.

1.3 Important Terms and Definitions

The following list of terms and definitions will be referred to and used throughout this thesis.

RCA(s) = recycled concrete aggregate(s) = aggregate(s) derived from the crushing and processing of demolished concrete structures (i.e., buildings, pavements, bridges, etc.). Only coarse RCA (i.e., particle sizes greater than 4.75 mm) has been investigated as part of this research study.

RCA Concrete = concrete produced using RCA as a full or partial replacement of natural aggregate. RCA concrete will also be referenced as RAC when used in tables or specimen identification.

NA concrete = natural aggregate concrete = concrete produced using natural (virgin) coarse aggregates. NA concrete will also be referenced as NAC when used in tables or specimen identification.

Original concrete = source concrete = concrete from which an RCA source was derived.

Original aggregates = the natural aggregates used to produce the original (or source) concrete from which an RCA source was derived.

Adhered mortar = AM = the attached mortar remaining on the original aggregates after crushing of the original (or source) concrete. The resulting agglomerate of the original aggregate and the adhered mortar is the recycled concrete aggregate or RCA.

1.4 Thesis Organization

This thesis has been organized into 11 chapters and three appendices. Chapter 2 presents a detailed literature review on properties of recycled concrete aggregates (RCAs), properties of concrete incorporating RCAs as a coarse aggregate replacement (RCA concrete), a review of

reinforcement bond in concrete and current research gaps. Chapter 3 outlines the research objectives and presents the experimental program. Chapter 4 presents the methods and results of the aggregate properties testing. Chapter 5 details the strategy by which the various mixture proportions were developed along with a summary of the finalized proportions and their applications. Chapter 6 details the procedures used to measure the fresh and hardened concrete properties. Chapters 7 and 8 contain the presentation and evaluation of the concrete test results for the direct replacement and strength-based mixture proportion types, respectively. Chapter 9 contains the presentation and evaluation of the beam-end bond specimen results along with an investigation of the interaction between RCA properties, RCA concrete properties and bond strength of RCA concrete with steel reinforcement. Chapter 10 utilizes selected findings of the previous chapters and presents a set of recommended guidelines for use of RCA in structural concrete applications. Chapter 11 provides a summary of the overall conclusions and contributions and identifies areas where future research work is required. Appendix A provides sample statistical calculations. Appendix B contains the bond-slip curves and crack patterns for the individual beam-end specimens. Appendix C provides a full overview of the beam-end test frame design assumptions and calculations. In addition, design drawings and sections of the test frame are included for use by other researchers intending to modify the frame for a specific testing application.

Chapter 2: Literature Review

2.1 General

The following chapter presents an overview of the current state-of-the-art of recycled concrete aggregates (RCAs) and the use of RCAs as a replacement of natural aggregate (NA) in new concrete (i.e., RCA concrete). The chapter is divided into three main sections: overview of RCAs, properties of RCA concrete, and bond of reinforcement in concrete. A summary and an identification of research gaps are presented at the end of the chapter which provide the basis for the overall objectives of this research project.

2.2 Recycled Concrete Aggregates (RCAs)

2.2.1 RCA Production Process

Once a concrete structure (i.e., concrete pavement, building, bridge, etc.) has been demolished, large pieces of concrete remain. Any steel reinforcement present is then removed using hydraulic shears, torches and electromagnets. The reinforcing steel and the concrete are then separated for further processing. The production of RCA from the demolished concrete debris involves several steps. Figure 2.1 outlines the production process of RCA recommended by ACI Committee 555 which includes removal of any deleterious material. Deleterious substances present in RCA could include: glass, plastic, plaster, oil droppings, wood, steel, clay, etc. and must be removed and sorted separately. Jaw crushers can provide an adequate particle size distribution necessary for quality RCA concrete production (ACI 555, 2001). Once the aggregates have been separated they must be classified according to size utilizing specified standards such as ASTM C 33 or CSA A23.1-09. After the RCA source has been sorted and graded it must be tested for strength, water absorption, abrasion, specific gravity, sulphate content and alkali-silica reaction potential before being considered for use as an aggregate.

Once the aggregates have been deemed suitable for use in new concrete, the mixture proportioning process can begin. Density and water absorption characteristics should be accounted for to ensure adequate workability, strength, and yield are achieved.

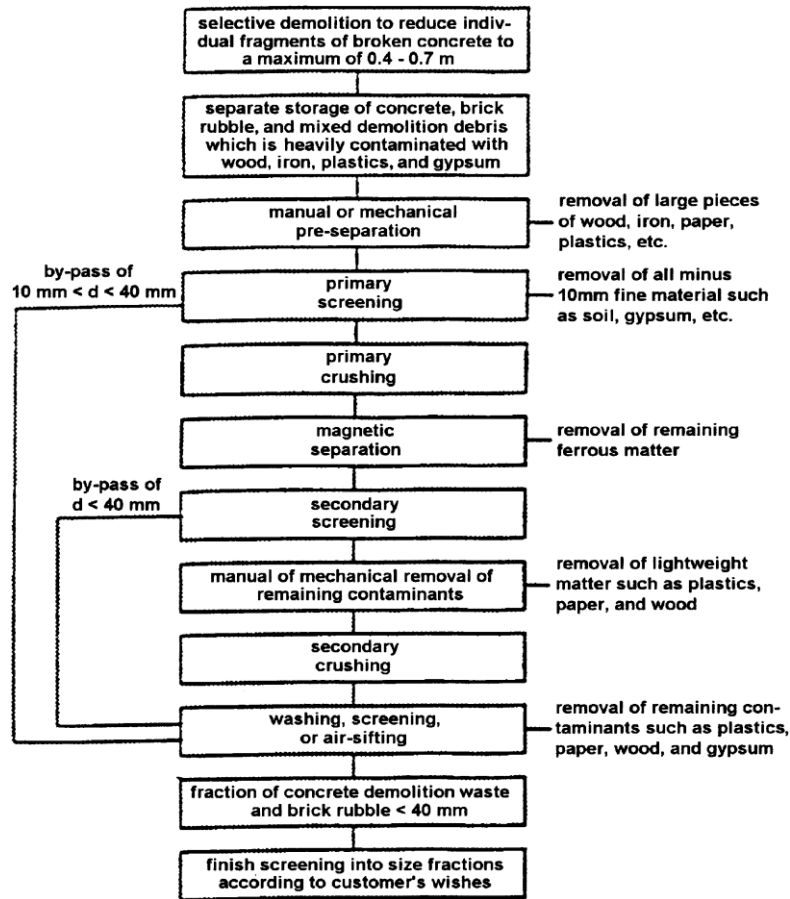


Figure 2.1 Production process for recycled concrete aggregates (ACI 555, 2001)

Tam and Tam (2007) recommend that different sources of RCA should be separately crushed and classified rather than processed in a combined form in a central location which could lower its overall quality and limit its applications. Nagataki et al. (2004) investigated producing RCA from the crushing of laboratory produced concrete blocks of varying compressive strengths. Blocks were stored for one year and exposed to exterior environmental conditions. Their main research involved investigating the effect of one and two-level processing of RCA. They found that using a jaw crusher and impact crusher followed by further mechanical grinding produced high-quality coarse RCA with reduced adhered mortar content.

2.2.2 Quantitative and Qualitative Aggregate Classification

The shape of a particle is defined using three different parameters: sphericity, form, and roundness (ICAR, 2004). Sphericity is a measure of the relative equivalence of the three principal axes or dimensions of a particle. Form is the measure of the relation between the three

dimensions of a particle based on ratios between the proportions of the long, medium, and short axes of the particle. Form, also called “shape factor,” is used to differentiate between particles that have the same sphericity values (ICAR, 2004). In terms of concrete aggregates, the roundness of an aggregate particle is a measure of the sharpness or angularity of the edges and corners of a particle (Neville, 1997). Texture or roughness of an aggregate affects its bond to the surrounding cement paste and influences the water demand of the concrete mixture. The surface texture of a particle can be classified as polished or dull, smooth or rough and can greatly influence the concrete’s ultimate strength in compression. As the surface of the aggregate becomes more roughened, the bond strength between the aggregate and cement paste increases (Neville, 1997).

Several qualitative and quantitative methods for characterizing the shape and texture of coarse aggregate are presented below:

1) ASTM D 3398, Index of Aggregate Particle Shape and Texture

This method provides a quantitative measure referred to as the particle index value which is used to indicate the effects of shape and texture on compaction and strength characteristics of soil aggregate and asphalt concrete mixtures. A washed and oven-dry sample is sieved into different size fractions and the bulk-dry specific gravity is determined. For each size fraction five cylindrical moulds of various diameters are used along with steel tamping rods of different weights. Each cylinder is filled in three layers with each layer receiving ten tamps. The procedure is then repeated with the same material but with each layer receiving 50 tamps. The particle index value is calculated using Equation 2.1.

$$I_a = 1.25V_{10} - 0.25V_{50} - 32.0 \quad \text{Equation 2.1}$$

Where,

I_a = particle index value;

V_{10} = voids in aggregate compacted at 10 drops per layer, %; and

V_{50} = voids in aggregate compacted at 50 drops per layer, %.

- 2) ASTM D 4791, Flat Particles, Elongated Particles, or Flat and Elongated Particles in Coarse Aggregate

This method evaluates aggregate shape by means of proportional calipers. The objective is to determine whether the particles have dimension ratios above or below a specified value. Particles are classified as cubical, flaky, elongated or flaky and elongated (ICAR, 2003).

- 3) British Standard BS EN 933-3: 1997 Tests for geometrical properties of aggregates. Determination of Particle Shape. Flakiness Index. This standard replaced the former BS 812-105 Flakiness Index and Elongation Index.

- 4) ASTM C-295, Petrography

Besides shape and texture, petrography can be used to determine physical and chemical characteristics of aggregates and to describe and classify constituents of a sample.

- 5) AASHTO TP 33, Modified, Uncompacted Void Content

In this test, a funnel is filled with aggregate and then left to flow from a fixed height into a cylinder. The uncompacted void content of the aggregate in the cylinder is measured. The uncompacted void content depends on the aggregate grading, shape, and surface texture. Only a single aggregate size should be used so the effect of the particle shape and texture can be evaluated (ICAR, 2004).

- 6) Image Analysis

There are currently no ASTM or AASHTO test methods for image analysis (ICAR, 2004). However, Fernlund (2005) proposed a method for determining the 3-D shape of coarse aggregate using image analysis. In this method only two images of the particles in the sample are required to obtain the shape and size distribution. In addition, the dimensions of all three axes of each individual particle can be measured very accurately.

- 7) Laser-Based Aggregate Scanning System (LASS)

Kim (2002) developed a new method of classifying aggregate shape, size, texture, angularity and grain-size distribution by using a combination of laser scanning and image analysis. A series of 3-D wavelet-based particle descriptors were used to analyze the three-dimensional data from the scanner and separate numerical indices were developed

for the individual classification of particle shape, texture, and angularity. According to Kim (2000), laser-based scanning, as opposed to other methods, can obtain true 3-D information on aggregates. Grain-size analysis and aggregate quality control are other potential applications of this scanning system.

2.2.3 Grading

Grading is the particle-size distribution of an aggregate as determined by a sieve analysis. Standards such as ASTM C136 or CSA A23.2-2A can be used to carry out a proper sieve analysis. Depending on their application, RCAs may be sieved to any variety of gradations. According to the Ontario Ministry of Transportation, aggregates for use in structural concrete should have gradation within the limits outlined in Table 2.1 (MTO, 2004).

Table 2.1 Gradation requirements for coarse aggregates for use in structural concrete, sidewalks, curb and gutter (MTO, 2004)

Nominal Maximum Size	19.0 mm	16.0 mm	13.2 mm	9.5 mm	6.7 mm
MTO Sieve Designation					
mm					
26.5	100	-	-	-	-
19.0	85 – 100	100	100	-	-
16.0	65 – 90	96 - 100	-	-	-
13.2	-	67 – 86	90 - 100	100	100
9.5	20 – 55	29 – 52	40 – 70	85 – 100	-
6.7	-	-	-	-	75 – 100
4.75	0 – 10	0 – 10	0 - 15	10 – 30	40 – 80
2.36	-	-	-	0 – 10	0 – 20

Hansen (1986) concluded that it is reasonably easy to produce well-graded RCA using a jaw crusher. Chen et al. (2002) found that using a crusher with the same maximum aggregate crushing size produces an RCA gradation similar to natural aggregate.

2.2.4 Absorption and Surface Moisture

Aggregates are naturally porous materials and water can be absorbed into the body of the particles (Mindess et al., 2003). The absorption capacity is defined as the total amount of water required to bring the aggregate to a saturated surface dry condition. Aggregates may exist in several moisture states: oven dry, air-dry, saturated surface dry, or moist. Figure 2.2 illustrates

the various moisture states of aggregates.

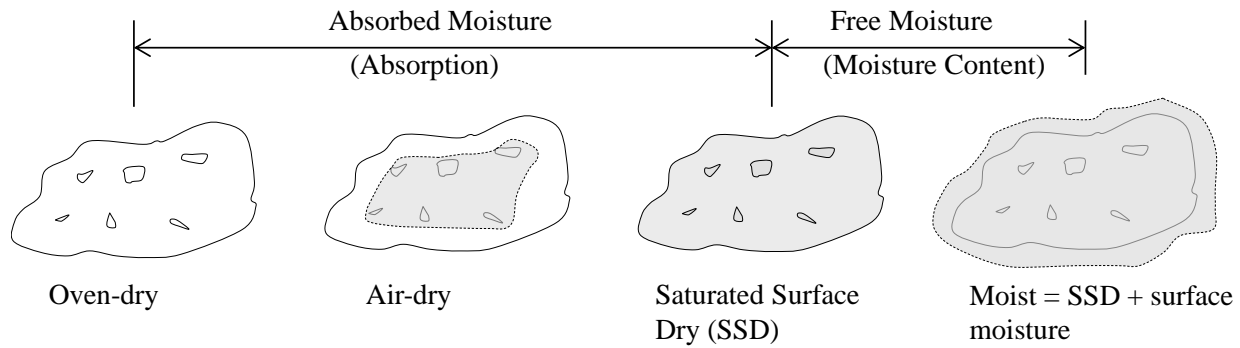


Figure 2.2 Various moisture states of aggregates (adapted from Neville, 1997)

A distinction must be made between the moisture that is absorbed by the aggregate and the additional water that adheres to the aggregates' surface. In concrete mixture proportions it is this surface or free moisture that is used to offset the required mixing water. Only free water is available for mixing in concrete and typically, it is this moisture which contributes directly to the water-cement ratio. In the field, stockpiled aggregates are usually much closer to a saturated surface dry condition (Mindess et al., 2003). An aggregate's ability to absorb water depends mainly on the size and number of internal pores (Neville, 1997). Hansen (1986) concluded that RCAs have a higher water requirement than natural aggregates due to the higher water absorption of old adhered mortar. In terms of impacting concrete workability, for the same slump, the free water requirement for RCA concrete may be around 5% higher than for NA concrete (ACI 555, 2001). The rate of absorption also plays an important role in concrete mixture proportioning incorporating RCA. In general, RCAs take longer to absorb moisture than natural aggregates and, as a result, may not reach full saturation during the mixing period. It has been suggested to pre-soak the RCAs to compensate for their slower absorption rate (Hansen, 1986).

Table 2.2 summarizes and presents some additional findings of previous researchers on absorption of coarse RCA. It is interesting to note the wide differences observed in absorption between the various studies (between 0.57 and 11.6%). In addition, there is a large data set for the absorption of RCA as this is the most critical parameter required by researchers involved in the study of RCA or RCA concrete.

Table 2.2 Summary of findings from previous researchers on absorption of coarse RCA

Researcher(s)	Number of RCA sources studied	Absorption range
Bordelon et al. (2009)	1	5.27%
Rahal (2007)	1	3.47%
Tam and Tam (2007)	10	0.57 to 8.74%
Lin et al. (2004)	1	6.99%
Casuccio et al. (2008)**	2	3.8 to 3.9%
Chen et al. (2003)	2	5.04 to 7.54%
Padmini et al. (2009)**	3	3.65 to 4.86%
Nagataki et al. (2004)*	3	4.88 to 6.27%
Poon et al. (2004)	1	6.28%
Movassaghi (2006)	2	5.2 to 11.6%
Etxeberria et al. (2007)	1	4.45%
Choi and Kang (2008)	3	2.64 to 6.25%
Obla and Kim (2009)	4	4.31 to 5.87%
Fathifazl (2009)	2	3.3 to 5.4%
Smith (2010)	1	4.3%
Shayan and Xu (2003)	1	4.7%
Gokce et al. (2004)	2	3.19 to 5.58%
Hansen and Narud (1983)	3	5.7 to 6.0%
Sagoe-Crentsil et al. (2001)	1	5.6%
Xiao and Falkner (2007)	1	9.25%

* Investigated a secondary crushing process which reduced the amount of adhered mortar and consequently, the absorption.

** Used laboratory produced original concrete with nominal aggregate size of 20 mm.

Levy and Helene (2004) found that as the percent RCA replacement increases, the water absorption rate increases. Specifically, they reported that the coarse and fine RCA were 6 to 10 times more water absorbent than the natural aggregates. Chen et al. (2002) used RCA and ceramic tiles in their mixtures and also found absorption rates of RCA to be much higher than for natural aggregate and they attributed this difference to the higher porosity of the RCA. Tam et al. (2008) suggested a method for measuring the water absorption of RCA that is different than traditional ASTM, CSA or British standards. It involves the use of a pycnometer and the real-time measurement of absorption. Oven-dry aggregate is first added to the pycnometer and immersed in water which is filled to a reference mark. An initial weight at time T_0 is recorded and as the aggregate pores begin to absorb water additional water is refilled to the reference mark and the process is repeated until no further water is absorbed.

2.2.5 Bulk Density

The bulk density is defined as the mass of aggregate particles at SSD that would fill a unit volume. This value is most commonly used in concrete mixture proportioning. Hansen and Narud (1983) found bulk densities at SSD for RCAs to be slightly less than for natural aggregates. This is the result of the lower density adhered mortar on the RCA. Table 2.3 summarizes and presents additional findings from previous researchers on the bulk density of RCA.

Table 2.3 Summary from previous researchers on bulk relative density of coarse RCA

Researcher(s)	Number of RCA sources studied	Bulk Density (Oven dry)	Bulk Density (SSD)	Bulk Density (Apparent)
Chen et al. (2003)	2	-	2.28 to 2.29	-
Obla and Kim (2009)	4	-	2.54 to 2.56	-
Etxeberria et al. (2007)	1	-	2.43	-
Smith (2010)	1	2.40	-	-
Tam and Tam (2007)	10	2.12 to 2.62	-	-
Tu et al. (2006)	1	2.35	2.48	-
Fathifazl (2009)	2	2.31 to 2.42	2.42 to 2.50	2.64
Movassaghi (2006)	2	2.05 to 2.28	2.28 to 2.40	2.58 to 2.68
Gokce et al. (2004)	2	-	2.41 to 2.50	-

2.2.6 Abrasion Resistance

Abrasion resistance of an aggregate is used often as a measure of its quality. Low abrasion resistance of an aggregate can increase the quantity of fines in the concrete and, as a consequence, can increase the water requirement of the concrete (Kosmatka et al., 2002). The most common test for abrasion resistance is the Los Angeles abrasion test. Under the CSA standards, the Micro-Deval apparatus is used to determine abrasion resistance of aggregates. The method involves placing a set amount of loose aggregate into a cylindrical steel drum with small steel ball bearings and water then spinning the drum for two hours. This action allows the aggregates and steel balls to knock off small pieces of aggregate. Due to the more brittle adhered mortar, RCAs have been found to have abrasion resistance values between 15 and 63% lower than natural aggregate (Hansen and Narud, 1983). Table 2.4 summarizes and presents additional findings from previous researchers on the abrasion resistance of coarse RCA.

Table 2.4 Summary from previous researchers on abrasion resistance of coarse RCA

Researcher(s)	Number of RCA sources studied	LA Abrasion Resistance	Micro-Deval Abrasion Resistance
Casuccio et al. (2008)	2	34 to 39%	-
Obla and Kim (2009)*	4	23.8 to 26.0%	-
Movassaghi (2006)	2	-	10.6 to 34.2%
Hansen and Narud (1983)*	3	26.4 to 36.7%	-
Shayan and Xu (2003)	1	32%	-
Tu et al. (2006)	1	29.3%	-
Smith (2010)	1	-	14.9%

* Note: only includes 2 of the 4 RCA sources and RCA sources were derived from returned concrete

2.2.7 Aggregate Crushing Strength

The strength of an aggregate can be a limiting factor in concrete compressive strength. To test the strength of bulk aggregate, an aggregate crushing value test (BS 812:1990) can be used to determine the aggregate crushing value (ACV). There is no direct correlation between the ACV and aggregate compressive strength although values will sometimes be in agreement. It may be possible that the influence of the aggregate on the strength of concrete is not only due to the aggregates' mechanical properties but also its absorption and bond characteristics (Neville, 1997). According to BS 882:1992, aggregates of various crushing values may be used for the following applications (excerpt from Rahman et al., 2009):

ACV < 25% Aggregates can be used in the production of concrete in heavy duty floors

25% < ACV < 45% Aggregates can be used in concrete for wearing surfaces

ACV > 45% Aggregates can be used in concrete for other purposes.

Limbachiya (2010) performed aggregate crushing value tests with one natural coarse aggregate source and two coarse RCA sources. The ACV for the natural aggregate was 12.4 and the RCAs had ACVs of 17.5 and 22.0.

Table 2.5 summarizes and presents additional findings from previous researchers on the aggregate crushing value of coarse RCA.

Table 2.5 Summary from previous researchers on aggregate crushing value of coarse RCA

Researcher(s)	Number of RCA sources studied	ACV
Padmini et al. (2009)*	3	23 to 26
Hansen and Narud (1983)	3	23.2 to 28.4
Sagoe-Crentsil et al. (2001)	1	23.1
Rakshvir and Barai (2006)	3	26.2 to 28.1
Limbachiya (2010)	2	17.5 to 22.0
Shayan and Xu (2003)	1	24
Katz (2003)	1	24.3

* RCA was produced from laboratory concrete with nominal aggregate size of 20 mm.

2.2.8 Adhered Mortar Content

Upon crushing old concrete, the resultant RCA contains both natural stone and old mortar. This old adhered mortar can account for, between 25 and 60 percent by volume of the aggregate itself. It should also be noted that the finer the aggregate, the higher the adhered mortar content (Hansen and Narud, 1983; Tu et al., 2006; and Juan and Gutierrez, 2009). The adhered mortar content can have negative effects on such concrete properties as absorption, density, abrasion resistance and sulphate content. The amount of adhered mortar remaining on RCAs depends largely on the crushing process by which the aggregates are produced. As the number of crushing processes increase, the amount of adhered mortar is reduced (Juan and Gutierrez, 2009, Nagataki et al., 2004). Etxeberria et al. (2007) found that by using an impact crusher a higher percentage of RCA without adhered mortar could be achieved. They also suggest that the adhered mortar in RCAs is lower in strength than the mortar produced in new concrete incorporating RCAs. As a result, they concluded that the weakest point in concrete produced with coarse RCA is governed by the strength of the RCA and their adhered mortar.

Several different methods have been devised to determine the percent of adhered mortar in RCAs. Hansen and Narud (1983) prepared RCA concrete cubes using red-coloured cement. After being cut into slices and polished, the new red-coloured mortar and the adhered old mortar on the RCA could be clearly distinguished. The adhered mortar content was determined using a linear traverse method similar in principle to ASTM C 457-71, Standard Recommendation Practice for Microscopical Determination of Air-Void Content and Parameters of the Air-Void System in Hardened Concrete.

Another common method used in the determination of adhered mortar content is by treatment with a solution of hydrochloric acid (Poon et al., 2004; Gokce et al., 2004; and Nagataki et al., 2004) or nitric acid (Movassaghi, 2006). This method focuses on the acid-dissolution of the cement paste as a way of separating the original aggregate from the old adhered mortar and has produced acceptable results. However, as noted by Juan and Gutierrez (2009), this method cannot be used on RCAs containing original limestone as the acid also attacks the aggregate. A combination of freeze-thaw and chemical breakdown has been another method used to determine the adhered mortar content. Proposed by Abbas et al. (2008), the freeze-thaw treatment method combines ASTM standard C 88-05, Standard test method for soundness of aggregates by use of sodium sulphate or magnesium sulphate and the MTO standard LS-614-2001 Method of test for freezing and thawing of coarse aggregate, to both mechanically and chemically breakdown the bond between the original aggregate and the attached mortar. The results of this test were validated by image analysis. One of the more recent methods used involves subjecting the RCAs to a thermal treatment to separate the adhered mortar (Juan and Gutierrez, 2009). Working on the principle that cement mortar begins to convert to quicklime at a temperature of 400°C, a muffle furnace is used to heat the aggregates and breakdown the adhered mortar. To induce further thermal stresses, the aggregates are rapidly cooled in water. Table 2.6 presents and summarizes the findings from previous researchers on the adhered mortar content of coarse RCA.

Table 2.6 Summary from previous researchers on adhered mortar content of coarse RCA

Researcher(s)	Number of RCA sources	Method of adhered mortar removal	Adhered mortar content
Nagataki et al. (2004)	3	Hydrochloric acid dissolution	30.2 to 55.0%
Gokce et al. (2004)	2	Hydrochloric acid dissolution	32.4 to 55.7%
Fathifazl (2008)	2	Freeze-thaw + sulphate attack	23 to 41%
Movassaghi (2006)	2	Nitric acid dissolution	37.6 to 62.6%
Liu et al. (2011)	2	Image analysis	42.2 to 46.5%
Juan and Gutierrez (2009)**	1	Thermal treatment	40 to 55%
Hansen and Narud (1983)*	3	Linear traverse method	41 to 43%

* Note: the linear traverse method is based on a percent volume of adhered mortar.

** The RCA sample came from one recycling plant however, 15 separate samples were tested.

2.2.9 Recycled Concrete Aggregate Preparation for use in Concrete

Researchers have experimented with different ways to prepare RCAs through different crushing methods and by accounting for their higher absorption capacity. Lin, Y.H. et al. (2004) recommend that RCAs be washed and regular chemical and mineral admixtures should be incorporated to ensure adequate compressive strength and workability.

2.2.10 National and International Standards and Guidelines for use of RCAs

Based on the current state-of-the-art of RCA research, the following guidelines and standards have been proposed by various international, technical, and design code committees.

2.2.10.1 Canadian Standards Association (CSA)

Current Canadian standards do not have a specific section on the use of RCA or RCA concrete. However, in CSA A23.1-09 Clause 4.2.3.1 (CSA A23.1, 2009) reference is given to using recycled concrete as aggregate. It states that aggregates should be evaluated in a similar manner to normal-density aggregates and the following parameters should be assessed: durability characteristics, deleterious materials, potential alkali-aggregate reactivity, chloride contamination, and workability characteristics of resulting concrete.

2.2.10.2 American Concrete Institute (ACI)

Similar to Canada, the United States' current building code for concrete, published by the American Concrete Institute (ACI 318, 2011) does not include specific provisions on using RCA concrete. Guidance on use of recycled materials in concrete is mainly provided by ACI technical committee 555 and their current state-of-the-art Report on Demolition and Reuse of Hardened Concrete (ACI 555, 2001). Section 5 of the report provides guidance on the production of concrete from recycled concrete and includes a discussion of aggregate production, aggregate properties, effects of aggregate properties on concrete properties and guidelines for RCA concrete mixture proportioning.

2.2.10.3 European Guidelines (RILEM)

A European specification for use of recycled aggregate in concrete was published in 1994 as a

recommendation report prepared by the former RILEM technical committee 121 (newly revised as committee 217). This report deals with coarse recycled aggregates derived from demolished masonry rubble (defined as Type 1), demolished concrete rubble (Type 2), and a combination of demolished concrete and natural aggregates (Type 3). Detailed ranges for various aggregate properties are outlined and used to classify a particular RCA source as either Type 1, 2 or 3. In addition, based on the RCA type, provisions for use as an aggregate concrete along with a set of durability compliance criteria are provided.

2.2.10.4 German Institute for Standardization

Recently updated in 2002, the German standard DIN 4226-100 allows the use of RCA in new concrete provided it satisfies the requirements of a particular aggregate class. Four separate classes of RCA are presented and classed according to Table 2.7.

Table 2.7 German standards on use of RCA in concrete (DIN, 2002)

Constituents (% by mass)	Type 1	Type 2	Type 3	Type 4
Concrete and natural aggregates acc. to DIN 4226-1	≥ 90	≥ 70	≤ 20	
Clinker, no porous clay bricks	≤ 10	≤ 30	≥ 80	≤ 80
Calcium silicate bricks			≤ 5	
Other mineral materials (e.g., porous brick, lightweight concrete, plaster, mortar, porous slag)	≤ 2	≤ 3	≤ 5	≤ 20
Asphalt	≤ 10	≤ 30	≤ 1	
Foreign substances (e.g., glass, plastic, metal, wood, paper, other)	≤ 0.2	≤ 0.5	≤ 0.5	≤ 1
Oven dry density (kg/m^3)	≥ 2000	≥ 2000	≥ 1800	≥ 1500
Maximum water absorption after 10 min (%)	10	15	20	No limit

2.2.10.5 Japanese Industrial Standard

The Japanese Standards Association separates recycled aggregates into two separate categories: low quality Class L and high quality Class H recycled aggregates. Class L aggregate concrete includes backfilling, filling and leveling concrete applications whereas Class H can be used for normal concrete applications. The standards for use of Class L and Class H recycled aggregates in concrete are JIS A 5023 (2006) and JIS A 5021 (2011), respectively. Table 2.8 outlines the physical properties requirements Class H recycled aggregates. Additional provisions are

provided on the limits of deleterious substance amounts in recycled aggregates.

Table 2.8 Japanese standards on use of high-quality RCA in concrete (JIS, 2011)

Items	Coarse aggregate	Fine aggregate
Oven-dry density, g/cm ³	not less than 2.5	not less than 2.5
Water absorption, %	not more than 3.0	not more than 3.0
Abrasion, %	not more than 35	NA
Solid volume percentage for shape determination, %	not less than 55	not less than 53
Amount of material passing test sieve 75µm, %	not more than 1.0	not more than 7.0
Chloride ion content	not more than 0.04	not more than 0.04

2.3 Properties of RCA Concrete

2.3.1 RCA Concrete Mixture Proportioning and Production

Most studies in the literature have adopted the absolute volume mixture proportioning method when proportioning RCA concrete mixtures (ACI 211, 1991). The following summarizes a set of guidelines provided by ACI Committee 555 (2001) for developing appropriate mixture proportions using RCA concrete.

To determine a target mean compressive strength on the basis of a required compressive strength, a higher standard deviation (4.83 MPa) should be used when proportioning a concrete mixture with RCA of variable quality. At the proportioning stage, it may be assumed that the w/c ratio for a required compressive strength will be the same for RCA concrete as for NA concrete when coarse RCA is used with natural sand. If trial mixtures show that the compressive strength is lower than assumed, an adjustment to lower the w/c ratio should be made. For the same slump, the free water requirement of RCA concrete is 5% more than for NA concrete. Specific gravity, unit weight, and absorption of aggregates should be determined before mixture proportioning. The mixture proportions should be based on the measured density of the recycled aggregates intended for use in the on-site concrete. The fine aggregate to coarse aggregate ratio for RCA concrete is the same as for NA concrete. Trial mixtures are absolutely mandatory and if the placing will include confined spaces and irregular shapes, trial placements should also be batched.

Some researchers recommend pre-wetting the RCAs prior to use to ensure that the water required to achieve the water-cement ratio is not absorbed into the aggregate (Xiao et al., 2005 and Lin et al., 2004). Other researchers such as Etxeberria et al. (2007) recommend not saturating the RCA as it could produce a less effective interfacial transition zone. Instead the aggregates should be kept at a humidity of 80% of their total absorption capacity. They also recommended investigating several RCA replacement percentages in order to determine the optimum RCA content. Eguchi et al. (2007) suggested a method for the on-site production of RCA concrete. Their proposed on-site batching method consists of three main steps: all concrete constituents except the RCA are batched at the batching plant, the RCA is then added on-site using a portable weighing ladder, and then the concrete truck's drum is used to mix together all the constituents. This method has the potential to reduce both economic and environmental costs.

Abbas et al. (2007) developed a new mixture proportioning method known as the Equivalent Mortar Volume (EMV) method specifically for the proportioning of RCA concrete. This method works by ensuring that the total amount of mortar in a RCA concrete mixture is equal to its companion NA concrete mixture. This method guarantees that the volume of total mortar in RCA concrete is equivalent to that in NA concrete. The method counts the residual (adhered) mortar content (RMC) on the RCA as part of the total mortar. Equation 2.2 gives the required volume of RCA by the equivalent mortar volume method.

$$V_{RCA}^{RAC} = \frac{V_{NA}^{NAC} \times (1 - R)}{(1 - RMC) \times \frac{SG_b^{RCA}}{SG_b^{OVA}}} \quad \text{Equation 2.2}$$

Where V_{RCA}^{RAC} is the volume fraction of coarse RCA in RCA concrete, V_{NA}^{NAC} is the volume fraction of natural aggregate in the companion NA concrete, RMC is the residual mortar content of RCA, R is the replacement ratio (volumetric ratio of natural aggregate in RCA concrete to natural aggregate in NA concrete), and SG_b^{RCA} and SG_b^{OVA} are the bulk specific gravities of RCA and original natural aggregate, respectively. This new mixture proportioning method has been shown to improve the RCA concrete workability, fresh and hardened mechanical properties, and to reduce the amount of fine aggregate and cement required.

2.3.2 Workability

It has been found throughout the literature that as the percent of RCA replacement is increased, the slump values decrease. Topcu and Sengel (2004) attributed this observation to the higher water absorption rate of the mortar adhered to the RCA. Specifically, they found that RCA concrete produced with 50% RCA replacement or more had significantly reduced workability. After testing both approaches, Sagoe-Crenstil et al. (2001) found that plant or commercially produced RCA is relatively smoother than laboratory produced RCA and found this to improve workability.

2.3.3 Wet Unit Weight and Air Content

In general, concrete incorporating RCA has a lower fresh unit weight due to the lower density of the mortar adhered to the RCA. Topcu and Sengel (2004) found that RCA concrete had a wet unit weight that was 6% lower than NA concrete. On average, most NA concrete contains about 2% of air voids due to the batching process alone. Abou-Zeid et al. (2005) found RCA concrete had slightly higher air content values of 3.5% versus 2.1% for the NA concrete.

2.3.4 Interfacial Transition Zone (ITZ)

The structure of concrete is made up of three main components, the cement mortar (includes fine aggregate), the coarse aggregate and the cement-coarse aggregate interface or the interfacial transition zone (ITZ). The ITZ has a much higher porosity than the surrounding hydrated cement paste and as a result, the ITZ will fail before the aggregate or cement mortar. In general, the ITZ is a location of stress concentration arising from a difference in Poisson's ratio and modulus of elasticity of the aggregate and cement mortar. In aggregates with a more porous outer layer, migration of mobile ions towards it are encouraged and as a result, lead to a more dense interfacial transition zone and improved mechanical interlock properties. Given that RCAs are heterogeneous materials, the microstructure of concrete incorporating RCAs becomes even more complex. Figure 2.3 depicts the microstructure for RCA concrete which contains three ITZs, one between the original aggregate and the old adhered mortar, one between the original aggregate and the new mortar, and one between the new mortar and the old adhered mortar.

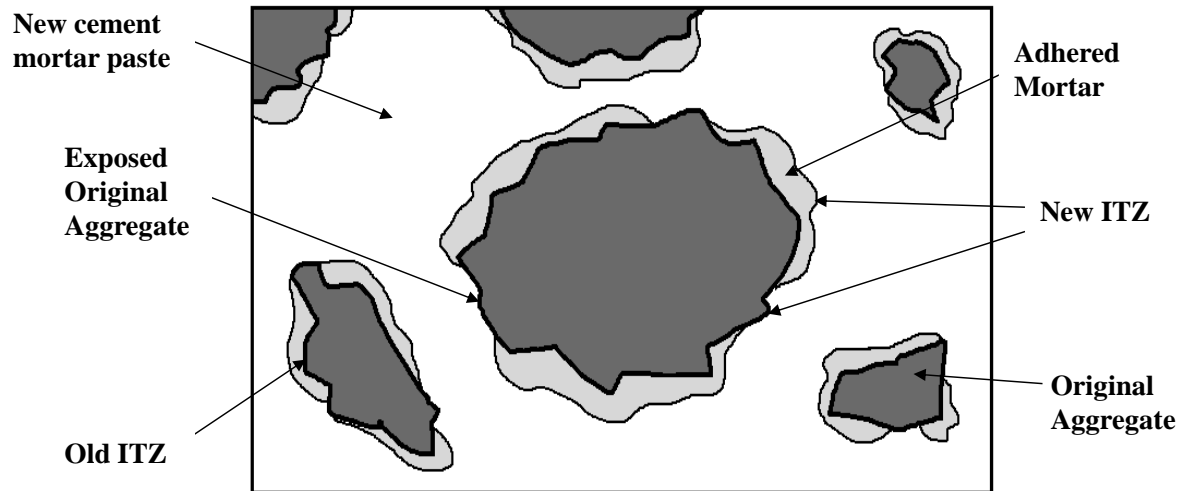


Figure 2.3 Interfacial transition zone in RCA concrete (Note: Adhered mortar + original aggregate = recycled concrete aggregate)

Otsuki et al. (2003) used the Vickers micro-hardness test to evaluate the ITZ characteristics in NA and RCA concrete. They found that the Vickers micro-hardness increases as the water-binder ratio decreases. In the case of the old ITZ formed on the RCAs, the compressive strength decreases with a decrease in adhered mortar strength because the strength of the old ITZ governs the strength of the RCA concrete. In concrete types with low water-binder ratio (0.25) they found the old ITZ to have lower Vickers micro-hardness. The opposite was observed in concrete with high water-binder ratio (0.55) as the new ITZ had lower Vickers hardness values.

Poon et al. (2004) used scanning electron microscopy to study the densities of both NA and RCA concrete. A higher density ITZ was observed in both the high-strength NA and RCA concretes. Comparing NAs and RCAs, the porosity of RCAs will be higher which will result in different ITZ microstructures. Etxeberria (2004) also used scanning electron microscopy to study the microstructure of RCA and found that the quality of the ITZ for RCA concrete was better than that of the adhered mortar. Therefore, the weakest point in RCA concrete is the adhered mortar and, consequently, the strength of the adhered mortar will determine the overall concrete strength and behaviour.

2.3.5 Compressive Strength

The concrete strength is generally regarded as the compressive strength tested by means of a uniaxial compressive strength test on a standard cylinder. The compressive strength is affected by a wide number of factors: water/cement ratio, type of cement, workability, addition of admixtures, supplementary cementing materials, aggregate size and type, moisture conditions during curing, temperature conditions during curing, age of concrete, maturity of concrete, and rate of loading. With regards to the aggregate used, its strength, surface texture and grading all determine its impact on the concrete compressive strength. The bond between the aggregate and the cement paste will directly influence the compressive strength. Crushed, angular and well-graded aggregates of nominal size tend to promote better bond and higher concrete strengths. Extensive testing has been carried out over the past three decades to determine the compressive strength of various RCA concrete mixtures. Table 2.9 presents and summarizes the findings of previous researchers on the compressive strength of RCA concrete.

Table 2.9 Summary of findings from previous researchers on compressive strength of RCA Concrete

Researcher(s)	Number of RCA sources studied	% Change in Compressive Strength from Control
Padmini et al. (2009)	3	10 to 35% decrease
Rahal (2007)*	1	3% decrease
Chen et al. (2003)	2	30 to 40% decrease
Etxeberria et al. (2007)**	1	20 to 25% decrease
Rakshvir and Barai (2006)	3	5 to 15% decrease
Katz (2003)	1	25% decrease
Topcu and Sengel (2004)	1	33% decrease
Tu et al. (2006)†	1	20 to 30% decrease
Sani et al. (2005)†	1	40% decrease

* Measured using cube specimens.

** RCA concrete with 100% RCA replacement.

† Fine RCA was used as a replacement for natural sand in the concrete mixtures.

‡ Compared to high performance NA concrete.

In addition to the findings of Table 2.9, Hansen and Narud (1983) found that the compressive strength of RCA concrete is largely controlled by the water/cement ratio of the original concrete when other factors are essentially identical. Sani et al. (2005) concluded that the compressive strengths of concrete made with 100% recycled coarse and fine aggregate was approximately 40% lower than for concrete utilizing natural aggregates. They also found that the compressive strength appeared to be inversely related to the porosity. They demonstrated that this reduction

in strength may be compensated for by incorporating fly ash into the mixture. In general, the compressive strength of RCA concrete decreases with an increase in percent of RCA replacement (Xiao et al., 2005). Lin et al. (2004) observed that the strength development was faster for RCA concrete with lower water-cement ratios of 0.5. In some cases, RCA concrete with strengths over 80 MPa have been produced using a combination of RCA replacement percentages, supplementary cementing materials and chemical admixtures (Ajdukiewicz and Kliszczewicz, 2002). In this case, the RCAs were obtained from an original concrete with compressive strengths of around 60MPa. In the research conducted by Sagoe-Crenstil et al. (2001), there was no significant difference between the strength of Portland cement concretes, as a function of aggregate type, for the grade of concrete investigated. Etxeberria et al. (2007) reported compressive strengths that were 20 to 25% less than NA concrete for 25%, 50%, and 100% RCA replacement. They recommended that RCA concrete could be used in medium strength applications only (20 to 45 MPa). In higher strength mixtures (45 to 60 MPa) the weakest point can be determined by the strength of the RCA or their adhered mortar content.

2.3.6 Tensile Strength

The tensile strength of concrete varies between 8 and 15% of the compressive strength. It is strongly affected by the type of test carried out to determine the tensile strength, the type of aggregate, the compressive strength, and the presence of a compressive strength that is transverse to the tensile stress (MacGregor and Bartlett, 2000). Typical tests for measuring the tensile strength of concrete include the direct tension test, the splitting tensile test using cylindrical specimens, and the flexural-tensile test using prismatic beam specimens. According to Neville (1997), the ratio of splitting tensile strength to compressive strength may be influenced by coarse aggregate properties. In general, as compressive strength increases, the tensile strength increases at a decreasing rate. In addition to the coarse aggregate properties, the method for measuring the tensile and compressive strength will affect the f'_c/f_t relationship. Etxeberria et al. (2007) found the splitting tensile strength of RCA concrete to be higher than the NA concrete. They attributed these findings to the absorption capacity of the adhered mortar on the RCA and the new interfacial transition zone formed between the RCA and the new cement mortar. Sagoe-Crenstil et al. (2001) found the splitting tensile strength to be a function of binder strength rather than aggregate type. They also measured the splitting tensile-to-compressive strength ratio which is

an indicator of the concretes resistance to tensile strain and is a function of coarse aggregate size and type, concrete voids, and curing and testing conditions. This ratio for RCA concrete was found to be in the range of NA concrete (between 0.89 and 1.21). Ajdukiewicz and Kliszczewicz (2002) observed that high performance concrete mixtures with natural aggregates always produced higher tensile strengths than high performance RCA concrete however the difference was never more than 10%. Table 2.10 summarizes and presents additional findings of previous researchers on the tensile strength of RCA concrete.

Table 2.10 Summary of findings from previous researchers on tensile strength of RCA Concrete

Researcher(s)	Number of RCA sources studied	% Change in Tensile Strength from Control
Etxeberria et al. (2007) [*]	1	18% increase, 2% decrease
Ajdukiewicz and Kliszczewicz (2002)	6	10% decrease
Safiuddin et al. (2011) [†]	1	No change
Rakshvir and Barai (2006)	3	10% decrease
Katz (2003) ^{**}	1	13% decrease

* Splitting tensile strength increased at the 50% replacement level but decrease at the 100% replacement level

** Splitting tensile strength is based on original concrete crushed at 28 days. Splitting tensile strength was found to be 19% higher based on original concrete crushed at 3 days.

† RCA concrete was considered to be high workability.

2.3.7 Flexural Strength

The flexural strength or modulus of rupture of normal-density concrete is approximated as 0.6 to 0.8 times the square root of compressive strength (based on metric units). It is usually used in design calculations for pavements and other slabs on grade. Abou-Zeid et al. (2005) found the flexural-compressive strength ratio for the RCA concrete to be slightly higher than the NA concrete. They attributed this to the superior bond between the RCA and the cement binder which is due to the rough surface and angularity of the aggregate. They also believed that it may be due to some form of reaction between the RCA concrete and the surrounding cement paste. Table 2.11 presents and summarizes the findings of previous researchers on the flexural strength of RCA concrete.

Table 2.11 Summary of findings from previous researchers on flexural strength of RCA Concrete

Researcher(s)	Number of RCA sources studied	% Change in flexural strength from control
Chen et al. (2003)	2	10 to 25% decrease
Rakshvir and Barai (2006)	3	10% decrease
Safiuddin et al. (2011)*	1	No change
Katz (2003)	1	15% decrease
Topcu and Sengel (2004)	1	13% decrease

* RCA concrete was considered to be high workability.

2.3.8 Linear Coefficient of Thermal Expansion

As temperature rises, concrete expands and the coefficient of thermal expansion (CTE) is a measure of the percent change in length of concrete under a 1°C change in temperature. Typically, for normal-density concrete this value is approximately $10 \times 10^{-6}/^{\circ}\text{C}$. Factors influencing the thermal expansion and contraction of concrete include, aggregate type, cement content, water-cementing material ratio, temperature range, concrete age, and relative humidity. Overall, aggregate type has the greatest influence (Kosmatka et al., 2002). A very limited number of studies have investigated the CTE of RCA concrete and the influence of aggregate properties on the CTE. Smith and Tighe (2009) performed CTE tests on concrete pavement cores containing concrete of several RCA replacement levels (0, 15, 30, 50%) using a simplified testing method. The RCA used for their research was considered to be of high quality. They found that as the percent replacement increased, the average CTE value decreased. Bekoe et al. (2010) also investigated the CTE of concrete for pavement applications at several replacement levels. Overall, they concluded that there was no clear difference between the NA concrete and the RCA concrete with various replacement percentages.

2.3.9 Modulus of Elasticity and Poisson's Ratio

The stiffness of a material characterizes its elastic behaviour and is quantified as the modulus of elasticity or the ratio between an applied stress and an instantaneous strain (Mehta and Monteiro, 2006). Although concrete is a non-linear material, an estimate of the elastic modulus is required to compute design stresses, moments, and deflections. The modulus of elasticity of concrete is ordinarily estimated as a function of the compression strength and the unit weight. Both ACI

318 and CSA A23.3 have expressions for modulus of elasticity as described in Equations 2.3 and 2.4, respectively. Note that both equations are based on metric units.

$$E_c = 0.403\gamma_c^{1.5}\sqrt{f'_c} \quad \text{Equation 2.3}$$

$$E_c = (3300\sqrt{f'_c} + 6900)(\gamma_c/2300)^{1.5} \quad \text{Equation 2.4}$$

Where, f'_c is the concrete compressive strength in MPa and γ_c is the unit weight of concrete in kg/m^3 . Several authors have studied the modulus of elasticity of RCA concrete. Rahal (2007) evaluated one type of RCA source and produced RCA concrete with compressive strengths between 20 and 50 MPa. The study found that for concrete between 25 and 30 MPa, the modulus of elasticity of the RCA concrete was 3% lower than the NA concrete. In addition, Equation 2.3 overestimated the secant modulus of both the NA and RCA concrete. Xiao et al. (2005) were able to measure the complete stress-strain behaviour of RCA concrete at several aggregate replacement levels (0, 30, 50, 70, and 100%). They found that as the percent replacement increased the modulus of elasticity decreased by up to 45% for the 100% RCA replacement mixtures. The researchers were also able to derive a constitutive relation for the RCA concrete tested and used regression to create a predictive model incorporating the percent of RCA replacement. Another study by Katz (2003) measured the modulus of elasticity of cube specimens and used a correction factor to normalize the results to equivalent cylinder values. Compared to the NA concrete, the RCA concrete had very similar elastic modulus values however; Equation 2.3 still over-predicted the modulus of elasticity values by 25%. They noted that the effect of the RCA on the modulus of elasticity is similar to that of lightweight aggregate. Bekoe et al. (2010) measured the elastic modulus of RCA concrete while investigating its use in pavement applications. The research used one source of RCA at several replacement levels (0, 25, and 50%) in concrete. They concluded that the elastic modulus decreases with an increase in replacement percentage and found, at 50% replacement level, a reduction of up to 10% compared to the control concrete. Chen et al. (2003) studied two sources of RCA and investigated the effect of washing the RCAs prior to batching on the mechanical properties of RCA concrete. They found that the RCA concrete mixtures on average, had elastic moduli that were 70% of the NA concrete for a given water-cement ratio. Another study by Etxeberria et al. (2007) which evaluated a single RCA source in multiple replacement percentages in new concrete found an

11% reduction (for 100% RCA replacement mixtures) in modulus of elasticity compared to the NA concrete.

Poisson's ratio is defined as the ratio between the lateral strain and the axial strain and generally remains constant within the linear-elastic range of a material. In concrete, the Poisson's ratio is mainly dependent on the properties of the aggregate and ranges between 0.15 and 0.22 and is generally the same under compressive or tensile loading (Neville, 1997). There have been a limited number of research studies on the Poisson's ratio of RCA concrete. Ajdukiewicz and Kliszczewicz (2002) studied six different RCA types and produced high strength RCA concrete. There was no significant difference in Poisson's ratio between the NA and RCA concretes for a range of compressive strengths (38.7 to 89.2 MPa). They reported 28 day Poisson's ratios that ranged between 0.17 and 0.22.

2.3.10 Fracture Energy

2.3.10.1 Fracture Energy of NA Concrete

In general, the total amount of energy absorbed in a tensile test to failure is represented by the area under the load-deformation curve for the specimen. This area also represents the amount of energy absorbed within the fracture process zone and is referred to as the fracture energy, "fracture toughness", or "work of fracture". Specifically, it represents the fracture energy per unit area of the fracture surface (projected area on a plane perpendicular to the stress direction) (Hillerborg et al., 1976).

The fracture process zone is created when microcracks in concrete originate from strain localization which develops ahead of the crack tip (Mehta and Monteiro, 2006). Numerous analytical models have been developed to attempt to model the fracture process zone. Hillerborg et al. (1976) developed the fictitious crack model which essentially modeled the fracture process zone as a "tied-crack" with a specified crack width, w and a specified stress-elongation (σ - w) relation. The model attempts to capture the complex behaviour of concrete in tension.

Figure 2.4 shows the stress-deformation curves for the concrete specimen for the additional deformation w within the fracture process zone. It is assumed that the deformation ϵ is uniform and the total elongation Δl can be expressed in terms of the total specimen length, $\Delta l = l\epsilon$. A

localized fracture zone starts to form after the peak load is reached and as the total elongation increases the stress decreases. Beyond the peak stress the total elongation of the specimen is the sum of the uniform deformation outside the fracture zone plus the additional localized deformation w within the fracture zone: $\Delta l = l\varepsilon + w$.

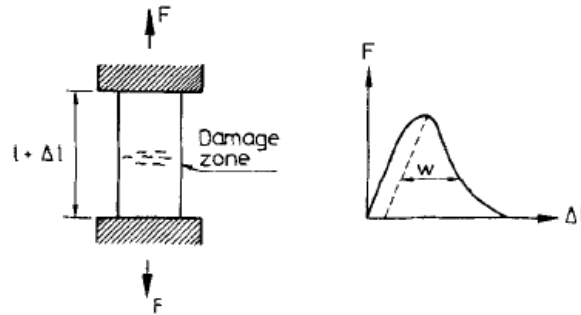


Fig. 1. - Load-deformation relation in a tensile test.

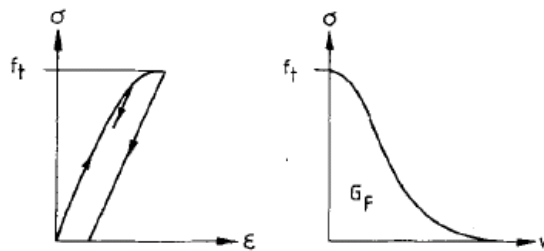


Figure 2.4 Stress-deformation curve for additional deformation within the fracture process zone (RILEM, 1985)

The fracture energy is thus equal to the area under the stress-elongation curve as described in Equation 2.5.

$$G_f = \int_0^{\infty} \sigma(w)dw \quad \text{Equation 2.5}$$

It should be recognized that the tensile behaviour of concrete is much different than for metals. Metals must yield before fracture subjecting them to shear deformations and large lateral deformations and stresses. This creates many complexities when attempting to describe their theoretical behaviour at fracture. As a result, the fracture behaviour of concrete can be represented by a much simpler theoretical model.

The most direct and effective way to determine the fracture energy of concrete is by performing a uniaxial tension test in which the entire load-deformation curve is measured. However, most testing facilities lack the proper equipment to conduct such tests. As a result, the fracture energy of concrete is usually determined by measuring the load-deformation curves of notched beams loaded in flexure. The value of G_f is then calculated by computing the area under the load-deflection curve and dividing it by the net cross-section of the specimen (see Figure 2.5). Hillerborg (1985) recommended that the fracture energy be calculated using Equation 2.6, which accounts for the self-weight of the concrete specimen.

$$G_f = (W_0 + mg\delta_f)/A \quad \text{Equation 2.6}$$

Where,

G_f = fracture energy;

W_0 = area under the load-deflection curve;

$m = m_1 + 2m_2$, m_1 = mass of the beam between supports;

m_2 = mass of loading frame not attached to the load machine that follows the specimen until failure;

g = acceleration due to gravity;

δ_f = final deflection of the beam, and

A = cross-sectional area of the beam above the notch (see Figure 2.5).

Usually, a linear trapezoidal function is used perform the numerical integration of the area under the curve (Equation 2.7).

$$\text{Area} = \sum_{i=0}^{n-1} (w_{i+1} - w_i)(P_i + P_{i+1})/2 \quad \text{Equation 2.7}$$

Where,

P = load at a given displacement, w .

n = number of data points recorded.

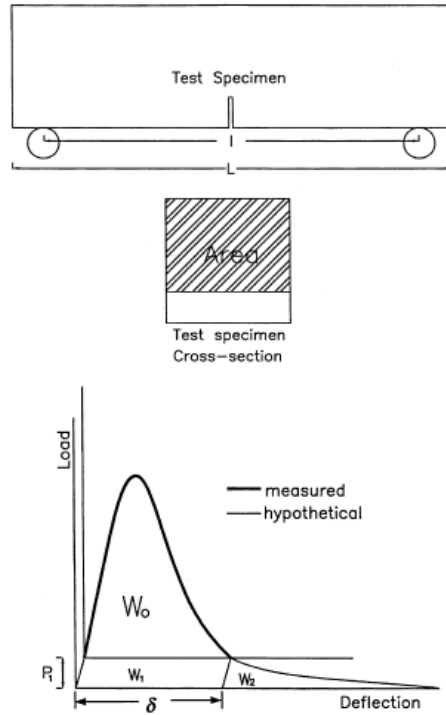


Figure 2.5 RILEM notched beam specimen and corresponding load-deflection curve for measuring the fracture energy of concrete (RILEM, 1985)

A correction must also be made in the determination of the fracture energy which accounts for the self-weight of the concrete itself. Based on empirical data, a relation between the fracture energy and the mean cylinder compressive strength was proposed in the CEB-FIP Model Code 90 (CEB-FIP, 1993) which is presented in Equation 2.8.

$$G_f = G_{F0} \left(\frac{f'_c}{f_{cm0}} \right)^{0.7} \quad \text{Equation 2.8}$$

Where,

G_f = fracture energy in N/mm;

G_{F0} = 25 N/m for $d_{max} = 8$ mm;

30 N/m for $d_{max} = 16$ mm;

58 N/m for $d_{max} = 24$ mm;

f'_c is the cylinder compressive strength; and

$$f_{cm0} = 10 \text{ MPa.}$$

Equation 2.6 is valid for concrete compressive strengths up to and including 80 MPa.

As concluded by Darwin et al. (2001), the fracture energy of concrete is mainly governed by the properties of the coarse aggregates. They found that concrete produced using basalt coarse aggregates had higher fracture energies than concrete produced with coarse limestone aggregates. The application of fracture mechanics in concrete modeling seems to be useful when studying shear and bond with reinforcement. Zuo and Darwin (2000) studied the splice strength in normal and high performance concrete and found that as fracture energy is increased, the resistance to crack propagation increases and delays splitting failures and increases splice length. ACI Committee 408 (2003) further summarizes these points by stating that as aggregate strength increases, an increase in bond strength is observed which appears to be related to the aggregates' effect on the tensile strength and fracture energy of the concrete. McCabe et al. (1992) applied the principles of fracture mechanics and finite element analysis to study steel-concrete bond in beam-end specimens. They found that they were able to use simple FEM concepts and elements to achieve excellent correlation with experimental results. Guinea et al. (2002) studied the effect of mortar-aggregate bond on the cracking mechanism and fracture properties of concrete. They found that the strength of the ITZ affects the fracture energy in different ways depending on the particle shape. Crushed versus rounded aggregates produced concrete with higher fracture energy values however, the interface was found to have no effect. This may be due to more significant mechanical interlock at the tail of the softening curve which compensates for the loss of energy consumption in the interfaces.

2.3.10.2 Fracture Energy of RCA Concrete

Given the unique nature of RCA concrete, the effect of specific RCA properties on the fracture energy is still relatively unknown as very few studies have been conducted on calculating the fracture energy of RCA concrete. With the increasing use of non-linear finite element analyses which use complex constitutive models for design of concrete structures, the fracture energy and post-peak softening response of RCA concrete are important input parameters for facilitating the

future design of RCA concrete-based structures. In addition, as discussed in ACI 408 (2003), a concrete with higher fracture energy may have improved bond strengths compared to a concrete with lower fracture energy and with similar tensile strength. Measuring the fracture energy of RCA concrete may therefore serve as preliminary indicator of its bond strength with reinforcing steel. Ong and Ravindrarajah (1987) studied fracture energy of low and high strength concrete produced using natural aggregates, RCAs, and a combination of natural aggregates and RCAs. They cast four 50 mm x 50 mm x 650 mm prisms with 25 mm notches cut at their mid-spans to determine the fracture energy. They found that the greater the volume of aggregate used, the larger the area of the cracking surface. In general, they concluded that the concrete produced using natural aggregates had higher fracture energies than the RCA concretes. They attributed this difference to the weaker bond between the cement paste and the RCAs which causes less complex micro-cracking and consumes less energy during crack propagation. Casuccio et al. (2007) noted similar trends with the RCA concrete having lower stiffness (13 – 18%) and significantly lower fracture energies (27 – 45%) than NA concrete. They attributed this difference to a decrease in elastic compatibility between the mortar and the coarse RCAs.

2.3.11 Bond Behaviour with Reinforcing Steel

There have been very few studies conducted on the bond performance with reinforcing steel in RCA concrete. Ajdukiewicz and Kliszczewicz (2002) performed pull-out tests on high performance RCA concrete using both round and ribbed and concrete mixtures with and without chemical admixtures. They found that in concrete with 100% coarse and fine RCA replacement the bond stress value at failure was up to 20% lower than for NA concrete. In the case where 100% coarse RCA with natural river sand was used; only an 8% reduction in bond stress was measured.

Xiao and Falkner (2007) performed a series of both pull-out and bond beam tests for several RCA replacement percentages and for both plain and ribbed reinforcing bars. They found the bond and development deterioration process for RCA concrete to be similar to NA concrete. Five stages were observed: micro-slip, internal cracking, pullout (peak stress), complete steel bar pullout, and residual (load is approximately half the peak value). Xiao and Falkner (2007) observed that for plain bars τ_{\max} decreased by 12% and 6% for 50% RCA replacement and 100%

RCA replacement, respectively. For deformed bars, τ_{\max} was very close to those for the control specimen. They postulated that the bond between the RCA concrete and the deformed bars is governed by the anchorage and friction resistance and therefore the percent of RCA replacement had little effect. However, the bond strength between RCA concrete and plain bars is governed by adhesion and in this case the aggregate type and percentage has an influence. The authors also developed an analytical expression that sufficiently models the entire bond-slip relationship between RCA concrete and plain and deformed reinforcing bars. Xiao and Falkner (2007) also concluded that the anchorage length for RCA concrete incorporating 100% RCAs could be the same as for NA concrete. Choi and Kang (2008) tested bond using pull-out specimens and several different RCA replacement percentages. They found for a water-cement ratio of 40% and with RCA replacement percentages of 50%, the bond stress-slip relationship was similar to normal concrete. For a water-cement ratio of 0.5 the bond stress-slip relationship becomes much more sensitive to the quality of the RCA and appears to be better than for NA concrete. They suggested that the ACI 408 expression for bond strength over-estimated the experimental values obtained whereas the CEB-FIP expression under-estimates the bond strength. The researchers recommend that new expressions for bond that consider the properties of the RCA be developed. Fathifazl (2008) tested beam-end specimens and found in general that RCA concrete specimens had lower bond strengths than NA concrete specimens. They found however, that the overall bond behaviour of specimens was independent of aggregate or concrete type. Table 2.12 presents and summarizes the findings of previous researchers on the compressive strength of RCA concrete.

Table 2.12 Summary of findings from previous researchers on bond strength of RCA concrete with reinforcing steel

Researcher(s)	Number of RCA sources studied	Bond Specimen Type(s)	Max. % Change in Bond Strength from Control
Fathifazl (2008)	2	Beam-ends	Similar
Choi and Kang (2008)*	3	Pull-out	Similar
Ajdukiewicz and Kliszczewicz (2002)**	6	Pull-out	20% decrease
Xiao and Falkner (2007)	1	Pull-out	12% decrease

* Used high-strength (800 MPa) 16mm diameter reinforcing bars.

** Investigated high-strength RCA concrete up to 80 MPa.

2.4 Bond of Reinforcement in Concrete

2.4.1 Overview

The bond of reinforcement in concrete is the critical parameter responsible for three main aspects of structural performance, namely (1) bond is used to anchor the ends of reinforcing bars, (2) bond transfers force into concrete in tension, thereby reducing the average strain in the flexural reinforcement and enhancing member stiffness (i.e., tension stiffening), (3), bond is used to maintain the composite action between the reinforcing bar and surrounding concrete (i.e., to ensure strain compatibility) (CEB-fip, 2000). In addition, bond action is also required to ensure an adequate level of ductility in structural members. In many cases, the bond must be able to withstand large steel strains along its embedded or anchored length to allow for the formation of bending cracks. In particular, when designing for seismic loading applications, it is the post-yield strength of the reinforcing steel that determines the structural ductility (CEB-fip, 2000).

In most design codes, bond is generally assumed as shear stress acting uniformly along the nominal surface area of a plane reinforcing bar. In reality, the bond stress varies along the length of the bar, being higher at the ends of the bar. Also, in ribbed bars (that are used most often); the transfer of load between the reinforcing bar and surrounding concrete is primarily through bearing of the ribs. This places the concrete in the vicinity of the ribs in a complex tri-axial stress state and often the concrete is cracked radially and conically. A relative displacement occurs between the concrete and the steel when their respective strains differ; this relative displacement is referred to as slip.

2.4.2 Mechanics of Bond

2.4.2.1 Failure Mechanism

When discussing the mechanics of bond between concrete and reinforcing bars there are three main mechanisms of transfer between concrete and steel.

1. Adhesion between the reinforcing bar and the concrete
2. Friction developed due to the roughness of the interface, forces transverse to the bar surface, and the relative slip between the reinforcing bar and surrounding concrete.

3. Mechanical bearing of the ribs against the concrete surface

After the initial slip, most of the bond is transferred by bearing. Friction starts to play a significant role when plain or epoxy-coated bars are used. Figure 2.6 illustrates the various bond transfer mechanisms on a reinforcing bar.

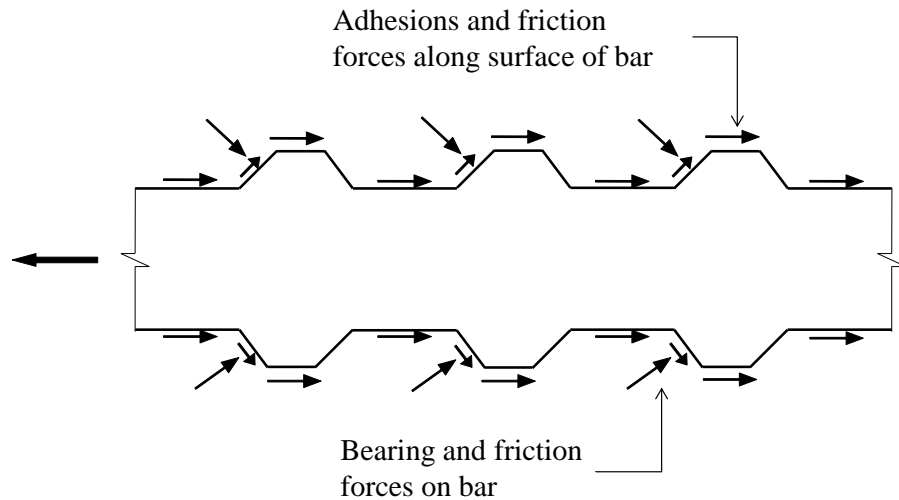


Figure 2.6 Bond transfer mechanisms for a reinforcing bar embedded in concrete (adapted from ACI 408, 2003)

Compressive bearing forces normal to the rib surface increase the value of the friction forces parallel to the surface. The forces acting on the bar surface become balanced by the compressive and shear forces. These compressive and shear forces are then resolved into tensile forces which caused cracking perpendicular and parallel to the reinforcing bar. Usually, splitting cracks may occur if insufficient spacing or cover is provided. In turn, if cover, spacing, and transverse reinforcement are insufficient to prevent splitting failure then shear failure originating at the top of the ribs of the bar will result and a pull-out failure will occur (ACI 408, 2003). In general, bond resistance is governed by the following factors:

- The mechanical properties of concrete and its constituents,
- Concrete cover and bar spacing,
- Transverse reinforcement (providing confinement to delay the onset of cracking),
- Surface condition of the bar (ribbed, plain, epoxy-coated, etc.), and
- Bar geometry (deformation height, spacing, width, face angle, etc.)

2.4.2.2 Derivation of Bond Forces

The change in force in the reinforcing bar, dT , does not only vary with the change in moment per unit length (or shear $V=dM/dl$), but simply with the force in the bar T . Figure 2.7 illustrates the change in bond force due to the change in moments in a beam.

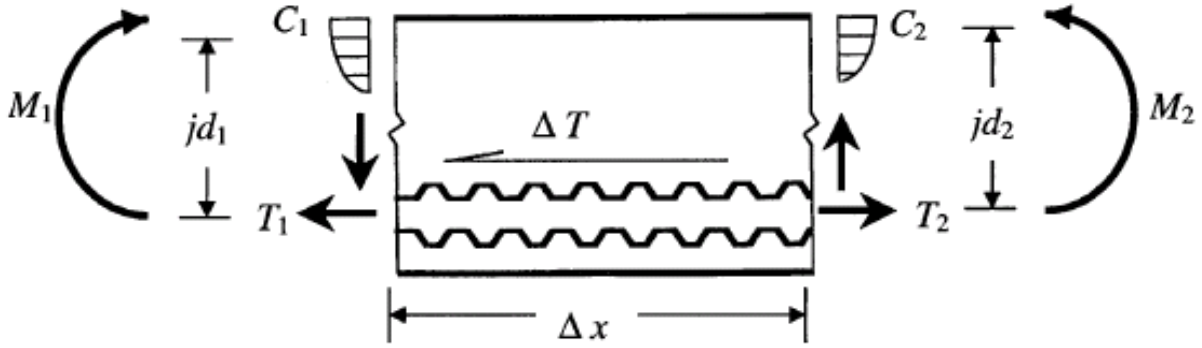


Figure 2.7 Change in bond force due to change in moment in a beam (ACI 408, 2003)

The force in the bar, T varies from high between flexural cracks to low or zero at the cracks. At crack locations, the concrete shares tensile stresses with the reinforcing steel. It is because of this fact that the real distribution of bond forces along the length of the bar cannot be predicted as the flexural crack locations and the amount of tensile stress carried by the concrete cannot be calculated. For design purposes, bond forces are treated to act uniformly along the anchored, developed or spliced, length of the reinforcement (ACI 408, 2003). The basic derivation of bond stress, u is summarized in Equation 2.9.

$$u = \frac{U}{\sum o} = \frac{\Delta T}{\Delta l \sum o} = \frac{\Delta f_s A_b}{\Delta l \sum o} = \frac{\Delta f_s d_b}{4 \Delta l} \quad \text{Equation 2.9}$$

Where,

U = bond force per unit length;

ΔT = difference in tensile force between the two bar ends;

$\sum o$ = sum of the perimeters of the bars developed at a section;

Δf_s = change in steel stress over length Δl ;

A_b = area of the bar; and

d_b = diameter of bar.

2.4.2.3 Bond-Slip Response

To better understand the nature of bond response, bond force-slip and bond stress-slip curves are generated. The bar forces are compared with the external slip of the reinforcing bar, measured with respect to the either the loaded or unloaded end of the bar. Bond force-slip and bond stress-slip curves are structural properties and depend on bar geometry, cover, transverse reinforcement, and the state of stress of the concrete surrounding the concrete. Figure 2.8 Typical bond-slip response curve shows a typical bond force versus slip curve.

Due mainly to adhesion between the bar and the surrounding concrete, the bond force-slip and bond stress-slip curves are initially very steep. As loading continues, cracks begin to form which causes the curves to gradually level off (ACI 408, 2003). Due to concrete shrinkage, cracks are initially present next to the reinforcing bar. These cracks can act as stress concentrations where cracks may initiate.

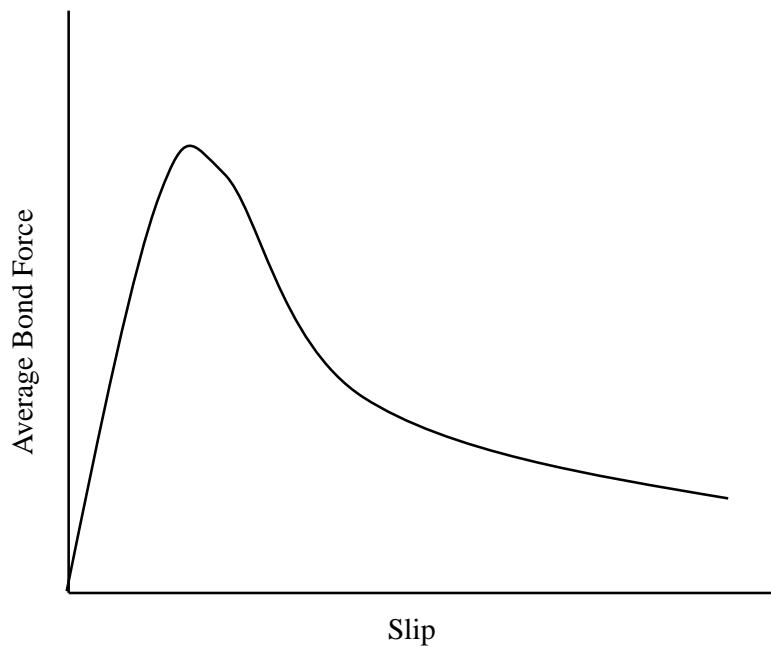


Figure 2.8 Typical bond-slip response curve

2.4.3 Factors Affecting Bond

2.4.3.1 Cover and Bar Spacing

With smaller cover and bar spacing, a splitting tensile failure is most likely to occur and is also the most common failure mode in reinforced concrete members (ACI 408, 2003). When concrete cover is large, pull-out failures are more likely.

2.4.3.2 Transverse Reinforcement

In the presence of transverse reinforcement, there is a small yet significant difference in bond strengths from the effect of the cracks between reinforcing bars. Transverse reinforcement confines developed and spliced bars by limiting the cracks and in turn increase the bond strength (ACI 408, 2003).

2.4.3.3 Bonded or Spliced Length

Increasing the development or spliced length will increase the bond strength. However, this increase will not be proportional but is nearly linear as the bond forces are not uniform along the length of the bar (ACI 408, 2003).

2.4.3.4 Bar Size

The total force developed at a bond failure is not just a function of spacing, cover and transverse reinforcement but also of bar area. Added bond strength provided by the transverse reinforcement increases as the size of the developed bar increases (ACI 408, 2003).

2.4.3.5 Compressive Strength

In concrete not confined by transverse reinforcement the bond stress, u , is proportional to $f'_c{}^{1/4}$. It was found for higher strength concretes, that when bond forces were normalized with respect to $f'_c{}^{1/2}$, the effect that f'_c has on bond strength becomes exaggerated and bond strength is overestimated. As f'_c increases the bond strength increases at a progressively slower rate (ACI 408, 2003).

2.4.3.6 Tensile Strength and Fracture Energy

Pullout failures mainly occur in cases of high confinement and small bonded lengths. Splitting cracks role in bond failure highlights the importance of the concrete tensile strength when considering bond properties. In concrete without confining reinforcement, the peak load is governed by the concrete tensile response. The tensile response involves more than just strength but also the fracture energy of the concrete or the ability of the concrete to dissipate energy generated by crack propagation. Concrete with higher fracture energy, G_f , will have improved bond strength even if the concrete has similar tensile strengths (ACI 408, 2003). It is generally agreed that tensile strength increases approximately with $f'_c^{1/2}$.

2.4.3.7 Slump and Workability

Usually, properly consolidated, low-slump concrete produces the best bond properties with reinforcing steel (ACI 408, 2003).

2.4.3.8 Aggregate Type

As the aggregate strength increases, both the concrete fracture energy and bond strength increase. In studies conducted by Darwin et al. (2001) that investigated using basalt and limestone aggregates, it was found that the higher fracture energies of the basalt controlled crack propagation better and resulted in higher bond strength because the fracture energy delayed a splitting failure.

For lightweight aggregate concrete, the bond strength bond strength of with reinforcing steel is lower due to than NA concrete due to: lower strength of the aggregate, lower concrete tensile strength, lower fracture energy, and lower local bearing capacity.

In general, bond strengths for lightweight aggregate concrete are between 65% and 100% that of normal weight concrete and as a result, development lengths for lightweight concrete must be longer (ACI 408, 2003).

2.4.4 Tests Specimens for Determining Bond Strength

2.4.4.1 Pullout Specimen

The pull-out specimen is the most widely used bond test specimen as it is relatively easy to construct and test. Figure 2.9 shows a typical pull-out test schematic.

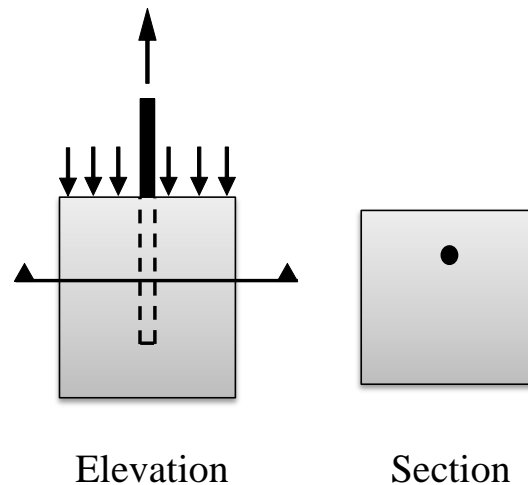


Figure 2.9 Typical bond pullout specimen

However, the stress fields created during the test are not consistent with realistic reinforced concrete members. As the bar is placed in tension, the concrete is placed in compression. Eventually compressive struts form between support points for the concrete and the reinforcing bar surface causing the reinforcing bar to be placed in compression. In reality, both the bar and the surrounding concrete are in tension. For this reason, ACI 408 (2003) recommends that pullout test specimens not be used as the sole basis for determining development length.

2.4.4.2 Beam-End Specimen

The modified-cantilever beam or beam-end specimen is also relatively simple to construct however, certain support conditions must be provided to ensure realistic reinforced concrete beam behaviour. Figure 2.10 illustrates the beam-end test specimen.

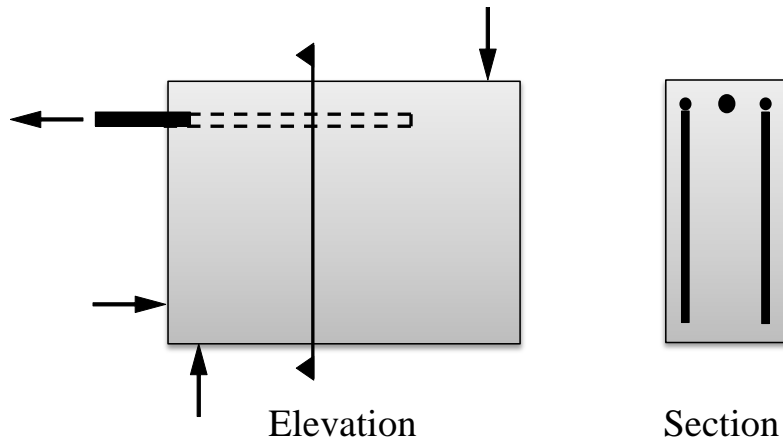


Figure 2.10 Beam-end test specimen

To prevent conical failure at the surface, a small length of bar is usually left unbonded. Stresses simulated with the beam-end test almost duplicate those generated in an actual reinforced concrete beam as both the reinforcing bar and the surrounding concrete are in tension. The bond strengths obtained from this test closely match values from other specimens designed to represent full-scale reinforced concrete members (ACI 408, 2003).

2.4.4.3 Beam Anchorage and Splice Specimens

Beam anchorage and splice specimens are larger specimens used to represent full-size members. They provide realistic data on development and splice length. Anchorage specimens simulate a member with a flexural crack and a known bonded length (see Figure 2.11).

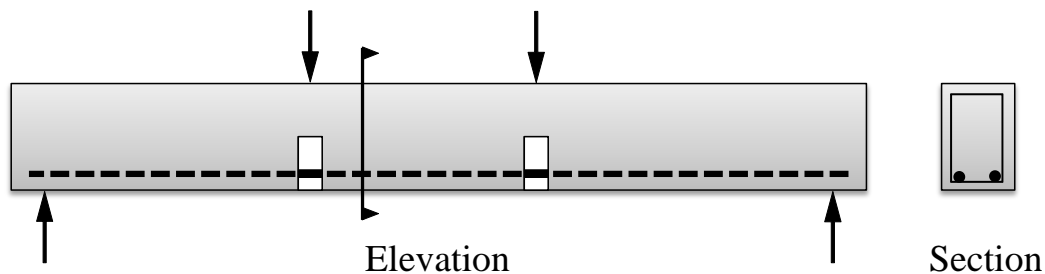


Figure 2.11 Typical beam anchorage specimen (ACI 408, 2003)

Splice specimens are easier to fabricated than anchorage specimens and as a result provide a large portion of the data used for development and splice lengths as reported in ACI 318 (ACI 318, 2009). Figure 2.12 shows a typical beam-splice specimen in four-point loading.

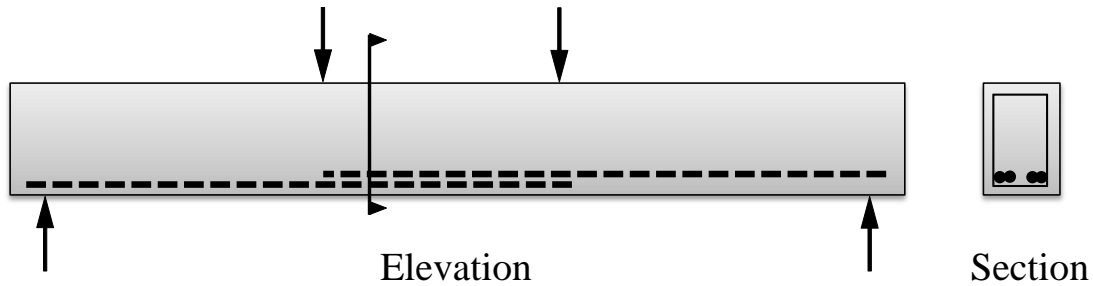


Figure 2.12 Typical beam-splice specimen

The splice length is usually constructed to overlap in the region of constant moment between the two loading points. Strain gauges can be installed in the cut grooves along the longitudinal reinforcement ribs. Another type of beam-splice specimen depicted in Figure 2.13 is the single overhanging cantilever beam developed by Ferguson (1973). The splice length is still within the constant moment region and this specimen has the advantage of being tested on its other span.

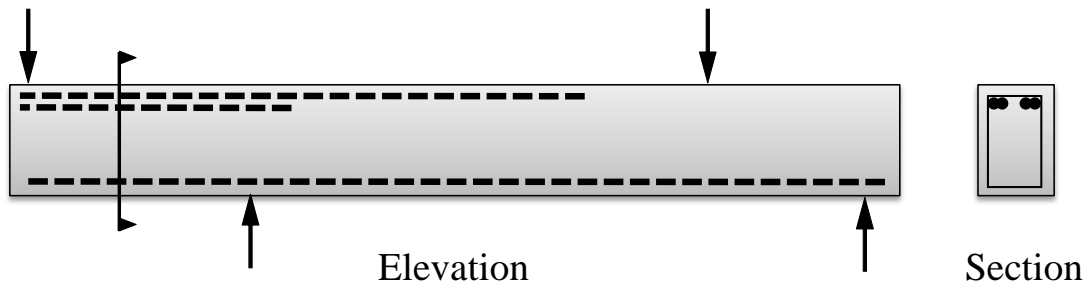


Figure 2.13 University of Texas beam (adapted from Ferguson, 1973)

2.4.5 Bond Models and Equations

The following section presents expressions that describe the bond strength of reinforcing bars in tension embedded in concrete. As there is currently no analytical theory-based model the bond models have been developed based on statistical comparisons with test results. All equations are based on S.I. units and were derived based on normal-weight concrete. In addition, the equations presented below apply to concrete members confined by transverse reinforcement whereas expressions for bond of unconfined concrete members can be found in ACI 408 (2003).

2.4.5.1 Orangun, Jirsa and Breen (1977)

Based on the results of 62 beam-splice specimens and, using statistical techniques, Orangun, Jirsa and Breen (1977) developed expressions to describe the bond strength of bars with and

without transverse (confining) reinforcement. Equation 2.10 describes their expression. Note that only the beam-splice specimens where the reinforcing steel did not yield were included in the development of the equation. Equation 2.10 was developed based on the premise that all bond failures occurred by splitting of the concrete cover and, as a result, a limit was placed on the amount of transverse reinforcement to avoid pullout failures (see Equation 2.11).

$$\frac{T_b}{\sqrt{f'_c}} = 0.25\pi l_d(c_{\min} + 0.4d_b) + 16.6A_b + \left(\frac{\pi l_d A_{tr}}{41.5sn}\right) f_{yt} \quad \text{Equation 2.10}$$

$$\frac{1}{d_b} \left(c_{\min} + 0.4d_b + \frac{A_{tr} f_{yt}}{10.34sn} \right) \leq 2.5 \quad \text{Equation 2.11}$$

Where,

T_b = maximum bond force developed (N);

f'_c = cylinder compressive strength (MPa);

l_d = embedded or bonded length of reinforcing bar (mm);

d_b = diameter of developed bar (mm);

c_{\min} = smaller of minimum concrete cover or 1/2 of the clear spacing between bars (mm);

s = spacing of transverse reinforcement (mm);

n = number of bars developed or spliced at the same location.

f_{yt} = yield strength of transverse reinforcing (MPa), and

A_{tr} = area of transverse reinforcement normal to plane of splitting through the anchored bars (mm²).

2.4.5.2 ACI Committee 408 (2003)

Based on further research conducted by Darwin et al. (1992), Darwin et al. (1996) and Zuo and Darwin (2000), Equation 2.10 was updated. The new expression was derived from the results of 635 beam-splice specimens which experienced bond failures due to splitting of the concrete cover and is presented in Equation 2.12. It should be noted that the ACI 408 expression normalizes the bond force with respect to f'_c ^{1/4} versus the traditional f'_c ^{1/2} proposed by Orangun,

Jirsa and Breen (1977). Darwin et al. (1996) found this normalization to provide a better fit to the data.

$$\frac{T_b}{f'_c{}^{1/4}} = [1.43l_d(c_{\min} + 0.5d_b) + 57.4A_b] \left(0.1 \frac{c_{\max}}{c_{\min}} + 0.90\right) + \left(8.9t_r t_d \frac{NA_{tr}}{n} + 558\right) \sqrt{f'_c}$$

Equation 2.12

Where,

T_b = maximum bond force developed (N);

f'_c = cylinder compressive strength (MPa);

l_d = embedded or bonded length of reinforcing bar (mm);

d_b = diameter of developed bar (mm);

c_{\max} = maximum (c_b , c_s);

c_{\min} = minimum (c_b , c_s);

c_b = bottom cover;

c_s = minimum [c_{so} , $c_{si} + 6.4$ mm];

c_{so} = side cover; and

c_{si} = 1/2 of the bar clear spacing.

A_b = cross-sectional area of developed or spliced bar (mm²);

$t_r = 9.6R_r + 0.28$

R_r = relative rib area (mm²);

$t_d = 0.72d_b + 0.28$

N = number of transverse bars in the development or splice length (mm);

A_{tr} = area of transverse reinforcement normal to plane of splitting through the anchored bars (mm²);

f_{yt} = yield strength of transverse reinforcing (MPa), and

n = number of bars developed or spliced at the same location.

2.4.6 Design Code Provisions for Development Length

The development length is a design parameter corresponding to the shortest length of reinforcing bar embedded in concrete required to develop a bar stress equal to the yield strength (f_y) (MacGregor and Bartlett, 2000). The following section presents the design equations for the development length of straight reinforcing bars in tension as part of the Canadian (CSA A23.3), United States (ACI 318) and European (CEB-FIP) codes.

2.4.6.1 CSA A23.3-04

The most recent concrete design code in Canada is CSA A23.3-2004 and includes provisions for development length of deformed bars in tension under clause 12.2. Equation 2.13 is the general development length equation which accounts for concrete that is both confined and unconfined by transverse reinforcement and was modeled after the ACI 318 code provisions for development length. It is important to note that the equations for development length were developed from empirically-derived relationships based on the beams that experienced splitting rather than pull-out failures (Orangun, Jirsa and Breen, 1977).

$$l_d = 1.15 \frac{k_1 k_2 k_3 k_4}{(d_{cs} + K_{tr})} \frac{f_y}{\sqrt{f'_c}} A_b \quad \text{Equation 2.13}$$

$$K_{tr} = \frac{A_{tr} f_{yt}}{10.5sn} \quad \text{Equation 2.14}$$

Where,

l_d = development length required to ensure the yielding of the reinforcing bar (mm);

$(d_{cs} + K_{tr}) \leq 2.5d_b$ in order to avoid pullout failures;

K_{tr} = coefficient to account for the effect of confinement by transverse reinforcement given by Equation 2.14.

d_{cs} = the smaller of:

- (a) the distance from the closest concrete surface to the centre of the bar being

developed (mm); or

(b) two-thirds of the centre-to-centre spacing of bars being developed (mm).

f_y = yield strength of bar being developed (MPa);

f'_c = cylinder compressive strength of concrete (MPa);

A_b = cross-sectional area of bar being developed or spliced (MPa);

k_1 = bar location factor;

k_2 = coating factor;

Where, $k_1 k_2 \leq 1.7$

k_3 = concrete density factor; and

k_4 = bar size factor.

s = spacing of transverse reinforcement (mm);

n = number of bars developed or spliced at the same location.

f_{yt} = yield strength of transverse reinforcing (MPa), and

A_{tr} = area of transverse reinforcement normal to plane of splitting through the anchored bars (mm^2).

2.4.6.2 ACI 318-09

Similar to the Canadian provisions, the American Concrete Institute building code for structural concrete provides provisions for development length in clause 12.1. Equation 2.15 was developed based on the work completed by Orangun, Jirsa and Breen (1977) and is applicable to concrete that is confined and unconfined by transverse reinforcement.

$$l_d = 0.9\alpha\beta\lambda\gamma \left(\frac{f_y}{\sqrt{f'_c} \left(\frac{c + K_{tr}}{d_b} \right)} \right) d_b \quad \text{Equation 2.15}$$

$$K_{tr} = \frac{A_{tr} f_{yt}}{10.34sn} \quad \text{Equation 2.16}$$

Where,

l_d = development length required to ensure the yielding of the reinforcing bar (mm);

K_{tr} = coefficient to account for the effect of confinement by transverse reinforcement given by Equation 2.16.

f_y = yield strength of bar being developed (MPa);

f'_c = cylinder compressive strength of concrete (MPa);

Where, $f'_c{}^{1/2} \leq 8$ MPa

c = the smaller of:

- (a) the distance from the closest concrete surface to the centre of the bar being developed (mm); or
- (b) one-half of the centre-to-centre spacing of bars being developed (mm).

d_b = diameter of bar being developed or spliced (MPa);

s = spacing of transverse reinforcement (mm);

n = number of bars developed or spliced at the same location.

f_{yt} = yield strength of transverse reinforcing (MPa), and

A_{tr} = area of transverse reinforcement normal to plane of splitting through the anchored bars (mm^2).

2.4.6.3 CEB-FIP Model Code 1990

The expression for required development length included in the 1990 CEB-FIP Model Code is similar to the expressions presented in the CSA A23.3 and ACI 318 codes with a few additional considerations. Equation 2.15 gives the expression for the design anchorage length as a function of some basic length, l_b (length necessary to transfer the yield strength of bar). This basic anchorage length is then given as a function of the design bond stress, f_{bd} . The design bond stress is then proportional to the design value of the concrete tensile strength. Another difference between the CEB-FIB equation and the previous equations is the presentation of the term that accounts for the contribution of transverse confinement on bond strength. Equation 2.17 is multiplied by a separate coefficient, α_4 , which accounts for the effect of confinement by transverse reinforcement. However, once applied, the coefficient α_4 , provides a similar expression to both the CSA A23.3 and ACI 318 expressions.

$$l_{b,net} = \alpha_1 \alpha_2 \alpha_3 \alpha_4 \alpha_5 l_b A_{s,cal} / A_{s,ef} \geq l_{b,min} \quad \text{Equation 2.17}$$

$$l_b = \frac{d_b f_{yd}}{4 f_{bd}} \quad \text{Equation 2.18}$$

Where,

$l_{b,net}$ = design anchorage length (mm);

$A_{s,cal}$ = calculated area of reinforcement required by the design (mm²);

$A_{s,ef}$ = area of reinforcement provided (mm²);

α_1 = bar form coefficient (straight, bent, loop);

α_2 = coefficient accounting for the influence of one or more welded transverse bars;

α_3 = coefficient accounting for the effect of confinement by concrete cover;

α_4 = coefficient accounting for the effect of confinement by transverse reinforcement;

α_5 = coefficient accounting for the effect of the pressure transverse to the plane of splitting along the design anchorage length.

l_b = basic length necessary for the transfer of yield force of a bar or wire defined by Equation 2.18;

f_{yd} = yield force of the bar (MPa);

f_{bd} = design bond stress (MPa) = $\eta_1 \eta_2 \eta_3 f_{ctd}$

f_{ctd} = design value of the concrete tensile strength (= $f'_{c,min} / 1.50$)

η_1 = bar surface factor = 1.0 for plain bars, 1.4 for indented bars and 2.25 for ribbed bars;

η_2 = bar location factor = 1.0 for good bond conditions, 0.7 for all other cases

η_3 = bar size factor = 1.0 for $d_b \leq 32$ mm, $(132 - d_b) / 100$ for $d_b > 32$ mm.

2.5 Identification of Research Gaps

Based on the current state-of-the art of RCA concrete research presented above, the following areas have been identified in which further research is required.

- a. Very limited studies have investigated the inter-relationships among the various RCA and natural aggregate properties such as shape, surface texture, density, absorption, adhered mortar content, abrasion resistance and crushing strength.
- b. Limited information is available on the aggregate properties of Canadian sources of RCA for use as a coarse aggregate replacement in concrete.
- c. Limited information is available that investigates the main mechanisms of RCA concrete failure and the aggregate properties influencing these mechanisms.
- d. There is limited information available on replacing natural aggregate with 100% RCA as coarse aggregate.
- e. Very few studies that have evaluated the effect that replacing coarse natural aggregates with RCAs has on mixture proportions.
- f. Very few studies have investigated the effect of RCA properties on the coefficient of thermal expansion of RCA concrete.
- g. Very few studies have investigated the fracture energy of RCA concrete
- h. Limited data on the bond performance of RCA concrete and reinforcing steel particularly using beam-end specimens is available. Within these studies, little has been investigated as to the main mechanisms of bond failure in the context of coarse aggregate properties.
- i. There is limited information on the development of predictive bond strength equations and comparisons to current expressions for bond strength.
- j. There are no current Canadian standards or guidelines for use of RCA as a replacement for natural coarse aggregate in concrete.

Chapter 3 presents a list of research objectives to address the gaps that have been identified in the current state-of-the-art described above.

Chapter 3: Research Objectives and Experimental Program

Based on the gaps identified within the current state-of-the-art, the following objectives form the basis for this research.

1. Develop a research program utilizing one local natural coarse aggregate as a control source and three sources of crushed concrete for use as RCAs. Investigate the inter-relationships among coarse aggregate properties such as, shape, surface texture, density, absorption characteristics, adhered mortar content, abrasion resistance, and crushing strength. Investigate the differences between natural coarse aggregate properties and RCA properties.
2. Investigate the effect that completely replacing natural aggregate with RCA has on concrete workability, hardened density, compressive strength, splitting tensile strength, linear coefficient of thermal expansion, modulus of elasticity, and Poisson's ratio. This would include identifying any statistically significant correlations between aggregate properties and concrete mechanical properties.
3. Develop concrete mixture proportions incorporating 100% RCA as coarse aggregate to achieve similar workability and compressive strength as NA concrete. Evaluate the effect of aggregate properties on the fundamental mixture proportions (i.e., water demand, cement content and water-cement ratio).
4. Provide additional data and investigate the effect of RCA properties on the fracture energy of RCA concrete. Testing variables will include various compressive strengths and aggregate types. Evaluate the relationship between various aggregate properties, concrete properties and fracture energy.
5. Investigate the effect that replacing natural aggregate with various RCA types has on the bond behaviour of reinforced RCA concrete members. This will be completed using beam-end bond specimens that incorporate several bonded lengths, several concrete compressive strengths and four coarse aggregate types. Design and construct a testing frame to facilitate beam-end testing using existing laboratory hydraulic testing systems. Evaluate current predictive bond strength equations based on their applicability for use with RCA concrete.

6. Develop a regression model based on the experimental data to predict bond strength of RCA concrete beam-end members. Use the regression model to make inferences on the effect of aggregate type on the required development length.
7. Develop best practice guidelines for using RCAs in new structural concrete. This guide would include a specified set of aggregate tests whose results will be used to assess and classify a particular RCA source for determining its adequacy for use as a coarse aggregate in structural concrete applications.

The experimental program was structured to provide a comprehensive study for achieving the research objectives stated above. To adequately understand the behaviour of reinforced RCA concrete members, the mechanical characteristics of the RCA concrete itself must be studied. Similarly, in order to fully evaluate and understand the mechanical properties of RCA concrete, the physical and mechanical properties of the RCAs must be well understood. Investigating the interaction between aggregate properties, concrete properties and reinforced concrete bond strength with reinforcing steel will help provide a more comprehensive understanding of the behaviour of RCA in structural applications.

A multi-stage experimental program was devised in which the various mechanical and physical properties of the RCA, RCA concrete and the reinforced RCA concrete members were investigated in succession. Various aggregate tests including absorption, density, crushing strength, adhered mortar content, abrasion resistance and physical size, shape and surface texture were included as part of the first stage of experimentation. Subsequently, 24 different concrete mixture proportions were developed in order to help understand the effect that the RCA has on concrete workability, hardened density, compressive strength, tensile strength, coefficient of thermal expansion, modulus of elasticity, Poisson's ratio, flexural strength (modulus of rupture), and fracture energy.

The concrete mixture proportions were developed based on three separate groupings: 1) control mixtures, 2) direct coarse aggregate replacement with constant water-cement ratio mixtures, and 3) strength-based mixtures with constant compressive strengths and slump ranges. The control mixtures used natural aggregate as coarse aggregate and served as a baseline for comparing with the RCA concrete mixtures. The direct replacement mixtures were used to investigate the effect

of coarse aggregate type on concrete slump, compressive strength splitting tensile strength, linear coefficient of thermal expansion, modulus of elasticity and Poisson’s ratio. Strength-based mixture proportions were developed to investigate the influence of aggregate properties on splitting tensile strength, modulus of elasticity, Poisson’s ratio, linear coefficient of thermal expansion, modulus of rupture, fracture energy, and reinforcement bond in concrete having the same compressive strength. During the final experimental stage, beam-end specimens were tested to study the bond strength and slip properties of the reinforced RCA concrete members.

Ultimately, the combination of observations and findings from each experimental stage has been used to study the effect of aggregate properties on the concrete and bond properties. In addition, guidelines for classification and selection of RCA sources for specific structural applications were developed based on the research expertise gained during this study. Figure 3.1 summarizes the experimental program structure.

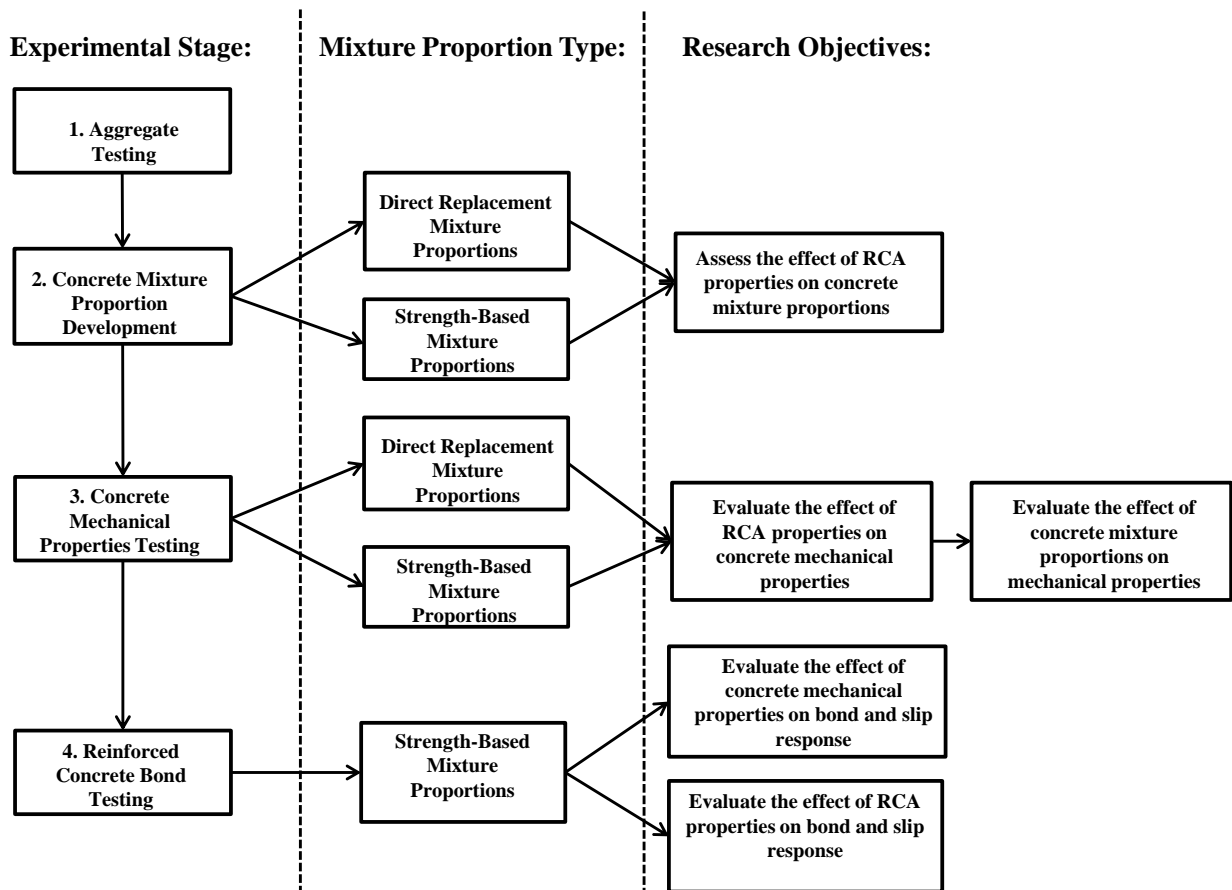


Figure 3.1 Experimental program staging, mixture proportion summary and corresponding research objectives

It should be noted that this research focused on assessing the strength properties of RCA and RCA concrete and therefore, short-term and/or long term durability properties such as alkali-aggregate reactivity, resistance to carbonation, drying shrinkage, sulphate resistance, freeze-thaw resistance, or chloride penetration were outside the scope of this research project and were not measured. Durability characteristics of RCA concrete are still of great concern and therefore, the reader is directed to several references provided in Section 10.3.7 for further information on this topic.

Chapter 4: Aggregate Testing Procedures, Results and Discussion

4.1 Overview

The following sections present and discuss the results from the numerous aggregate tests that were conducted as part of this research. Each coarse aggregate source is classified based on their qualitative and quantitative properties. A comprehensive evaluation of each aggregate source was used to identify relationships between the various aggregate properties.

4.2 Aggregate Sources and Preparation

Four coarse aggregate types were evaluated as part of this research. Combined rounded river gravel and crushed limestone gravel from southern Ontario supplied by a local aggregates supplier was used as the control natural aggregate sample (NA). The NA source satisfied all requirements of CSA A23.1 for a coarse aggregate for use in concrete. The three other aggregate types were obtained from crushed concrete. The first type of recycle concrete aggregate (RCA-1), was produced from the crushing of non-structural concrete used in sidewalks, curbs, and gutters throughout the Region of Waterloo. The second source (RCA-2) was produced from the crushing of runway, apron, and terminal structures from Pearson International Airport in Toronto, Canada. The third source (RCA-3) was produced from the crushing of concrete that had been returned to a ready-mix plant and was never used in service. This source contains crushed concrete from a concrete source that was not properly cured and may have had additional water added creating high water-cement ratios and low concrete strengths. The natural aggregate, RCA-1 and RCA-3 were pre-graded to satisfy the MTO requirements (OPSS 1002) for use as coarse aggregate in concrete (MTO, 2004). However, the RCA-2 had originally been graded to serve as granular base (granular A) for use as base material for new airport runways and apron structures. In total, more than 100 hours were spent handling, sieving, and re-grading RCA-2 to satisfy the requirements of OPSS 1002. First, all the raw RCA-2 had to be sieved and separated into the various required size fractions: 25 mm, 19.0 mm, 16.0 mm, 9.5 mm, and 4.75 mm. All material 25 mm or larger was discarded as well as the majority of the material passing the 4.75 mm sieve which was considered as recycled fine aggregate.

Afterwards, the RCA-2 was re-combined to produce the desired grading according to OPSS 1002. After sieving and re-grading, approximately 50% of the raw RCA-2 was used to make up the concrete stone and a significant amount of both fine and oversized RCA-2 made up the residual 50%. Figure 4.1 shows the various particle sizes generated from the raw RCA-2 source.

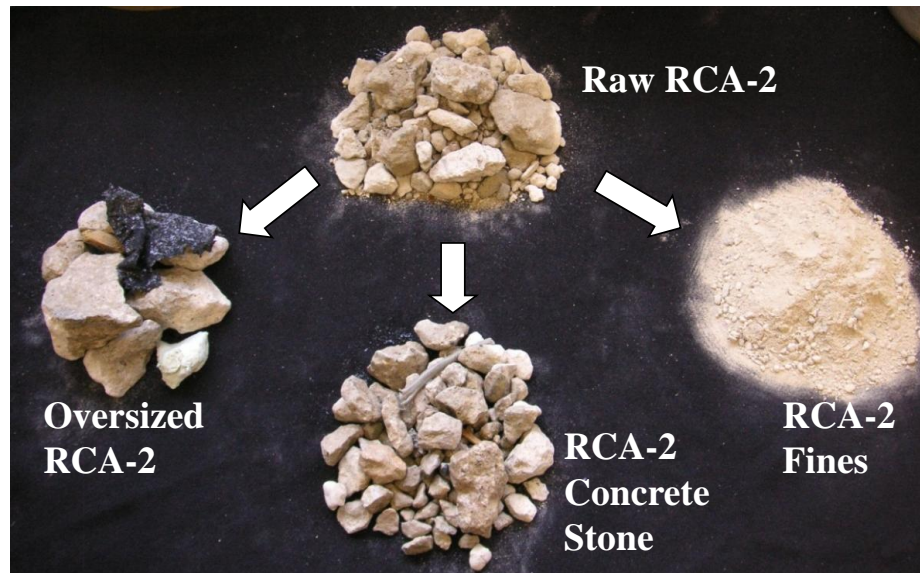


Figure 4.1 RCA-2 various gradations

Concrete sand was used as the fine aggregate for all natural aggregate and RCA concrete mixtures. The sand was produced in accordance with the Ontario Provincial Standard Specifications (OPSS 1002) for fine aggregate for use in concrete.

4.3 Aggregate Physical Classification and Grading

4.3.1 Physical classification

A qualitative procedure was followed to classify the four aggregate types used in this project. Three separate characteristics, particle size, shape and surface texture, were used to distinguish between each aggregate type. Each aggregate type had a nominal maximum particle size of 19.0 mm and the gradation followed the Ontario Ministry of Transportation's guidelines for concrete stone (OPSS 1002). Both the particle shape and surface textures were characterized according to British Standard BS 812: Part 1:1975.

Table 4.1 and Table 4.2 outline the various descriptions associated with the aggregate particle shape and surface texture, respectively. Following the BS 812 descriptions, the natural aggregate, RCA-1, RCA-2, and RCA-3 were classified as listed in Table 4.3.





Table 4.1 Particle shape classification using BS 812 Part 1: 1975 (adapted from Neville, 1997)





Classification	Description	Examples
Rounded	Fully water-worn or shaped by attrition	River or seashore gravel; desert, seashore and wind-blown sand
Irregular	Naturally irregular, or partly shaped by attrition and having rounded edges	Other gravels; land or dug flint
Flaky	Material of which the thickness is small relative to the other two dimensions	Laminated rock
Angular	Possessing well-defined edges formed at the intersection or roughly planar faces	Crushed rocks of all types; talus; crushed slag
Elongated	Material, usually angular, in which the length is considerably larger than the other two dimensions	—
Flaky and Elongated	Material having the length considerably larger than the width, and the width considerably larger than the thickness	—

Table 4.2 Surface texture of aggregates using BS 812 Part 1: 1975 (adapted from Neville, 1997)

Group	Surface Texture	Characteristics	Examples
1	Glassy	Conchoidal fracture	Black flint, vitreous slag
2	Smooth	Water-worn, or smooth due to fracture of laminated or fine-grained rock	Gravels, chert, slate, marble, some rhyolites
3	Granular	Fracture showing more or less uniform rounded grains	Sandstone, oolite
4	Rough	Rough fracture of fine- or medium-grained rock containing no easily visible crystalline constituents	Basalt, felsite, porphyry, limestone
5	Crystalline	Containing easily visible crystalline constituents	Granite, gabbro, gneiss
6	Honeycombed	With visible pores and cavities	Brick, pumice, foamed slag, clinker, expanded clay

Table 4.3 Aggregate particle shape and surface texture classifications and descriptions for natural aggregate, RCA-1, RCA-2 and RCA-3

Aggregate Type	Particle Shape Classification	Surface Texture Classification
Natural	<p>Rounded/Irregular – shaped by a combination of attrition and crushing</p> 	<p>Smooth/Rough – combination of river stone and crushed gravel</p> 
RCA-1	<p>Angular/Irregular – shows fairly well-defined edges at the intersection of plane surfaces</p> 	<p>Rough – noticeable roughened fracture surfaces resembling crushed limestone</p> 

<p>RCA-2</p>	<p>Irregular – resembles crusher run gravel but with a large amount of adhered mortar. Particles are not angular like the RCA-1</p> 	<p>Granular – due to the large amount of adhered mortar, the surface of the RCA-2 is more brittle and as a result has more loose adhered rounded mortar particles</p> 
<p>RCA-3</p>	<p>Irregular/Rounded – resembles crusher run gravel but with significant amounts of adhered mortar</p> 	<p>Granular – adhered mortar is quite brittle resulting in a large amount of adhered surface fines</p> 

In addition to the information provided in Table 4.3, it should also be noted that RCA-2 contains considerable amounts of deleterious materials such as wood chips, asphalt, metal, plastics, Styrofoam, and tile. Figure 4.2 shows some of the deleterious material found within the RCA-2 as a result of crushing and combining of terminal building concrete and apron concrete.



Figure 4.2 Deleterious materials present within RCA-2

The deleterious materials were considered to be part of the RCA-2 aggregate and, as a result, were not removed when used in concrete for this study. Compared to the natural aggregate and RCA-2 and RCA-3, RCA-1 appears to have the most roughened surface texture. This may have a significant influence on the bond between the cement paste and the aggregate; a rougher surface results in a better bond due to increased mechanical interlocking effects (Rao and Prasad, 2002). Higher mortar-aggregate bond strength in concrete incorporating RCA-1 may result in higher concrete compressive and flexural strengths as compared to a natural aggregate concrete. These points will be further investigated and discussed in later sections.

4.3.2 Grading

In general, all aggregates satisfied the grading limits for concrete stone to be used to produce structural concrete set by the Ontario Ministry of Transportation (MTO): OPSS 1002 Specification for Aggregates. Table 4.4 presents the gradation requirements for the fine aggregates used in this study according to OPSS 1002. Table 4.5 outlines the grading percentages for 19 mm nominal size concrete stone under the MTO guidelines for use in structural concrete.

Table 4.4 Fine aggregate gradation requirements

Gradation Requirements:	
Sieve Size	Percent Passing
9.5 mm	100
4.75 mm	95 – 100
2.36 mm	80 – 100
1.18 mm	50 – 85
600 mm	25 – 60
300 mm	10 – 30
150 mm	0 – 10
75 mm	0 – 3

Table 4.5 OPSS 1002 Gradation requirements for coarse aggregates for use in structural concrete

MTO Sieve Designation	Percent Passing
25.0 mm	100
19.0 mm	85 - 100
16.0 mm	65 - 90
9.5 mm	20- 55
4.75 mm	0 - 10

Separate sieve analyses according to CSA standard A23.2-2A were conducted on each aggregate type to ensure that each aggregate met the MTO specifications. Figure 4.3 and Figure 4.4 present the gradation curves for the fine and coarse aggregates, respectively. Upon inspection, all aggregate gradations met the requirements of MTO OPSS 1002 for concrete sand and concrete stone, respectively.

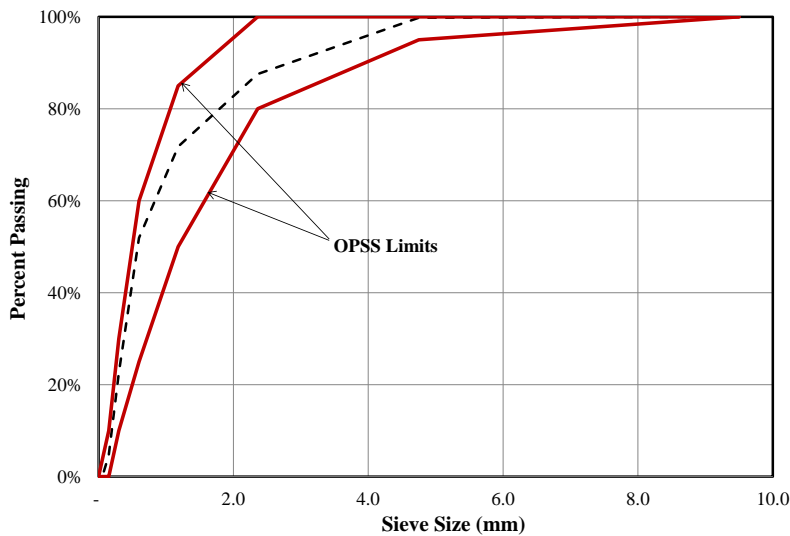


Figure 4.3 Fine aggregate gradation

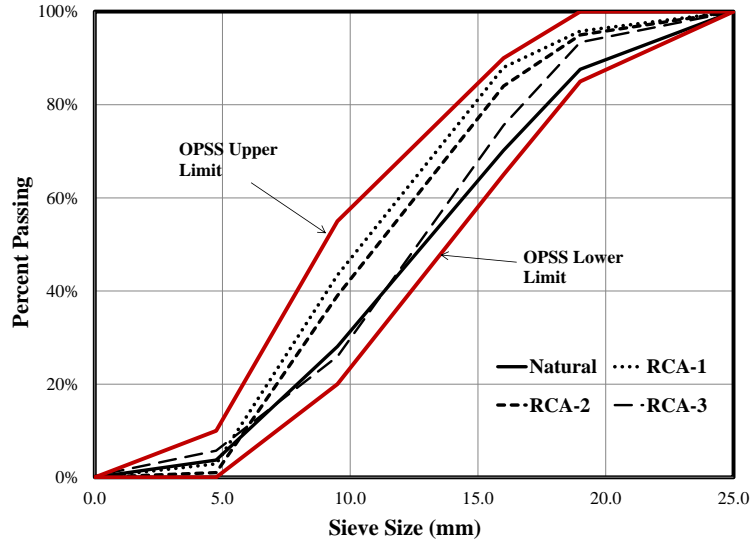


Figure 4.4 Particle size distributions for the natural aggregate, RCA-1, RCA-2 and RCA-3

4.4 Aggregate Testing Procedures

4.4.1 Adhered Mortar Content of Recycled Concrete Aggregates

The adhered mortar portion of the recycled concrete aggregate consists of both hydrated and unhydrated cement particles and the original fine aggregate (sand). All other particles are considered to be the original coarse aggregates (see Figure 4.5).



Figure 4.5 RCA-1 old adhered mortar and original aggregates

At present, there is no standard test procedure for the determination of the amount of adhered mortar on recycled concrete aggregates. However, based on current literature, three methods were selected and the results were compared to determine the amount of adhered mortar in the three recycled concrete aggregates (RCA-1, RCA-2 and RCA-3). The amount of adhered mortar was calculated for all three methods based on Equation 4.1.

$$\% \text{ A.M.} = \frac{\text{Mass of RCA} - \text{Mass of RCA after removal of mortar}}{\text{Mass of RCA}} \times 100\% \quad \text{Equation 4.1}$$

Where,

% A.M. = amount of adhered mortar (by percent weight);

Mass of RCA = M_{RCA} = oven dry mass of the RCA (includes original aggregate plus the adhered mortar);

Mass of RCA after removal of mortar = $M_{\text{R,RCA}}$ = mass of RCA after removal of mortar by one of the three methods of removal: nitric acid dissolution, freeze-thaw, or thermal treatment.

4.4.1.1 Nitric Acid Dissolution Method

Dissolution in acid is the most common method found in the literature for separating the adhered mortar and natural aggregate in recycled concrete aggregates. Essentially, the method involves immersing aggregate samples in nitric acid to dissolve the adhered mortar, leaving behind only the original aggregate (see Figure 4.6). Aggregates were graded according to MTO OPSS 1002 for concrete stone as given in Table 4.6. Aggregate particle sizes less than 9.5 mm were not used so that the original aggregates present within the adhered mortar matrix were of sufficient size for separation (i.e., larger than 4.75 mm).



Figure 4.6 Heating of RCA in nitric acid bath

Table 4.6 Aggregate gradations as used for nitric acid dissolution testing

Sieve Size*	Percent Retained			Percent Passing			MTO** Spec.
	RCA-1	RCA-2	RCA-3	RCA-1	RCA-2	RCA-3	
19 mm	4	5	7	96	95	93	85 - 100
16 mm	8	11	8	88	84	76	65 - 90
9.5 mm	45	45	50	43	39	26	20 - 55

Note: * Recycled concrete aggregate particles smaller than 9.5 mm were not used so that the attached original aggregates present within the adhered mortar matrix were not too small for separation

**Both aggregates meet the MTO specifications for aggregates used in structural concrete

The test procedure was partially adapted from the work of Movassaghi (2006) and can be summarized as follows:

- All aggregate types (RCA-1, RCA-2, and RCA-3) were thoroughly washed and then dried in an oven at 105 °C for 24 hrs.
- All noticeable impurities such as wood chips, plastics, metals, Styrofoam, asphalt, tile, brick, etc., were removed.
- Once the RCAs were oven-dry, 500 gram samples (M_{RCA}) of each RCA type were measured out for use in the test.
- Each specimen was digested in a 20% nitric acid solution (1 litre total = 800 mL H_2O + 200 mL HNO_3).
- The solution was heated on a hot plate and the aggregates were stirred gently with the flattened end of a glass rod. This process continued until adhered cement mortar began to

dissolve (typically 10 minutes).

- Each aggregate mixture was covered and heated to near boiling temperatures (around 85°C) for two to three hours. At this point, the mortar and aggregate in all RCA samples were still not completely separated.
- The sample was removed from the hot plate and left over a 48 hour period to determine how long term exposure to nitric acid would degrade the adhered mortar
- The samples were then gently heated again for a remaining 3 hours. Although extensive degradation of the adhered mortar had occurred, adhered mortar still remained.
- The aggregates were then removed from the nitric acid solution, drained and rinsed.
- In an attempt to remove the remaining deteriorated mortar, the sample was placed in the Micro-Deval machine for 15 minutes without metal balls. There was no observed difference in appearance or mass after this final step.
- The samples were then washed and dried in an oven at 105°C for 24 hrs and weighed again ($M_{R,RCA}$). The amount of adhered mortar for each aggregate was then calculated using Equation 4.1.

4.4.1.2 Freeze-Thaw Method

This method combines the use of mechanical stresses and chemical attack to breakdown the adhered mortar of the RCAs. A sodium sulphate solution was used to begin the degradation of the adhered mortar; Abbas et al. (2008a) compared several chemical solutions and found that sodium sulphate was the most effective at degrading the mortar. The RCAs were then subjected to several freeze-thaw cycles (while still immersed in Na_2SO_4) to impose internal mechanical stresses induced by the cyclical expansion and contraction of the recycled concrete aggregates. The test procedure was adapted by Abbas et al., (2008a) from ASTM standard C 88-05, Standard Test Method for Soundness of Aggregates by Use of Sodium Sulphate or Magnesium Sulphate and the MTO standard LS-614-2001 Method of Test for Freezing and Thawing of Coarse Aggregate. The test procedure is summarized as follows:

- Representative oven dried samples of the RCAs were obtained in the amounts of 1000 g for the 4.75 mm and 9.5 mm size fractions and 2000 g of the 16 mm and 19 mm size fractions (total of four samples per aggregate type). These were recorded as M_{RCA} .

- Samples were then immersed in a 26% (by weight) sodium sulphate solution.
- While still immersed in the sodium sulphate solution, the RCAs were subjected to five daily cycles of freezing and thawing consisting of 16 hours at -17°C followed by 8 hours at 80°C . A large walk-in freezer and a small oven were used to achieve these temperatures.
- After the final freeze-thaw cycle, the solution was drained from the samples and the aggregates were washed and sieved over a No. 4 (4.75 mm) sieve and then once again placed in an oven for 24 hours at 105°C .
- The final oven-dry mass was recorded ($M_{R,RCA}$) and observations were made.
- Equation 4.1 was used to calculate the amount of adhered mortar for each size fraction (i.e., % A.M. for the 4.75 mm and 9.5 mm size fractions, and % A.M. for the 16.0 mm and 19.0 mm size fractions)
- To calculate the amount of adhered mortar based on the entire aggregate gradation (i.e., all size fractions combined), a weighted average (based on the various aggregate size fractions) of the percent adhered mortar was calculated for each RCA type.

4.4.1.3 Thermal Expansion Method

The third method used to determine the adhered mortar content for the recycled concrete aggregate involved subjecting the aggregates to large and sudden temperature variations. This approach is based on the knowledge that at temperatures in excess of 400°C , calcium hydroxide dehydration occurs, causing gradual disintegration of the cement mortar (Zoldners, 1971). The following procedure has been adapted from the study by Juan and Gutierrez (2009).

- Oven-dry samples of each RCA type were separated into two size fractions (smaller size fraction retained on the 4.75 mm and 9.5 mm sieves, and a larger size fraction, retained on the 16 mm and 19 mm sieves).
- 250 grams of each size fraction were then immersed in cool water for 24 hours to saturate the adhered mortar and underlying aggregate.
- The RCA samples were then drained and immediately placed into a muffle furnace set to a temperature of 500°C for two hours (see Figure 4.7).



Figure 4.7 Muffle furnace for use with the thermal expansion test

- The RCA samples were then quickly removed from the furnace and placed directly into cold water causing a sudden reduction in the aggregate temperature and creating internal thermal stresses. Upon cooling, the adhered mortar became very brittle and could easily be broken off by hand. Any remaining adhered mortar was removed using a rubber hammer.
- Samples were then placed back into an oven for 24 hours at 110°C. Each sample was then sieved over a 4.75 mm sieve and any fine particles less than 4.75 mm or retained mortar particles larger than 4.75 mm were discarded. Final weights of the original aggregates were recorded as $M_{R,RCA}$ and the amount of adhered mortar was calculated (Equation 4.1).

4.4.2 Density and Absorption of Fine and Coarse Aggregates

The bulk density, relative density and absorption capacity of both the fine and coarse aggregates were carried out in accordance with the test procedures outlined in CSA A23.2-04, Methods of Test and Standard Practices for Concrete (CSA A23.2, 2004). The relative density and absorption capacity of the fine aggregate were evaluated using CSA A23.2-6A. First, a one kilogram sample of fine aggregate (concrete sand) was dried to constant mass at 110°C for 24 hours. Following drying, the sample was soaked for 24 hours to ensure that the sand particles were fully saturated. To remove the surface water, the sand was spread out over a stainless steel

countertop and stirred while passing a hot-air heating gun over its surface to expedite drying. Once the sand approached a “free-flowing” condition a portion was placed into a stainless steel mould cone and tamped 25 times. The mould was then slowly removed and revealed that the sand had retained the mould shape. This process was repeated until the sand slumped slightly after removal of the mould. At this condition, the sand was considered to be saturated surface dry (SSD). A pycnometer was then filled with water and its mass plus the mass of water was recorded as “B”. Next, the pycnometer was emptied and then partially filled with 500 g of the saturated surface dry sand, recorded as mass, M_f , and then filled to its calibration mark (approximately 90% of the capacity) with water. The sand and water mixture was then rolled and inverted within the pycnometer to eliminate all air bubbles. Once all air bubbles were expelled, the total mass of the pycnometer, water and sand were measured and recorded as mass, “C”. The sand was then removed from the pycnometer and dried to a constant mass for 24 hours at 110°C and then weighed and recorded as mass “A”. Using the recorded masses, several calculations could be carried out using Equations 4.2 to 4.5.

$$\text{Bulk Relative Density} = \frac{A}{B + M_f - C} \quad \text{Equation 4.2}$$

$$\text{Bulk Relative Density (SSD)} = \frac{M_f}{B + M_f - C} \quad \text{Equation 4.3}$$

$$\text{Apparent Relative Density} = \frac{A}{B + A - C} \quad \text{Equation 4.4}$$

$$\text{Absorption} = \frac{M_f - A}{A} \quad \text{Equation 4.5}$$

The bulk density of the coarse natural and recycled concrete aggregates was evaluated using CSA A23.2-10A. Approximately 8 kilograms of oven dry coarse aggregate was required for the test. A steel cylinder with known volume, “V”, was filled in thirds with the aggregate and rodded 25 times per layer. The mass of the aggregate filling the cylindrical measure was recorded as “M” and the oven dry bulk density was calculated using Equation 4.6.

$$\text{Oven Dry Bulk Density} = \frac{M}{V} \quad \text{Equation 4.6}$$

Absorption and relative density of each coarse aggregate type were evaluated using CSA A23.2-12A. Approximately 3 kg of coarse aggregate was used for the test. First, the aggregate was soaked for 24 hours and then drained and towel dried so that only the surface moisture was removed leaving the aggregate in the saturated surface dry condition. The aggregate was then weighed in air and its mass was recorded as “B”. Immediately after, the sample was placed in a wire basket with 1.25 mm mesh width and weighed while submerged in water and its mass recorded as “C”. Finally, the sample was placed in an oven and dried to constant mass for 24 hours and then weighed a final time as mass “A”. Using the recorded masses, the following coarse aggregate physical properties could be calculated from Equations 4.7, 4.8 and 4.9.

$$\text{Bulk Relative Density (SSD)} = \frac{B}{B - C} \quad \text{Equation 4.7}$$

$$\text{Apparent Relative Density} = \frac{A}{A - C} \quad \text{Equation 4.8}$$

$$\text{Absorption} = \frac{B - A}{A} \times 100\% \quad \text{Equation 4.9}$$

4.4.3 Rate of Absorption of Coarse Aggregates

A separate study was conducted to measure the time required for each coarse aggregate type at an oven dry condition to reach a saturated surface dry condition. Several time increments were used during which, each aggregate type was soaked in water and both their oven-dry and surface dry weights were recorded. To monitor the moisture content changes of each aggregate over time, measurements of moisture content were taken at ½ hour, 1 hour, 2 hour, 4 hour, 8 hour and 24 hour time intervals. For each time interval, 1000 gram samples of each aggregate type were prepared. After being soaked for a given time increment, aggregates were surface dried, weighed and their masses recorded as M_1 , before being placed into an oven for 24 hours at 110°C. Once the samples were oven-dried their weights were recorded as M_2 and their moisture contents were calculated using Equation 4.10.

$$\text{Moisture Content} = \frac{M_1 - M_2}{M_2} \times 100\% \quad \text{Equation 4.10}$$

Once all moisture contents and their respective immersion times were recorded, the length of time for each aggregate to become fully saturated could be determined.

4.4.4 Moisture Content and Adhered Surface Moisture of Pre-Soaked Coarse Aggregates

The term adhered surface moisture refers to the moisture content in excess of SSD after aggregates have been soaked for 24 hours. When using RCAs (which have higher absorption than natural aggregates) as coarse aggregates in concrete mixtures, they are often pre-wetted or pre-soaked because they tend to absorb water more slowly during mixing. This slower absorption may cause variation in the fresh properties of the RCA concrete and the specified water-cement ratio may not be achieved.

A method for measuring the adhered surface moisture was developed for the purposes of developing the concrete mixture proportions for this study (refer to Chapter 5 for more details on mixture development). Approximately 1500 g of properly graded coarse aggregate was allowed to soak for 24 hours (or, at a minimum, the measured time required for total absorption). Samples were then drained over a 1.18 mm sieve to minimize loss of fines. Once satisfactorily drained, samples were immediately weighed to the nearest 0.1 gram and then placed in an oven to dry at 110°C ±5°C for 24 hours. Samples were then removed from the oven and weighed again. The total moisture content after 24 hours of soaking followed by draining over a 1.18 mm sieve (MC₂₄) was then obtained using Equation 4.11.

$$\text{MC}_{24} = \left(\frac{M_{\text{TOT}} - M_{\text{OD}}}{M_{\text{OD}}} \right) \times 100\% \quad \text{Equation 4.11}$$

The adhered surface moisture was then obtained by calculating the difference between MC₂₄ and the absorption capacity of the aggregate as described in Equation 4.12.

$$\% \text{ Adhered Surface Moisture} = \text{MC}_{24} - \text{Absorption} \quad \text{Equation 4.12}$$

4.4.5 Absorption of Original Aggregates and Adhered Mortar

The absorption capacity of the recycled concrete aggregates is dependent on two separate sources: the original aggregate and the adhered mortar. For this reason, the absorption capacity of the original aggregates was estimated to determine the relative contribution from the adhered mortar and the original aggregates to the total absorption capacity of the RCA. Since the source of the original aggregates from the RCA was unknown, measurements were performed using the original coarse aggregate left over after subjecting the RCA to the thermal treatment method of adhered mortar removal. Test method CSA A23.2-12A and Equation 4.9 were used to obtain these results.

4.4.6 Abrasion Resistance

The abrasion resistance of each aggregate was determined using the Micro-Deval method to provide a measure of the aggregates' resistance to abrasion under moist conditions. The test was carried out in accordance with CSA test method A23.2-29A. Test samples were first washed and oven-dried for a 24 hour period at 110°C. A 1500 g oven-dried sample was then prepared using the following gradation: 750 g passing 20 mm sieve and retained on the 14 mm sieve; and 750 g passing the 14 mm sieve and retained on the 10 mm sieve. The final combined mass (approximately 1500 g) is recorded as mass "A" to the nearest 1 g. The sample was then saturated in 2.0 L of water for one hour and then placed in the stainless steel Micro-Deval abrasion jar and combined with 5000 g of magnetic 9.5 mm diameter stainless steel balls. The jar lid was then fastened and the apparatus was placed in the Micro-Deval machine and subjected to 100 revolutions per minute for two hours. The samples were then removed from the jar and poured over two superimposed 5 mm and 1.25 mm sieves. Using a magnetic rod, the stainless steel balls and aggregate were separated. Material left on the 5 mm and 1.25 mm sieved was combined and placed in an oven, and material smaller than 1.25 mm was discarded. After 24 hours of drying the sample was weighed and its mass recorded as "B". The Micro-Deval abrasion loss was calculated using Equation 4.13.

$$\text{Abrasion Loss} = \frac{A - B}{A} \times 100\% \quad \text{Equation 4.13}$$

4.4.7 Aggregate Crushing Value (ACV)

To determine the compressive strength of loose aggregate, British Standard BS 812-110: 1990 was employed to determine the aggregate crushing value (ACV) of each aggregate type. This test involves the use of a case-hardened, open-ended steel cylinder with an internal diameter of 154 mm, a wall thickness of 16 mm and a separate 10 mm thick steel base plate. A separate solid steel plunger with an exterior diameter of 152 mm fits into the steel cylinder to act as the crushing head. A separate steel cylindrical measure is used in combination with a steel rod to obtain the proper volume of coarse aggregate. Figure 4.8 illustrates the test apparatus. The basic principle of the test is to compact and crush the loose aggregate specimen in the test cylinder by applying a constant load rate of 40 kN/min through the plunger. After the load reaches 400 kN, the applied load is removed and the aggregates are emptied from the test cylinder and sieved to determine the extent of crushing. The extent to which the aggregates have been crushed is determined by the amount of crushed particles passing a 2.36 mm sieve. The total percent mass loss is represented as the aggregate crushing value (ACV).

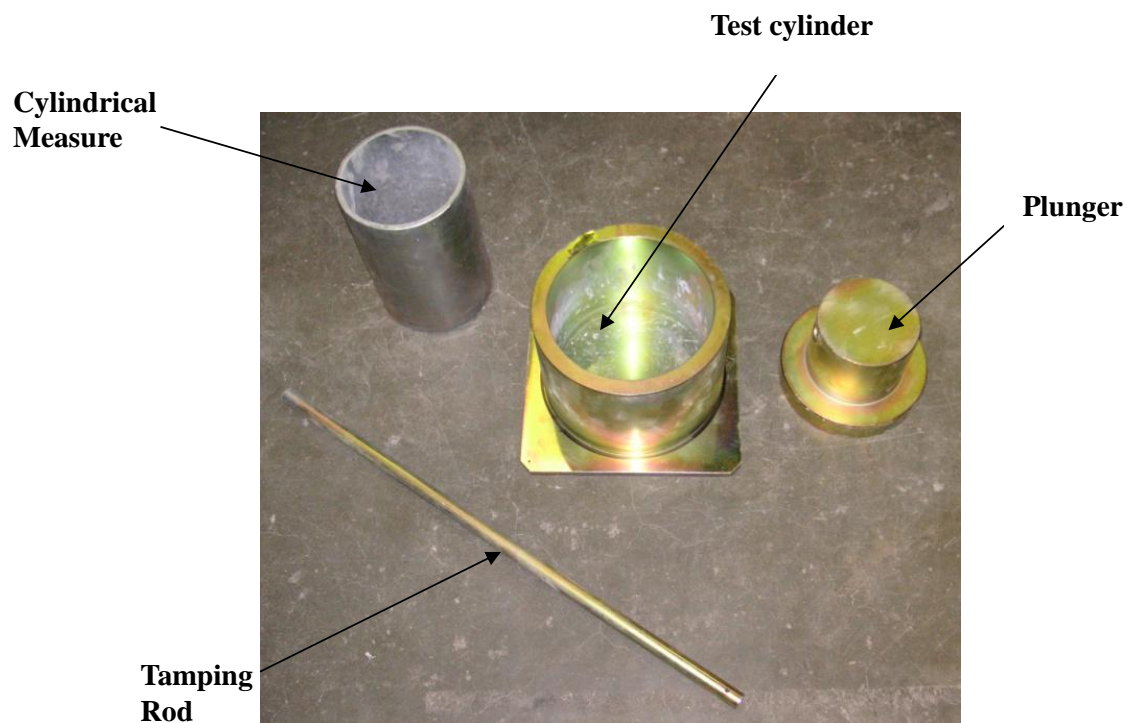


Figure 4.8 Aggregate crushing value test apparatus

The test proceeds as follows:

- An oven-dry 25 kg sample of aggregate is sieved to achieve a gradation that lies between 9.5 mm and 16 mm.
- The steel cylindrical measure is filled in three equal layers with aggregate and rodded 25 times per layer to obtain the required specimen volume.
- The test cylinder was placed on the base plate and the aggregate sample was transferred from the cylindrical measure to the test cylinder in 3 equal layers with 25 strokes from the tamping rod per layer.
- The surface of the aggregate was levelled in the test cylinder and the plunger was inserted into the cylinder and left to rest horizontally on the aggregate surface.
- The entire apparatus was placed into a 500 kN test frame where it was loaded at a uniform rate of 40 kN/minute up to a load of 400 kN.
- Once the load was released the crushed material was removed from the cylinder by hammering on the outside with a rubber mallet whilst holding the cylinder over a metal tray of known weight.
- All crushed material was then sieved over a 2.36 mm sieve and the weights were recorded. M_1 was the mass of the crushed test specimen after transfer from the test cylinder and M_2 was the mass of the material passing the 2.36 mm test sieve.
- The aggregate crushing value (ACV) was then calculated using Equation 4.14.

$$ACV = \frac{M_2}{M_1} \times 100 \quad \text{Equation 4.14}$$

- Three samples of each aggregate type were tested and the ACV was reported as their average.

Physically, the aggregate crushing value represents the degree to which the aggregate sample has been crushed. The higher the ACV, the more susceptible the aggregate is to crushing which implies lower strength. Figure 4.9 shows the aggregate crushing value test in progress.



Figure 4.9 Aggregate crushing value test in progress

4.5 Discussion and Analysis of Results

The following sections present the results of all aggregate tests and describe correlations between the various physical properties tested. Conclusions based on these results are summarized at the end of the chapter.

4.5.1 Adhered Mortar Content of Recycled Concrete Aggregates

4.5.1.1 Nitric-Acid Dissolution

Dissolution in nitric acid was not able to completely remove the adhered mortar in the RCA samples. Also, the nitric acid dyed some of the aggregates with a yellowish colour which may indicate the presence of limestone in the original aggregate. While significant mass loss occurred, the remaining mortar was still firmly attached to the original aggregates for all three types of RCA investigated. Figure 4.10 shows the extent of the deterioration for each RCA type.

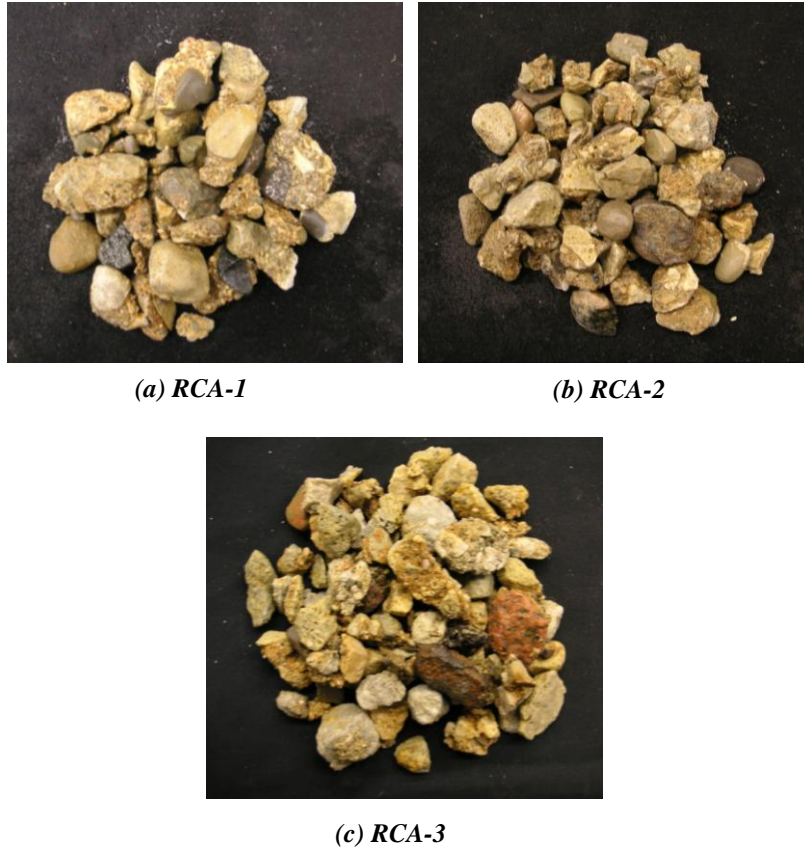


Figure 4.10 RCA samples after nitric acid dissolution

As visible in the above figure, significant destruction of the cement mortar occurred in all RCAs exposing the original coarse aggregates. Following a 15 minute cycle in the Micro-Deval apparatus, the mortar remained firmly attached to the original aggregate. Further scratching and hammering using a rubber mallet still failed to remove the remaining mortar. This suggests that this method works by dissolving only the outer layer or surface of the mortar but does not fully breakdown the mortar-aggregate bond. It is possible that a longer exposure at higher concentrations of nitric acid could dissolve greater amounts of the remaining cement mortar. Upon inspection, it is difficult to determine which aggregate experienced a higher dissolution of mortar. Table 4.7 presents the adhered mortar content values after nitric acid dissolution.

Table 4.7 Adhered mortar content* – Nitric acid dissolution method

Aggregate Type	% Adhered Mortar*
RCA-1	20.4
RCA-2	32.1
RCA-3	36.1

*Actually represents percent mass loss after nitric acid digestion

Failing the complete removal of mortar, final masses of the aggregates were still recorded and instead were considered to represent the aggregate resistance to nitric acid digestion. Although the results reported are not the actual adhered mortar percentages it is interesting to note that a notable difference was observed between the three recycled concrete aggregates: RCA-3 lost 36.1% of its mass, RCA-2 lost 32.1%, and RCA-1 lost only 20.4%.

4.5.1.2 Freeze-Thaw Method

The next method used to determine the amount of adhered mortar involved subjecting the recycled concrete aggregates to freezing and thawing action combined with saturation in a sodium sulphate solution. It is estimated through visual inspection that approximately 90% of the mortar was removed by this method. Figure 4.11 shows the aggregates after the test was completed.

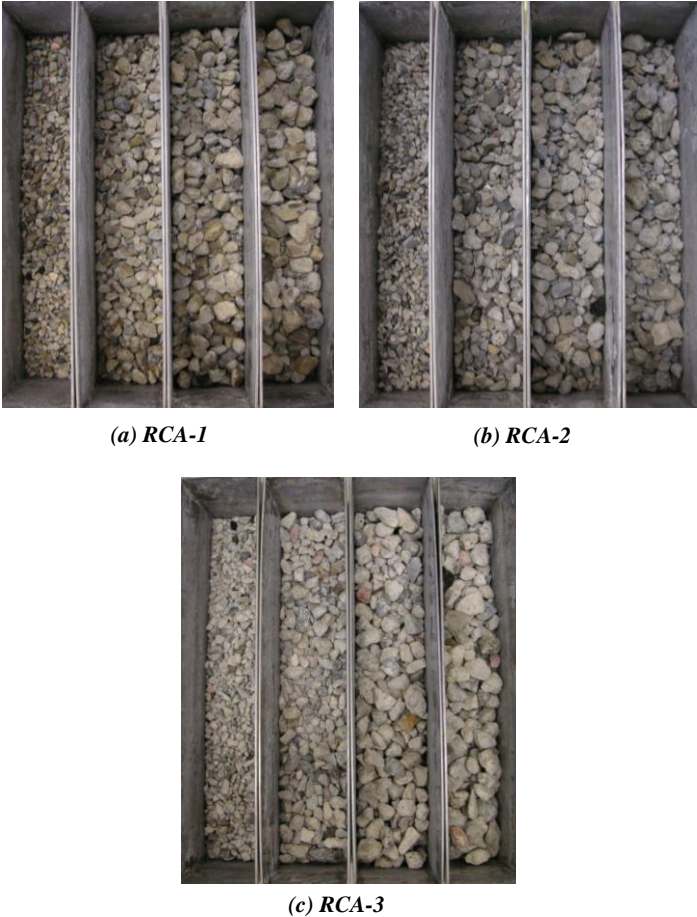


Figure 4.11 RCA samples after freeze-thaw test (size fractions from left to right: 4.75 mm, 9.5 mm, 16.0 mm, 19.0 mm)

Upon close visual inspection, this method seemed to remove more of the adhered mortar than the nitric acid dissolution. Hammering using a rubber mallet to remove the remaining mortar was recommended after the last freeze-thaw cycle. It was obvious that significant deterioration of the cement paste had been achieved and that the mortar-aggregate bond had been broken down as removal by hand of the remaining attached mortar could be done with ease. By comparison of the material passing the 4.75 mm sieves, it is evident that RCA-2 had a higher percentage of adhered mortar than either RCA-1 or RCA-3. Results of this test method are summarized in Table 4.8.

Table 4.8 Adhered mortar content – Freeze-thaw method*

Size Fraction	RCA-1	RCA-2	RCA-3
4.75 mm	40.1%	50.7%	35.6%
9.5 mm	22.3%	33.6%	23.9%
16.0 mm	23.6%	38.6%	17.3%
19.0 mm	15.5%	40.9%	14.9%
Weighted Average	29.6%	41.1%	24.5 %

*Note: Values actually represent percent mass loss after combined freezing and thawing and sodium sulphate exposure.

Once again, this method failed to completely remove the attached mortar even after hammering and scratching. While the results reported are not the true adhered mortar contents, a significant difference in mass loss between the three RCA types was still observed. The RCA-2 lost 41.1% of its adhered mortar versus only 29.6% for RCA-1 and 24.5% for RCA-3 after the five freeze-thaw cycles and being saturated in the sodium sulphate solution.

4.5.1.3 Thermal Expansion Method

The final method used to determine the adhered mortar content involved subjecting the recycled concrete aggregates to a sudden temperature change to create thermal stresses. Table 4.9 summarizes the results of this test.

Table 4.9 Adhered mortar content – Thermal treatment method

Size Fractions	RCA-1	RCA-2	RCA-3
4.75 mm and 9.5 mm	46.7%	43.9%	37.6%
16.0 mm and 19.0 mm	55.3%	57.5%	54.0%
Weighted Average	46.4%	55.7%	49.6%

By visual inspection, this method succeeded to remove nearly 100% of the adhered mortar from the recycled concrete aggregates. However, the difference in adhered mortar content between the three RCA types has been reduced with RCA-2 containing only 17% and 11% more adhered mortar than RCA-1 and RCA-3, respectively. Figure 4.12, Figure 4.13, and Figure 4.14 show the original aggregates without any adhered mortar for all RCA types.

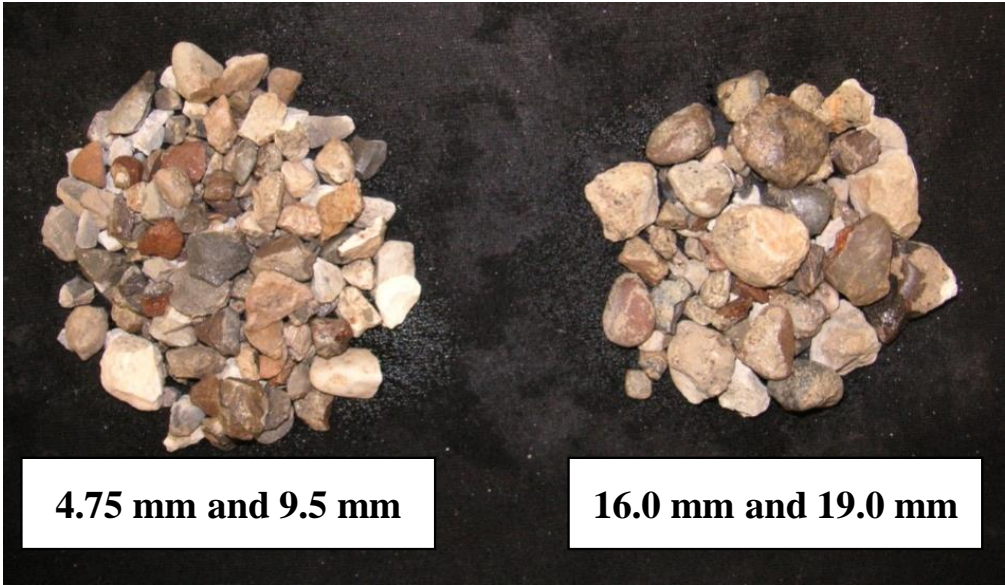


Figure 4.12 RCA-1 original aggregates after thermal treatment (separate size fractions)

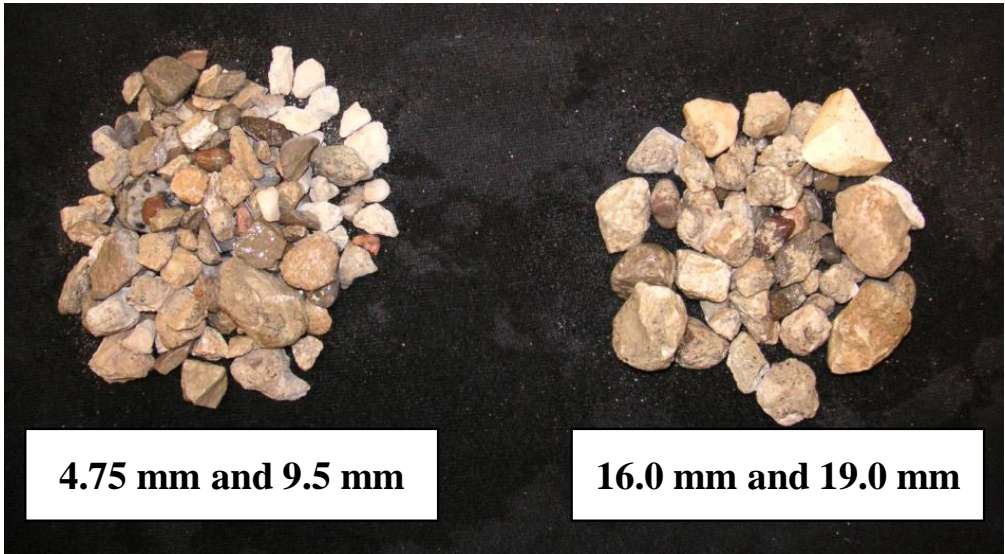


Figure 4.13 RCA-2 original aggregates after thermal treatment (separate size fractions)

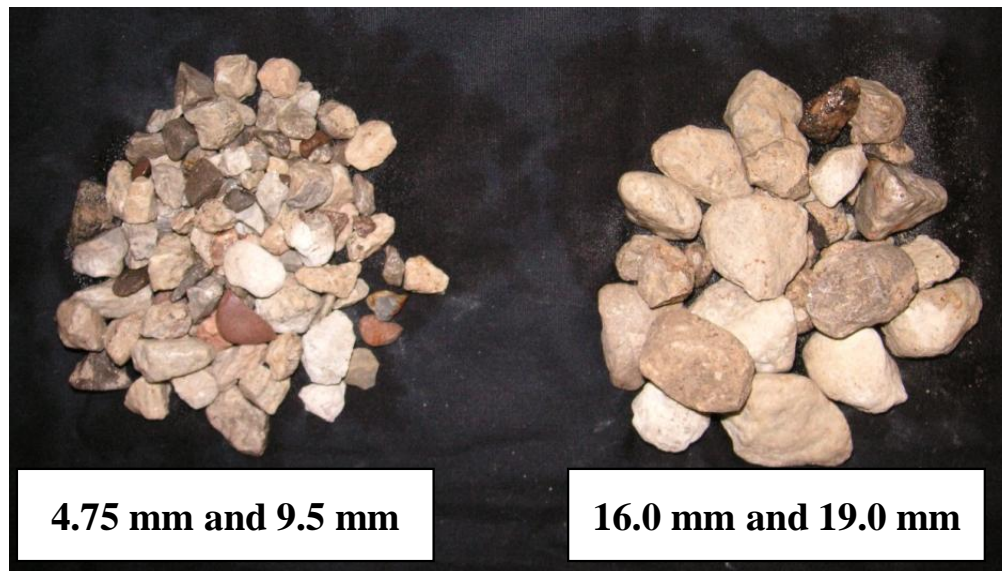


Figure 4.14 RCA-3 original aggregates after thermal treatment (separate size fractions)

After considering all three methods, it is apparent that RCA-2 has a larger percentage of adhered mortar than RCA-1 or RCA-3. There are two possible explanations for this difference. First, it is possible that RCA-1 was produced from a lower grade of concrete and thus, may have contained less cement than the concrete that produced RCA-2. Given that RCA-1 was derived from the crushing of sidewalks, curbs and gutters, RCA-3 was derived from the crushing of returned and improperly cured returned concrete and RCA-2 was derived from the crushing of apron and airport terminal structures which may have contained concrete of higher quality and higher mortar volumes, this explanation seems plausible. Another explanation for this difference may be due to the type of crusher and crushing method used to produce each RCA type. As the number of crushing cycles increases, the amount of adhered mortar has been found to decrease (Nagataki et al, 2004). Also, the type of crusher and crushing process used can influence how efficiently the original concrete is crushed and how much adhered mortar is left on the surface. Impact crushers for instance have been shown to produce RCAs with relatively lower mortar content than jaw crushers (Etxeberria et al., 2007). It is also probable that both explanations are correct and the original concrete used to produce RCA-2 may have had a higher cement content than either RCA-1 or RCA-3 and had been crushed using a less refined crushing method. Both factors would explain the higher adhered mortar content of RCA-2.

4.5.2 Density and Absorption of Fine and Coarse Aggregates

Table 4.10 presents the various fine aggregate properties and Figure 4.10 presents the coarse aggregate densities and absorption capacities.

Table 4.10 Fine aggregate properties

Fine Aggregate Property	
Fineness Modulus (FM) =	2.66
Bulk Relative Density =	2.66
Bulk Relative Density (SSD) =	2.70
Absorption =	1.63%

Table 4.11 Coarse aggregate densities and absorption capacities

Property/Aggregate Type	NA	RCA-1	RCA-2	RCA-3
Bulk Relative Density (SSD) =	2.70	2.47	2.45	2.41
Apparent Relative Density =	2.77	2.63	2.67	2.70
Bulk Relative Density (Oven-dry) =	2.66	2.37	2.31	2.23
Oven-dry rodded bulk density =	1733 kg/m ³	1539 kg/m ³	1458 kg/m ³	1395 kg/m ³
Absorption =	1.52 %	4.66 %	6.15 %	7.81 %
Moisture Content (24 hrs in water) =	3.26 %	8.95 %	7.92 %	12.02 %
Adhered surface moisture =	1.72 %	5.97 %	2.20 %	4.39 %

RCA-3 is the least dense of all the aggregates followed by RCA-2, RCA-1 and NA. Both the bulk relative densities in the oven-dry and saturated surface dry condition (SSD) follow the same trend as the oven-dry bulk density. This trend may be due to both the adhered mortar content and the lower density adhered mortar on the RCA-3 compared to the higher density adhered mortar on the RCA-1 and RCA-2 (Section 4.5.5 presents further discussion). The absorption capacities of the RCAs were significantly higher than the natural aggregate. This trend is consistent with the literature (Eguchi et al., 2007, Choi and Kang, 2008 and Obla and Kim, 2009), and may be explained by the presence of adhered mortar on the RCAs. It has been typically accepted that as the amount of adhered mortar increases, the absorption capacity also increases (Juan and Gutierrez, 2009). However, this trend was not the case when comparing RCA-2 and RCA-3. While RCA-3 had an absorption capacity 25% higher than RCA-2, it had an adhered mortar content that was 12% lower (i.e., 49.6% versus 55.7%). This result will be explained through further investigation of the absorption of the original aggregates and the adhered mortar for each RCA type (refer to Section 4.5.5).

4.5.3 Rate of Absorption of Coarse Aggregates

The amount of time required for an aggregate to reach a saturated surface dry condition is expected to increase as the absorption capacity increases. Figure 4.15 through Figure 4.18 present the absorption versus time plots and corresponding complete saturation times for each aggregate. Note that after reaching SSD, for all aggregate types, the measured absorptions were often slightly higher or lower than those reported in Table 4.11. This is a result of the inherent variability in measuring the absorption of coarse aggregates.

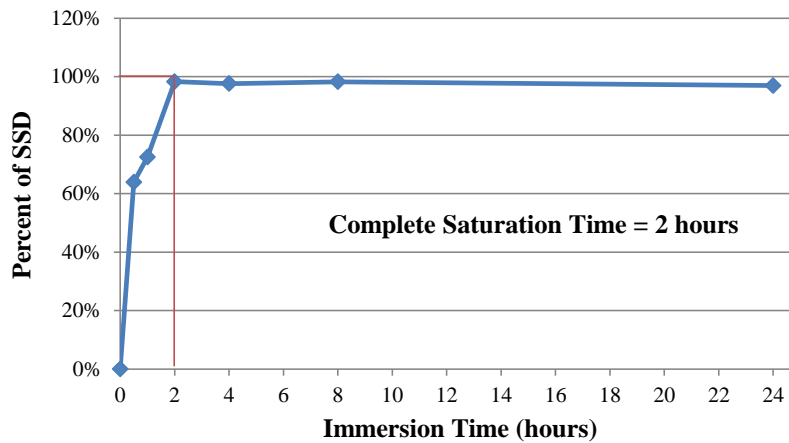


Figure 4.15 Moisture absorption over time for natural aggregate

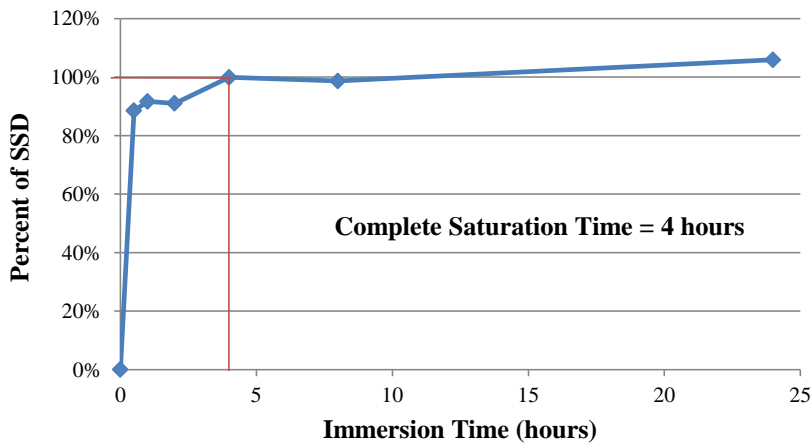


Figure 4.16 Moisture absorption over time for RCA-1

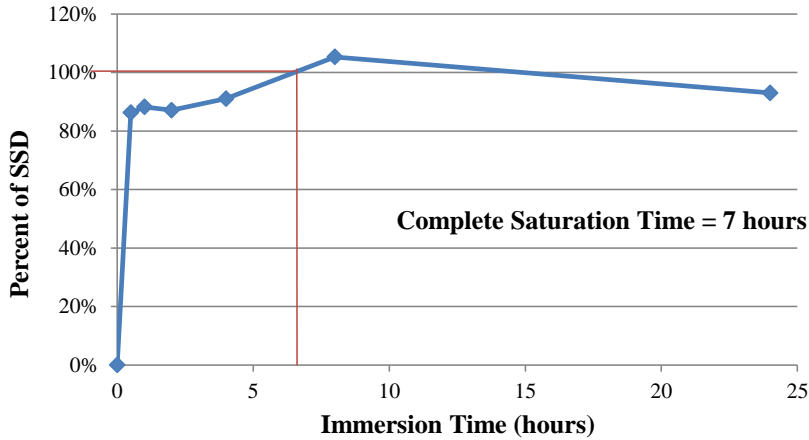


Figure 4.17 Moisture absorption over time for RCA-2

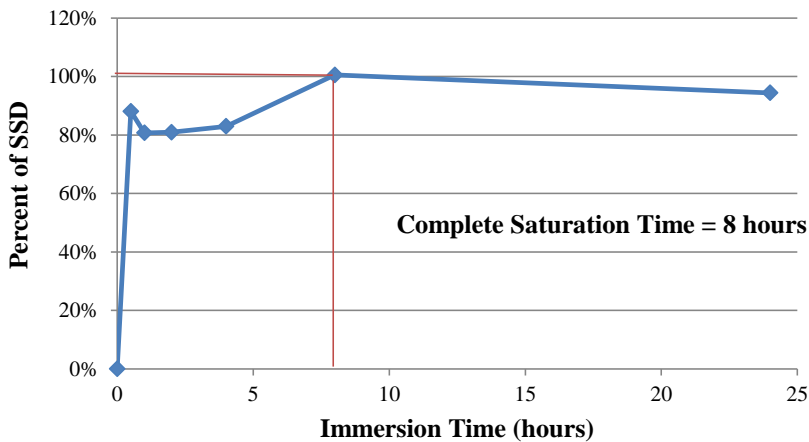


Figure 4.18 Moisture absorption over time for RCA-3

RCA-3 had the highest absorption capacity of 7.81%, and took the longest time to reach SSD at approximately 8 hours. This may be due to the more porous adhered mortar on RCA-3 which could potentially absorb water more quickly (refer to Section 4.5.5 for adhered mortar absorption). RCA-2, with an absorption capacity of 6.15% took approximately 7 hours to reach SSD, RCA-1, with an absorption capacity of 4.66% took only 4 hours and the natural aggregate with an absorption capacity of 1.52% took only 2 hours to reach complete saturation.

Absorption rates are important to consider when developing concrete mixture proportions incorporating RCAs. Concrete mixtures are proportioned assuming that both coarse and fine aggregates are in a saturated surface dry (SSD) condition. Aggregates whose moisture contents are less than SSD at the time of mixing will absorb mixing water which will affect workability

and the water-cement ratio. Thus, batch proportions must be adjusted to compensate for this difference in mixing water to ensure that the desired water-cement ratio and consistent workability is attained. Portland cement concrete cured at room temperature takes approximately three hours from the time of batching to reach initial set (Kosmatka et al., 2002). Therefore, the rate of absorption of aggregates with high absorption capacities must be considered in order to achieve proper workability and actual or desired water-cement ratios. Further discussion on the absorption rate of aggregates and how it relates to concrete mixture proportioning is included in Chapter 5.

4.5.4 Moisture Content and Adhered Surface Moisture of Pre-Soaked Aggregates

As presented in Section 4.4.4, the total moisture content of aggregates after 24 hours of soaking followed by draining over a 1.18 mm sieve (MC_{24}) and the absorption was required for determination of the adhered surface moisture (moisture in excess of SSD). The adhered surface moisture is a critical quantity in the proportioning of concrete mixtures. Therefore, to minimize variations in concrete properties, variations in the determination of the adhered surface moisture must also be minimized. Given that the adhered surface moisture is dependent on the MC_{24} (as shown in Equation 4.12), the variability associated with the measurement of the MC_{24} values will govern the variability associated with the adhered surface moisture values. In total, 20 samples of each aggregate type were used to gauge the variation in MC_{24} through the calculation of the standard deviation and the coefficient of variation. Moisture contents were measured using the procedures in Section 4.4.2. The adhered surface moisture was then calculated as the difference between the MC_{24} and the absorption of the aggregate (Equation 4.12). The results of this statistical moisture analysis are presented in Table 4.12.

Table 4.12 Statistical moisture analysis of pre-soaked coarse aggregates

	Natural Aggregate	RCA-1	RCA-2	RCA-3
Absorption	1.52%	4.66%	5.20%	7.81%
Mean moisture content after 24 hours of soaking, MC_{24} (20 samples)	3.06%	7.34%	7.33%	10.08%
Standard deviation	0.41%	0.49%	0.41%	0.56%
Coefficient of variation	0.135	0.066	0.049	0.055
Adhered surface moisture content *	1.54%	2.68%	2.18%	2.27%

* Adhered surface moisture (refer to Equation 4.12) = MC_{24} - Absorption

Standard deviation values for the MC_{24} values were similar for both the natural aggregate and the RCAs. The coefficient of variation values of RCAs range between 5 and 7% whereas the natural aggregate value is 13% (the latter value reflecting the lower mean pre-soaked moisture content of the natural aggregate). The adhered surface moisture content of RCA-1 was 1.7, 1.2 and 1.2 times larger than that of the natural aggregate, RCA-2 and RCA-3, respectively. This difference may be explained by the more roughened surface texture of the RCA-1 as compared to the smoother surface texture of natural aggregate and granular surface of RCA-2 and RCA-3. Therefore, this measure of adhered surface moisture may be used to provide a quantitative and indirect measure of coarse aggregate surface texture. In addition, a roughened aggregate surface generally results in better bond between the mortar and coarse aggregate and may produce higher concrete compressive strengths (Neville, 1997).

4.5.5 Absorption of Original Aggregates and Adhered Mortar

Table 4.13 presents the absorption capacities of the original aggregates in RCA-1, RCA-2 and RCA-3 as measured after removing the adhered mortar using the thermal treatment method.

Table 4.13 Absorption of the RCA original aggregates and adhered mortar

Absorption	Natural Aggregate	RCA-1	RCA-2	RCA-3
Absorption of original aggregates ¹ $MC_{original}$	1.52 %	3.66 %	3.44 %	2.77 %
Contribution of adhered mortar ²	N/A	1.00 %	2.71 %	5.04 %

¹Original aggregates used were those produced using the thermal expansion method, thus nearly 100% of the adhered mortar had been removed from the aggregate particles. Absorption was measured on the basis of mass.

²Contribution of Adhered Mortar = Absorption - $MC_{original}$

The results presented indicate that while the adhered mortar content of RCA-3 is lower than RCA-2, its higher absorption capacity is mainly attributed to the higher absorption capacity of its adhered mortar (5.04%). It was found that the contribution of the adhered mortar to the absorption capacity of RCA-3 was 5.0 and 2.7 times higher as compared to that of the RCA-1 and RCA-2, respectively. This suggests that the porosity of the adhered mortar on the RCA-3 particles is higher than that on the RCA-1 and RCA-2 particles. Consequently, it may be inferred that mortar with a higher porosity will have lower strength. This inference seems plausible given that RCA-3 was produced from the crushing of returned concrete that may have been mixed with additional water (i.e., added from concrete truck drivers or from natural

precipitation) thereby increasing the water-cement ratio and increasing the mortar porosity.

It should be noted that the absorption capacity of the original aggregates were similar among the three RCAs (between 2.77 and 3.66%). However, the natural aggregate absorption (1.52%) was approximately two times lower than the RCA original aggregates. This may be due to the small traces of adhered mortar remaining on the RCAs and the result of possible micro-cracking in the RCA original aggregates caused by the crushing process used to produce the RCA and the thermal treatment method of adhered mortar removal.

4.5.6 Abrasion Resistance

Once the aggregates had been subjected to one cycle in the Micro-Deval machine, a noticeable difference in their overall shape and textures was observed. In general, all aggregate types were more rounded in shape. The recycled concrete aggregates still retained some attached mortar which had also been rounded by the abrasion action of the Micro-Deval apparatus. Table 4.14 presents the Micro-Deval abrasion loss values for each coarse aggregate type.

Table 4.14 Micro-Deval abrasion loss percentages for each coarse aggregate type

Aggregate Type	Micro-Deval Abrasion Loss
Natural aggregate (NA)	11.9 %
RCA-1	15.1 %
RCA-2	22.1 %
RCA-3	25.0 %

As expected, the natural aggregate had a lower abrasion loss than the RCAs since it had no adhered mortar. The natural aggregate had a 26% higher abrasion resistance than RCA-1, an 86% higher abrasion resistance than RCA-2 and a 110% higher abrasion resistance than RCA-3. In comparison, RCA-3 experienced a 12% and 40% higher abrasion loss than the RCA-2 and RCA-1, respectively. This difference in abrasion resistance between the different RCA types may be explained by their differences in relative density and amount of adhered mortar that are a direct result of the original source concrete from which they were derived. The source concrete from which RCA-3 was improperly cured and would have contained higher amounts of water and, as a result, would tend to have higher water-cement ratios, higher mortar porosity and consequently, lower adhered mortar density. Conversely, the source concrete from which RCA-

1 and RCA-2 were produced had lower water-cement ratios, were properly cured and consolidated and contained less water leading to lower mortar porosity and higher adhered mortar density.

Figure 4.19 and Figure 4.20 show the aggregates before and after testing in the Micro-Deval machine. It appears that both attached mortar and original aggregate in the RCAs had been abraded and rounded after the test. After the test, a clear distinction between the original aggregates and the adhered mortar in the RCAs was observed.

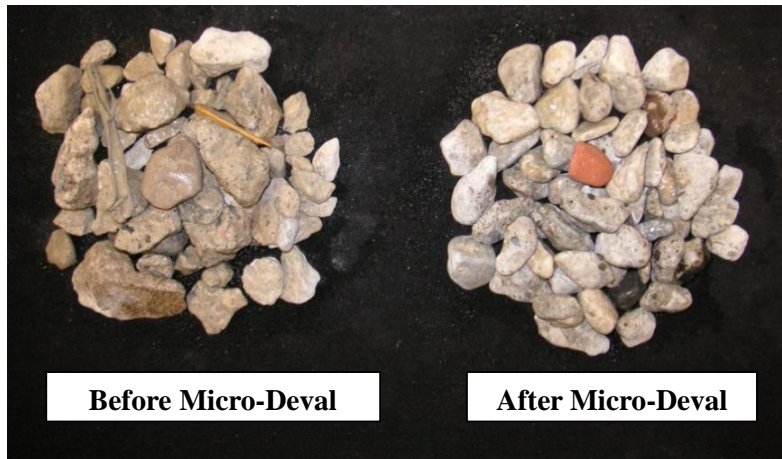


(a) Natural Aggregate

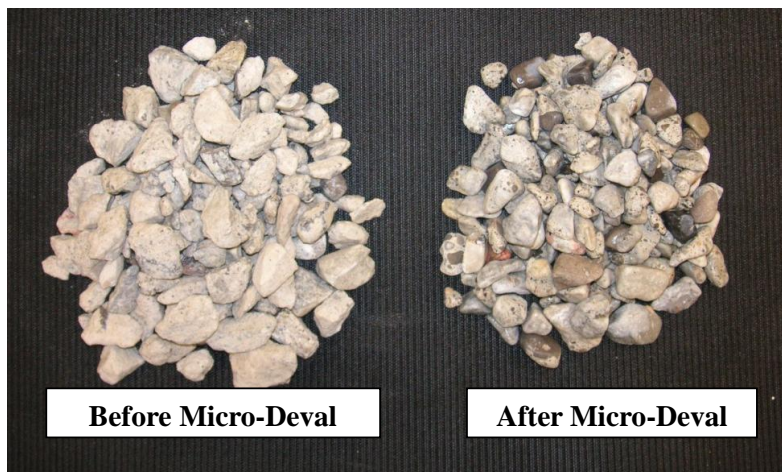


(b) RCA-1

Figure 4.19 Natural aggregate and RCA-1 samples before and after micro-deval abrasion testing



(a) RCA-2



(b) RCA-3

Figure 4.20 RCA-1 and RCA-3 samples before and after micro-deval abrasion testing

4.5.7 Aggregate Crushing Value (ACV)

Each ACV test took about 10 minutes for load application followed by 5 minutes of sieving, weighing, and recording final masses. Audible cracking sounds could be heard in the cylinder apparatus up to a load level of about 250 kN. After the test was over the aggregates were noticeably crushed and wedged against the cylinder wall. Considerable hammering on the outside of the cylinder with a rubber mallet was required to loosen and eventually remove the crushed aggregate. Figure 4.21 shows the crushed RCA-1 sample in the test apparatus at the end of the test. Noticeable differences in texture, shape and size were observed in each aggregate after crushing. Figure 4.22 shows the loose crushed natural aggregate, RCA-1, RCA-2, and RCA-3 samples at the end of the test.



Figure 4.21 Crushed RCA-1 and cylinder mould after aggregate crushing value test



(a) Natural Aggregate



(b) RCA-1



(c) RCA-2



(d) RCA-3

Figure 4.22 Loose crushed aggregate samples after aggregate crushing value test

In general, all aggregates became more roughened as many of the rounded and smooth particles were crushed. This observation proved to be most evident in the smaller sized particles which became flake-like in shape. RCA-3 appeared to have a higher percentage of fines after crushing than the RCA-2, RCA-1 or the natural aggregate. These qualitative observations were consistent with the aggregate crushing values that are summarized in Table 4.15. The natural aggregate has the lowest ACV (highest strength), followed by RCA-1, RCA-2 and RCA-3 with the highest ACV (lowest strength). The natural aggregate has a crushing strength 27% higher than RCA-1, 43% higher than RCA-2, and 57% higher than RCA-3. This trend in ACV results was the same as that observed in the abrasion resistance tests.

Table 4.15 Aggregate crushing value results

Aggregate Type	Measurement	Trial #1	Trial #2	Trial #3
Natural	Mass of test specimen (M_1) =	2924.7 g	2927.2 g	2923.7 g
	Mass of material passing 2.36 mm sieve (M_2) =	557.9 g	518.0 g	522.5 g
	ACV = $M_2/M_1 \times 100$ =	19.1	17.7	17.9
	Mean ACV =	18.2		
RCA-1	Mass of test specimen (M_1) =	2521 g	2511.5 g	2541.4 g
	Mass of material passing 2.36 mm sieve (M_2) =	583.7 g	581.1 g	581.0 g
	ACV = $M_2/M_1 \times 100$ =	23.2	23.1	22.9
	Mean ACV =	23.1		
RCA-2	Mass of test specimen (M_1) =	2479.7 g	2454.2 g	2481.3 g
	Mass of material passing 2.36 mm sieve (M_2) =	645.9 g	627.8 g	651.0 g
	ACV = $M_2/M_1 \times 100$ =	26.0	25.6	26.2
	Mean ACV =	26.0		
RCA-3	Mass of test specimen (M_1) =	2670.7	2622.6	2596.2
	Mass of material passing 2.36 mm sieve (M_2) =	753.6	751.5	746.8
	ACV = $M_2/M_1 \times 100$ =	28.2	28.7	28.8
	Mean ACV =	28.5		

Based on the findings of the preceding tests, it may be expected that concrete produced with a lower aggregate crushing value (i.e., higher strength), in which aggregate strength was the governing factor (i.e., as is the case with higher strength concrete), could produce concrete with higher compressive strengths than concrete produced with lower strength aggregate. For example, the results seem to suggest that for concrete produced with the same volume of RCA-1

and RCA-2, the concrete produced with RCA-1 would have higher strengths because it has a lower aggregate crushing value indicating a higher crushing strength.

4.5.7.1 Response of Confined Bulk Aggregate to Crushing

A further analysis was conducted using the ACV test data to evaluate the average stress-strain response of loose rodded bulk aggregate. In addition to measuring the ACV, load and displacement values were recorded during the test. Load values were converted into stresses by dividing them by the area of the interior portion of the ACV test cylinder. Displacement values were converted into strains by dividing them by the initial height (100 mm) of aggregate sample above the base of the ACV cylinder. Figure 4.23 depicts the above mentioned length dimensions and the pre- and post-crushing behaviour of the ACV aggregate sample.

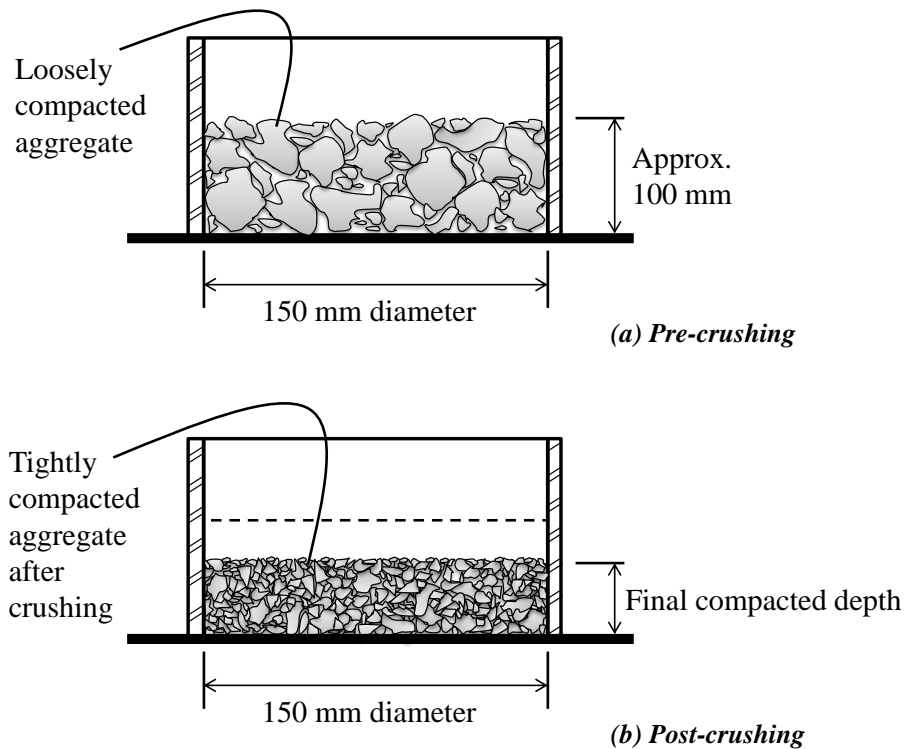


Figure 4.23 Pre- and post-crushing behaviour of ACV test samples

Two important assumptions were made while calculating the average stress-strain response of the ACV aggregate samples:

- (1) The stress values calculated are considered to be average axial stresses as the area over which the plunger is in contact with the individual aggregate particles cannot be calculated readily. Instead, the gross area of the interior of the ACV cylinder was taken as the area over which the load compresses the aggregate sample.
- (2) The initial depth of the rodded aggregate sample was assumed to be approximately 100 mm given that each sample was prepared using the same steel cylindrical measure.

The stress-strain response of confined bulk aggregate in compression is presented in Figure 4.24. The stress-strain response curves for each aggregate sample seem to follow a similar trend by initially displaying linear behaviour prior to crushing and then begin to become increasingly non-linear as aggregate particles begin to crush and compact.

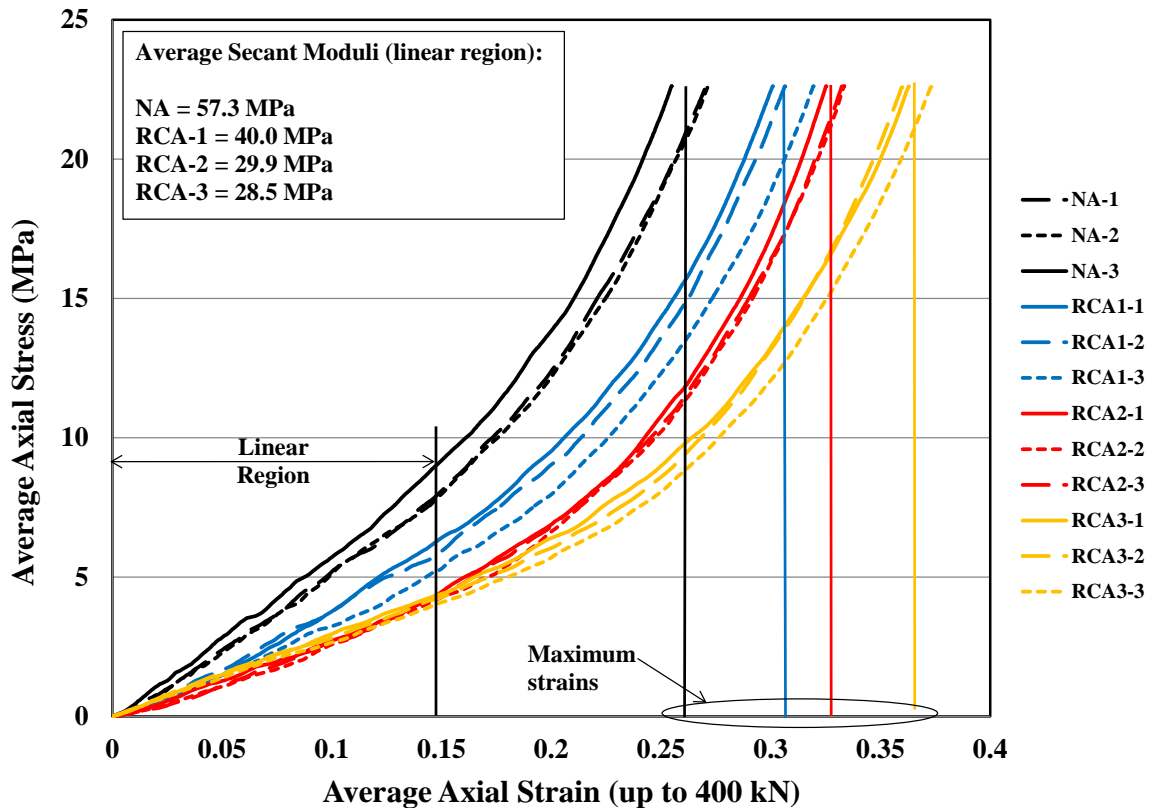


Figure 4.24 Stress-strain response of rodded aggregate during ACV testing

The linear region was identified as the portion of the stress-strain curve up to an average axial strain value of 0.15 mm/mm. Using this region, an average secant modulus of bulk aggregate (E_{ACV-s}) was calculated using Equation 4.15.

$$E_{ACV-s} = \frac{(\sigma_{avg-2} - \sigma_{avg-1})}{(\varepsilon_{avg-2} - \varepsilon_{avg-1})} \times 100\% \quad \text{Equation 4.15}$$

Where,

σ_{avg-2} = maximum average axial stress within the linear region,

σ_{avg-1} = average axial stress value corresponding to the initial average axial strain (ε_{avg-1})

ε_{avg-2} = average axial strain defining the extent of the linear region = 0.15,

ε_{avg-1} = initial average axial strain = 0.005

The calculated average secant moduli for each bulk aggregate sample are summarized in Figure 4.24 and Table 4.16. There were three separate samples per aggregate type for a total of 12 and the variation in stress-strain response between samples was minimal.

Table 4.16 ACV secant bulk moduli and maximum strain values

Agg. Type	Measurement	Trial #1	Trial #2	Trial #3
Natural	ACV secant modulus (MPa)	54.79	54.80	62.35
	Maximum strain (at load of 400kN)	0.2702	0.2713	0.2550
	Mean ACV secant modulus =	57.3		
	Mean maximum strain =	0.2655		
RCA-1	ACV secant modulus (MPa)	43.46	40.28	36.15
	Maximum strain (at load of 400kN)	0.3011	0.3067	0.3196
	Mean ACV secant modulus =	40.0		
	Mean maximum strain =	0.3091		
RCA-2	ACV secant modulus (MPa)	30.43	29.67	29.61
	Maximum strain (at load of 400kN)	0.3254	0.3336	0.3326
	Mean ACV secant modulus =	29.9		
	Mean maximum strain =	0.3305		
RCA-3	ACV secant modulus (MPa)	29.56	28.46	27.34
	Maximum strain (at load of 400kN)	0.3630	0.3600	0.3733
	Mean ACV secant modulus =	28.5		
	Mean maximum strain =	0.3655		

Both the mean ACV average secant modulus and maximum strain values seem to be related to the aggregate crushing values as displayed in Figure 4.25 and Figure 4.26. This is an interesting result as the aggregate crushing value is really an indication of mass loss due to crushing whereas maximum strain and elastic moduli are considered mechanical properties of the material itself.

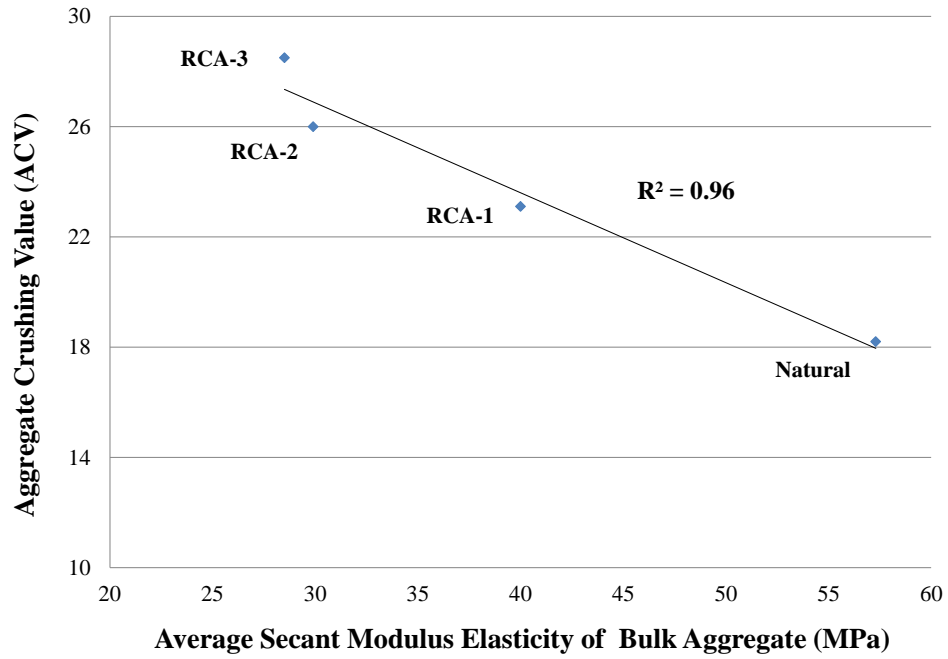


Figure 4.25 Relation between average secant modulus of bulk aggregate and aggregate crushing value

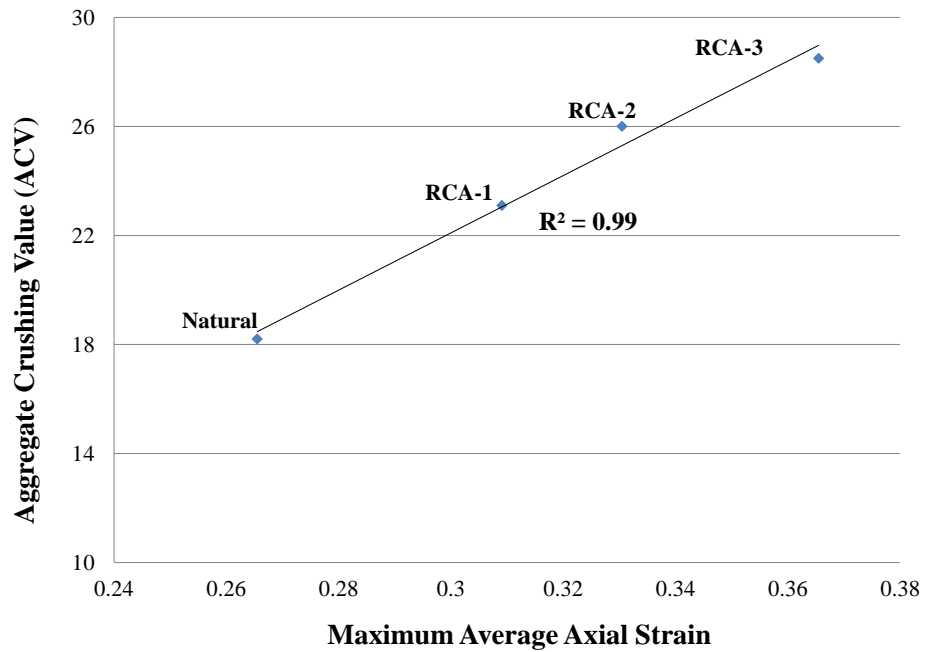


Figure 4.26 Relation between maximum average axial strain and aggregate crushing value

According to Lydon and Balendran (1986), the modulus of elasticity of aggregate is proportional to the aggregate bulk density squared. Figure 4.27 confirms this relationship with a high R^2 value of 0.97. This suggests that the average secant modulus of bulk aggregate measured during the ACV test is proportional to the actual modulus of elasticity of the RCA. As the modulus of elasticity of natural aggregate concrete is related to the modulus of elasticity of natural aggregate, it is possible that there may be a similar relation between the modulus of elasticity of RCA concrete and the ACV secant modulus of bulk aggregate. This relation is investigated further in Chapters 7 and 8.

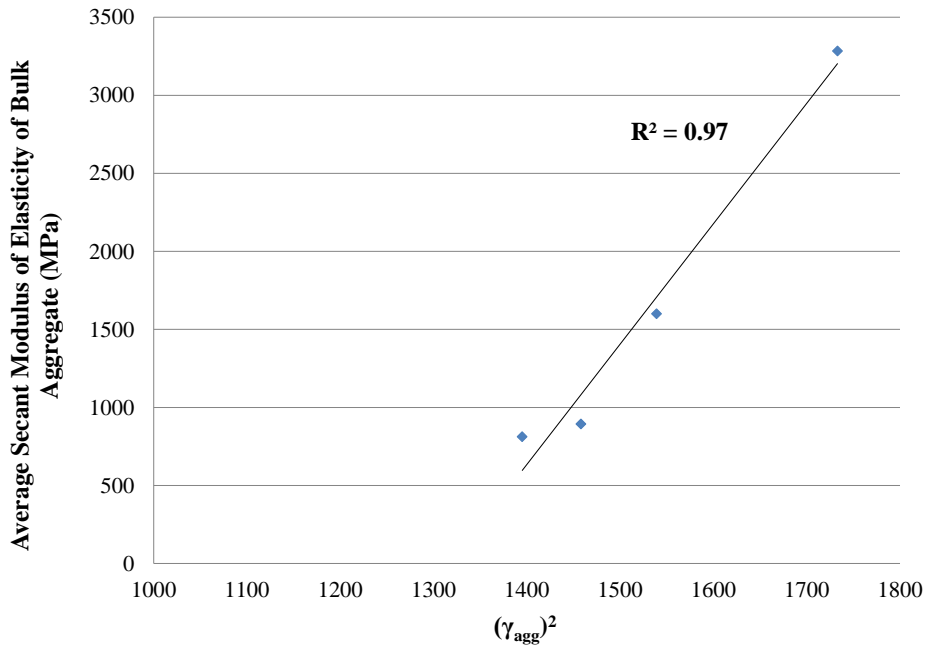


Figure 4.27 Relationship between the bulk density of aggregate squared and the average secant modulus of elasticity of bulk aggregate

4.5.8 Relationship between Aggregate Properties

Based on the results and observations presented in the preceding sections, it is clear that the various aggregate properties are influenced by a wide range of factors. One of the main goals of this study has been to investigate how the various aggregate properties influence one another in order to develop better quality control measures for RCA. Several correlations were found to exist among various aggregate properties. Figure 4.28 illustrates that as the oven dry bulk density increases, the absorption decreases. This result seems fairly intuitive and generally

confirms similar observations in the literature (Mehta and Monteiro, 2006). Similarly, as bulk density increases, the aggregate crushing value decreases indicating an increase in crushing strength (see Figure 4.29).

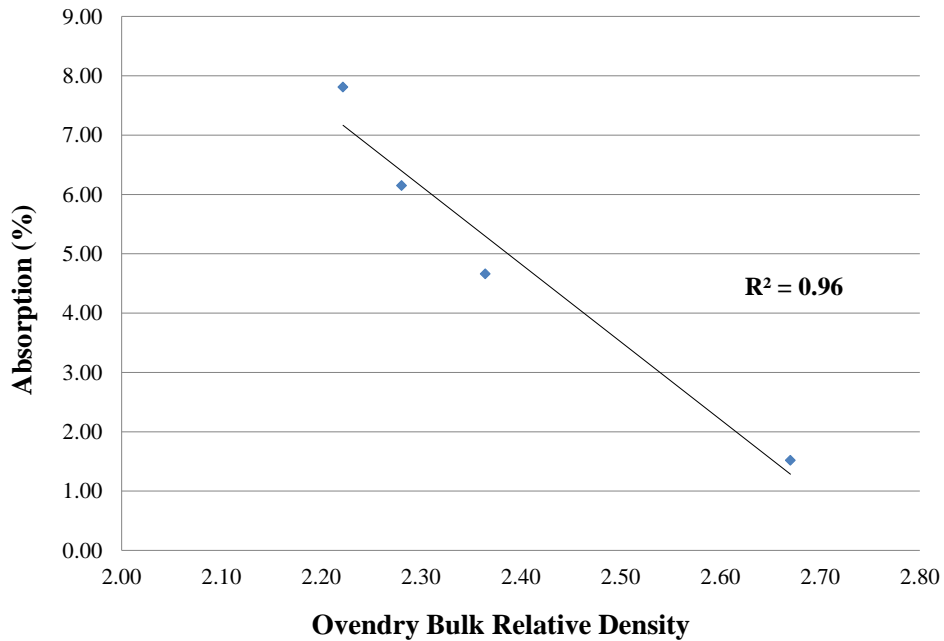


Figure 4.28 Relationship between oven dry bulk density and absorption of coarse aggregate

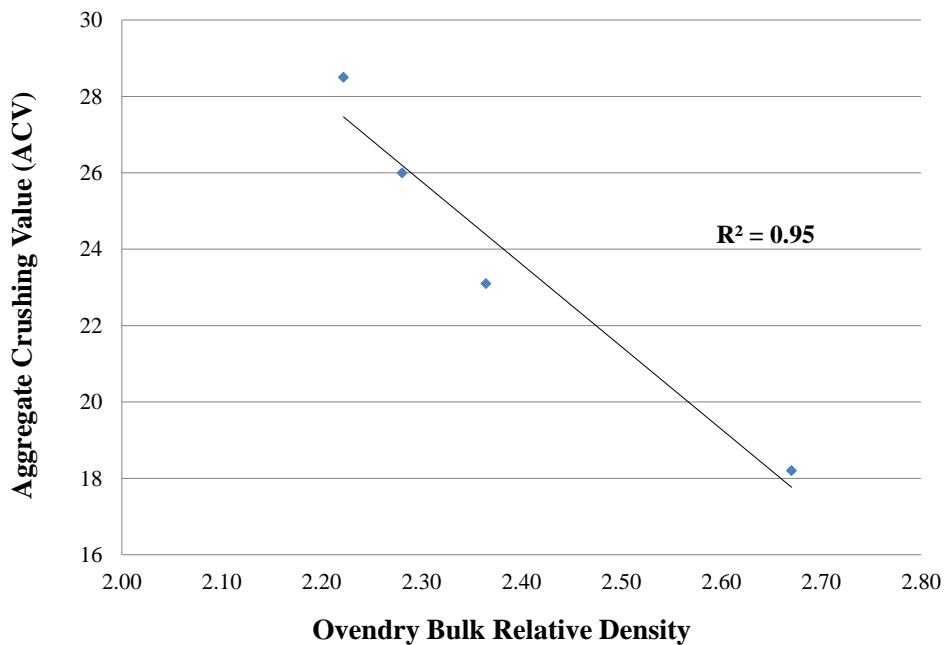


Figure 4.29 Relationship between oven dry bulk density and aggregate crushing value

As bulk density and absorption are related, it was reasonable to assume that absorption and aggregate crushing value may also be well correlated. This correlation was confirmed with a very high correlation ($R^2 = 0.99$) as presented in Figure 4.30.

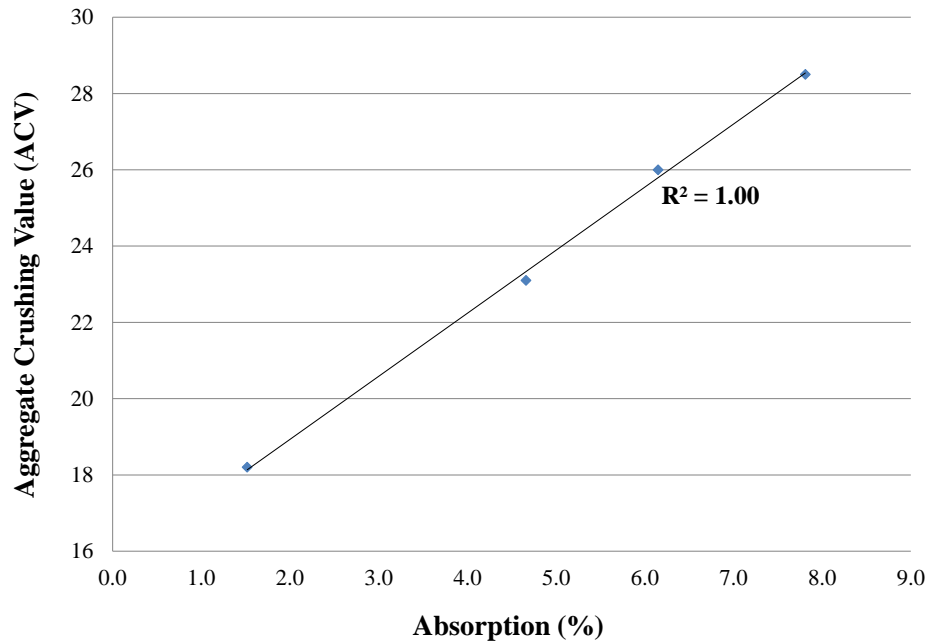


Figure 4.30 Relationship between absorption and aggregate crushing value

As mentioned previously, abrasion resistance and aggregate crushing values are generally in agreement. This relation was confirmed in Figure 4.31 which indicates a fairly high correlation (R^2 of 0.93) between ACV and micro-deval abrasion resistance. This relationship may be related to the overall strength of the aggregate particle and its degree of brittleness when it comes in contact and is compressed against other aggregate particles.

Based on the correlations noted above and on the other findings of this research, the relationships between aggregate properties are illustrated by the network of interactions in Figure 4.32.

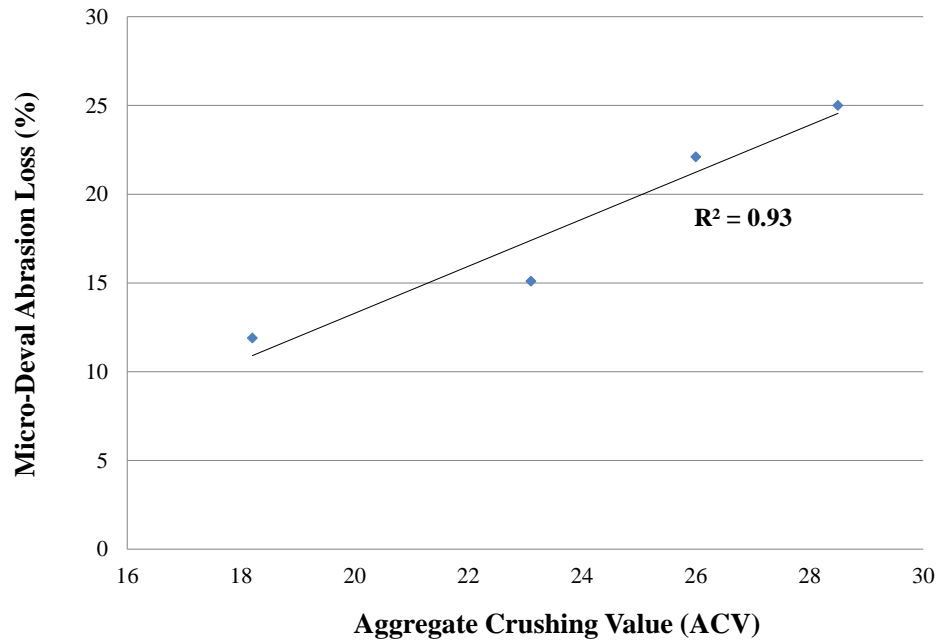


Figure 4.31 Relationship between aggregate crushing value and micro-deval abrasion resistance

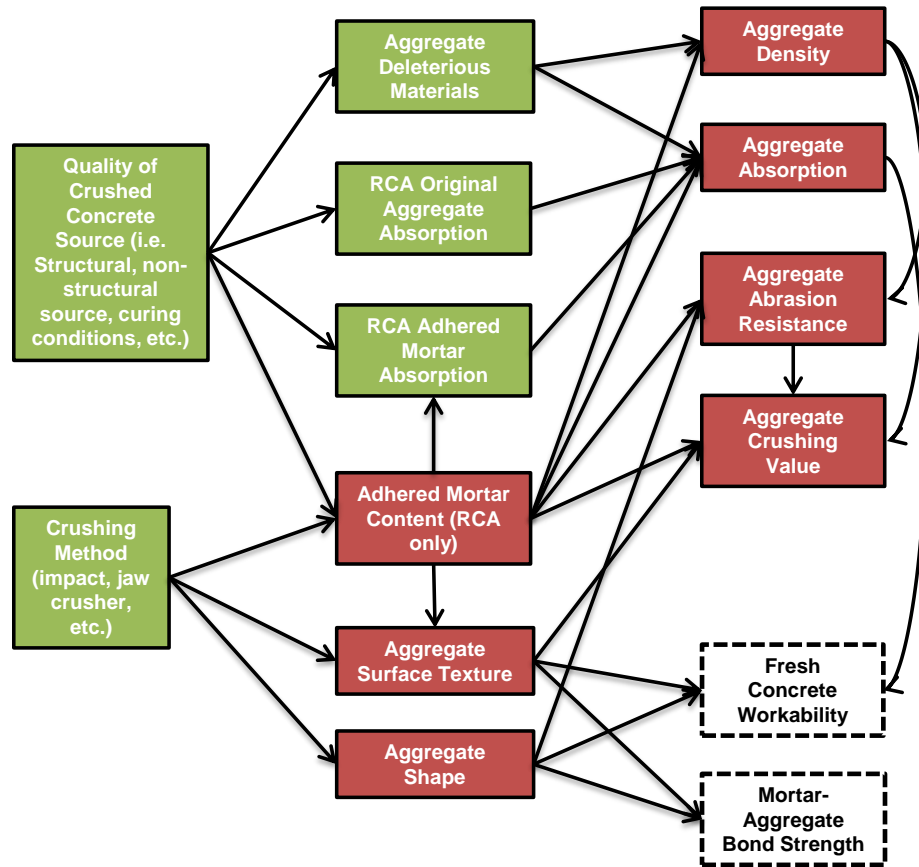


Figure 4.32 Relationships between aggregate properties

As illustrated in Figure 4.32, the quality of the source concrete and the crushing process by which the RCA is produced will govern the resulting RCA source and its properties. However, if RCA is to be produced on a commercial scale, it is likely that crushed concrete from multiple sources will be combined into several sources of varying quality and information about the source concrete and crushing method may not be available. Therefore, the frequent testing and monitoring of incoming RCA sources is paramount to the adequate control and efficient use of these materials.

It is also evident from Figure 4.32 that the adhered mortar content of the RCA governs many of the other aggregate properties such as, density, absorption, abrasion resistance, crushing value and surface texture. In addition to the adhered mortar content, the aggregate shape and surface texture also govern important aggregate properties such as the abrasion resistance and crushing value. As will be discussed in later sections, the aggregate shape and surface texture play an important role in mortar-aggregate bond strength (and consequently compressive and tensile strength) of hardened concrete, and can greatly affect the workability of fresh concrete. Deleterious materials present within RCA sources will affect the density and absorption such as is the case with RCA-2. In summary, the adhered mortar content, particle shape, and surface texture are the fundamental RCA properties which need to be measured to assess their relative impact on other aggregate properties that influence properties of concrete incorporating RCAs.

4.6 Conclusions

The following conclusions were made after investigating and testing the various properties and characteristics of the natural and recycled concrete aggregates.

1. The thermal treatment method, required the least amount of effort, and proved to be the most effective method for removing adhered mortar from the RCAs. By visual inspection, it was able to remove over 95% of the adhered mortar. Adhered mortar contents of 46.4%, 55.7% and 49.6% were measured for the RCA-1, RCA-2 and RCA-3, respectively.
2. After measuring the absorption rates of each aggregate it was concluded that the natural aggregate took the least time to become fully saturated (2 hours) followed by the RCA-1 (4 hours), RCA-2 (7 hours) and the RCA-3 (8 hours). Based on these findings, it was

decided to soak each aggregate in water for 24 hours prior to concrete batching. This would minimize variability in workability and actual water-cement ratio resulting from absorption of water by the RCA during mixing.

3. Upon visual comparison of the shape and surface texture of the four aggregate types it was found that the RCA-1 had the most roughened surface. When the amount of excess surface water (above SSD) present after a 24 hour soaking period was compared between each aggregate, RCA-1 had the highest percent by weight. This method could provide an indirect measure of surface texture for the various aggregate types.
4. The absorption and the amount of adhered mortar of RCAs were found not to be proportional as the absorption of RCA particles is dependent not only on the amount of adhered mortar but also on the quality (porosity) of the adhered mortar itself. This finding explained why RCA-3, which had the highest absorption (7.81%), had a smaller amount of adhered mortar than RCA-2 (49.6% versus 55.7%). The adhered mortar portion of RCA-3 accounted for 5.04% out of the 7.81% total absorption versus 2.71% out of 6.15% for the RCA-2.
5. Similar to results in the literature, it was confirmed that as the amount of adhered mortar increases, the bulk density decreases and the absorption capacity increases.
6. Upon examination of the aggregate crushing values and Micro-Deval abrasion resistance values for each aggregate type, a similar trend was discovered; the natural aggregate had the lowest crushing value and highest abrasion resistance followed by RCA-1, RCA-2 and RCA-3.

Chapter 5: Development of Concrete Mixture Proportions

5.1 Overview of Mixture Proportion Types and Phases

Once all of the aggregate sources were tested and characterized, concrete mixtures were proportioned to achieve a specified set of fresh and hardened properties. In total, twenty four different mixture proportions were developed as part of this research. In the development of these mixture proportions, a total of 89 mixture proportions were batched. Appendix A provides a summary of the mixture proportions for the trial batching (mainly control and strength-based mixtures) and illustrates the successive mixture proportion adjustments required to achieve the specified slump and compressive strength requirements of each mixture proportion. Based on the trial batches, it became obvious that pre-soaking of coarse aggregates and maintaining the fine aggregate at a constant air-dry moisture condition prior to batching was essential for achieving adequate batch-to-batch repeatability. The twenty-four mixtures are separated into three separate categories, (1) control mixtures, (2) direct replacement mixtures, and (3) strength-based mixtures. All mixtures were proportioned for interior exposure conditions and as such, no air-entraining admixtures were used and no assessment of durability properties (i.e., alkali-silica reactivity, shrinkage, resistivity, freeze-thaw resistance, etc.) was performed.

5.1.1 Control Mixtures

The control mixtures used both natural coarse and fine aggregates and were proportioned to achieve compressive strengths of 30, 40, 50 and 60 MPa with slump values between 75 and 125 mm. This workability range was chosen as it satisfies the requirements of CSA A23.1-09 Clause 4.3.2.3.2. These mixtures represented the baseline data set from which all RCA concrete mixtures were compared.

5.1.2 Direct Replacement Mixtures

The direct replacement mixtures were developed by replacing the natural aggregate (100% replacement) from the control mixtures with equivalent volumes of RCA-1, RCA-2 and RCA-3 with no other changes to the mixture proportions. Due to the varying densities of the three aggregate types, a direct replacement by volume ensured that the total yield remained constant.

These mixtures were used to gauge the effect of natural coarse aggregate replacement with RCA on concrete compressive strength and workability (i.e., constant water content, cement content and water-cement ratio). Once the direct replacement mixtures were developed, the influence of aggregate type on the workability, hardened density, compressive strength, splitting tensile strength, modulus of elasticity, Poisson's ratio, and the coefficient of thermal expansion of concrete could be studied.

5.1.3 Strength-Based Mixtures

The strength-based mixture proportions also used 100% replacement of natural aggregate by RCA, however the mixture proportions (w/c ratio, water and cement content) were modified to achieve the same strength and workability targets as the control mixtures (i.e., 30, 40, 50 or 60 MPa compressive strengths and slumps between 75 and 125 mm). The strength-based mixtures were developed for three reasons: (1) to determine the effect of various RCA types and their corresponding properties on the fundamental concrete mixture components (i.e., water demand, cement content and water-cement ratio), (2) to assess the differences in concrete fresh and hardened properties when proportioning mixtures for constant w/c ratio and aggregate volume (direct replacement) versus proportioning mixtures for constant strength and slump ranges (strength-based) and (3), to determine the effect that natural aggregate replacement (by volume) with RCA has on splitting tensile strength, modulus of rupture, fracture energy and bond with reinforcement for concrete with similar compressive strengths.

5.1.4 Mixture Proportion Phases and Summary

In addition to the three mixture proportion types, the research program was divided into two phases (Phase 1 and Phase 2) with several main differences between each phase:

1. Different compressive strength targets (i.e., Phase 1 with 30 and 50 MPa, and Phase 2 with 40 and 60 MPa)
2. Different suppliers of the same type GU cement.
3. Different ages of cement at time of batching (due to material availability issues).
4. Addition of a third recycled concrete aggregate (RCA-3) source for use in Phase 2 mixtures.

All mixture proportions and their naming conventions are summarized in Table 5.1. The

concrete mixtures are referenced with respect to aggregate type (NA = natural aggregate, RCA-1, RCA-2, RCA-3), concrete compressive strength (30, 40, 50 or 60 MPa) and mixture proportioning scenario: Control (C), Direct Replacement (D), and Strength-Based (S). For example, RAC1-40S refers to concrete that was produced using RCA of type 1 (RCA-1), proportioned to achieve a compressive strength of 40 MPa and was a strength-based mixture type (S).

Table 5.1 Summary of all mixture proportions and associated naming conventions

No.	Mixture ID	Phase 1 (30 and 50 MPa) or Phase 2(40 and 60 MPa)	Coarse Aggregate Type	Target Compressive Strength	Control (C), Direct Replacement (D) or Strength-Based (S) Mixture Type			
1	NAC-30C	1	Natural (NA)	30 MPa	Control			
2	NAC-50C			50 MPa				
3	NAC-40C			40 MPa				
4	NAC-60C			60 MPa				
5	RAC1-30D	1	RCA-1	30 MPa	Direct Replacement			
6	RAC1-50D			50 MPa				
7	RAC1-40D	2		RCA-1	40 MPa	Direct Replacement		
8	RAC1-60D				60 MPa			
9	RAC1-30S	1			RCA-1	30 MPa	Strength-Based	
10	RAC1-50S					50 MPa		
11	RAC1-40S		2			RCA-1		40 MPa
12	RAC1-60S							60 MPa
13	RAC2-30D	1	RCA-2	30 MPa			Direct Replacement	
14	RAC2-50D			50 MPa				
15	RAC2-40D	2		RCA-2	40 MPa		Direct Replacement	
16	RAC2-60D				60 MPa			
17	RAC2-30S	1			RCA-2	30 MPa	Strength-Based	
18	RAC2-50S					50 MPa		
19	RAC2-40S		2			RCA-2		40 MPa
20	RAC2-60S							60 MPa
21	RAC3-40D	2	RCA-3	40 MPa			Direct Replacement	
22	RAC3-60D			60 MPa				
23	RAC3-40S			2	RCA-3		40 MPa	Strength-Based
24	RAC3-60S						60 MPa	

5.2 Mixing Procedure, Aggregate Preparation and Curing Program

5.2.1 Absolute Volume Method of Mixture Proportioning

Concrete mixtures were proportioned in accordance with ACI's committee 211 *Standard Practice for Selecting Proportions for Normal, Heavyweight and Mass Concrete* (ACI 211, 1997). Specifically, the absolute volume method was employed which uses the relative densities of the various constituents to calculate the absolute volume of each that will occupy one cubic metre of concrete. Specific properties of coarse aggregate that are required for use in the absolute volume mixture proportioning method include: nominal maximum coarse aggregate size, oven-dry bulk relative density, oven-dry bulk rodded density, absorption capacity, and the in-situ moisture content at time of batching. Fine aggregate properties include: oven-dry relative density, fineness modulus, absorption capacity, and the in-situ moisture content at time of batching. The general use (GU) portland cement had an assumed relative density of 3.15 that was required for the mixture proportioning calculations. All aggregate properties were summarized and discussed in Chapter 4.

The absolute volume method is outlined in several steps:

- 1) *Determine the water requirement for a given slump range and maximum coarse aggregate size.* This was determined based on Table 9-5 in Kosmatka et al. (2002). From this table the percent entrapped air content was also estimated.
- 2) *Select a suitable water cement ratio based on a target 28 day compressive strength.* Initial w/c values were based on Table 9-3 in Kosmatka et al. (2002) for non-air-entrained concrete.
- 3) *Calculate the cement content (kg/m^3) based on the selected water content and water-cement ratio.*
- 4) *Determine the oven-dry mass of coarse aggregate.* These values were selected using table 9-4 in Kosmatka et al. (2002) given the fineness modulus of the sand and the nominal maximum size of coarse aggregate is given by Equation 5.1:

$$\text{WCA}_d = \text{VCA}_d \times \text{DCA}_d \quad \text{Equation 5.1}$$

Where, WCA_d is the oven-dry mass of coarse aggregate (kg per m^3 of concrete), VCA_d is

the bulk volume of oven-dry rodded coarse aggregate determined from Table 9-4 (Kostamatka et al., 2002), and DCA_d is the oven-dry bulk relative density of coarse aggregate (kg/m^3).

5) *Calculate the volume of all ingredients:*

$$\text{Vol. of water per m}^3 \text{ of concrete} = (\text{Water content})/(\text{DW} \times 1000)$$

$$\text{Vol. of cement per m}^3 \text{ of concrete} = (\text{Cement content})/(\text{DC} \times 1000)$$

$$\text{Vol. of coarse aggregate per m}^3 \text{ of concrete} = (\text{Oven-dry mass of C.A.})/(\text{DCA} \times 1000)$$

Where, DW, DC and DCA are the relative densities of water, cement and coarse aggregate, respectively.

$$\text{Vol. of entrapped air per m}^3 \text{ of concrete} = (\% \text{ Entrapped air})/100$$

The total volume of the above ingredients was calculated so that,

$$\text{Vol. of fine aggregate per m}^3 \text{ of concrete, } (VFA_d) = 1 \text{ m}^3 - (\text{Total Vol.})$$

Then, the oven-dry mass of fine aggregate could be calculated using Equation 5.2:

$$WFA_d = VFA_d \times DFA_d \times 1000 \quad \text{Equation 5.2}$$

6) *Compensate for in-situ moisture content of the coarse and fine aggregate.* In this step the mass of the coarse aggregate (WCA_d), fine aggregate (WFA_d) and water are adjusted according to the aggregate's absorption capacity and the in-situ moisture contents (%MC).

$$\text{Adjusted C.A. mass} = WCA_d \times (1 + \%MC_{CA}/100)$$

$$\text{Adjusted F.A. mass} = WFA_d \times (1 + \%MC_{FA}/100)$$

$$\text{Surface water contributed by C.A., } SW_{CA} = \text{Absorption capacity of C.A.} - \%MC_{CA}$$

$$\text{Surface water contributed by F.A., } SW_{FA} = \text{Absorption capacity of F.A.} - \%MC_{FA}$$

$$\text{Adjusted water mass} = (\text{Water Content} - (WCA_d \times SW_{CA}/100) - (WFA_d \times SW_{FA}/100)) \times 1000$$

Note that the surface water value for the coarse or fine aggregate may have a negative value indicating that the in-situ moisture content is less than the absorption capacity or saturated surface dry condition.

7) *Scale all material masses (kg per m³ of concrete) to the desired trial batch size.*

Note that some of the strength-based RCA-2 and RCA-3 concrete mixtures required the use of small amounts of high-range water reducer (Glenium 7700) which was added in dosages of mL per 100 kg of cement as per the manufacturer's recommendations and as required to achieve the desired slump.

5.2.2 Mixing Procedure and Batching Methods

Due to the various volumes of concrete being produced for different applications, and laboratory resource changes between the time of Phase 1 and Phase 2 testing, the use of several concrete batching methods was required.

5.2.2.1 Mixing Procedure

A mixing procedure adapted from CSA standard A23.2-2C Making Concrete Mixes in the Laboratory, was used throughout the research program and proceeds as follows (CSA A23.2, 2004):

1. The coarse aggregate was added first followed by addition of one third of the mixing water, and when required, the admixtures. The mixture was then mixed for 30 seconds.
2. The fine aggregate was then added with the cementing materials, and the remaining two thirds of water. During this stage the mixer ran continuously.
3. After all ingredients were in the mixer, the concrete was mixed for three minutes followed by a three minute rest, followed by two minutes of final mixing.

In between mixtures, the mixing pan and mixer paddles were thoroughly cleaned and any excess water was removed using towels to ensure there was no contamination of the next mixture.

5.2.2.2 Batching Method A

A small 0.05 m³ (50 L) capacity pan mixer (high shearing type) was used for the majority of the concrete batching (see Figure 5.1a). In addition, the coarse aggregates were pre-soaked in buckets with lids for 24 hours and drained over a 1.18 mm sieve prior to batching. This ensured that the aggregates reached a saturated surface dry condition. A more thorough discussion of this pre-soaking procedure is described in Section 5.2.3. Batching Method A was mainly used for casting cylinders for trial batches and to assess initial workability, compressive strength, splitting tensile strength, modulus of elasticity, poisson's ratio, hardened density, and the coefficient of thermal expansion of concrete during both Phase 1 and Phase 2.

5.2.2.3 Batching Method B

A 0.2 m³ (200 L) pan mixer (see Figure 5.1b) was used for batching larger concrete specimens such as the beam-end specimens, fracture energy specimens and their associated cylinders for Phase 1. As depicted in Figure 5.2, coarse aggregates were pre-wetted in 1.33 m³ hoppers for five minutes and then covered with plastic sheeting 30 minutes prior to batching to minimize evaporation of the water required to maintain the coarse aggregates at a saturated surface dry condition. This will be described later Section 5.2.3.

5.2.2.4 Batching Method C

Batching Method C involved using a 0.3 m³ (300 L) pan mixer (see Figure 5.1c) to batch larger concrete specimens such as: the beam-end specimens, fracture energy specimens and their associated cylinders for Phase 2. Once again, coarse aggregates were pre-wetted in 1.33 m³ hoppers for five minutes and then covered with plastic sheeting 30 minutes prior to batching to minimize evaporation of the water required to maintain the coarse aggregates at a saturated surface dry condition (see Figure 5.2).



Figure 5.1 Range of concrete pan mixers used for batching



Figure 5.2 Aggregate hopper systems and pre-wetting of coarse aggregates in hoppers as per batching methods B and C

5.2.3 Aggregate Preparation and Controlling the Actual Water-Cement Ratio

The high water absorption of the RCA can result in changes in workability and the actual or effective water-cement ratio of the fresh concrete during mixing and placement due to absorption of the mixing water by unsaturated RCA. The changes in the fresh properties may occur even if the moisture content of the aggregate is known and moisture corrections are applied to the concrete batch quantities since the absorption rate of the aggregate is not instantaneous. A

summary of absorption times is presented in Table 5.2 below and further discussion of coarse aggregate absorption rates is included in Section 4.5.3.

Table 5.2 Pre-soaking time required for aggregates to reach SSD

Aggregate Type	Time Required to Reach SSD Condition (hours)
Natural	2
RCA-1	4
RCA-2	7
RCA-3	8

Consequently, it was noticed that all the mixing water was not fully absorbed by each aggregate type within the first 30 minutes of being added to the mixer (the usual maximum time for aggregates to absorb mixing water, Neville, 1997). Also, in mixtures with higher cement content, the aggregate particles could potentially become quickly coated with mortar and unable to absorb sufficient water to reach their absorption capacity. If this were to happen, it may create an additional source of variation in the actual water-cement ratio during the first 30 minutes of batching. In order to minimize this occurrence, typical production practice is to pre-wet the RCA to reduce the amount of moisture absorbed by the RCA during mixing; moisture corrections are still applied for aggregate moisture contents other than saturated-surface dry (SSD). Table 5.3 summarizes three methods for coarse RCA pre-treatment prior to batching in RCA concrete.

For the purposes of the current research, Option #1 was used in which all coarse aggregates (natural and RCA) were soaked for 24 hours and then drained immediately prior to batching to ensure that the aggregate was fully saturated (at or above SSD) to eliminate absorption of the mixing water during concrete production and placement. The aggregate moisture content after 24 hours of soaking (MC_{24}) was determined, and the excess surface moisture (above SSD) was considered to be available as mixing water (refer to Sections 4.4.4 and 4.5.4). Accordingly, the batch proportions were adjusted to compensate for this additional moisture and to maintain a consistent water-cement ratio as suggested by Poon et al. (2004b).

Table 5.3 Coarse aggregate pre-treatment methods

	Option #1	Option #2	Option #3
Pre-Wetting Procedure	Soak coarse aggregates for 24 hours prior to batching	“Pre-wet” coarse aggregates for 24 hours prior to batching	Use coarse aggregates in their in-situ moisture condition
Moisture Condition after pre-wetting	Ensures that the aggregates have reached the SSD condition.	Does not ensure aggregates are fully saturated however, will be very close to SSD. Varying amounts of adhered surface moisture will be present.	Usually in-situ moisture contents will be less than SSD. If kept in an air-dry condition, in-situ moisture contents will eventually stabilize and remain constant
Impact on actual water-cement ratio	Using this method will ensure that all water has been absorbed by the coarse aggregate and the moisture condition from sample-to-sample does not vary significantly	Using this method does not ensure that the coarse aggregate will be saturated. In addition, the moisture condition may vary significantly from sample-to-sample.	Particularly in the case of RCA that has low absorption rates and high absorption capacities, all of the additional mixing water required to offset coarse aggregate absorption will not be fully absorbed in the first 30 minutes after batching. This may have a significant impact on the actual water-cement ratio. In addition, in mixtures with higher cement contents and paste volumes, the coarse aggregates may become covered with paste preventing the absorption of water required for the aggregates to reach their SSD condition.
Critical measurement procedures	Absorption capacity and adhered surface moisture (see Section 4.4.4 for definition and calculation)	Absorption capacity and adhered surface moisture at regular time intervals prior to batching	Absorption capacity and in-situ moisture content
Practical implications of applying method to mass-production of RCA concrete	Mass soaking 24 hours prior to batching followed by draining of coarse aggregates would be impractical. The resources and effort required for this option may not be feasible on a large-scale production of RCA concrete.	Mass pre-wetting of coarse aggregates 24 hours prior to batching requires additional effort compared to using coarse aggregate in-situ however, this could still be practical using appropriate misting or sprinkler systems.	Using the RCA in-situ would require the least effort however; excessive water absorption by the RCA may impact the actual water-cement ratio and affect both the fresh and hardened properties of RCA concrete.

It should be noted that since water absorption by the coarse aggregate during mixing is eliminated by pre-soaking of the aggregates, it may affect the fresh properties of the concrete in comparison to concrete made with pre-wetted aggregate (i.e., Option #2) or where no pre-treatment is applied (i.e., Option #3). However, assuming that the batch moisture corrections are done properly, the effect on the hardened properties of the concrete should not be significant except in cases where the RCA is very dry prior to batching. Nevertheless, the results of this

research study are applicable to pre-soaked aggregates, and further study is required to determine the effect, if any, of other aggregate treatment methods on the concrete properties.

This study used one type of concrete sand (fine aggregate) in the “air-dry” state (in-situ moisture content of 0.20%) which had a water absorption capacity of 1.61%. Therefore, additional mixing water was required to offset the additional water absorbed by the sand (fine aggregate).

5.2.4 Curing Program

During the first trial batches, two curing protocols were adapted to study the effect on compressive strength. The first protocol involved curing the specimens for 28 days in an air dry condition. The concrete laboratory was considered to be at a constant relative humidity of 50%±10% and temperature of 21°C±2°C for 365 days of the year. The second curing protocol involved moist-curing the specimens for the first 7 days and then air-curing them for the remaining 21 days. This method was used to simulate typical construction site curing practices. It was found that the second curing method increased compressive strengths by up to 13% and all subsequent concrete specimens were cured following this procedure. Note that the curing procedure changed slightly depending on which batching method was used (see Section 5.2.2).

5.3 Control Concrete Mixture Proportions

In total, 32 trial mixtures were carried out to develop the four control concrete mixture proportions used in this research. The trial testing included two rounds of confirmation batching associated with Phase 1 and Phase 2 of the research. The finalized control mixture proportions for Phase 1 and Phase 2 are summarized in Table 5.4 and Table 5.5, respectively. It should be noted that the decreases in water-cement ratios from Phase 1 to Phase 2 were very small (i.e., 0.60 to 0.59 and 0.38 to 0.37) relative to the increase in compressive strength (i.e., 10 MPa increase between 30 MPa and 40 MPa, 50 MPa and 60 MPa). This may be a result of the different cement supplier, quality and age of cement used in Phase 1 versus Phase 2. Older cement has a higher likelihood of being exposed to moist air and becoming partially hydrated and, as a result, can lose strength (Kosmatka et al., 2002 and ACI 225, 2009). As will be discussed in later chapters, the variations in slump between the Phase 1 and Phase 2 mixtures may be attributed to the age and relative quality of the cement sources used during each phase.

In general, the appearance of the fresh control concretes with lower strengths (i.e. 30 and 40 MPa) and higher water-cement ratios was stonier and exhibited some signs of bleeding during consolidation. In contrast, the appearance of the fresh concrete with higher strengths (50 and 60 MPa) with lower water-cement ratios was noticeably smoother due to the higher mortar volume and exhibited negligible bleeding during consolidation.

Table 5.4 Phase 1 (30 and 50MPa) control concrete mixture proportions

	NAC-30C	NAC-50C
Water (kg/m ³)*	160	180
Cement (kg/m ³)*	267	474
Coarse aggregate (kg/m ³)*	1106	1106
Vol. coarse aggregate per m ³ of concrete	0.411	0.411
Fine aggregate (kg/m ³)*	861	633
Water-cement ratio*	0.60	0.38

* Water content values reported do not include adjustments for aggregate water absorption
 Note: NAC-30C Control concrete with a target compressive strength of 30 MPa

Table 5.5 Phase 2 (40 and 60MPa) control concrete mixture proportions

	NAC-40C	NAC-60C
Water (kg/m ³)*	160	180
Cement (kg/m ³)*	271	487
Coarse aggregate (kg/m ³)*	1099	1099
Vol. coarse aggregate per m ³ of concrete	0.412	0.412
Fine aggregate (kg/m ³)*	861	625
Water-cement ratio*	0.59	0.37

* Water content values reported do not include adjustments for aggregate water absorption
 Note: NAC-40C Control concrete with a target compressive strength of 40 MPa

5.4 Direct Replacement Concrete Mixture Proportions

Once the control mixture proportions were finalized the direct replacement mixtures proportions were created by simply replacing the natural aggregate volume by an equivalent volume of RCA-1, RCA-2 and RCA-3. For similar reasons as described above, the water-cement ratios did not vary significantly between the Phase 1 and Phase 2 direct replacement mixtures due to the varying cement quality and age at time of casting. The finalized direct replacement mixture

proportions for Phase 1 and Phase 2 are summarized in Table 5.6 and Table 5.7. Note that the only proportions that change between mixtures are the coarse aggregate content in kg/m^3 . This change is related to the natural aggregate which was replaced by an equivalent volume of RCA-1, RCA-2, and RCA-3. The RCA have different bulk densities and are reflected in these values.

Table 5.6 Phase 1 (30 and 50MPa) direct replacement concrete mixture proportions

	RAC1-30D	RAC1-50D	RAC2-30D	RAC2-50D
Water (kg/m^3)*	160	180	160	180
Cement (kg/m^3)*	267	474	267	474
Coarse aggregate* (kg/m^3)	975	975	949	949
Vol. coarse Aggregate per m^3 of concrete	0.411	0.411	0.411	0.411
Fine aggregate (kg/m^3)*	863	635	863	635
Water-cement ratio*	0.60	0.38	0.60	0.38

* Water content values reported do not include adjustments for aggregate water absorption

Note: RAC1-40C = concrete mixture incorporating RCA-1 as coarse aggregate with a target compressive strength of 40 MPa and proportioned as a direct replacement mixture (i.e., constant w/c ratio)

Table 5.7 Phase 2 (40 and 60MPa) direct replacement concrete mixture proportions

	RAC1-40D	RAC1-60D	RAC2-40D	RAC2-60D	RAC3-40D	RAC3-60D
Water (kg/m^3)*	160	180	160	180	160	180
Cement (kg/m^3)*	271	487	271	487	271	487
Coarse aggregate* (kg/m^3)	974	974	940	940	912	912
Vol. coarse aggregate per m^3 of concrete	0.412	0.412	0.412	0.412	0.412	0.412
Fine aggregate (kg/m^3)*	861	625	861	625	861	625
Water-cement ratio*	0.59	0.37	0.59	0.37	0.59	0.37

* Water content values reported do not include adjustments for aggregate water absorption

Note: RAC2-60D = concrete mixture incorporating RCA-2 as coarse aggregate with a target compressive strength of 60 MPa and proportioned as a direct replacement mixture (i.e., constant w/c ratio)

5.5 Strength-Based Concrete Mixture Proportions

The proportioning of the strength-based mixtures proceeded systematically by first adjusting the w/c ratio to achieve target compressive strengths of 30, 40, 50 and 60 MPa. The compressive strength data obtained and prior knowledge gained from the direct replacement mixture results assisted in reducing the number of w/c ratio iterations. Once the compressive strength targets

(and corresponding w/c ratios) had been achieved, water and cement contents were adjusted (while still maintaining previously determined w/c ratios) until slump values between 75 and 125 mm were achieved. A total of 37 trial batches were prepared in order to establish the final 10 strength-based mixture proportions (refer to Appendix D for a summary of trial mixture proportions). Confirmation batches of all strength-based mixture proportions were then completed to ensure adequate repeatability of fresh and hardened concrete properties. Given the differences in cement quality (i.e., supplier and age), comparisons of the effect of RCA properties on fundamental concrete mixture proportions (i.e., w/c ratio, water demand, and cement content) between Phase 1 and Phase 2 were not possible. Instead, separate comparisons and conclusions were made for Phase 2 mixtures only and are discussed in detail in Chapter 8.

The finalized strength-based mixture proportions for Phase 1 and Phase 2 are summarized in Table 5.8 and Table 5.9, respectively. In order to reach the compressive strength and workability targets, a polycarboxylate-based high range water reducer was required for the RAC2-60S and RAC3-60S mixtures. Several trial mixtures were batched without using a water reducer and relied on increasing the water content alone to achieve the slump targets without success. The mixtures became too sticky and the cement contents required for maintaining the low water cement ratios given the high water contents became too high (e.g., more than 600kg/m³) and impractical.

Table 5.8 Phase 1 (30 and 50MPa) strength-based concrete mixture proportions

	RAC1-30S	RAC1-50S	RAC2-30S	RAC2-50S
Water (kg/m ³)*	175	190	165	190
Cement (kg/m ³)*	243	404	262	500
Coarse aggregate* (kg/m ³)	970	970	919	919
Vol. coarse aggregate per m ³ of concrete	0.409	0.409	0.398	0.398
Fine aggregate (kg/m ³)*	848	672	889	621
Water-cement Ratio*	0.72	0.47	0.63	0.38

* Water content values reported do not include adjustments for aggregate water absorption

Note: RAC1-50S = concrete mixture incorporating RCA-1 as coarse aggregate with a target compressive strength of 50 MPa and proportioned as a strength-based mixture (i.e., constant compressive strength and slump range)

Table 5.9 Phase 2 (40 and 60MPa) strength-based concrete mixture proportions

	RAC1-40S	RAC1-60S	RAC2-40S	RAC2-60S	RAC3-40S	RAC3-60S
Water (kg/m ³)*	180	190	170	180	165	180
Cement (kg/m ³)*	281	463	293	487	337	600
Coarse aggregate* (kg/m ³)	970	970	919	919	879	879
Vol. coarse aggregate per m ³ of concrete	0.410	0.410	0.403	0.403	0.397	0.397
Fine aggregate (kg/m ³)*	802	621	839	648	841	567
Water reducer in mL/100kg cement	0	0	0	450	0	700
Water-cement ratio*	0.64	0.41	0.58	0.37	0.49	0.30

* Water content values reported do not include adjustments for aggregate water absorption

Note: RAC3-40S = concrete mixture incorporating RCA-3 as coarse aggregate with a target compressive strength of 40 MPa and proportioned as a strength-based mixture (i.e., constant compressive strength and slump range)

5.6 Summary of Mixture Proportions and Applications

Once the various control, direct replacement, and strength-based mixture proportions had been developed for Phases 1 and 2, various concrete properties (e.g., slump, compressive strength, splitting tensile strength, modulus of elasticity, linear coefficient of thermal expansion, modulus of rupture, and fracture energy) were measured and investigated. For each concrete property, a comparison was made between the RCA concrete and the equivalent control (natural aggregate) concrete mixture to gauge the effect of RCA properties on a particular concrete property. Various relationships between both aggregate and concrete properties were identified and evaluated. Once all the various concrete properties were tested, beam-end specimens were cast using the control and strength-based concrete mixtures and were tested to measure the effect of RCA and RCA concrete properties on bond strength and slip response.

Figure 5.3 summarizes all of the concrete mixture proportion types, the separate phases and batching methods used, the various coarse aggregates, and the associated concrete and bond properties measured. Chapters 7, 8 and 9 present and discuss the results of the concrete mechanical properties and bond-slip testing.

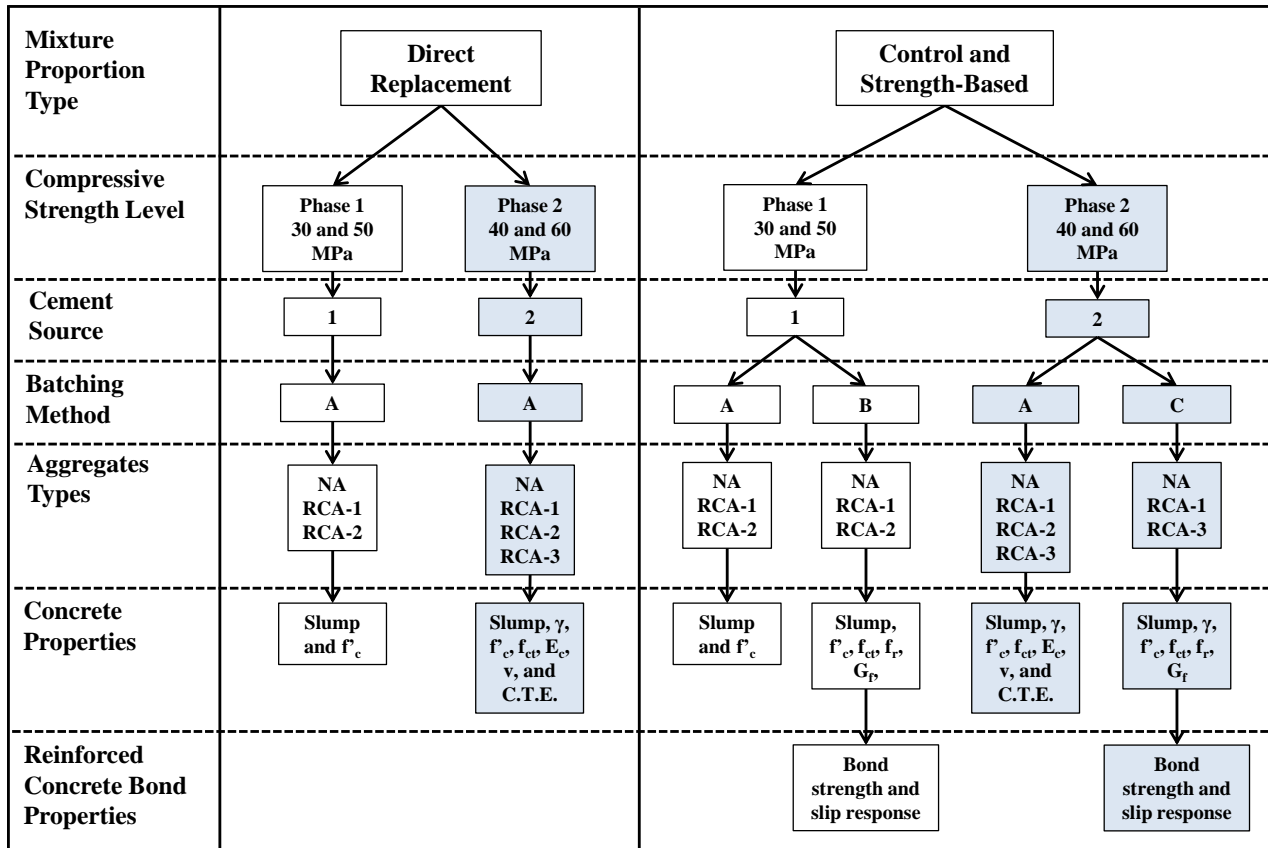


Figure 5.3 Summary of mixture proportion types and applications

Chapter 6: Concrete Properties Testing Procedures

6.1 Overview

This chapter details the procedures followed for the determination of fresh and hardened concrete properties. A detailed description of the steps followed, any relevant instrumentation setup, and the type of measured values has also been described. The majority of the procedures adhere closely to various Canadian Standards Association (CSA) and American Society for Testing and Materials (ASTM) standards while in a few cases, other standards have been either developed or adapted from CSA or ASTM standards. Workability of fresh concrete was assessed by measuring the slump. As all concrete mixture proportions were designed for interior exposure applications, no air entraining admixtures were used. Therefore, the air content of the fresh concrete was not measured. Similarly, since General Use (GU) Portland cement was used without any set retarding or accelerating admixtures, the measurement of fresh concrete temperature was not critical. Numerous hardened concrete properties were measured including, density, compressive strength (7 day and 28 day), splitting tensile strength, secant modulus of elasticity, Poisson's ratio, coefficient of thermal expansion, modulus of rupture (flexural strength), and fracture energy.

6.2 Testing Procedures

6.2.1 Workability

The workability of the concrete was assessed indirectly based on slump (CSA A23.2, 2009). The slump of concrete is defined as the measure of consistency of fresh concrete following the subsidence of the sample measured to the nearest 5 mm after removal of the slump cone. Figure 6.1 depicts the slump cone, tamping rod and a typical slump test in progress. Once the concrete was batched, the slump test was performed in accordance with CSA standard A23.2-5C. Slump values were used to gauge the effect of replacing natural aggregate with RCA on workability. Strength-based mixture proportions were developed to achieve slumps within a working range of 75 to 125 mm. Slump values were also used to assess batch-to-batch variation and in determining the inherent variability in the measurement of aggregate absorption capacity.



Figure 6.1 Slump cone apparatus and measurement

6.2.2 Measurement of Hardened Density

A volumetric measurement of hardened density was performed on concrete produced from Phase 2 mixture proportions (40 and 60MPa). Cylindrical specimens (200 mm long and 100 mm diameter) were used to measure the density. A minimum of six cylinders were used to determine the average hardened density for a given concrete type. A digital caliper was used to measure the overall height, H and the diameter at mid-height at two diametrically opposite points, d_1 and d_2 (see Figure 6.2). The two values of diameter were then averaged to calculate the diameter, d which was used to calculate the volume of the specimen. The mass of the cylinder in air was then measured to the nearest gram and recorded as M . The hardened density was then calculated using Equation 6.1.

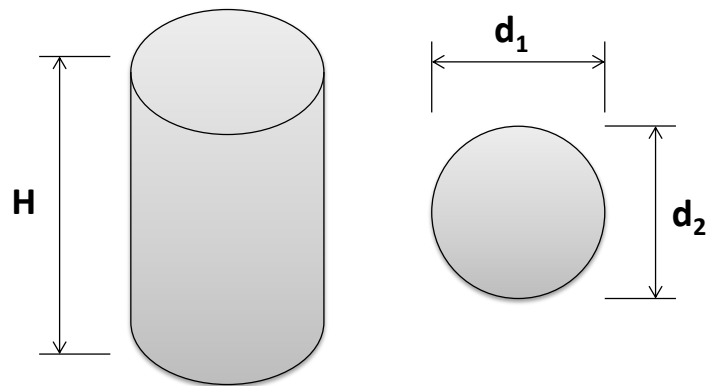


Figure 6.2 Cylindrical specimen used for measurement of density of hardened concrete

$$\gamma_c = \frac{4M}{\pi Hd^2} \quad \text{Equation 6.1}$$

Where,

γ_c = density of hardened concrete (kg/m³);

M = mass of cylindrical concrete specimen (kg);

H = measured height of concrete specimen (m); and

d = average diameter of concrete specimen = (d₁+ d₂)/2 (m).

Density values were reported to the nearest 1 kg/m³. Hardened density values were used to compare the effect that coarse aggregate density has on hardened density of concrete and density was required for modulus of elasticity calculations.

6.2.3 Compressive Strength

The compressive strength of concrete was measured using CSA A23.2-9C, Compressive Strength of Cylindrical Concrete Specimens (CSA A23.2, 2009). Specimens were cylinders measuring 200 mm long with a diameter of 100 mm. A minimum of three specimens were tested per concrete type (and age) and the compressive strength of a particular concrete type was reported as the average of all three specimens. Specimens were prepared using single-use plastic molds. After two days of curing, concrete specimens were removed from the molds. The ends of the cylinders were then ground to achieve adequate planeness using an end grinder prior to testing using a hydraulic compression tester with a 1500 kN capacity as depicted in Figure 6.3. Specimens were tested in an air-dry condition (after 7 days curing under moist conditions followed by 21 days of curing in air). The maximum stress (in MPa) and the fracture pattern were recorded. Figure 6.4 illustrates the various fracture patterns of cylindrical concrete specimens. In addition to the fracture pattern, careful observations of the fracture surface were used to determine whether fracture occurred through the coarse aggregate, through the mortar or around the coarse aggregate particles (e.g., through the interfacial transition zone or ITZ). These failure modes were used as a basis for comparing and interpreting differences in compressive strengths between natural aggregate concrete and RCA concrete.



Compressive strength tester



Concrete cylinder end grinder

Figure 6.3 Compressive strength tester and three-cylinder concrete end grinder

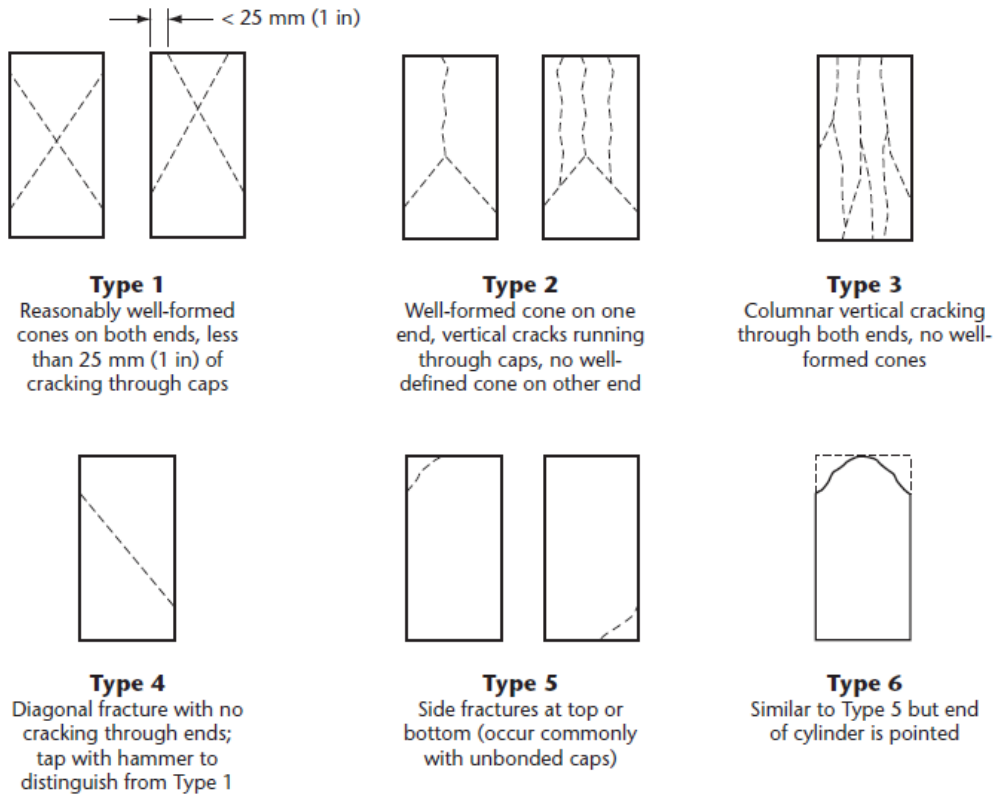


Figure 6.4 Sketches of types of fracture of cylindrical concrete cylinders loaded under uniaxial compression (excerpted from CSA A23.2-9C, 2009)

6.2.4 Splitting Tensile Strength

The splitting tensile strength of concrete was measured using CSA A23.2-13C, Splitting Tensile Strength of Cylindrical Concrete Specimens (CSA A23.2, 2009). In general, the splitting tensile strength is greater than the direct tensile strength and lower than the flexural strength or modulus of rupture (CSA A23.2-09). Cylindrical specimens 100 mm diameter and 200 mm long were prepared in the same way as the compressive strength specimens. Specimens were tested in an air-dry condition (after 7 days curing under moist conditions followed by 21 days of curing in air). A minimum of three specimens were tested per concrete type (and age) and the splitting tensile strength of a particular concrete type was reported as the average of all three specimens. To ensure proper alignment during testing, the specimen was positioned using an aligning apparatus and bearing strips were placed at the top and bottom of the specimen as depicted in Figure 6.5. The aligning apparatus and specimen were then centered directly beneath the centre of thrust of the spherical bearing block.

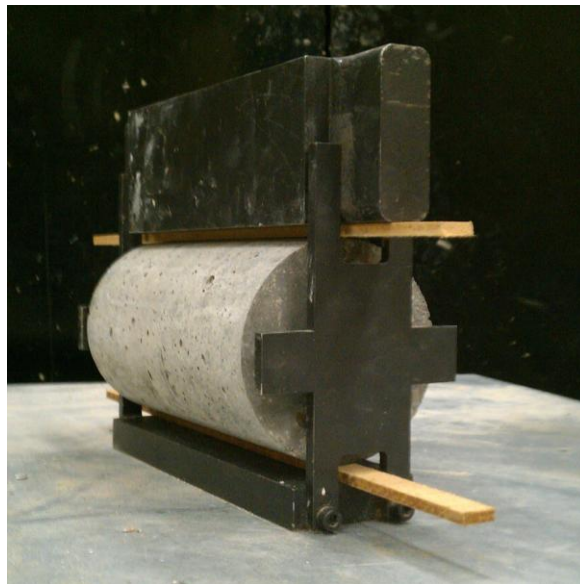


Figure 6.5 Aligning apparatus and bearing strips used to position splitting tensile strength specimens

The length and diameter of the specimens were measured prior to testing. Loading was applied using the same hydraulic strength tester used in the measurement of compressive strength (Figure 6.3). The splitting tensile strength of a cylindrical concrete specimen was calculated using Equation 6.2.

$$f_{ct} = \frac{2P}{\pi ld} \quad \text{Equation 6.2}$$

Where,

f_{ct} = splitting tensile strength, MPa

P = maximum applied load, N

l = length of cylindrical specimen, mm

d = diameter of cylindrical specimen, mm

The maximum load at failure was recorded along with the observed failure pattern of the specimen. The splitting tensile strength was measured for all concrete types to assess the influence that coarse aggregate properties have on tensile strength.

6.2.5 Linear Coefficient of Thermal Expansion

A standard test method for determining the linear coefficient of thermal expansion (LCTE) of concrete does not exist therefore, the method used in this study was similar to one carried out by Sharaf et al. (2005). Cylindrical specimens 100 mm diameter and 200 mm long were prepared in the same way as the compressive strength specimens and were used in combination with a DEMEC mechanical strain gauge to measure the strain due to thermal expansion under varying temperature (see Figure 6.6). A minimum of two specimens were tested per concrete type (and age) and the LCTE for a particular concrete type was reported as the average of both specimens. Two pairs of stainless steel DEMEC locating discs were mounted with epoxy at a gauge length of 150 mm along the longitudinal axis of the cylinder specimens at diametrically opposite points on the specimen circumference (see Figure 6.7). All specimens were air dry at the time of testing.

An invar standard DEMEC rod was used to mount the locating discs at a precise gauge length apart from each other (see Figure 6.6). Initial gauge readings were taken after the specimens had been at room temperature (21°C) for 24 hours. Specimens were then placed in a freezer set at -15°C and after 24 hours specimens were removed and gauge readings were taken immediately. This created a temperature difference of 36°C. Ambient temperatures were measured using a

digital thermometer. The temperature cycle was repeated to obtain average strain values. Specimens were kept at each temperature for 24 hours prior to strain measurement to ensure they had reached the ambient temperature.

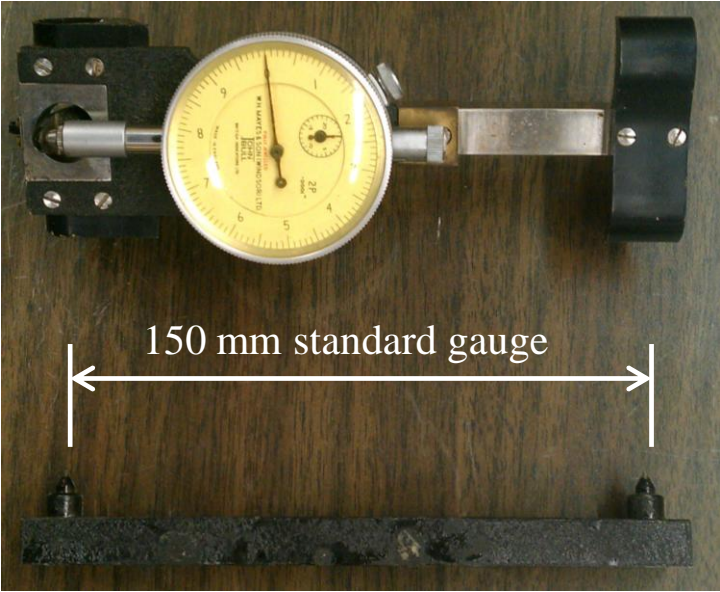


Figure 6.6 Specimen test setup and instrumentation for measurement of the coefficient of thermal expansion of concrete

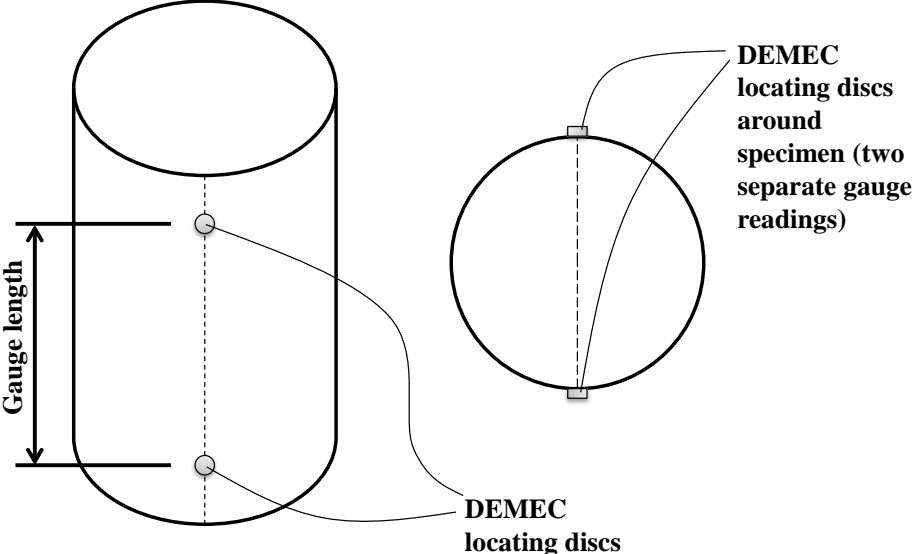


Figure 6.7 Specimen test setup and instrumentation for measurement of the coefficient of thermal expansion of concrete

The coefficient of thermal expansion was calculated using Equation 6.3:

$$\alpha = \frac{\varepsilon_2 - \varepsilon_1}{T_1 - T_2} \quad \text{Equation 6.3}$$

Where,

α = linear coefficient of thermal expansion, 1/°C

ε_1 = strain at temperature 1 (mm/mm)

ε_2 = strain at temperature 2 (mm/mm)

T_1 = reference temperature 1 (°C)

T_2 = reference temperature 2 (°C)

6.2.6 Static Modulus of Elasticity and Poisson's Ratio

The modulus of elasticity and Poisson's ratio of concrete were measured using ASTM C469-02, Standard Test Method for Static Modulus of Elasticity and Poisson's Ratio of Concrete in Compression (ASTM C469, 2002). The static modulus of elasticity is generally lower than the dynamic modulus of elasticity with other testing conditions being the same. Working values of modulus of elasticity and Poisson's ratio are generally within a stress range of 0 to 40% of the ultimate load. Cylindrical specimens 100 mm diameter and 200 mm long were prepared in the same way as the compressive strength specimens. To determine the linear stress range of the concrete in compression (i.e., up to 40% of the ultimate compressive strength) companion cylindrical specimens were tested following the procedure outlined in Section 6.2.3. All specimens were air dry at the time of testing. A minimum of three specimens were tested per concrete type (and age) and the modulus of elasticity and the Poisson's ratio for a particular concrete type were reported as the average of all three specimens. A combined compressometer-extensometer fitted with two linear variable differential transformers (LVDTs) to measure the vertical and transverse strain was mounted to the cylindrical specimen. The LVDTs used were capable of measuring changes in length of 0.0001 mm. The test setup and combined compressometer-extensometer are depicted in Figure 6.8 and Figure 6.9 illustrates the calculation of the elastic modulus and Poisson's ratio.

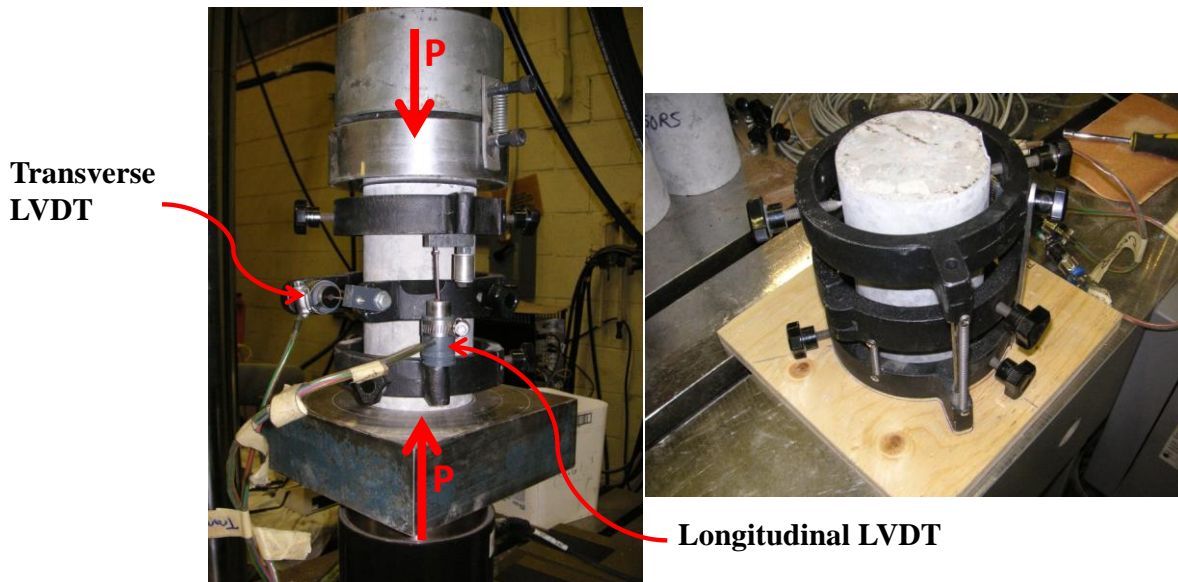


Figure 6.8 Modulus of elasticity and Poisson's ratio test setup and compressometer-extensometer

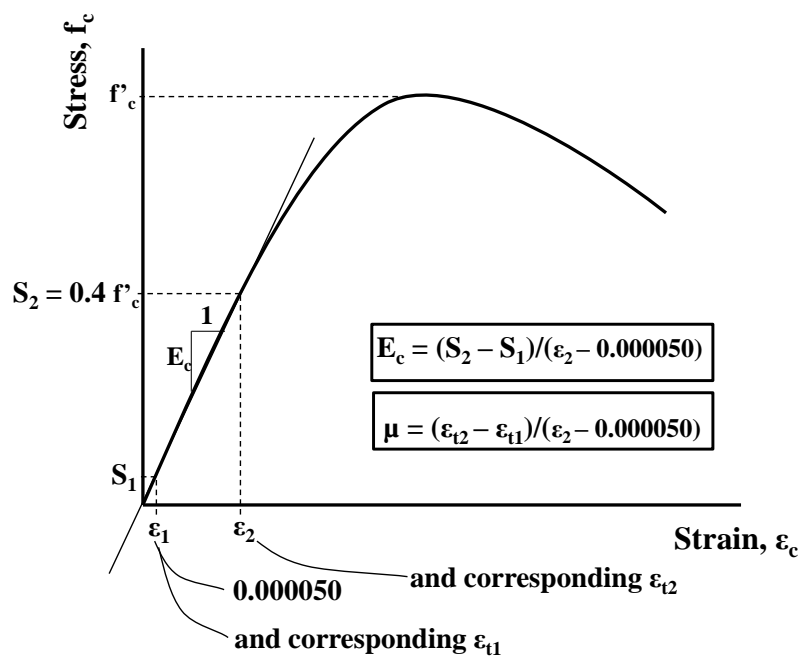


Figure 6.9 Stress-strain response and calculation of the static modulus of elasticity and Poisson's ratio of concrete in uniaxial compression

The secant modulus of elasticity and corresponding Poisson's ratio were defined by the slope of a line passing through two points on the stress vs. longitudinal strain and stress vs. transverse strain curves, respectively. The first point was the compressive stress corresponding to 40% of the ultimate compressive strength, S_2 , and the corresponding longitudinal and transverse strains,

ε_2 and ε_{t2} , respectively. The second point was taken as a longitudinal strain of 0.000050, ε_1 , and its corresponding transverse strain, ε_{t1} and the corresponding compressive stress, S_1 .

A closed-loop servo-hydraulic testing system with a capacity of 500 kN was used. Loading, longitudinal displacement, and transverse displacement were all recorded continuously during the test. Loading was applied at a rate of 240 kPa/s (1.89 kN/s) up until a maximum load corresponding to 40% of the peak compressive strength (f'_c). Each specimen was loaded from 0 to $0.4f'_c$ over three separate cycles. The initial cycle was primarily for the seating of the gauges while the second and third cycles were used to obtain an average slope (modulus of elasticity and Poisson's ratio). Adjustment factors accounting for the longitudinal and transverse gauge lengths of the compressometer-extensometer had to be applied to convert the recorded LVDT readings into equivalent strains.

6.2.7 Fracture Energy and Modulus of Rupture

The area below the stress versus crack opening displacement in a tensile test represents the energy absorbed in the plastic or damage zone and is denoted by, G_f (Hillerborg, 1986). This value is also known as the fracture energy per unit area of the fracture surface (projected area perpendicular to the stress direction). No standard method has been adapted for the testing of fracture energy of concrete and therefore, a new test method was developed by adapting the procedures and specimen configurations from several previous studies in the literature (RILEM, 1985, Darwin et al., 2001, and Martin et al., 2007). The newly developed specimen and test procedure was also used to calculate the flexural tensile strength (modulus of rupture) of concrete.

Using the strength-based mixtures from Phase 1 and Phase 2, fracture energy specimens were cast in conjunction with the beam-end specimens for the main purpose of investigating the effect of fracture energy on bond strength with reinforcing steel. A summary of the various fracture energy test procedures developed in the literature along with a summary of the proposed test method is presented in Table 6.1.

Table 6.1 Summary of the various fracture energy test procedures

Test Procedure Factor	RILEM (1985)	Darwin et al. (2001)	Martin et al. (2007)	Proposed Test Method (2011)
Specimen Dimensions	200mm x 100mm x 1200mm long with a span of 1130 mm	100mm x 100mm x 350mm with a span of 300 mm (3:1 span-to-depth ratio)	150mm x 150mm x 530mm with steel counterweights to counteract the self-weight and create a small net negative moment (1% of the expected peak positive moment at testing).	100mm x 100mm x 700mm long with a clear span of 350mm. Use beam self-weight at overhangs to counteract initial positive moment between supports.
Specimen Curing	Cured in lime-saturated water until 30 minutes prior to testing.	Cured in lime-saturated water until the time of testing at which time they were covered in plastic wrap.	Before testing specimens were stored in sealed plastic bags containing moist towels.	Moist-cured for 7 days under burlap and plastic then cured in air until testing.
Notch Dimensions	100 mm deep (half the depth of the specimen) with a width no greater than 10mm	25 mm deep (1/4 the specimen depth) by 3 mm wide	25 to 75mm deep and widths ranging between 6 and 9mm	30mm deep by 5mm wide
Notch Installation	Cutting recommended	Saw cutting	Cast-in-place flexible form	Saw cutting
Instrument and test frame setup	Closed-loop servo controlled with high stiffness Crack mouth opening displacement shall be used as the control value for displacement rate Deformation of the center of the specimen shall be determined with regard to a line between two points on the beam above the supports	150 kN Closed-loop servohydraulic testing system Crack mouth opening displacement control 0.08mm/min Two LVDTs mounted on the specimen itself were used to measure the midspan deflection	1300 kN universal testing machine using a 13 kN S-type load cell Direct measurement of the beam deflection was used to control the load rate 0.18mm/minute Four potentiometers were used to measure the midspan deflection of the beam	100 kN closed-loop servo-hydraulic controlled testing system. Crack mouth opening displacement control and LVDTs mounted on specimen to measure midspan deflection.
Fracture Energy Calculation	$G_f = (W_o + mgd_f)/A_{fracture}$ Where W_o = area under the load- displacement curve, $A_{fracture}$ = projection of the fracture zone on a plane perpendicular to the beam axis, and d_f = final deflection of the beam, and m is the mass of the beam between supports plus the weight of any instrumentation attached	Same as RILEM However, it uses the area under the load vs. mid-span deflection. Mid-span deflection is measured on specimen.	The fracture energy was computed from the area under the complete, and self-weight corrected load-deflection curve divided by the cross-sectional fracture area.	Compute fracture energy using RILEM recommended formula but subtract the self-weight counteracted by the overhangs.

After reviewing the tests proposed in the literature, single-edge notched double-cantilevered (SENDC) specimens were developed as part of this research for measuring the fracture energy and modulus of rupture. Each specimen had dimensions of 700 mm length, 100 mm width, 100 mm height, and a notch depth of 30 mm. Notches were saw-cut after curing for at least 14 days and were 5 mm in width. The specimens were 700 mm in length but had clear spans of 350 mm; this provided cantilever sections on each end with lengths of 175 mm whose weight counteracted the mass of the specimen within the clear span (see Figure 6.10 and Figure 6.11). Therefore, self-weight corrections as proposed by RILEM can be omitted when using this type of specimen, thereby eliminating any errors associated with its calculation.

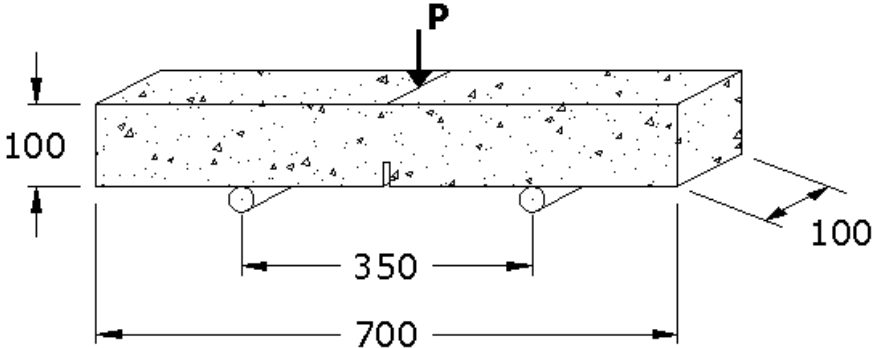


Figure 6.10 Single-edge notched double cantilevered (SENDC) fracture energy specimen

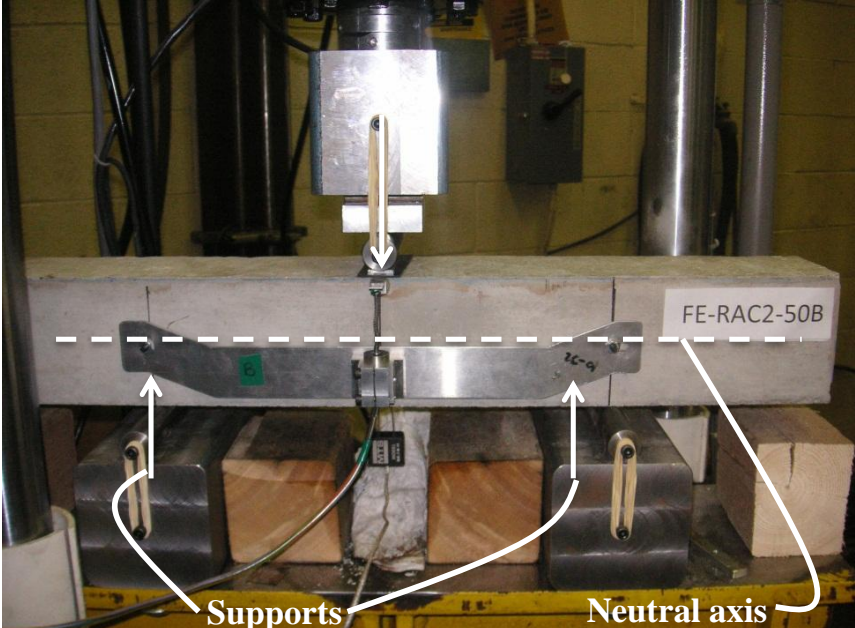


Figure 6.11 Fracture energy SENDC specimen test setup and instrumentation

A closed-loop servo-hydraulic testing system with a 100 kN capacity was used to perform this test using the crack mouth opening displacement (CMOD), measured using a clip gauge, as the feedback channel (see Figure 6.12). All specimens (NA and RCA concrete) were tested in an air dry condition. Tests were run at a constant CMOD of 0.075 mm per minute to ensure that the peak load was reached within 30 to 60 seconds of the start of the test. The test was run until the specimens had become completely separated into two halves.

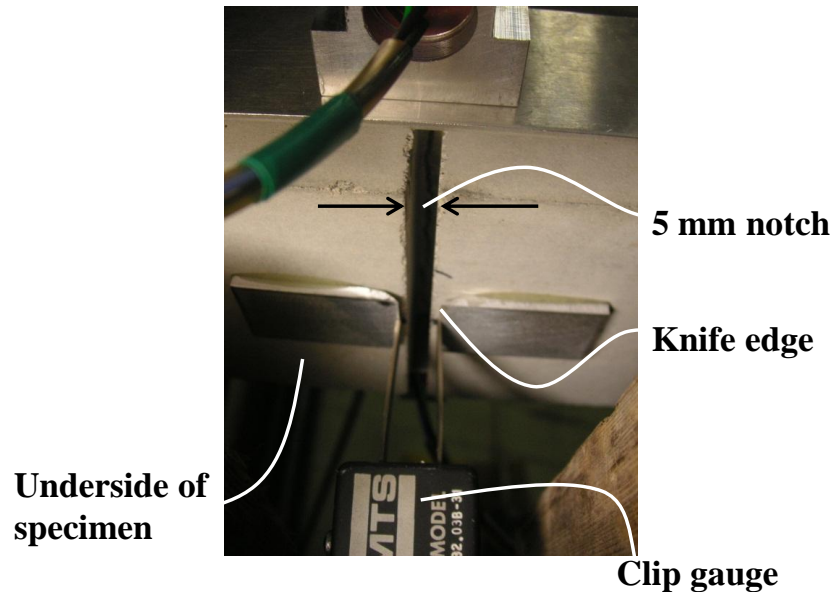


Figure 6.12 Underside of fracture energy test specimen and clip gauge setup

The mid-span displacement was measured relative to the specimen using aluminum brackets attached over the supports and mounted on either side of the specimen. Two linear variable differential transformers (LVDTs) with an accuracy of 0.0001 mm were mounted on the aluminum brackets to measure the mid-span displacement on either side of the specimen (see Figure 6.13).

Data collected included the midspan LVDT readings (two readings), the applied load, and the crack mouth opening displacement (CMOD). The fracture energy was then calculated as the area under the load versus midspan deflection plot divided by the area of fracture (see Figure 6.14). In addition, the crack tip opening displacement at the peak load, $CTOD_{peak}$ was recorded as the value presented in Figure 6.14.

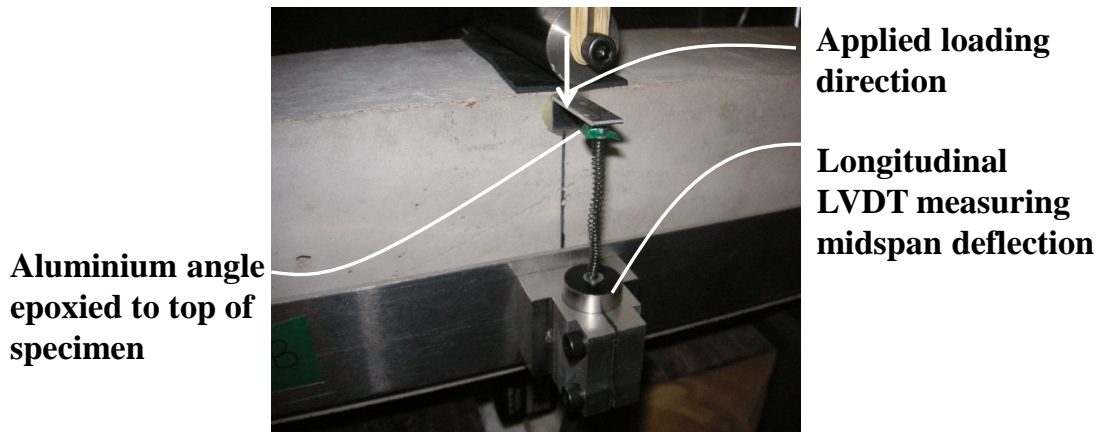


Figure 6.13 Side view of fracture energy test specimen and LVDT for midspan displacement measurement

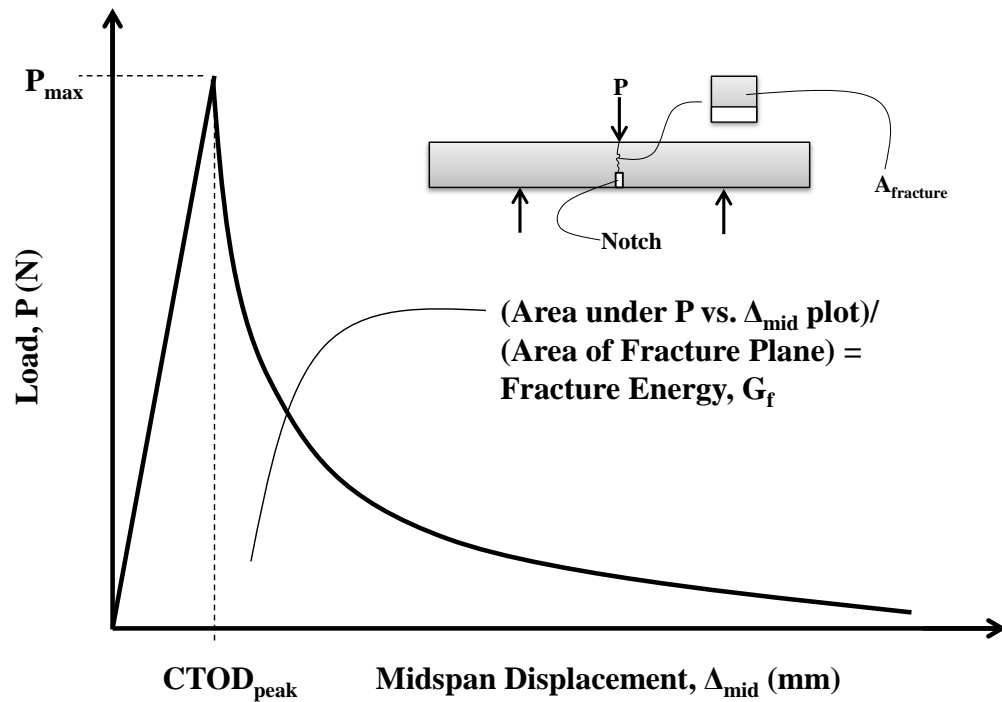


Figure 6.14 Load vs. displacement plot for calculation of fracture energy of concrete using single-notched double-cantilevered specimen

The area under the load versus midspan deflection plot was calculated using numerical integration and the fracture energy was then calculated using Equation 6.6.

$$G_f = \frac{W_0}{A_{\text{fracture}}} \quad \text{Equation 6.6}$$

Where,

G_f = fracture energy (N/mm);

W_0 = area under the load-deflection curve (N-mm); and

A_{fracture} = cross-sectional area of the beam above the notch (mm) (see Figure 6.14).

Note that unlike the expression for the calculation of fracture energy proposed by Hillerborg (1985) (Equation 2.6), the calculation of the additional work carried out by the self-weight of the specimen between supports is not required in Equation 6.6 as the overhangs of the specimen counteract this work. The modulus of rupture was measured using the same SENDC specimens used to determine the fracture energy. Equation 6.7 was used to calculate the modulus of rupture,

$$f_r = \frac{3}{2} \frac{PL}{b(h-a)^2} \quad \text{Equation 6.7}$$

Where,

f_r = modulus of rupture (MPa);

P = maximum load (N);

L = clear span of prism (mm) = 350 mm;

b = width of prism (mm) = 100 mm = h = height of prism = 100 mm; and

a = notch depth (mm) = 30 mm

6.3 Summary

The procedures outlined in this chapter were used for testing concrete in this research. Most test procedures come directly from CSA or ASTM standards. However, in the case of the coefficient of thermal expansion and fracture energy, test methods were developed based on previous research by others. Chapters 7, 8 and 9 present the testing results and evaluation of the various concrete mechanical properties associated with the control, direct replacement and strength-based mixtures based on these test methods.

Chapter 7: Evaluation of Direct Replacement Mixture Test Results

7.1 Overview

The direct replacement mixtures were designed using the same mixture proportions (water-cement ratio, cement content and coarse aggregate volume) as the NA concrete mixtures for the purpose of isolating the effect that a particular coarse aggregate type has on the mechanical properties of concrete (refer to Section 5.1.2). The following sections present and discuss the fresh and hardened properties of the direct replacement mixtures, including: workability (slump), hardened density, compressive strength (early age and nominal), splitting tensile strength, linear coefficient of thermal expansion, modulus of elasticity, and Poisson's ratio. Chapter 6 detailed all the concrete testing procedures used. Compressive strength and splitting tensile results are explained in terms of their failure mechanisms. A detailed description of the failure modes of RCA concrete is also presented. In addition, the effect of particular aggregate properties on concrete mechanical properties as they pertain to the direct replacement mixtures are also identified and discussed. Results for Phases 1 and 2 are presented separately and overall conclusions are summarized at the end of the chapter.

7.2 Failure Modes of RCA Concrete

Natural aggregate concrete is a complex heterogeneous material whose response to stress is dependent on both the response of individual components and on the interaction between each component (Mindess et al., 2003). NA concrete is considered a three phase material in which the weakest phase becomes the source of the failure mechanism. The three phases in NA concrete consist of the coarse aggregate particles, the mortar (matrix), and the mortar-aggregate interface or interfacial transition zone (ITZ). RCA concrete is considered a five phase material as the RCA particles produced from crushing of NA concrete also consist of three phases. Two additional phases are introduced when RCA is re-used in new concrete: a new mortar phase and a new interfacial transition zone. The strength of RCA concrete therefore is ultimately governed by the weakest of the five phases. Figure 7.1 summarizes the five possible failure modes of RCA concrete and the RCA properties which influence these failure modes.

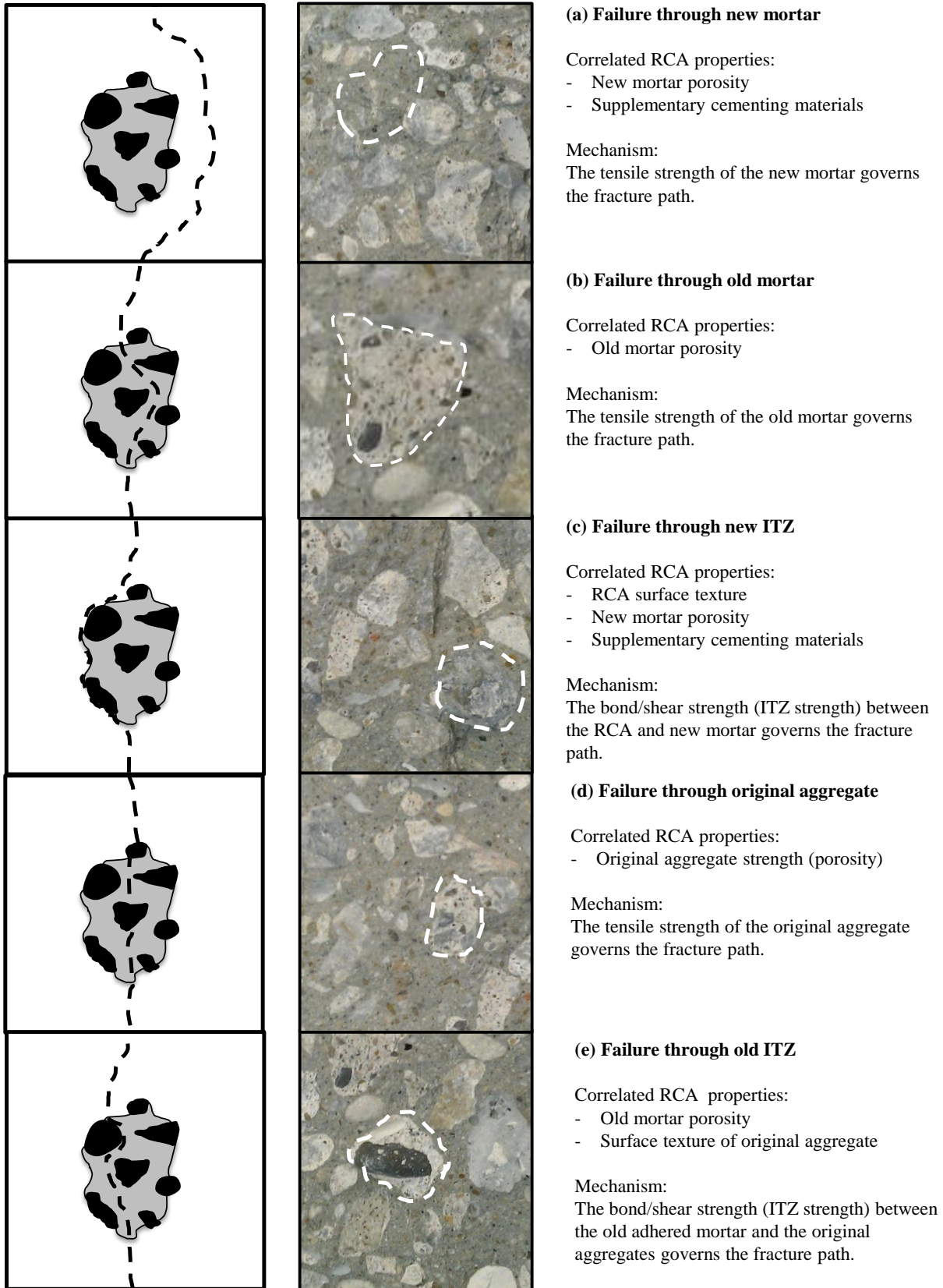


Figure 7.1 Failure modes of RCA concrete

The majority of the failures that occurred in compressive, splitting tensile, fracture energy, or bond strength specimens were modes b, c and d. Given that all of the direct replacement mixtures of a given strength class (i.e., 30, 40, 50 or 60 MPa) had identical coarse aggregate volumes and water-cement ratios, it is reasonable to assume that the tensile strength of mortar within a particular strength class was the same regardless of concrete (and aggregate) type. Therefore, by observing the fracture planes of the compressive strength and splitting tensile strength specimens to assess whether failure mode b, c or d occurred, any variation in compressive and splitting tensile strength could be explained based either on the tensile strength of the original aggregate, the tensile strength of the old mortar, and/or the bond or shear strength of the ITZ (which is influenced by the surface texture of the aggregate particle). It should be noted that in most cases it is difficult to differentiate between failure modes b and d as the failure through old mortar and through original aggregate often occur simultaneously. In most cases, it may also be quite difficult to differentiate between failure modes b and e, unless, the original aggregate is clearly separated from the old mortar (as depicted in Figure 7.1e).

In general, the tensile strength of the entire RCA particle itself will be dependent on the tensile strength of the old mortar and the tensile strength of the original aggregate. Therefore, for the purposes of the following analyses, failures were visually identified as:

- Occurring around more than 50% of the aggregate (NA or RCA) particles, or
- Occurring through more than 50% of the aggregate (NA or RCA), particles or
- Occurring approximately equally around and through the aggregate particles (NA or RCA).

In the case of failures occurring equally around and through coarse aggregate particles, the mortar-aggregate bond strength (ITZ strength) in combination with the aggregate tensile strength governs the concrete strength. Note that particular failure modes were approximated based on visual inspection.

7.3 Phase 1 Direct Replacement Mixtures (30 and 50MPa)

The following section presents the results and evaluation of the Phase 1 direct replacement mixtures (refer to Chapter 3 for a description of mixture proportion phases).

7.3.1 Workability

Slump values for the Phase 1 direct replacement mixtures have been summarized in Figure 7.2. Slumps were measured to the nearest 5 mm in accordance with CSA A23.2-5C (refer to Chapter 6 for procedure). Pre-soaking the RCA-1 and RCA-2 should have eliminated any slump loss due to coarse aggregate absorption of mixing water during batching. However, a significant reduction in slump between the NA concrete mixtures and the RCA concrete mixtures was observed (up to 75% and 55% reduction for the RCA-1 and RCA-2 concrete mixtures, respectively). The lower slump values in the RCA concrete mixtures result from the more angular shape and roughened surface texture of the RCAs which increased the inter-particle friction in the fresh concrete.

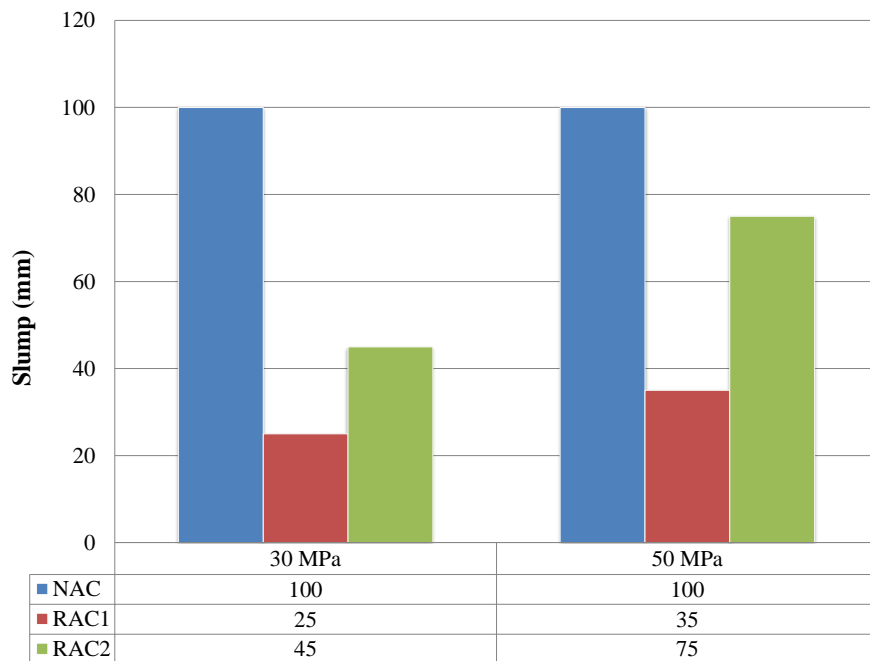


Figure 7.2 Slump values for Phase 1 direct replacement mixtures

Recall that in Section 4.5.4 the amount of adhered surface moisture was defined and used as an indirect measure of aggregate surface texture. A strong relationship (R^2 value of 0.91) between the adhered surface moisture of the aggregate and the slump (assuming aggregates have been pre-soaked) exists as depicted in Figure 7.3. This relationship exists because the adhered surface moisture of an aggregate particle may provide an indirect indication of the aggregate particle

surface texture. Another possible contributor to the higher slump values of the RCA-2 concrete as compared to the RCA-1 concrete is the slight increase in mortar volume due to the abrasion of the weaker adhered mortar on the RCA-2 particles. Increasing the mortar volume increases the lubrication properties of the concrete mixture and reduces the inter-particle friction. A study conducted by Safiuddin et al. (2011), concluded that RCA particles could lose up to 8% of their mass via aggregate-aggregate collisions during one minute of concrete mixing, hence increasing mortar volume.

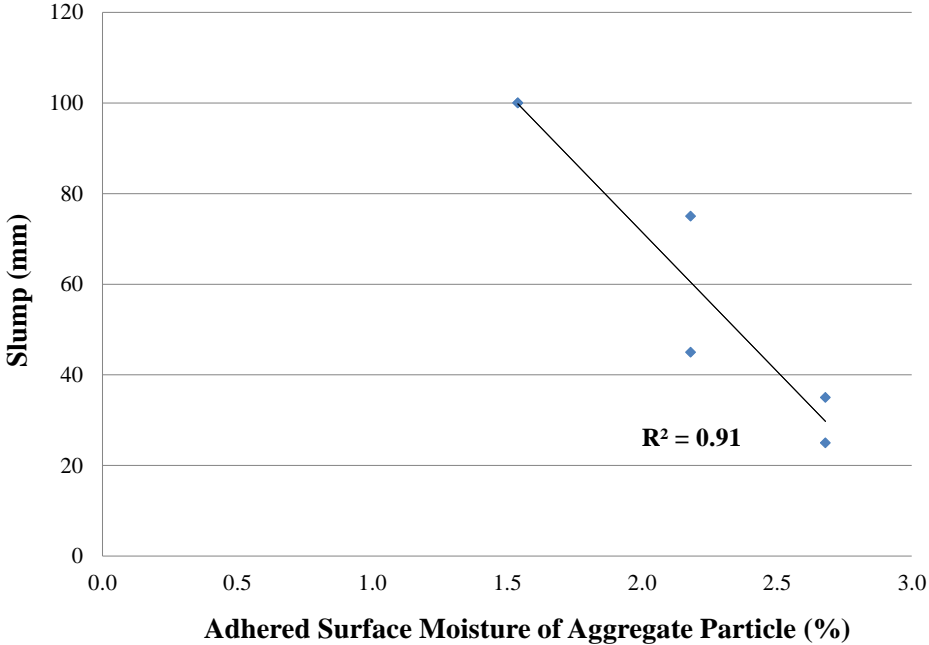


Figure 7.3 Relationship between slump and adhered surface moisture of aggregate particle (Phase 1 direct replacement mixtures)

7.3.2 Compressive Strength Results

Early (7 day) and nominal (28 day) compressive strengths and their statistics for each Phase 1 direct replacement mixture are summarized in Figure 7.4 and Figure 7.5. The compressive strength values reported are averages of three cylinders with dimensions 100 mm by 200 mm and were measured in accordance with CSA A23.2-9C. All early strength (7 day) specimens were tested under moist conditions whereas all 28 day strength specimens were tested in an air dry condition). Examining the early (7 day) compressive strengths indicated that the 30 MPa RCA-1 concrete had the highest compressive strength followed by the RCA-2 and NA concretes. In the 50 MPa mixtures, the RCA-1 concrete had the highest strength followed by the NA and RCA-2

concretes. A similar trend existed when comparing the 28 day compressive strength mixtures.

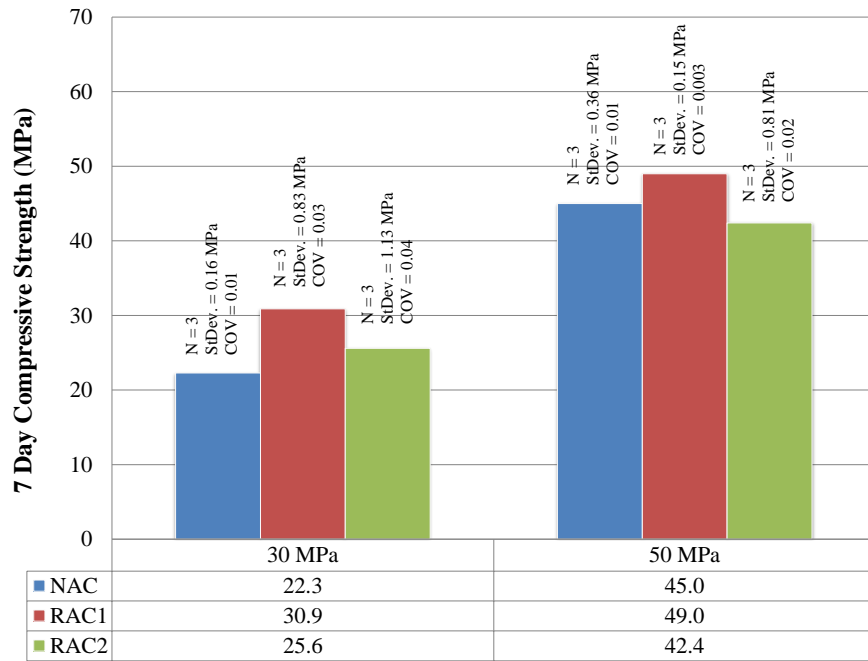


Figure 7.4 Early (7 day) compressive strength test results and statistics for Phase 1 direct replacement mixtures

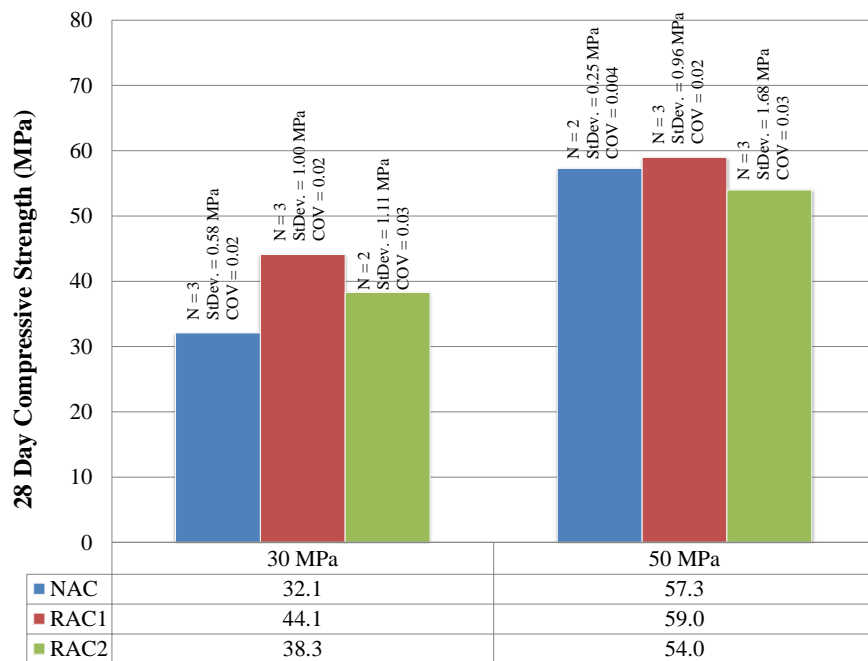


Figure 7.5 Nominal (28 day) compressive strength test results and statistics for Phase 1 direct replacement mixtures

After 28 days of curing, the 30 and 50 MPa RCA-1 concrete mixtures achieved compressive strengths that were 37% and 3% higher than the NA concrete, respectively. The 30 and 50 MPa RCA-2 concrete mixtures produced compressive strengths that were 19% higher and 5% lower than the NA concrete, respectively. These values are in contrast with trends found in the literature that have reported a decrease in compressive strength when natural aggregate is replaced with RCA (Xiao and Zhang, 2005, Chen et al., 2003, Topcu and Sengel, 2004, Etxeberria et al., 2007). Overall, within batch variation of compressive strengths were fairly low at both the 30 and 50 MPa compressive strength levels (i.e., coefficient of variation values ranged between 0.4% and 3%). Compared to the control standards recommended by ACI Committee 214 (ACI 214, 2011), this range of coefficient of variation in compressive strengths for laboratory-produced concrete is considered “very good” to “excellent”. Figure 7.6 shows the early compressive strength normalized to the 28 day strength (f'_c). At the 30 MPa strength level, all three concrete types had equal normalized strength, indicating that at lower compressive strengths, replacing natural aggregate with RCA has little effect on early age strength gain. At the 50 MPa strength level, the NA and RCA-2 concrete mixtures had similar normalized strength (78.5% of f'_c at 7 days) whereas the 7 day strength of the RCA-1 was closer to its 28 day compressive strength (83.1% of f'_c at 7 days).

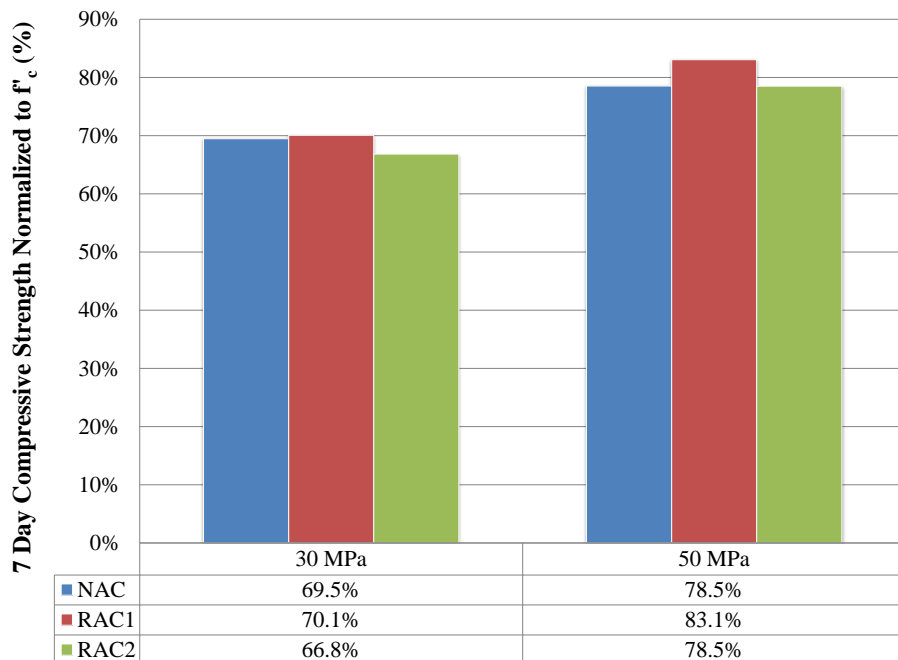


Figure 7.6 Early compressive strength normalized to 28 day strength for Phase 1 direct replacement mixtures

7.3.2.1 Statistical Significance of Compressive Strength Results

To determine whether the relative differences in 28 day compressive strengths between the various Phase 1 direct replacement mixtures were statistically significant, a least significant difference (LSD) value was calculated at the 5% significance level. Using analysis of variance (ANOVA) and a modification to the Bonferroni t-test, the 5% LSD values for the 30 and 50 MPa direct replacement mixtures were calculated as 2.7 MPa and 3.8 MPa, respectively. As presented in Figure 7.5, the difference in nominal compressive strength values at the 30 MPa strength level between the NA concrete and the RCA-1 concrete and the NA concrete and the RCA-2 concretes were greater than the 5% LSD value. This indicates that relative differences in compressive strength between the NA concrete mixtures and the RCA-1 and the RCA-2 concrete direct replacement mixtures are statistically significant at the 95% confidence level. Therefore, this difference in the compressive strength results can be directly attributed to the effect of the RCA-1 and RCA-2 properties. However, at the 50 MPa level, the difference in nominal compressive strength values for both the RCA-1 and RCA-2 concretes were less than the 5% LSD value. This result indicates that the relative differences in compressive strength between the NA concrete mixtures and the RCA-1 and the RCA-2 concrete direct replacement mixtures are not statistically significant. Refer to Appendix B for sample LSD calculations.

7.3.2.2 Failure Mechanism and Effect of RCA Properties on Compressive Strength

To explain the effect that RCA has on concrete compressive strength, the failure planes of concrete cylinders for each concrete type were examined and were found to be mainly around or mainly through the RCA (failure mode b or d, see Figure 7.1). A summary of the 28 day compressive strengths and associated failure modes is presented in Table 7.1, Figure 7.7 and Figure 7.8 to facilitate the following discussion. As previously mentioned, failure planes that occur around the aggregate indicate that the mortar-aggregate interface or interfacial transition zone (ITZ) is the limiting strength factor. When considering RCAs (i.e., RCA-1 and RCA-2) that contain original natural aggregates and adhered mortar, this suggests that either the old or the new ITZ is the limiting strength factor. Failure planes that occur through the coarse aggregate indicate that the strength of the coarse aggregate (NA or RCA) itself is the limiting strength factor.

Table 7.1 Summary of nominal compressive strengths and failure modes (Phase 1 control and direct replacement mixtures)

Mix ID	28 day f'_c (MPa)	Failure Mode
NAC-30-C	32.1	Around more than 50% of aggregates
RAC1-30-D	44.1*	Around more than 50% of aggregates
RAC2-30-D	38.3*	Around more than 50% of aggregates
NAC-50-C	57.3	Through more than 50% of aggregates
RAC1-50-D	59.0	Through more than 50% of aggregates
RAC2-50-D	54.0*	Through more than 50% of aggregates

* Indicates that the difference in f'_c from the NA concrete is statistically significant at the 95% confidence level. Recall 5% LSD for 30 MPa = 2.7 MPa and 5% LSD for 50 MPa = 3.8 MPa.

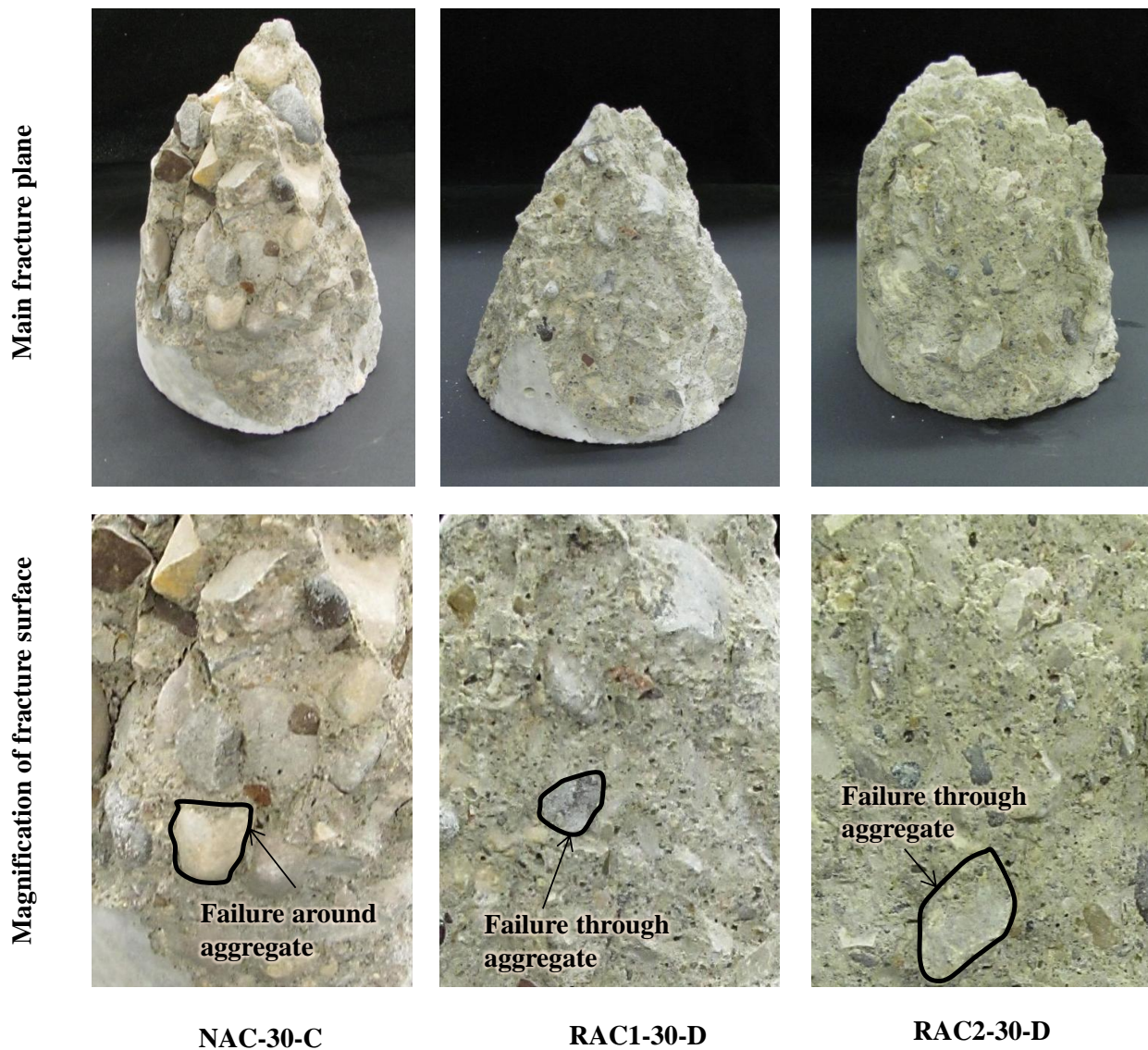


Figure 7.7 Fracture surfaces of the Phase 1 30 MPa direct replacement compressive strength specimens

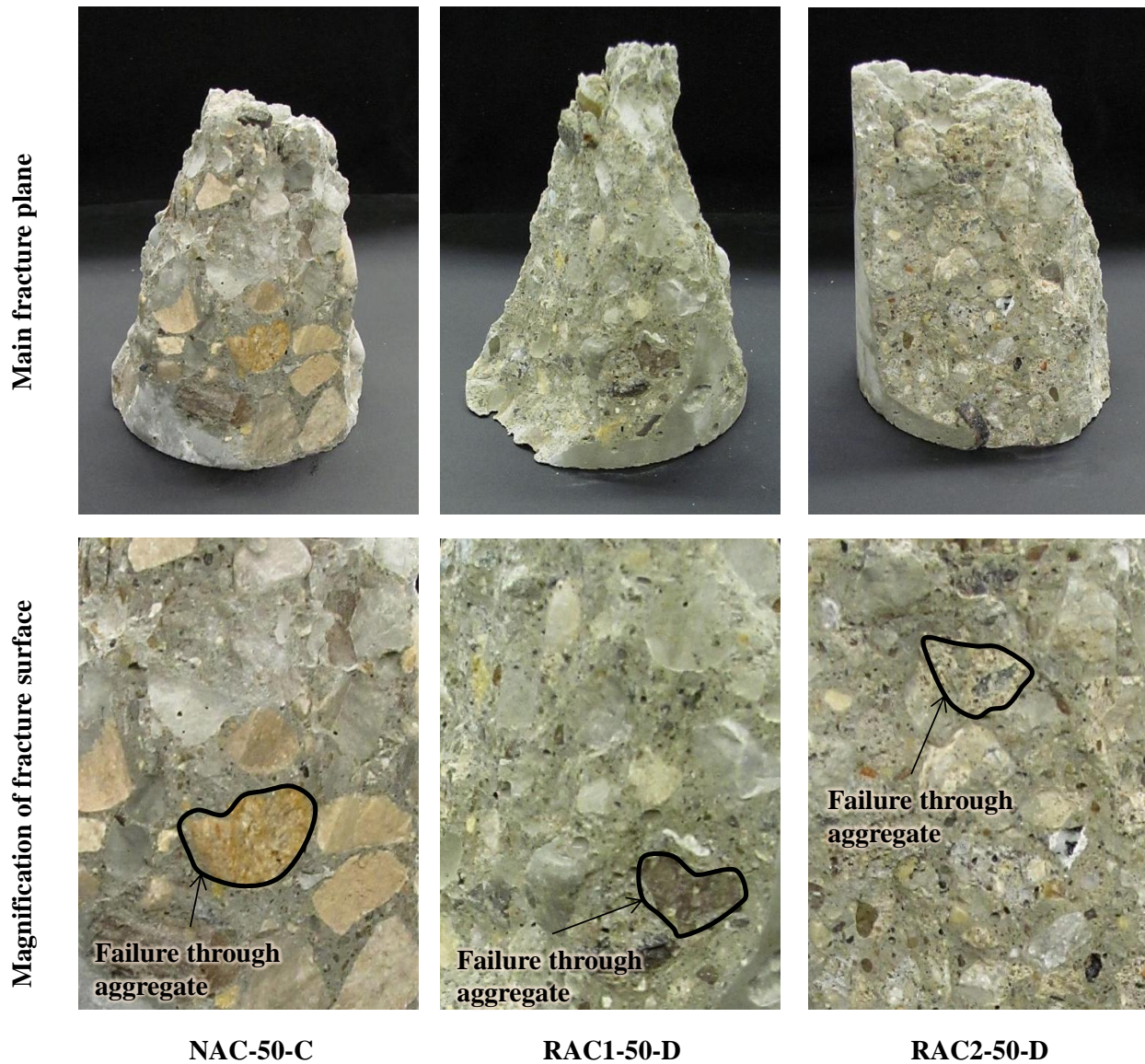


Figure 7.8 Fracture surfaces of the Phase 1 50 MPa direct replacement compressive strength specimens

In the 30 MPa specimens, the failure planes occurred mainly around the aggregate for all three aggregate types. Recall that all direct replacement mixtures have the same water-cement ratio and proportions and, as a result, have the same mortar strengths. Therefore, given that the 30 MPa RCA-1 direct replacement concrete specimens had higher compressive strengths than the NA concrete specimens, it appears that the mortar-aggregate bond strength (ITZ strength) between the new mortar and the RCA-1 is higher than the mortar-aggregate bond strength between new mortar and the NA. As suggested by Rao and Prasad (2002), this increase in ITZ strength is attributed to the more roughened surface texture of the RCA particles compared to the

smoother surface texture of the natural aggregate particles.

In the 50 MPa specimens, the failure planes occurred mainly through the aggregate for all three aggregate types. This suggests that the tensile strength of the natural aggregate and the tensile strength of the original natural aggregate (in the RCA) were the limiting factors rather than mortar-aggregate bond. Since the RCA-2 concrete had a compressive strength that was statistically different from the NA concrete, it follows that the strength of the RCA-2 was the governing factor of concrete compressive strength. Compared to the NA, RCA-2 had a higher ACV value (26.0 versus 18.2) and lower crushing strength which explains why the compressive strength of the RCA-2 concrete was also lower. Figure 7.9 presents the relationship between the adhered surface moisture of an aggregate particle versus the compressive strength for both the 30 and 50 MPa mixtures.

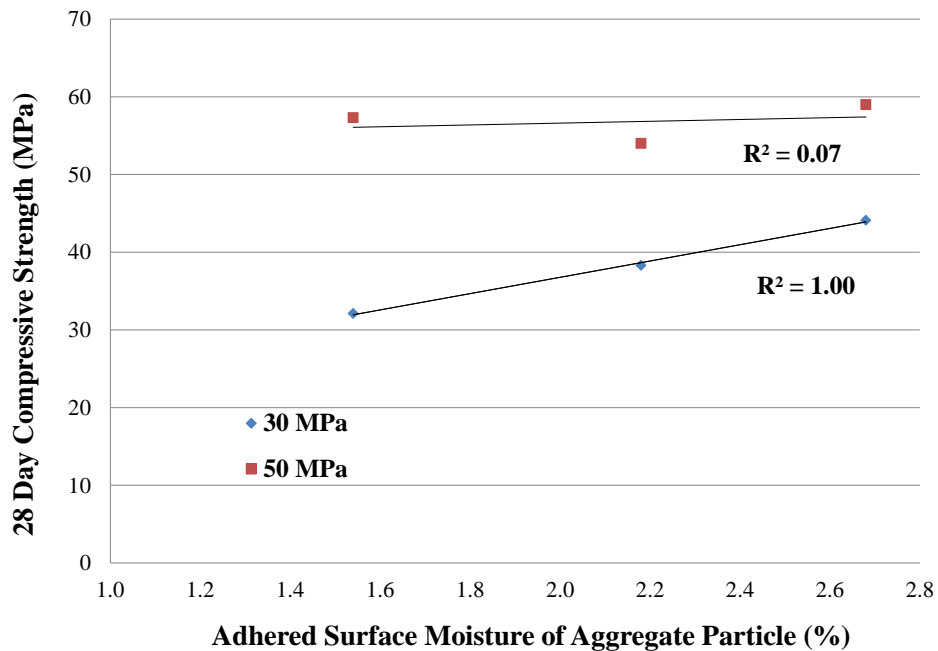


Figure 7.9 Relationship between adhered surface moisture of aggregate particle and compressive strength (Phase I direct replacement mixtures)

As explained in Section 4.5.4, the adhered surface moisture provides an indirect measure aggregate surface roughness; a higher amount of adhered surface moisture on an aggregate particle is associated with a rougher surface texture. Based on the evaluations presented above, a strong relationship ($R^2 = 0.97$) exists between adhered surface moisture (indirect surface texture)

and compressive strength for the 30 MPa mixtures where the failure was governed by the bond between aggregate surface and mortar. In the case of the 50 MPa mixtures, there was found to be no relationship (i.e., $R^2 = 0.07$) between the adhered surface moisture and compressive strength.

7.3.3 Conclusions from Phase 1 Mixtures

The following conclusions have been made based on the results and analysis of the Phase 1 direct replacement concrete mixtures:

1. After replacing the natural aggregate with an equivalent volume of RCA and maintaining an equivalent water-cement ratio, the measured slump values for the RCA-1 and RCA-2 concretes decreased up to 75 and 55%, respectively, in comparison to the NA concrete. Given that the coarse aggregates were pre-soaked prior to batching, the reduction in slump was attributed to the more roughened surface texture of the RCA particles which increased the inter-particle friction in the fresh concrete.
2. A strong correlation exists between adhered surface moisture of aggregate particles (which, as presented in Section 4.5.4, provides an indirect measure of surface roughness) and slump for both the 30 and 50 MPa mixtures.
3. In the 30 MPa direct replacement mixtures, both RCA-1 and RCA-2 concretes had higher compressive strength values than the NA concrete. This is likely due to the stronger mortar-aggregate bond between the RCA particles and the new mortar. In the 50 MPa direct replacement mixtures, RCA-1 concrete had compressive strength values that were statistically similar to the NA concrete and the RCA-2 concrete had lower compressive strength values than the NA concrete. For the RCA-2 concrete, the lower aggregate strength (as represented by the ACV) of the RCA-2 particles as compared to the NA particles appeared to govern the resulting compressive strength.
4. A very good correlation between adhered surface moisture of aggregate particles (indirect measure of surface texture) and compressive strength was found for the 30 MPa samples. This provides confirmation of the influence of aggregate surface texture on the mortar-aggregate bond strength which governed the compressive strength of the 30 MPa mixtures.

7.4 Phase 2 Direct Replacement Mixtures (40 and 60MPa)

The following section presents the results and evaluation of the Phase 2 direct replacement mixtures (refer to Chapter 5 for a description of mixture proportioning).

7.4.1 Workability and Hardened Density Results

7.4.1.1 Workability

Slump values for the Phase 2 direct replacement mixtures have been summarized in Figure 7.10.

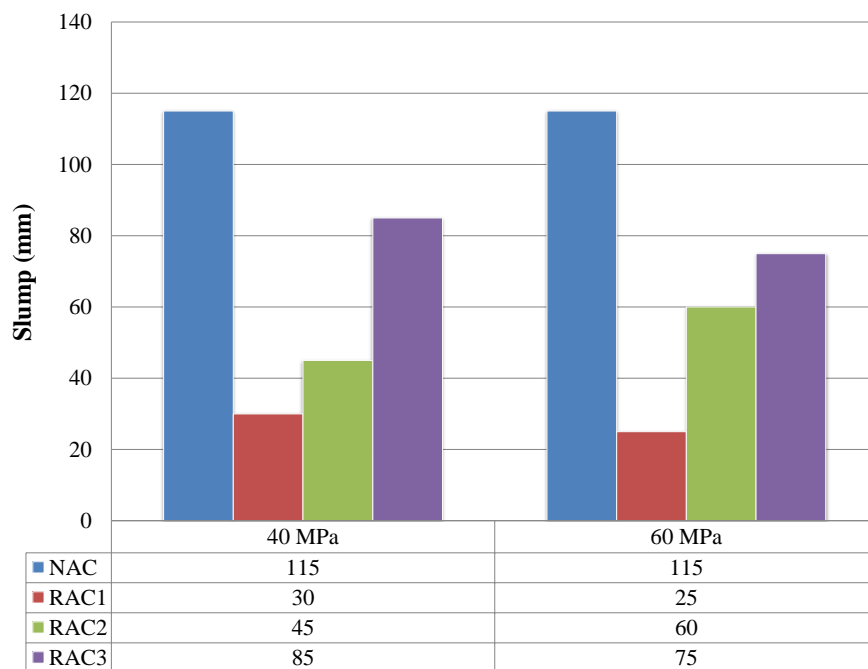


Figure 7.10 Slump values for Phase 2 direct replacement mixtures

Pre-soaking the RCA-1, RCA-2 and RCA-3 particles should have eliminated any slump loss due to coarse aggregate absorption of mixing water during batching. However, similar to Phase 1, a significant reduction in slump between the NA concrete mixtures and the RCA concrete mixtures was observed. The slumps of the RCA-1, RCA-2 and RCA-3 concretes were up to 78, 61, and 35% lower than the corresponding NA concrete mixture, respectively. Based on the previous analysis, the lower slump values in the RCA concrete mixtures result from the more angular shape and roughened surface texture of the RCAs which increased the inter-particle friction in fresh concrete. A fairly strong relationship exists between the adhered surface texture of the

aggregate and the slump (assuming aggregates have been pre-soaked) as depicted in Figure 7.11 with an R^2 value of 0.84.

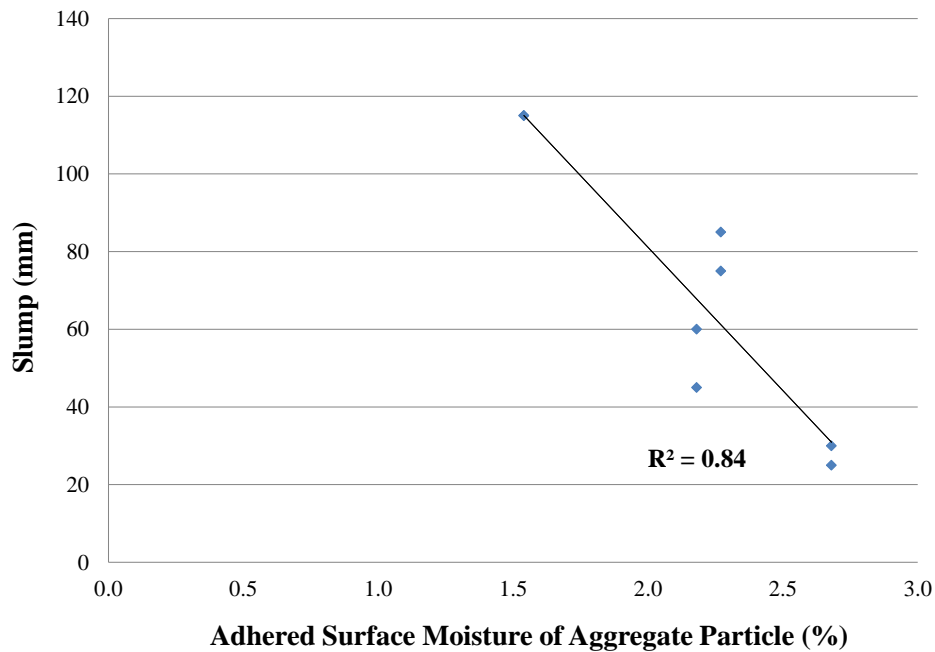


Figure 7.11 Relationship between slump and adhered surface moisture of aggregate particle (Phase 2 direct replacement mixtures)

As previously explained, this relationship exists because the adhered surface moisture (moisture in excess of SSD; refer to Section 4.5.4 for definition) of an aggregate particle may provide an indirect indication of the aggregate particle surface texture. In addition, another possible contributor to the higher slump values of the RCA-2 and RCA-3 concretes as compared to the RCA-1 concrete is a possible increase in mortar volume due to the abrasion of the weaker adhered mortar on the RCA-2 and RCA-3 particles. Weaker adhered mortar tends to have lower abrasion resistance which may cause a larger portion of adhered mortar to be lost during the concrete mixing process.

7.4.1.2 Hardened Density

The density of hardened concrete was measured using the procedure outlined in Chapter 6. Measurements were taken when the concrete specimens were 28 days old and the results are presented in Figure 7.12.

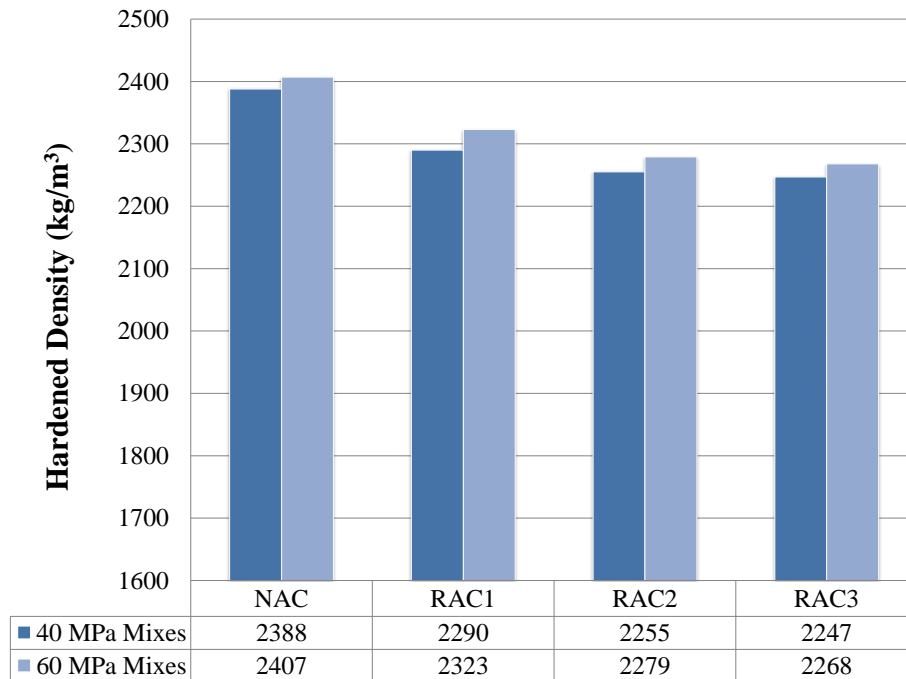


Figure 7.12 Hardened density results for the phase 2 direct replacement mixtures

In general, the NA concrete had higher densities at both the 40 and 60 MPa strength levels followed by the RCA-1, RCA-2 and RCA-3 concretes. As suspected, given that all mixtures had equal volumes of coarse aggregate (i.e., direct replacement), a strong correlation between aggregate density and concrete density was observed. Figure 7.13 depicts a strong relationship (given the high R^2 values) between concrete hardened density and the bulk density of coarse aggregate. Figure 7.14 depicts the strong relationship between concrete hardened density and the aggregate crushing value with R^2 values of 0.91 and 0.89 for the 40 and 60 MPa compressive strengths, respectively. This relationship follows well with the findings in Section 4.5.8 which showed a strong relationship between the aggregate crushing value and the aggregate bulk density. Further discussion of the effect of concrete hardened density and the aggregate crushing value on the bond strength is included in Section 9.7.4. No significant correlation was found between concrete hardened density and the compressive strength or splitting tensile strength of concrete.

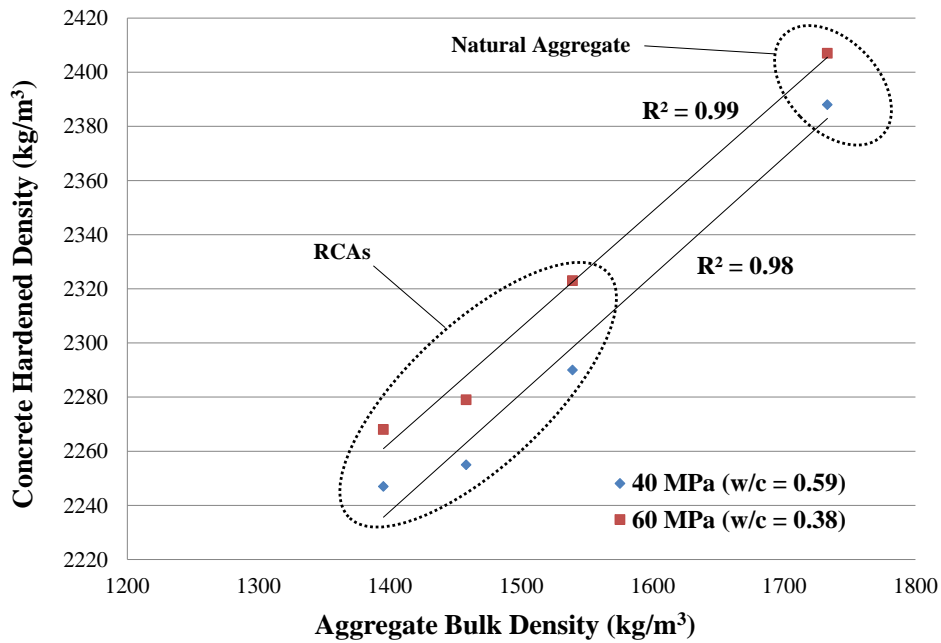


Figure 7.13 Relationship between aggregate bulk density and concrete hardened density (Phase 2 direct replacement mixtures)

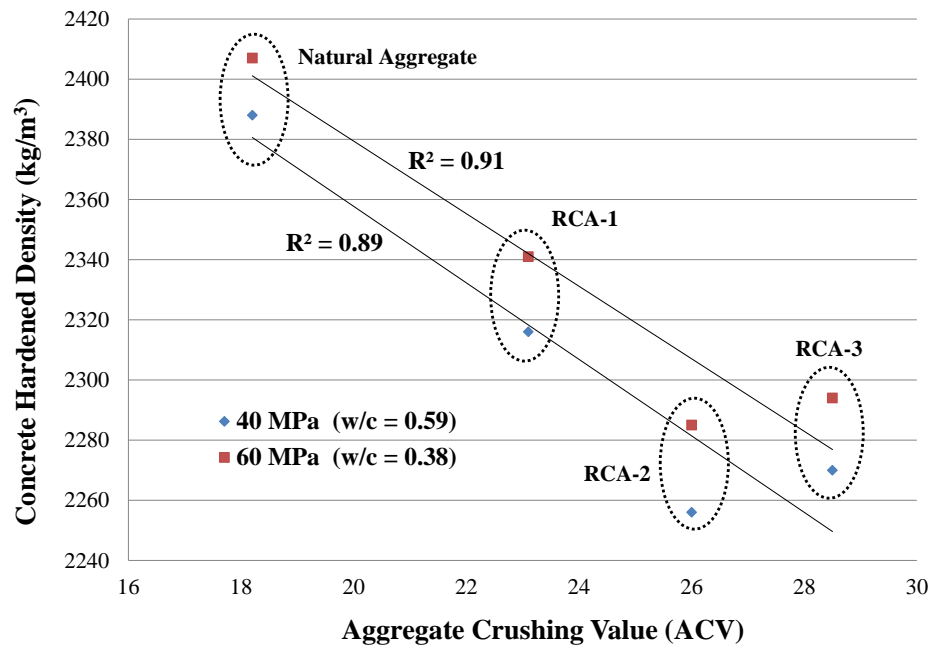


Figure 7.14 Relationship between aggregate crushing value and concrete hardened density (Phase 2 direct replacement mixtures)

7.4.2 Compressive Strength Results

Early (7 day) and nominal (28 day) compressive strengths and their statistics for each Phase 1 direct replacement mixture are summarized in Figure 7.15 and Figure 7.16. Compressive strength values reported are averages of three cylinders with dimensions 100 mm by 200 mm and were measured in accordance with CSA A23.2-9C. All early strength (7 day) specimens were tested under moist conditions whereas all 28 day strength specimens were tested in an air dry condition).

Examining the early (7 day) compressive strengths indicated that the 40 MPa RCA-1 concrete had the highest compressive strength followed by the natural, RCA-2 and RCA-3 concretes (i.e., similar trend to Phase 1 results). In the 60 MPa mixtures, the RCA-1 concrete had the highest strength followed by the NA, RCA-2 and RCA-3 concretes.

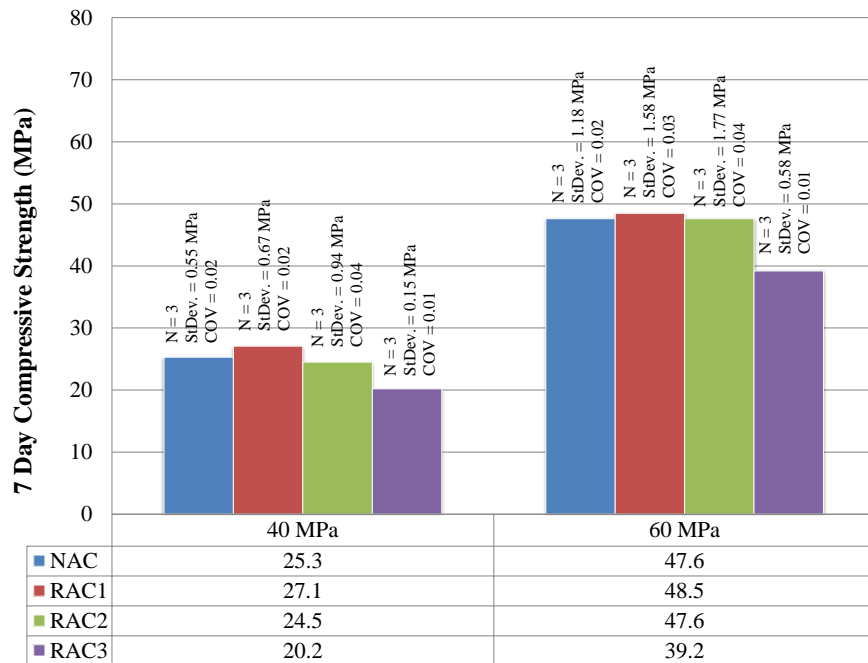


Figure 7.15 Early (7 day) compressive strength results and statistics for Phase 2 direct replacement mixtures

A similar trend existed when comparing the nominal (28 day) compressive strength results. After 28 days of curing, the 40 and 60 MPa RCA-1 concrete mixtures achieved compressive strengths that were 10% and 12% higher than the NA 40 and 60 MPa concrete, respectively.

Once again, these values are in contrast with trends found in the literature that have reported a decrease in compressive strength when natural aggregate is replaced with RCA (Xiao and Zhang, 2005, Chen et al., 2003, Topcu and Sengel, 2004, Etxeberria et al., 2007).

The 40 and 60 MPa RCA-2 concrete mixtures produced compressive strengths that were essentially the same as the NA concrete at 3% lower and 1% lower, respectively. The 40 and 60 MPa RCA-3 concrete mixtures produced compressive strengths that were significantly lower (19% each) than the NA concrete mixtures.

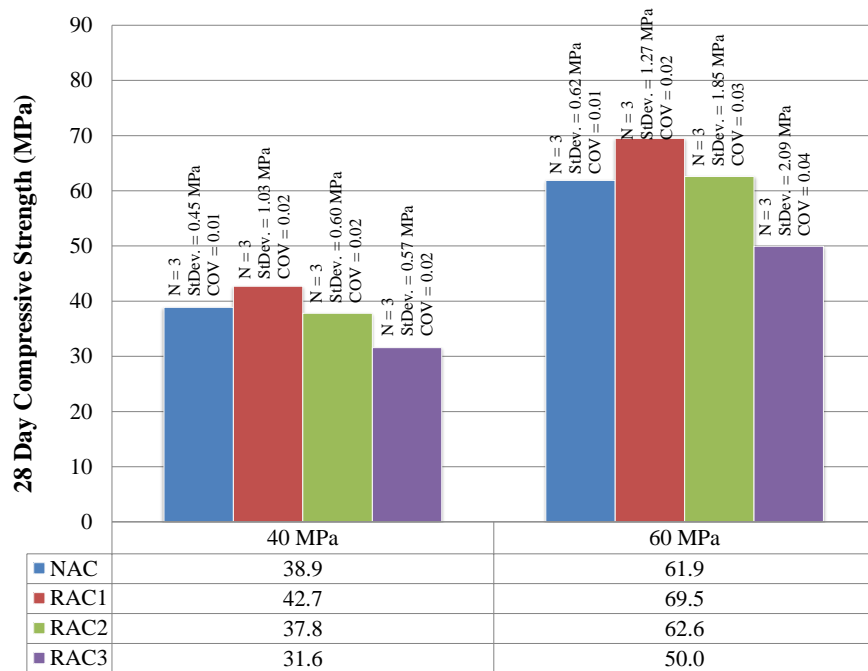


Figure 7.16 Nominal (28 day) compressive strength results and statistics for Phase 2 direct replacement mixtures

Overall, within batch variation of compressive strengths were fairly low at both the 40 and 60 MPa compressive strength levels (i.e., coefficient of variation values ranged between 1% and 4%). Compared to the control standards recommended by ACI Committee 214 (ACI 214, 2011), this range of coefficient of variation in compressive strengths for laboratory-produced concrete is considered “good” to “excellent”.

Figure 7.17 shows the early compressive strength normalized to the 28 day strength (f'_c). At the 40 MPa strength level, there was negligible difference in normalized early strength between all

four concrete types indicating that similar to the 30 MPa mixtures, replacing natural aggregate with RCA had little effect on early age strength gain. At the 60 MPa strength level, the NA concrete and RCA-2 concrete mixtures had similar normalized strengths (76% of f'_c at 7 days). The RCA-1 concrete achieved a higher percentage of its compressive strength after 7 days of curing (83.1% of f'_c at 7 days) than RCA-3 concrete (78.5% of f'_c).

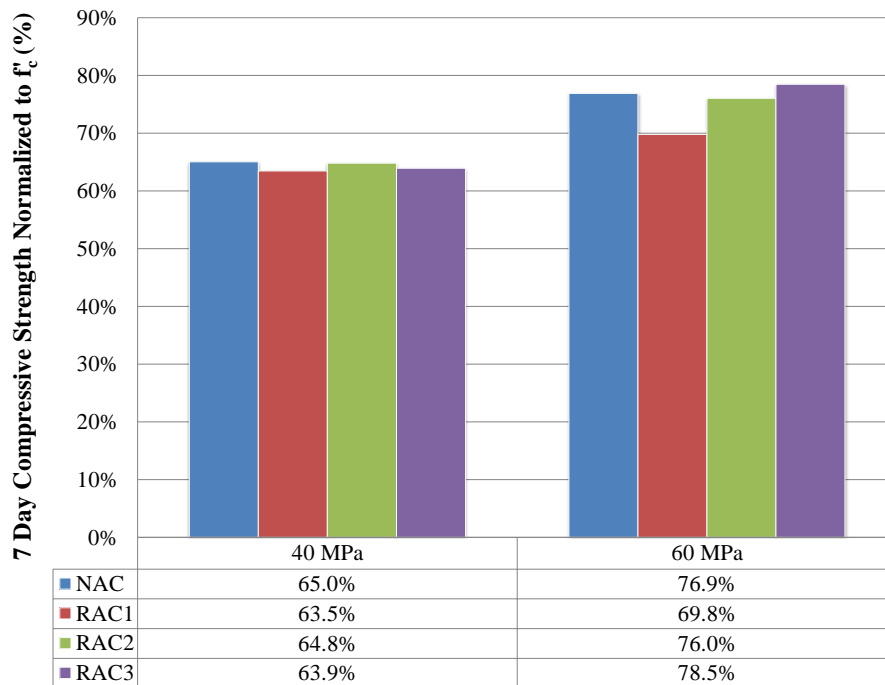


Figure 7.17 Early compressive strength normalized to 28 day strength for Phase 2 direct replacement mixtures

7.4.2.1 Statistical Significance of Compressive Strength Results

To determine whether the relative difference in 28 day compressive strengths between the various phase 2 direct replacement mixtures were statistically significant, a least significant difference (LSD) value was calculated using the data from each strength set. Using analysis of variance (ANOVA) and a modification to the Bonferroni t-test, the 5% LSD values for the 40 and 60 MPa direct replacement mixtures were calculated as 2.0 MPa and 4.4 MPa, respectively. As presented in Figure 7.16 and Table 7.2, the difference in 28 compressive strength values (at both 40 and 60 MPa strength levels) between the NA concrete and the RCA-1 concrete and the NA concrete and the RCA-3 concretes were greater than the 5% LSD value. This indicates that relative differences in compressive strength between the NA concrete mixtures and the RCA-1

and the RCA-3 concrete direct replacement mixtures are statistically significant. Therefore, this difference in the compressive strength results can be directly attributed to the effect of the RCA-1 and RCA-3 properties. Refer to Appendix B for sample LSD calculations.

7.4.2.2 Failure Mechanism and Effect of RCA Properties on Compressive Strength

To explain the effect that RCA has on concrete compressive strength, the failure planes of concrete cylinders for each concrete type were examined and were classified as being mainly around or mainly through the coarse aggregate (failure mode b or d, see Figure 7.1). A summary of the nominal compressive strengths and associated failure modes is presented in Table 7.2, Figure 7.18 and Figure 7.19 to facilitate the following discussion.

Table 7.2 Summary of nominal compressive strengths and failure modes (Phase 2 control and direct replacement mixtures)

Mix ID	28 day f'_c (MPa)	Failure Mode
NAC-40-C	38.9	Around more than 50% of aggregates
RAC1-40-D	42.7*	Equally around and through aggregates
RAC2-40-D	37.8	Through more than 50% of aggregates
RAC3-40-D	31.6*	Through more than 50% of aggregates
NAC-60-C	61.9	Equally around and through aggregates
RAC1-60-D	69.5*	Through more than 50% of aggregates
RAC2-60-D	62.6	Through more than 50% of aggregates
RAC3-60-D	50.0*	Through more than 50% of aggregates

* Indicates that the difference in f'_c from the NA concrete is statistically significant at the 95% confidence level. Recall 5% LSD for 40 MPa = 2.0 MPa and 5% LSD for 60 MPa = 4.4 MPa.

As previously mentioned, given that the direct replacement mixtures all had the same water-cement ratios (and correspondingly similar mortar strengths), failure planes that occur around the aggregate indicate that the mortar-aggregate interface or interfacial transition zone (ITZ) is the limiting strength factor. Failure planes that occur through the coarse aggregate indicate that the strength of the coarse aggregate itself is the limiting strength factor.

In the 40 MPa specimens, the failure planes occurred mainly around the aggregate for the NA concrete specimens, both around and through RCA-1 concrete specimens and mainly through the aggregate for the RCA-2 and RCA-3 specimens. Given that all direct replacement mixtures have the same water-cement ratios, the mortar strengths should also be similar. The only statistically significant differences in compressive strength exist between the NA and the RCA-1 and RCA-3

concrete mixtures. The higher compressive strength of the 40 MPa RCA-1 mixture is likely due to the stronger mortar-aggregate bond resulting from the more roughened RCA-1 surface texture in combination with its crushing strength. The lower strength of the RCA-3 particle itself seems to be the governing factor for concrete compressive strength as the failure planes passed mainly through the RCA-3 particles.

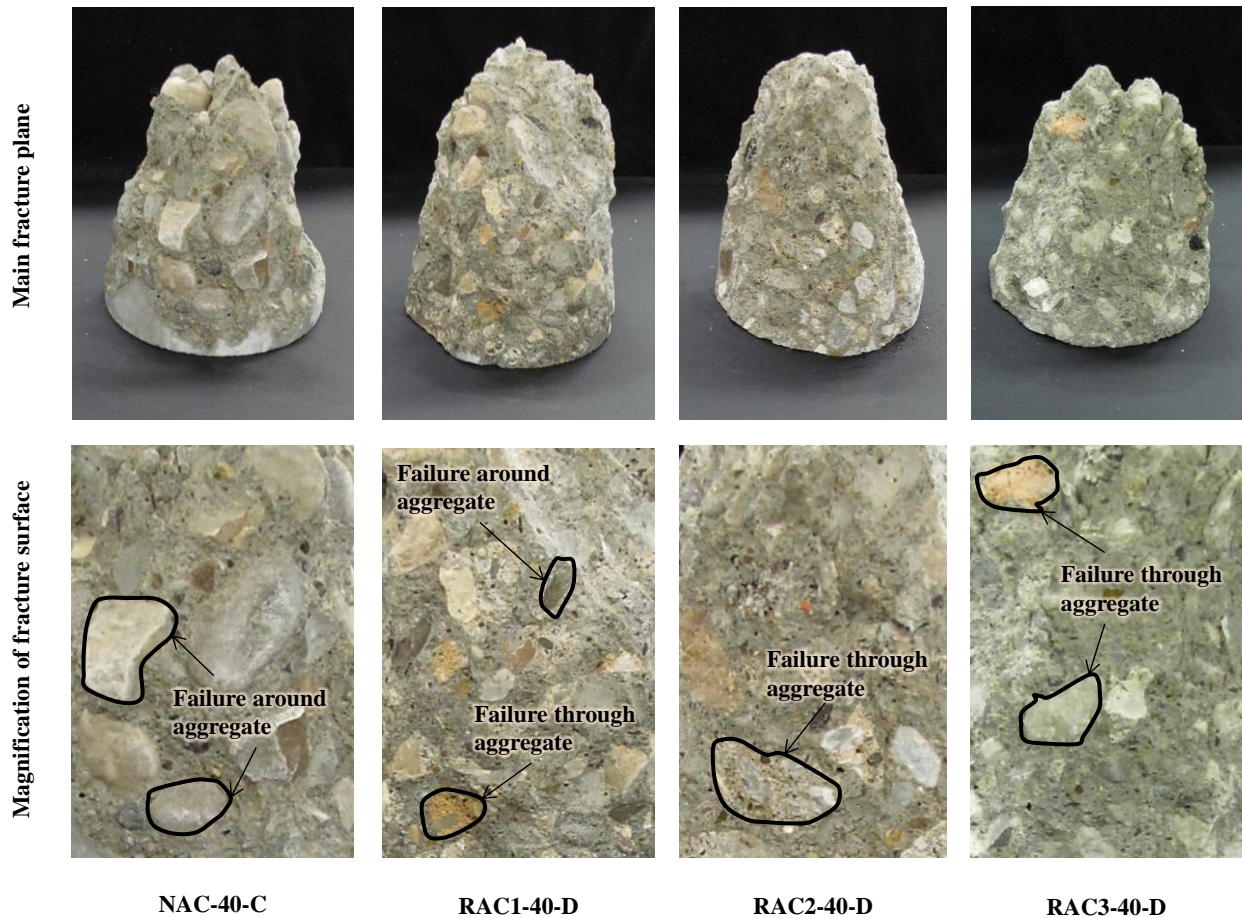


Figure 7.18 Fracture surfaces of the Phase 2 40 MPa direct replacement compressive strength specimens

In the 60 MPa specimens, the failure planes occurred both around and through the aggregate for the NA concrete specimens and mainly around the aggregate for the remaining RCA concrete specimens. It was also observed that the failure planes passing around the natural coarse aggregate occurred around the smoother river gravel component, whereas failures passing through the natural coarse aggregate occurred through the crushed angular component. For the NA concrete specimens, this suggests that the mortar-aggregate bond strength in combination with the tensile strength of the natural aggregate governed the concrete compressive strength. It

may also be inferred that if the natural coarse aggregate consisted of only angular particles then failures would have occurred mainly through the aggregate particles. Consequently, this would have increased the resulting compressive strength of the NA concrete. Statistically, the differences in compressive strength between the NA and the RCA-2 concrete were not significant. Therefore, it can be inferred that the tensile strength of the RCA-2 and the combination of mortar-aggregate bond strength and tensile strength of the natural aggregate are similar. The RCA-3 concrete had a significantly lower compressive strength than the NA concrete (i.e., 50.0 MPa versus 61.9 MPa), which suggests that the tensile strength of RCA-3 is considerably lower than the combined mortar-aggregate bond and tensile strength of the natural aggregate.

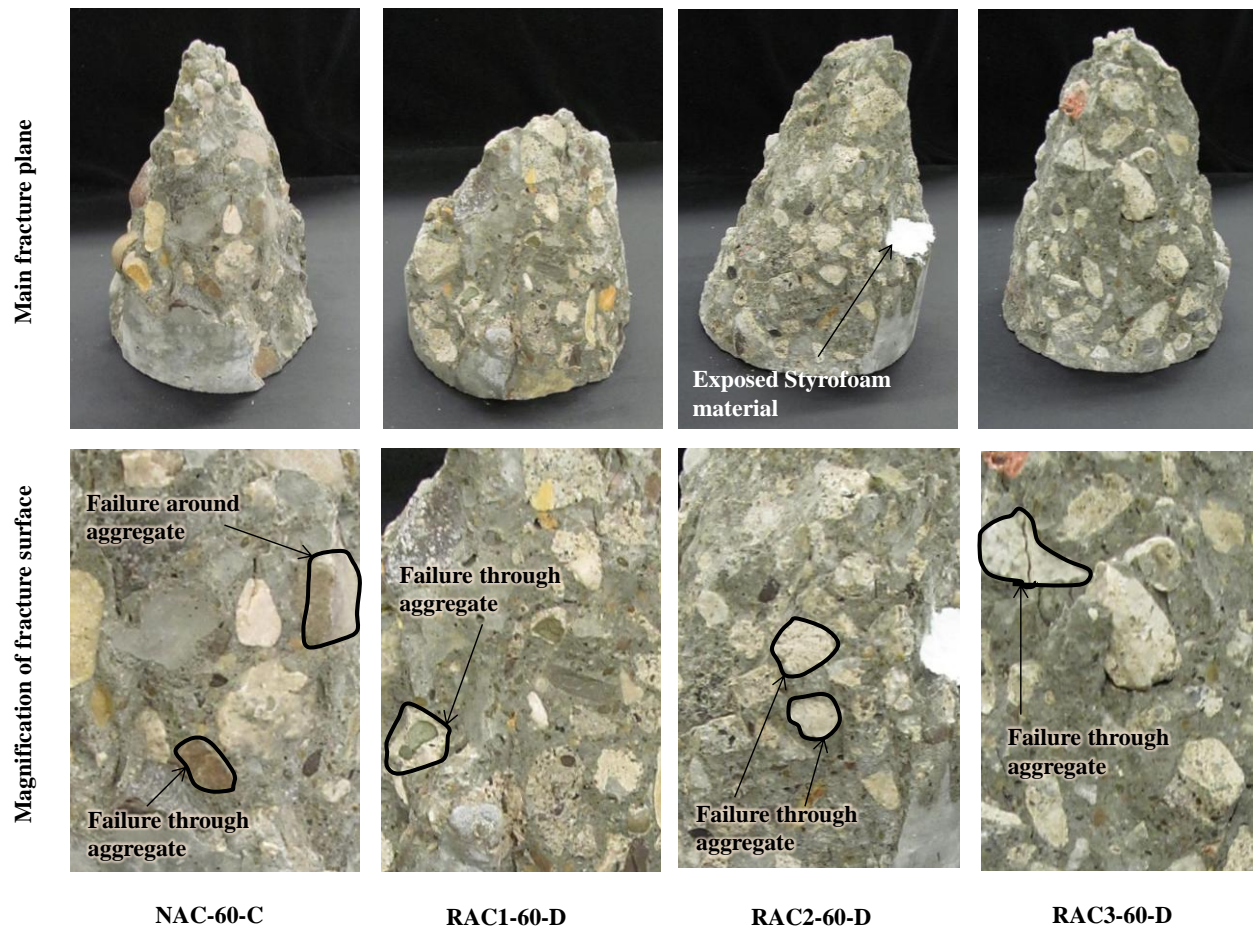


Figure 7.19 Fracture surfaces of the phase 2 60 MPa direct replacement compressive strength specimens

The RCA-1 concrete had a significantly (according to the calculated 5% LSD values) higher

compressive strength than the NA concrete (i.e., 69.5 MPa versus 61.9 MPa). Given that the fracture planes passed mainly through the RCA-1 particles and both around and through the natural aggregate particles, it may be inferred that the tensile strength of the RCA-1 is higher than the combined strength of the mortar-aggregate bond and tensile strength of the natural aggregate. Given that the crushing strength of the natural aggregate is higher than the RCA-1 (i.e., ACV of 18.2 and 23.1 for the natural aggregate and RCA-1, respectively), the NA concrete may have had the higher compressive strength if the failure planes passed mainly through the aggregate particles (i.e., if the natural aggregate particles consisted mainly of crushed/angular particles).

7.4.3 Splitting Tensile Strength Results

The Phase 2 direct replacement splitting tensile strength specimens were prepared using Batching Method A (smaller mixer with pre-soaking of coarse aggregates for 24 hours; refer to Section 5.2.2). The splitting tensile strength was measured for each of the Phase 2 direct replacement mixtures at 28 days and the results are presented in Figure 7.20.

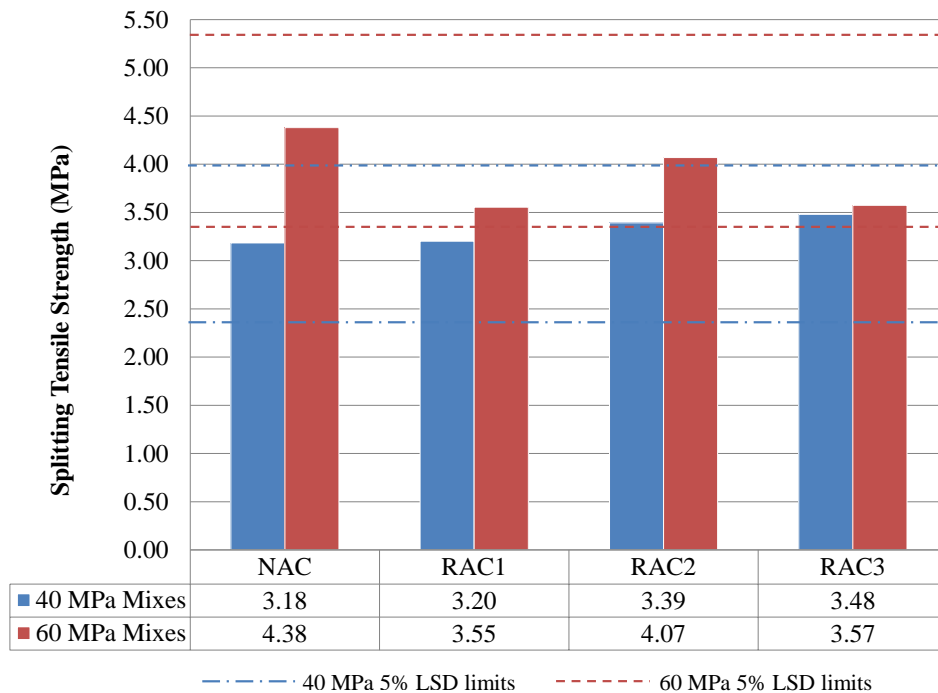


Figure 7.20 Splitting tensile strength results and least significant difference (LSD) limits

All splitting tensile strength specimens were tested in an air dry condition. In general, the 40

MPa mixtures produced splitting tensile strengths that were lower than the 60 MPa mixtures. No discernible trend between the relative splitting tensile strengths and properties of the aggregates was discovered. A statistical analysis of the data will be performed in Section 7.4.3.1 to assess whether the differences in splitting tensile strength are statistically significant.

The relationship between the splitting tensile strength and compressive strength of concrete has been well established for normal weight concrete. Neville (1997), the Oluokun (1991) and Mirza et al. (1979) have all proposed expressions that relate concrete splitting tensile strength to compressive strength, as presented in Equations 7.1, 7.2 and 7.3, respectively.

$$f_{ct} = 0.3(f'_c)^{2/3} \quad \text{Equation 7.1}$$

$$f_{ct} = 0.214(f'_c)^{0.69} \quad \text{Equation 7.2}$$

$$f_{ct} = 0.53\sqrt{f'_c} \quad \text{Equation 7.3}$$

Where,

f_{ct} = splitting tensile strength (MPa), and

f'_c = compressive strength (MPa).

The experimental splitting tensile strength results were plotted along with the above expressions and are presented in Figure 7.21. Note that each data point plotted on Figure 7.21 represents an average of three splitting tensile test results.

Equation 7.3 proposed by Mirza et al. (1979) provided the best fit of the experimental data. There is a general ascending trend line (solid line in Figure 7.21) which indicates that splitting tensile strength increases for an increase in compressive strength. However, a larger data set is required to eliminate some of the scatter shown on the plot.

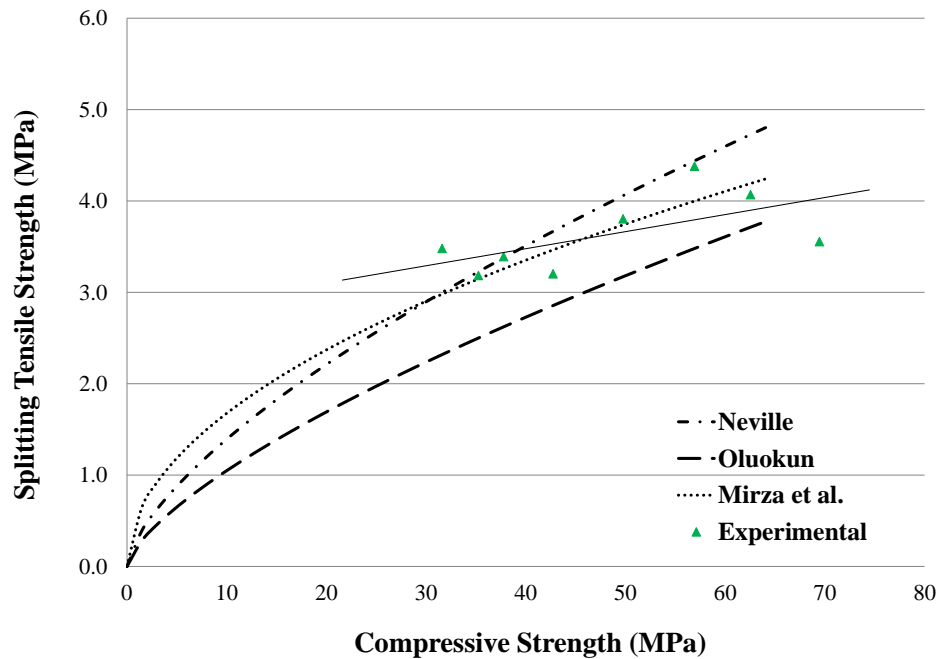


Figure 7.21 Relationship between compressive strength and splitting tensile strength (Phase 2 direct replacement mixtures)

7.4.3.1 Statistical Significance of Splitting Tensile Strength Results

To determine whether the relative difference in 28 day compressive strengths between the various Phase 2 direct replacement mixtures were statistically significant, a least significant difference (LSD) value was calculated using the data from each strength set. Using analysis of variance (ANOVA) and a modification to the Bonferroni t-test, the 5% LSD values for the splitting tensile strength values for the 40 and 60 MPa direct replacement mixtures were calculated and are tabulated in Table 7.3.

As presented in Table 7.3, the difference in 28 day splitting tensile strength values (at both 40 and 60 MPa strength levels) between the NA concrete and the RCA concrete were lower than the 5% LSD value. This indicates that relative differences in splitting tensile strength between the NA concrete mixtures and the RCA concrete direct replacement mixtures are not statistically significant. Therefore, the splitting tensile strength of all the RCA concrete types is statistically the same as the NA concrete at both the 40 and 60 MPa strength levels.

Table 7.3 Splitting tensile results, statistics and failure modes for Phase 2 direct replacement mixtures

Mix ID	f_{ct} (MPa)	Standard Deviation (MPa)	Coeff. of Variation	Failure Mode
NAC-40	3.18	0.15	0.05	Through more than 50% of aggregates
RAC1-40	3.20	0.20	0.06	Through more than 50% of aggregates
RAC2-40	3.39	0.41	0.12	Through more than 50% of aggregates
RAC3-40	3.48	0.26	0.08	Through more than 50% of aggregates
<i>5% LSD</i>	<i>0.78</i>			
NAC-60	4.38	0.15	0.03	Through more than 50% of aggregates
RAC1-60	3.55	0.07	0.02	Through more than 50% of aggregates
RAC2-60	4.07	0.50	0.12	Through more than 50% of aggregates
RAC3-60	3.80	0.47	0.12	Through more than 50% of aggregates
<i>5% LSD</i>	<i>1.00</i>			

7.4.3.2 Failure Mechanism and Effect of RCA Properties on Splitting Tensile Strength

Upon inspection of the fracture surfaces of the splitting tensile strength specimens (Figure 7.22 and Figure 7.23), it appears that the majority of the fracture planes for both the 40 and 60MPa specimens occurred mainly through the coarse aggregate.

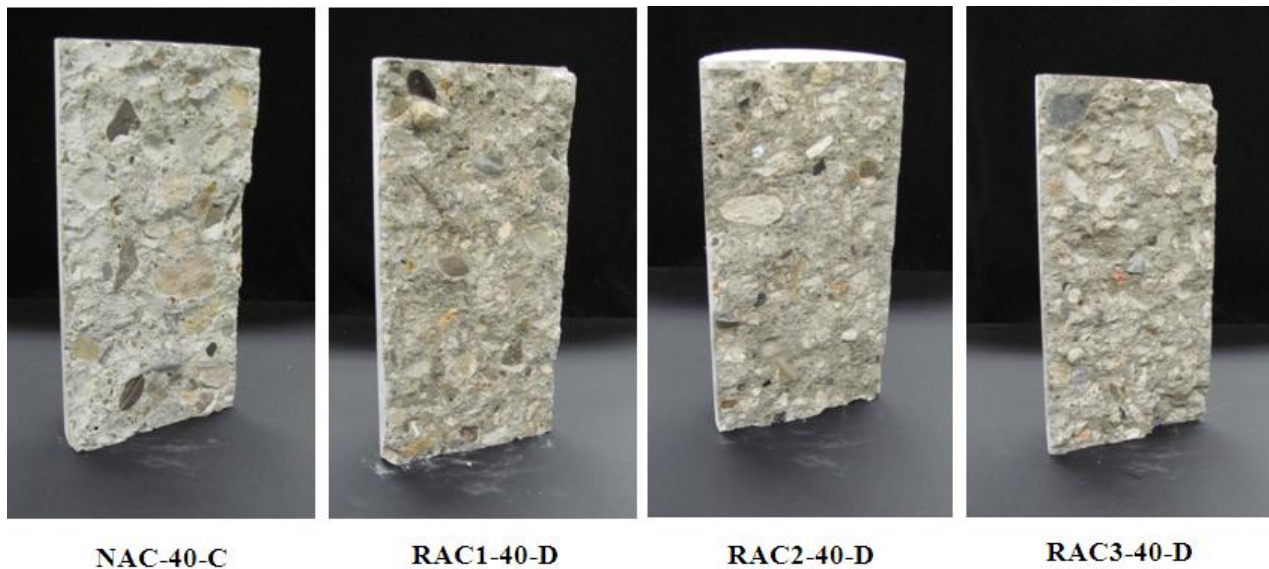


Figure 7.22 Fracture surfaces of the phase 2 40 MPa direct replacement splitting tensile strength specimens

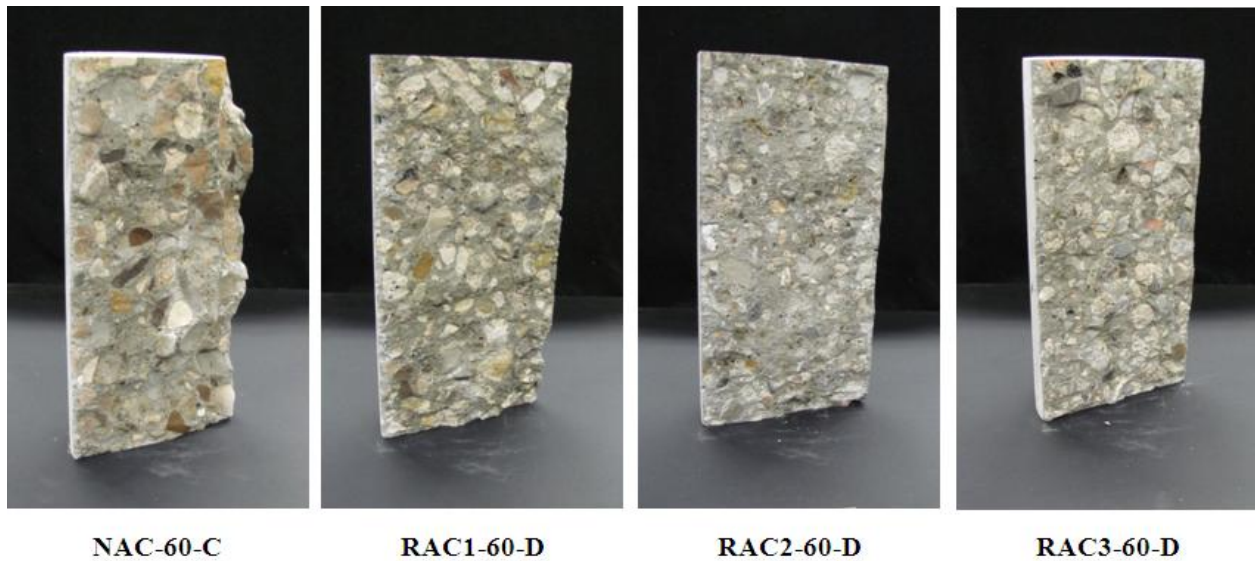


Figure 7.23 Fracture surfaces of the phase 2 60 MPa direct replacement splitting tensile strength specimens

This failure mode suggests that the strength of the coarse aggregate was the governing factor in determining the splitting tensile strength of the concrete specimens. As noted above, the relative differences in splitting tensile strengths (and $f_{ct}/f'_c{}^{1/2}$ values) between the four concrete types were not statistically significant. This suggests that for equal volume fractions of coarse aggregate and for equal water-cement ratios, splitting tensile strengths (and $f_{ct}/f'_c{}^{1/2}$ values) are insensitive to the properties of the RCAs used in this research. Given that the differences in compressive strengths between RCA and NA concrete were found to be statistically significant, the fact that the splitting tensile strengths were statistically insignificant indicates a relatively low relationship between compressive strength and splitting tensile strength for the RCA mixtures tested. Further discussion of the effect of aggregate strength (ACV) on concrete splitting tensile strength is provided later in Section 8.4.1.

7.4.4 Linear Coefficient of Thermal Expansion Results

To assess the effect of aggregate type on the thermal expansive properties of concrete, the linear coefficient of thermal expansion (LCTE) was measured for each concrete type. In general, the LCTE is the resultant of the thermal coefficient of hydrated cement paste, the thermal coefficient of the aggregate and the aggregate content in the mix (Neville, 1997). The procedures outlined in Chapter 6 were followed to determine the LCTE.

LCTE results are presented in Table 7.4 and Figure 7.24 and consist of an average of two companion specimens (A and B) that are themselves averages of two separate gauge measurements (see Section 6.2.6). Note that all LCTE specimens were kept in an air dry moisture condition throughout the duration of testing.

Table 7.4 Linear coefficient of thermal expansion test results (Phase 2 control and direct replacement mixtures)

Concrete Type	LCTE Specimen A $\times 10^{-6}/^{\circ}\text{C}$	LCTE Specimen B $\times 10^{-6}/^{\circ}\text{C}$	Average LCTE $\times 10^{-6}/^{\circ}\text{C}$
NAC-40	8.44	7.51	7.97
RAC1-40	8.62	9.27	8.95
RAC2-40	8.81	8.16	8.48
RAC3-40	8.62	8.53	8.58
5% LSD			1.84
NAC-60	9.73	8.99	9.36
RAC1-60	9.55	9.92	9.73
RAC2-60	9.46	9.36	9.41
RAC3-60	9.46	9.83	9.64
5% LSD			1.28

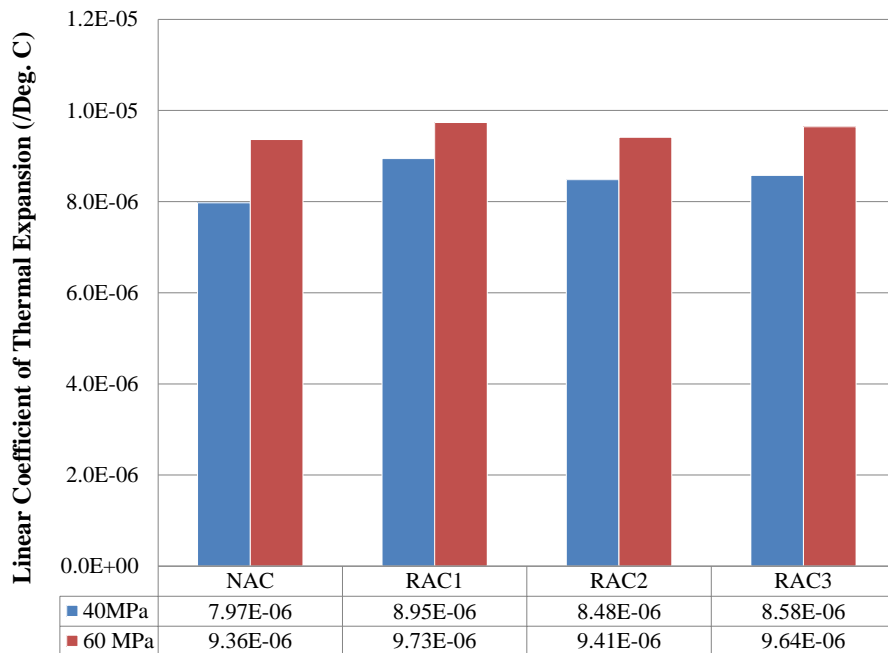


Figure 7.24 Linear coefficient of thermal expansion test results (Phase 2 direct replacement mixtures)

Given that LCTE varies with aggregate content and given that all the direct replacement mixtures

(within a given strength level) had identical water-cement ratios (i.e., hydrated paste properties), it seems reasonable that there were no statistical differences in LCTE values. Since LCTE varies with the coefficient of thermal expansion of aggregate the data also suggest that all aggregate types (natural and RCA) have similar LCTE values. Although the LCTE values were not statistically different when comparing the NA concrete to the RCA concretes, a difference does exist between the 40 and 60 MPa samples. This suggests that more than just the aggregate volume influences the LCTE values.

Figure 7.25 presents the relationship between LCTE, water-cement ratio and aggregate density. A strong relationship ($R^2 = 0.88$) exists between the LCTE, water-cement ratio and aggregate density. Note that only the aggregate density varies between concrete types of a certain strength level. Therefore, although differences in LCTE are statistically insignificant, there is still an effect of changing coarse aggregate density on the LCTE of concrete.

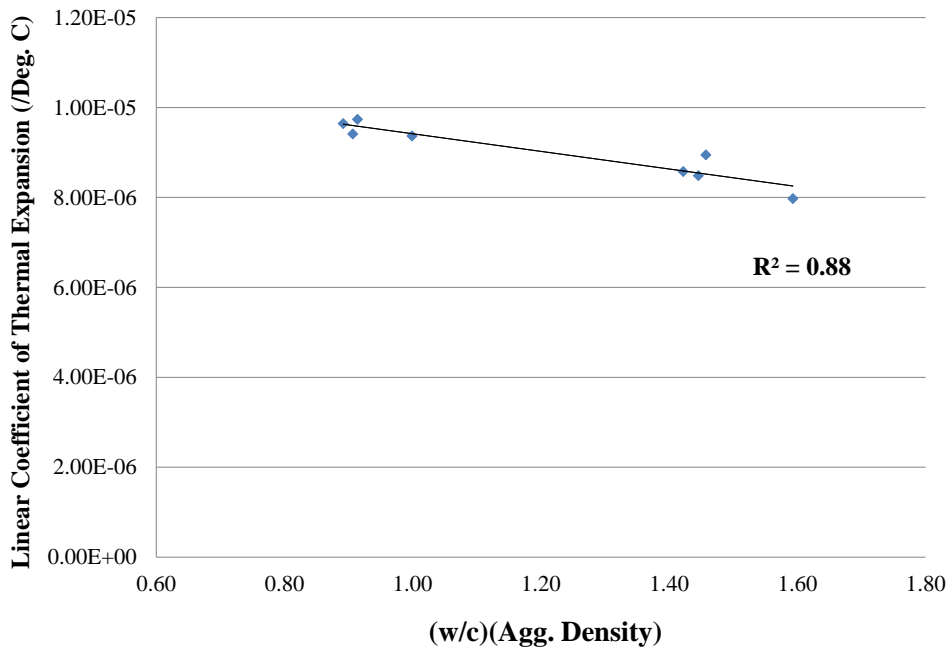


Figure 7.25 Relationship between LCCTE, water-cement ratio and aggregate density (Phase 2 direct replacement mixtures)

7.4.5 Modulus of Elasticity and Poisson's Ratio Results

The modulus of elasticity was measured for the Phase 2 direct replacement mixtures to determine the effect that replacing natural aggregate with RCA has on concrete stiffness. Refer to Chapter

6 for test setup, procedures and instrumentation. All modulus of elasticity specimens were tested in an air dry condition. Figure 7.26 presents the modulus of elasticity results for the 40 and 60 MPa mixtures. The 40 MPa NAC specimens on average had elastic modulus values that were 1%, 9%, and 19% higher than the RCA-1, RCA-2, and RCA-3 concrete specimens, respectively. The 60 MPa specimens on average had elastic modulus values that were 6%, 12%, and 21% higher than the RCA-1, RCA-2, and RCA-3 concrete specimens, respectively. The differences in moduli of elasticity are in part due to the varying compressive strengths. Therefore, the experimental values were normalized with respect to $f_c^{1/2}$.

Based on the values presented in Figure 7.27, the 40 MPa NAC specimens had normalized elastic modulus values that were 6%, 8%, and 10% higher than the RCA-1, RCA-2, and RCA-3 concrete specimens, respectively. The 60 MPa NAC specimens had normalized elastic modulus values that were 11%, 13%, and 13% higher than the RCA-1, RCA-2, and RCA-3 concrete specimens, respectively. This reduction in modulus of elasticity results seems to be in agreement with published results (Rahal, 2007 and Etxeberria et al., 2006), and reflect the influence of RCA type on the modulus of elasticity irrespective of compressive strength.

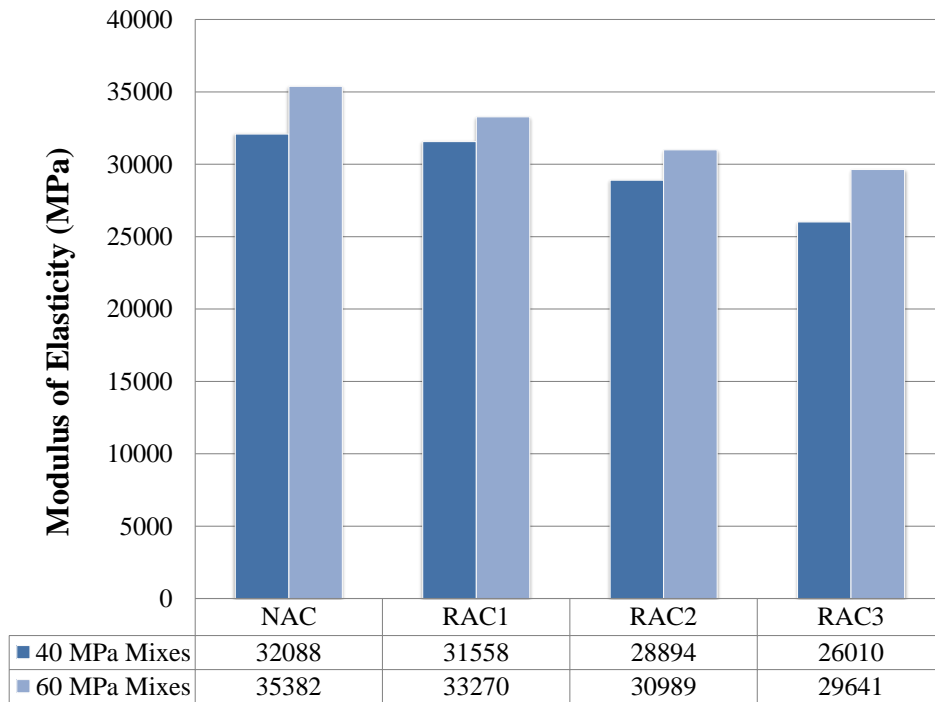


Figure 7.26 Modulus of elasticity results (Phase 2 direct replacement mixtures)

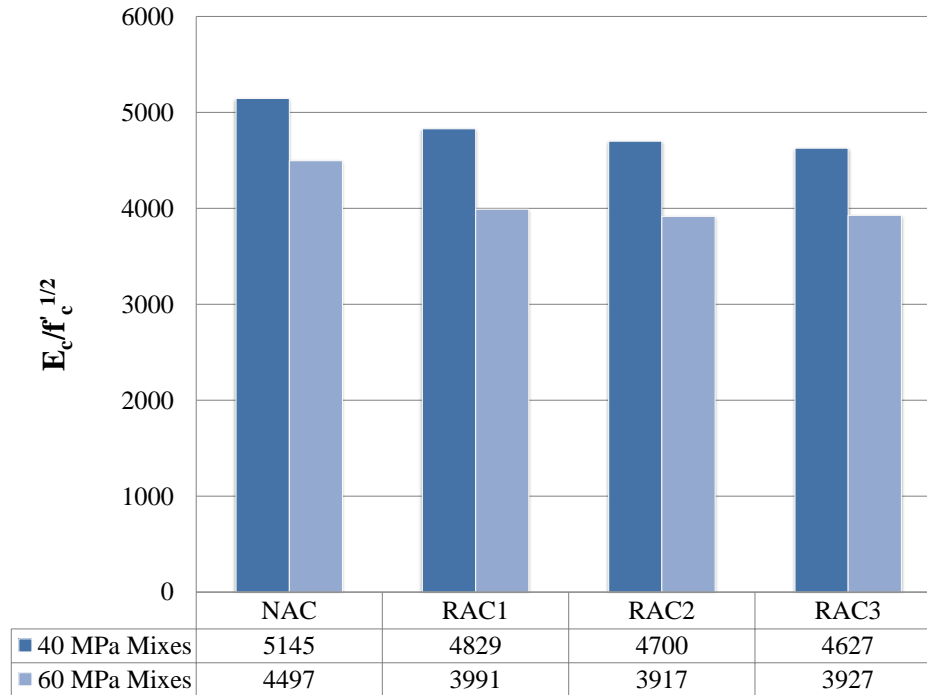


Figure 7.27 Modulus of elasticity results normalized with respect to $f_c^{1/2}$ (Phase 2 direct replacement specimens)

7.4.5.1 Statistical Significance of Modulus of Elasticity Results

Least significant difference (LSD) values were calculated using the data from each strength set (i.e., 40 and 60 MPa) once again to determine whether the relative difference in moduli of elasticity and $E_c/f_c^{1/2}$ values between the various Phase 2 direct replacement mixtures were statistically significant. The 5% LSD values for the modulus of elasticity and $E_c/f_c^{1/2}$ values for the 40 and 60 MPa direct replacement mixtures along with their sample statistics (i.e., standard deviation and coefficient of variation) were calculated and are tabulated in Table 7.5. Note that each modulus of elasticity value reported represents an average of three specimens. In general, specimen-to-specimen coefficient of variation values were relatively low (i.e., 5% or lower).

As presented in Table 7.5, the difference in moduli of elasticity (at both 40 and 60 MPa strength levels) between the NA concrete and the RCA-1 concrete were lower than the 5% LSD value. This indicates that relative differences in modulus of elasticity (E_c) between the NA concrete mixtures and the RCA-1 concrete direct replacement mixtures are not statistically significant. The differences in E_c between the NA concrete mixture and the RCA-2 and RCA-3 mixtures however, were statistically significant.

Table 7.5 Modulus of elasticity results and statistics for Phase 2 direct replacement mixtures

Mix ID	E_c (MPa)	Standard Deviation (MPa)	Coeff. of Variation	$E_c/f_c^{1/2}$
NAC-40	32088	1135	0.04	5145
RAC1-40	31558	747	0.02	4829
RAC2-40	28894	908	0.03	4700
RAC3-40	26010	1179	0.05	4627
<i>5% LSD</i>	<i>2861</i>			<i>475</i>
NAC-60	35382	843	0.02	4497
RAC1-60	33270	559	0.02	3991
RAC2-60	30989	875	0.03	3917
RAC3-60	29641	969	0.03	3927
<i>5% LSD</i>	<i>2345</i>			<i>307</i>

In order to eliminate the effect of compressive strength on modulus of elasticity and determine whether significant differences exist between the RCA and NA concretes, the 5% LSD values for the $E_c/f_c^{1/2}$ values must be evaluated. Based on the results presented in Table 7.5, at the 40 MPa strength level, only the $E_c/f_c^{1/2}$ value for RCA-3 concrete was statistically different from the NA concrete. At the 60 MPa level, all RCA concretes (RCA-1, RCA-2, and RCA-3) had $E_c/f_c^{1/2}$ values that were statistically different from the NA concrete. This finding illustrates that at higher compressive strength levels, and with equivalent water-cement ratios, replacing natural aggregate with RCA can lead to a significant reduction in modulus of elasticity of the resulting concrete.

7.4.5.2 Effect of RCA Properties on Modulus of Elasticity

The modulus of elasticity of concrete is dependent on the concrete compressive strength, the volumetric proportion of aggregate and the modulus of elasticity of the aggregate (Neville, 1997). Given that each direct replacement mix had the same coarse aggregate volume and each modulus of elasticity value was normalized with respect to $f_c^{1/2}$ the difference in coarse aggregate elastic moduli must explain the differences between the various concrete types. Often, the modulus of elasticity of the aggregate is unknown and CSA A23.3-04 (Clause 8.6.2.2) and other expressions typically use the density of concrete raised to the power of 1.5 as an indirect estimate of this property (Pauw, 1960) as in Equation 7.5.

$$E_c = (3300\sqrt{f'_c} + 6900)(\gamma_c/2300)^{1.5} \quad \text{Equation 7.5}$$

Where,

E_c = static modulus of elasticity of concrete in compression (MPa)

f'_c = concrete cylinder compressive strength (MPa)

γ_c = concrete hardened density (kg/m^3)

Once elastic modulus values were normalized with respect to compressive strength and the concrete hardened density, the differences between the various concrete types decreased significantly, as evidenced by Figure 7.28. Figure 7.29 was plotted to confirm that the modulus of elasticity is proportional to the hardened density of concrete. Using the relationship defined in Figure 7.13 which presents the relationship between aggregate density and concrete hardened density along with the relationship provided by Figure 7.29, it may be deduced that the bulk density of coarse aggregate (natural and RCA) is proportional to the modulus of elasticity of concrete. This inference was confirmed in Figure 7.30 that shows a fairly strong correlation between the coarse aggregate bulk density and concrete elastic modulus, especially for the 60 MPa specimens.

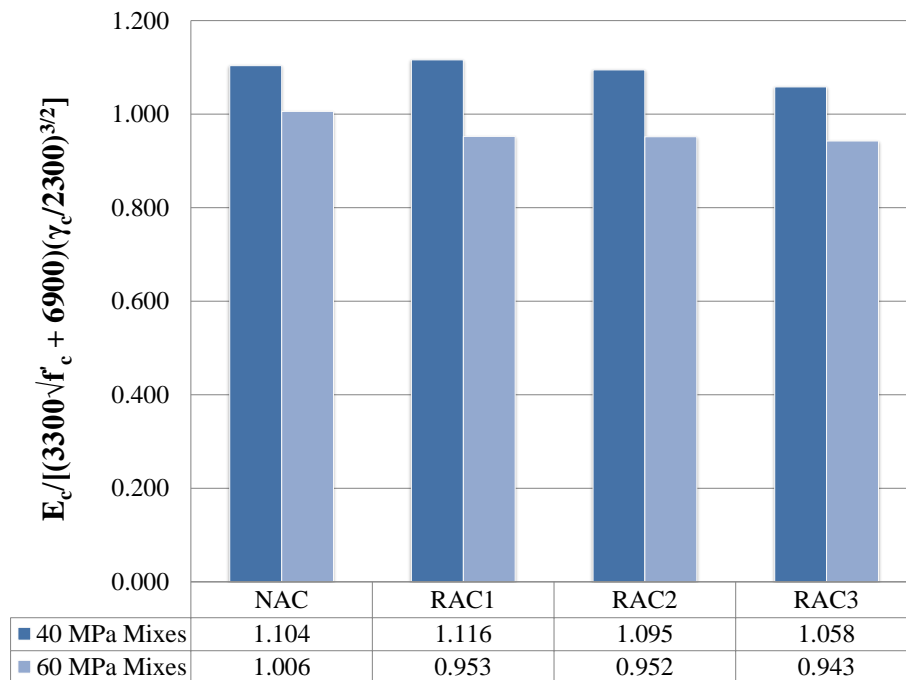


Figure 7.28 Modulus of elasticity results normalized with respect to f'_c and hardened density

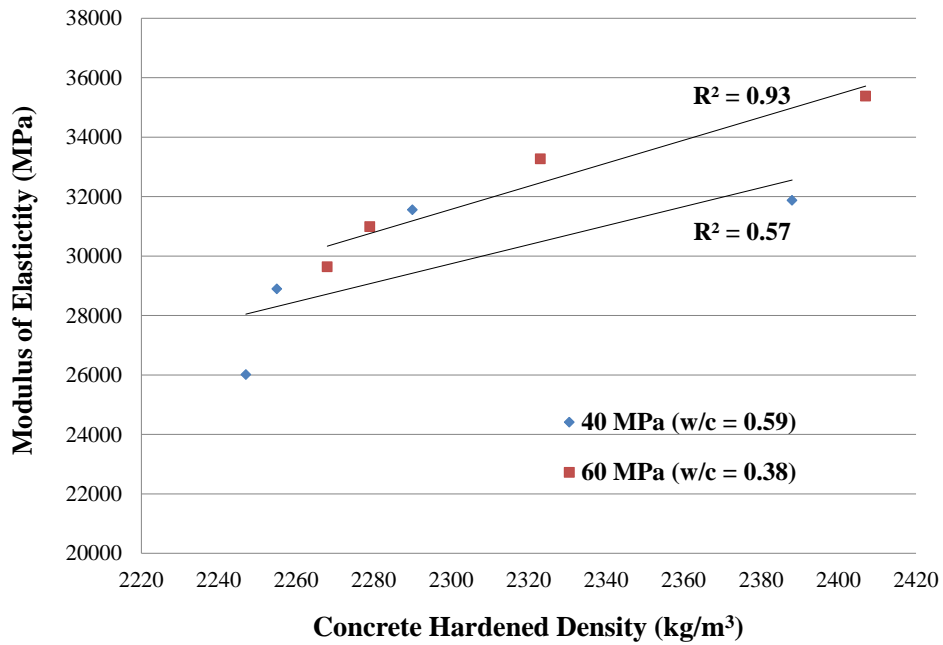


Figure 7.29 Relationship between modulus of elasticity and concrete hardened density

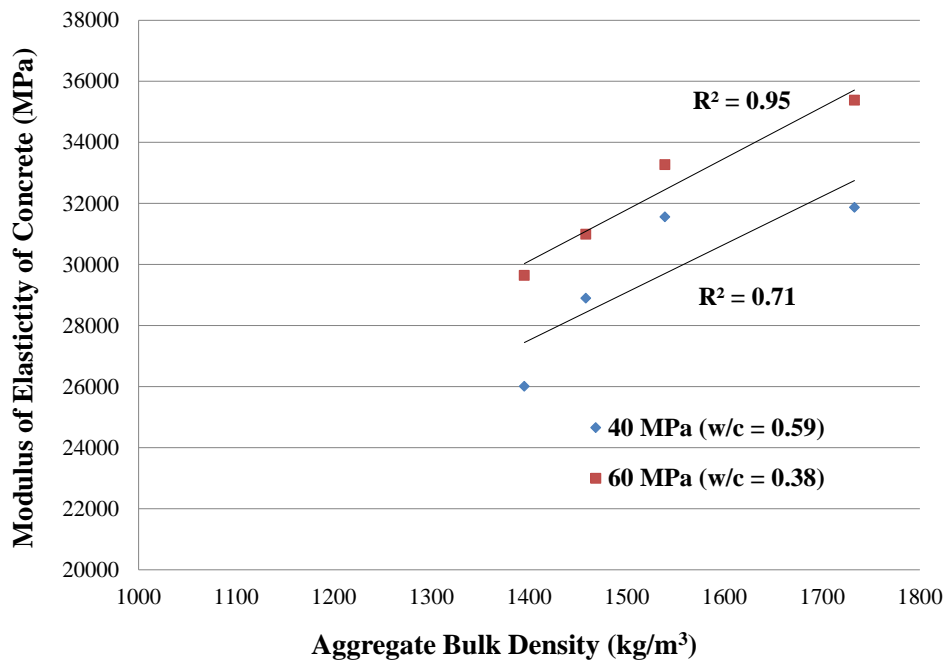


Figure 7.30 Relationship between coarse aggregate bulk density and modulus of elasticity of concrete (Phase 2 direct replacement mixtures)

The modulus of elasticity of concrete seems to be directly related to the elastic modulus of the

coarse aggregate itself of which, coarse aggregate bulk density is an indirect indication. In the case of RCA, the original modulus of elasticity of the concrete from which it was derived is rarely known, and consequently the actual modulus of elasticity of RCA is rarely known. Recall that in Chapter 4, the average secant modulus of elasticity of bulk aggregate measured during the ACV test was determined to be a proportional measure of the actual modulus of elasticity of aggregate. Figure 7.31 presents the relationship between the modulus of elasticity of concrete and the average secant modulus of bulk aggregate determined using the ACV test.

A very strong correlation was found for the 40 MPa mixtures whereas a less significant relation exists for the 60 MPa mixtures. These results provide a promising means of estimating the elastic modulus of RCA concrete given the modulus of elasticity of bulk coarse RCA. In addition, using the ACV test to calculate an average secant modulus of elasticity of confined bulk aggregate is a feasible method of obtaining a proportional modulus of elasticity of coarse RCA. These results also provide further explanations for the differences in elastic modulus measured between the NA concrete and the RCA concretes.

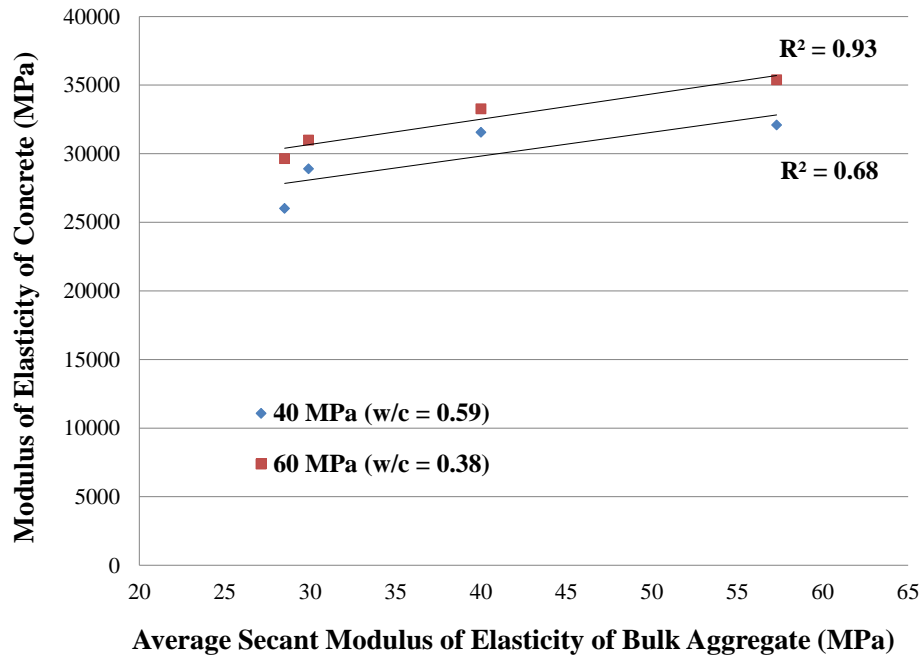


Figure 7.31 Relationship between modulus of elasticity of concrete and modulus of elasticity of bulk aggregate (Phase 2 direct replacement mixtures)

7.4.5.3 Poisson's Ratio Test Results

Table 7.6 presents the Poisson's ratios for the control and direct replacement mixtures along with the coefficient of variation (C.O.V.) between the Poisson's ratios of the various concrete types, and the 5% least significant difference (5% LSD) values for each strength level data set. By examining the Poisson's ratio data and the 5% LSD values, the results show that no significant difference exists between the NA and the RCA concretes. In addition, the coefficient of variation values between each concrete type are fairly low which further validates that no significant difference in Poisson's ration exists between the NA and RCA concretes. Therefore, the volume replacement of natural aggregate with RCA did not have an effect on the Poisson's ratio of the resulting concrete. In comparing the 40 and 60 MPa mixtures, there appears to be a significant difference in Poisson's ratio (i.e., 0.20 versus 0.26). A further discussion and comparison of the Poisson's ratios measured for the direct replacement and strength-based mixtures and the overall effect of RCA properties on the Poisson's ratio is included in a later Section 8.3.5.2.

Table 7.6 Poisson's ratio test results (Phase 2 control and direct replacement mixtures)

Concrete Type	Poisson's Ratio	Standard Deviation	C.O.V.
NAC-40	0.21	0.016	0.076
RAC1-40	0.20	0.008	0.038
RAC2-40	0.19	0.018	0.093
RAC3-40	0.21	0.011	0.052
Average	0.20		
C.O.V.	0.05		
5% LSD	0.04		
NAC-60	0.25	0.028	0.107
RAC1-60	0.25	0.002	0.008
RAC2-60	0.27	0.028	0.103
RAC3-60	0.25	0.010	0.040
Average	0.26		
C.O.V.	0.04		
5% LSD	0.06		

7.4.6 Conclusions from Phase 2 Mixtures

The following conclusions are based on the evaluation and findings of the Phase 2 direct replacement mixture testing.

1. After replacing the natural aggregate with equivalent volumes of RCA and maintaining equivalent water-cement ratios, slump values of the RCA-1, RCA-2 and RCA-3 concretes were up to 78%, 61%, and 35% lower, respectively. Slump loss values were a result of the more roughened surface texture of the RCA particles which increased the inter-particle friction in the fresh concrete.
2. The strong correlation found to exist in the Phase 1 direct replacement mixtures between adhered surface moisture of aggregate particles (which provides an indirect measure of surface roughness) and slump was confirmed in the Phase 2 direct replacement mixtures testing.
3. The NA concrete mixtures had the highest hardened densities followed by the RCA-1, RCA-2, and RCA-3 mixtures. This trend is a direct result of the excellent correlation ($R^2 = 0.98$) between bulk density of coarse aggregate and hardened density of concrete.
4. Within the 40 MPa direct replacement mixtures, the RCA-1, RCA-2 and RCA-3 mixtures had compressive strengths that were 10% higher, 3% lower, and 19% lower than the NA concrete, respectively. The higher compressive strength values of the 40 MPa RCA-1 concrete mixtures are likely due to the stronger mortar-aggregate bond between the RCA and the new mortar. The lower compressive strength of the 40 MPa RCA-3 concrete mixtures is likely due to the reduced strength of the RCA-3 particles themselves (i.e., as indicated by a higher ACV compared to the natural aggregate).
5. Within the 60 MPa direct replacement mixtures, the RCA-1, RCA-2 and RCA-3 concrete mixtures had higher compressive strengths that were 12% higher, 1% lower, and 19% lower than the NA concrete, respectively. Upon examination of the fracture surface of the NA concrete and RCA-1 concrete, the higher strength of the RCA-1 concrete is due to the higher strength of the RCA-1 as compared to the combined strength of the mortar-aggregate bond and tensile strength of the natural aggregate. The lower compressive strength of the RCA-3 concrete is due to the lower strength of the RCA-3 particles.
6. The relative differences in splitting tensile strengths and $f_{ct}/f_c^{1/2}$ values for the various concrete types (i.e., the NA and RCA concretes) were found to be statistically insignificant. This was most likely a result of all direct replacement mixtures having equivalent volumes of coarse aggregate.
7. LCTE values for the 60 MPa mixtures were higher than the 40 MPa mixtures.

Differences in LCTE values between the various concrete types were found to be statistically insignificant.

8. It was concluded that for equal volume fractions of coarse aggregate and for equal water-cement ratios, values of $f_{ct}/f_c^{1/2}$ were insensitive to the properties of the aggregates used in this experimental study.
9. In general, fully replacing natural aggregate with RCA while maintaining a constant water-cement ratio reduces the modulus of elasticity. The 40 MPa NA concrete specimens had $E_c/f_c^{1/2}$ values that were 6%, 9%, and 11% higher than the RCA-1, RCA-2, and RCA-3 concrete specimens, respectively. The 60 MPa NA concrete specimens had $E_c/f_c^{1/2}$ values that were 5%, 8%, and 10% higher than the RCA-1, RCA-2, and RCA-3 concrete specimens, respectively. It was found that the elastic modulus of concrete correlates well with both the average secant modulus of elasticity of bulk aggregate (determined during ACV testing) and the aggregate bulk density.

7.5 Overall Conclusions

The following conclusions are those derived from the combined findings of the Phase 1 and 2 direct replacement mixtures.

1. After replacing the natural aggregate with equivalent volumes of RCA and maintaining equivalent water-cement ratios, slump values of the RCA concretes were up to 78% lower. Slump loss values were a direct result of the more roughened surface texture of the RCA particles which increased the inter-particle friction in the fresh concrete.
2. A good correlation (R^2 of 0.84 and 0.91) exists between adhered surface moisture of aggregate particles (which provides an indirect measure of surface roughness) and slump.
3. The NA concrete mixtures had the highest hardened densities followed by the RCA-1, RCA-2, and RCA-3 concrete mixtures. This trend is a direct result of the excellent correlation ($R^2 = 0.98$) between bulk density of coarse aggregate and hardened density of concrete.
4. On average, the RCA-1, RCA-2, and RCA-3 concrete specimens had compressive strengths that were between 7 and 22% higher, 1% lower and 7% higher, and 19% lower than the NA concrete specimens, respectively. Overall, the RCA concrete tested as part

of this study had compressive strengths ranging between 81 and 122% of the compressive strength of NA concrete. In the case of the lower strength mixtures (i.e., 30 and 40 MPa), the mortar-aggregate bond strength seemed to be the limiting strength factor. In the higher strength mixtures (i.e., 50 and 60 MPa), a combination of mortar-aggregate bond strength and aggregate tensile strength was the limiting factor controlling the compressive strength.

5. The relative differences in splitting tensile strengths and $f_{ct}/f_c^{1/2}$ values for the various concrete types were found to be statistically insignificant. This was most likely a result of all direct replacement mixtures having equivalent volumes of coarse aggregate.
6. Differences in LCTE values between the various concrete types were found to be statistically insignificant. However, a very good correlations ($R^2 = 0.88$) was found to exist between the LCTE, water-cement ratio, and aggregate density. Note that only the aggregate density varies between concrete types of a certain strength level. Therefore, although differences in LCTE are not statistically significant, there is still an effect of changing coarse aggregate density on the LCTE of concrete.
7. For equal volume fractions of coarse aggregate (i.e., in direct replacement mixtures), values of $f_{ct}/f_c^{1/2}$ were insensitive to the properties of the aggregates used in this experimental study.
8. By fully replacing natural aggregate with RCA, modulus of elasticity values normalized with respect to $f_c^{1/2}$ were reduced by as much as to 10% as compared to equivalent NA concrete. Strong correlations were found between the elastic modulus of concrete and both the average secant modulus of elasticity of bulk aggregate (determined during ACV testing) and the aggregate bulk density.

Chapter 8: Evaluation of Strength-Based Mixture Test Results

8.1 Overview

As discussed in Section 5.1.3, the strength-based mixtures were designed to achieve similar compressive strength and slump values as the NA concrete mixtures. The following sections present and discuss the fresh and hardened properties of the strength-based mixtures. Properties measured include, workability (slump), hardened density, compressive strength (early age and nominal), splitting tensile strength, linear coefficient of thermal expansion, modulus of elasticity, Poisson’s ratio, modulus of rupture and fracture energy. Refer to Chapter 6 for a detailed outline of all the concrete testing procedures. Evaluation of the results for Phase 1 and 2 are presented separately and then a combined evaluation is presented at the end of the chapter. To further clarify the purpose of the strength-based mixtures, Figure 8.1 summarizes the various concrete properties tested in this chapter and the motivation for their testing and evaluation.

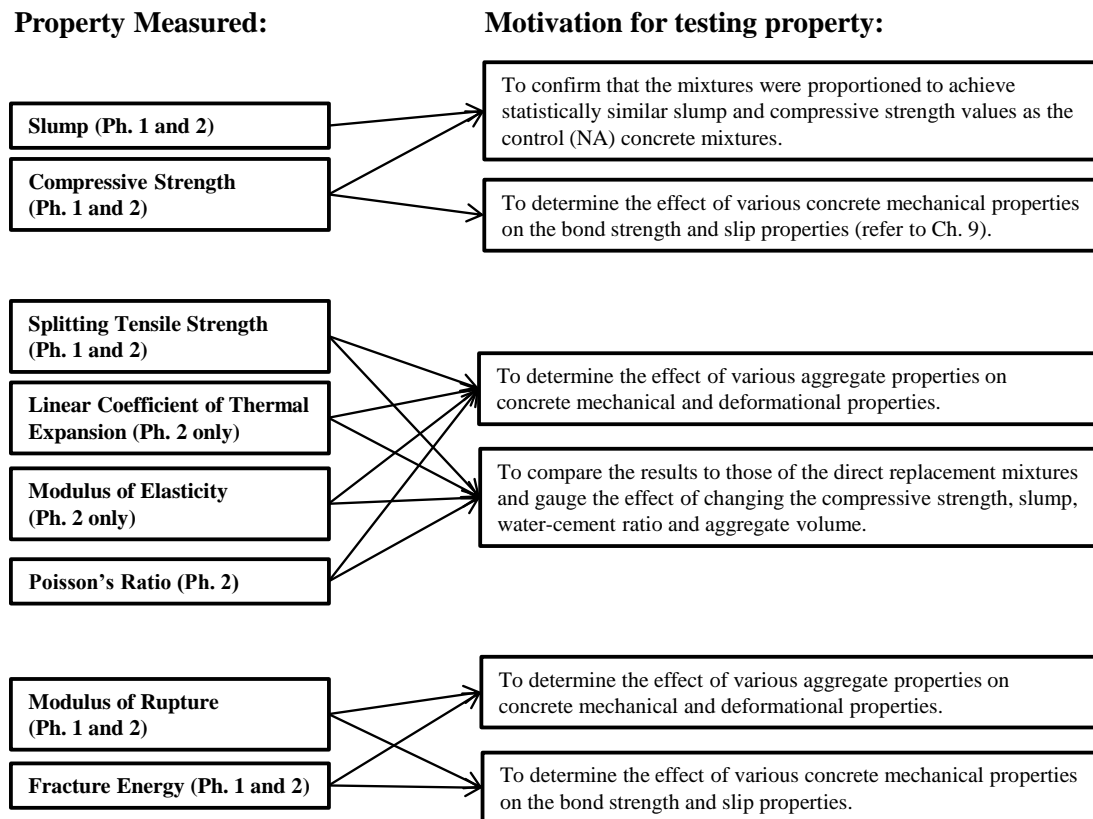


Figure 8.1 Overview of strength-based mixtures properties and motivation for testing

In addition to the information presented in Figure 8.1, the effect of particular aggregate properties on basic concrete mixture proportions (i.e., cement content, water demand and water-binder ratio) as they pertain to the direct replacement mixtures is also evaluated.

8.2 Phase 1 Strength-Based Mixtures (30 and 50 MPa)

The following discussion of the strength-based mixture properties is based on the results from mass batching of Phase 1 beam-end and fracture energy specimens (refer to Section 5.6 for a description of mixture proportion phases). These mixtures were batched using batching Method B in which the aggregates were pre-wetted prior to batching, and a larger 0.1 m³ concrete pan mixer was used (see Section 5.2.2 for details). It should be noted that the slump and compressive strength results of the Phase 1 strength-based mixtures batched using Method A (refer to Section 5.6) have not been reported in this thesis as the difference in compressive strength between the NA mixtures and the RCA-1 and RCA-2 concrete mixtures were statistically significant. Therefore, based on these results, it was not possible to isolate the effect of the aggregate on the concrete properties that may be influenced by the compressive strength. Similarly, the effect of RCA properties on the required concrete mixtures proportions for the Phase 1 mixtures could not be assessed because the direct replacement mixtures were batched using Method A and the strength-based mixtures were batched using Method B (see further discussion in Section 8.5).

8.2.1 Workability

All strength-based mixtures were proportioned to achieve slump values between 75 and 125 mm. As presented in Figure 8.2, all slump values were within the specified 75 to 125 mm range.

In general, the 30 MPa mixtures had a more stony and granular consistency than the 50 MPa mixtures which had a more creamy consistency. Differences in consistency between the NA concrete and the RCA concrete mixtures were negligible. Once again the slump results presented in Figure 8.2 are those measured from the concrete batched using Batching Method B (refer to Section 5.2.2 for a description of Batching Methods).

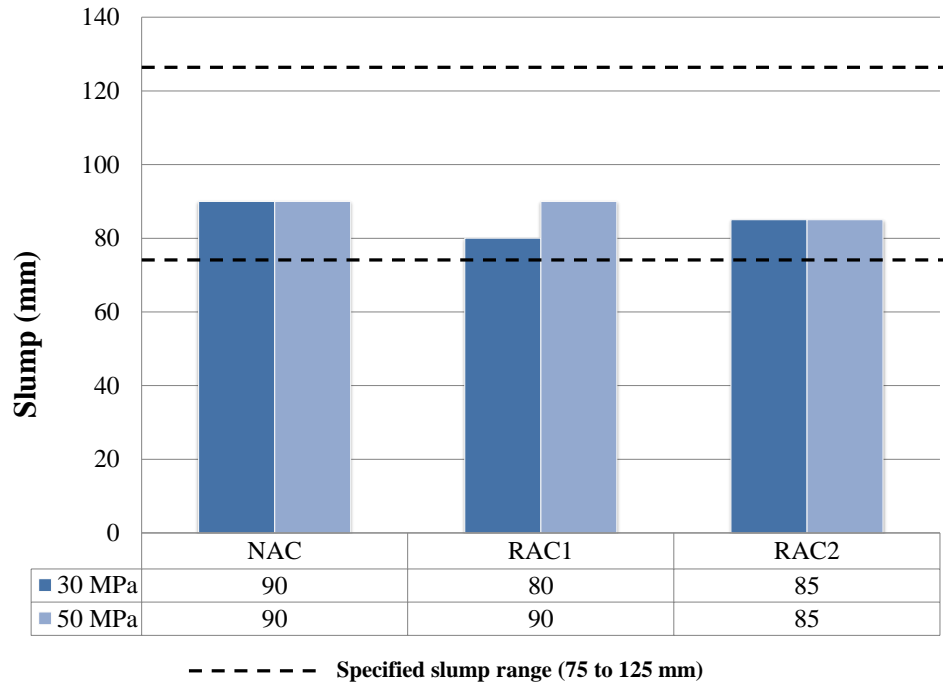


Figure 8.2 Slump values for Phase 1 strength-based mixtures

8.2.2 Compressive Strength Results

Compressive strength testing was performed 28 days after concrete batching and results are presented in Figure 8.3. It must be noted that the compressive strengths of the Phase 1 NA mixtures presented in Figure 8.3 are different from those presented in Section 7.3.2 (i.e., 33.4 MPa vs. 32.1 MPa and 48.8 MPa vs. 57.3 MPa) in the evaluation of the direct replacement mixture results. This is a result of the different batching methods used for the direct replacement mixtures (i.e., Batching Method A: using a smaller mixer with pre-soaked aggregates) and the strength-based mixtures presented (i.e., Batching Method B: using a larger mixer with pre-wetted aggregates). Using the statistical techniques presented in Chapter 7 (i.e., analysis of variance and the modified Bonferroni t-test), the 5% LSD values for the 30 and 50 MPa strength-based mixtures were calculated as 1.5 MPa and 1.6 MPa, respectively.

By observation, the differences in the compressive strengths in the 50 MPa mixtures are less than their respective 5% LSD values indicating that the slight variation in compressive strengths between NA and RCA concretes are statistically insignificant. However, for the 30 MPa mixtures, the difference between the compressive strength of the NA concrete and the RCA-1 and RCA-2 concretes were larger than the 5% LSD value and therefore, are considered

statistically significant. This result enables the direct comparison between the 50 MPa concrete types while attributing any differences in other concrete mechanical properties dependent on compressive strength to the properties of the coarse aggregate.

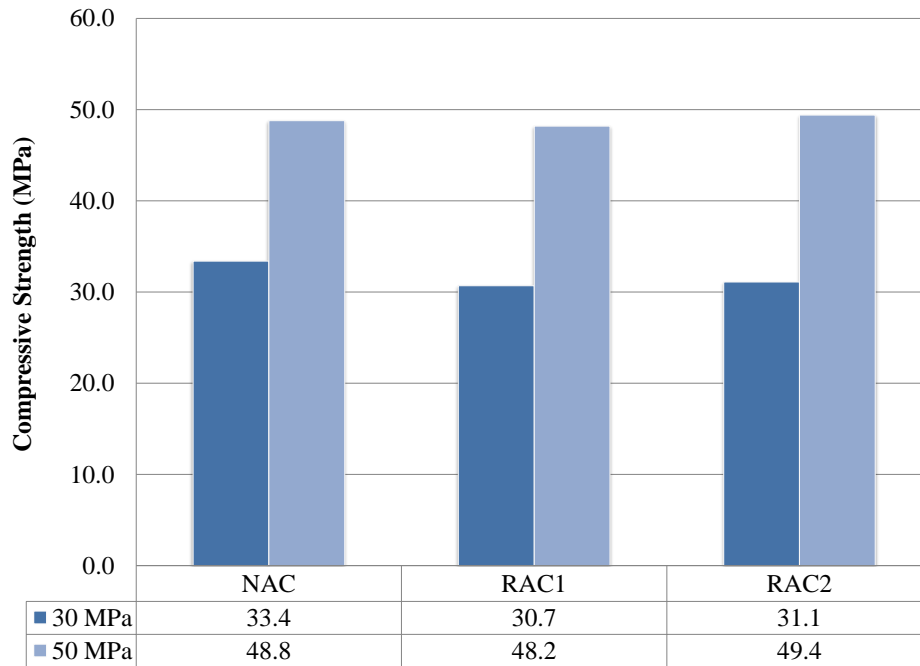


Figure 8.3 Nominal (28 day) compressive strength test results (Phase 1 strength-based mixtures)

In the case of the 30 MPa mixtures, the difference in compressive strength between the NA concrete and RCA concrete may have a significant effect on other concrete properties (i.e., splitting tensile strength and modulus of rupture). Therefore, to facilitate the proper comparison of values, the splitting tensile strength, modulus of rupture and average bond strength must all be normalized with respect to some power of the compressive strength (e.g., f'_c , $f'_c{}^{1/2}$, $f'_c{}^{1/4}$).

8.2.3 Splitting Tensile Strength Results

Phase 1 splitting tensile strength testing was carried out in conjunction with fracture energy testing and specimens were cast along with beam-end specimens (i.e., using Batching Method B). Splitting tensile strength testing was carried out in accordance with the procedure outlined in Chapter 6 and results are reported in Figure 8.4. Note that each splitting tensile strength value reported represents an average of three specimens.

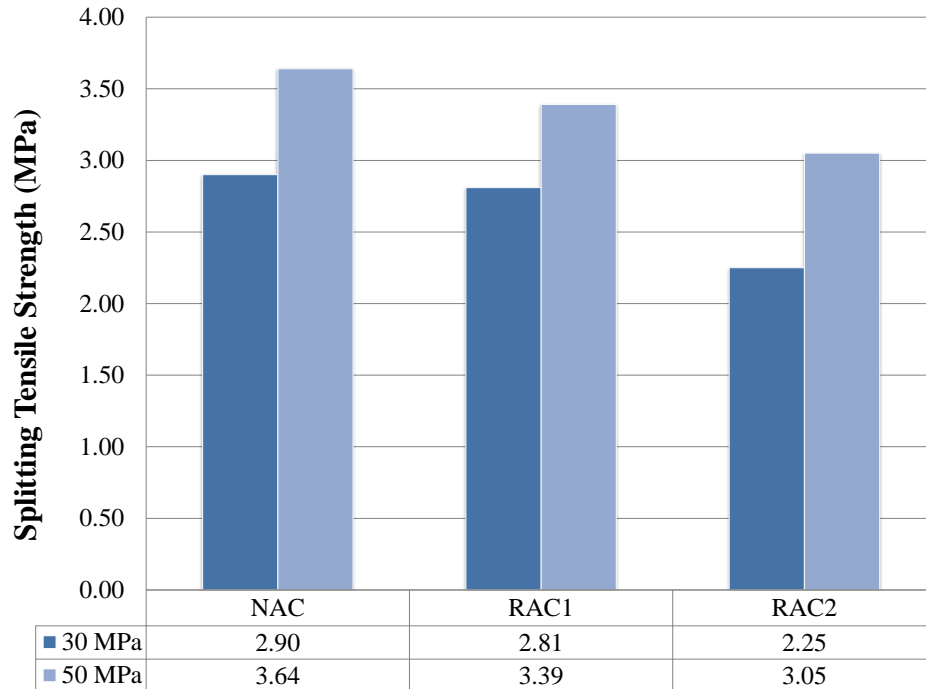


Figure 8.4 Splitting tensile strength results (Phase 1 strength-based mixtures)

Upon inspection of the splitting tensile strength results, a general trend exists in which the NA concrete had the highest splitting tensile strengths followed by the RCA-1 and RCA-2 concrete. The 30 MPa NA concrete had splitting tensile strengths that were 3% and 22% higher than the RCA-1 and RCA-2 concrete mixtures, respectively. The 50 MPa NA concrete had splitting tensile strengths that were 7% and 16% higher than the RCA-1 and RCA-2 concrete mixtures, respectively. Similar decreases in splitting tensile strength of RCA concrete have been reported by other researchers (Ajdukiewicz and Kliszczewicz, 2002 and Rakshvir and Barai, 2006).

To eliminate the effect of concrete compressive strength, splitting tensile strength values were normalized with respect to $f'_c{}^{1/2}$. The normalized splitting tensile strengths are presented in Figure 8.5. Note that these splitting tensile strength values were normalized with respect to $f'_c{}^{1/2}$ measured on the day of testing. A slight deviation in the trend observed in Figure 8.4 exists in Figure 8.5 as the 30 MPa RCA-1 concrete had a slightly higher $f_{ct}/f'_c{}^{1/2}$ value than the NA and RCA-2 concretes.

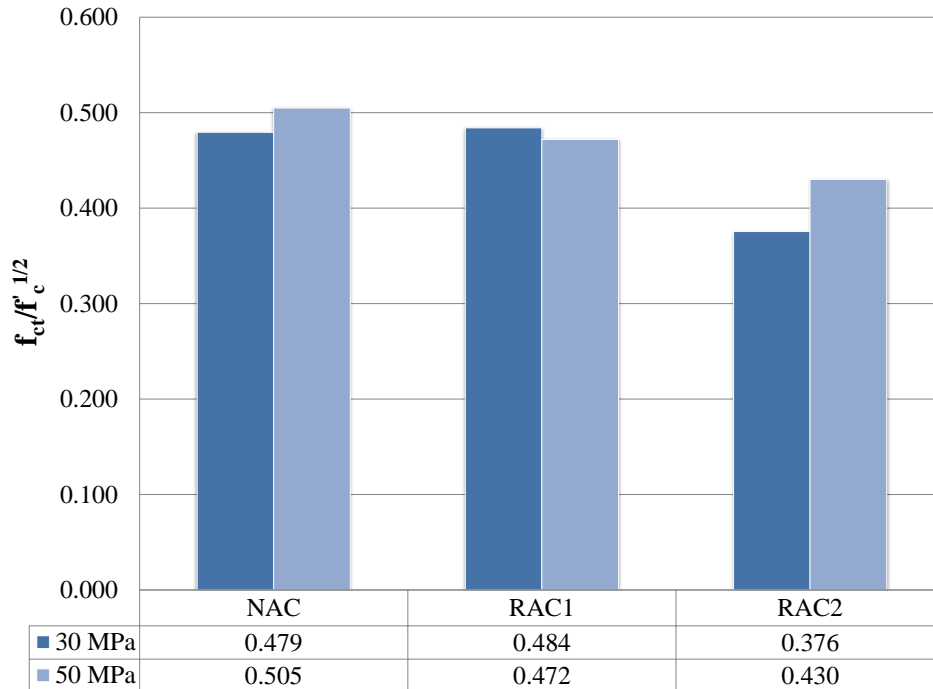


Figure 8.5 Normalized splitting tensile strength results (Phase 1 strength-based mixtures)

The relationship between the splitting tensile strength and the ACV is presented in Figure 8.6. It should be mentioned that splitting tensile strengths were normalized to $f_c'^{1/2}$ for several reasons, (1) when investigating the relationship between f_{ct} and ACV, normalizing with respect to $f_c'^{1/2}$ gave the highest coefficient of determination value in both Phase 1 and Phase 2 (refer to Section 8.3.3) results; (2) it has been found that coarse aggregate shape effects the tensile strength of concrete and therefore, will also effect $f_{ct}/f_c'^{1/2}$ (Mindess et al., 2003); and (3) in structural design codes and in many studies in the literature, the term $f_c'^{1/2}$ is used most often to provide an indication of tensile strength. Based on the lower coefficient of determination value, no significant relation between splitting tensile strength and ACV for the 30 MPa specimens existed whereas a fairly strong correlation ($R^2 = 0.95$) was observed for the 50 MPa specimens. This finding suggests that the strength of coarse aggregate (i.e., ACV) at lower compressive strength levels does not govern the splitting tensile strength of concrete. At higher concrete strengths (i.e., 50 MPa), the splitting tensile strength seems to be more influenced by the strength of the coarse aggregate. By investigating the fracture planes of the splitting tensile specimens, the 30 MPa specimens had fractures that occurred both around and through the coarse aggregate particles suggesting that the mortar-aggregate bond was the main failure mechanism. This

agrees with the findings presented for the Phase 2 direct replacement mixtures in Section 7.4.3.2.

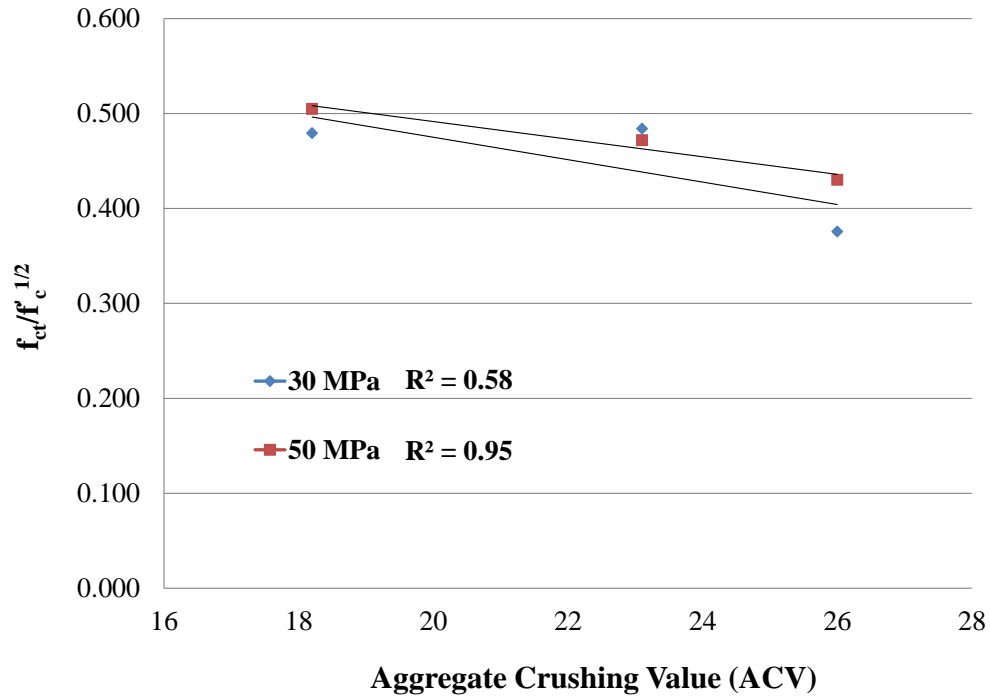


Figure 8.6 Relationship between $f_{ct}/f_c^{1/2}$ and aggregate crushing value (Phase 1 strength-based mixtures)

The RCA-1 particles were previously described (see Section 4.5.4) as having a more roughened surface texture than the NA or RCA-2 which could lead to a stronger mortar-aggregate bond, and may explain why the RCA-1 concrete had the highest $f_{ct}/f_c^{1/2}$ value. In the 50 MPa specimens, failure occurred mainly through the coarse aggregate particles indicating that the aggregate strength was the main failure mechanism. Recall from Section 4.5.7 that the natural aggregate had the highest crushing strength (i.e., lowest ACV). This explains why the NA concrete had the highest splitting tensile strength.

8.2.4 Modulus of Rupture Results

The modulus of rupture (flexural tensile strength) was measured using the same specimens used for measuring the fracture energy (i.e., single-edge notched double-cantilevered prisms). Average values (two specimens, A and B) of modulus of rupture for each concrete type are presented in Figure 8.7.

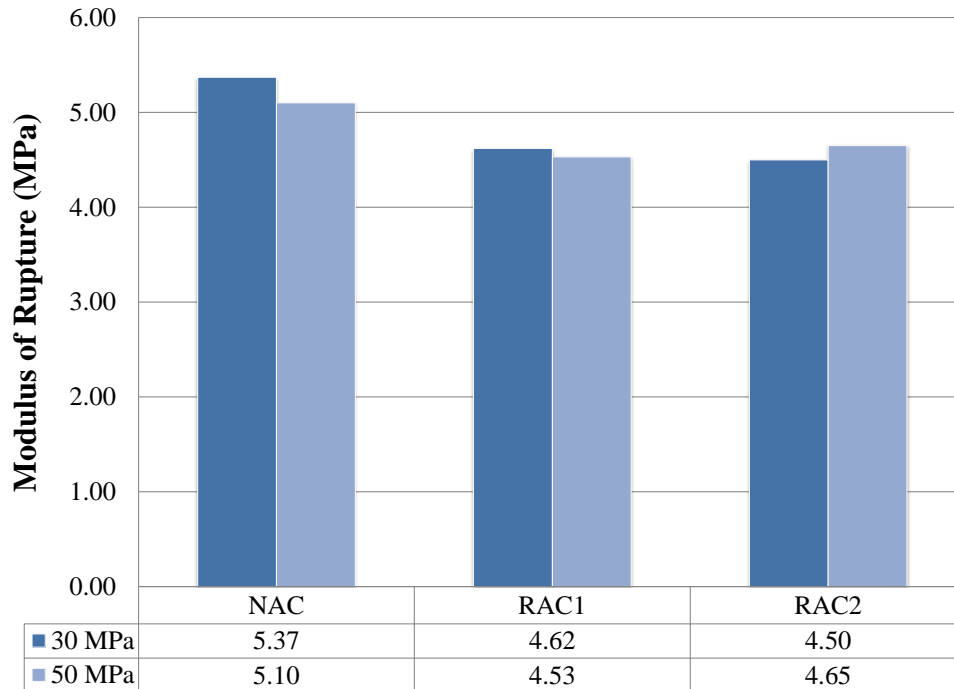


Figure 8.7 Modulus of rupture (flexural strength) results (Phase 1 strength-based mixtures)

Based on the results presented in Figure 8.7, the NA concrete had the highest f_r at both the 30 and 50 MPa strength levels. The 30 MPa NA concrete had f_r values that were, on average, 14% and 16% higher than the RCA-1 and RCA-2 concretes, respectively. The 50 MPa NA concrete had a mean f_r value that was 11% and 1% higher than the RCA-1 and RCA-2 concretes, respectively. These decreases in flexural strength of RCA concrete compared to the NA concrete are in a similar range to those measured in other research studies (Chen et al., 2003 and Rakshvir and Barai, 2006). To eliminate the influence of compressive strength on flexural strength and what is typically used in design equations for concrete, modulus of rupture values were normalized with respect to $f_c^{1/2}$ and are summarized in Figure 8.8.

After normalizing the modulus of rupture values with respect to $f_c^{1/2}$, the general trend in the modulus of rupture results changed significantly. The NA concrete had the highest modulus of rupture value followed by the RCA-1 and RCA-2 concretes. Values of $f_r/f_c^{1/2}$ ranged between 0.65 and 0.91. Shayan and Xu (2003) reported a similar $f_r/f_c^{1/2}$ value (i.e., approximately 0.95). Figure 8.9 illustrates the relationship between $f_r/f_c^{1/2}$ and aggregate crushing value.

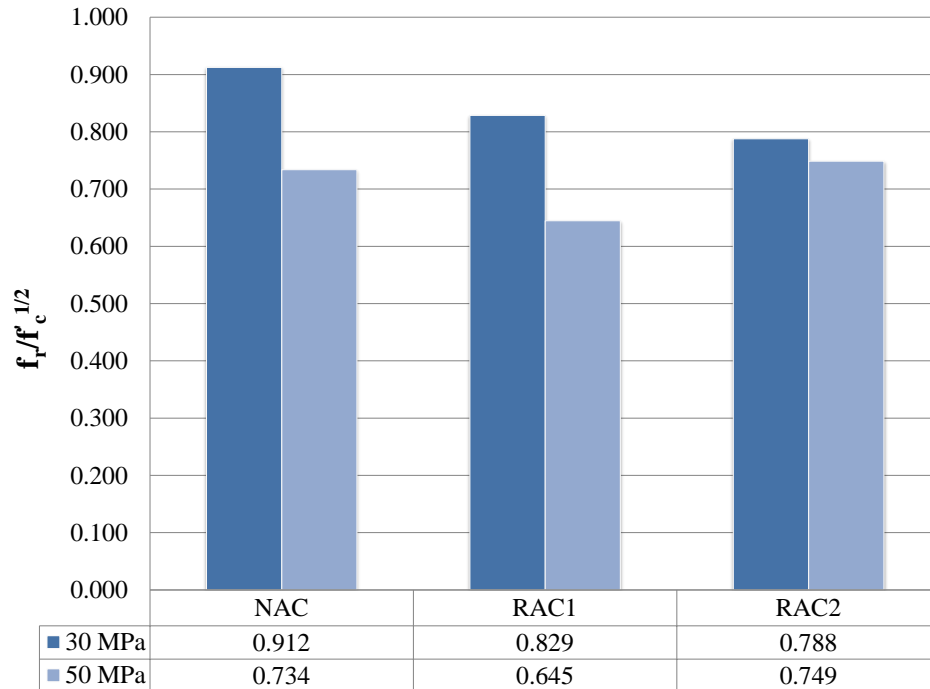


Figure 8.8 Normalized modulus of rupture (flexural strength) test results (Phase 1 strength-based mixtures)

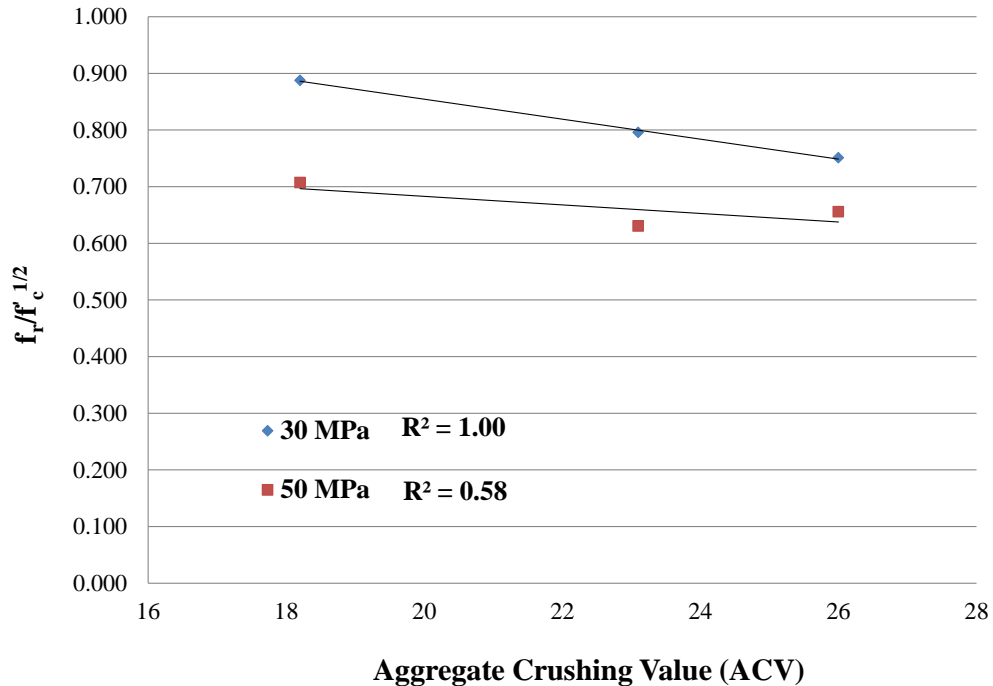


Figure 8.9 Relationship between aggregate crushing value and $f_r/f_c^{1/2}$ (Phase 1 control and strength-based mixtures)

As illustrated in Figure 8.9, the 30 MPa samples demonstrated an excellent correlation ($R^2 =$

1.00) between f_r and the ACV whereas a less significant relation ($R^2 = 0.58$) was found for the 50 MPa samples. This demonstrates that as compressive strength increases, the relationship between ACV and the modulus of rupture or $f_r/f_c^{1/2}$ becomes more variable. Further results and discussion of these trends are presented for the Phase 2 modulus of rupture specimens (Section 8.3.6).

8.2.5 Fracture Energy Results

Single edge-notched double-cantilevered (SENDC) fracture energy specimens were cast in conjunction with beam-end specimens, compressive strength and splitting tensile cylinders. Based on the work by Zuo and Darwin (2000) that proposed a strong dependence of concrete-steel bond strength on the fracture energy of concrete, an experimental program was devised to measure the effect of the fracture energy of RCA concrete on bond strength. As a secondary objective, the effect of various aggregate and concrete properties on the fracture energy of concrete was evaluated.

The initial study (Phase 1) involved the testing of 12 fracture energy specimens consisting of three aggregate types (natural, RCA-1, and RCA-2), two compressive strengths (30 and 50 MPa) and duplicate specimens. The full test setup, definitions, specimen dimensions and calculation methods were presented in Chapter 6. Based on the availability of laboratory testing equipment and technical resources, the fracture energy specimens were tested nearly 6 weeks after the beam-end specimens. As a result, separate compressive strength and splitting tensile strength cylinders were cast to provide data for correlation with fracture energy and modulus of rupture results.

As there is currently no standard definition for the region over which the fracture energy should be calculated, a displacement-based limit was adopted for this research. All fracture energy values reported represent the fracture energy calculated up until an average midspan deflection of 1.0 mm (i.e., $G_{f,1mm}$). By limiting the fracture energy data to this displacement level, a relative comparison between various concrete types and compressive strengths could be made. Note that the correlation results between fracture energy and bond strength for Phase 1 are presented in Chapter 9. Table 8.1 presents the fracture energy testing results along with the concrete compressive strength, concrete splitting tensile strength and the peak load.

Table 8.1 Fracture energy test results (Phase 1 strength-based mixtures)

Specimen ID	f'_c	f_{ct}	Peak Load	$G_{f,1mm}^*$
	[MPa]	[MPa]	[N]	[N/m]
NAC-30A			5111	98.9
NAC-30B			4909	109.1
Avg.	36.6	2.90	5010	104.0
RAC1-30A			4421	89.5
RAC1-30B			4207	134.4
Avg.	33.7	2.81	4314	112.0
RAC2-30A			4197	100.1
RAC2-30B			4206	103.8
Avg.	35.9	2.25	4202	102.0
NAC-50A			4672	100.0
NAC-50B			4849	93.6
Avg.	52.0	3.64	4761	96.8
RAC1-50A			4072	91.3
RAC1-50B			4376	56.2
Avg.	51.6	3.39	4224	73.8
RAC2-50A			4341	114.6
RAC2-50B			5089	113.0
Avg.	50.3	3.05	4715	113.8

* Represents the fracture energy up until an average midspan deflection of 1 mm. In cases where the specimens did not reach a maximum midspan deflection of 1 mm, the fracture energy was calculated using the total area under the load-deflection plot.

Based on the fracture energy results of the 30 MPa specimens, the NA concrete had an average fracture energy that was 2% and 29% higher than the RCA-1 and RCA-2 concretes, respectively. In comparing the 50 MPa specimens, the RCA-2 concrete had the highest average fracture energy that was 2% and 15% higher than the NA and RCA-1 concretes, respectively. Casuccio et al. (2008) used single-edge notched beam specimens and reported fracture energies for RCA concrete in a similar range (i.e., between 81 and 155 N/mm). They reported that fully replacing natural aggregate with RCA reduced fracture energies by up to 45%. However, in this study, the 50 MPa RCA-2 concrete had an average fracture energy that was 15% higher than NA concrete. It should be noted that although distinct differences in fracture energy were observed between NA and RCA concrete specimens, the specimen-to-specimen variation may be too high in some cases to make conclusive statements on the effect of replacing NA with RCA on the fracture energy of the resulting concrete.

By observation, the largest specimen-to-specimen variation in fracture energy results exists in

the RCA-1 concrete specimens (i.e., 89.5 and 134.4 N/mm for the 30 MPa specimens and 91.3 and 56.2 N/mm for the 50 MPa specimens). No identifiable explanation other than the actual material property variation was found to explain the variability of these results. The higher fracture energies of the RCA-2 concrete samples may be explained by examining the fracture surfaces themselves. This will be discussed further in a following section. No significant correlations between fracture energy, aggregate crushing value, splitting tensile strength and modulus of rupture were found to exist.

8.2.5.1 Load-Deflection Response of Phase I Fracture Energy Specimens

The load versus midspan deflection relationship for each fracture energy specimen is presented in Figure 8.10 to Figure 8.15.

In general, all load versus midspan deflection curves consisted of a nearly linear ascending branch up until the peak load was reached followed by a convex descending branch which asymptotically approached the horizontal axis until zero load. Overall, the 50 MPa samples had shorter tails (i.e., less deformation after 1 mm midspan deflection had been reached) than the 30 MPa samples which suggest more brittle behaviour. On average, both the 30 and 50 MPa NA concrete specimens appear to have a slightly steeper initial descending branch than the corresponding RCA-1 and RCA-2 samples. In certain cases, this may explain why higher fracture energies were measured for some of the RCA specimens as the amount of energy absorbed prior to failure would have been higher in the RCA specimens.

By examining the load deflection curves of the RCA-1 specimens (Figure 8.11 and Figure 8.14), a noticeable difference in behaviour was observed between duplicate specimens. This difference in load-deflection behaviour is reflected in the calculated fracture energy values for the RCA-1 specimens.

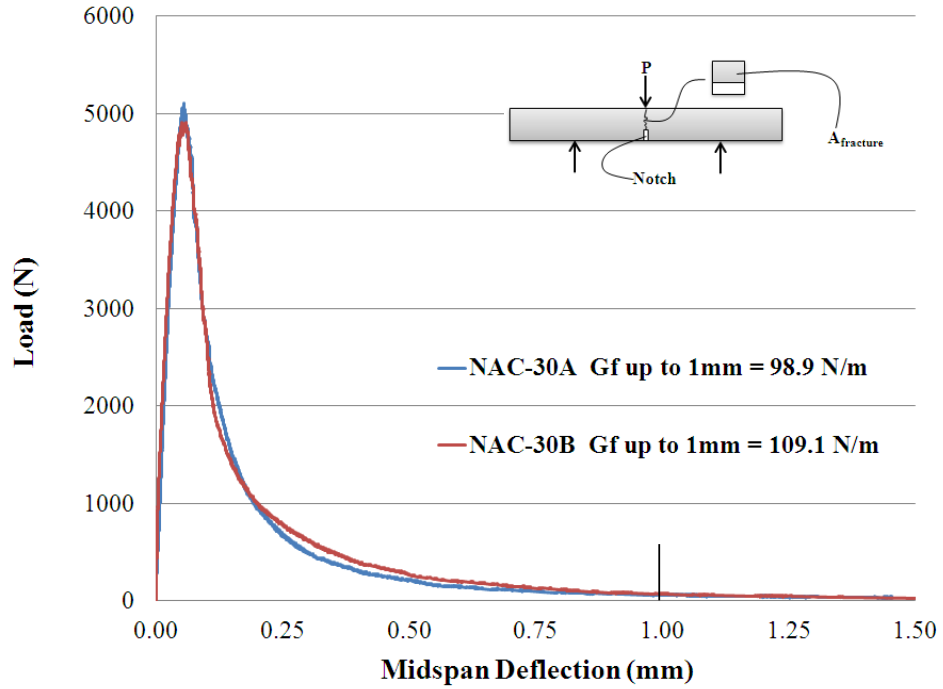


Figure 8.10 Load vs. midspan deflection for NAC-30 fracture energy specimens (Phase I)

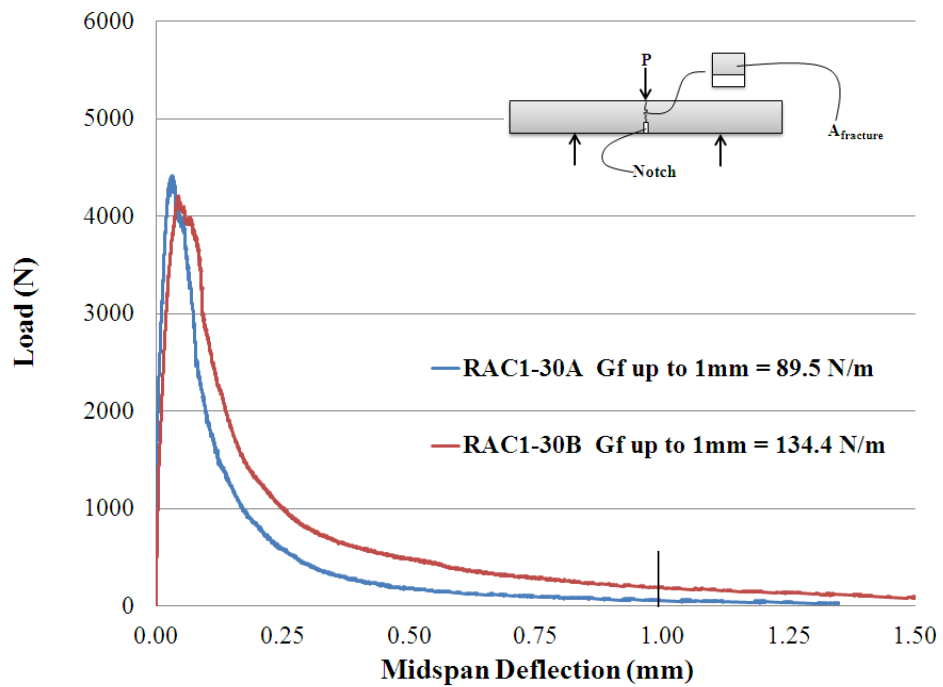


Figure 8.11 Load vs. midspan deflection for RAC1-30 fracture energy specimens (Phase I)

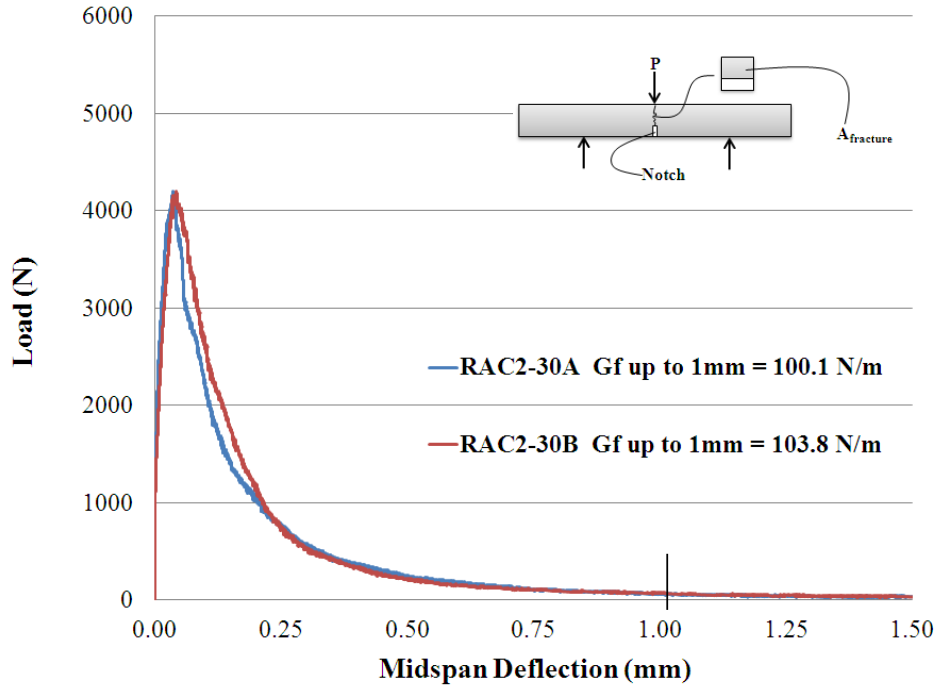


Figure 8.12 Load vs. midspan deflection for RAC2-30 fracture energy specimens (Phase 1)

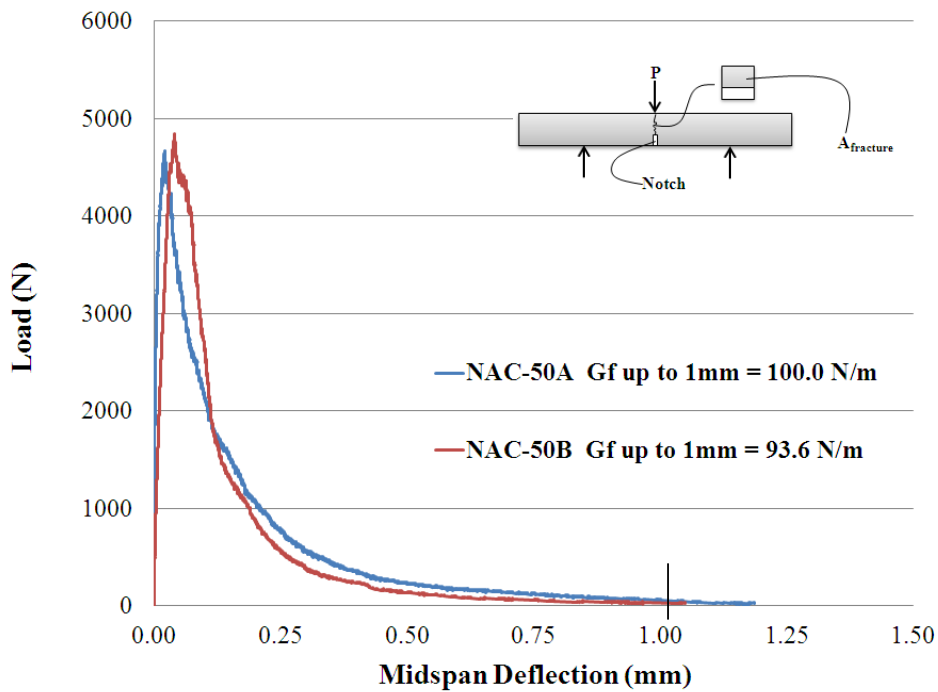


Figure 8.13 Load vs. midspan deflection for NAC-50 fracture energy specimens (Phase 1)

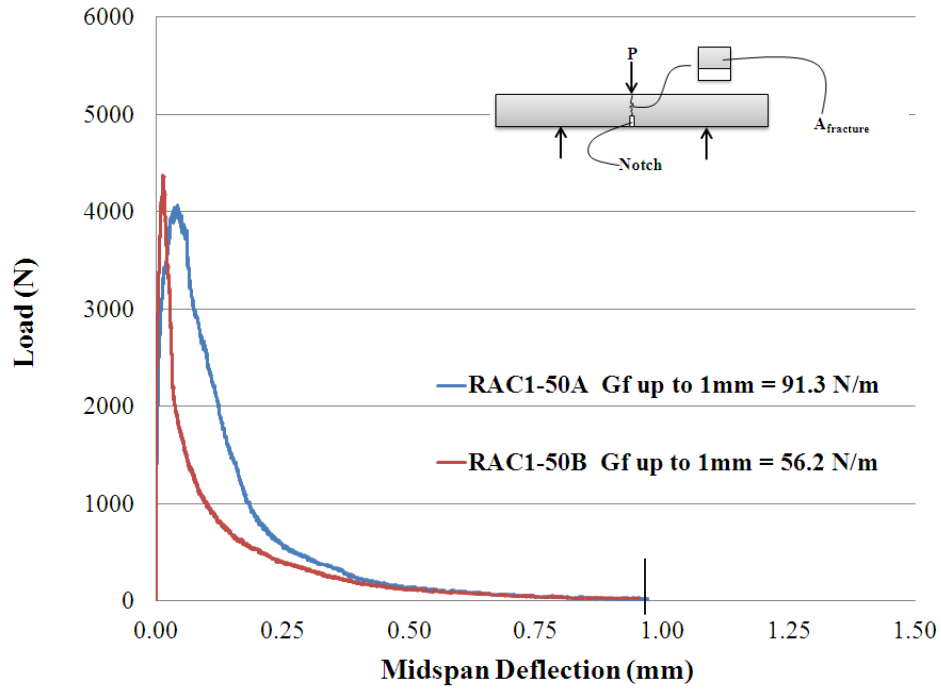


Figure 8.14 Load vs. midspan deflection for RAC1-50 fracture energy specimens (Phase I)

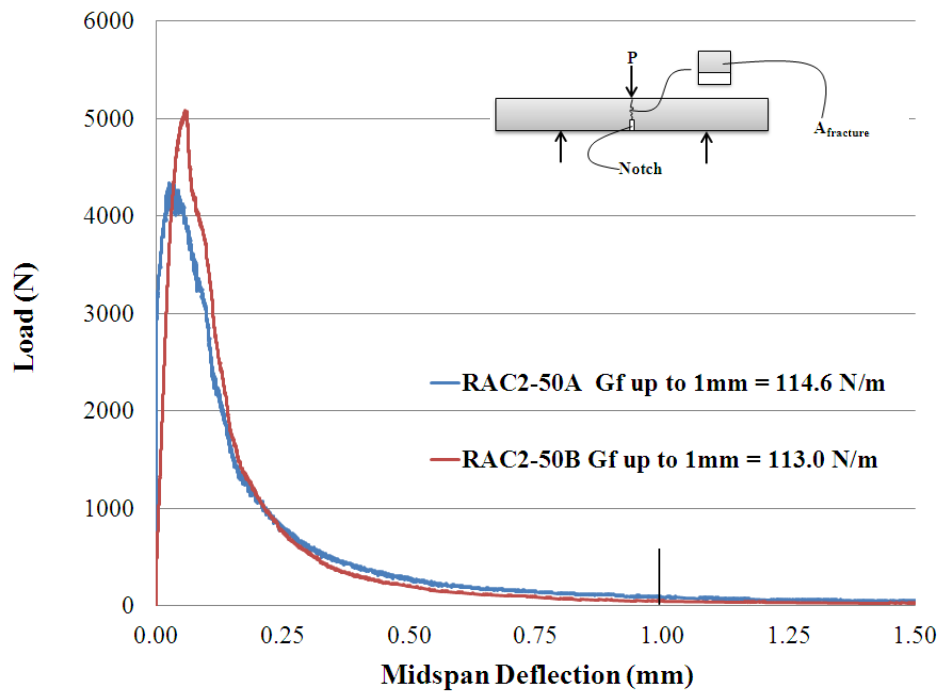


Figure 8.15 Load vs. midspan deflection for RAC2-50 fracture energy specimens (Phase I)

8.2.5.2 Examination of Fracture Surfaces

Once fracture energy specimens were tested, the fracture surface for each specimen was photographed, measured (to obtain an area of fracture surface) and observed. Note that because the strength-based mixtures had varying water-cement ratios, the mortar strengths also varied among the several concrete types. Therefore, the process of isolating the resulting fracture mechanism of the strength-based mixtures becomes slightly more complex compared to that previously carried out for the direct replacement mixtures. In this case, the fracture energy may be influenced by a number of factors including, the mortar strength, aggregate strength, mortar-aggregate bond properties (and indirectly, coarse aggregate surface texture), coarse aggregate shape, volume of coarse aggregate, and the quantity and properties of deleterious materials.

Figure 8.16 depicts the fracture surfaces of the 30 MPa specimens. In general, a higher percentage of fracture planes passed through rather than around the coarse aggregates for the NA concrete specimens as compared to the RCA concrete specimens. This failure mechanism suggests that the strength of the coarse aggregate rather than the mortar-aggregate bond (which is a function of the aggregate surface texture) has a greater influence on the fracture energy of RCA concrete.

Figure 8.17 depicts the fracture surfaces of the 50 MPa specimens. The NA concrete fracture planes passed mainly through the aggregates. Compared to the RCA-1 and RCA-2 concrete fracture surfaces, the NA concrete fracture plane was more uniform and less tortuous. As previously observed, the RCA-1 concrete specimens had the highest specimen-to-specimen variability in fracture energy. Based on their fracture surfaces, no discernible difference was observed that could account for the large variability in fracture energy between duplicate specimens. Additional sources for this variability may include: specimen alignment, specimen dimensions, support conditions, concrete consolidation, etc. Examination of the fracture surfaces revealed some low-strength deleterious materials (e.g., wood chips) were found to pass through or in the vicinity of the RCA-1 and RCA-2 concrete fracture surfaces which could act as additional crack arrestors. This may also explain some of the variability in the fracture energy test results.

Specimen A

Specimen B

NAC-30



RAC1-30



RAC2-30



Figure 8.16 Fracture zones of fracture energy prisms (Phase 1 30 MPa specimens)

Specimen A

Specimen B

NAC-50



RAC1-50



RAC2-50



Figure 8.17 Fracture zones of fracture energy prisms (Phase 1 50 MPa specimens)

8.2.6 Conclusions from Phase 1 Mixtures

Based on the analysis and findings of the Phase 1 strength-based mixtures, the following conclusions have been compiled.

1. By varying the water content and the water-cement ratio it was possible to produce RCA-1 and RCA-2 concrete with slump values ranging between 75 and 125 mm and compressive strengths of 30 and 50 MPa.
2. Splitting tensile strengths for the 30 MPa NA concrete mixtures were up to 22% higher than the equivalent RCA concrete mixture. Splitting tensile strengths for the 50 MPa NA concrete mixtures were up to 16% higher than the equivalent RCA concrete mixture.
3. A strong correlation between the splitting tensile strength and aggregate crushing value was found for both the 30 and 50 MPa mixtures. Also, a strong correlation was found between $f'_s/f_c^{1/2}$ and the coarse aggregate volume.
4. After normalizing with respect to $f_c^{1/2}$, a good correlation between the modulus of rupture and the aggregate crushing value was found for both the 30 and 50 MPa mixtures.
5. The 30 MPa RCA concrete had average fracture energies that were 98% and 108% in comparison to the equivalent NA concrete. Whereas the 50 MPa RCA concrete had average fracture energies that were between 76% and 118% in comparison to the equivalent NA concrete.
6. In general, the NA concrete fracture energy specimens have a slightly steeper initial descending branch than the corresponding RCA-1 and RCA-2 concrete specimens.
7. The RCA-1 concrete fracture energy specimens had the highest specimen-to-specimen variability. This may be explained by differences in specimen alignment, specimen dimensions, concrete quality and consolidation, and quantity and properties of deleterious materials bridging the fracture plane.
8. No significant relationship was found between the fracture energy and the aggregate strength (ACV) at either strength level.

8.3 Phase 2 Strength-Based Mixtures (40 and 60 MPa)

The following discussion is based on the strength-based mixtures (refer to Section 5.6 for a description of mixture proportion phases) that were batched using Batching Method A in which the aggregates were pre-soaked prior to batching and a 0.05 m³ concrete pan mixer was used (see Section 5.2.2 for details). The compressive strength and slump results of the Phase 2 strength-based mixtures were evaluated to ensure that they were statistically similar. Other concrete mechanical properties including the splitting tensile strength, coefficient of thermal expansion, the modulus of elasticity, Poisson's ratio, the modulus of rupture, and the fracture energy are presented and evaluated based on their dependence on various aggregate properties. In addition, the splitting tensile strength, linear coefficient of thermal expansion, and the modulus of elasticity results of the Phase 2 RCA concrete strength-based mixtures (constant compressive strength and slump) were compared to those of the Phase 2 RCA concrete direct replacement mixtures (constant water-cement ratio and coarse aggregate volume). This comparison was aimed at assessing the influence of compressive strength, slump, and coarse aggregate volume (independent of the aggregate type) on these properties (refer to Figure 8.1 for further explanation).

8.3.1 Workability and Hardened Density Results

8.3.1.1 Workability

All strength-based mixtures were proportioned to achieve slump values between 75 and 125 mm. Slump tests were carried out in accordance with the procedure outlined in Chapter 6. As presented in Figure 8.18 all slump values were within the specified slump range.

In general, when freshly mixed the 40 MPa mixtures had a more stony and granular appearance than the 60 MPa mixtures which had a more creamy appearance. Differences in appearance between the NA concrete and the RCA concrete were negligible. Overall, both NA and RCA concretes were fairly easy to consolidate and excessive bleeding was not an issue.

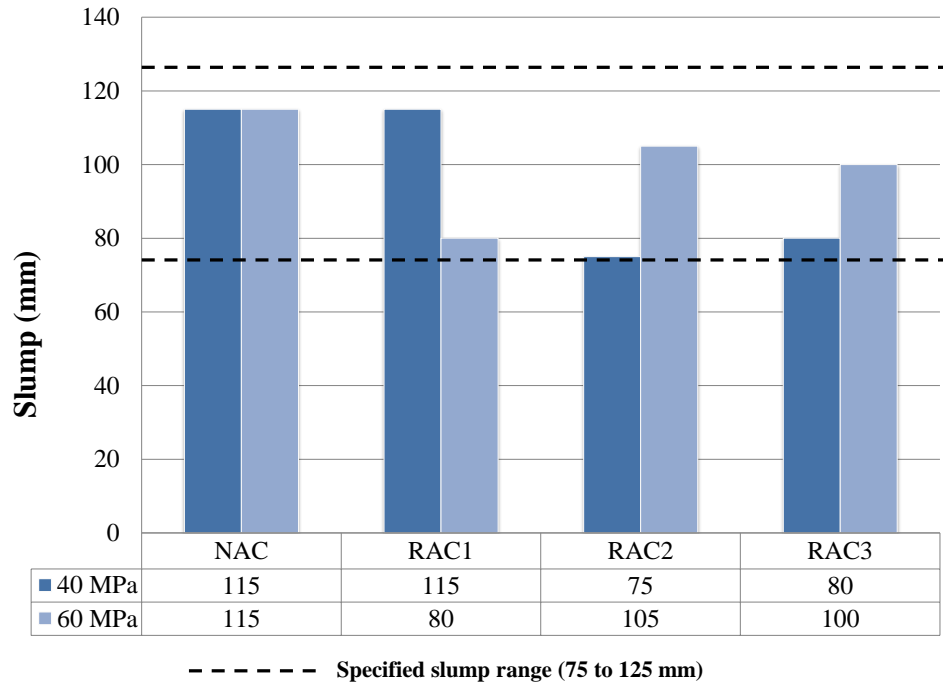


Figure 8.18 Slump values for Phase 2 strength-based mixtures

8.3.1.2 Hardened Density

The density of hardened concrete for the Phase 2 strength-based mixtures was measured using the procedure outlined in Chapter 6. Density results measured will be compared to those of the direct replacement mixtures to assess the effect that aggregate volume has on hardened density. In addition, the results will be used in the normalization of modulus of elasticity results. Measurements were taken when the concrete specimens were 28 days old and the results are presented in Figure 8.19.

Overall, the NA concrete had the highest hardened density as compared the RCA concretes. By comparing the hardened density results of the strength-based mixtures to those obtained from the direct replacement mixtures (see Section 7.4.1.2), changing the aggregate volume and water-cement ratio seems to have had a negligible effect.

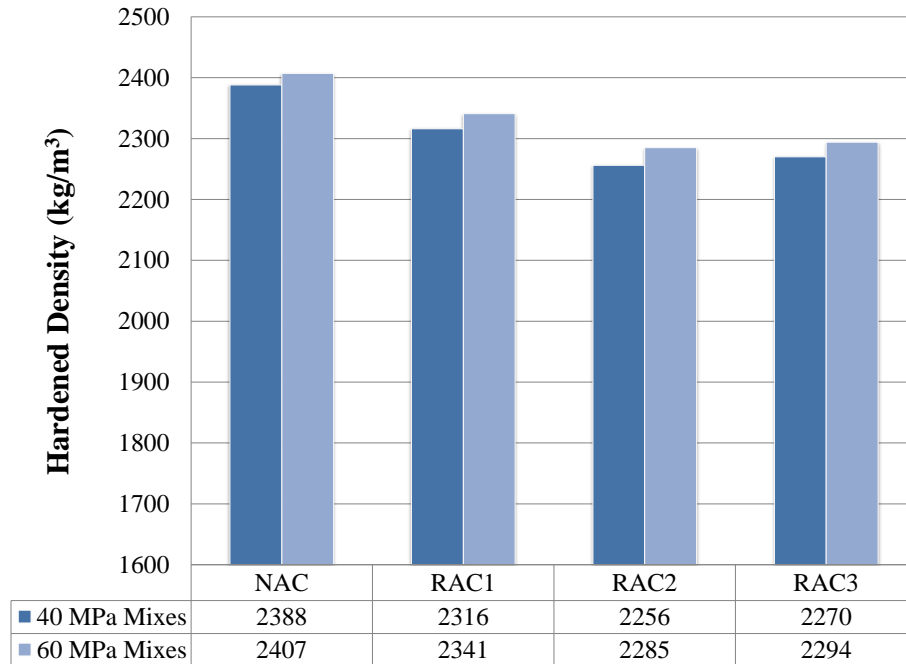


Figure 8.19 Hardened density results for the Phase 2 strength-based mixtures

8.3.2 Compressive Strength Results

Similar to the Phase 1 mixtures, compressive strength testing was performed after 28 days of concrete batching and in accordance with the procedure outlined in Chapter 6. The compressive strength results for the Phase 2 strength-based mixtures are presented in Figure 8.20. Based on statistical method outlined previously, the 5% LSD values for the 40 and 60 MPa strength-based mixtures were calculated as 2.1 MPa and 3.7 MPa, respectively. In comparing the differences in compressive strengths of the 40 and 60 MPa mixtures, their respective 5% LSD values indicate that the slight variation in compressive strengths between NA and RCA concretes are statistically insignificant.

Similar to Phase 1, this result enables the direct comparison between concrete types while attributing any differences in other concrete mechanical properties dependent on compressive strength to the properties of the coarse aggregate. In addition, given that both the Phase 2 direct replacement mixtures and strength-based mixtures were batching using the same batching process (i.e., batching method A) the effect of RCA type on changes in mixture proportions can also be accurately assessed.

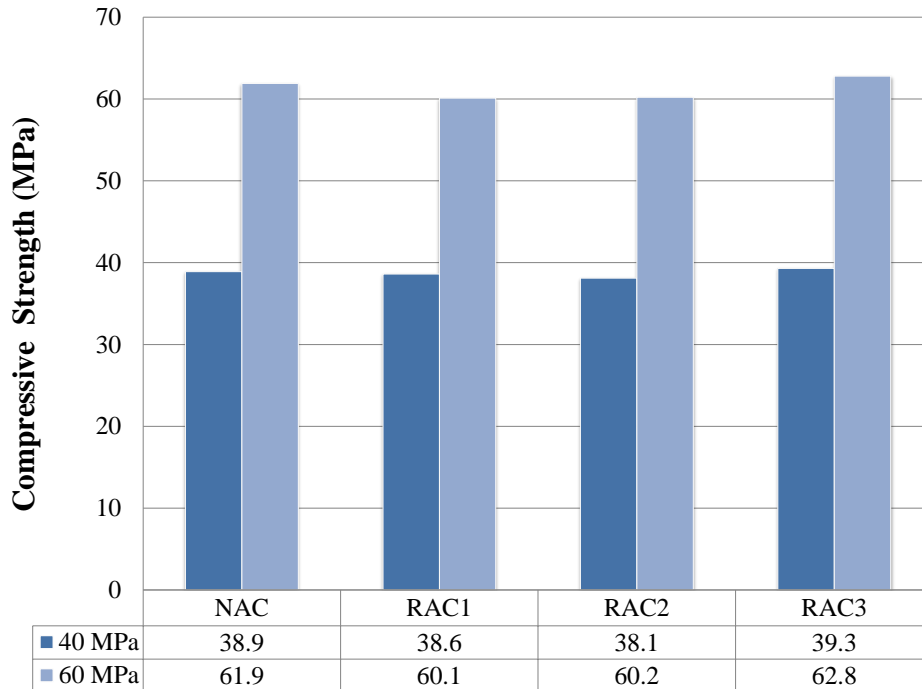


Figure 8.20 Nominal (28 day) compressive strength results (Phase 2 strength-based mixtures)

8.3.3 Splitting Tensile Strength Results

The splitting tensile strength of the Phase 2 strength-based mixtures specimens were prepared using Batching Method A (smaller mixer with pre-soaking of coarse aggregates for 24 hours; refer to Section 5.2.2). Testing was carried out in accordance with the procedure outlined in Chapter 6 and results are reported in Figure 8.21. General conclusions will be made at the end of this section (Section 8.3.3.2) as to the effect of compressive strength and aggregate volume on splitting tensile strength by comparing the splitting tensile strength results of the Phase 2 direct replacement mixtures (refer to Section 7.4.3) to the Phase 2 strength-based mixtures.

Each splitting tensile strength value reported represents an average of at least three samples. Note that all modulus of elasticity specimens (NA and RCA concrete) were kept in an air dry moisture condition throughout the duration of testing. A statistical analysis of the data will be presented in Section 8.3.3.1 to assess whether the differences in splitting tensile strength are statistically significant.

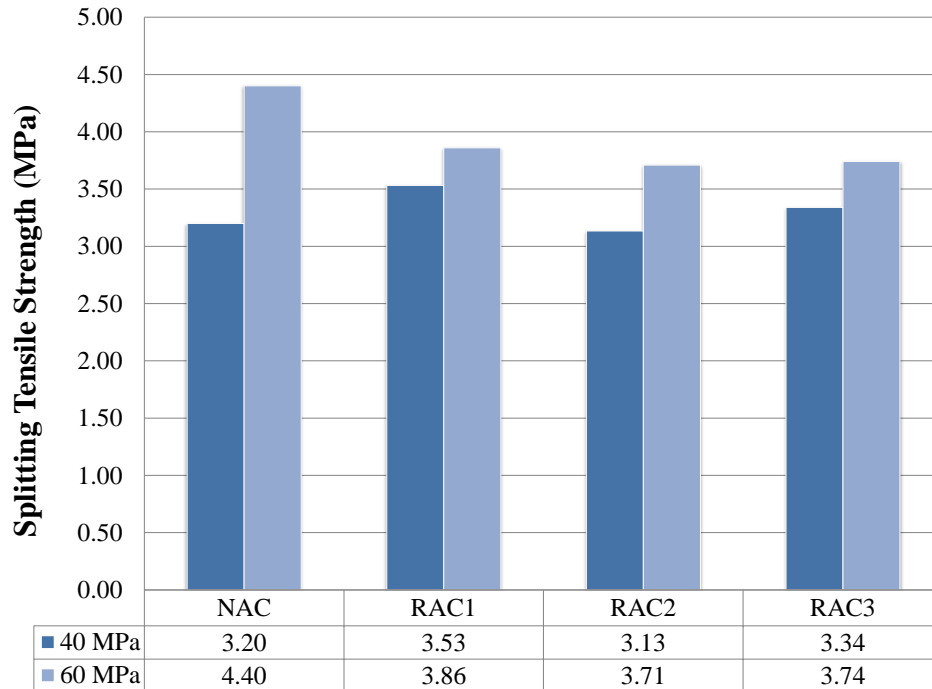


Figure 8.21 Splitting tensile strength results (Phase 2 strength-based mixtures)

In comparing the 40 MPa samples, the RCA-1 concrete had the highest splitting tensile strength that was 9%, 11%, and 5% greater than the NAC, RCA-2 and RCA-3 samples, respectively. To eliminate any effect of differences in compressive strength and for other reasons mentioned in Section 8.2.3, splitting tensile strength values were normalized with respect to $f'_c{}^{1/2}$ and are presented in Figure 8.22.

The 60 MPa NA concrete had the highest $f_{ct}/f'_c{}^{1/2}$ values followed by the RCA-1, RCA-2 and RCA-3 concretes. The 40 MPa RCA-1 concrete had the highest $f_{ct}/f'_c{}^{1/2}$ values followed by the NA, RCA-2 and RCA-3 concretes. As demonstrated in Figure 8.23, a fairly strong relationship was found to exist between $f_{ct}/f'_c{}^{1/2}$ and the ACV at the higher (60 MPa) strength level. This confirms the similar behaviour observed in the Phase 1 50 MPa samples: the splitting tensile strength is dependent on the strength of the coarse aggregate.

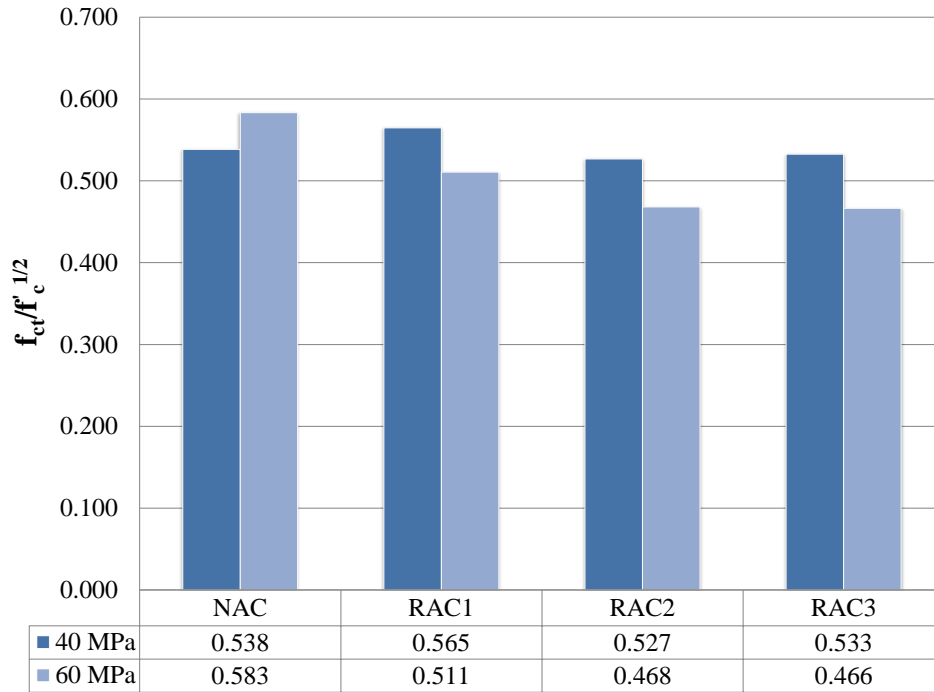


Figure 8.22 Normalized splitting tensile strength values (Phase 2 control and strength-based mixtures)

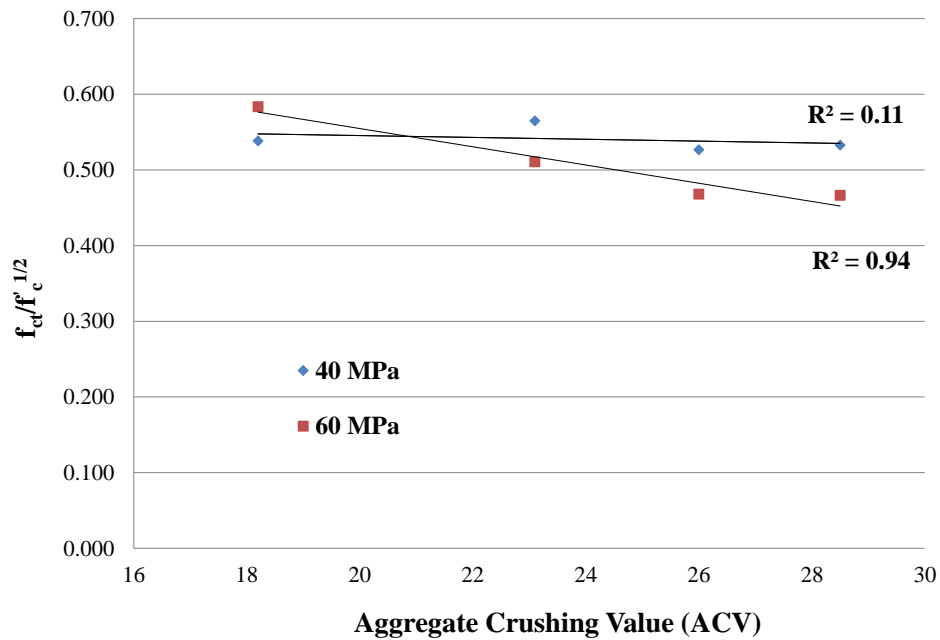


Figure 8.23 Relationship between aggregate crushing value and $f_{ct}/f_c^{1/2}$ (Phase 2 control and strength-based mixtures)

8.3.3.1 Statistical Significance of Tensile Strength Results

To determine whether the relative difference in 28 day splitting tensile strengths between the various Phase 2 strength-based mixtures were statistically significant, a least significant difference (LSD) value was calculated using the data from each strength set. Using analysis of variance (ANOVA) and a modification to the Bonferroni t-test, the 5% LSD values for the splitting tensile strength values for the Phase 2 (40 and 60 MPa) strength-based mixtures were calculated and are tabulated in Table 8.2. Note that the failure mode of the splitting tensile strength specimens was determined by visual approximation of the fracture surface. The difference in 28 day splitting tensile strength values (at both 40 and 60 MPa strength levels) between the NA concrete and the RCA concrete were lower than the 5% LSD value. This indicates that relative differences in splitting tensile strength between the NA concrete mixtures and the RCA concrete strength-based mixtures are not statistically significant. Therefore, the splitting tensile strength of all the RCA concrete types is statistically similar to the NA concrete at both the 40 and 60 MPa strength levels.

Table 8.2 Splitting tensile results, statistics and failure modes for Phase 2 strength-based mixtures

Mix ID	f_{ct} (MPa)	Standard Deviation (MPa)	Coeff. of Variation	Failure Mode
NAC-40	3.18	0.15	0.05	Through more than 50% of aggregates
RAC1-40	3.51	0.18	0.05	Through more than 50% of aggregates
RAC2-40	3.11	0.37	0.12	Through more than 50% of aggregates
RAC3-40	3.30	0.49	0.15	Through more than 50% of aggregates
<i>5% LSD</i>	<i>0.93</i>			
NAC-60	4.38	0.15	0.03	Through more than 50% of aggregates
RAC1-60	3.84	0.39	0.10	Through more than 50% of aggregates
RAC2-60	3.70	0.33	0.09	Through more than 50% of aggregates
RAC3-60	3.72	0.30	0.08	Through more than 50% of aggregates
<i>5% LSD</i>	<i>0.87</i>			

Based on modification factors presented in design codes for development length and splice length (e.g., CSA A23.3, 2004), modifications for concrete density are used to represent the effect of splitting tensile strength on the bond strength of concrete with reinforcing steel. Further discussion on the effect of concrete density on the bond strength of RCA concrete members is presented in Chapter 9. A good relationship between the splitting tensile strength and concrete hardened density was discovered and is presented in Figure 8.24. Although the ACV and

concrete hardened density are independent of one another, they both appear to have a significant influence on the splitting tensile strength of concrete.

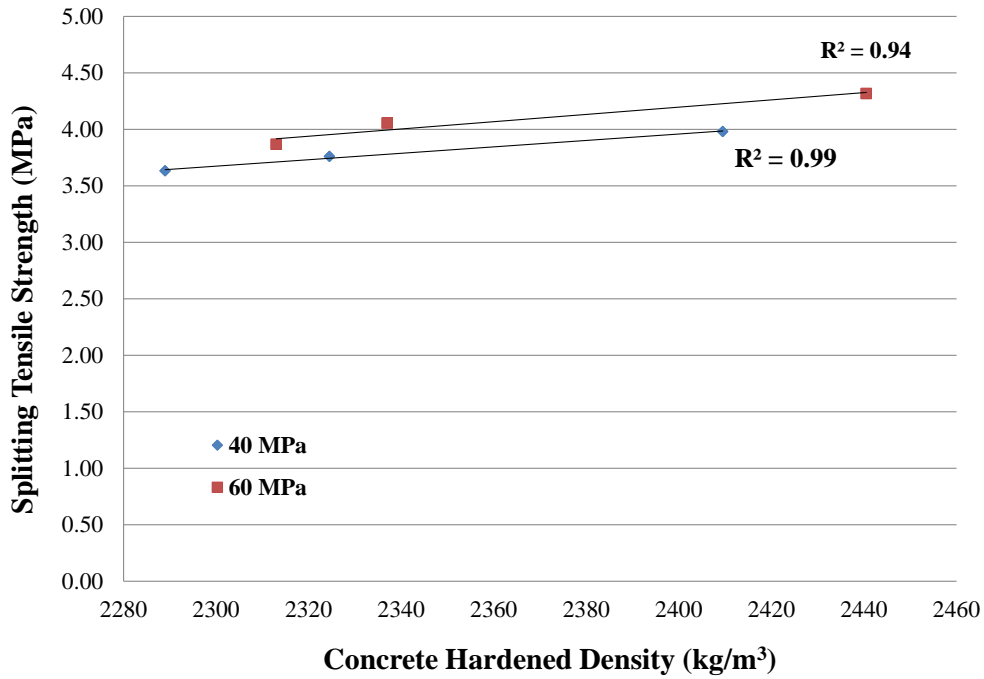


Figure 8.24 Relationship between concrete hardened density and splitting tensile strength (Phase 2 control and strength-based mixtures)

8.3.3.2 Comparison of Strength-Based and Direct Replacement Mixture Results

To assess the differences in splitting tensile strength values between the Phase 2 RCA concrete direct replacement (constant water-cement ratio) and Phase 2 RCA concrete strength-based mixtures (constant compressive strength and slump), a statistical analysis based on the 5% LSD (least significant difference) values was carried out. Note that this comparison between strength-based and direct replacement is only possible for the Phase 2 results as both mixture proportion types were batched using Method A whereas the Phase 1 direct replacement mixtures were batched using Method A and the strength-based mixtures were batched using Method B (refer to Section 5.2.2 for a description of batching methods).

The analysis was carried out separately for the 40 MPa and 60 MPa mixtures and the results are summarized in Table 8.3.

Table 8.3 Statistical comparison of the mean splitting tensile strength values between the RCA concrete direct replacement and RCA concrete strength-based mixtures

	40 MPa		60 MPa	
	*D.R. (MPa)	*S.B. (MPa)	D.R. (MPa)	S.B. (MPa)
RAC1	3.20	3.51	3.55	3.84
RAC2	3.39	3.11	4.07	3.70
RAC3	3.48	3.30	3.80	3.72
Mean	3.36	3.31	3.81	3.75
Diff. in Means	0.05		0.06	
5% LSD	0.32		0.35	

* D.R.= direct replacement mixtures, S.B. = strength-based mixtures

Based on the 5% LSD values presented above, the difference in mean splitting tensile strength values between the direct replacement and strength-based mixtures are not statistically significant. This suggests that a change in aggregate volume, slump, compressive strength and water-cement ratio (i.e., mortar properties) associated with the strength-based mixtures does not have a significant effect on the splitting tensile strength of RCA concrete. From the findings of the previous Section 8.3.3.1, it appears that it is mainly the aggregate strength (i.e., ACV) that affects the splitting tensile strength of RCA concrete, regardless of mixture proportioning type (i.e., strength-based or direct replacement).

8.3.4 Linear Coefficient of Thermal Expansion Results

To assess the effect of aggregate type on the thermal expansive properties of concrete, the linear coefficient of thermal expansion (LCTE) was measured for each concrete type. As discussed in Section 7.4.4, the LCTE is the resultant of the thermal coefficient of hydrated cement paste, the thermal coefficient of the aggregate and the aggregate content in the mix (Neville, 1997). The procedures outlined in Chapter 6 were followed to determine the LCTE.

LCTE results are presented in Table 8.4 and consist of an average of two companion specimens (A and B) that are themselves averages of two separate gauge measurements (see Section 6.2.6). Note that all LCTE specimens (NA and RCA concrete) were kept in an air dry moisture condition throughout the duration of testing.

Table 8.4 Linear coefficient of thermal expansion test results (Phase 2 control and strength-based mixtures)

Concrete Type	LCTE Specimen A $\times 10^{-6}/^{\circ}\text{C}$	LCTE Specimen B $\times 10^{-6}/^{\circ}\text{C}$	Average LCTE $\times 10^{-6}/^{\circ}\text{C}$
NAC-40	8.44	7.51	7.97
RAC1-40	8.44	7.79	8.11
RAC2-40	7.97	8.16	8.07
RAC3-40	8.34	7.88	8.11
5% LSD			2.12
NAC-60	9.73	8.99	9.36
RAC1-60	9.55	8.81	9.18
RAC2-60	8.90	9.64	9.27
RAC3-60	9.73	10.01	9.87
5% LSD			2.25

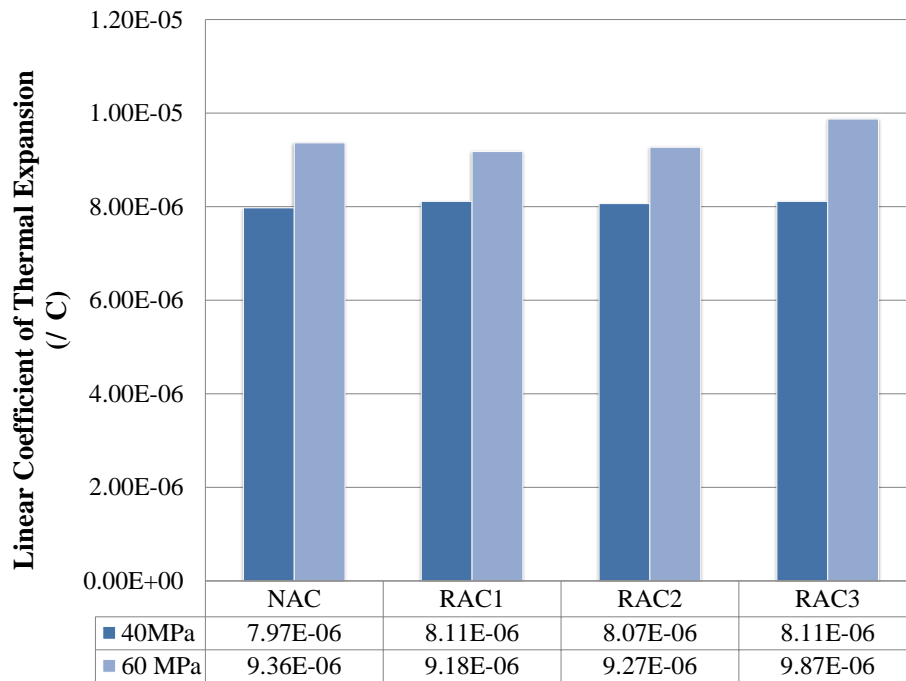


Figure 8.25 Linear coefficient of thermal expansion results (Phase 2 strength-based mixtures)

Within the 40 MPa mixtures, the NA concrete had the lowest LCTE whereas the RCA-1 concrete had the lowest LCTE in the 60 MPa. However, upon statistical analysis of the test data 5% LSD values (see Table 8.4), the relative difference between the NA and the RCA concrete was found to be statistically insignificant.

Given that LCTE varies with aggregate content and given that all the strength-based mixtures had varying water-cement ratios (i.e., hydrated paste properties) and aggregate volumes, there should have been a significant difference in LCTE values. However, similar to the direct replacement mixtures (refer to Section 7.4.4), no significant difference in LCTE values was found between the 40 and 60 MPa samples. This suggests that compressive strength and water-cement ratio may not have a significant effect on the LCTE of RCA concrete. Bekoe et al. (2010) also found no significant variation in LCTE values with varying water-cement ratios between 0.43 and 0.53.

8.3.4.1 Comparison of Strength-Based and Direct Replacement Mixtures Results

To assess the differences in LCTE values between the Phase 2 RCA concrete direct replacement (constant water-cement ratio) and Phase 2 RCA concrete strength-based mixtures (constant compressive strength and slump), a statistical analysis based on the 5% LSD (least significant difference) values was carried out. The analysis was carried out separately for the 40 MPa and 60 MPa RCA concrete mixtures and the results are summarized in Table 8.5.

Table 8.5 Statistical comparison of the mean LCTE values between the RCA concrete direct replacement and RCA concrete strength-based mixtures

	40 MPa		60 MPa	
	*D.R. $\times 10^{-6}/^{\circ}\text{C}$	*S.B. $\times 10^{-6}/^{\circ}\text{C}$	D.R. $\times 10^{-6}/^{\circ}\text{C}$	S.B. $\times 10^{-6}/^{\circ}\text{C}$
RAC1	8.95	8.11	9.73	9.18
RAC2	8.48	8.07	9.41	9.27
RAC3	8.58	8.11	9.64	9.87
Mean	8.67	8.10	9.59	9.44
Diff. in Means	0.57		0.15	
5% LSD	0.32		0.53	

*D.R.= direct replacement mixtures, S.B. = strength-based mixtures

The direct replacement LCTE values were generally higher than the strength-based mixture values. Based on the 5% LSD values presented above, the difference in mean LCTE values between the direct replacement and strength-based mixtures for the 40 MPa mixtures are statistically significant. This suggests that for the 40 MPa mixtures, changes in aggregate volume, slump, compressive strength and water-cement ratio (i.e., mortar properties) associated with the strength-based mixtures has a significant effect on the LCTE of RCA concrete.

For the 60 MPa mixtures, the 5% LSD value was higher than the differences in means between the strength-based and direct replacement mixtures suggesting no statistical difference between each set. This suggests, at the 60 MPa strength level, that the LCTE is insensitive to changes in aggregate volume, slump, compressive strength and water-cement ratio associated with the strength-based mixtures.

8.3.5 Modulus of Elasticity and Poisson's Ratio Results

The modulus of elasticity was measured for the Phase 2 strength-based mixtures to determine the effect that aggregate volume and type has on the concrete stiffness for equivalent compressive strengths (i.e., to gauge the difference between direct replacement and strength-based mixture proportions). The test setup, procedures and instrumentation for the measurement of modulus of elasticity and the Poisson's ratio are described in Chapter 6. An overall comparison between the direct replacement and strength-based mixtures' modulus of elasticity and Poisson's ratio results is presented at the end of this section. Note that all modulus of elasticity specimens (NA and RCA concrete) were kept in an air dry moisture condition throughout the duration of testing.

Modulus of elasticity and normalized modulus of elasticity results for the Phase 2 strength-based mixtures are presented in Figure 8.26, Figure 8.27, and Figure 8.28.

Overall, the NA concrete had significantly higher modulus of elasticity values (up to 15% higher) than the RCA concretes after being normalized with respect to $f'_c{}^{1/2}$ and the concrete hardened density. In Section 7.4.5.1, the concrete modulus of elasticity was found to be directly related to the aggregate modulus of elasticity. However, as was discussed, the modulus of elasticity of the original concrete (i.e., concrete from which the RCAs are derived), and consequently the modulus of elasticity of the RCA is unknown. Recall from Section 4.5.7.1 that the average secant modulus of bulk aggregate (measured during the ACV test) was determined to be a proportional measure of the actual modulus of elasticity of aggregate. Figure 8.29 presents the relationship between the modulus of elasticity of concrete and the average secant modulus of bulk aggregate.

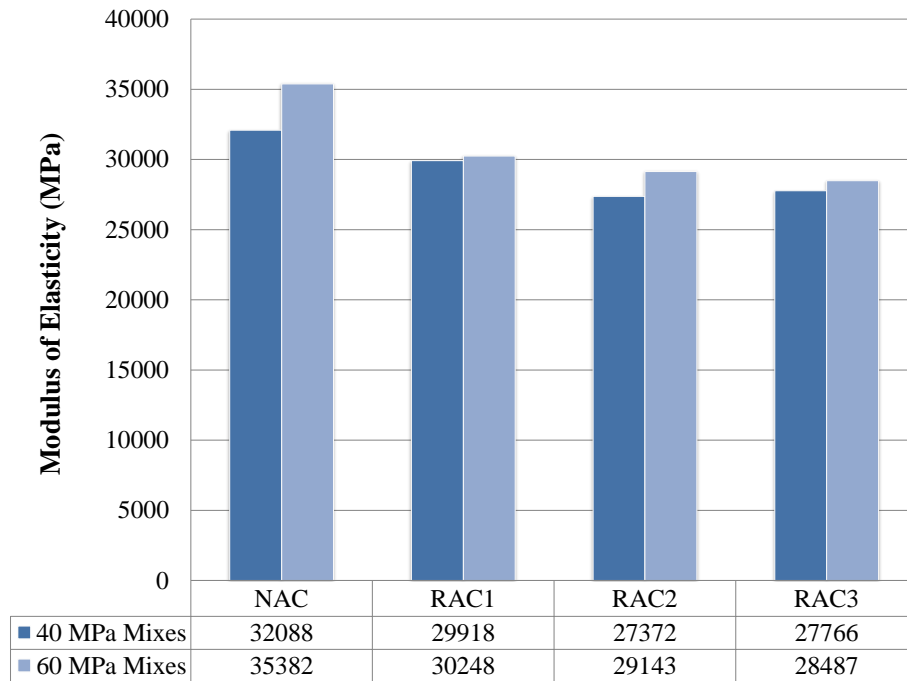


Figure 8.26 Modulus of elasticity results

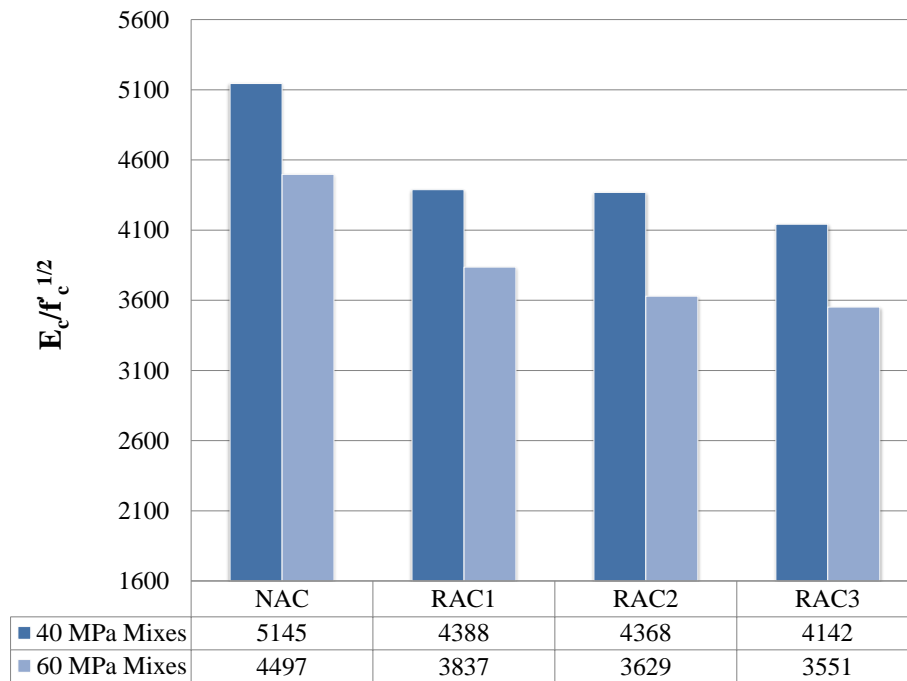


Figure 8.27 Modulus of elasticity results normalized with respect to $f_c^{1/2}$

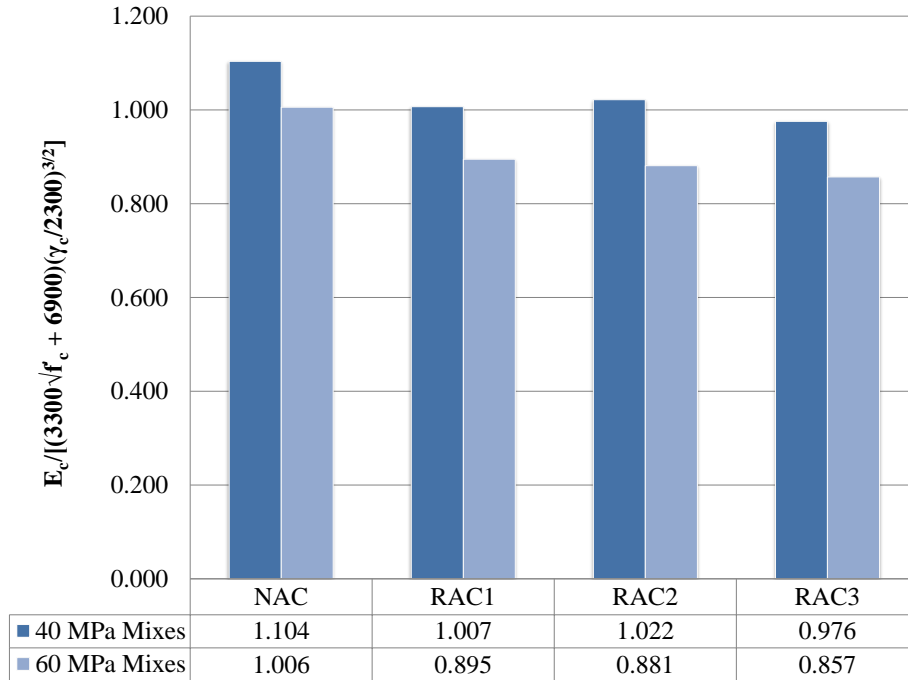


Figure 8.28 Modulus of elasticity results normalized with respect to f'_c ^{1/2} and hardened density (Phase 2 strength-based mixtures)

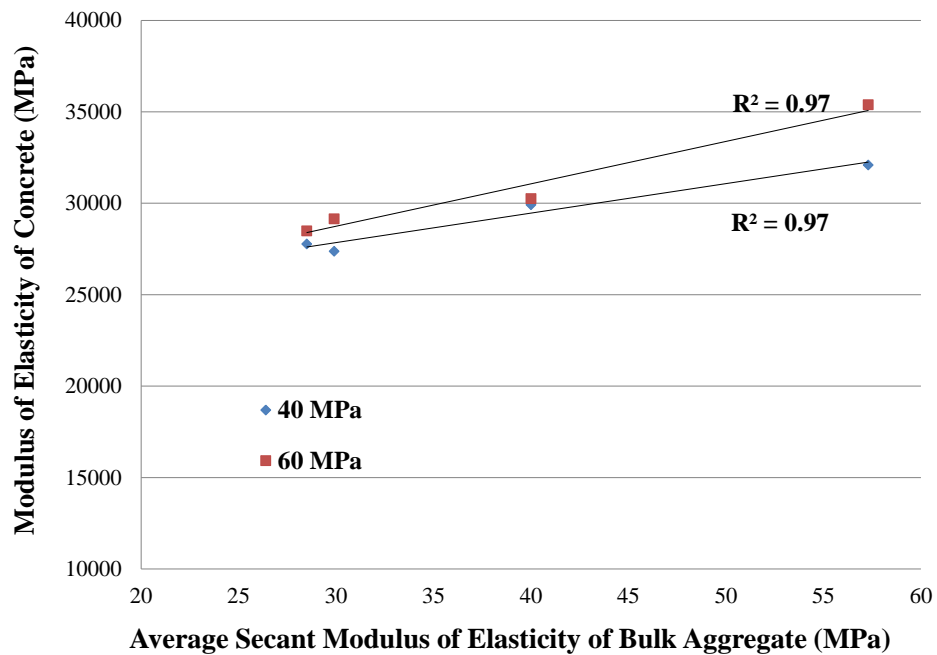


Figure 8.29 Relationship between modulus of elasticity of concrete and average secant modulus of elasticity of bulk aggregate

Recall from Section 7.4.5 that the modulus of elasticity is dependent on the concrete compressive strength, the volumetric proportion of aggregate and the modulus of elasticity of the aggregate. The strength-based mixtures have constant compressive strength but variable coarse aggregate volumes. Similar to the direct replacement results (see Section 7.4.5), a strong correlation was found between the average secant modulus of elasticity of bulk aggregate and the modulus of elasticity of concrete. These results also help to explain the differences observed in the modulus of elasticity values between the NA and RCA concrete specimens. The natural aggregate had a higher average secant modulus of elasticity of bulk aggregate value than the RCA-1, RCA-2 or RCA-3, which translated into higher modulus of elasticity values of the NA concrete (assuming concrete compressive strengths similar to the RCA concrete). Therefore, the average secant modulus of elasticity of bulk aggregate (as measured during the ACV test) may be used to assess the relative influence of various aggregates on the elastic modulus of concrete mixtures incorporating these materials as coarse aggregates.

8.3.5.1 Comparison of Strength-Based and Direct Replacement Mixtures Results

To assess the differences in modulus of elasticity values between the direct replacement (constant water-cement ratio) and strength-based mixtures (constant compressive strength and slump), a statistical analysis based on the 5% LSD (least significant difference) values was carried out. The analysis was carried out separately for the 40 MPa and 60 MPa mixtures. Table 8.6 summarizes the results of the analysis.

Table 8.6 Statistical comparison of the mean $E_c/f_c^{1/2}$ values between the direct replacement and strength-based mixtures

	40 MPa		60 MPa	
	*D.R.	*S.B.	D.R.	S.B.
RAC1	4388	4829	3837	3991
RAC2	4368	4700	3629	3917
RAC3	4142	4627	3551	3939
Mean	4299	4719	3672	3949
Diff. in Means	420		277	
5% LSD	211		189	

* D.R.= direct replacement mixtures, S.B. = strength-based mixtures

Based on the 5% LSD values presented in Table 8.6, the difference in mean values of $E_c/f_c^{1/2}$

between the direct replacement and strength-based mixtures are statistically significant. This suggests that both a change in aggregate volume and water-cement ratio (i.e., mortar properties) associated with the strength-based mixture proportions has a significant effect on the normalized modulus elasticity of RCA concrete.

8.3.5.2 Poisson's Ratio Test Results

Table 8.7 presents the average (based on three specimens) Poisson's ratios for the control and strength-based mixtures along with the coefficient of variation (C.O.V.) between the Poisson's ratios of the various concrete types, and the 5% least significant difference (5% LSD) values for each strength level. Note that all Poisson's ratio specimens (NA and RCA concrete) were kept in an air dry moisture condition throughout the duration of testing.

Table 8.7 Poisson's ratio test results (Phase 2 control and strength-based mixtures)

Concrete Type	Poisson's Ratio	Standard Deviation	C.O.V.
NAC-40	0.21	0.02	0.07
RAC1-40	0.26	0.01	0.03
RAC2-40	0.26	0.02	0.08
RAC3-40	0.15	0.03	0.23
Average	0.22		
C.O.V.	0.23		
5% LSD	0.06		
NAC-60	0.25	0.03	0.12
RAC1-60	0.28	0.01	0.02
RAC2-40	0.21	0.07	0.31
RAC3-60	0.20	0.03	0.14
Average	0.24		
C.O.V.	0.15		
5% LSD	0.11		

By examining the Poisson's ratio data and the 5% LSD values, it is evident that the 40 MPa RCA-3 concrete has a Poisson's ratio that is significantly lower than the NA, RCA-1 or RCA-2 concretes. This difference in Poisson's ratio may be attributed to a 17% lower water-cement ratio of the RCA-3 concrete as compared to the NA concrete which would produce a stronger mortar phase and may result in lower lateral strains (transverse strains of the specimen diameter) under uniaxial compression. Lower mortar strengths may result in less micro-cracking for similar concrete compressive strengths. The water-cement ratios of the other two RCA concretes

were more similar to that of the NA concrete: the RCA-1 and RCA-2 had water-cement ratios that were 8% higher and 2% lower than the NA concrete at the 40 MPa level. No significant difference exists between the NA and the RCA concretes at the 60 MPa strength level. In comparing the 40 and 60 MPa mixtures, there appears to be a slight difference in Poisson's ratio (i.e., 0.22 versus 0.24).

Differences in Poisson's ratio between the direct replacement (constant water-cement ratio) and strength-based mixtures (constant compressive strength and slump) were assessed using a statistical analysis based on the 5% LSD (least significant difference). The analysis was carried out separately for the 40 MPa and 60 MPa mixtures and the results are presented in Table 8.8.

Based on the 5% LSD values, the difference in mean values of the Poisson's ratios between the direct replacement and strength-based mixtures are not statistically significant. However, Poisson's ratios for the direct replacement mixtures (Section 7.4.5.3) are less variable than the strength-based mixtures as is demonstrated by the lower coefficients of variation values (refer to Table 8.7). This indicates that although the 5% LSD values show no statistical difference in most of the values, changing the aggregate volume and water-cement ratio (i.e., strength-based mixtures), has an effect as compared to leaving the aggregate volume and water-cement ratio constant (i.e., direct replacement mixtures).

Table 8.8 Statistical comparison of the mean Poisson's ratio values between the direct replacement and strength-based mixtures

	40 MPa		60 MPa	
	*D.R.	*S.B.	D.R.	S.B.
RAC1	0.20	0.26	0.25	0.28
RAC2	0.19	0.26	0.27	0.21
RAC3	0.21	0.15	0.25	0.20
Mean	0.20	0.22	0.26	0.23
Diff. in Means	0.02		0.03	
5% LSD	0.08		0.06	

* D.R.= direct replacement mixtures, S.B. = strength-based mixtures

It should be noted that some of the Poisson's ratio values reported in Table 8.8 (direct replacement and strength-based mixtures) are higher than the typical range (i.e., between 0.15 and 0.22) as reported in the literature for NA concrete and RCA concrete (Neville, 1997 and Ajdukiewicz and Kliszczewicz, 2002). However, given that no significant difference in

Poisson's ratio between the NA and RCA concretes was found to exist (except in the case of the RCA-3 60 MPa concrete), if the Poisson's ratio results reported are used exclusively to gauge the effect of replacing RCA with NA on the Poisson's ratio then this deviation of values from the typically reported range is not critical.

8.3.6 Modulus of Rupture Results

Similar to Phase 1, modulus of rupture (flexural strength) was measured using the same specimens used for measuring the fracture energy (i.e., single-edge notched double-cantilevered prisms). Testing for the modulus of rupture (f_r) was performed in accordance with the procedure outlined in Chapter 6. Average values (two specimens, A and B) of modulus of rupture for each concrete type are presented in Figure 8.30. The 40 MPa specimens present a similar trend as the 30 MPa specimens of Phase 1: the NA concrete had the highest f_r followed by the RCA-1, RCA-2 and RCA-3 concretes. The 40 MPa NA concrete had f_r values that were, on average, 10% higher than any of the RCA concretes. The trend changed significantly when examining the 60 MPa specimens where the NA concrete had the lowest f_r value followed by the RCA-3, RCA-2 and the RCA-1 concrete which had the highest f_r value. To eliminate the influence of compressive strength on the flexural strength and to be consistent with what is typically used in design equations, f_r values were normalized with respect to $f_c'^{1/2}$ and are summarized in Figure 8.31.

After normalizing the f_r values the trend in the 40 MPa specimens remained unchanged: the NA concrete had the highest $f_r/f_c'^{1/2}$ values followed by the RCA-1, RCA-2 and RCA-3 concretes. In the case of the 60 MPa specimens, the RCA-1 specimens had $f_r/f_c'^{1/2}$ values that were 27% higher than the NA concrete specimens. These results are in contrast to previous researchers, who have consistently reported decreases in flexural strength when comparing RCA concretes to NA concretes (Chen et al., 2003, Topcu and Sengel, 2004, and Katz, 2003). Similar to the Phase 1 specimens, a stronger correlation ($R^2 = 0.82$) between f_r and the ACV for the lower strength (40 MPa) specimens was found (Figure 8.32). This confirms that as compressive strength increases, the relationship between ACV and modulus of rupture becomes more variable. Further investigation of the failure surfaces and the main mechanism for failure will be carried out in Section 8.3.7.2 where the fracture energy results will be evaluated. An overall comparison of the

Phase 1 and 2 results is presented in Section 8.4.2.

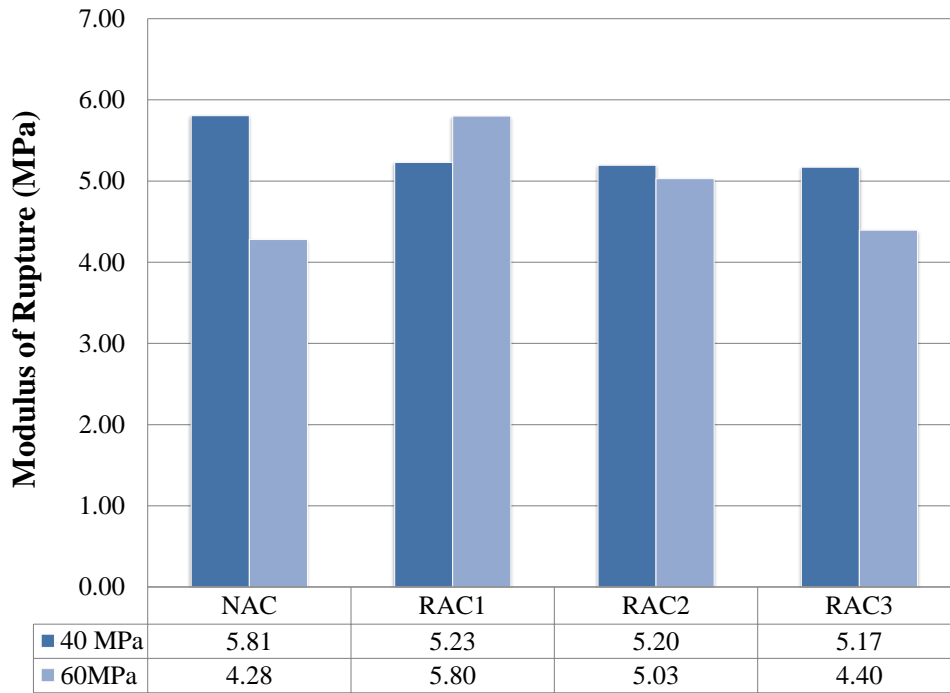


Figure 8.30 Modulus of rupture (flexural strength) results (Phase 2 control and strength-based mixtures)

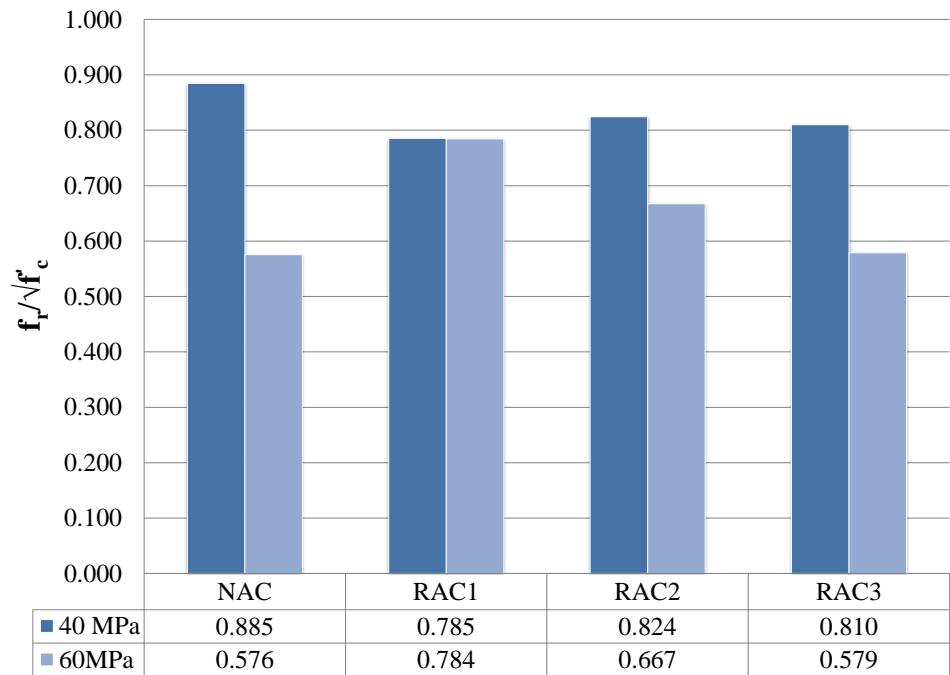


Figure 8.31 Normalized Modulus of rupture (flexural strength) results (Phase 2 control and strength-based mixtures)

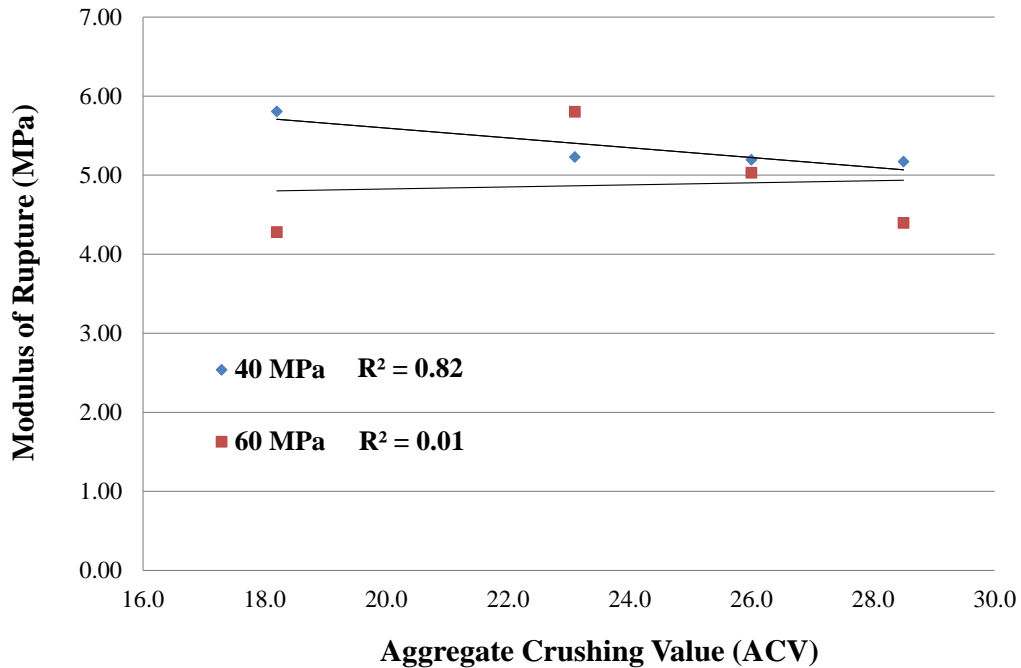


Figure 8.32 Relationship between aggregate crushing value and modulus of rupture (Phase 2 control and strength-based mixtures)

8.3.7 Fracture Energy Results

Similar to Phase 1, single edge-notched double-cantilevered (SENDC) fracture energy specimens were cast in conjunction with beam-end specimens, compressive strength and splitting tensile cylinders. The secondary study (Phase 2) involved the testing of 16 fracture energy specimens consisting of four aggregate types (NA, RCA-1, RCA-2 and RCA-3), two compressive strengths (40 and 60 MPa) and duplicate specimens. The full test setup, definitions, specimen dimensions and calculation methods are presented in Section 6.2.7.

The main objective of the Phase 2 fracture energy experimental program was to measure the effect of the fracture energy of RCA concrete on bond strength and confirm trends observed during Phase 1. As a secondary objective, the effect of various aggregate and concrete properties on the fracture energy of RCA concrete was evaluated. The NA, RCA-1 and RCA-3 fracture energy specimens were cast in conjunction with the Phase 2 beam-end specimens for use of gauging the effect of fracture energy on bond strength. The RCA-2 concrete specimens were cast 13 weeks after the NA, RCA-1 and RCA-3 specimens and were used in the evaluation of the effect of aggregate and concrete properties on fracture energy of RCA concrete. Based on the

availability of laboratory testing equipment and technical resources, the fracture energy specimens were tested at 18 weeks (RCA-2 concrete specimens) and 30 weeks (NA, RCA-1 and RCA-3 concrete specimens) after batching. As a result, separate compressive strength and splitting tensile strength cylinders were cast to provide data for correlation with fracture energy and modulus of rupture results. Table 8.9 presents the fracture energy testing results along with the concrete compressive strength, concrete splitting tensile strength and the peak load for the Phase 2 specimens.

Table 8.9 Fracture energy test results (Phase 2 control and strength-based mixtures)

Specimen ID	Age [days]	f_c [MPa]	f_{ct} [MPa]	Peak Load [N]	$G_{f,1mm}^*$ [N/m]
NAC-40A		44.1	3.84	5422	144.3
NAC-40B		42.2	3.36	6380	116.9
Mean	217	43.2	3.60	5901	130.6
RAC1-40A		46.0	3.13	5146	106.3
RAC1-40B		42.8	3.47	5149	123.1
Mean	216	44.4	3.30	5148	114.7
RAC2-40A		39.7	2.79	5756	126.7
RAC2-40B		39.7	2.79	4532	104.2
Mean	123	39.7	2.79	5144	115.5
RAC3-40A		40.3	3.67	6015	119.1
RAC3-40B		41.2	3.61	5130	84.2
Mean	215	40.8	3.64	5573	101.7
NAC-60A		52.7	3.76	5337	125.2
NAC-60B		58.1	3.80	5298	149.0
Mean	217	55.4	3.78	5318	137.1
RAC1-60A		54.7	3.85	4341	111.1
RAC1-60B [†]		49.9	3.61	-	-
Mean	216	52.3	3.73	4341	111.1
RAC2-60A		56.8	3.30	5029	103.8
RAC2-60B		56.8	3.30	5090	82.3
Mean	123	56.8	3.30	5060	93.1
RAC3-60A		56.4	3.71	4476	120.7
RAC3-60B		59.0	3.54	4398	86.7
Mean	215	57.7	3.63	4437	103.7

* Represents the fracture energy up until an average midspan deflection of 1 mm. In cases where the specimens did not reach a maximum midspan deflection of 1 mm, the fracture energy was calculated using the total area under the load-deflection plot.

[†] Equipment malfunction, no fracture energy data available for specimen.

As discussed in Section 8.2.5, there is currently no standard definition for the region over which the fracture energy should be calculated, a displacement-based limit was adopted for this

research. Therefore, all fracture energy values reported represent the fracture energy calculated up until an average midspan deflection of 1.0 mm (i.e., $G_{f,1mm}$). Limiting the fracture energy data to this displacement level allows for the relative comparison between various concrete types and compressive strengths. Note that the correlation results between fracture energy and bond strength for Phase 2 are presented in Chapter 9.

Overall, the NA concrete had the highest fracture energies at both the 40 and 60 MPa strength levels followed by the RCA-1 concrete. This trend is different from that observed in Phase 1 where the RCA-1 and RCA-2 concrete had the highest average fracture energy at the 30 MPa and 50 MPa strength levels, respectively. On average, the Phase 2 NA concrete specimens had fracture energies that were between 12% and 32% higher than the RCA concretes. This range coincides with values reported in the literature (Casuccio et al., 2008 and Ong and Ravindrarajah, 1987). Similar to Phase 1, it must be noted that although distinct differences in fracture energy were observed between NA and RCA concrete specimens, the specimen-to-specimen variation may be too high in some cases to make conclusive statements on the effect of replacing NA with RCA on the fracture energy of the resulting concrete.

Figure 8.33 presents the relationship between aggregate strength (ACV) and the fracture energy.

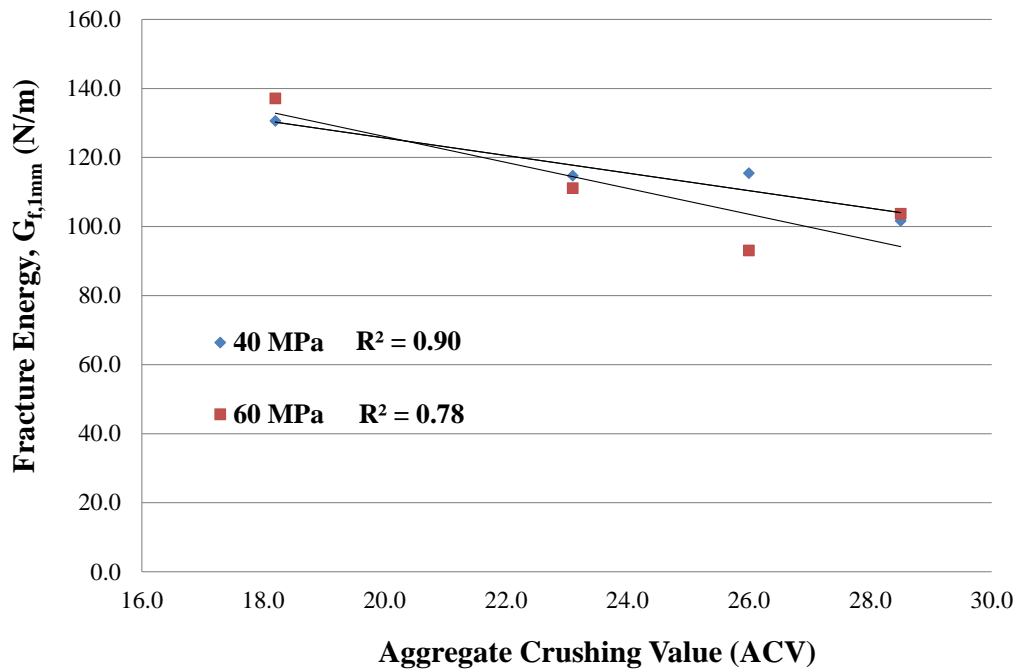


Figure 8.33 Relationship between aggregate strength (ACV) and fracture energy

Overall, a fairly good correlation ($R^2 = 0.90$) was found for the 40 MPa specimens whereas a slightly poorer relation ($R^2 = 0.78$) was found for the higher strength, 60 MPa specimens. In general, the trend lines indicate that as fracture energy decreases, the ACV increases (aggregate strength decreases). This finding is similar to that presented by Darwin et al. (2001) who noted the influence of coarse aggregate strength on fracture energy of concrete. They found that concrete incorporating high strength natural basalt as coarse aggregate produced fracture energies that were higher than concrete incorporating lower strength natural limestone. This trend will be further discussed in Section 8.4.3 in the overall evaluation of the combined results of Phase 1 and Phase 2. Additional relationships were investigated including the relationship between fracture energy and compressive strength, fracture energy and splitting tensile strength, and fracture energy and modulus of rupture however, no significant correlations were found.

8.3.7.1 Load-Deflection Response of Phase 2 Fracture Energy Specimens

The load-deflection responses for each fracture energy specimen are presented in Figure 8.34 to Figure 8.41. The same general response was observed as the Phase 1 specimens: all load versus midspan deflection curves consisted of a nearly linear ascending branch up until the peak load was reached followed by a convex descending branch which asymptotically approached the horizontal axis until zero load.

Overall, the 60 MPa samples had shorter tails (i.e., less deformation after 1 mm midspan deflection had been reached) than the 40 MPa samples which suggest more brittle behaviour. No significant difference in initial stiffness (i.e., slope of ascending linear branch) was observed between the NA and the RCA concretes. By examining the load deflection curves of the NA concrete specimens (Figure 8.34 and Figure 8.35) and the RCA-3 concrete specimens (Figure 8.40 and Figure 8.41) noticeable differences in behaviour was observed between duplicate specimens. This difference in load-deflection behaviour is reflected in the calculated fracture energy values for the NA and RCA-3 concrete specimens.

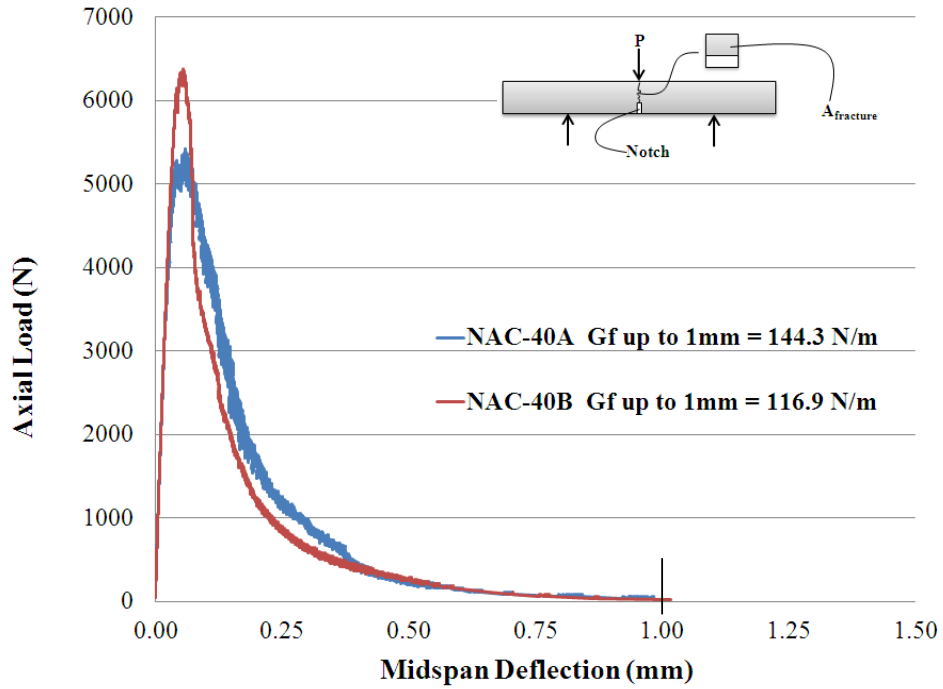


Figure 8.34 Load vs. midspan deflection for 40 MPa NA concrete fracture energy specimens (Phase 2)

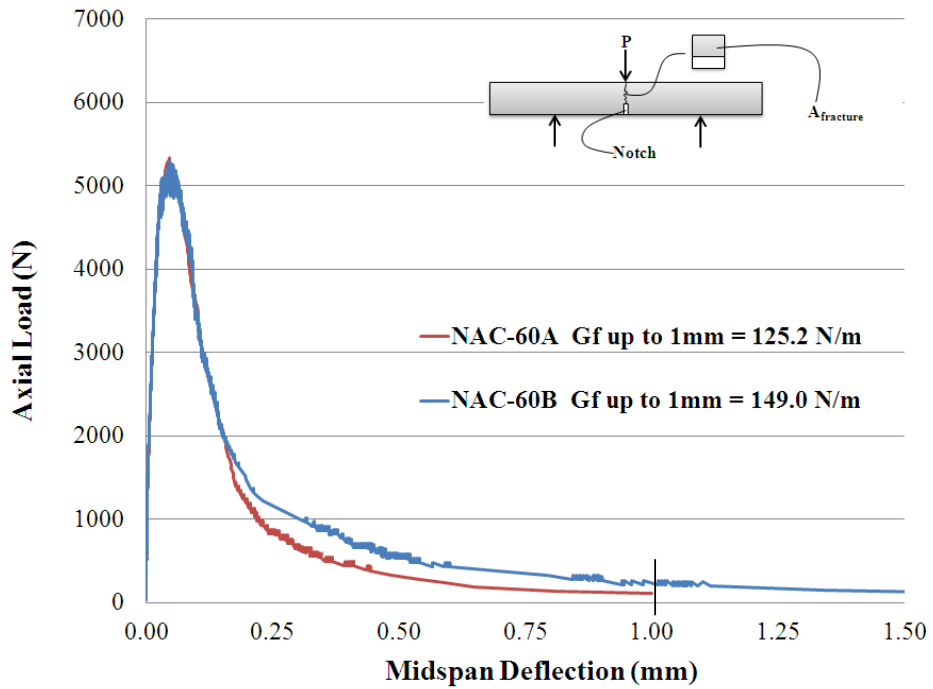


Figure 8.35 Load vs. midspan deflection for 60 MPa NA concrete fracture energy specimens (Phase 2)

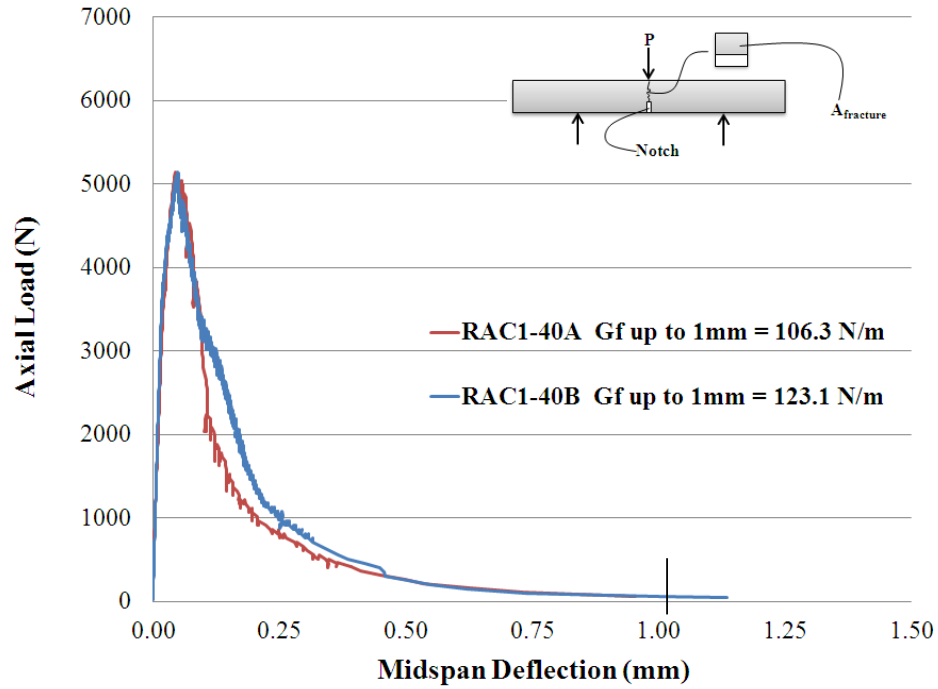


Figure 8.36 Load vs. midspan deflection for 40 MPa RCA-1 concrete fracture energy specimens (Phase 2)

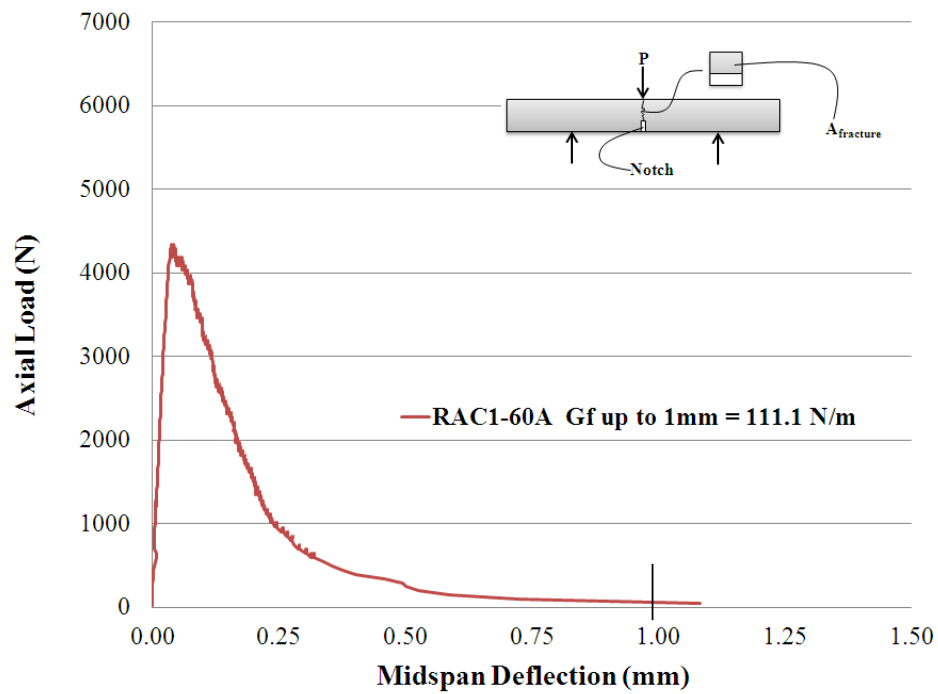


Figure 8.37 Load vs. midspan deflection for 60 MPa RCA-1 concrete fracture energy specimens (Phase 2)

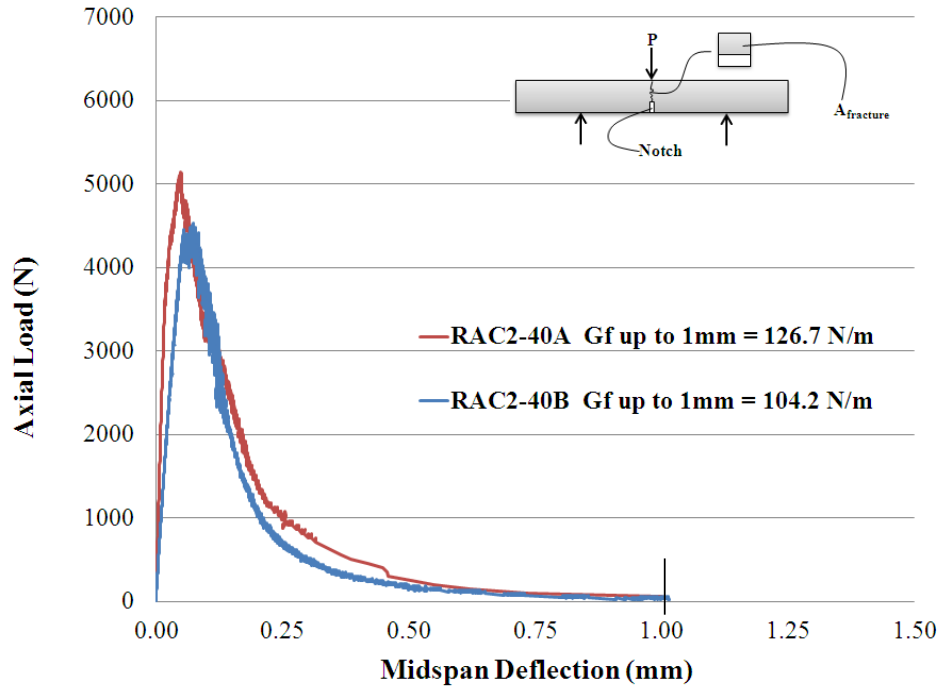


Figure 8.38 Load vs. midspan deflection for 40 MPa RCA-2 concrete fracture energy specimens (Phase 2)

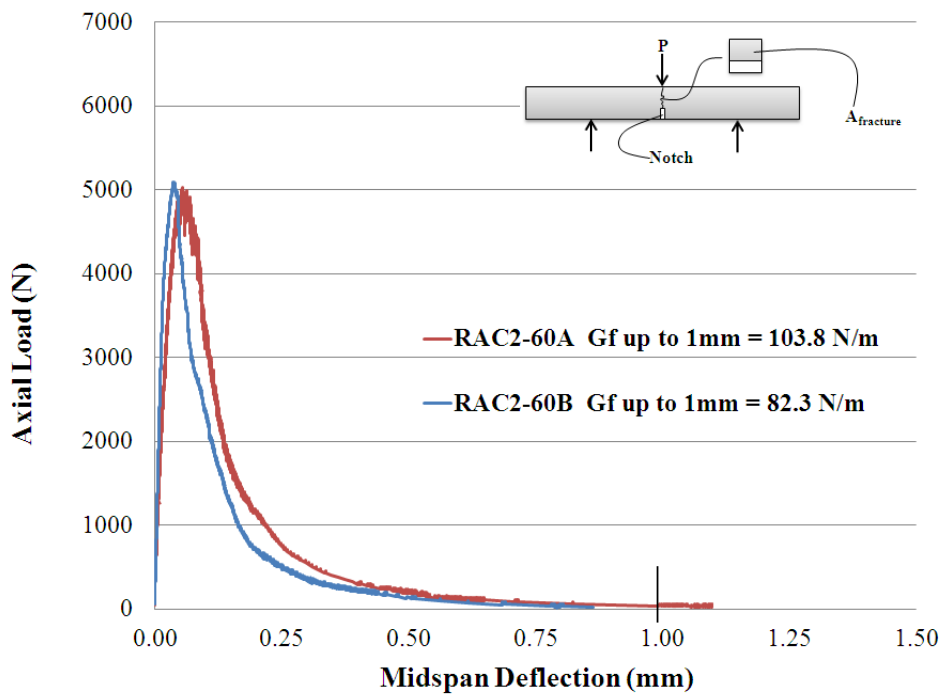


Figure 8.39 Load vs. midspan deflection for 60 MPa RCA-2 concrete fracture energy specimens (Phase 2)

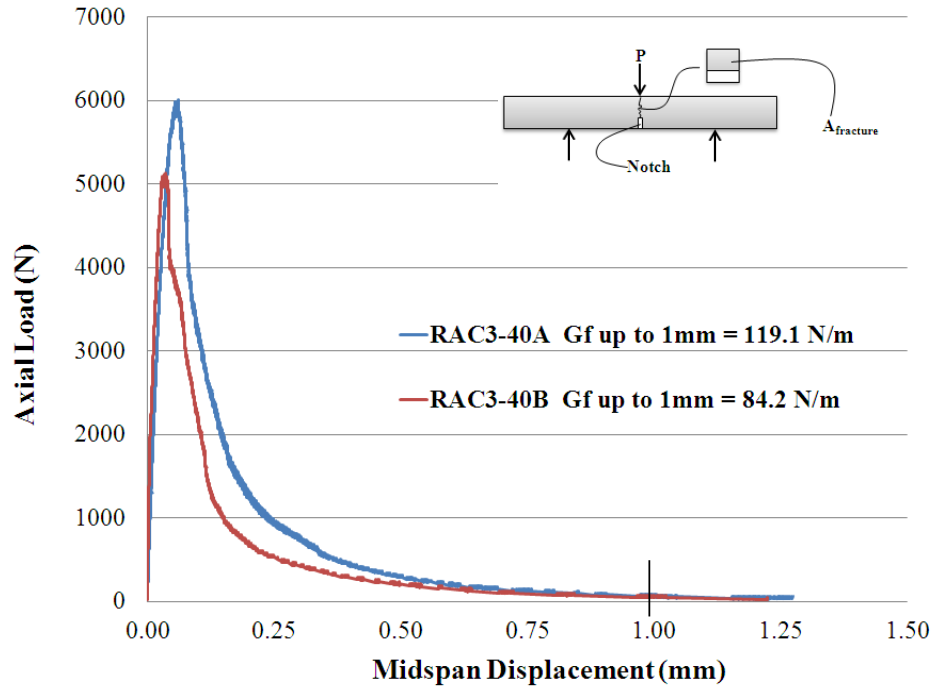


Figure 8.40 Load vs. midspan deflection for 40 MPa RCA-3 concrete fracture energy specimens (Phase 2)

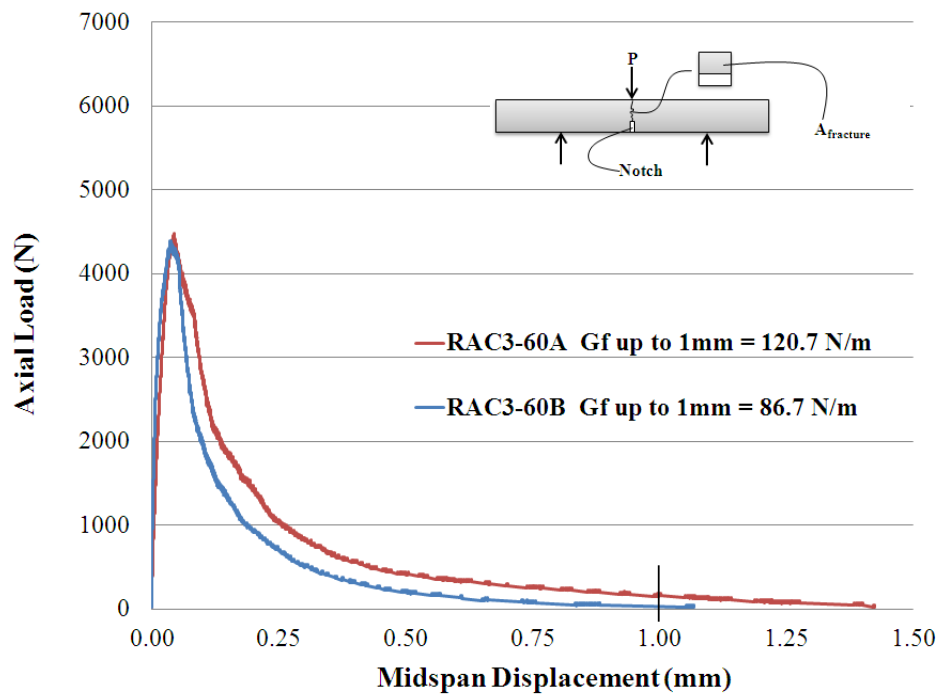


Figure 8.41 Load vs. midspan deflection for 60 MPa RCA-3 concrete fracture energy specimens (Phase 2)

8.3.7.2 Examination of Fracture Surfaces of the Fracture Energy and Modulus of Rupture Specimens

Following the same procedure as Phase 1, once fracture energy (and modulus of rupture) specimens were tested; the fracture surface of each specimen was photographed, measured (to obtain an area of fracture surface) and observed. As mentioned previously in Section 8.2.5.1, the strength-based mixtures had varying water-cement ratios which equates to varying mortar strengths among the several concrete types. Therefore, the process of isolating the resulting failure mechanism of the strength-based mixtures is more complex compared to that of the direct replacement mixtures. In the case of strength-based mixtures, the fracture energy (and modulus of rupture) may be influenced by a number of factors including, the mortar strength, aggregate strength, mortar-aggregate bond properties (and indirectly, coarse aggregate surface texture), coarse aggregate shape, volume of coarse aggregate, and the quantity and properties of deleterious materials.

Figure 8.42 depicts the fracture surfaces of the 40 MPa specimens and Figure 8.43 depicts the fracture surfaces of the 60 MPa specimens. In general, fracture planes occurred mainly through the coarse aggregates for both the NA concrete specimens and RCA concrete specimens. This indicates that coarse aggregate strength governed the fracture energy of the concrete in the Phase 2 specimens. This observed failure mechanism further supports the very good correlation found in Figure 8.33 between ACV and fracture energy (i.e., as aggregate strength increases, fracture energy increases). Some slight variability in the fracture energy results may be explained by the observation of the corresponding fracture surfaces. The 60 MPa NA concrete Specimen B had a fracture energy that was 16% higher than Specimen A which may be a result of the protruding smooth natural aggregate particle as seen in Figure 8.43. In addition, pieces of deleterious substances (e.g., wood chips, Styrofoam, metal, asphalt, etc.) can be observed along the RCA-2 concrete fracture planes in Figure 8.43.

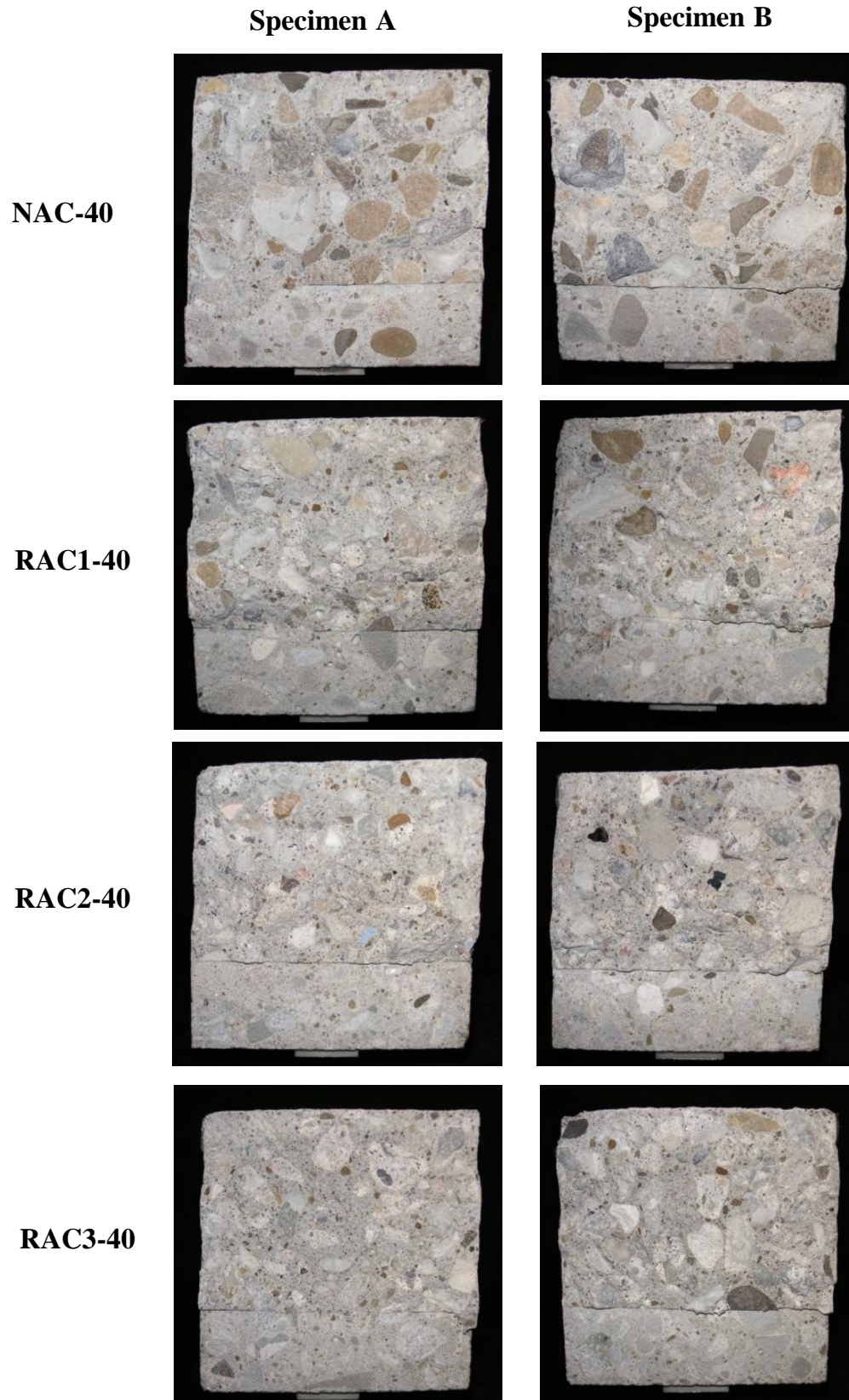


Figure 8.42 Fracture zones of fracture energy prisms (Phase 2 40 MPa specimens)

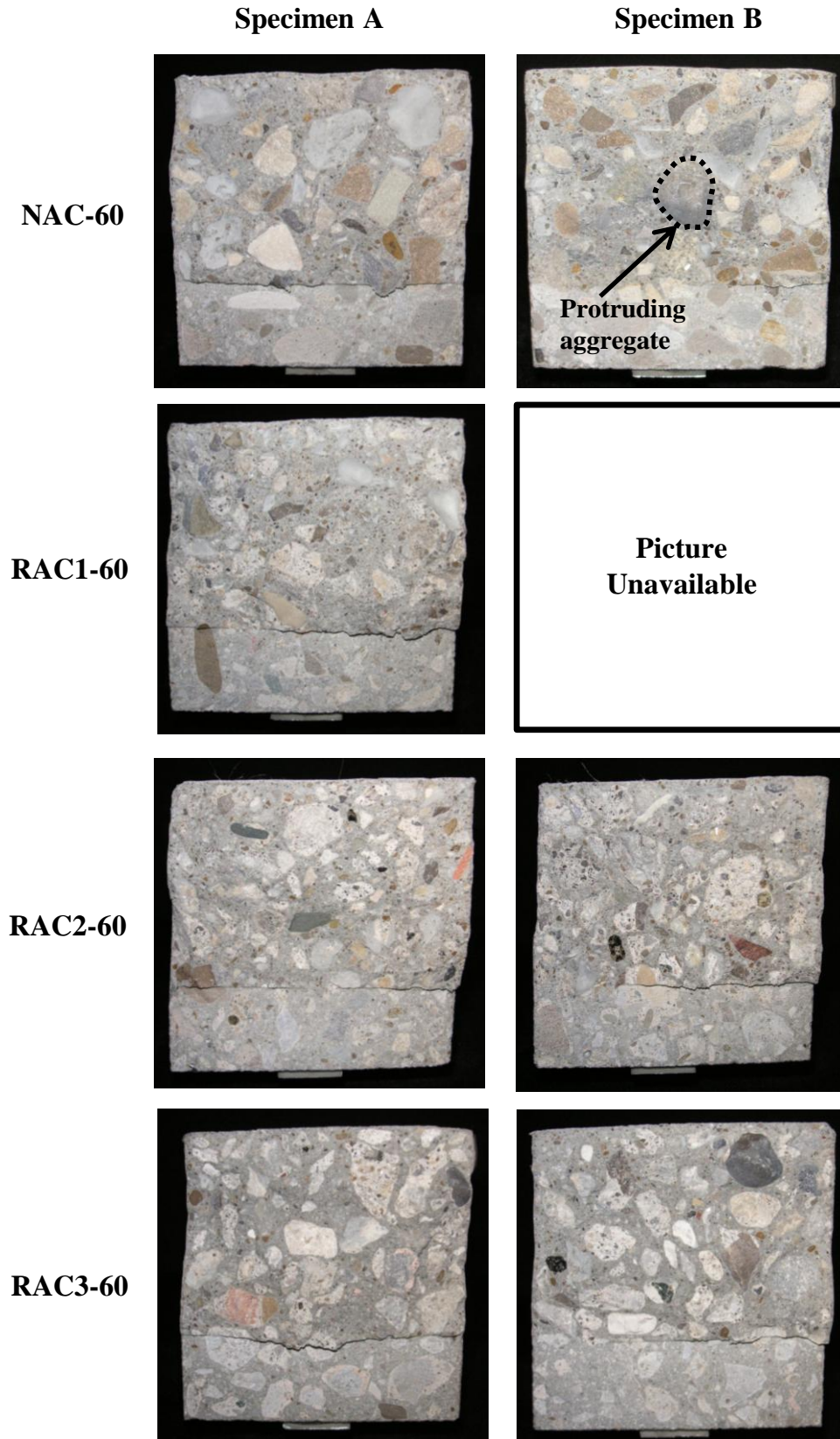


Figure 8.43 Fracture zones of fracture energy prisms (Phase 2 60 MPa specimens)

8.3.8 Conclusions from Phase 2 Mixtures

Based on the analysis and findings of the Phase 2 strength-based mixtures, the following set of conclusions have been compiled.

1. Through small adjustments of mixture proportions and through the use of water-reducing admixtures, using RCA-1 and RCA-2 as a replacement for natural aggregate in concrete up to 60 MPa is feasible. However, producing higher strength RCA-3 concrete requires a significant increase in the cement content and therefore, may not be practical for use in concrete with strengths of 60 MPa or higher (or with w/c ratios of 0.30 or lower).
2. Replacing natural coarse aggregate with RCA-1 requires less cement than an equivalent NA concrete. This is a direct result of the stronger-mortar aggregate bond properties of the RCA-1 which leads to higher compressive strengths for equivalent cement contents.
3. The NA concrete had the highest f_{ct}/f'_c values followed by the RCA-1, RCA-2 and RCA-3 concretes. Strong relationships exist between f_{ct}/f'_c , ACV and concrete hardened density.
4. Overall, the differences in LCTE between the NA concrete and the RCA concretes were statistically insignificant. However, a strong relationship was found to exist between the LCTE and the water-cement ratio (related to thermal properties of cement paste) and the aggregate density (related to thermal properties of aggregate).
5. The NA concrete had elastic modulus values up to 15% higher than an RCA concrete with similar compressive strength. The relationship between the average secant modulus of bulk aggregate and the concrete modulus of elasticity discovered in Phase 1 was confirmed through a strong correlation.
6. Only the 40 MPa RCA-3 concrete had a Poisson's ratio that was statistically different from the NA, RCA-1 and RCA-2 concretes. This may be a result of the lower water-cement ratio of the RCA-3 concrete as compared to the other concretes. A lower water-cement ratio would produce mortar of higher strength which may reduce the amount of mortar cracking and assist in reducing the lateral strains produced from the uniaxial compressive stress.
7. The NA concrete had normalized modulus of rupture ($f_r/f'_c{}^{1/2}$) values that were up to 27% higher than for an equivalent RCA concrete. At lower concrete strengths (i.e., 40 MPa),

the modulus of rupture appears to be dependent on the strength of coarse aggregate. In this case, the NA concrete had the highest modulus of rupture followed by the RCA-1, RCA-3 and RCA-2 concretes. In contrast, at higher concrete strengths (i.e., 60 MPa), the strength of coarse aggregate has little or no effect on the modulus of rupture.

8. Overall, the NA concrete had fracture energies that were between 12% and 32% higher than the RCA concretes. Very good correlations between aggregate strength (i.e., ACV) and the average fracture energy were found at the 40 and 60 MPa strength levels. This suggests a strong dependence of fracture energy on aggregate strength which is in contrast with the results of Phase 1.

8.4 Evaluation of Combined Results from Phases 1 and 2

After systematically examining the testing results of the Phase 1 and 2 strength-based and direct replacement mixtures separately, this final section examines overall trends found when combining the results of each mixture proportion type and phase.

8.4.1 Effect of Aggregate Properties on Splitting Tensile Strength

Based on the results of the Phases 1 and 2 strength-based mixtures, a fairly strong relationship was found between the aggregate crushing value and $f_{ct}/f_c^{1/2}$. Although the coefficient of determination is low, Figure 8.44 illustrates the general trend that as the aggregate crushing value increases (aggregate crushing strength decreases), the normalized splitting tensile strength, f_{ct}/f_c , also decreases. In addition, it is noticed that at higher compressive strengths (i.e., 50 MPa or higher), there is a very good correlation between ACV and f_{ct}/f_c .

As discussed in Sections 8.2.3 and 8.3.3, the fracture planes occurred mainly through the aggregates in the 50 and 60 MPa samples indicating that the aggregate strength governed the splitting tensile strength. This suggests that using lower strength RCA as full replacement of natural aggregate in concrete with compressive strengths of 50 MPa or higher (even with statistically similar compressive strengths) could significantly reduce the splitting tensile strength of the resulting concrete. In addition to the strength of the aggregate, the volume of the aggregate in the concrete mixture was also found to have a significant effect on $f_{ct}/f_c^{1/2}$ as shown in Figure 8.45.

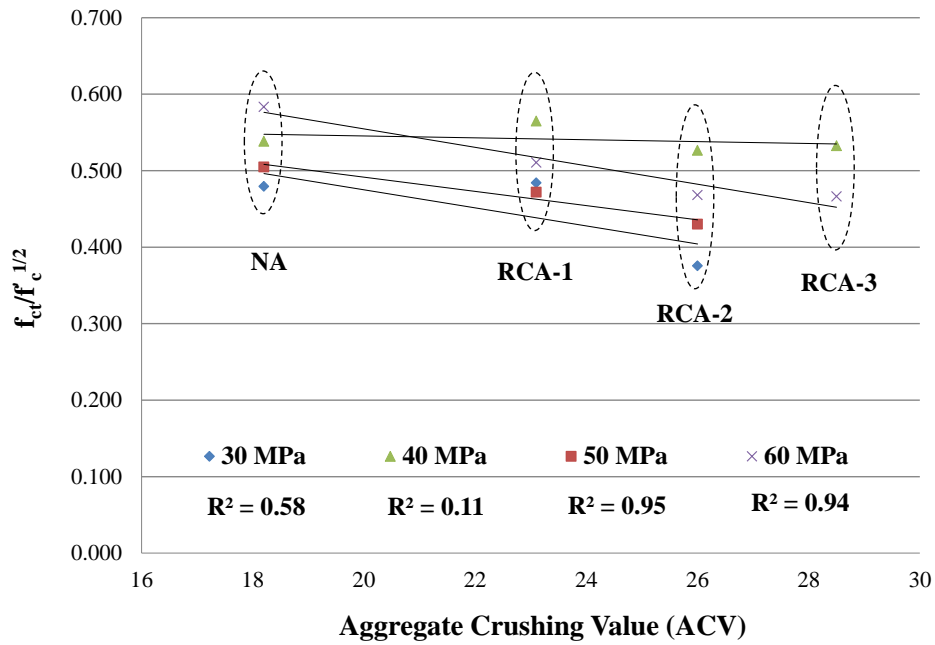


Figure 8.44 Relationship between splitting tensile strength normalized to compressive strength and aggregate crushing value

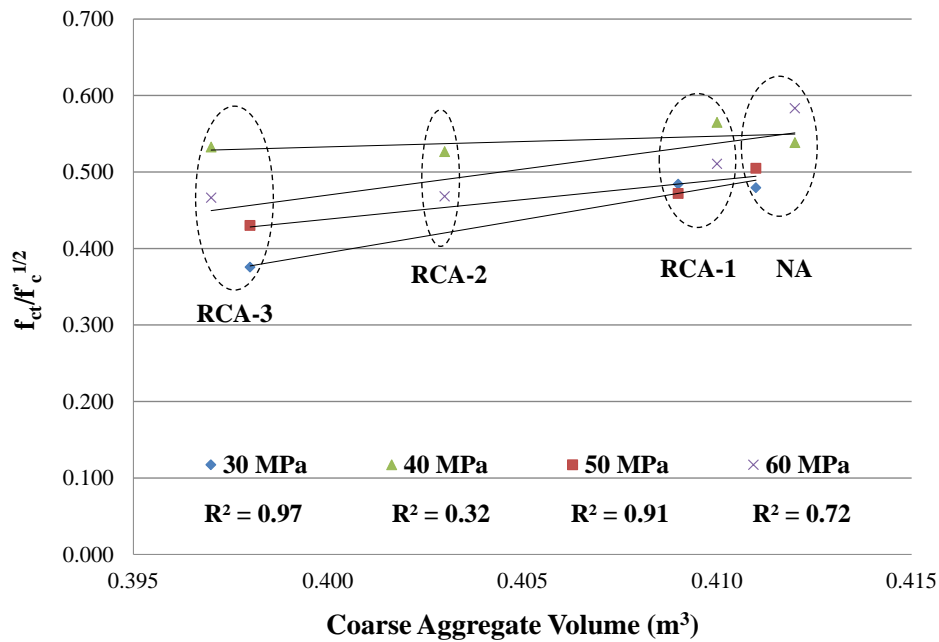


Figure 8.45 Relationship between splitting tensile strength normalized to compressive strength and coarse aggregate volume in concrete

The influence of other aggregate properties such as the abrasion resistance, relative density and

adhered surface moisture (indirect measure of surface roughness) on $f_{ct}/f_c^{1/2}$ was assessed, although no significant relationships were found at any of the four compressive strength levels.

8.4.2 Effect of Aggregate Strength on Modulus of Rupture

Based on the results presented in Phase 1 and Phase 2, an overall evaluation of the effect of aggregate strength (measured via the ACV) on the modulus of rupture normalized with respect to the compressive strength ($f_r/f_c^{1/2}$) is presented through the use of Figure 8.46 and Figure 8.47.

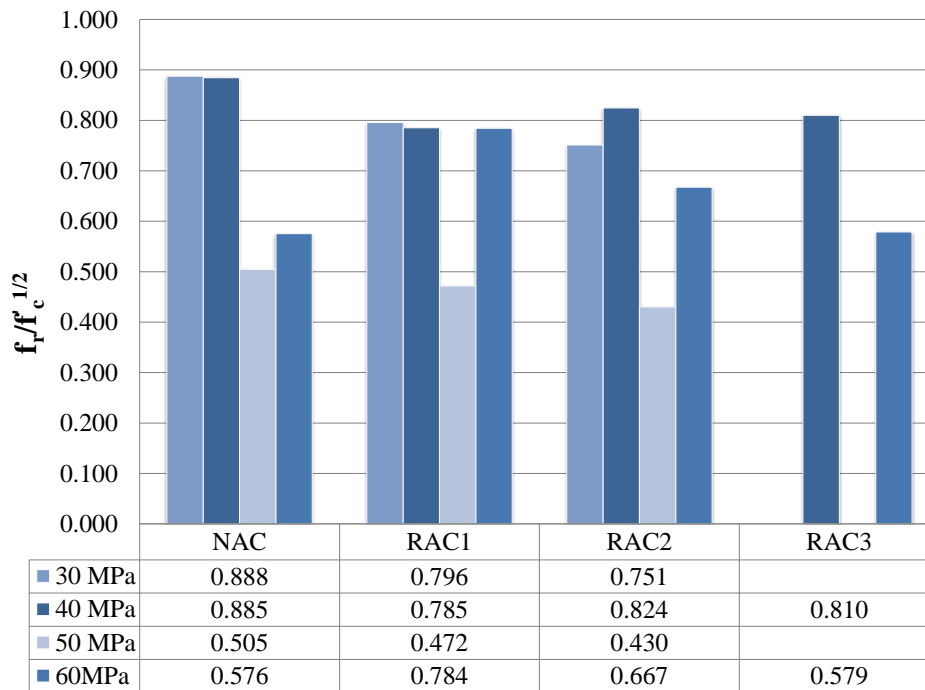


Figure 8.46 Modulus of rupture test results (Combined Phase 1 and 2 control and strength-based mixtures)

The influence of other aggregate properties such as the abrasion resistance, relative density and adhered surface moisture (indirect measure of surface roughness) on $f_r/f_c^{1/2}$ was assessed however, no significant relationships were found at any of the four compressive strength levels. In addition, no significant relationship was found between the coarse aggregate volume and the modulus of rupture or $f_r/f_c^{1/2}$.

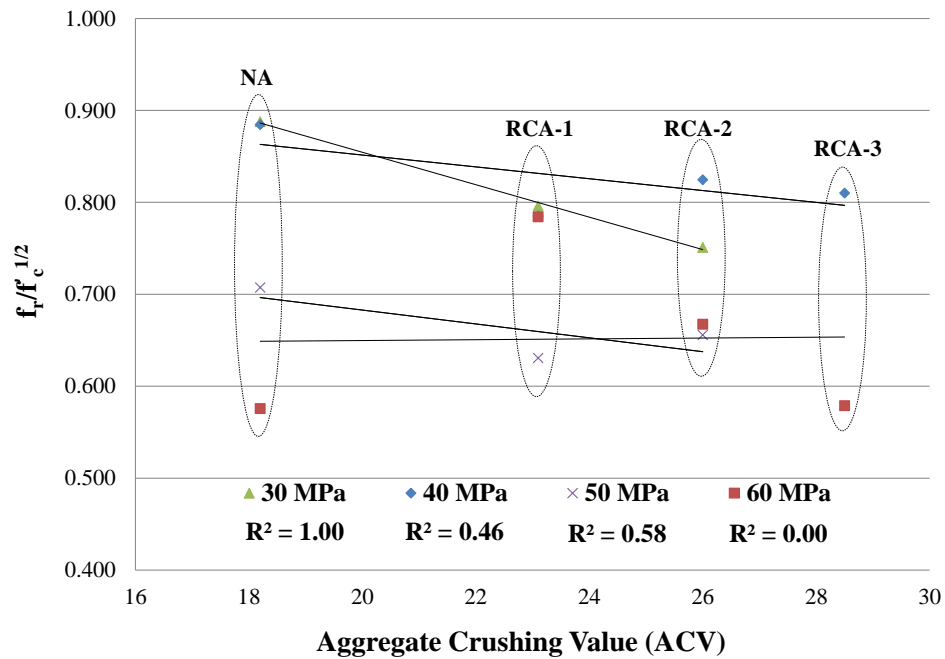


Figure 8.47 Relationship between aggregate crushing value and $f_r/f_c^{1/2}$ (Combined Phase 1 and 2 results)

Based on the trends presented in Figure 8.47, several observations and conclusions can be made:

- 1) As concrete compressive strength increases, the effect of coarse aggregate strength (as measured by the ACV) on $f_r/f_c^{1/2}$ decreases. This is particularly evident in the case of high strength concrete (i.e., 60 MPa or higher) where aggregate strength appears to have no effect on $f_r/f_c^{1/2}$. Perhaps at higher concrete strengths the failure mechanism changes (i.e., fracture planes now pass mainly through the aggregate instead of around) where the coarse aggregate strength becomes the governing factor for $f_r/f_c^{1/2}$.
- 2) At lower concrete strengths (i.e., 40MPa or lower), increasing the coarse aggregate strength (i.e., decreasing ACV) equates to an increase in $f_r/f_c^{1/2}$. Perhaps at higher concrete compressive strengths, the mortar strength (as governed by the water-cement ratio) has a higher influence on $f_r/f_c^{1/2}$.
- 3) At lower concrete strengths, replacing natural aggregate with RCA (while maintaining similar compressive strengths and slump values) decreases the $f_r/f_c^{1/2}$ of the resulting concrete.

8.4.3 Overall Evaluation of the Fracture Energy of RCA Concrete

In general, the fracture energies measured during this research study (i.e., combined Phase 1 and Phase 2 results) are highly variable, even within identical specimens. The Phase 1 results identified that fracture energy was independent of aggregate strength (ACV) whereas, the Phase 2 results indicated the opposite trend showing a strong relationship between aggregate strength and fracture energy. In both phases, fracture energy was found to be independent of concrete compressive strength, splitting tensile strength and flexural strength. To assess the overall effect that replacing natural aggregate with RCA has on the fracture energy of concrete, a relative comparison between typical ranges of fracture energies for NA concretes found in the literature was compared to the fracture energy results of the RCA concretes tested in this research study. Table 8.10 summarizes the fracture energy test statistics for the combined Phase 1 and 2 results.

Table 8.10 Summary of fracture energy test results statistics (Combined Phase 1 and 2)

	Phase 1 (NA + RCA Concrete)	Phase 2 (NA + RCA Concrete)	NA Concrete	RCA Concrete
Range of f_c (MPa)	33.7 to 52.0	39.7 to 59.0	36.6 to 58.1	33.7 to 59.0
Range of $G_{f,1mm}$ (N/m)	56.2 to 134.4	82.3 to 149.0	93.6 to 149.0	56.2 to 134.4
Mean $G_{f,1mm}$ (N/m)	100.4	113.6	117.1	103.7
Std. Deviation (N/m)	18.6	19.8	20.9	18.8
Coeff. of Variation	0.19	0.17	0.18	0.18

By comparing the data presented in Table 8.10, the NA concrete overall has mean fracture energies that are 11% higher than the RCA concretes and both data sets have similar coefficients of variation. Table 8.11 summarizes the findings of other researchers who have measured the fracture energy of NA concrete.

If the experimental data is compared to the NA concrete fracture energy results reported in Table 8.11, it is noticed that both the experimental NA concrete and RCA concrete fracture energy ranges fall within the ranges reported in the literature. It should be noted that the results presented in Table 8.11 represent concrete types incorporating either limestone or granite coarse aggregate.

Table 8.11 Summary of fracture energy data for NA concrete specimens reported by other researchers

Researchers:	Aggregate Type(s) Assessed	Notched Beam Dimensions ** (H x W x L (N))	Concrete Compressive Strength Range (MPa)	NA Concrete Fracture Energy Range (N/m)
Martin et al. (2007)	Natural rounded and angular	100 x 75 x 533 (25)	39.5 to 48.1	85.8 to 120.8
Darwin et al. (2001)*	Crushed natural limestone	100 x 100 x 350 (25)	30.3 to 85.7	36 to 70
Casuccio et al. (2008)†	Crushed natural granite	105 x 75 x 400 (50)	18.1 to 48.4	143 to 155
Ong and Ravindrarajah (1987) †	Crushed natural granite ††	50 x 50 x 600 (25)	24.0 to 42.5	60.5 to 82.5
Overall Range:			18.1 to 85.7	36 to 155

* Results reported include only those from concrete incorporating natural limestone coarse aggregates.

** L = height, W = width, L = clear span, N = notch depth, with all dimensions in mm.

† Results reported include only the results of the natural coarse aggregate concrete.

†† Maximum coarse aggregate size was 10 mm.

Although replacing the NA with RCA may affect (decrease or increase) the fracture energy, the inherent variability associated with the fracture energy of NA concrete (i.e., 30 to 60 MPa) is such that an overall conclusion on whether NA or RCA concrete has higher fracture energies is not possible based on the current data. In the study by Darwin et al. (2001), two types of aggregate were used: limestone and high-strength basalt. They found significant differences in fracture energy ranges between the limestone and basalt-based concretes (i.e., limestone: $G_f = 36$ to 70 N/m and basalt: $G_f = 117$ to 227 N/m). Perhaps the difference in strengths between the natural limestone aggregate and the RCAs used in this study are too small to create a significant difference in the fracture energies of the resulting concretes.

8.5 Effect of Natural Aggregate Replacement with RCA on Mixture Proportions

By comparing the mixture proportions of the RCA concrete strength-based mixtures to those of the corresponding direct replacement mixtures, the effect of RCA on water demand, cement content and water-cement ratio could be assessed. As mentioned in Section 8.2.2, the compressive strengths reported for the Phase 1 strength-based mixtures are those associated with

concrete batched using batching Method B (i.e., large-scale batching using pre-wetted aggregates). Since the Phase 1 direct replacement mixtures were batched using Method A (i.e., small-scale batching using pre-soaked aggregates), a comparison between both mixture proportion types (i.e., the direct replacement and strength-based mixtures) for the purposes of assessing the effect of RCA properties on the fundamental mixture proportions was not possible. Therefore, only the Phase 2 direct replacement and strength-based mixtures which were both batched using batching Method A could be compared to determine the effect of RCA properties on the mixture proportions. Figure 8.48 and Figure 8.49 summarize the relative differences in cement content, water demand and water-cement ratio of the Phase 2 mixtures for the 40 MPa and 60 MPa mixtures, respectively.

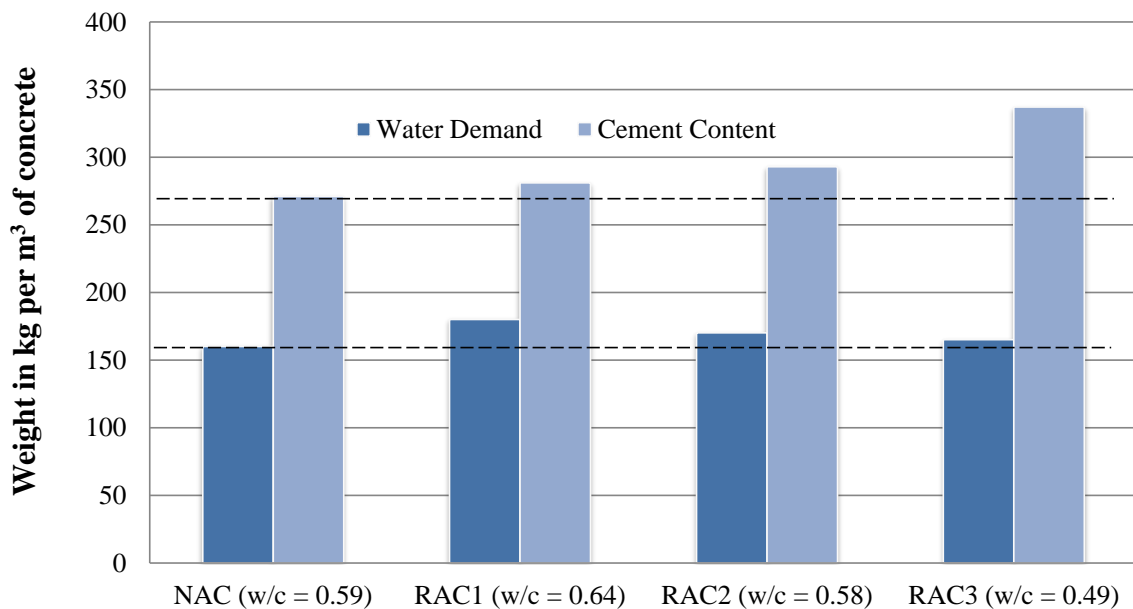


Figure 8.48 Water and cement demands for the Phase 2 40MPa strength-based mixtures

The 40 MPa mixture results indicated a consistent increase in the required cement content for the RCA concrete mixtures with the RCA-3 concrete requiring the highest increase followed by the RCA-2 and RCA-1 concretes. Depending whether the failure planes of the concrete compressive strength cylinders were mainly around or through the coarse aggregate particles, the governing concrete constituent (i.e., the coarse aggregate, mortar or mortar-aggregate interface) could be identified. Fracture planes passing through the coarse aggregate were due to lower aggregate strength (measured using ACV). Fracture planes passing around the coarse aggregate were due

to an inferior mortar-aggregate bond that is related to the aggregate surface texture which was categorized visually or measured indirectly using the amount of adhered surface moisture (i.e., moisture content above SSD). In addition, for fracture planes passing both around and through the coarse aggregates, both the strength of aggregate and the mortar-aggregate bond strength controlled the failure (refer to Section 7.4.2.2 for further explanation of compressive strength failure modes). In some cases, the RCA had a more roughened surface texture equating to a better mortar-aggregate bond and increased concrete compressive strength for the same water-cement ratio. In other cases, the natural aggregate produced concrete with higher compressive strength due to its higher strengths and/or superior mortar-aggregate bond.

The RCA-2 and RCA-3 concretes required 8 and 24% more cement than the equivalent NA concrete mixture to achieve similar strengths, respectively. Minor adjustments to the water content of the RCA concrete mixtures were required to achieve slumps within the target range. The RCA-1 concrete required an 8% higher water-cement ratio to achieve similar compressive strength and slump values as the NA concrete. While the water-cement ratio increased, the required water content to achieve slump values between 75 and 125 mm (3 and 5 in.) increased by 13% and, as a result, the cement content had to increase by 4% to maintain a constant water-cement ratio. This additional water was required due to the more roughened surface texture of the RCA-1 particles which acted to increase the inter-particle friction in the fresh concrete.

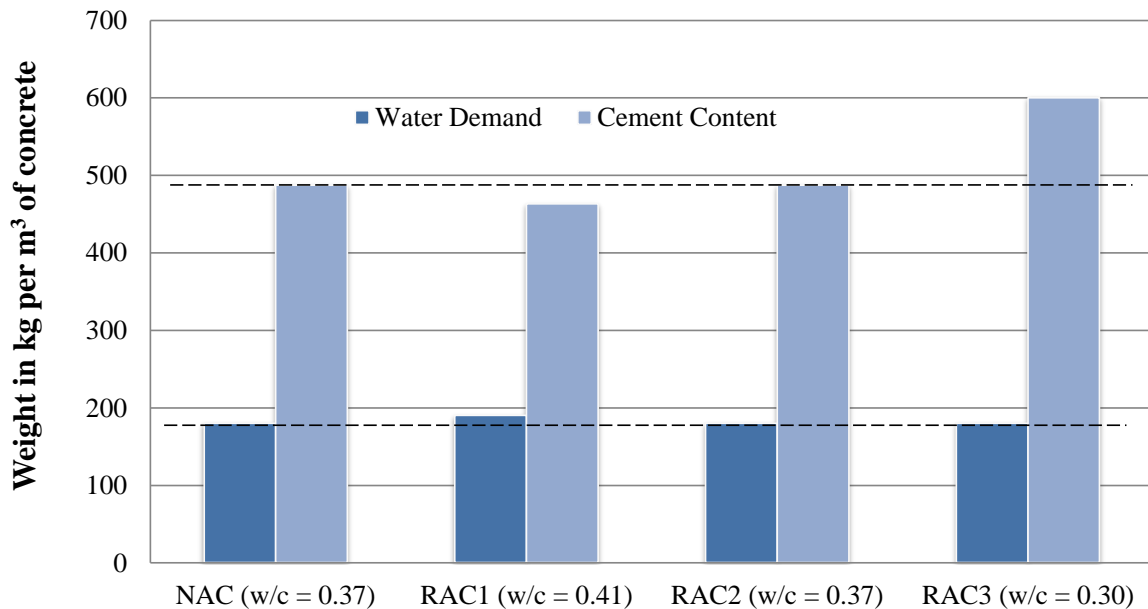


Figure 8.49 Water and cement demands for the Phase 2 60MPa strength-based mixtures

The 60 MPa mixture results indicated that the RCA-1 concrete required 5% less cement than the equivalent NA concrete mixture. However, to maintain slumps within a similar range, the water requirement for the RCA-1 concrete was 6% greater than the NA concrete mixture. As discussed in Section 7.4.1, reductions in slump were mainly due to the more roughened surface texture of the RCA particles which increased the inter-particle friction of fresh concrete. This translated to a water cement ratio that was 8% higher for the RCA-1 concrete as compared to the equivalent NA concrete. This indicates that the replacement of NA with RCA-1 can reduce the amount of cement required to achieve specified strengths and, consequently, can reduce the energy demands associated with the production of cement. The 60 MPa RCA-2 concrete mixtures required the same cement content as the NA concrete mixture to achieve similar strength. However, to achieve similar workability as the NA concrete mixture, use of a high-range water reducer was required. To achieve the required strength for the RCA-3 concrete mixture, the cement content had to be increased by 23% and the water cement ratio was reduced by 19%. In addition, a high-range water reducer was required to achieve slump values within the target range.

Overall, RCA-1 and RCA-2 when used as coarse aggregates in concrete required minimal adjustments to the mixture proportions to achieve similar compressive strengths and slumps as the NA concrete however, the RCA-3 concrete required a significantly higher cement content that may not make its use practical in high-strength concrete applications.

8.6 Overall Conclusions

Based on the combined analysis and findings of the Phase 1 and 2 strength-based mixtures, the following set of general conclusions has been compiled.

1. In general, based on the results from the direct replacement mixtures and the strength-based mixtures, full replacement of natural aggregate with RCA was found to have no statistically significant effect on the LCTE of concrete.
2. Based on the combined findings of Phases 1 and 2, both the aggregate strength (ACV) and the coarse aggregate volume have a significant influence on the splitting tensile strength. As ACV decreases (i.e., aggregate strength increases), the splitting tensile strength increases. As the coarse aggregate volume increases, the splitting tensile

strength also increases.

3. The average secant modulus of elasticity of bulk aggregate as measured during the ACV testing was found to have a very good correlation with the modulus of elasticity of concrete. This confirmed findings found with the direct replacement mixture results. This strong relationship seems to agree with the literature where it is noted that for constant compressive strength, the modulus of elasticity of concrete is a function of the modulus of elasticity of aggregate and the volumetric proportion of aggregate. Therefore, the average secant modulus of elasticity of bulk loose RCA (computed based on the ACV test) may be used to assess how replacing a natural aggregate with a particular RCA will affect the modulus of elasticity of the resulting RCA concrete.
4. Based on the combined results of Phase 1 and 2, at lower concrete strengths (i.e., 30 and 40 MPa specimens), the aggregate strength (measured by the ACV) has the most significant influence on the modulus of rupture ($f_r/f_c^{1/2}$). As the ACV decreases (i.e., aggregate strength increases), the modulus of rupture increases.
5. Evaluation of the fracture energy has provided some indication that as coarse aggregate strength increases (and ACV decreases), the fracture energy of the resulting concrete will increase. However, the inherent variability in fracture energy testing is such that a relative comparison between the fracture energy of NA concrete and RCA concrete may not be possible for natural coarse aggregates of normal strength (i.e., limestone and granite).
6. Overall, it is possible to produce concrete incorporating 100% RCA as coarse aggregate by adjusting the water content, cement content and water-cement ratio with compressive strengths of 30, 40, 50 and 60 MPa with slumps between 75 and 125 mm. It should be noted however that with inferior strength RCA sources (e.g., RCA-3), it may be necessary to use a high-range water reducer and/or other admixtures to achieve the performance requirements. While it may be possible to produce RCA concrete of higher strengths using inferior strength RCA, the large cement contents that may be required may deem such mixtures economically impractical and may offset the environmental benefits of using RCA in concrete.
7. Overall, RCA with a more roughened surface texture may require more water than a concrete with equivalent mixture proportions that uses natural aggregate. This is due to

the more roughened surface texture of the RCA particle that increases the inter-particle friction in the fresh concrete. However, the more roughened surface of the RCA particle may also lead to a superior mortar-aggregate bond in the resulting RCA concrete. An improvement in the mortar-aggregate bond could produce concrete that requires less cement to achieve compressive strengths equivalent to that of a NA concrete.

In addition to the set of conclusions presented above, and based on the combined findings from previous chapters, Figure 8.50 presents a visual summary of the various relationships between aggregate and concrete properties. Note that Figure 8.50 is an expansion of the results presented in Section 4.5.8 that includes the aggregate-concrete properties relationships from the findings of Chapters 7 and 8.

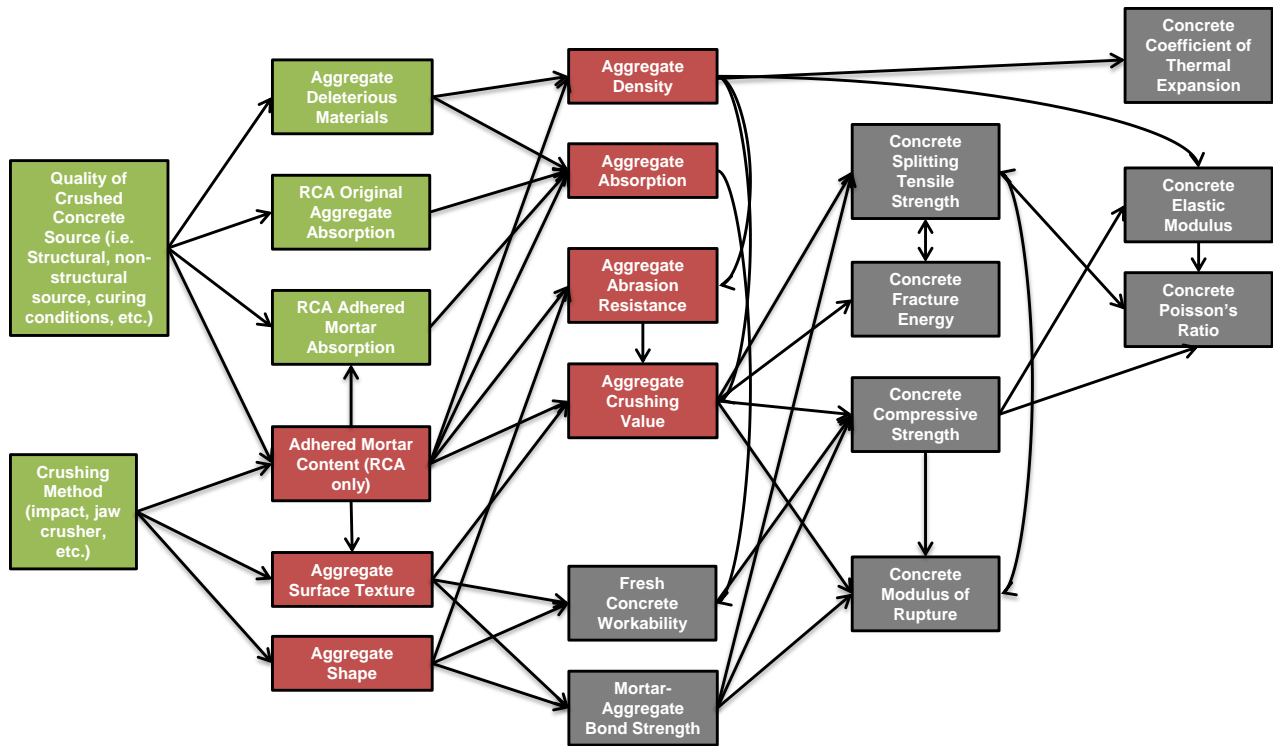


Figure 8.50 Overview of relationships between various aggregate and concrete properties

It is apparent from Figure 8.50 that the aggregate strength (or ACV) has a significant influence on a variety of important concrete properties such as the compressive strength, splitting tensile strength, fracture energy and the flexural strength (modulus of rupture). Therefore, the ACV is a fundamental aggregate property in determining how a particular RCA source will perform as a replacement for natural coarse aggregate in concrete.

Chapter 9: Bond Testing and Evaluation of Beam-End Specimens

9.1 Overview

The following sections present and discuss the results of the bond strength and slip testing of the NA and RCA concretes. In lieu of more traditional pull-out or bond beam specimens, beam-end specimens were cast to measure bond strength and slip. Unlike pull-out specimens, beam-end specimens are intended to replicate the concrete and reinforcing steel stress states present at the end of a reinforced concrete flexural member where both the tension steel and surrounding concrete are placed in tension. Compared to full-scale beam specimens, beam-ends are relatively simple to construct and test. In general, good agreement in bond strength results has been found between traditional bond beams and beam-end specimens (ACI 408, 2003). Beam-ends were designed specifically for the purposes of studying bond-splitting failures as these types of failures are most likely to occur in real structures (CEB-fip, 2000). ASTM A944-05 was followed when designing the test setup, instrumentation and beam-end specimens.

A new test frame apparatus was designed and constructed to allow for integration with current laboratory testing equipment. Along with bond strength values, bond stress-slip response curves were plotted and compared for the natural and RCA concrete specimens. After testing, a select number of beam-end specimens were dissected to examine the concrete failure planes and reinforcing bar length and condition. The effects of various aggregate and concrete mechanical properties on the bond strength and slip values were investigated in terms of their statistical correlations.

9.2 Experimental Program

Beam-end testing involved a small pilot study of two phases of primary testing. The pilot study involved casting two beam-end specimens in order to evaluate the new frame design and the necessary instrumentation. The first phase involved the mass batching of 24 beam-end specimens using Phase 1 (30 and 50 MPa) strength-based mixture proportions and batching Method B as described in Chapter 5. The second phase involved the mass batching of an additional 24 beam-end specimens using Phase 2 (40 and 60 MPa) strength-based mixture

proportions and batching Method C as described in Chapter 5.

9.2.1 Pilot Study

The main focus of the pilot study was to investigate the effect of bonded length on bond splitting failure and to verify the adequacy of the test frame. It was necessary to select bonded lengths such that bond failure would occur prior to yielding of the reinforcement. Two initial bonded lengths of 125 mm ($5d_b$) and 375 mm ($15d_b$) were selected. Also, since the test setup and test frame apparatus were custom built for this test, the second focus of the pilot study was to develop an adequate testing procedure and verify the adequacy of the instrumentation. Two trial beam-end specimens, with bonded lengths of 125 mm and 375 mm were cast using normal aggregate, C-1 exposure class concrete supplied by a local ready-mix concrete supplier. These beam-end specimens, along with 12 concrete cylinders, were allowed to moist cure under burlap and polyethylene sheathing for 7 days before curing in air until they were tested. Specimens were tested at 37 days and the results recorded indicated that the new test frame design was adequate and that all instrumentation performed as predicted. Construction and testing of Phase 1 beam-end specimens began soon afterwards. The recorded results for the pilot program included the peak load, peak bond stress and associated load vs. slip plots and are summarized in Table 9.1.

Table 9.1 Pilot study beam-end test results

	BE-TRIAL-125	BE-TRIAL-375
37 day Compressive Strength		40.9 MPa
Peak Load	61.9 kN	164.5 kN
Peak Bond Stress	6.25 MPa	5.54 MPa
Loaded-End Slip at Peak Load	0.143 mm	0.533 mm
Free-End Slip at Peak Load	0.316 mm	0.116 mm
Failure Type	Splitting failure	

9.2.2 Phase 1 Beam-End Batching

The purpose of the Phase 1 beam-end testing was to provide an assessment of the effect of RCA types 1 and 2 on the bond strength of reinforcing steel and to determine whether correlations between bond strength and various aggregate and concrete properties exist. The testing program involved the mass batching of concrete to produce 24 beam-end specimens and 68 200 mm by

100 mm diameter test cylinders. Concrete cover and reinforcement bar diameter were both kept constant at 30 mm and 25.2 mm, respectively. These values were chosen to represent typical values for interior exposure concrete and for a beam-end cross-section of the size selected. Several experimental design variables were established as summarized in Table 9.2.

Table 9.2 Phase 1 Beam-end testing control variables

Experimental Design Variable	Level		
	1	2	3
Aggregate Type	NA	RCA-1	RCA-2
Concrete Compressive Strength	30 MPa	50 MPa	-
Bonded Length	125 mm	375 mm	-

In addition to the control variables outlined, the Phase 1 beam-ends were batched using a 0.10 m³ rotating pan type (high shear) mixer and coarse aggregates (natural and recycled) were pre-wetted in hoppers for 30 minutes prior to batching (described in Chapter 5 as batching method B). A typical factorial design approach was taken in which the three control variables and their associated levels formed a total of 12 different specimen configurations per phase. To allow for repeatability of results, duplicates of each specimen configuration were cast.

The beam-end specimens were cast in conjunction with 12 fracture energy specimens and 27 additional 200 mm by 100 mm diameter cylinders in an attempt to establish a correlation between bond strength and fracture energy for NA and RCA concrete. The two bonded lengths were chosen such that they were shorter than the development lengths for a 25M bar and concrete strengths of 30 and 50 MPa calculated using Clause 12.2.2 of CSA A23.3-04 (CSA A23.3, 2004). This would ensure that failure of the beam-end would be a bond failure rather than yielding of the reinforcing steel. Table 9.3 outlines the beam-end specimen identification and their associated control variable values for Phase 1.

Table 9.3 Phase 1 Beam-end specimen identification and test matrix

Specimen ID	Aggregate Type	Compressive Strength	Bonded Length
BE-NAC-30-125A	NA	30 MPa	125 mm
BE-NAC-30-125B			125 mm
BE-NAC-30-375A			375 mm
BE-NAC-30-375B			375 mm
BE-NAC-50-125A	NA	50 MPa	125 mm
BE-NAC-50-125B			125 mm
BE-NAC-50-375A			375 mm
BE-NAC-50-375B			375 mm
BE-RAC1-30-125A	RCA-1	30 MPa	125 mm
BE-RAC1-30-125B			125 mm
BE-RAC1-30-375A			375 mm
BE-RAC1-30-375B			375 mm
BE-RAC1-50-125A	RCA-1	50 MPa	125 mm
BE-RAC1-50-125B			125 mm
BE-RAC1-50-375A			375 mm
BE-RAC1-50-375B			375 mm
BE-RAC2-30-125A	RCA-2	30 MPa	125 mm
BE-RAC2-30-125B			125 mm
BE-RAC2-30-375A			375 mm
BE-RAC2-30-375B			375 mm
BE-RAC2-50-125A	RCA-2	50 MPa	125 mm
BE-RAC2-50-125B			125 mm
BE-RAC2-50-375A			375 mm
BE-RAC2-50-375B			375 mm

9.2.3 Phase 2 Beam-End Batching

The second phase of beam-end testing had three main objectives. The first objective was to expand the overall bond strength data set by including two new compressive strength levels at 40 and 60 MPa and by investigating the use of an additional RCA source (i.e., RCA-3). Secondly, the Phase 2 testing program aimed to confirm the trends and correlations found in Phase 1. Lastly, by considering the larger data set from Phase 1 and 2 combined (total of 48 beam-ends), Phase 2 aimed to investigate any additional correlations and trends. The testing program involved the mass batching of concrete to produce an additional 24 beam-end specimens and 108

200 mm by 100 mm diameter test cylinders. Concrete cover and reinforcement bar diameter were kept the same as in Phase 1 at 30 mm and 25.2 mm, respectively. Several experimental design variables were established as listed in Table 9.4.

Table 9.4 Phase 2 beam-end specimen control variables

Experimental Design Variable	Level		
	1	2	3
Aggregate Type	NA	RCA-1	RCA-3
Concrete Compressive Strength	40 MPa	60 MPa	-
Bonded Length	125 mm	450 mm	-

Based on the results of the Phase 1 beam-end testing, it was decided to increase the bonded length from 375 to 450 mm to confirm trends in behaviour and correlations between aggregate properties and bond strength. This also provided a wider range of design variables upon which to develop regression models. The increased bonded length of 450 mm was still shorter than the development length calculated for a 25M reinforcing bar and concrete strengths of 40 and 60MPa using Clause 12.2.2 of A23.3-04 (CSA A23.3, 2004). This would ensure that failure of the beam-end would be due to a bond failure rather than yielding of the reinforcing steel. *Error! Reference source not found.* outlines the beam-end specimen identification and their associated control variable values for Phase 2.

In addition to the experimental design variables outlined, the Phase 2 beam-ends were batched using a 0.10 m³ rotating pan type mixer and coarse aggregates (natural and recycled) were pre-wetted in hoppers for 30 minutes prior to batching (described in Chapter 5 as batching method C). A typical factorial design approach was taken in which the three control variables and their associated levels formed a total of 12 different specimen configurations per phase. To allow for repeatability of results, duplicates of each specimen configuration were cast. The beam-end specimens were cast in conjunction with 16 fracture energy specimens and 72 additional 200 mm by 100 mm diameter cylinders in an attempt to establish a correlation between bond strength, compressive strength, splitting tensile strength, modulus of rupture, and fracture energy for NA and RCA concrete.

Table 9.5 Phase 2 beam-end identification and test matrix

Specimen ID	Aggregate Type	Compressive Strength	Bonded Length
BE-NAC-40-125A	NA	40 MPa	125 mm
BE-NAC-40-125B			125 mm
BE-NAC-40-450A			450 mm
BE-NAC-40-450B			450 mm
BE-NAC-60-125A	NA	60 MPa	125 mm
BE-NAC-60-125B			125 mm
BE-NAC-60-450A			450 mm
BE-NAC-60-450B			450 mm
BE-RAC1-40-125A	RCA-1	40 MPa	125 mm
BE-RAC1-40-125B			125 mm
BE-RAC1-40-450A			450 mm
BE-RAC1-40-450B			450 mm
BE-RAC1-60-125A	RCA-1	60 MPa	125 mm
BE-RAC1-60-125B			125 mm
BE-RAC1-60-450A			450 mm
BE-RAC1-60-450B			450 mm
BE-RAC3-40-125A	RCA-3	40 MPa	125 mm
BE-RAC3-40-125B			125 mm
BE-RAC3-40-450A			450 mm
BE-RAC3-40-450B			450 mm
BE-RAC3-60-125A	RCA-3	60 MPa	125 mm
BE-RAC3-60-125B			125 mm
BE-RAC3-60-450A			450 mm
BE-RAC3-60-450B			450 mm

9.3 Test Frame Design

The design of the beam-end testing frame was adapted from the suggested setup presented in ASTM A944-05, *Standard Test Method for Comparing Bond Strength of Steel Reinforcing Bars to Concrete Using Beam-End Specimens*. A vertical orientation rather than horizontal was chosen to accommodate the use of an existing testing frame. Figure 9.1 and Figure 9.2 show the two test frame configurations and the final constructed test frame.

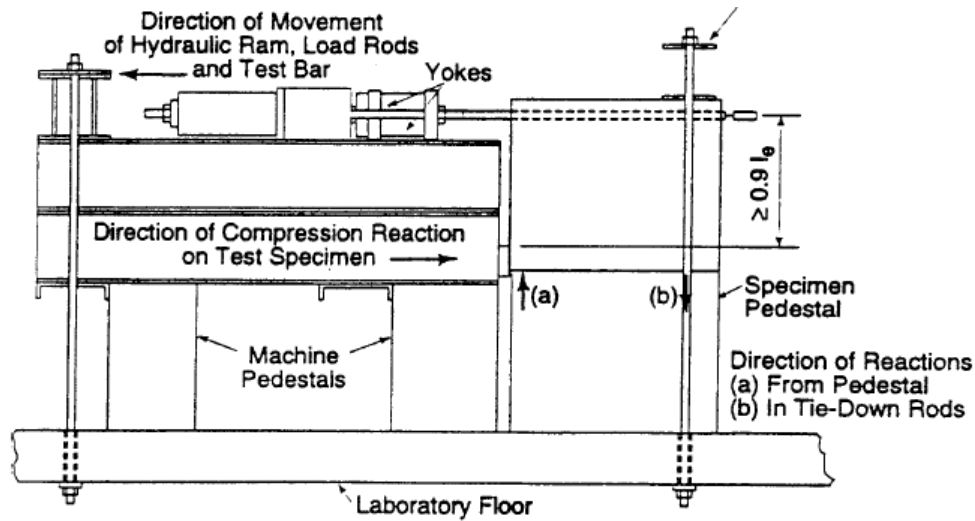


Figure 9.1 Beam-end test frame apparatus as per ASTM A944-05

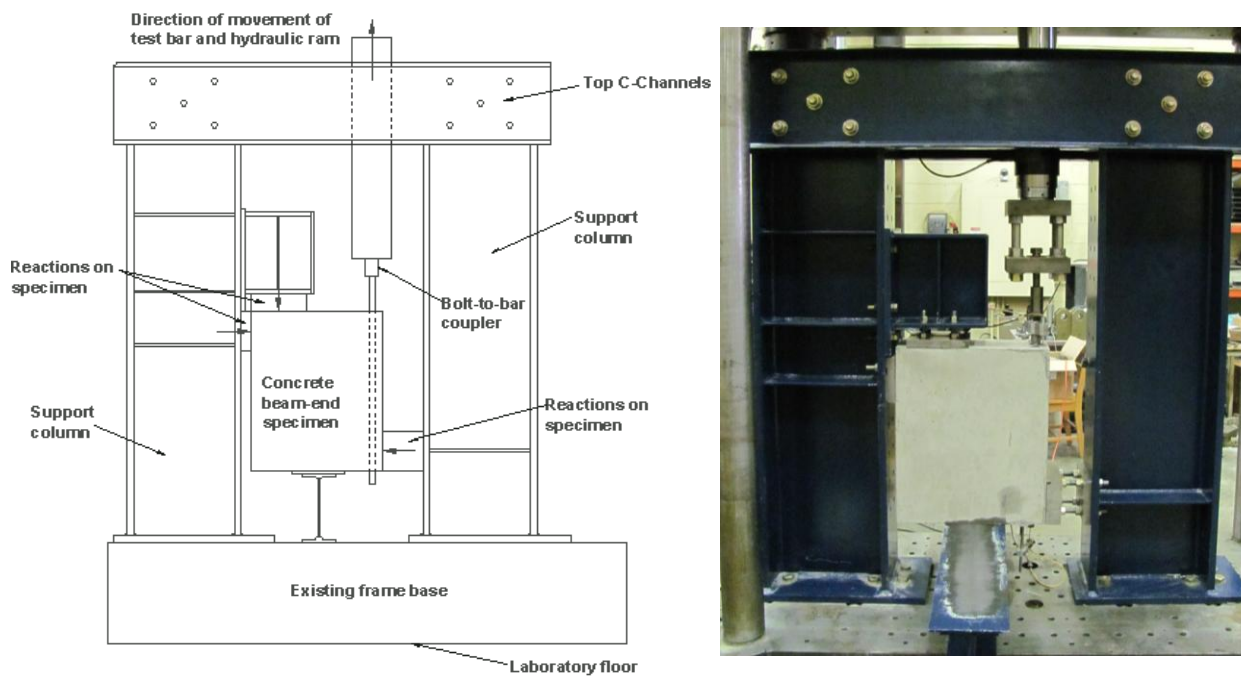


Figure 9.2 Modified, vertically oriented beam-end test frame apparatus

The beam-end specimen simulates the conditions experienced by the end of a beam subjected to four-point loading. As depicted in Figure 9.2, three support reactions had to be resisted by the test frame to simulate realistic forces experienced by the beam-end specimen. The bottom right reaction simulates a support reaction whereas the top frame reactions represent the internal compression force and one of the load points. The tension force applied to the bar by the

hydraulic actuator represents the internal tension force in the beam. Figure 9.3 outlines the structural idealization as well as the internal forces and strut-end-tie diagram for the beam-end specimen.

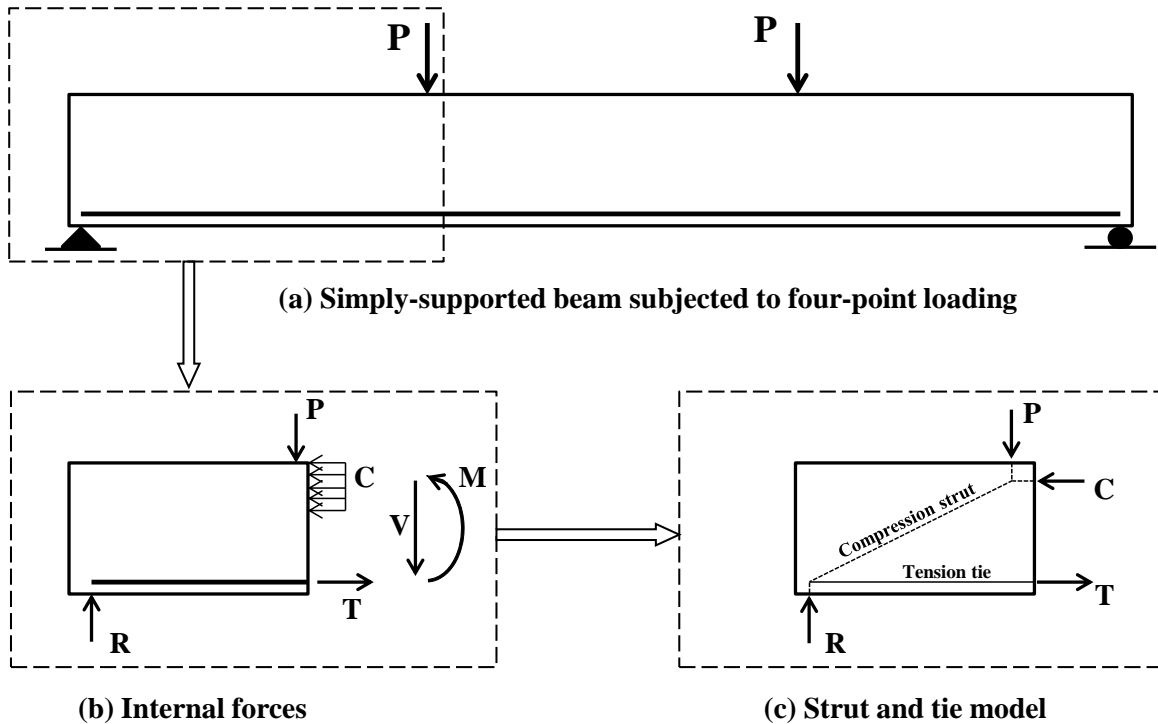


Figure 9.3 Beam-end structural idealization

Given a simply supported beam with an applied loading (Figure 9.3a), the internal couple moment, M is equilibrated through a compression zone at the top of the beam, C and a tension tie, T at the bottom. The applied load P is then equal to the support reaction R at the end of the beam (Figure 9.3b). As a result of these internal forces, a diagonal compression strut will connect the end reaction and compression force placing the middle section of the specimen in compression (Figure 9.3c). The frame itself was designed to accommodate a variety of beam-end specimen sizes and configurations. As a result, a simple optimization approach was taken to determine the maximum design forces, moments and displacements exerted on the structure. Several structural models incorporating varying dimensions and applied forces were constructed and analyzed using SAP 2000. A load of 500 kN was set as the maximum tensile force that could be applied to the test bar which was based on the maximum capacity of the test frame. Due to the sensitivity required when measuring bond slip, a stiffness-based design was favoured

over a strength-based approach. The maximum lateral deflection of the top of the left test frame column was limited to 1.00 mm (0.06% of total frame height). The deflection criteria governed over the ultimate load criteria (i.e., considering both material and member resistances) in all structural components. Full design notes, calculations, and technical drawings are contained in Appendix C.

9.4 Design and Construction of Beam-End Specimens

Beam-end specimens with dimensions of 600 mm x 500 mm x 225 mm were chosen based on guidelines provided in ASTM A944-05. To prevent conical failure at the loaded-end, bond-breakers were installed at the specimen surface. The beam-end cross section and its reinforcement layout are presented in Figure 9.4. Beam-end specimens with dimensions of 600 mm x 500 mm x 225 mm were chosen based on guidelines provided in ASTM A944-05. Material properties for the 25M test reinforcing bar provided as mill certificates from the reinforcing steel supplier are presented in Table 9.6.

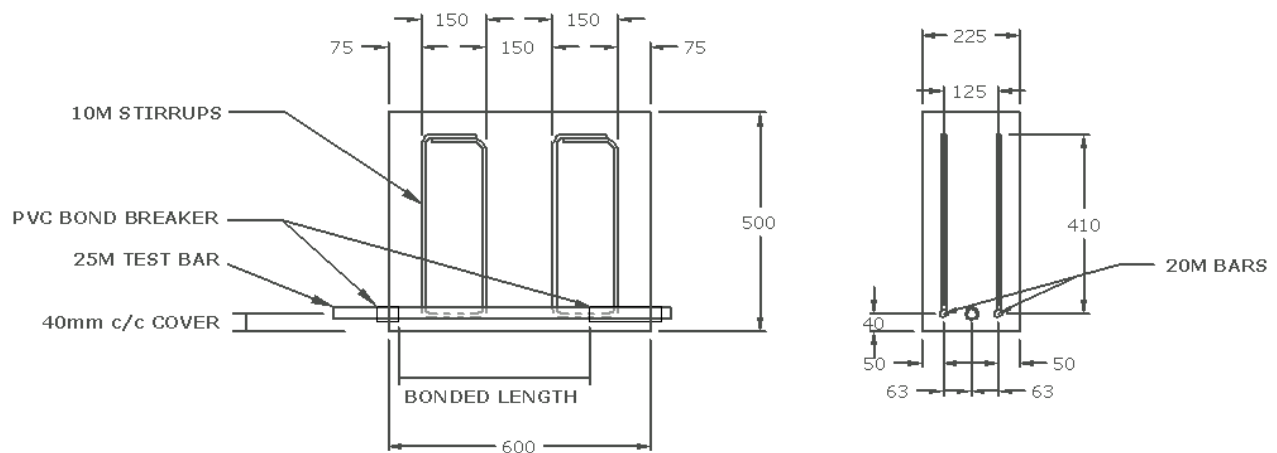


Figure 9.4 Beam-end specimen cross-section dimensions and reinforcement layout

Table 9.6 Material properties for 25M reinforcing steel test bar (Obtained from mill certificates courtesy of reinforcing supplier)

Material Property	
Yield Strength (MPa)	466.5
Ultimate Strength (MPa)	643.0
Maximum Elongation (%)	18.0

In addition to the main 25M test bar, two 20M bars were placed in the same plane to provide one half of the cross-sectional area of the test bar to provide adequate reinforcement against flexural failure of the specimen. Shear reinforcement was placed in the same plane as the longitudinal reinforcement so as not to intercept any longitudinal splitting crack resulting from bond failure (i.e., to eliminate the contribution of confining effects to bond strength).

Formwork had to be specially designed to allow for ease of construction and placement of concrete. Forms were built in three separate sections containing eight beam-end forms each. Spacers and metal tie wire were used to initially secure stirrups in the forms. Figure 9.5 depicts typical beam-end formwork beds and the individual specimen reinforcement arrangement. This formwork arrangement allowed for both easy handling and transport of each form and removal of the hardened beam-end specimens. The ends of each bond breaker had to be sealed with duct tape to ensure no cement paste could enter and bond to the reinforcing bar. Special anchor inserts were cast into every specimen to facilitate easy hoisting and transportation between testing.



Figure 9.5 Typical beam-end formwork casting beds and reinforcement

Once the forms were two-thirds filled with fresh concrete, the spacers and tie wire were removed and stirrups were adjusted to ensure they maintained a vertical orientation. The forms were filled in lifts and were vibrated to ensure adequate consolidation of concrete within the forms. The tops of each specimen were screeded to remove excess concrete and to provide a surface level with the tops of the forms. Specimens were allowed to cure for several hours before their surfaces were finished using metal trowels, and were then covered with dampened burlap and polyethylene sheeting. Figure 9.6 depicts the beam-end casting and curing processes using

dampened burlap and polyethylene sheeting.



Figure 9.6 Beam-end casting and curing techniques

All accompanying cylinders were cured in a similar manner. Burlap was dampened each day for the first seven days after casting. Following seven days of curing, the burlap and polyethylene sheeting were removed. After approximately one week of air-curing, beam-end specimens were removed from their forms and their accompanying cylinders were demoulded. The beam ends and cylinders were then cured in air until testing. Beam-end specimens for Phase 1 were cast over a period of three days in June 2009 and beam-end specimens for Phase 2 were cast over a period of three days in July 2011.

9.5 Test Setup and Procedure

The first step of the test setup involved properly aligning the beam-end specimen such that the test frame applied a tensile force parallel to the orientation of the embedded reinforcing bar. The alignment process utilized a combination of ratchets and shims to shift the concrete specimen to line up with the bolt-coupler system. Once the specimen was aligned, the threaded-end of the bar was secured into the bolt-coupler system which eliminated the possibility of slip between the test bar and the coupler unlike wedge grip systems. Figure 9.7 illustrates the loaded and free-end LVDT setup.

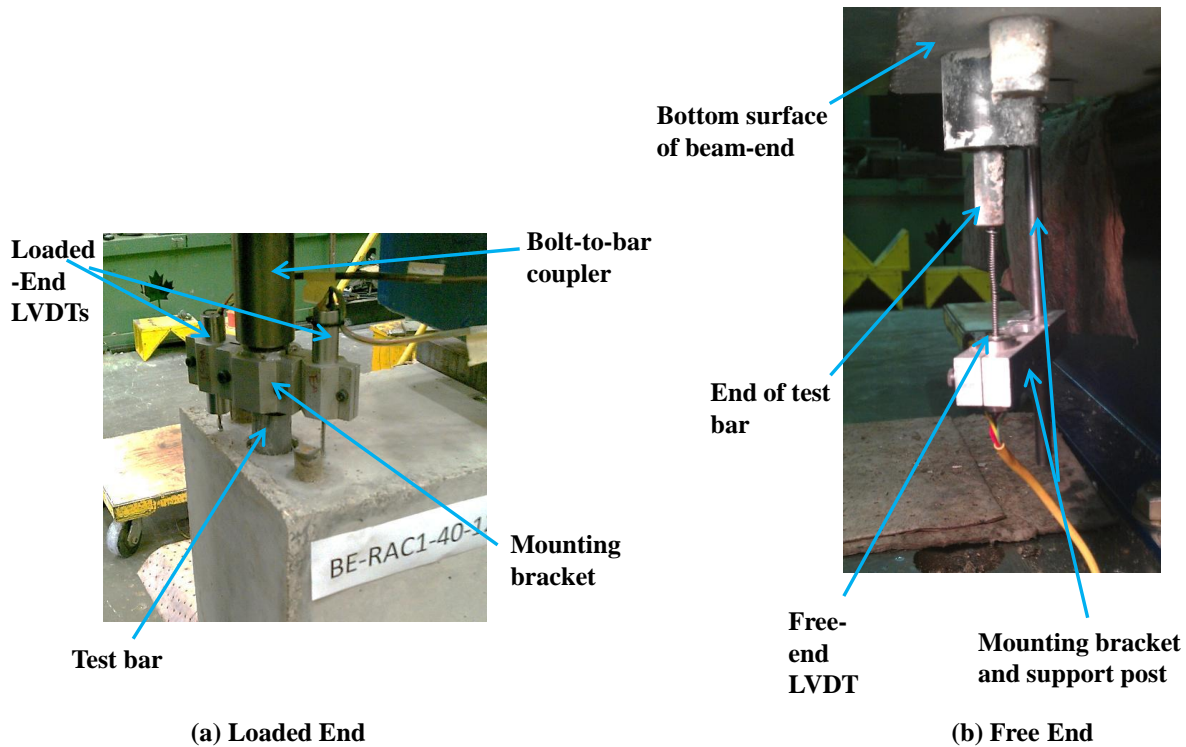


Figure 9.7 *Beam-end loaded-end and free-end LVDT mounting setup*

Instrumentation consisted of three linear variable differential transformers (LVDTs) used to measure slip. Two LVDTs were mounted to the loaded-end of the bar to obtain an average measure of the loaded-end slip, and the third was mounted to the bottom of the specimen to measure free-end slip. Concrete Rawplugs were used to attach a mounting post and bracket to hold the free-end LVDT. All slip displacement values were measured relative to the concrete specimen. Load was measured using a 500 kN load cell and the test was run using a closed-loop servo-hydraulic testing system using the axial displacement of the actuator as the control channel. A constant axial displacement rate of 0.3 mm/min was used to capture the behaviour after slip for each specimen, and to ensure that slip or other failure did not occur in less than three minutes after the start of the test. Data was collected at frequency of 3 Hz and tests were run until a significant portion of the post-peak behaviour of each specimen was captured.

9.6 Evaluation of Bond-Slip Response of Phase 1 (30 and 50 MPa) Specimens

The following section presents and discusses the bond strength and slip data for all Phase 1 beam-end specimens. Bond strength, slip and stress-slip curves were compared and contrasted

between the NA and RCA concrete specimens. The effects of various aggregate and concrete properties on the bond strength and slip results were examined through the use of correlation plots. Following testing, several beam-end specimens were dissected and a macro-scale forensic analysis was carried out to determine actual bonded lengths and investigate concrete failure mechanisms.

9.6.1 Summary and Discussion of Test Results

Aggregate crushing values, splitting tensile strengths, compressive strengths, average bond strengths (τ_b), and slip values for the Phase 1 beam-end specimens have been summarized in Table 9.7. A large percentage of free-end slip measurements were inaccurate due to the LVDT setup used to measure free-end slip. When bond failure and splitting cracks occurred, the free-end LVDT became dislodged from its mounting bracket and was no longer parallel to the direction of bar movement causing errors in readings and sudden jumps in the bond-slip response plots (refer Appendix D for the bond-slip response curves of each beam-end specimen). Table 9.7 has these measurements denoted N/A. Note that each average bond stress and slip values reported represents the average value of two identical beam-end specimens (i.e., A and B). Average bond stress values for the 125 mm and 375 mm bonded lengths are summarized in Figure 9.8a and Figure 9.8b, respectively. These results have been normalized by $f'_c{}^{1/2}$ to account for the specimen to specimen variation in f'_c .

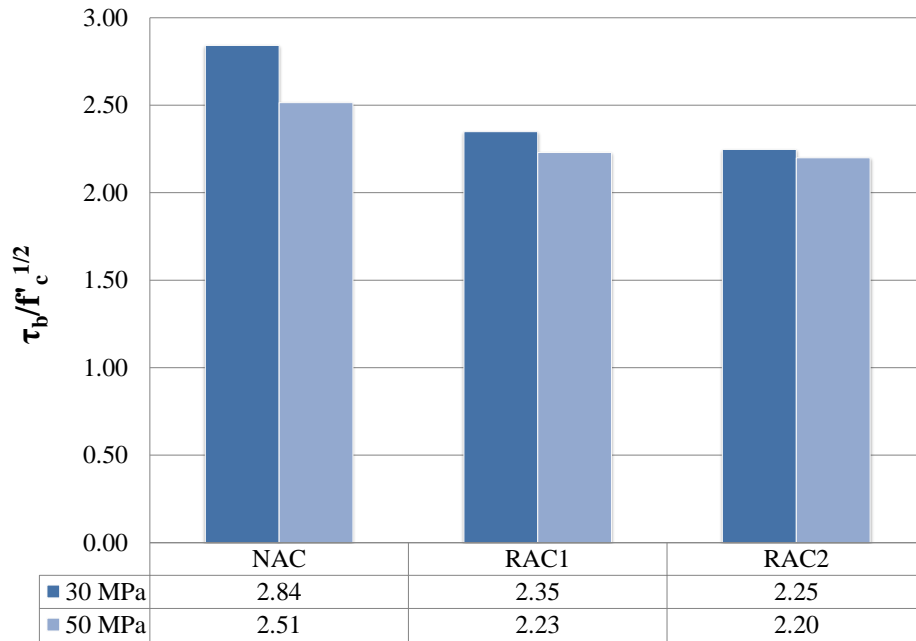
The NA concrete beam-end specimens with bonded lengths of 125 mm had $\tau_b/f'_c{}^{1/2}$ values that were 11 to 17 % higher than the RCA-1 concrete specimens, and 12 to 21 % higher than the RCA-2 specimens. The NA concrete beam-end specimens with bonded lengths of 375 mm had $\tau_b/f'_c{}^{1/2}$ values that were 10 % higher than the RCA-1 concrete specimens and 8 to 12 % higher than the RCA-2 concrete specimens. In general, the NA concrete beam-end specimens achieved higher bond strengths than the RCA concrete specimens at both the 30 and 50 MPa compressive strength levels. On average, the RCA-1 concrete specimens achieved higher bond strengths than the RCA-2 specimens except for the case of specimen type BE-RAC2-50-375 which had an average bond strength of 5.31 MPa compared to 5.25 MPa for the equivalent RCA-1 concrete specimen type, BE-RAC1-50-375.

Table 9.7 Phase 1 beam-end bond strength test data (30 and 50 MPa; NAC, RAC1 and RAC2)

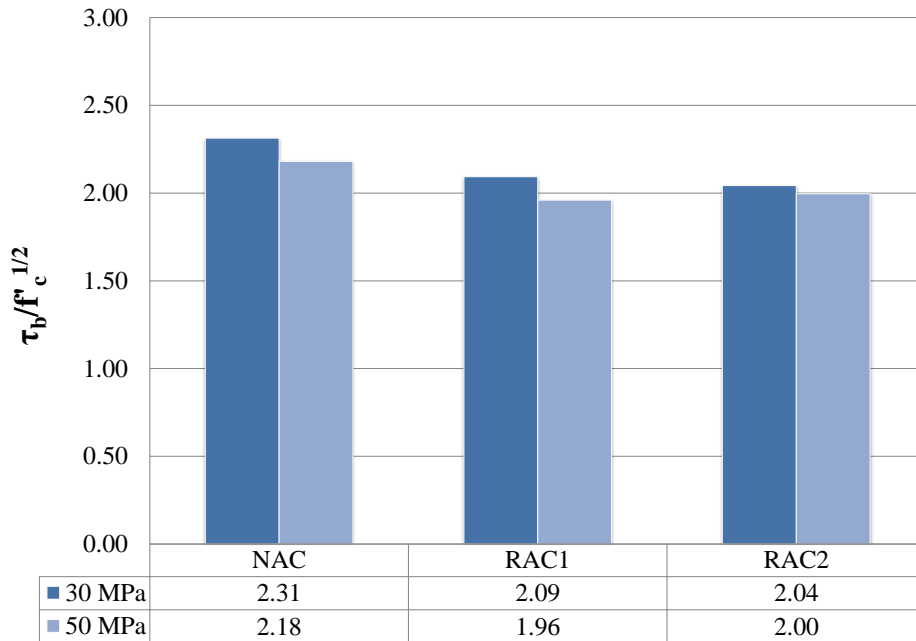
Specimen ID [†]	ACV	$f_{ct}/f'_c{}^{1/2}$	f'_c (MPa)	T_b (kN)	Average τ_b (MPa)	Loaded- End Slip at Failure [‡] (mm)	Free-End Slip at Failure (mm)
BE-NAC-30-125A	18.2	0.479	34.5	65.4	6.99	0.078	0.090
BE-NAC-30-125B				74.1			
BE-NAC-30-375A				169.9	5.69	0.308	N/A
BE-NAC-30-375B							
BE-NAC-50-125A		0.505	49.0	66.9	6.75	0.077	0.084
BE-NAC-50-125B				67.8			
BE-NAC-50-375A				179.5	5.86	0.340	0.181
BE-NAC-50-375B							
BE-RAC1-30-125A	23.1	0.484	30.9	56.2	5.66	0.083	0.093
BE-RAC1-30-125B				56.7			
BE-RAC1-30-375A				150.8	5.04	0.293	N/A
BE-RAC1-30-375B							
BE-RAC1-50-125A		0.472	47.9	61.4	5.98	0.073	N/A
BE-RAC1-50-125B				57.8			
BE-RAC1-50-375A				161.9	5.25	0.336	0.101
BE-RAC1-50-375B							
BE-RAC2-30-125A	26.0	0.376	31.3	50.6	5.50	0.069	0.078
BE-RAC2-30-125B				59.1			
BE-RAC2-30-375A				148.8	5.00	0.255	N/A
BE-RAC2-30-375B							
BE-RAC2-50-125A		0.430	49.4	57.7	5.86	0.090	0.065
BE-RAC2-50-125B				59.2			
BE-RAC2-50-375A				164.6	5.31	0.226	0.330
BE-RAC2-50-375B							

[†] Specimens have been labelled as follows: BE = Beam-End, RAC1 = Recycled Aggregate Concrete incorporating RCA-1, 50 = compressive strength in MPa, 375 = bonded length in mm, and the letters A and B denote identical specimens A and B.

[‡] Top slip values have been corrected for axial elongation of the free length of the test bar (i.e., $s_{top,corr} = s_{top} - (PL)/(A_b E_s)$, where $L = 75$ mm, $A_b = 500$ mm², and $E_s = 200\ 000$ MPa).



(a) 125 mm Bonded Length Specimens



(b) 375 mm Bonded Length Specimens

Figure 9.8 Summary charts of bond strength normalized to $f'_c{}^{1/2}$ (Phase 1)

In general, no trend was found within the loaded or free-end slip value at failure between the NA concrete or RCA concretes, or between the 30 and 50 MPa specimens. The 375 mm bonded

length specimens had peak slip values that were between 2.5 and 4.5 times larger than their equivalent peak slip values of the 125 mm bonded lengths. This indicates that the change in peak slip values was not proportional to the change in bonded length (i.e., $375\text{mm}/125\text{mm} = 3$ times longer). Note that loaded-end slip values were corrected to account for the axial elongation of the unbonded length (75 mm typically) of the reinforcing bar (refer to footnote on Table 9.7 for calculation).

9.6.1.1 Bond-Slip Response and Failure Mechanism of Beam-End Specimens

The typical stages of bond-slip response for the beam end specimens are presented in Figure 9.9. The stages observed during Phase 1 testing and the stages presented in Figure 9.9 closely resemble those described in CEB-fip (2000). The top view shows the circumferential tension field originating from the reinforcing bar. The bottom view depicts the surface splitting cracks that are initiated and propagated as the circumferential tension field expands due to an increase in bar force (applied axial load). The side view provides an elevation of the growing circumferential tension field in relation to the length of the embedded bar. Stage 1 represents the state of uncracked concrete bonded to reinforcing steel. Chemical adhesion and micromechanical friction are the main contributors to bond (refer to Section 2.4.2.1). Any slip that occurs during Stage 1 is primarily due to the shear deformations in the concrete. At increasing bond stresses (due to increase axial load), chemical adhesion and micromechanical friction no longer contribute to bond as it is the mechanical interlock (bearing forces) between the reinforcement ribs and the surrounding concrete that begin to take effect. Micro-cracking begins to occur at the tips of the reinforcement ribs allowing the bar to slip relative to the concrete. By Stages 2 and 3, splitting cracks begin to form as and the circumferential tension field developed by the wedging action begins to grow with increasing load and exceeds the tensile strength of the concrete. Slip between the steel and the surrounding concrete continues to increase, surface cracks are visible by the end of Phase 3 and failure is imminent. By Stage 4, the splitting cracks reaches the end of the bar and a sudden failure occurs as the bar slips and the longitudinal splitting cracks widen. This is commonly referred to as a splitting-induced pullout failure. When the bar is no longer bonded to the surrounding concrete, the tensile stress present at the end of bonded length of the bar causes a transverse splitting crack as the concrete alone is not capable of carrying this additional tensile load.

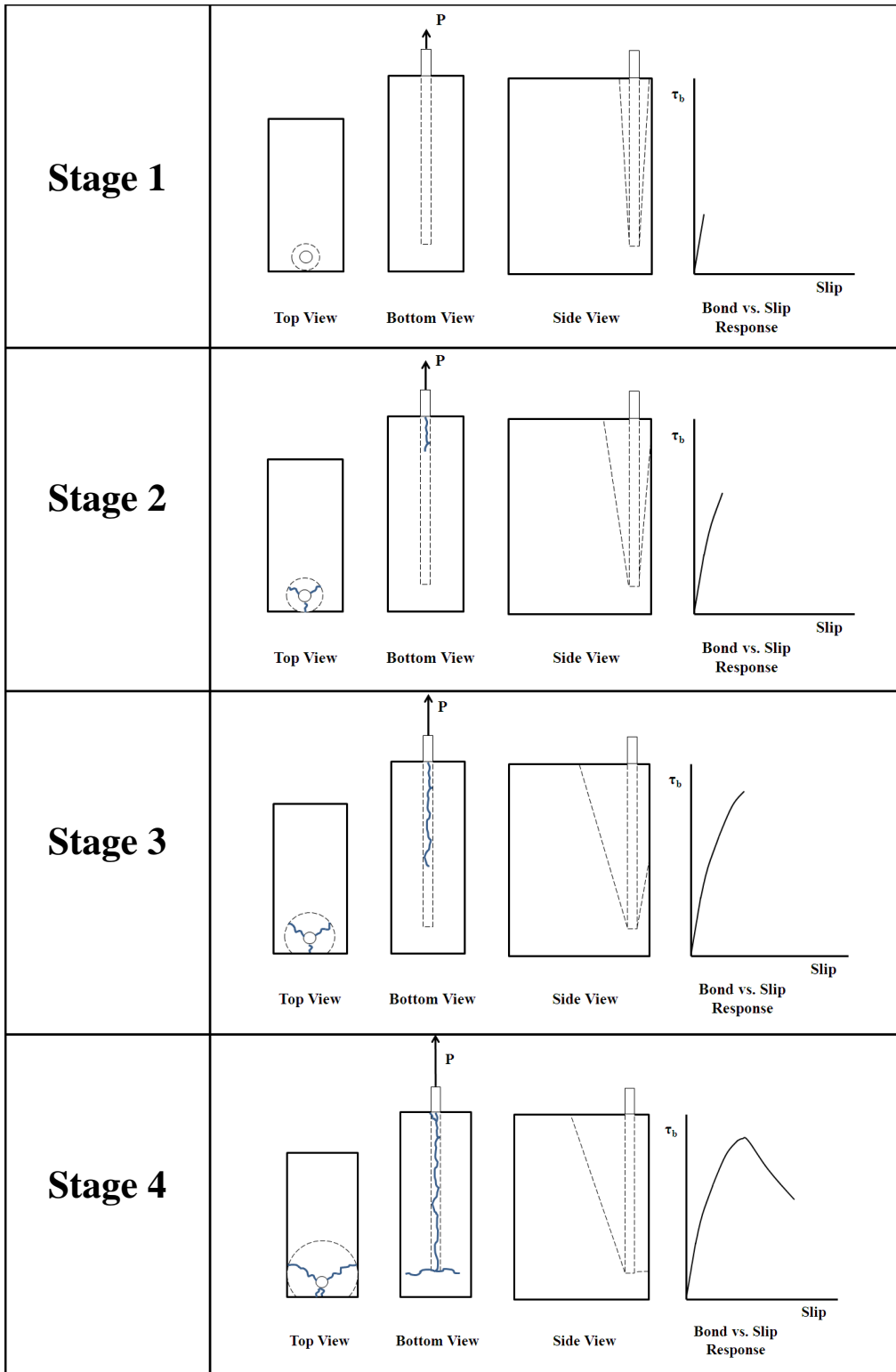


Figure 9.9 Typical observed stress fields and cracking of beam-end specimens

In general, splitting failures occurred in all specimens (Figure 9.10) regardless of their

compressive strength or bonded length. Longitudinal splitting cracks ran along the bonded length of the test bar. This type of failure (rather than a pull-out failure) was expected for the bar size (i.e., 25M), bar spacing and level of concrete cover (i.e., 30 mm). In addition, bond failures rather than yielding of the steel reinforcement were expected as the bonded lengths used during Phase 1 (i.e., 125 and 375 mm) were both less than the calculated development length based on CSA A23.3-04 (CSA A23.3, 2004).

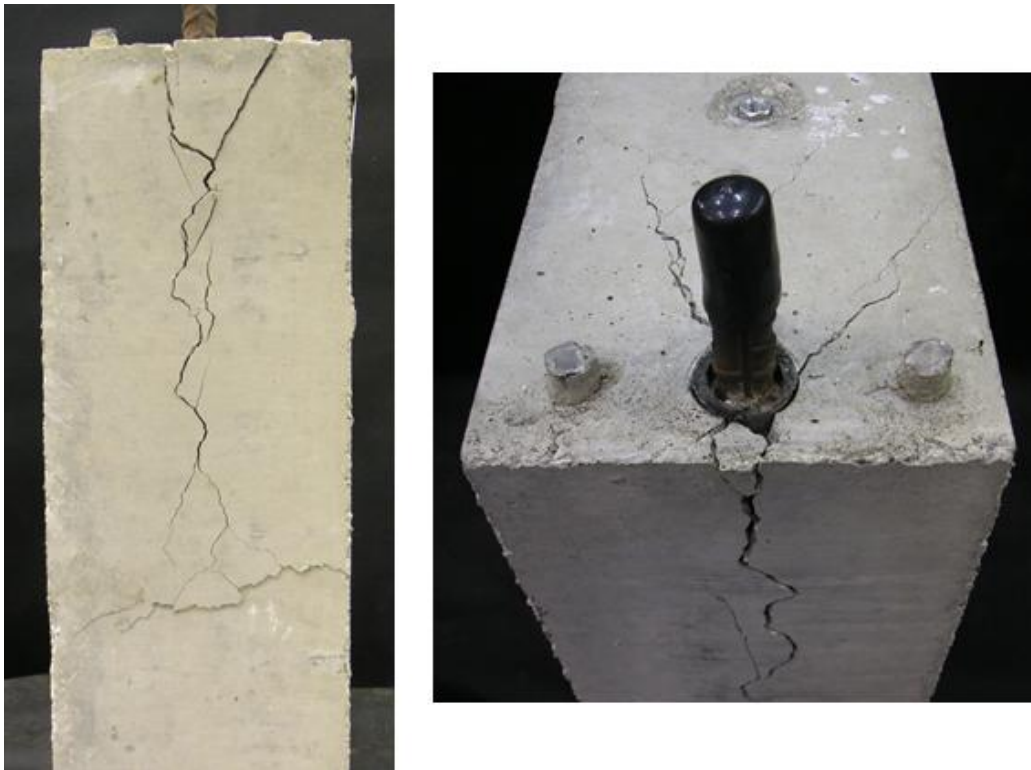


Figure 9.10 Typical splitting failure for beam-end specimens (BE-RAC2-50-375B)

Figure 9.11 is a typical bond stress vs. slip plot for both the loaded and free-end slip values. As the bond stress increases, the curve starts to increase non-linearly until the bond capacity of the beam-end is reached, at which time the load suddenly drops off to reach a plateau and begins a gradual decent. The free-end slip LVDT initially lags behind the loaded-end slip LVDT until the peak is reached and then both LVDT readings begin to approach constant values as the splitting cracks begin to widen and the load begins to decrease (bond-slip curve flattens). The remaining bond capacity after initial slip can be attributed to the friction between the bar ribs and the surrounding concrete (i.e., residual friction bond strength).

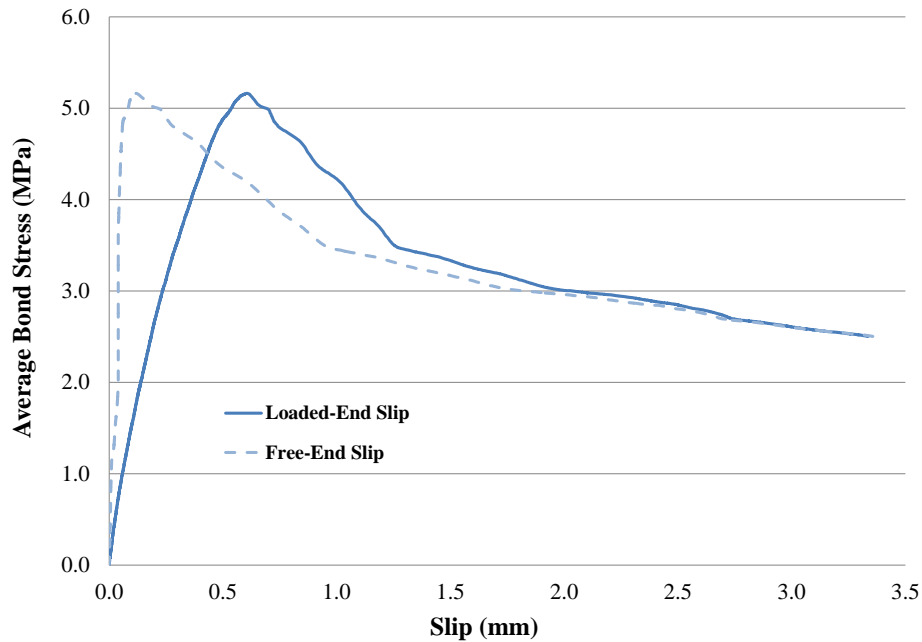


Figure 9.11 Typical bond-slip response of beam-end specimen (BE-RAC3-40-450B)

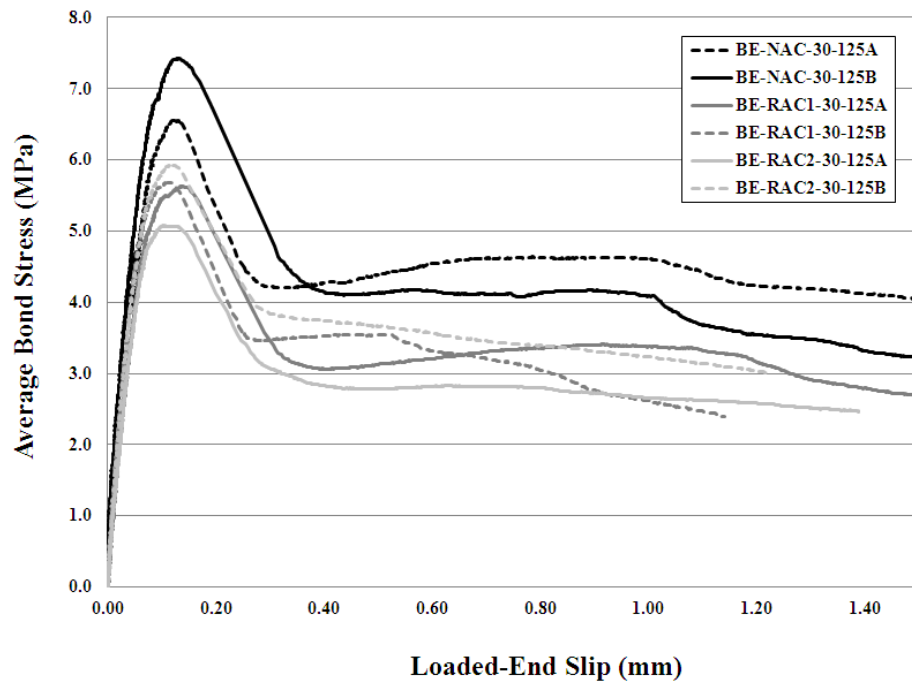
Figure 9.12 and Figure 9.13 compare the bond-slip responses for the 30 and 50 MPa beam-end specimens, respectively. Comparing the 125 mm and the 375 mm bonded length specimens, it appears that the post failure response differs. The 125 mm bonded length specimens have post peak responses that reach a horizontal plateau (refer to Figure 9.12) whereas the 375 mm bonded length specimens have plateaus that become increasingly sloped as compressive strength increases (refer to Figure 9.13). This is due to the condition of the concrete keys surrounding the reinforcing bar. In the 125 mm bonded length specimens, the shorter splitting cracks created more post-cracking confinement than the 375 mm bonded length specimens. In addition, the concrete keys were still intact and continued to sustain load while the slip continued to increase as the splitting cracks continued to widen. This caused the plateau of the bond – slip curve to remain relatively horizontal. In the 375 mm bonded length specimens, the longer splitting cracks in combination with the concrete keys being damaged or sheared off due to the higher bar forces sustained at failure created less post-cracking confinement as compared to the 125 mm bonded length specimens. This is evident from the forensic analysis performed on the beam-end specimens which revealed larger amounts of concrete adhered to the bar deformations for the longer bonded length specimens (refer to Section 9.6.8). The concrete keys could no longer

sustain loads and the splitting cracks continued to widen causing the plateau of the bond – slip response curve to decrease.

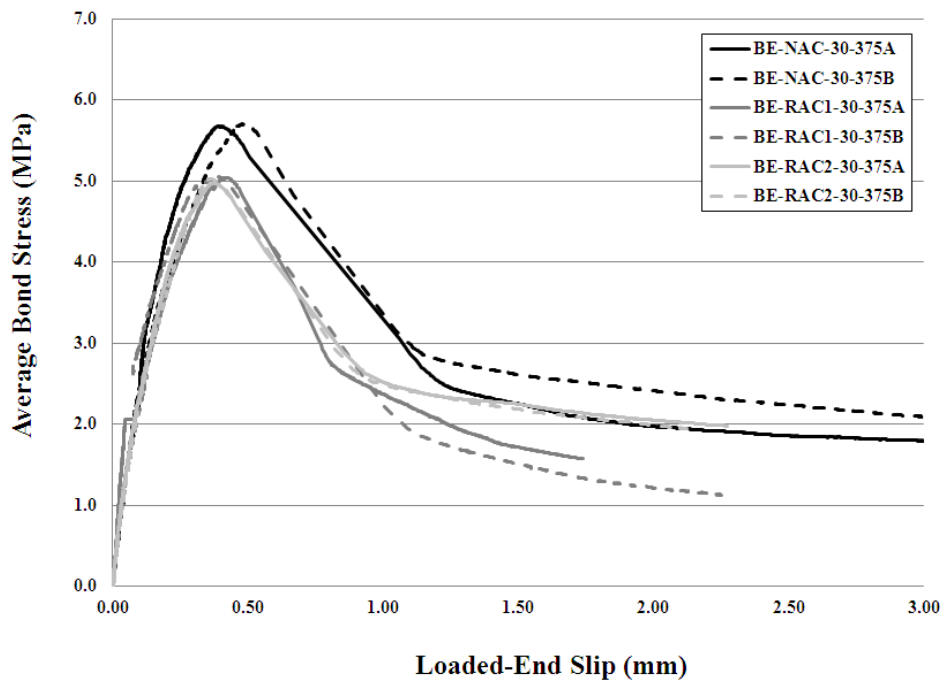
By comparing the 30 MPa and 375 mm bonded length specimens (Figure 9.12b), the NAC and RCA-1 specimens reached a friction plateau of approximately 2 MPa whereas the RCA2 specimens approached a plateau of approximately 1.5 MPa. The lower residual (frictional) bond strength in the 375 mm bonded length specimens may be a result of the higher tensile stresses developed within the bonded bar causing more extensive damage to the surrounding bonded concrete.

The 50 MPa beam-end specimens display similar behaviour to the 30 MPa specimens as shown in Figure 9.13a and Figure 9.13b. For the 125 mm bonded length specimens there are similar peak slip values and the residual bond strength plateau is once again approximately 4 MPa. For the 50 MPa 375 mm bonded length specimens, there are similar peak slip values to the 30 MPa specimens and the residual bond strength plateau is once again approximately 2 MPa. This suggests that for bonded lengths (5 and 15 bar diameters), concrete compressive strength has little impact on the bond-slip response and residual bond strength.

In comparing the 30 MPa and 125 mm bonded length specimens (Figure 9.12a), the NA concrete specimens reach a plateau of around 4.0 MPa whereas the RCA-1 and RCA-2 concrete beam-end specimens seem to reach a plateau of around 3 MPa. It appears that the NA concrete 30 MPa specimens were capable of maintaining higher residual bond strength due to friction than the RCA specimens. The lower crushing strength of the RCA (measured by the ACV) as compared to the natural coarse aggregate may be responsible for this decrease of residual bond strength of the RCA beam-end specimens. In real structures, this difference in post-failure behaviour of bond between NA and RCA concrete may not be a significant factor in the design of reinforced concrete structures as it is the average bond stress at failure that are relevant in the development of equations for bond and anchorage. Aside from lower bond strengths and slight variations in residual bond strength, the bond-slip responses of the Phase 1 RCA concrete beam-ends were very similar to the NA concrete specimens. Individual bond-slip curves and crack patterns for each beam-end specimen have been included in Appendix D.

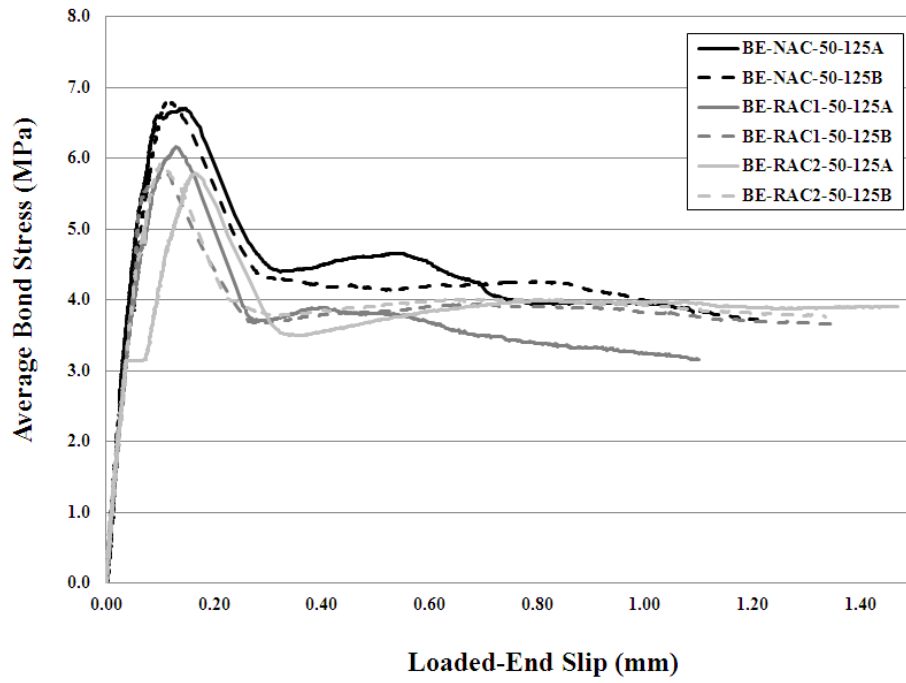


(a) 125 mm Bonded Length Specimens

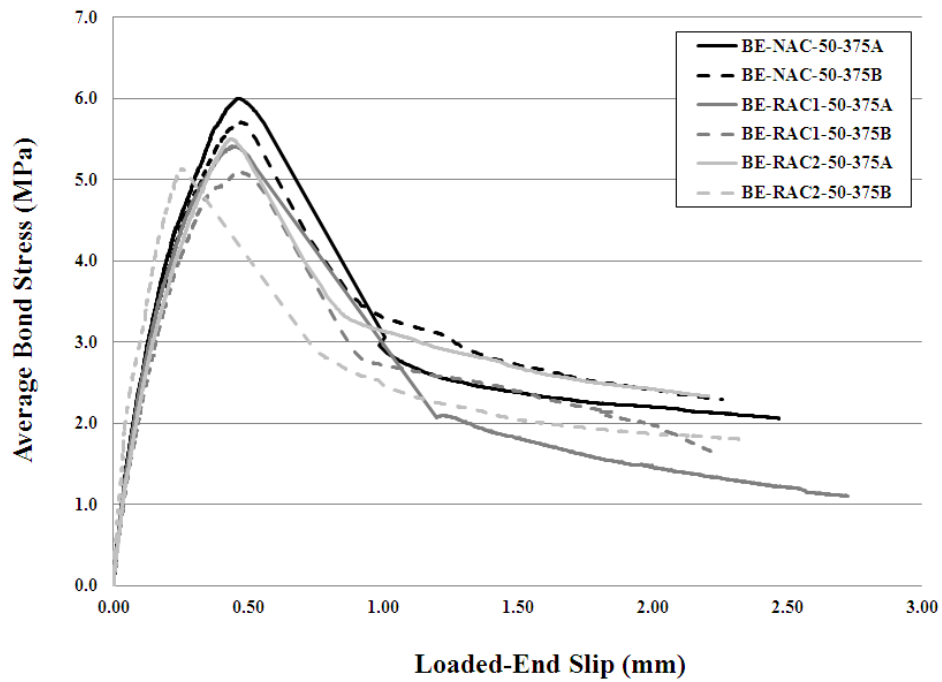


(b) 375 mm Bonded Length Specimens

Figure 9.12 Comparison of bond-slip responses for 30 MPa Phase 1 beam-end specimens



(a) 125 mm Bonded Length Specimens



(b) 375 mm Bonded Length Specimens

Figure 9.13 Comparison of bond-slip responses for 50 MPa Phase 1 beam-end specimens

9.6.2 Effect of Aggregate Crushing Value on Bond Behaviour

A good correlation between the aggregate crushing value and the average bond stress was observed as illustrated in Figure 9.14 for the 30 MPa and 50 MPa specimens.

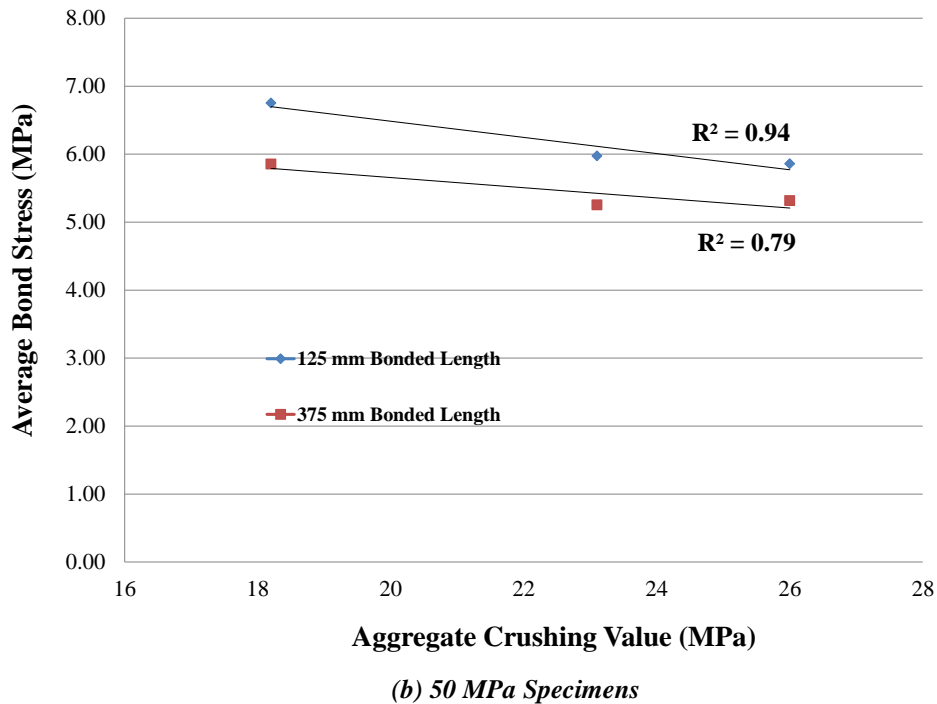
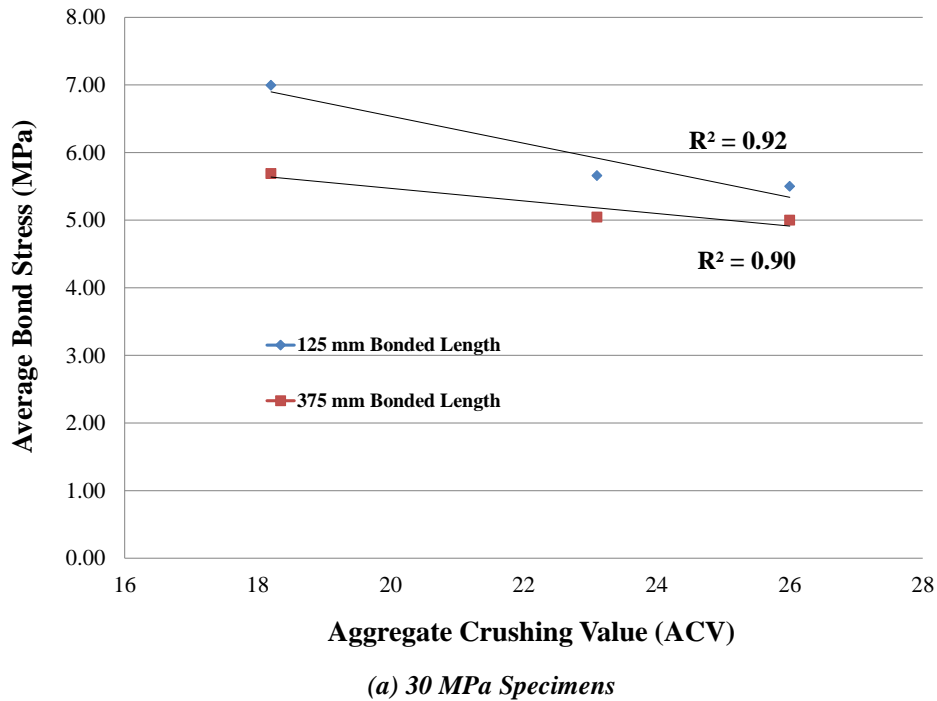
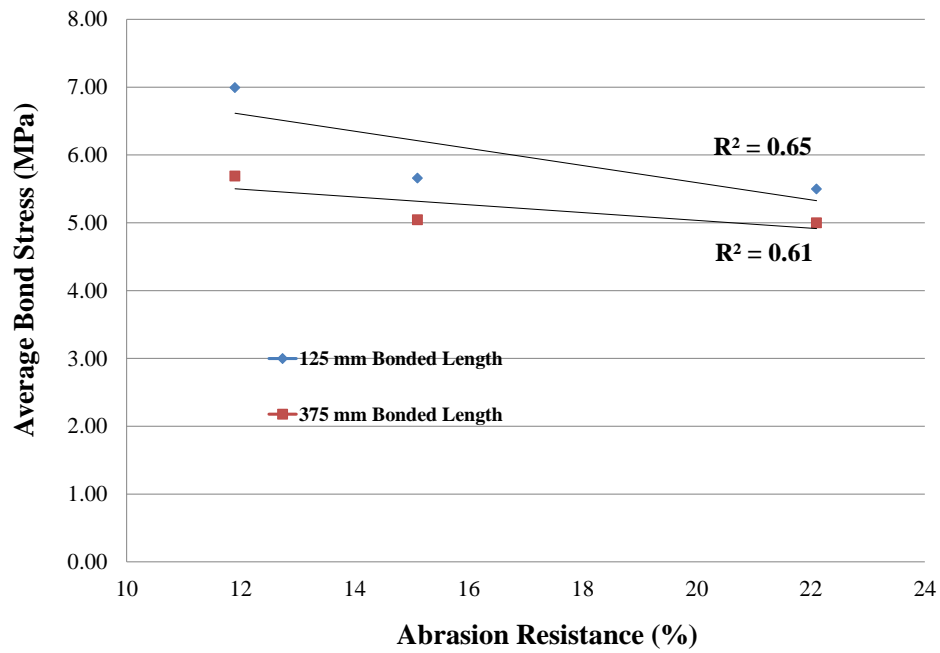


Figure 9.14 Relationship between average bond strength and aggregate crushing value (Phase 1 specimens)

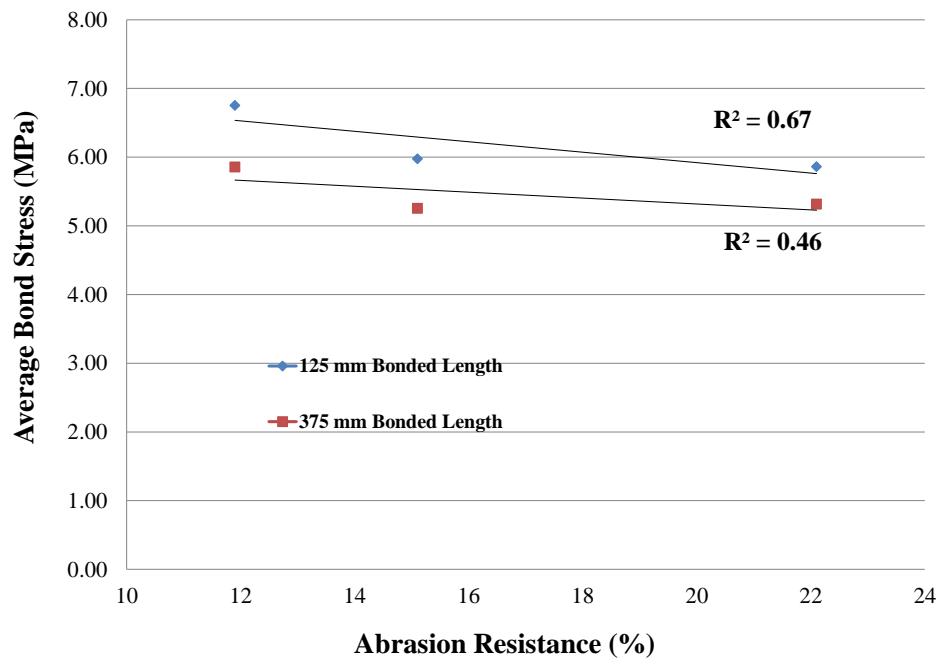
Note that each value on the plots represents the average bond strength of two duplicate beam-end specimens (i.e., A and B). The 30 MPa specimens displayed excellent correlation between the bond strength and ACV as demonstrated by R^2 values of 0.92 and 0.90 for the 125 mm and 375 mm bonded lengths, respectively. Similarly, the 50 MPa specimens had high R^2 values of 0.94 and 0.79 for the 125 mm and 375 mm bonded lengths, respectively. These trends indicate that for various values of bonded length and concrete compressive strength, the average bond stress may be related to the crushing strength of coarse aggregate (ACV). As suggested by other researchers (Darwin et al., 2001, Zuo and Darwin, 2000), this may be due to the influence of coarse aggregate on fracture energy of concrete which has been related to the bond strength between concrete and steel reinforcement. Higher strength aggregates have been shown to produce concretes with higher fracture energies (Darwin et al., 2001) and higher splice strengths (Zuo and Darwin, 2000). The lower aggregate crushing values of the RCA-1 and RCA-2 may explain why the NA concrete beam-ends had higher bond strengths. It should be noted however, that the change in average bond stress vs. ACV (i.e., the slope of the trend line) seems fairly low, especially in the case of the 50 MPa specimens. Sections 9.8.2 and 9.8.7 compare the results of the Phase 1 and 2 beam-end specimens to determine whether the change in average bond stress as a function of ACV is statistically significant.

9.6.3 Effect of Aggregate Abrasion Resistance on Bond Behaviour

The relationship between the abrasion resistance (by the Micro-Deval method) and the average bond stress is illustrated in Figure 9.15 for the 30 MPa and 50 MPa specimens, respectively. Note that each value on the plots represents the average bond strength of two duplicate beam-end specimens (i.e., A and B). A slight trend was found between abrasion resistance and average bond strength in which as abrasion resistance increases (i.e., lower material loss), the average bond strength increases. Although this general trend exists, the R^2 values were fairly low (i.e., 0.65 and 0.67 for the 30 and 50 MPa 125 mm bonded length specimens, respectively and; 0.61 and 0.46 for the 30 and 50 MPa 375 mm bonded length specimens, respectively) compared to those found when comparing ACV and the average bond strength. This weaker correlation was expected as the abrasion resistance of an aggregate does not directly contribute to the resistance of tensile cracking in concrete. However, a general trend does exist due to a strong correlation (R^2 of 0.93) between aggregate crushing value and abrasion resistance (see Figure 4.37).



(a) 30 MPa Specimens

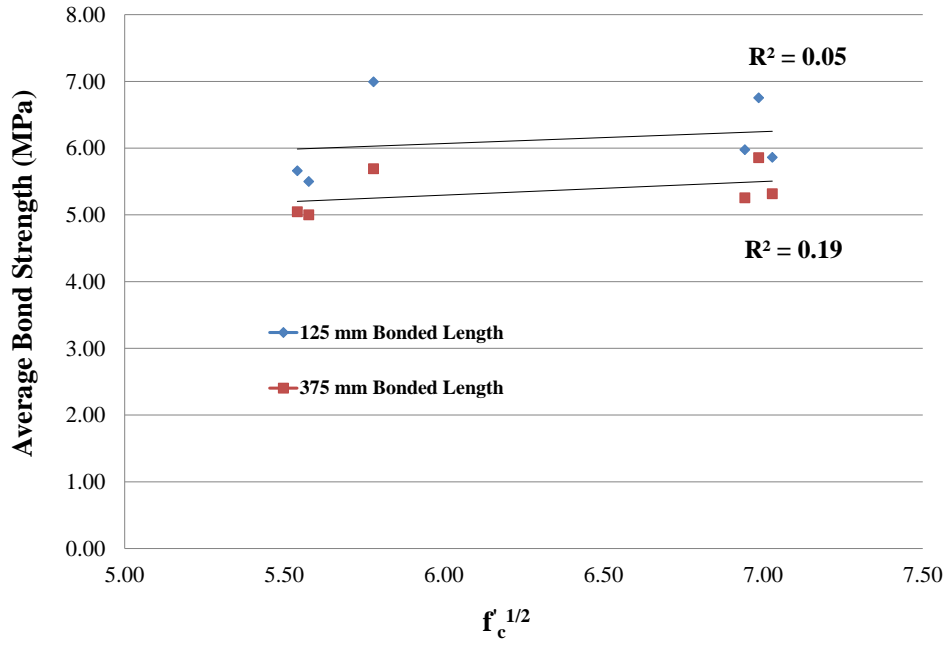


(b) 50 MPa Specimens

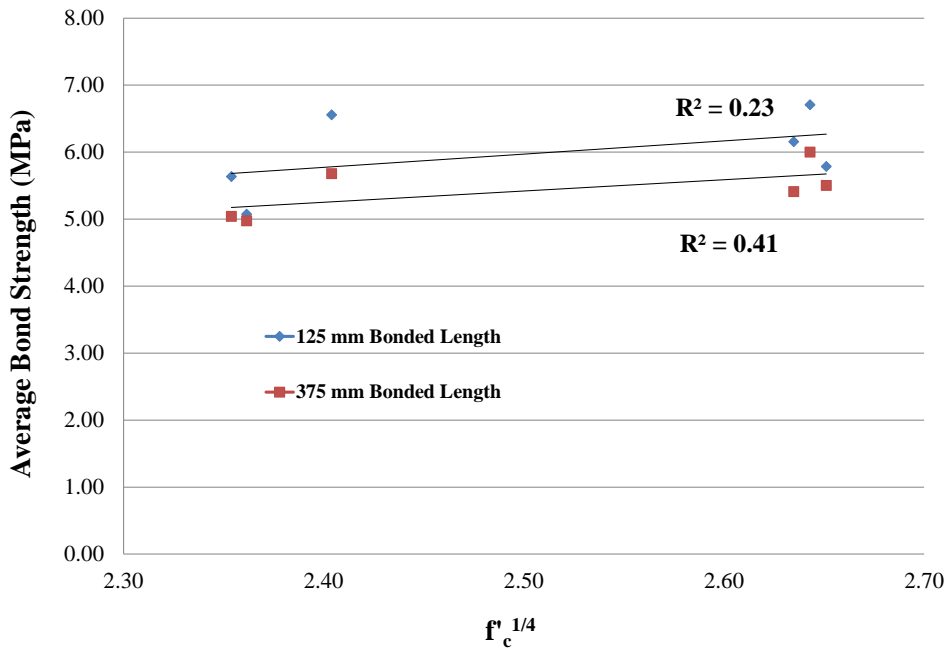
Figure 9.15 Relationship between average bond strength and abrasion resistance (Phase 1 specimens)

9.6.4 Effect of Compressive Strength on Bond Behaviour

The relationship between the average bond strength and compressive strength normalized with respect to $f'_c{}^{1/2}$ and $f'_c{}^{1/4}$ is illustrated in Figure 9.16a and Figure 9.16b, respectively.



(a) Relationship between τ_b and $f'_c{}^{1/2}$



(b) Relationship between τ_b and $f'_c{}^{1/4}$

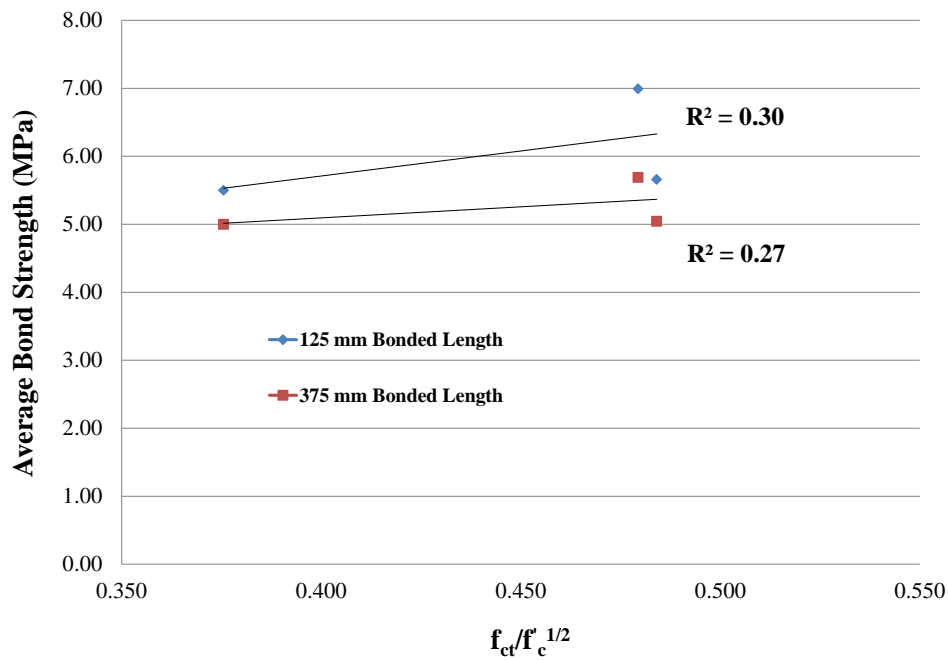
Figure 9.16 Relationship between average bond strength and compressive strength (Phase 1 beam-end specimens)

Each value on the plots represents the average bond and compressive strength of a single beam-end specimen and the results of both the 30 and 50 MPa specimens are combined. Contrary to the findings in the literature (refer to Section 2.4.3.5), no significant correlation was found between bond strength and $f_c^{1/2}$ or $f_c^{1/4}$. An overall assessment of the effect of compressive on the bond strength is included in Section 9.8.3.

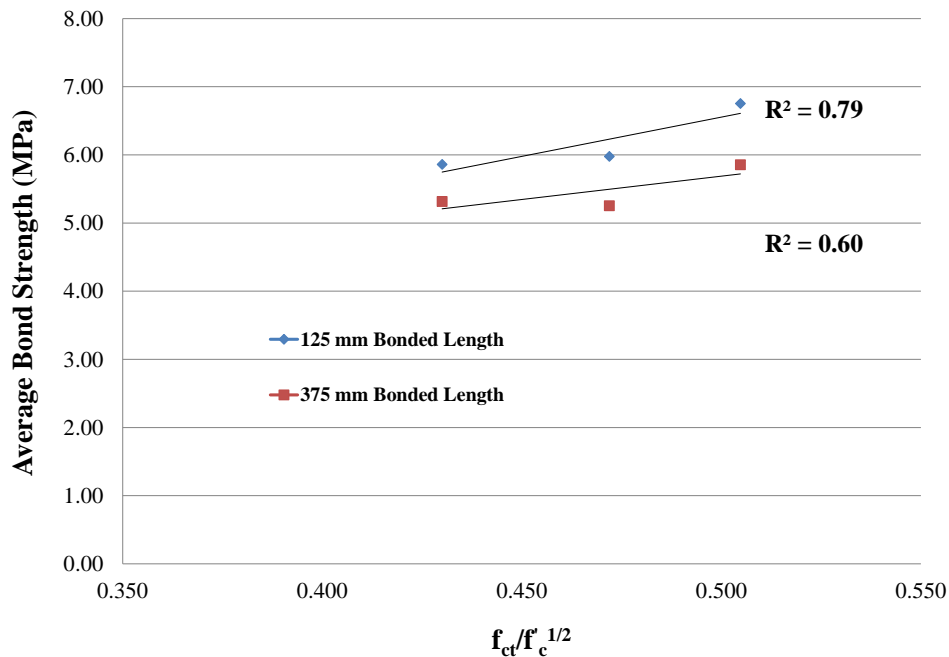
9.6.5 Effect of Splitting Tensile Strength on Bond Behaviour

The splitting tensile strength testing was performed in conjunction with the fracture energy testing, nearly 40 days after the beam-end specimens were tested. In order to eliminate the differences in compressive strength and to isolate the effect of aggregate type on splitting tensile strength and bond, splitting tensile strength values were normalized with respect to $f_c^{1/2}$ values at the time of fracture energy testing. These values are also summarized in the previous Table 9.7.

Figure 9.17 provides an indication of the influence of splitting tensile strength of concrete on bond strength. Note that each value on the plots represents the average bond strength of two duplicate beam-end specimens (i.e., A and B)



(a) 30 MPa Specimens



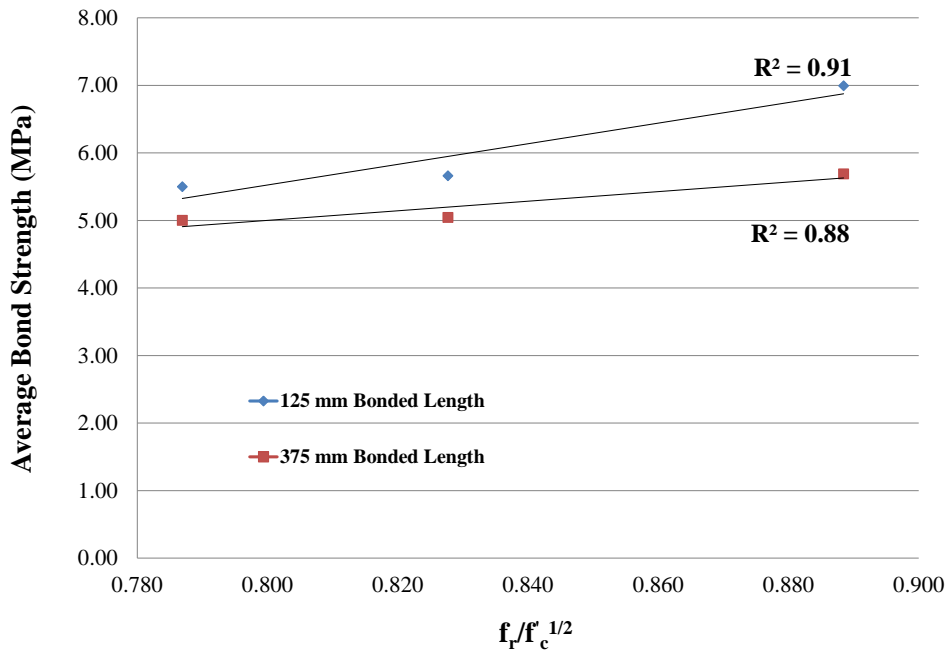
(b) 50 MPa Specimens

Figure 9.17 Relationship between average bond strength and splitting tensile strength (Phase 1 specimens)

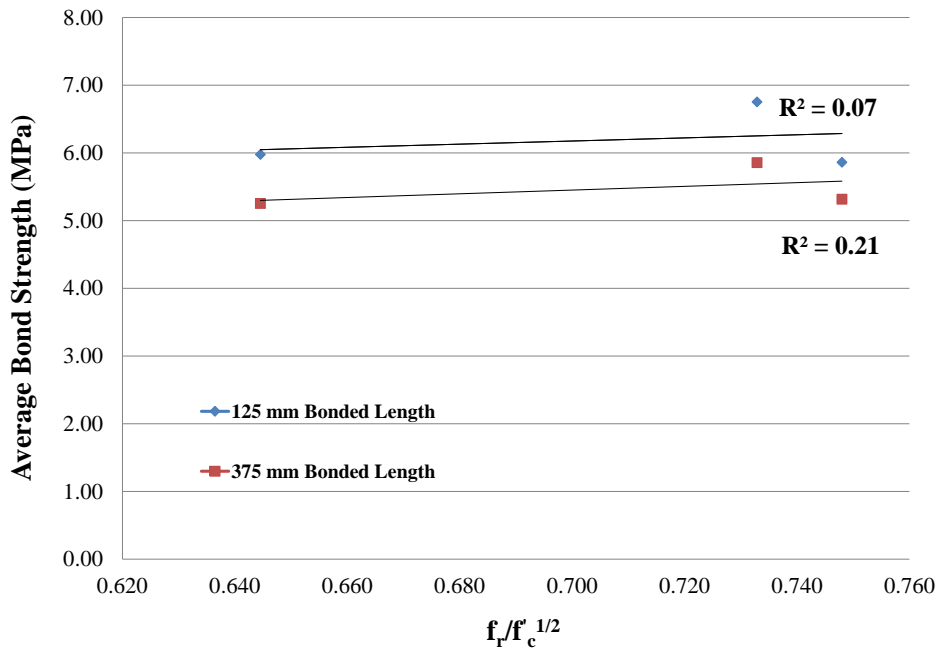
In general, no significant correlation was observed to exist between splitting tensile strength and average bond strength for the 30 MPa specimens (Figure 9.16a). Slightly better correlations were observed for the 50 MPa specimens (R^2 values of 0.79 and 0.60 for the 125 and 375 mm bonded lengths, respectively). Overall, general trend lines in Figure 9.17 suggest that as splitting tensile strength increases, average bond stress increases.

9.6.6 Effect of Modulus of Rupture on Bond Behaviour

The modulus of rupture of concrete was measured using the fracture energy single-edge notched double cantilevered (SENDC) specimens (refer to Chapter 6 for test procedure). The relationship between modulus of rupture normalized to $f_c^{1/2}$ ($f_r/f_c^{1/2}$) and average bond strength is presented in Figure 9.18. Note that each plotted value represents an average of two specimens (i.e., Specimen A and B for both the fracture energy and beam-end specimens). A strong correlation exists between $f_r/f_c^{1/2}$ and the bond strength for the 30 MPa specimens. However, there appears to be little relation between $f_r/f_c^{1/2}$ and $\tau_{b,avg}$ for the 50 MPa specimens. The influence of aggregate strength (i.e., ACV) on the modulus of rupture will be evaluated based on the combined results of Phase 1 and 2 in Section 9.8.5.



(a) 30 MPa Specimens



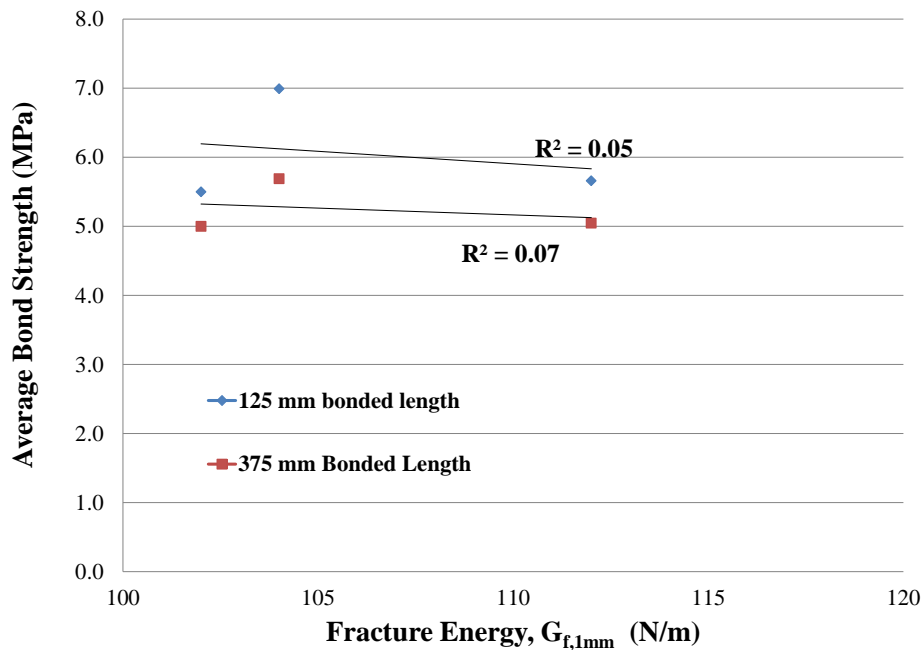
(b) 50 MPa Specimens

Figure 9.18 Relationship between average bond strength and $f_r/f_c^{1/2}$ (Phase I specimens)

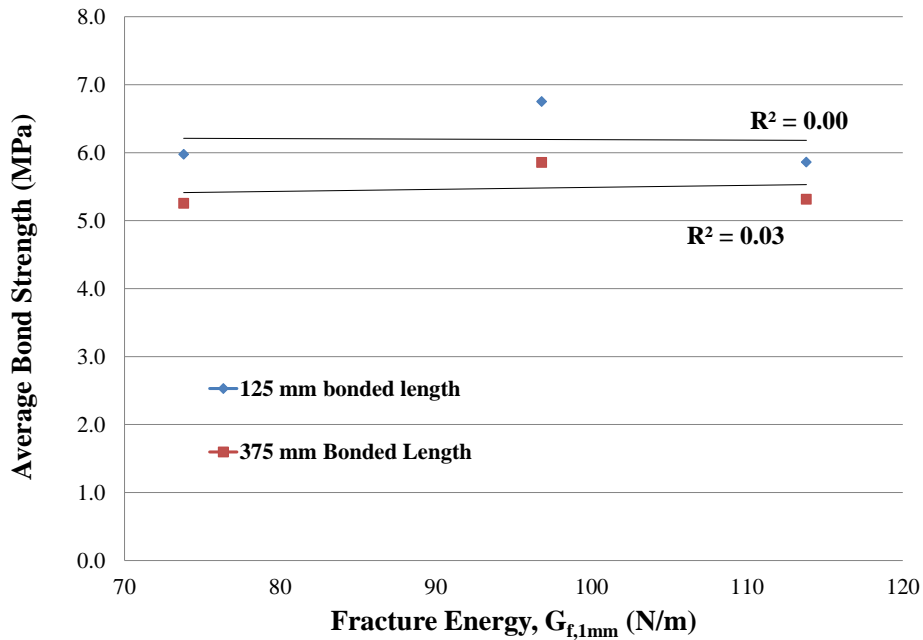
9.6.7 Effect of Fracture Energy on Bond Behaviour

The fracture energy of concrete was measured using single-edge notched double-cantilevered (SENDC) beam specimens in accordance with the procedures outlined in Section 6.2.7. Specimens were cast in conjunction with beam-end specimens to allow for the correlation of bond strength and fracture energy to be assessed.

Figure 9.19 depicts the relationship between average bond strength and fracture energy for the 30 and 50 MPa Phase 1 beam-end specimens. Note that each plotted value represents an average of two specimens (i.e., Specimen A and B for both the fracture energy and beam-end specimens). As evidenced by the low R^2 values, there was no significant relation between fracture energy and average bond strength for either the 30 or 50 MPa specimens. This finding is in contrast to the proposals of ACI committee 408 (2003) and Zuo and Darwin (2000) which suggest that an increase in fracture energy results in a higher resistance to splitting crack propagation which ultimately increases splice strength. The combined results of Phase 1 and 2 will be evaluated in Section 9.8.6 to determine the overall effect of fracture energy of RCA concrete on the average bond strength.



(a) 30 MPa Specimens



(b) 50 MPa Specimens

Figure 9.19 Relationship between average bond strength and fracture energy (Phase 1 specimens)

9.6.8 Dissection and Forensic Analysis of Beam-Ends

After reviewing the results of the Phase 1 beam-ends tests, five specimens were selected for dissection and forensic analysis. The main purpose of this dissection phase was to,

- 1) Understand the failure mechanism associated with beam-end specimens;
- 2) Identify signs of slip attributed to crushing of concrete in the vicinity of the reinforcement ribs, and;
- 3) Investigate the influence of aggregate type on bond failure mode.

Dissections were performed systematically on each specimen through the use of a portable concrete cut-off saw. Figure 9.20 outlines the beam-end dissection process.

Once the beam-ends were dissected, the individual components (i.e., surrounding concrete and reinforcing bar) were photographed. The main reinforcing bar was examined and the actual bonded length was measured. Note that the average bond stress results reported in Section 9.6.1 incorporate the measured bonded lengths derived from the forensic analysis in their calculation. A macro-level forensic analysis was then performed which entailed observing the individual

fracture surfaces under low-magnification magnifying glass and noting the crack patterns, the condition of the rib indentations and amounts of adhered concrete on the test bar. The type of bond failure was also identified based on the classification presented in Figure 9.21.

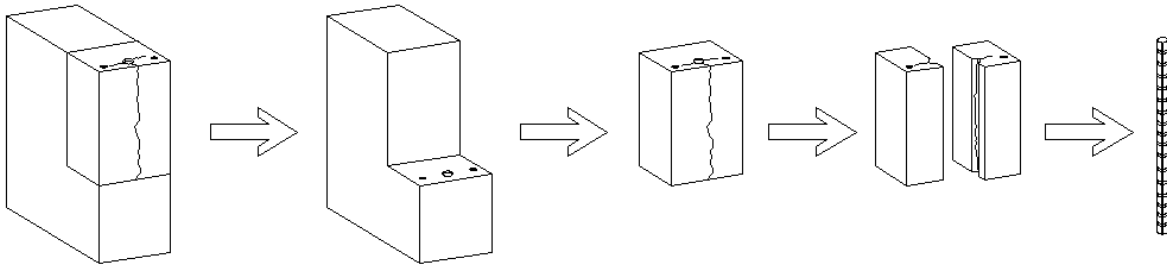


Figure 9.20 Schematic of the beam-end dissection procedure

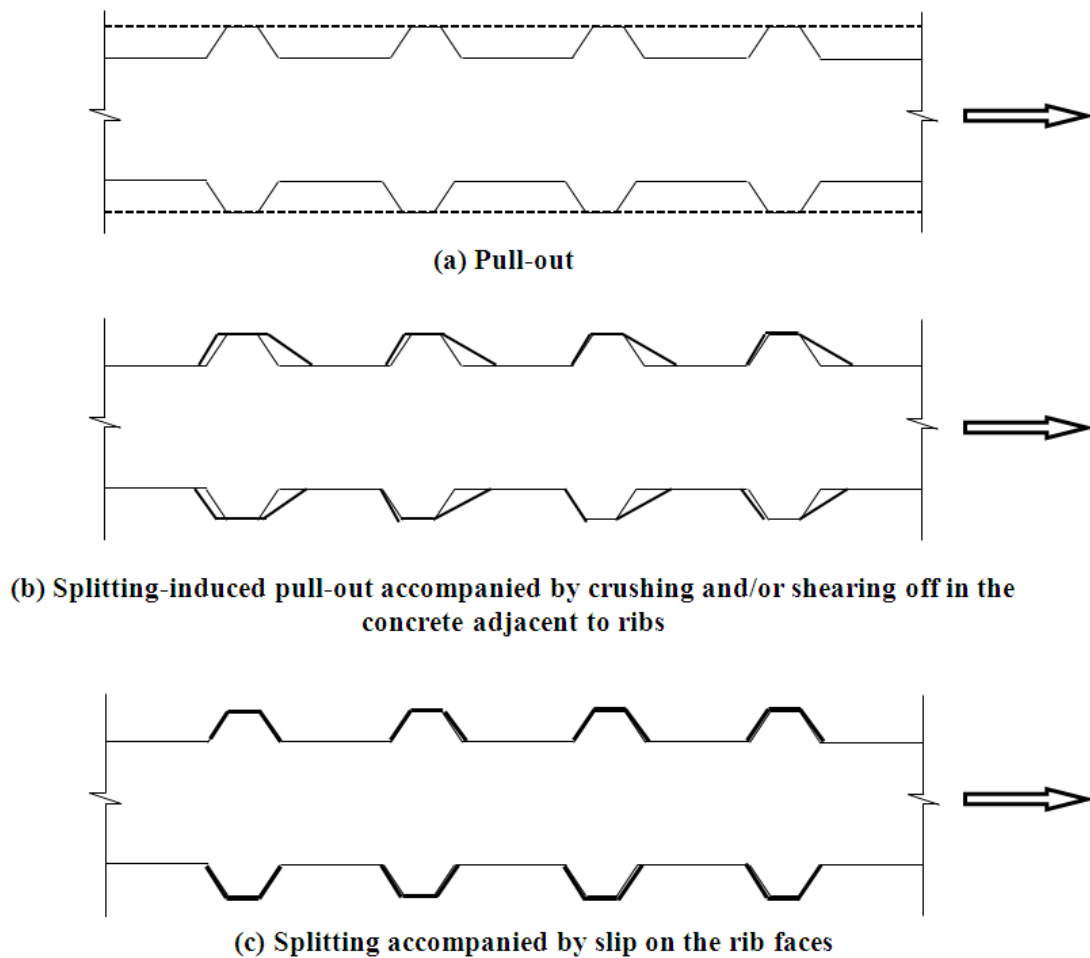


Figure 9.21 Modes of bond failure (adapted from CEB-FIP, 2000)

9.6.8.1 Specimen BE-NAC-30-375A

Beam-end specimen BE-NAC-30-375A failed at a pull-out load of 169.9 kN and an average concrete compressive strength of 34.5 MPa. Figure 9.22 indicates the splitting crack patterns along the interior face of the concrete indentations. A bonded length of 380 mm was measured as depicted in Figure 9.24. It can be observed in Figure 9.23 that the tensile hoop stresses generated from the stress cone during loading caused fracture planes to occur both around and through the coarse natural aggregates. This figure also indicates that the rib indentations are more prominent closer to the free-end of the bar which is a result of the lower bond stresses at this end (i.e., because the extent of concrete crushing is reduced). It is also interesting to note that along the main bar rib indentations there are no exposed aggregate only mortar which was in direct contact with the bar surface. This was typical of all dissected beam-end specimens. This is most likely due to the vibration and consolidation procedures in which the bar became coated with mortar prior to initial set of the concrete. The strength of this thin mortar layer may govern the chemical adhesive strength component of the overall bond capacity (refer to Section 2.4.2.1 for overview of bond failure mechanisms). Figure 9.24 shows the main test bar with pieces of adhered mortar wedged between the rib face and the bar face. It also shows some slight wear of the concrete rib indentations and a significant amount of adhered concrete on the ribs indicating a splitting-induced pull-out failure (see Figure 9.21b).

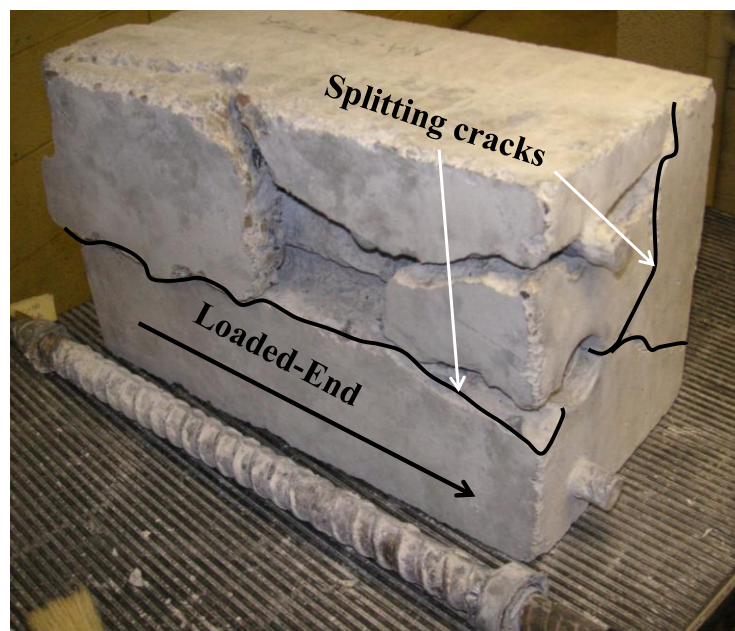


Figure 9.22 Main anchorage zone and splitting crack pattern (dissected BE-NAC-30-375A)

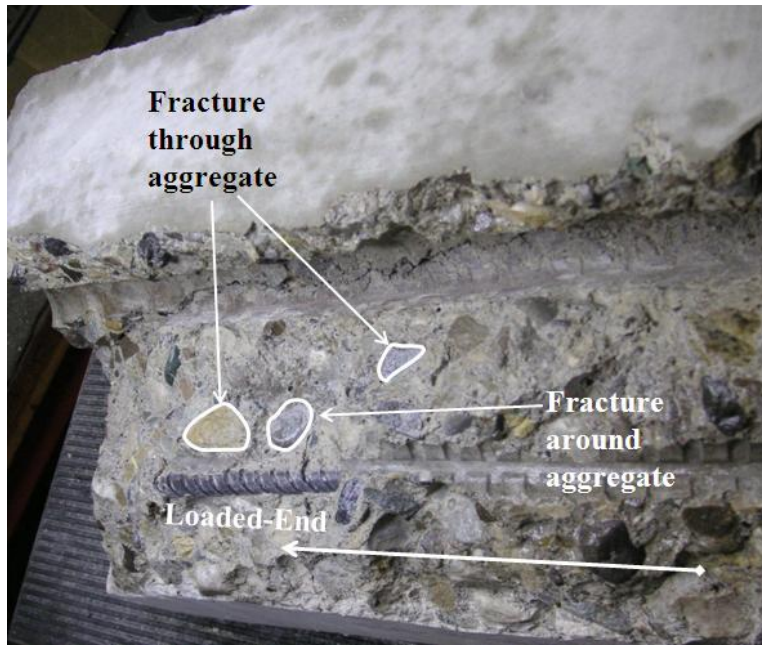


Figure 9.23 Main failure planes through concrete cover (dissected BE-NAC-30-375A)

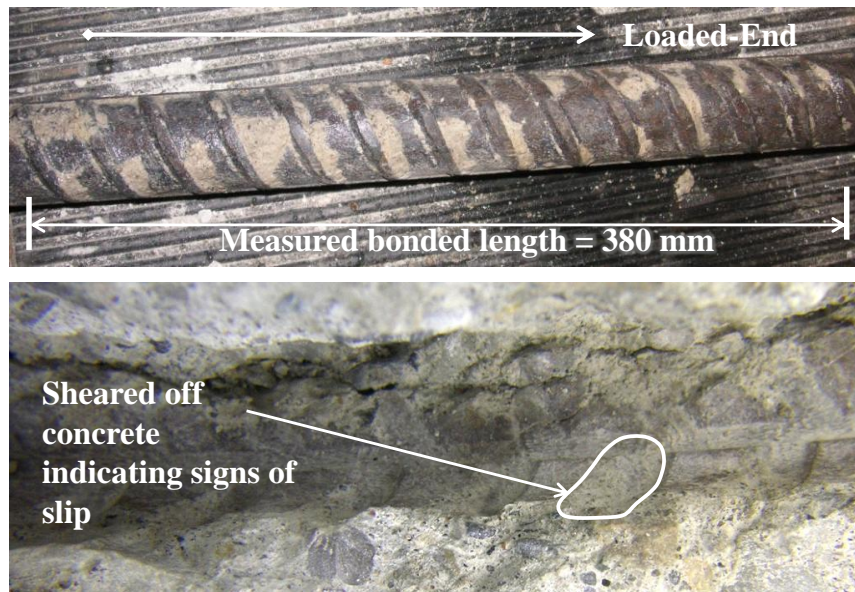


Figure 9.24 Main test bar, measured bonded length, and concrete rib indentations (dissected BE-NAC-30-375A)

9.6.8.2 Specimen BE-NAC-50-375A

Beam-end specimen BE-NAC-50-375A failed at a pull-out load of 179.5 kN and an average concrete compressive strength of 49.0 MPa. Figure 9.25 depicts the main anchorage zone for the dissected 50 MPa NA concrete specimen with a 375 mm bonded length. The main splitting

cracks ran from the concrete surface to the surface of the test bar. Figure 9.26 depicts the main failure planes along the splitting cracks. Splitting cracks passed both around and through the natural aggregate particles. It was noticed that concrete rib indentations were more pronounced at the free-end where bond stresses were lower. Figure 9.27 shows the test bar and crushing of concrete rib indentations. Both the crushing of concrete ribs and the significant amount of adhered concrete remaining on the test bar indicate the bond failure was a splitting-induced pull out (see Figure 9.21b). A bonded length of 375 mm was measured as depicted in Figure 9.27.



Figure 9.25 Main anchorage zone and splitting crack pattern (dissected BE-NAC-50-375A)

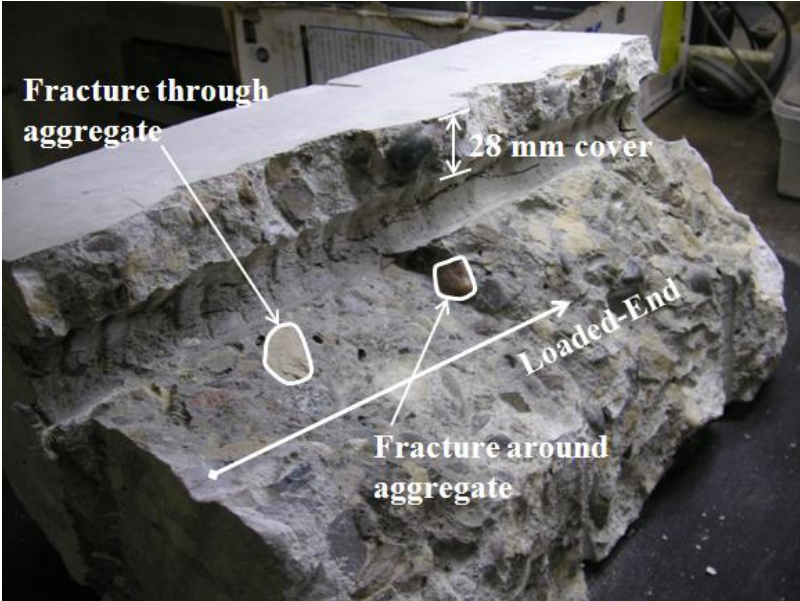


Figure 9.26 Main failure planes through concrete cover (dissected BE-NAC-50-375A)

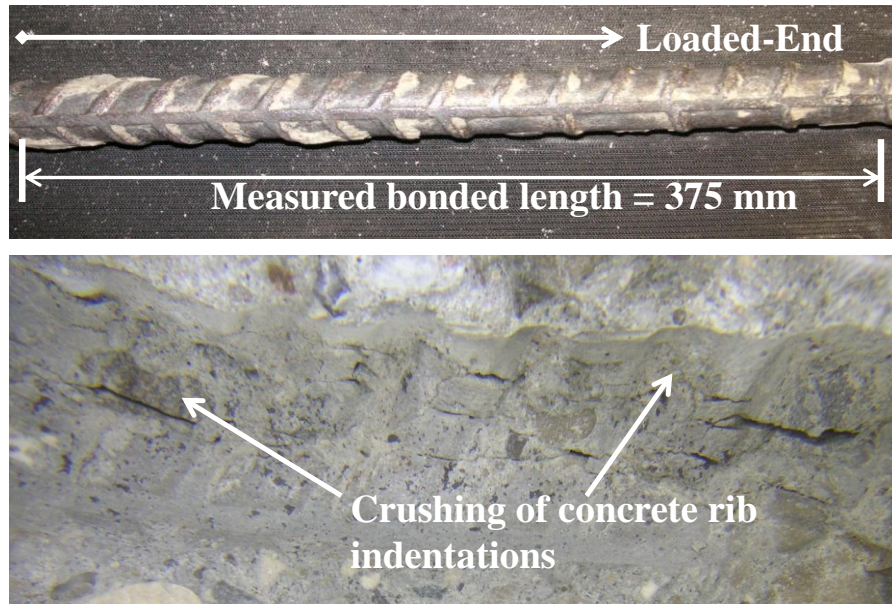


Figure 9.27 Main test bar, measured bonded length, and crushing of concrete rib indentations (dissected BE-NAC-50-375A)

9.6.8.3 Specimen BE-RAC1-30-375A

Beam-end specimen BE-RAC1-30-375A failed at a pull-out load of 150.8 kN and an average concrete compressive strength of 30.9 MPa. Figure 9.28 shows the main anchorage zone of the 30 MPa RCA-1 concrete beam-end specimen with a bonded length of 375 mm. Typical splitting cracks along the bottom face of the specimen run from the concrete surface through the main concrete cover to the top surface of the testing bar. Splitting cracks along the plane perpendicular to the test bar radiate out from the location of the test bar. Figure 9.29 shows the failure planes through the main concrete cover and along the splitting plane of the test bar. A cover of 30 mm was measured for this specimen. Also depicted in Figure 9.29 is a smooth aggregate particle (original aggregate in RCA-1) arresting the splitting crack running along the bar location. This illustrates the role that aggregate strength plays on bond behaviour. Figure 9.30 shows the test bar with an actual measured bonded length of 380 mm. A significant amount of adhered concrete remained on the test bar which indicates the bond failure was a splitting-induced pull out (see Figure 9.21b).

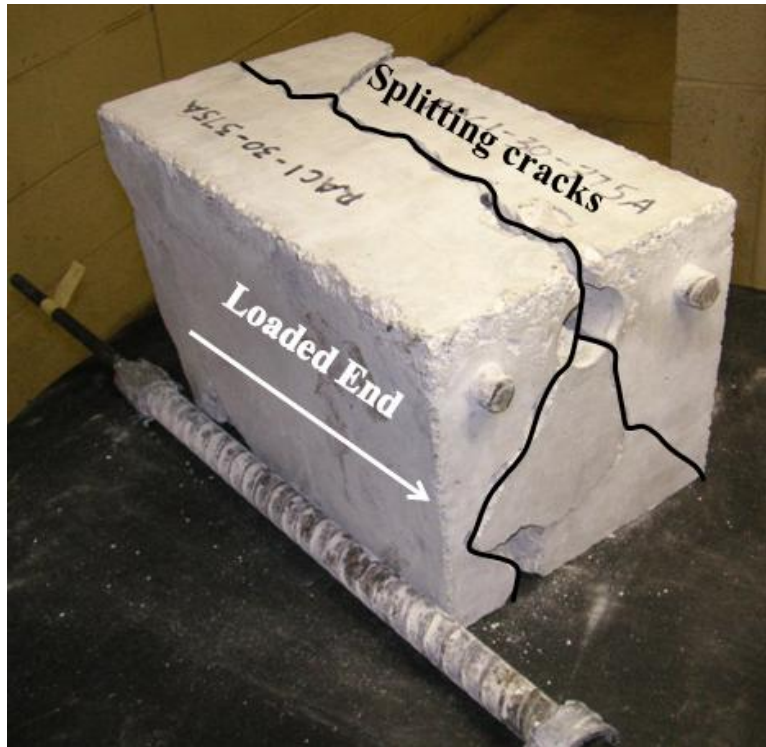


Figure 9.28 Main anchorage zone and splitting crack pattern (dissected BE-RAC1-30-375A)

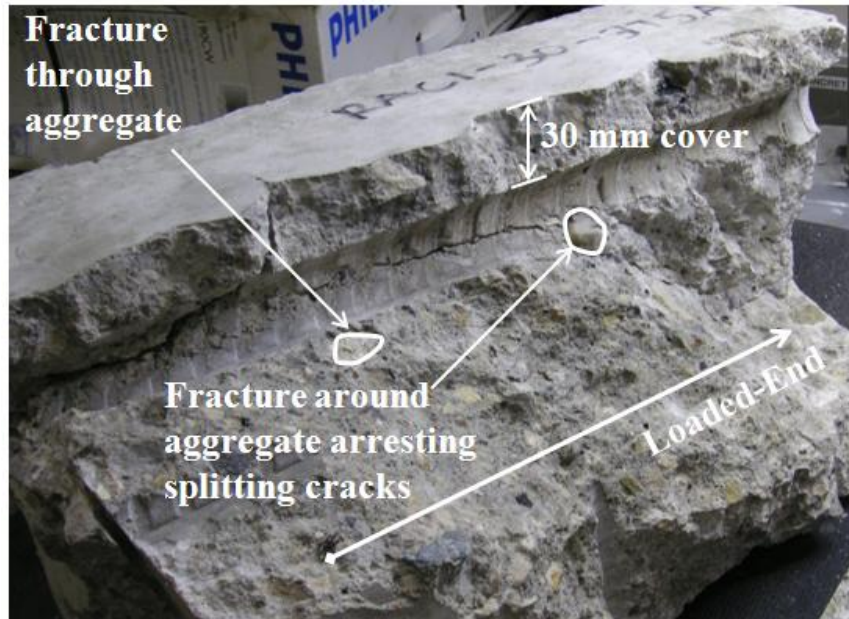


Figure 9.29 Main failure planes through concrete cover (dissected BE-RAC1-30-375A)



Figure 9.30 Main test bar, measured bonded length, and adhered concrete (dissected BE-RAC1-30-375A)

9.6.8.4 Specimen BE-RAC2-30-125B

Beam-end specimen BE-RAC2-30-125B failed at a pull-out load of 59.1 kN and an average concrete compressive strength of 31.3 MPa. Figure 9.31 shows the main anchorage zone and splitting crack pattern. Similar to the 375 mm bonded length specimens, the splitting cracks run the length of the bonded region of the bar passing from the bar surface, through the concrete cover up to the concrete surface. Figure 9.32 shows the failure planes passing both around and through the RCA-2 coarse aggregate. Smaller pieces of deleterious materials (i.e., wood chips) are also shown passing through the fracture surface.

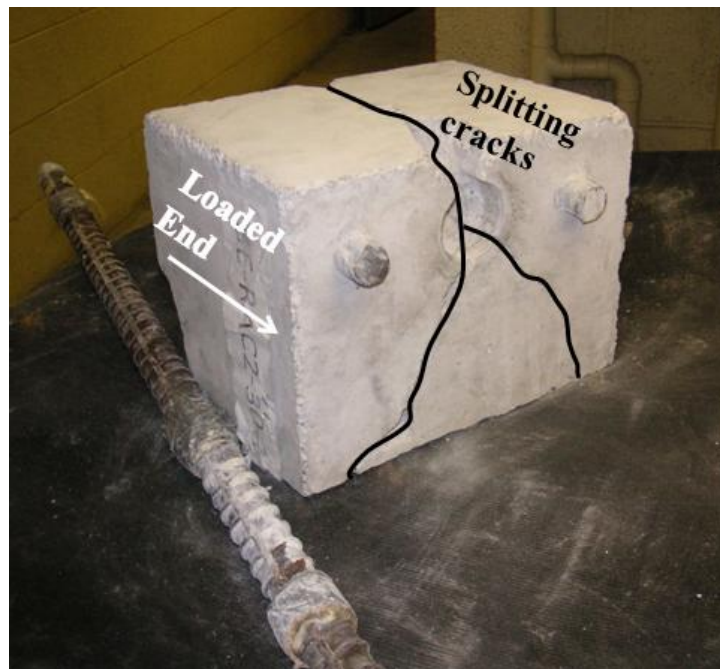


Figure 9.31 Main anchorage zone and splitting crack pattern (dissected BE-RAC2-30-125B)

Figure 9.33 shows the main test bar and sheared off concrete within the ribs indicating a

splitting-induced pull-out failure. This suggests that this type of failure is independent of aggregate type and bonded length and is most likely influenced by the rib face angle (CEB-FIP, 2000). Figure 9.27 also shows the actual measured bonded length of 125 mm.

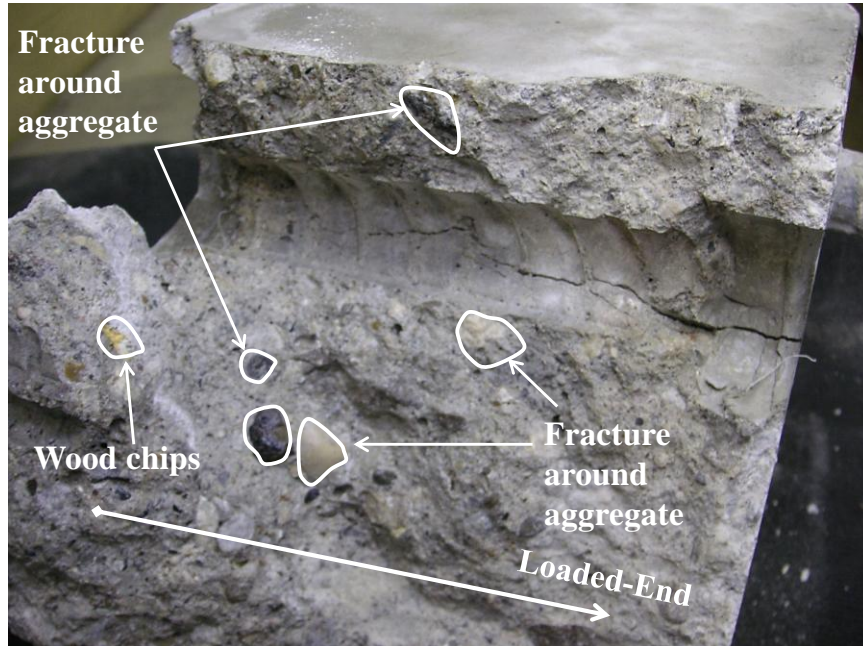


Figure 9.32 Main failure planes through concrete cover (dissected BE-RAC2-30-125B)



Figure 9.33 Main test bar, measured bonded length and adhered concrete (dissected BE-RAC2-30-125B)

9.6.8.5 Specimen BE-RAC2-50-375A

Beam-end specimen BE-RAC2-50-375A failed at a pull-out load of 164.6 kN and an average concrete compressive strength of 49.4 MPa. Figure 9.34 illustrates the splitting cracks within the main anchorage zone and test bar. This splitting pattern was typical amongst the 375 mm bonded length specimens. Figure 9.35 illustrates the failure planes through the concrete cover and along the bonded length. The majority of the failure planes fractured through the RCA-2

particles indicating that aggregate strength is closely related to the bond strength (see Section 9.6.2). There were also pieces of asphalt that passed through the failure plane going through the main concrete cover. Once again, the concrete rib indentations are more intact closer to the free-end of the bar which is a result of the lower bond stresses at this location (i.e., because the extent of concrete crushing is reduced). Figure 9.36 depicts the test bar and shearing off in the concrete against the reinforcing steel ribs indicating splitting-induced pull-out failure (see Figure 9.22b). Figure 9.36 also shows the measured bonded length of 380 mm. Further crushing of concrete rib indentations can be seen in Figure 9.37 acting parallel to the orientation of the test bar.

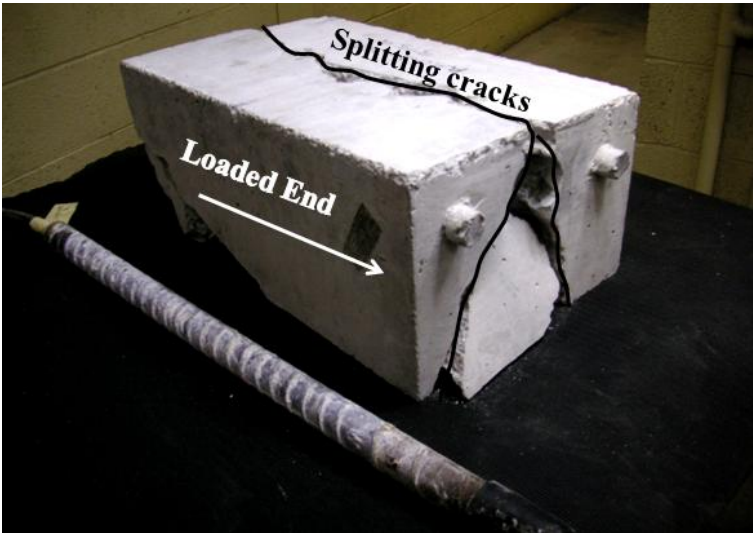


Figure 9.34 Main anchorage zone and splitting crack pattern of (dissected BE-RAC2-50-375A)

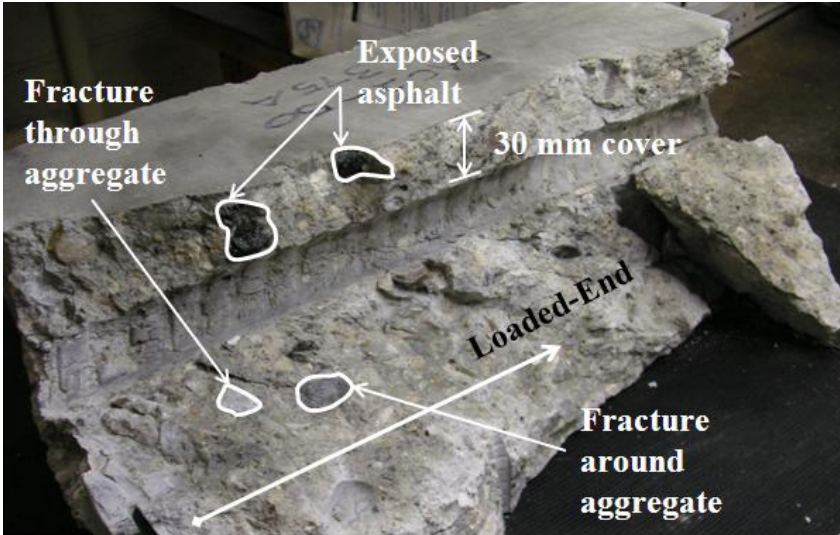


Figure 9.35 Main failure planes through concrete cover (dissected BE-RAC2-50-375A)

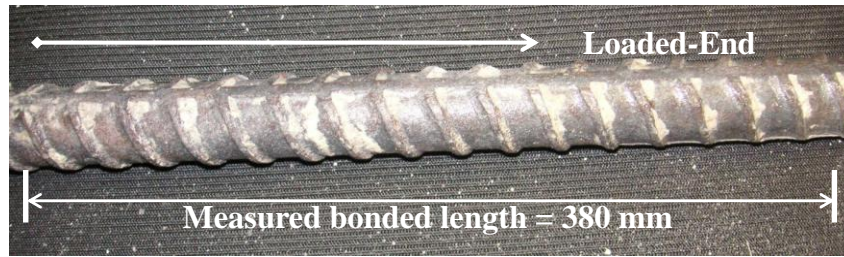


Figure 9.36 Main test bar, measured bonded length and adhered concrete (dissected BE-RAC2-50-375A)

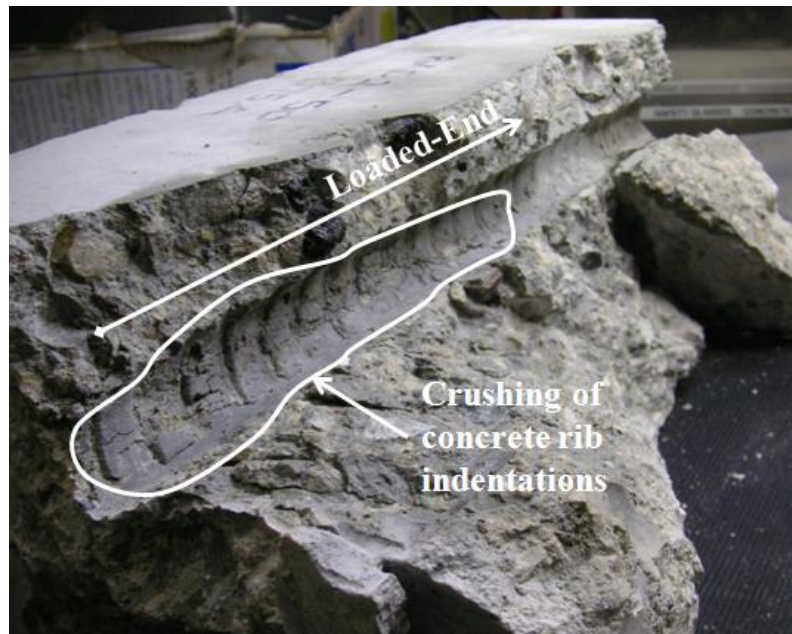


Figure 9.37 Evidence of crushing of concrete rib indentations (dissected BE-RAC2-50-375A)

9.6.8.6 Summary and Conclusions from Phase 1 Dissections and Forensic Analysis

The following conclusions were based on the observations and measurements taken during the dissection of Phase 1 beam-end specimens.

- 1) In all specimens, the bond failure mode was splitting-induced by crushing and/or shearing of the concrete adjacent to the ribs. Therefore, at the 30 and 50 MPa concrete strength level, for bonded lengths of 125 and 375 mm, and for natural, RCA-1 and RCA-2 aggregates, the type of aggregate had no apparent influence on the bond failure mode.
- 2) Splitting occurs due to circumferential tension field that develops due to bearing of ribs on the surrounding concrete. Signs of slip were identified in all specimens by observing the reinforcing bar ribs displaced from the cast-in concrete rib indentations. Based on the

failure mechanism of the beam-end specimens, slip of the reinforcing bar occurred due to micro-cracking at the tips of the reinforcement ribs which was followed by the formation of longitudinal splitting cracks.

- 3) In all cases, the fracture planes passed mainly through the coarse aggregate particles highlighting the influence of aggregate strength on bond strength.

9.6.9 Conclusions from Phase 1 Bond Testing

The following conclusions can be drawn from the beam-end testing results from Phase 1 (f'_c of 30 and 50 MPa, and bonded lengths of 125 and 375 mm):

1. The NA concrete beam-end specimens had τ_b/f'_c values that were between 10 and 21% higher than the RCA concrete beam-end specimens for compressive strengths of 30 and 50 MPa and bonded lengths of 125 and 375 mm.
2. Replacing natural coarse aggregate with either RCA-1 or RCA-2 did not have a discernible effect on the general bond stress-slip response. While the maximum bond strengths for the NA concrete specimens were higher than the RCA concrete specimens, the residual bond strength values were generally similar. In general, any differences in post-peak bond-slip behaviour between the NA concrete or RCA concrete beam-end specimens is considered insignificant as it is the peak bond force that is commonly useful in design of reinforced concrete structures.
3. Overall, based on the results from Phase 1, the aggregate crushing value is the aggregate property which has the highest influence on bond strength. Excellent correlations were found between the aggregate crushing value and the average bond strength. As coarse aggregate crushing strength decreases (ACV increases), the average bond strength decreases. However, the change in average bond stress vs. ACV (i.e., the slope of the trend line) was fairly low, especially in the case of the 50 MPa specimens. An analysis is performed at the end of this chapter to confirm that the effect of ACV on bond strength is statistically significant.
4. Although the R^2 values were relatively low, it was found that as abrasion resistance increases (decrease in micro-deval abrasion loss), the average bond strength increases.

This was believed to be an indirect relationship resulting from the strong relationship that exists between ACV and micro-deval abrasion resistance.

5. In contrast to published studies in the literature for normal weight (natural aggregate) concrete, no significant relationship existed between concrete compressive strength (f'_c , $f'_c{}^{1/2}$, and $f'_c{}^{1/4}$) and the average bond strength and between the splitting tensile strength (f_{ct}) and the average bond strength.
6. An excellent correlation between modulus of rupture and average bond strength exists for the 30 MPa specimens. However, no correlation exists for the 50 MPa specimens. A discussion at the end of this chapter will address the relation between modulus of rupture and bond strength for all 48 beam-end specimens.
7. For the 50 MPa samples, it appears that the splitting tensile strength normalized with respect to $f'_c{}^{1/4}$ is the concrete property which has the greatest influence on bond strength. This may be a direct result of the strong correlation between splitting tensile strength and ACV for the 50 MPa specimens.
8. After dissection and macro-level forensic analyses were performed on a select number of beam-end specimens, general beam-end structural behaviour and failure mechanism was confirmed. All specimens failed by splitting-induced pull-out followed by crushing and/or shearing off in the concrete adjacent to the ribs. This failure mechanism was confirmed as excessive rib crushing and shearing were observed during the dissection process, especially in the 375 mm bonded length specimens. Examination of fracture planes passing mainly through the coarse aggregate confirmed the influence of the coarse aggregate strength (i.e., ACV) on bond strength.

9.7 Evaluation of Bond-Slip Response of Phase 2 (40 and 60 MPa) Specimens

The following section presents the bond and slip data for all Phase 2 beam-end specimens. Bond strength, slip and stress-slip curves were compared and contrasted between the natural and RCA concrete specimens. The effects of various aggregate and concrete properties on the bond strength and slip results were examined through the use of correlation plots. Following testing, several beam-end specimens were dissected and a macro-scale forensic analysis was carried out to determine actual bonded lengths and investigate failure mechanisms. A detailed discussion and comparison of the Phase 1 and 2 results and trends has been included in Section 9.8.

9.7.1 Summary and Discussion of Test Results

Aggregate crushing values, splitting tensile strengths, compressive strengths, average bond strengths (τ_b), and slip values have been summarized in Table 9.8. Note that each average bond stress and slip value reported represents the average value of two identical beam-end specimens (i.e., A and B).

Due to the change in batching method (i.e., batching method A versus C), as described in Section 5.2.2, the compressive strengths for the 60 MPa mixtures were, on average lower than those measured during trial batching. As Batching Method C used a different pre-treatment process for the coarse aggregates than Batching Method A (i.e., pre-wetting via spraying versus pre-soaking in buckets), the in-situ moisture of coarse aggregates was more variable. In addition, Batching Method C used a pan mixer that was six times larger (300 L versus 50 L) than the pan mixer used in Batching Method A which provided a larger interior surface area on which excessive cement paste could become adhered resulting in a change to the specified water-cement ratio. However, it was assumed that the mixture proportions were most sensitive to the in-situ moisture content of both the fine and coarse aggregates. Therefore, given that the compressive strengths were lower than the trial mixtures, the actual water-cement ratios must have been higher than specified, indicating that the actual moisture contents of the coarse aggregates and/or fine aggregate were higher than those included as part of the mixture proportion moisture corrections.

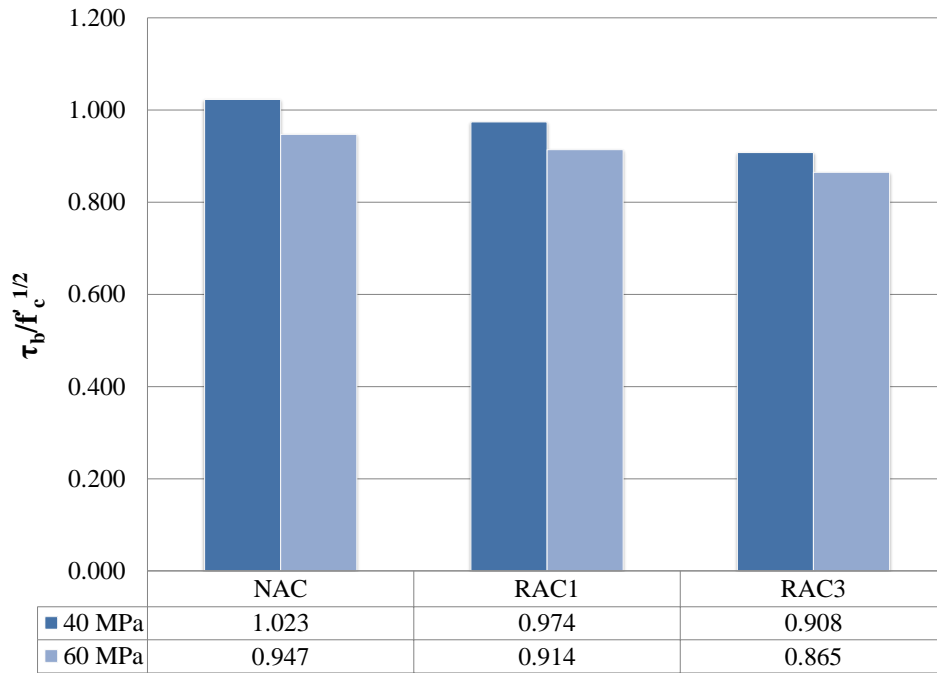
Compressive strengths averaged 54 MPa for the NA concrete mixtures, 52 MPa for the RCA-1 concrete mixtures and 56.5 MPa for the RCA-3 concrete mixtures (see Table 9.8). Therefore, in order to isolate the effect of aggregate type on bond, the average bond strength values were normalized with respect to $f'_c{}^{1/2}$, and are summarized in Figure 9.38.

Table 9.8 Phase 2 beam-end bond-slip response test data

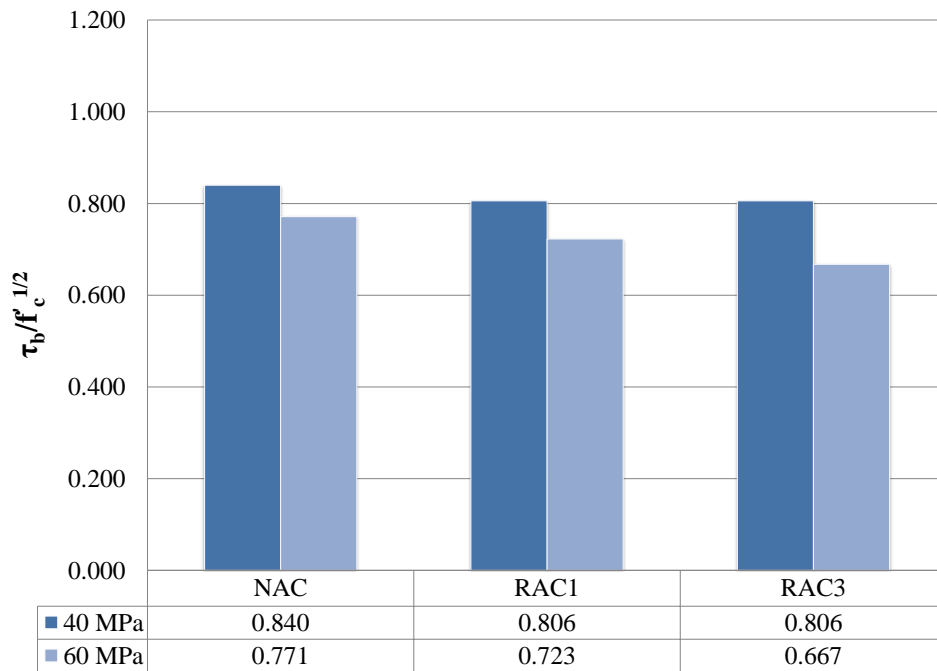
Specimen ID [†]	ACV	f_{ct}/f'_c	f'_c (MPa)	T_b (kN)	τ_b (MPa)	Loaded-End Slip at Failure [‡] (mm)	Free-End Slip at Failure (mm)
BE-NAC-40-125A	18.2	0.089	40.5	61.0	6.46	0.143	0.158
BE-NAC-40-125B		0.111	39.4	67.9			
BE-NAC-40-450A		0.089	40.5	205.2	5.31	0.493	0.127
BE-NAC-40-450B		0.111	39.4	180.5			
BE-NAC-60-125A		0.074	53.8	67.2	6.95	0.114	0.111
BE-NAC-60-125B		0.086	53.8	71.4			
BE-NAC-60-450A		0.074	53.8	199.2	5.66	0.534	0.132
BE-NAC-60-450B		0.086	53.8	207.0			
BE-RAC1-40-125A	23.1	0.087	43.7	60.6	6.39	0.114	0.082
BE-RAC1-40-125B		0.087	42.6	68.8			
BE-RAC1-40-450A		0.087	43.7	190.6	5.29	0.488	0.127
BE-RAC1-40-450B		0.087	42.6	189.5			
BE-RAC1-60-125A		0.071	53.8	62.8	6.57	0.124	0.132
BE-RAC1-60-125B		0.087	49.9	68.3			
BE-RAC1-60-450A		0.071	53.8	182.2	5.20	0.560	0.137
BE-RAC1-60-450B		0.087	49.9	191.2			
BE-RAC3-40-125A	28.5	0.088	41.4	63.8	5.84	0.099	0.103
BE-RAC3-40-125B		0.087	41.5	55.2			
BE-RAC3-40-450A		0.088	41.4	187.0	5.19	0.502	0.133
BE-RAC3-40-450B		0.087	41.5	185.4			
BE-RAC3-60-125A		0.071	56.2	65.9	6.51	0.103	0.113
BE-RAC3-60-125B		0.066	57.0	63.9			
BE-RAC3-60-450A		0.071	56.2	181.3	5.02	0.447	0.071
BE-RAC3-60-450B		0.066	57.0	179.3			

[†] Specimens have been labelled as follows: BE = Beam-End, RAC1 = Recycled Aggregate Concrete incorporating RCA-1, 60 = compressive strength in MPa, 450 = bonded length in mm, and the letters A and B denote identical specimens A and B.

[‡] Top slip values have been corrected for axial elongation of the free length of the test bar (i.e., $s_{top,corr} = s_{top} - (PL)/(A_b E_s)$, where $L = 75$ mm, $A_b = 500$ mm², and $E_s = 200\,000$ MPa).



(a) 125mm bonded length specimens



(b) 450mm bonded length specimens

Figure 9.38 Summary charts of average bond strength normalized to $f'_c{}^{1/2}$ (Phase 2)

The NA concrete beam-end specimens with bonded lengths of 125 mm had $\tau_b/f'_c{}^{1/2}$ values that were 3 to 5 % higher than the RCA-1 concrete specimens and 9 to 11 % higher than the RCA-3

concrete specimens. The NA concrete beam-end specimens with bonded lengths of 450 mm had $\tau_b/f_c^{1/2}$ values that were 4 to 6 % higher than the RCA-1 concrete specimens and 4 to 13 % higher than the RCA-3 concrete specimens. In general, the NA concrete beam-end specimens achieved higher bond strengths than the RCA concrete specimens at both the 40 and 60 MPa compressive strength levels. On average, the RCA-1 concrete specimens achieved higher bond strengths than the RCA-3 specimens.

Similar to the Phase 1 beam-end specimens, no trend was found within the loaded or free-end slip value at failure between the NA concrete and RCA concretes, or between the 40 and 60 MPa specimens. The 450 mm bonded length specimens had peak slip values that were, on average, three times larger than their equivalent peak slip values of the 125 mm bonded lengths. This confirms the findings of Phase 1 that the changes in peak slip values were not proportional to the change in bonded length (i.e., 450mm/125mm = 3.6 times longer). To account for the axial elongation of the unbonded length (75 mm typically) of the reinforcing bar, loaded-end slip values were corrected using the calculation provided in the footnote on Table 9.8.

9.7.1.1 Bond-Slip Response and Failure Mechanism of Beam-End Specimens

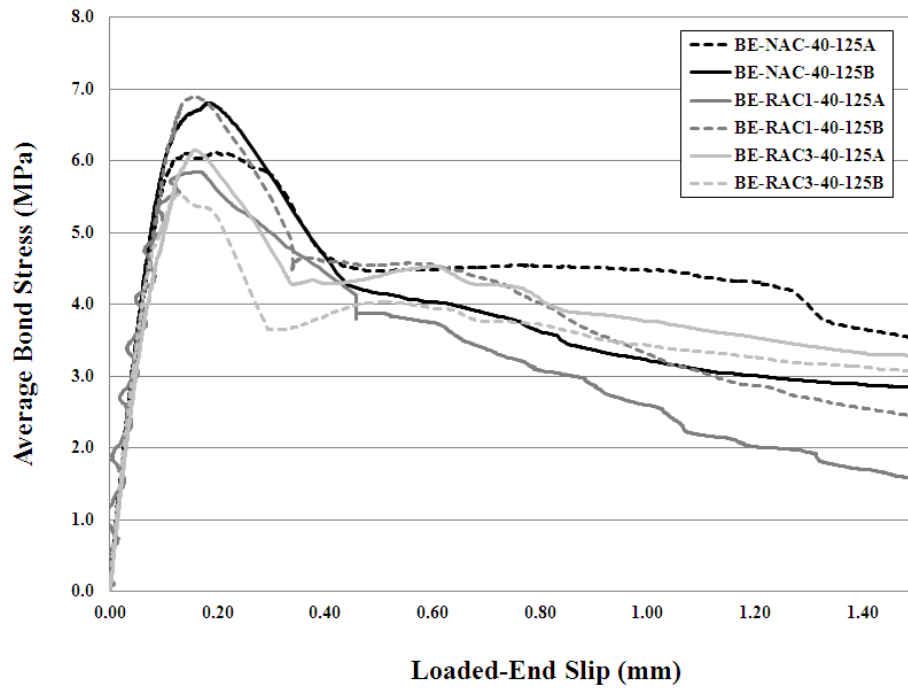
As presented as part of the Phase 1 evaluation of bond strengths (Section 9.6.1.1), the typical stages of bond-slip response for the beam end specimens are presented in Figure 9.9. The stages observed during the Phase 1 testing and the stages presented in Figure 9.9 closely resemble those described in CEB-fip (2000). Similar to Phase 1 specimens, splitting failures occurred in all Phase 2 specimens (see Figure 9.10) regardless of the compressive strength or bonded length. Splitting cracks ran along the bonded length of the test bar. Figure 9.11 is a typical bond stress vs. slip plot observed in the Phase 2 beam-end specimens.

Figure 9.39 and Figure 9.40 compare the bond-slip responses for the 40 and 60 MPa beam-end specimens, respectively. In comparing the 40 MPa and 125 mm bonded length specimens (Figure 9.39a), all beam-end specimens seem to reach a plateau of around 4 MPa. By comparing the 40 MPa and 450 mm bonded length specimens (Figure 9.39b), all beam-end specimens reached a residual (friction) plateau of approximately 3 MPa. Similar to the Phase 1 375 mm bonded length specimens, the lower residual (frictional) bond strength in the 450 mm bonded length specimens may be a result of the higher tensile stresses developed within the bonded bar

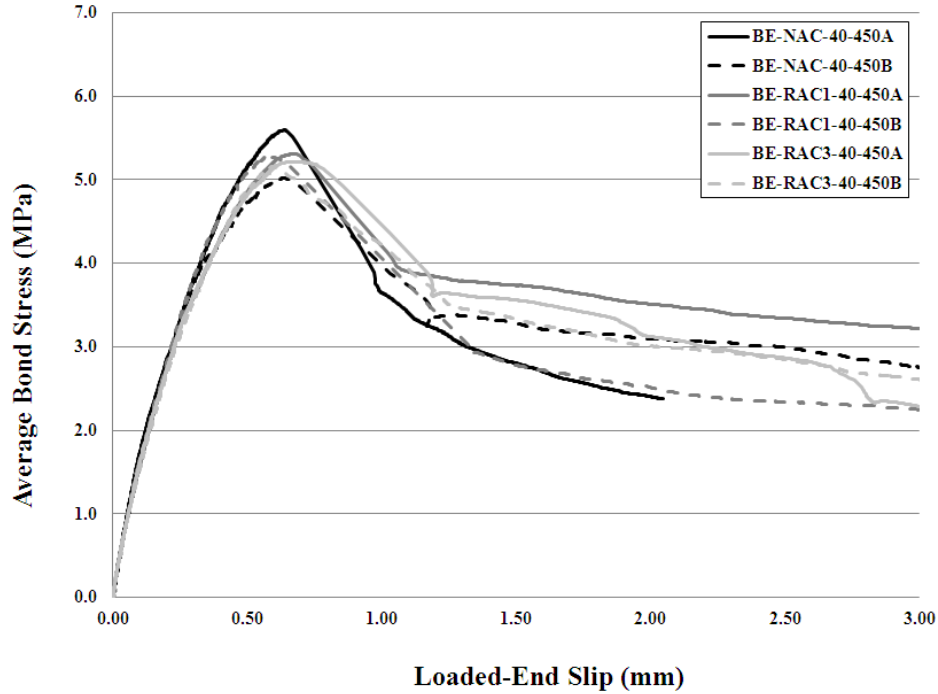
causing more extensive damage to the surrounding bonded concrete. This will become evident from the forensic analysis performed on the beam-end specimens in which higher amounts of concrete adhered to the bar deformations were found for the longer bonded length specimens.

The post failure response differs when comparing the 125 mm and the 450 mm bonded length specimens. Similar to what was observed with the Phase 1 specimens, the 125 mm bonded length specimens have post peak responses that reach a horizontal plateau whereas the 450 mm bonded length specimens have plateaus that gradually decrease as compressive strength increases. This is due to the condition of the concrete surrounding the reinforcing bar. In the 125 mm bonded length specimens, the shorter splitting cracks created more post-cracking confinement than the 450 mm specimens. In addition, the concrete keys were still intact and continued to sustain load while the slip continued to increase as the splitting cracks continued to widen. This caused the plateau of the bond – slip curve to remain relatively horizontal. The longer splitting cracks in the 450 mm specimens combined with the crushed or sheared off concrete keys due to the higher bar forces at failure, created less confinement as compared to the 125 mm bonded length specimens. The forensic analysis performed on the beam-end specimens confirms this behaviour as higher amounts of concrete adhered to the bar deformations were found for the longer bonded length specimens (refer to Section 9.7.9). Similar to what was described in Section 9.6.1.1 for the Phase 1 specimens, after the concrete keys could no longer sustain loads and the splitting cracks continued to widen causing the bond – slip response curve to gradually decrease.

The 60 MPa 125 mm bonded length beam-end specimens display similar behaviour to the 40 MPa specimens as displayed in Figure 9.40. For the 125 mm bonded length specimens there are similar peak slip values and the residual bond strength plateau is once again approximately 4 MPa. However, for the 60 MPa 450 mm bonded length specimens there are similar peak slip values to the 40 MPa specimens but the residual bond strength plateau is slightly higher at approximately 3 MPa. This suggests that for shorter bonded lengths (5 bar diameters), concrete compressive strength has little impact on the bond-slip response and residual bond strength.

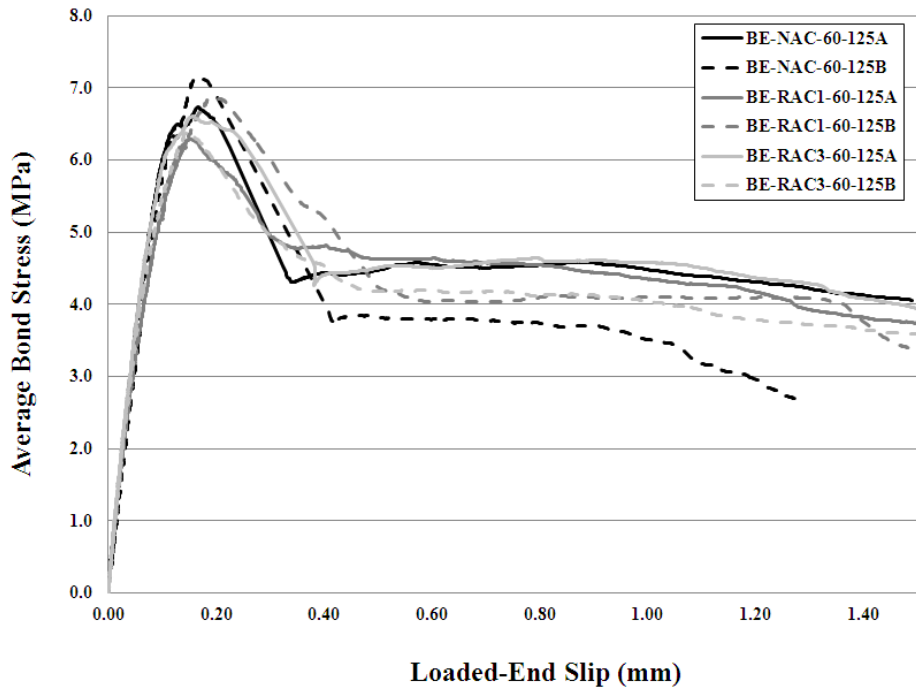


(a) 125 mm Bonded Length Specimens

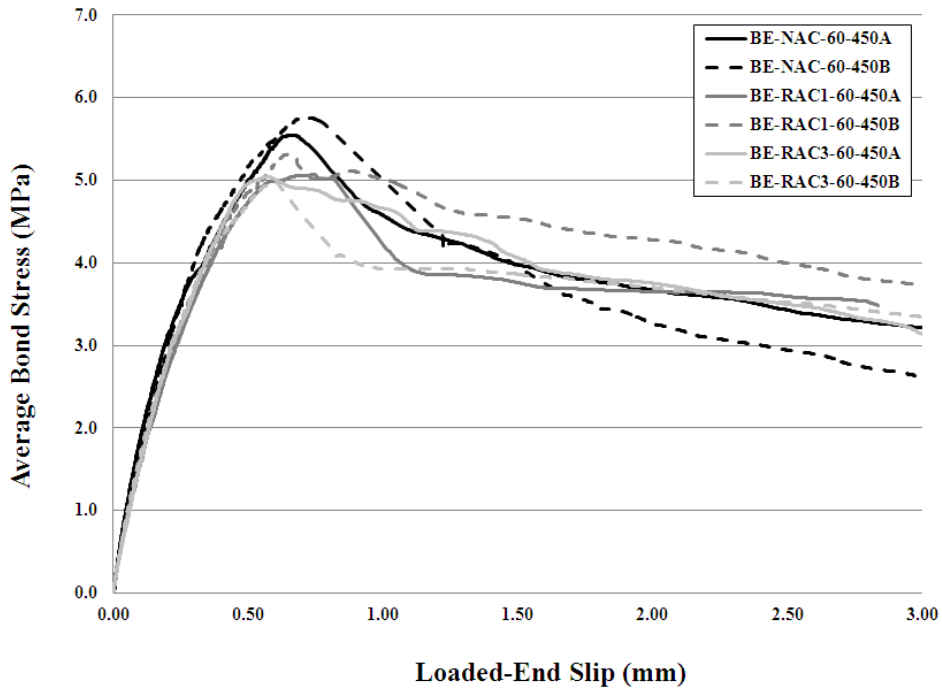


(b) 450 mm Bonded Length Specimens

Figure 9.39 Comparison of bond-slip responses for 40 MPa Phase 2 beam-end specimens



(a) 125 mm Bonded Length Specimens



(b) 450 mm Bonded Length Specimens

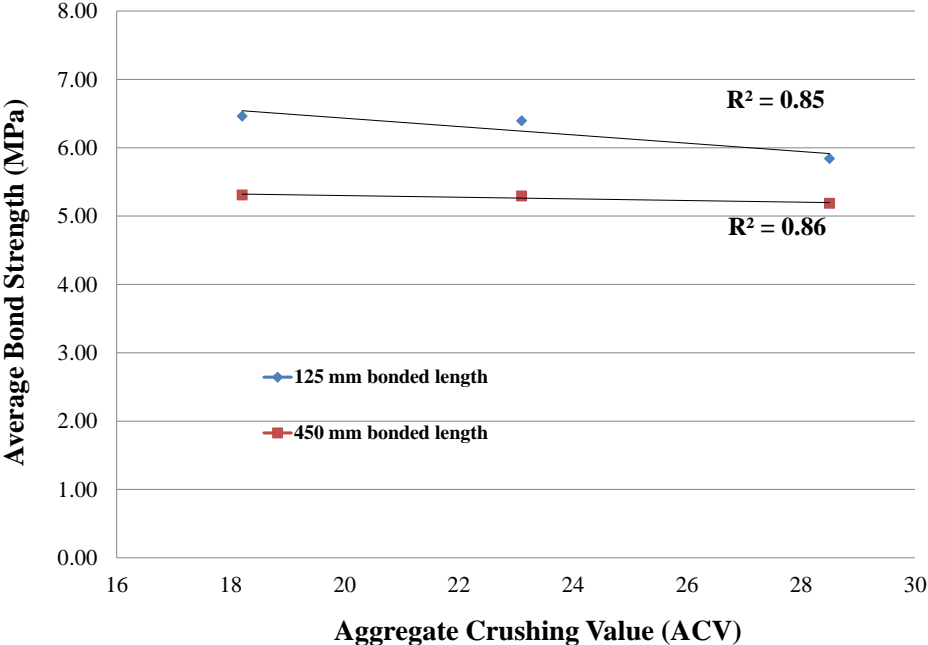
Figure 9.40 Comparison of bond-slip responses for 60 MPa Phase 2 beam-end specimens

As mentioned in Section 9.6.1.1, differences in post-failure behaviour of bond between NA and RCA concrete are not significant in the design of reinforced concrete structures as it is the average bond stress at failure (i.e., the bond strength) that is relevant in the development of equations for anchorage design of a reinforced concrete member.

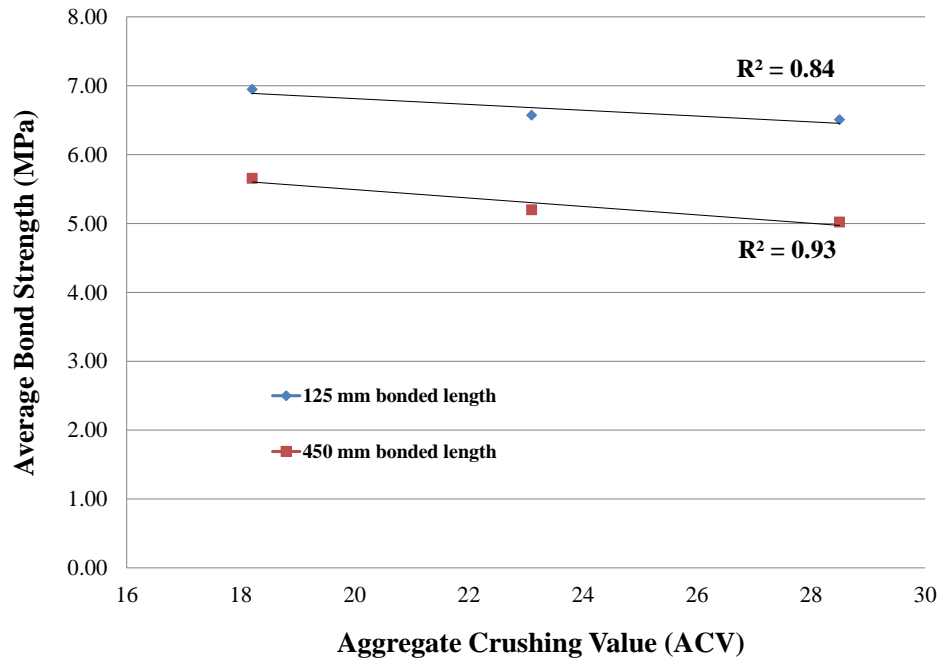
Similar to the Phase 1 bond testing results, aside from lower bond strengths and slight variations in residual bond strength, the bond-slip responses of the Phase 2 RCA concrete beam-ends were very similar to the NA concrete specimens. Individual bond-slip curves and crack patterns for each beam-end specimen have been included in Appendix D.

9.7.2 Effect of Aggregate Crushing Value on Bond Behaviour

Very good correlations between aggregate crushing value and the average bond strength was found during Phase 2 beam-end testing as presented in Figure 9.41. Note that each value on the plots represents the average bond strength of two duplicate beam-end specimens (i.e., A and B).



(a) 40 MPa Specimens



(b) 60 MPa Specimens

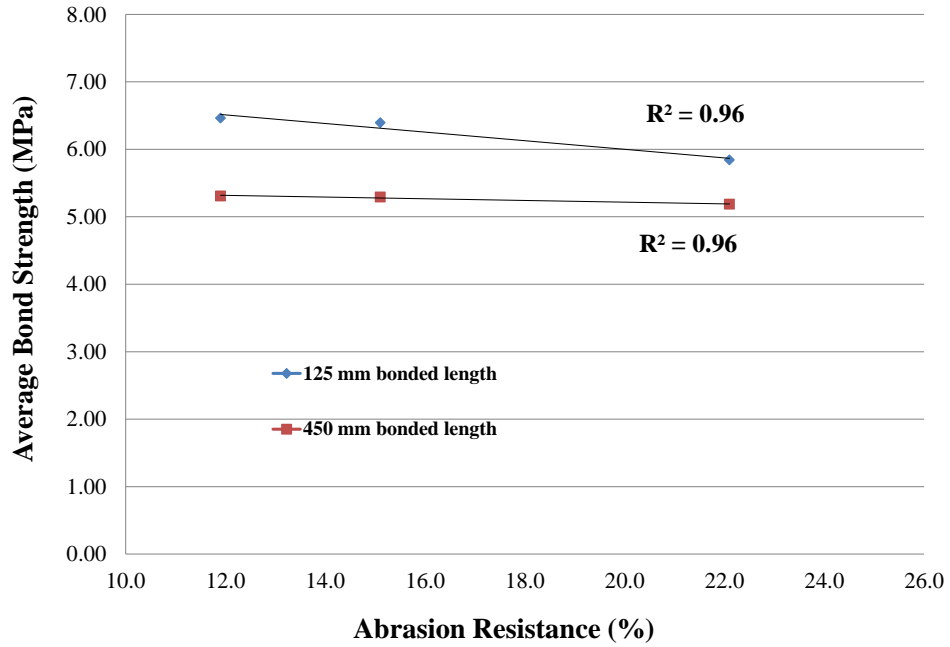
Figure 9.41 Relationship between average bond strength and aggregate crushing value (Phase 2 specimens)

The 40 MPa specimens displayed excellent correlation between the bond strength and ACV as demonstrated by R^2 values of 0.87 and 0.86 for the 125 mm and 450 mm bonded lengths, respectively. Similarly, the 60 MPa specimens had high R^2 values of 0.84 and 0.93 for the 125 mm and 450 mm bonded lengths, respectively. Combined with the trends from Phase 1, these correlations indicate that for various values of bonded length and concrete compressive strength, there may be a significant relationship between the average bond stress and the crushing strength of bulk coarse aggregate (ACV). It should be noted however, that the change in average bond stress vs. ACV (i.e., the slope of the trend line) seems fairly low, especially in the case of the 40 MPa specimens. Sections 9.8.2 and 9.8.7 compare the results of the Phase 1 and 2 beam-end specimens to determine whether the change in average bond stress as a function of ACV is statistically significant.

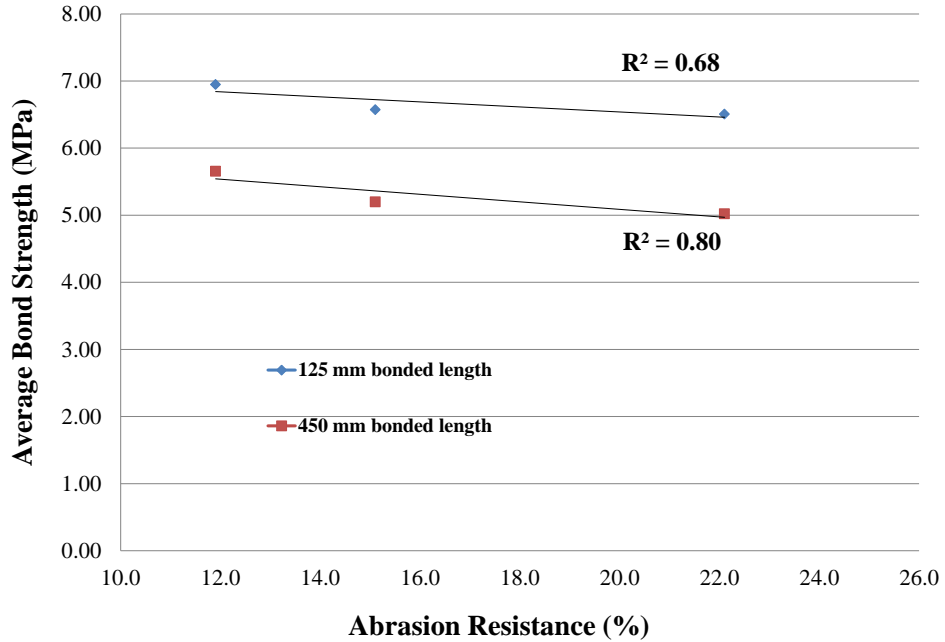
9.7.3 Effect of Aggregate Abrasion Resistance on Bond Behaviour

The relationship between abrasion resistance (by the Micro-Deval method) and the average bond strength for the 40 MPa and 60 MPa specimens is presented in Figure 9.42. Each value on the

plots represents the average bond strength of two duplicate beam-end specimens (i.e., A and B).



(a) 40 MPa Specimens



(b) 60 MPa Specimens

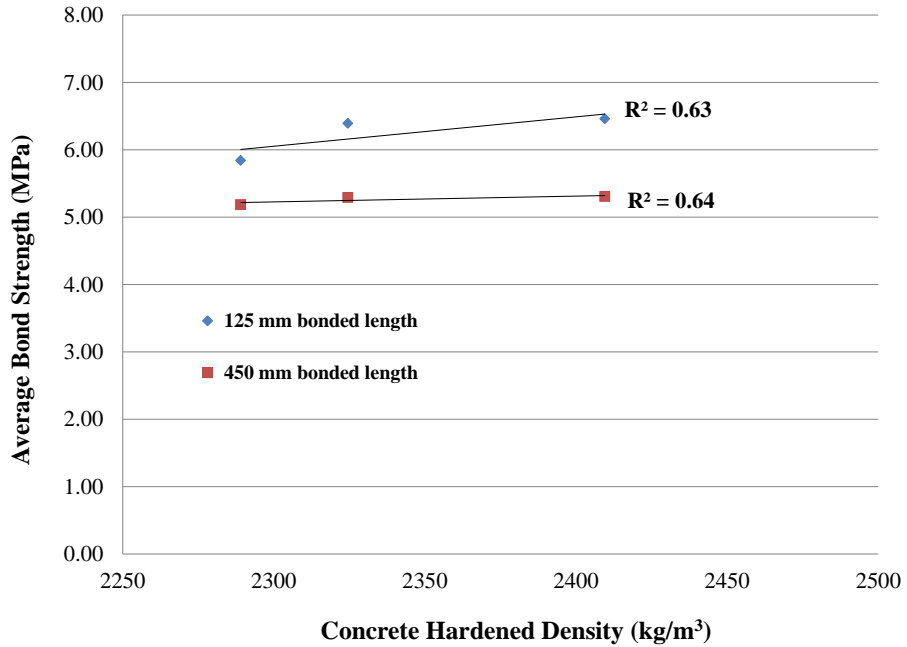
Figure 9.42 Relationship between average bond strength and abrasion resistance (Phase 2 specimens)

A fairly strong trend was found between abrasion resistance and average bond strength in which as abrasion resistance increases (i.e., lower abrasion loss), the average bond strength increases. The R^2 values for the 40MPa specimens were very high with R^2 values of 0.96 and 0.96 for the 125 and 450 mm bonded length specimens, respectively. The R^2 values for the higher strength 60 MPa specimens were considerably lower with R^2 values of 0.68 and 0.80 for the 125 and 450 mm bonded length specimens, respectively. Similar to the Phase 1 test results, the weaker correlation may exist because the abrasion resistance of an aggregate does not directly contribute to the mitigation of tensile (bond-splitting) cracking in concrete. However, as previously mentioned, a general trend does exist due to a strong correlation (R^2 of 0.93) between aggregate crushing value and abrasion resistance (see Figure 4.37).

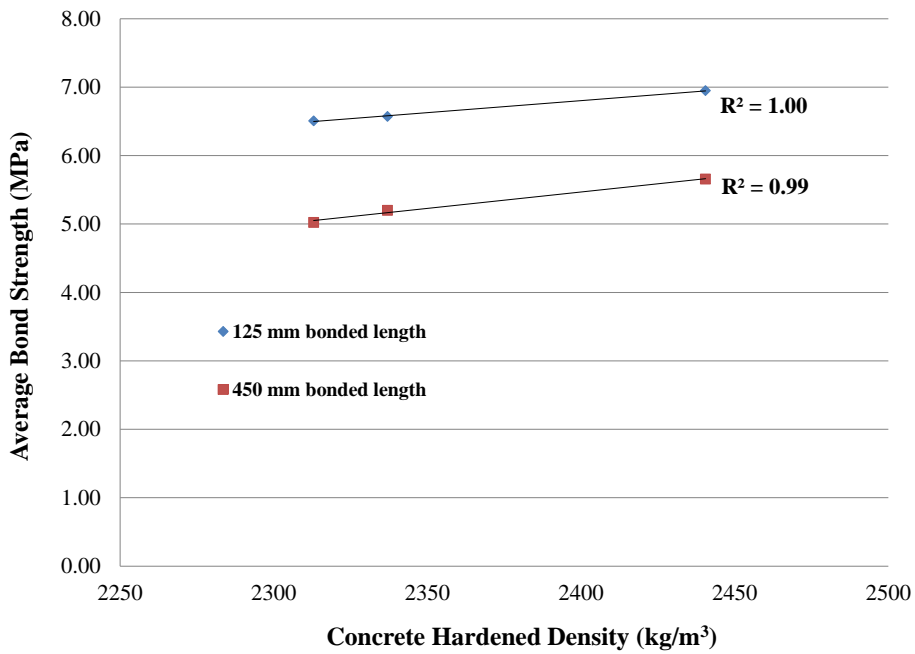
9.7.4 Effect of Concrete Hardened Density on Bond Behaviour

The hardened density of concrete is an indirect factor that affects bond strength; it is the aggregate strength itself that is the governing material property influencing the bond strength of reinforced RCA concrete members. Similar to lightweight aggregate concrete, RCA concrete has lower hardened density values. Given current development length modifications used for lightweight aggregate concrete, a similar impact may result when considering RCA concrete. For this reason, the hardened density of RCA concrete was measured during Phase 2 testing to determine its effect on bond behaviour of RCA concrete beam-ends. Figure 9.43 presents the relationship between the average bond strength and the hardened density of concrete. Note that each plotted value represents an average of two specimens (i.e., Specimen A and B for both the fracture energy and beam-end specimens). When evaluating the 40 MPa specimens results (Figure 9.43a), a moderate correlation exists between hardened density and average bond strength with R^2 values of 0.63 and 0.64 for the 125 mm and 450 mm bonded length specimens, respectively. Although the R^2 values are fairly low, the general trend seems to indicate that as concrete hardened density increases so does the average bond strength. In the evaluation of the 60 MPa specimens test results (Figure 9.43b), a very strong correlation existed between hardened density and average bond strength reflected by R^2 values of 0.99 for both the 125 mm and 450 mm bonded lengths specimens. The influence of concrete hardened density on bond strength seems to be a direct result of the relation between aggregate crushing strength (ACV) and concrete hardened density (refer to Section 7.4.1.2) which had a strong correlation with an R^2

value of 0.85. Therefore, the concrete hardened density is a by-product of aggregate strength (i.e., ACV) correlating with hardened density.



(a) 40 MPa Specimens

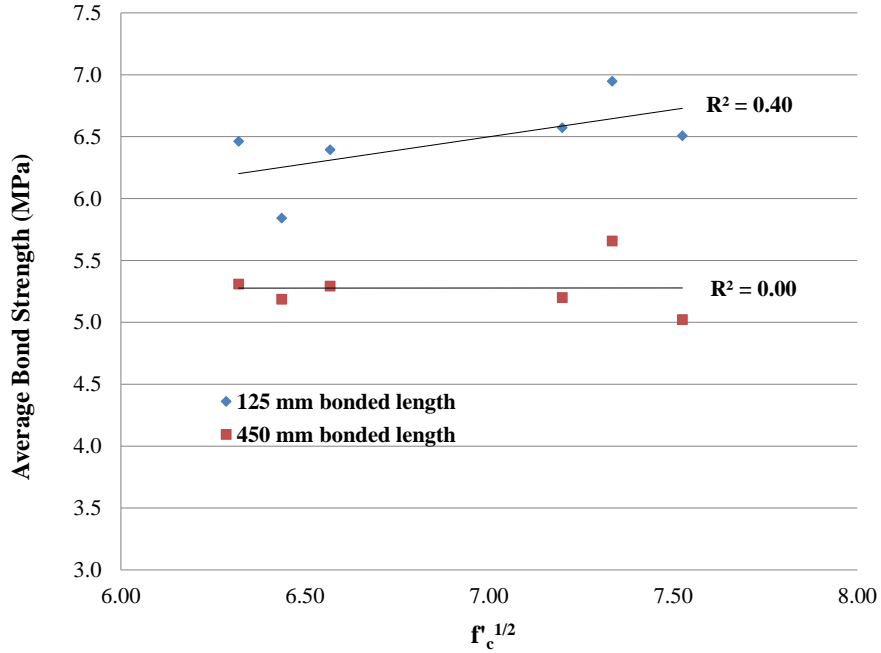


(b) 60 MPa Specimens

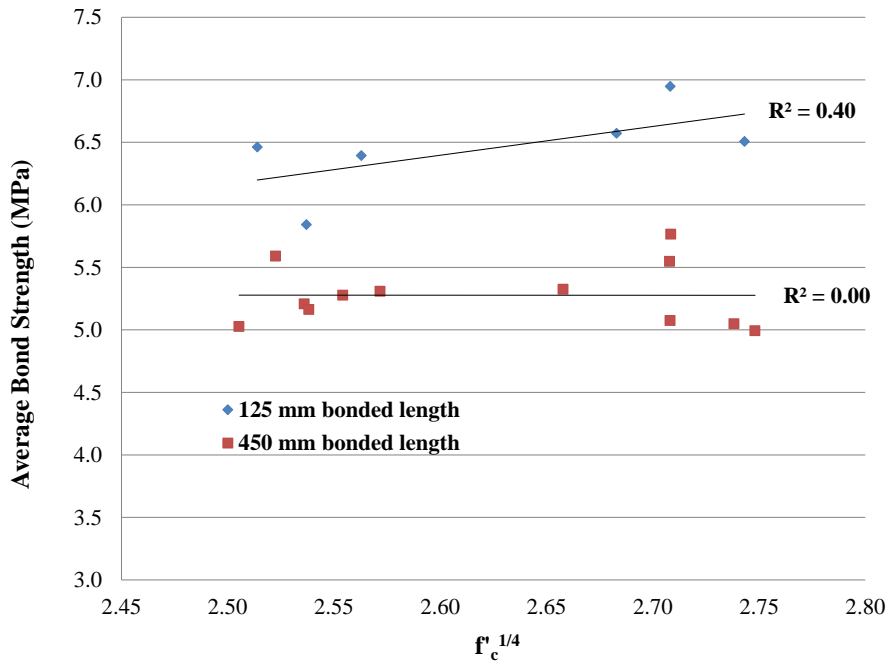
Figure 9.43 Relationship between average bond strength and concrete hardened density (Phase 2 specimens)

9.7.5 Effect of Compressive Strength on Bond Behaviour

Figure 9.44 presents the relationship between the average bond strength (τ_b) and $f'_c{}^{1/2}$ and $f'_c{}^{1/4}$.



(a) Relationship between τ_b and $f'_c{}^{1/2}$



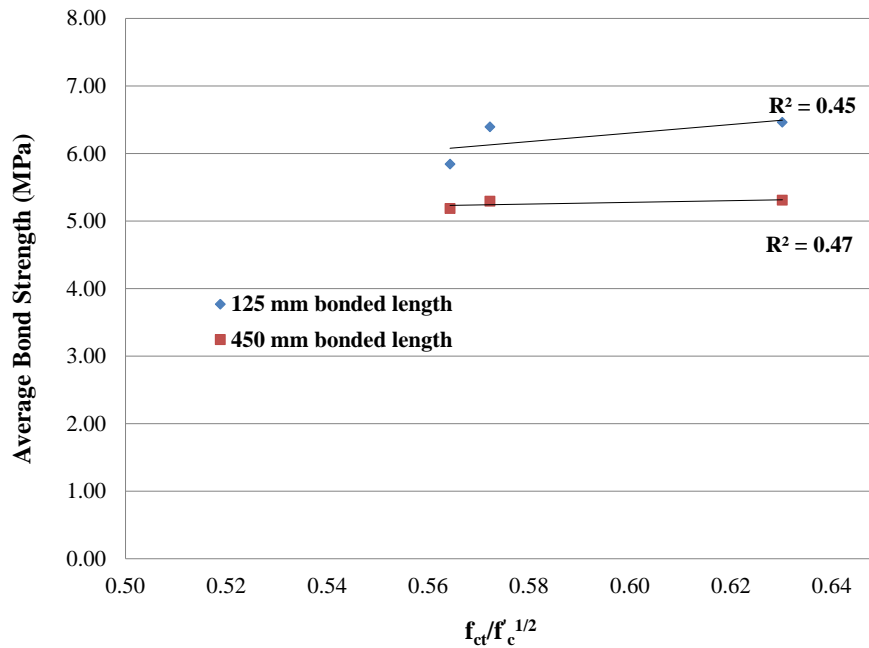
(b) Relationship between τ_b and $f'_c{}^{1/4}$

Figure 9.44 Relationship between average bond strength and compressive strength (Phase 2 beam-end specimens)

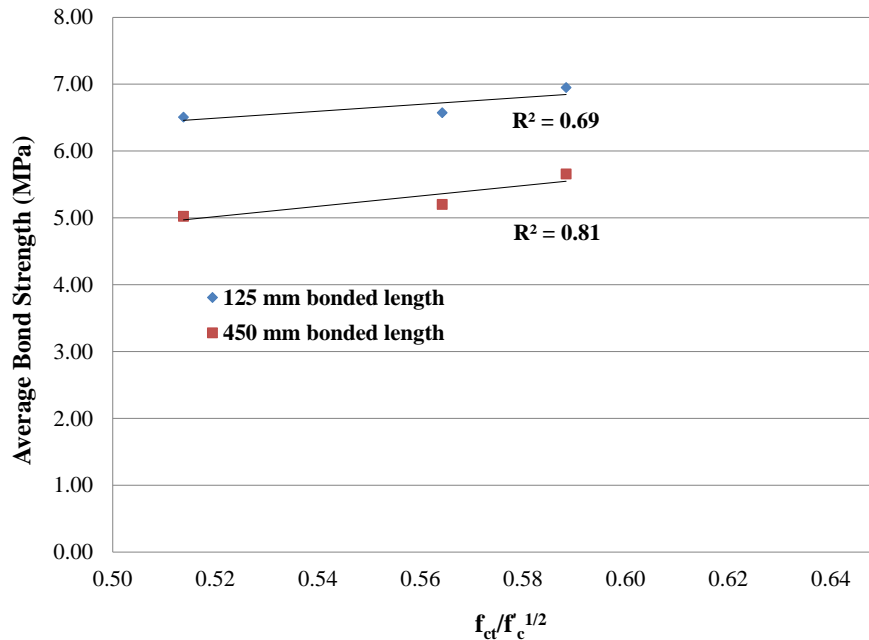
Although it is generally regarded in the literature that bond strength (τ_b) varies with $f_c^{1/2}$ and even $f_c^{1/4}$, the bond test results of Phase 2 confirm the findings of the Phase 1 test results showing no such correlation. Each value on the plots represents the bond strength of one beam-end specimen. An overall assessment of the effect of compressive on the bond strength is included in Section 9.8.3.

9.7.6 Effect of Splitting Tensile Strength on Bond Behaviour

Figure 9.45 depicts the relationship between average bond strength and the normalized concrete splitting tensile strength ($f_{ct}/f_c^{1/2}$). Note that each plotted value represents an average of two specimens (i.e., Specimen A and B for both the fracture energy and beam-end specimens). Overall, there seems to be a fairly weak correlation between the average bond strength and the splitting tensile strength as evidenced by R^2 values of 0.45 to 0.47 and 0.69 to 0.81 for the 40 MPa and 60 MPa specimens, respectively. Given that the main failure mechanism observed in the beam-end specimens was splitting-induced pullout failure, and that this mechanism arises from a circumferential tension field surrounding the reinforcing bar and surrounding concrete, it is intuitive that the concrete tensile strength is a closely related property of this type of failure.



(a) 40 MPa specimens



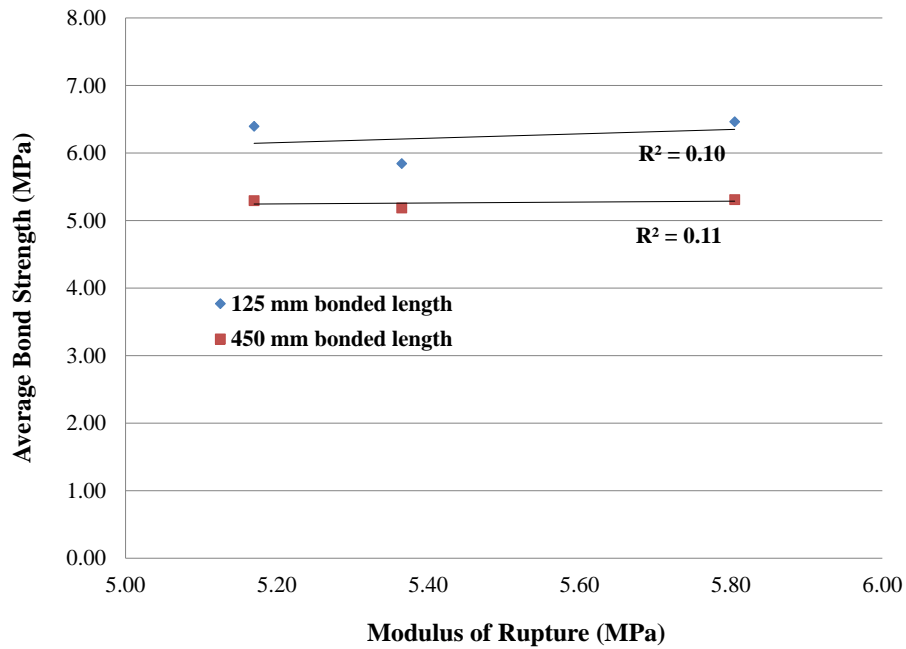
(b) 60 MPa specimens

Figure 9.45 Relationship between average bond strength and splitting tensile strength (Phase 2 specimens)

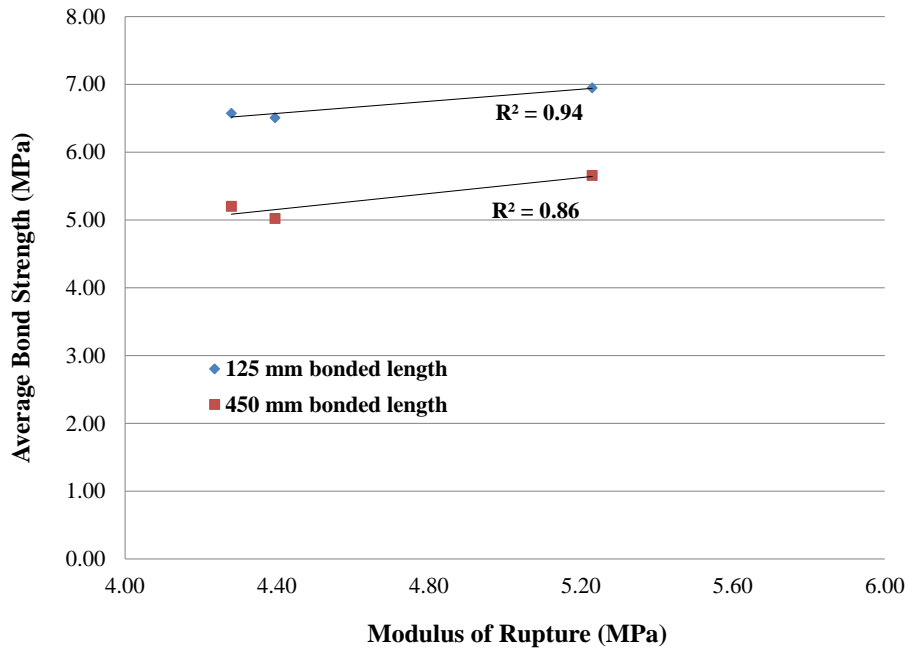
Compared to the findings of Phase 1 (refer to Figure 9.17), there appears to be a slightly stronger relation between the $f_{ct}/f_c^{1/2}$ values and the bond strength. This difference in trends between Phase 1 and Phase may be due to the fact that the Phase 1 splitting tensile specimens were tested 30 to 40 days after beam-end testing and their results were normalized with respect to $f_c^{1/2}$, whereas the Phase 2 splitting tensile specimens were tested on the day of beam-end testing.

9.7.7 Effect of Modulus of Rupture on Bond Behaviour

The modulus of rupture of concrete was measured using the same fracture energy single-edge notched double cantilevered (SEND) specimens (refer to Section 6.2.7 for test procedure). The relationship between modulus of rupture and average bond strength is presented in Figure 9.46. Note that each plotted value represents an average of two specimens (i.e., Specimen A and B for both the fracture energy and beam-end specimens).



(a) 40 MPa Specimens



(b) 60 MPa Specimens

Figure 9.46 Relationship between average bond strength and modulus of rupture (Phase 2 specimens)

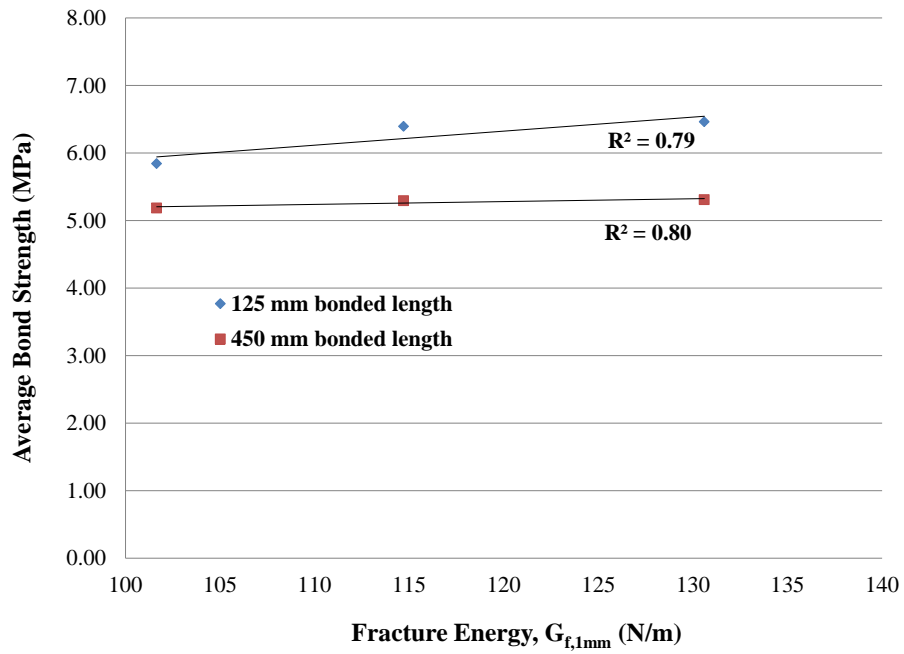
A strong correlation (i.e., $R^2 = 0.86$ and 0.94 for the 125 mm and 450 mm bonded lengths, respectively) exists between the modulus of rupture and the bond strength for the 60 MPa

specimens. However, there appears to be little relation between f_r and $\tau_{b,avg}$ for the 40 MPa specimens. This is in contrast to the findings in Phase 1 where the lower strength (30 MPa) specimens had a stronger correlation between f_r and $\tau_{b,avg}$, but where the higher strength (50 MPa) specimens had a lower correlation. The overall effect of modulus of rupture on the bond strength of RCA concrete will be evaluated in Section 9.8.5.

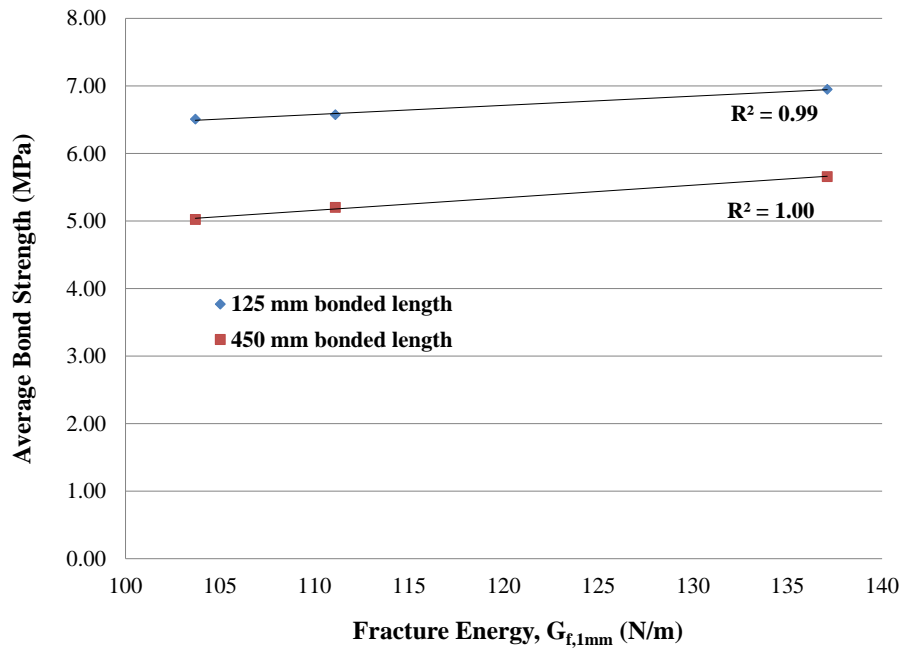
9.7.8 Effect of Fracture Energy on Bond Behaviour

As described in Phase 1 (Section 9.6.7), the fracture energy of concrete was measured using single-edge notched double-cantilevered (SEND) beam specimens in accordance with the procedures outlined in Section 6.2.7. Specimens were cast in conjunction with beam-end specimens to allow for the correlation of bond strength and fracture energy to be assessed. Figure 9.47 presents the relationship between average bond strength and fracture energy for the Phase 2 beam-end specimens. Note that each plotted point represents an average of two specimens (i.e., Specimen A and B for both the fracture energy and beam-end specimens). Fairly strong correlations were found for the 40 MPa specimens and very strong correlations were found for the 60 MPa specimens. However, in the case of the 40 MPa specimens with a bonded length of 450 mm, while the correlation is fairly high ($R^2 = 0.80$), the slope of the line is nearly zero indicating a negligible effect of fracture energy on average bond strength.

Overall, the trends depicted in Figure 9.47 seem to indicate that as the fracture energy of concrete increases, the average bond strength also increases. This finding is in contrast to the findings from the Phase 1 specimens. However, it confirms the proposals of ACI committee 408 (2003) and Zuo and Darwin (2000) which suggest increasing fracture energy would result in a higher resistance to splitting crack propagation which could ultimately increase splice (or bond) strength. The overall effect of fracture energy on the bond strength of RCA concrete will be evaluated in Section 9.8.6.



(a) 40 MPa Specimens



(b) 60 MPa Specimens

Figure 9.47 Relationship between fracture energy and average bond strength (Phase 2 specimens)

9.7.9 Dissection and Forensic Analysis of Beam-Ends

After reviewing the results of the Phase 2 beam-end testing, six specimens were selected for dissection and forensic analysis. The main purpose of this dissection phase was to,

- 1) Investigate causes for outlying bond strength results by comparing actual bonded lengths and cover depths,
- 2) Identify signs of slip attributed to crushing of concrete in the vicinity of the reinforcement ribs, and
- 3) Investigate the influence of aggregate type on bond failure mode.

Dissections were performed systematically as described in Section 9.6.8. Note that the average bond stress results reported in Section 9.7.1 incorporate the measured bonded lengths derived from the forensic analysis in their calculation.

9.7.9.1 Specimen BE-NAC-40-450A

Beam-end specimen BE-NAC-40-375A failed at a pull-out load of 205.2 kN and an average concrete compressive strength of 40.5 MPa. The main anchorage zone and exterior splitting cracks for BE-NAC-40-450A are shown in Figure 9.48. Splitting cracks ran from top of the specimen to the end of the bonded length through the main concrete cover to the bar surface. The main fracture surface and test bar are shown in Figure 9.49. Fracture planes pass both around and through the coarse natural aggregate particles. The main concrete cover to the test bar was measured to be 30 mm. Rib indentations from the 20M secondary steel bars are also shown with part of the exposed 10M stirrup. A measured bonded length of 460 mm was recorded as depicted in Figure 9.50. Adhered concrete is also present on the test bar due to the shearing and/or crushing of the concrete adjacent to the ribs indicating a splitting-induced pull-out failure (see Figure 9.21b). Figure 9.50 shows the bar ribs shifted out of the surrounding concrete indentations which represents slip between the reinforcing bar and the concrete. This slip likely occurred prior to the formation of the longitudinal splitting cracks.

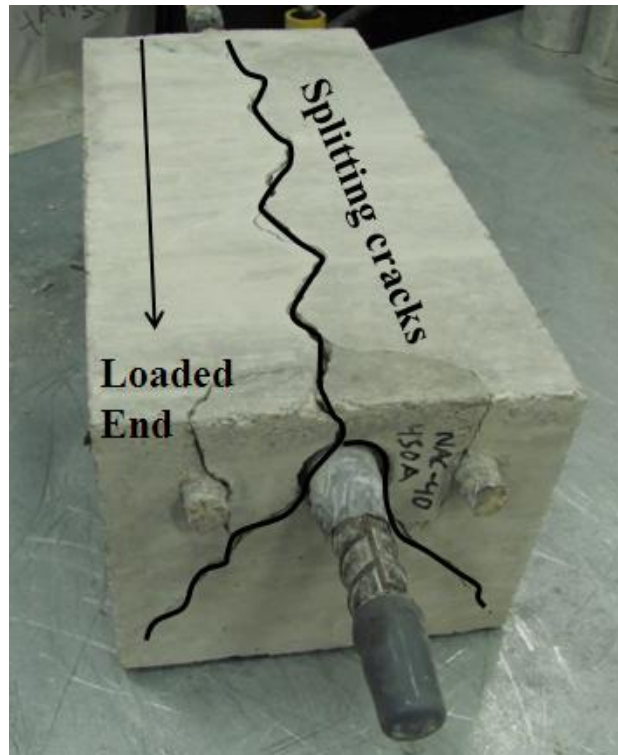


Figure 9.48 Main anchorage zone and splitting crack pattern (dissected BE-NAC-40-450A)

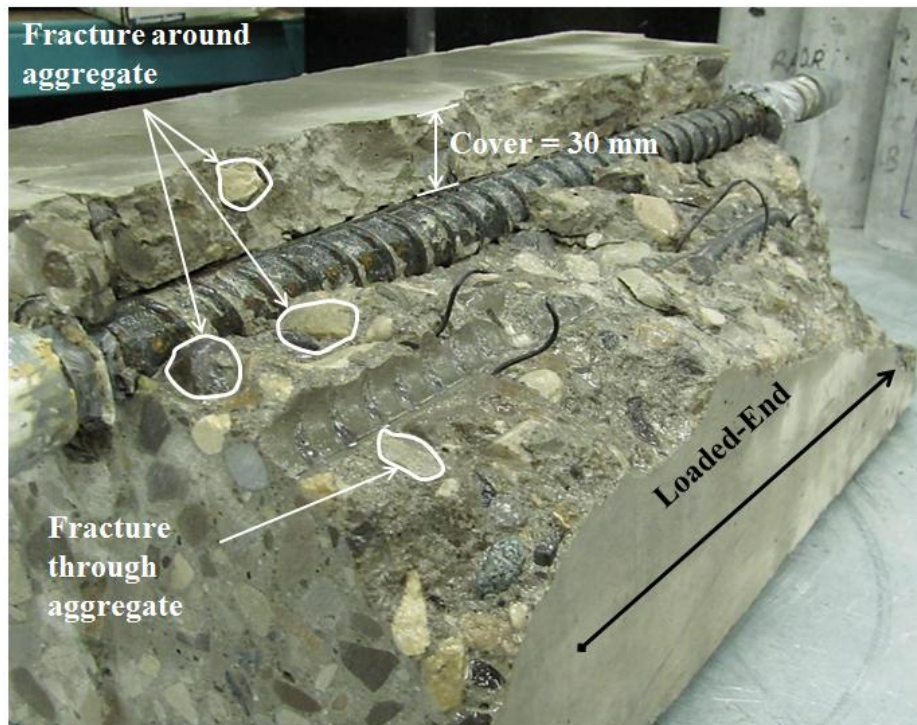


Figure 9.49 Main failure planes through concrete cover (dissected BE-NAC-40-450A)

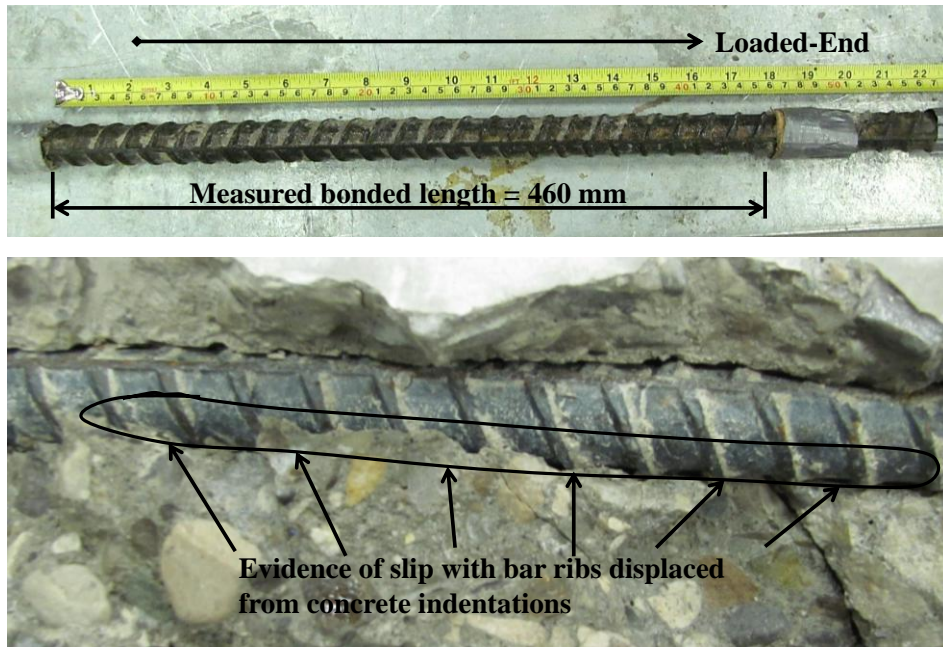


Figure 9.50 Main test bar, measured bonded length, and evidence of slip (dissected BE-NAC-40-450A)

9.7.9.2 Specimen BE-NAC-40-450B

Beam-end specimen BE-NAC-40-375B failed at a pull-out load of 180.5 kN (14% lower than BE-NAC-40-375A) and an average concrete compressive strength of 39.4 MPa. This specimen had a similar splitting crack pattern to its counterpart (BE-NAC-40-375A) as is depicted in Figure 9.51. Some exterior damage to the dissected specimen occurred whilst attempting to wedge open the anchorage zone and expose the test bar. Figure 9.52 shows the splitting failure-induced fracture planes and local concrete rib crushing at the free-end. This observation is contrary to what would be expected as the higher bond stresses would exist near the loaded-end leaving the concrete rib indentations at the free-end intact. Perhaps the concrete in this section was slightly weaker and rib crushing initiated before crushing in other locations. Figure 9.52 also shows the top concrete cover as 25 mm. Figure 9.53 shows the test bar with a measured bonded length of 450 mm. A larger amount of adhered concrete exists on the free-end of the bar which could explain the rib crushing identified in Figure 9.52. The longer bonded length in combination with a smaller top cover distance of specimen BE-NAC-40-450B may also partially suggest why this specimen had significantly lower bond strength than its counterpart specimen BE-NAC-40-450A (180.5 kN versus 205.2 kN). The mode of bond failure was the same as BE-NAC-40-450A; splitting-induced pull-out.

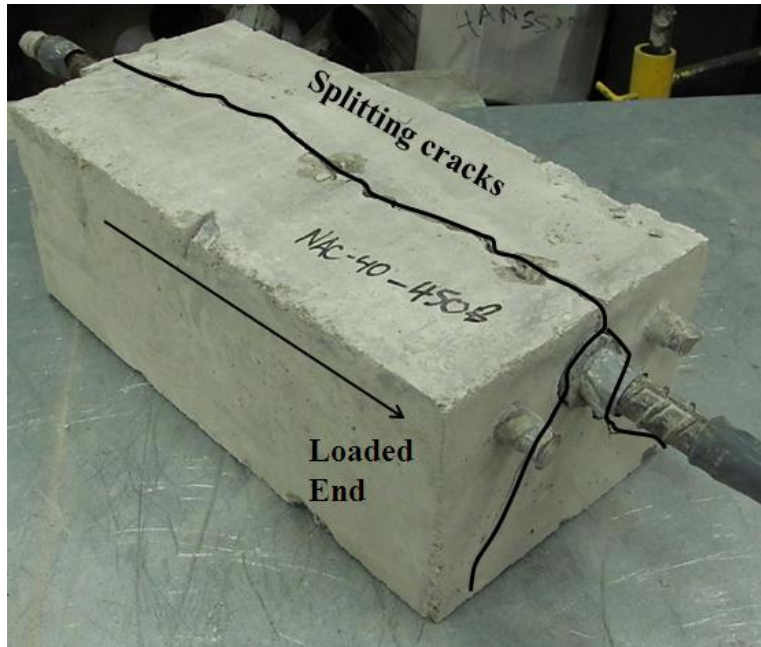


Figure 9.51 Main anchorage zone and splitting crack pattern (dissected BE-NAC-40-450A)

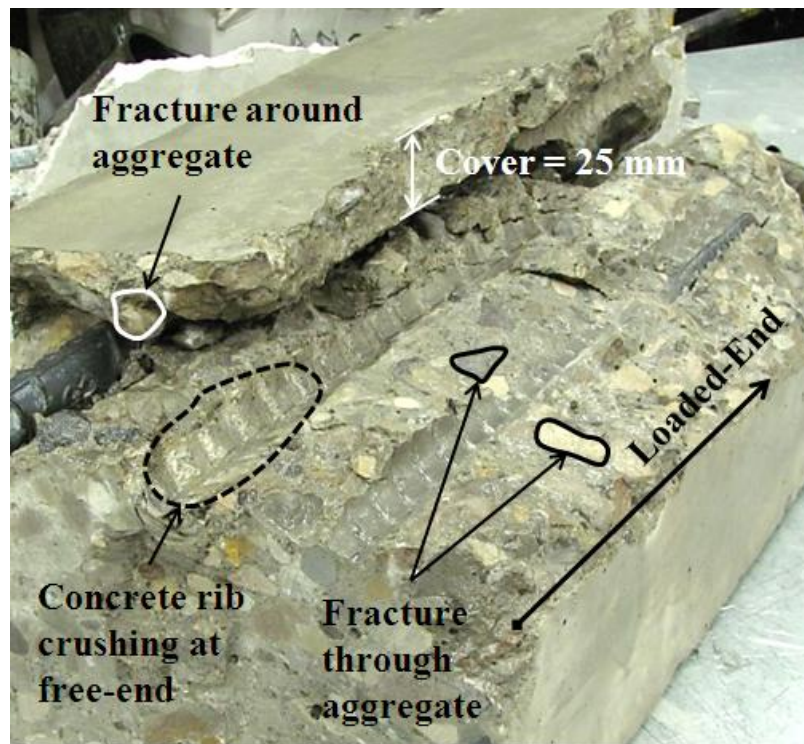


Figure 9.52 Main failure planes through concrete cover (dissected BE-NAC-40-450A)



Figure 9.53 Main test bar, measured bonded length, and adhered concrete (dissected BE-NAC-40-450B)

9.7.9.3 Specimen BE-RAC1-40-125A

Beam-end specimen BE-RAC1-40-125A failed at a pull-out load of 60.6 kN and an average concrete compressive strength of 43.7 MPa. Figure 9.54 presents the main anchorage zone and splitting crack pattern for beam-end specimen RAC1-40-125A. Unlike the 40MPa NAC 375 mm bonded length specimens, side splitting cracks occurred between the main test bar and the secondary 20M bars.

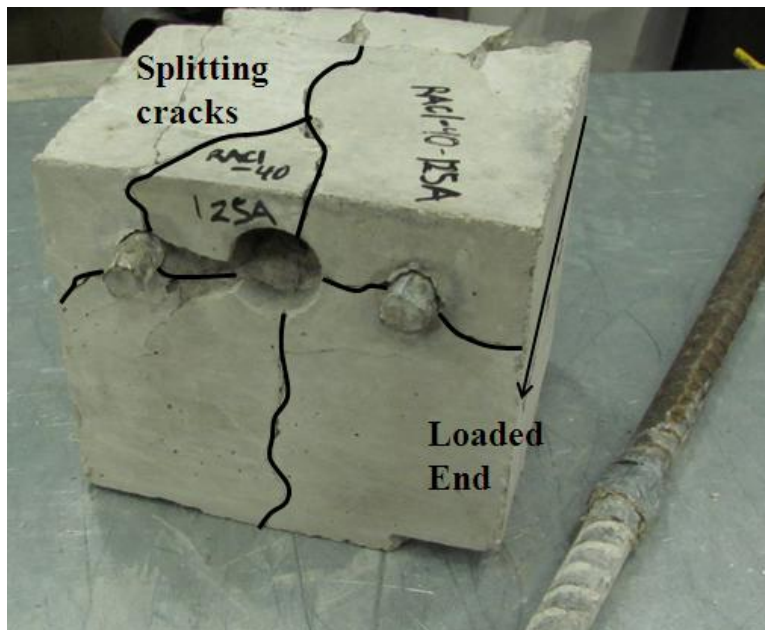


Figure 9.54 Main anchorage zone and splitting crack pattern (dissected BE-RAC1-40-125A)

The main fracture plane (Figure 9.55) passed both around and through the RCA-1 particles and the main concrete cover was measured to be 27 mm. Splitting cracks can be seen acting along the test bar with minor concrete rib crushing at the loaded-end of the bar. Both exposed original aggregate and old mortar can be seen along the fracture plane. The actual bonded length was

measured to be 130 mm, 5 mm longer than assumed. Figure 9.56 shows the adhered concrete that was sheared off during testing. The majority of the adhered concrete is present within the free-end zone of the bar. This pattern once again indicates a splitting-induced pull-out bond failure.

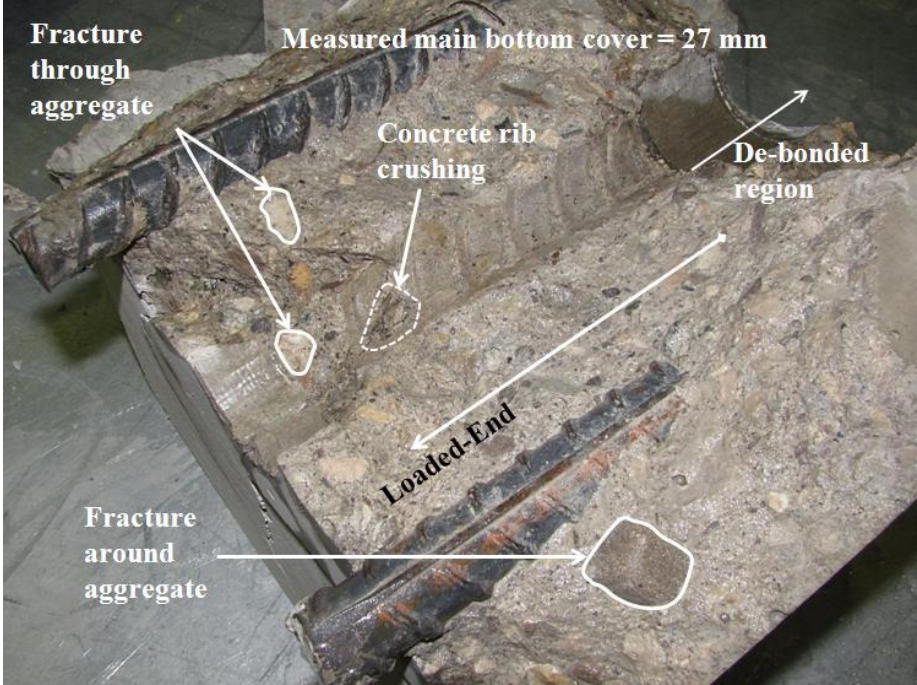


Figure 9.55 Main failure planes through concrete cover (dissected BE-RAC1-40-125A)

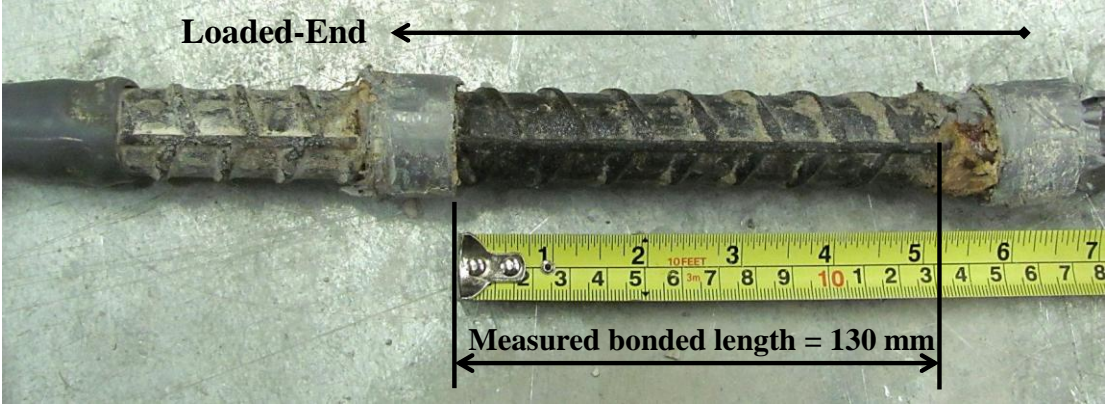


Figure 9.56 Main test bar, measured bonded length, and adhered concrete (dissected BE-RAC1-40-125A)

9.7.9.4 Specimen BE-RAC1-40-125B

Beam-end specimen BE-RAC1-40-125B failed at a pull-out load of 68.8 kN (12% higher than BE-RAC1-40-125A) and an average concrete compressive strength of 42.6 MPa. Figure 9.57 illustrates the main anchorage zone and typical splitting crack pattern displaying side splitting cracks along the plane of the primary (25M bar) and secondary (20M bars) reinforcing. Figure 9.58 depicts the fracture zones passing both around and through the RCA-1 particles. Splitting cracks can also be seen running along the orientation of the main testing bar and being slightly wider near the loaded-end where bond stresses were higher. The main bottom cover was measured to be 25 mm from the bar surface to the external concrete surface. Figure 9.59 shows the main test bar with adhered concrete mainly near the free-end and an actual bonded length of 125 mm was measured. Evidence of slip was also found when investigating that the test bar ribs were displaced slightly from the concrete indentations. With similar concrete compressive strengths, the longer bonded length and larger cover of the BE-RAC1-40-125B specimen seems to contradict its lower bond pull-out force as compared to its counterpart, BE-RAC1-40-125A. Therefore, the difference in strength may be attributed to any number of differences in specimen construction and concrete quality including differences in concrete quality in the two anchorage zones, differences in consolidation of concrete around the test bar, etc.

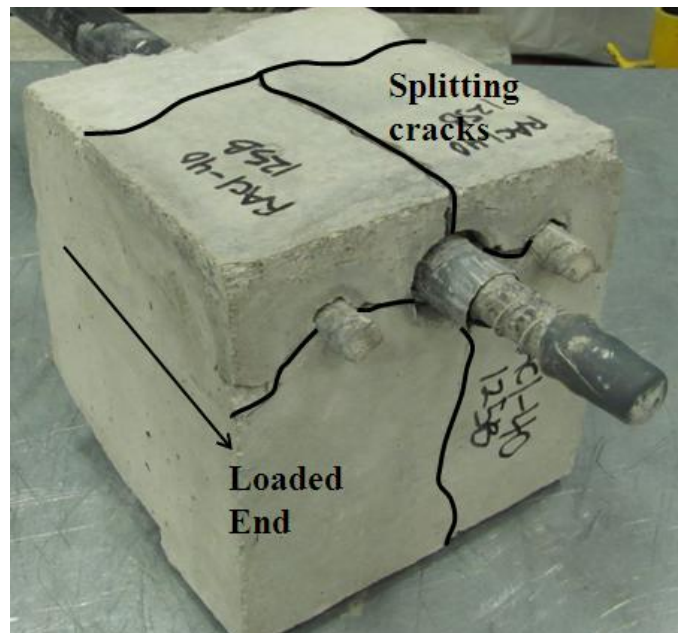


Figure 9.57 Main anchorage zone and splitting crack pattern (dissected BE-RAC1-40-125B)

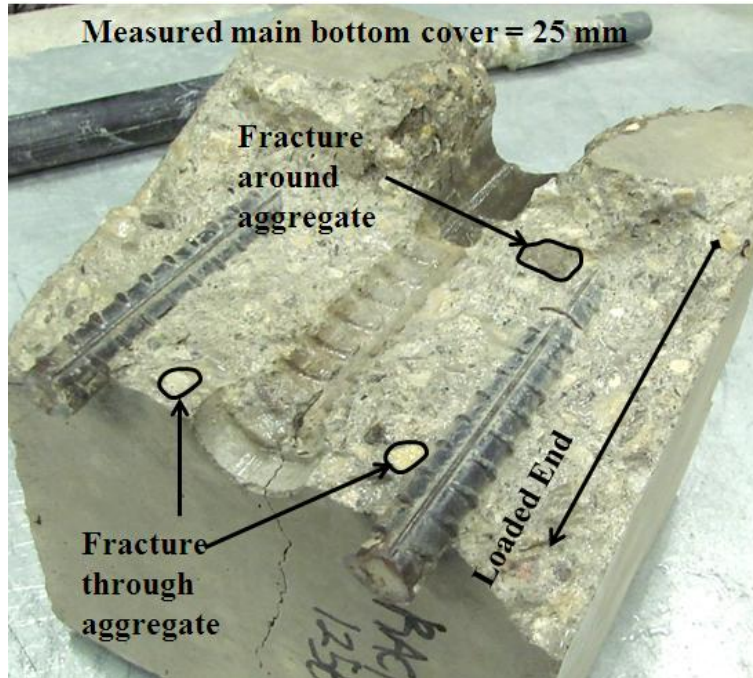


Figure 9.58 Main failure planes through concrete cover (dissected BE-RAC1-40-125B)

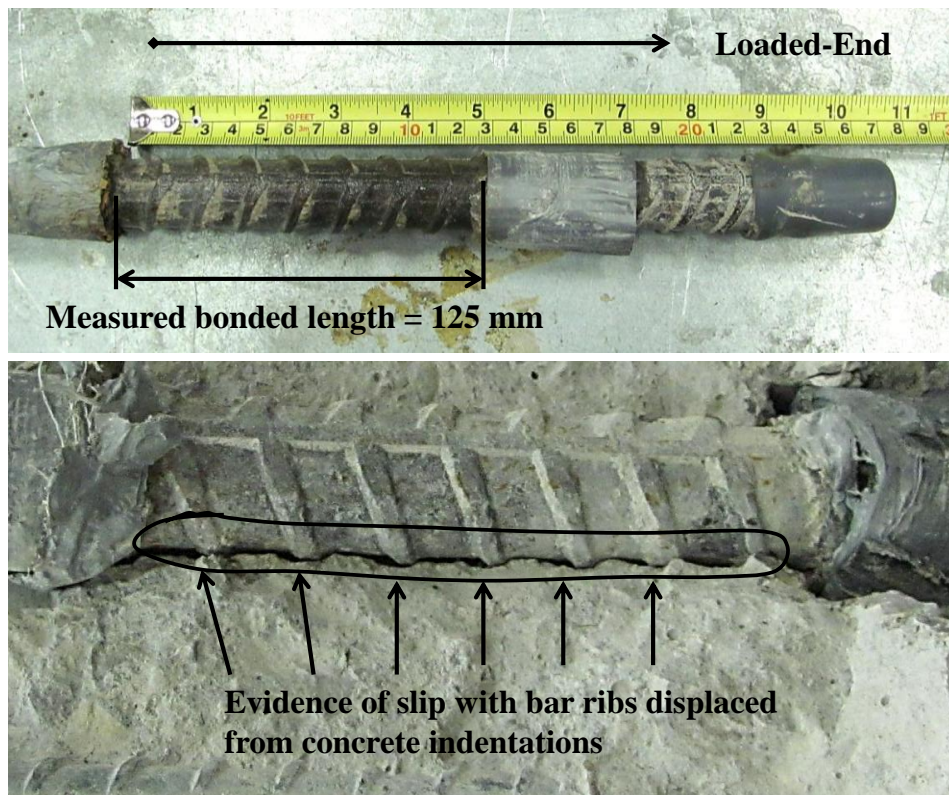


Figure 9.59 Main test bar, measured bonded length, and evidence of slip (dissected BE-RAC1-40-125B)

9.7.9.5 Specimen BE-RAC3-40-125A

Beam-end specimen BE-RAC3-40-125A failed at a pull-out load of 63.8 kN and an average concrete compressive strength of 41.4 MPa. Figure 9.60 shows the typical splitting crack pattern with similar side splitting as the 40 MPa RCA-1 concrete beam specimens with 125 mm bonded lengths. Once again the splitting cracks ran the full bonded length of the bar before diverging in the transverse direction where the concrete alone resists tension forces. The actual main bottom covered was measured to be 27 mm.

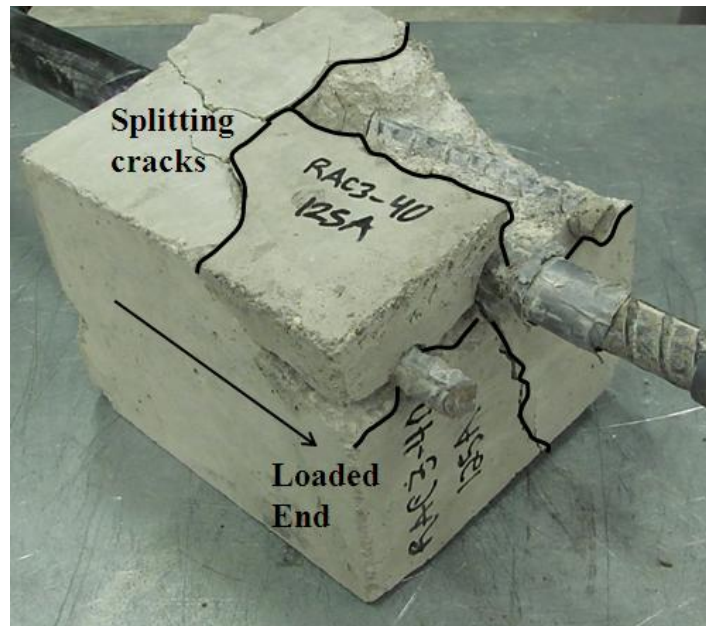


Figure 9.60 Main anchorage zone and splitting crack pattern (dissected BE-RAC3-40-125A)

Figure 9.61 illustrates the fracture plane passing mainly through the RCA-3 particles indicating that the strength of aggregate was the governing property influencing splitting crack propagation. Splitting cracks are wider near the loaded-end of the specimen where radial tension stresses were higher. The actual bonded length of the specimen was measured to be 130 mm. Figure 9.62 shows the main test bar and the adhered concrete wedged against the ribs which indicates shearing and/or crushing of the concrete adjacent to the ribs. This would also signal a splitting-induced pull-out bond failure typical of what was observed in previous specimens.

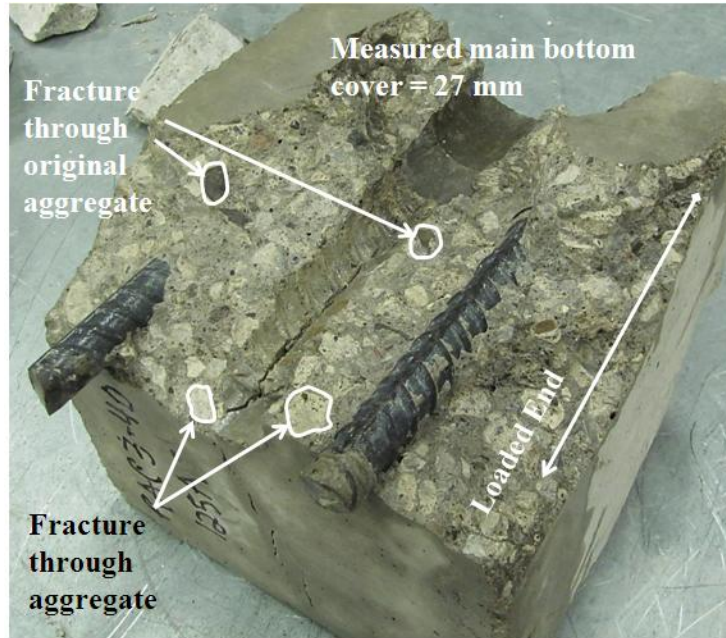


Figure 9.61 Main failure planes through concrete cover (dissected BE-RAC3-40-125A)

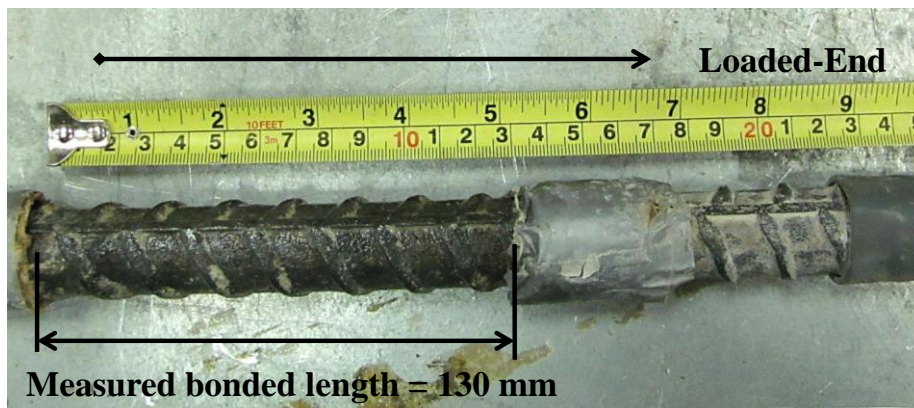


Figure 9.62 Main test bar, measured bonded length, and adhered concrete (dissected BE-RAC3-40-125A)

9.7.9.6 Specimen BE-RAC3-40-125B

Beam-end specimen BE-RAC3-40-125B failed at a pull-out load of 55.2 kN (16% lower than BE-RAC3-40-125B) and an average concrete compressive strength of 41.5 MPa. Splitting cracks propagated similarly as observed in BE-RAC3-40-125A, however, side splitting occurred on only one side and was not as extensive (see Figure 9.63). The actual main bottom cover was measured to be 25 mm.

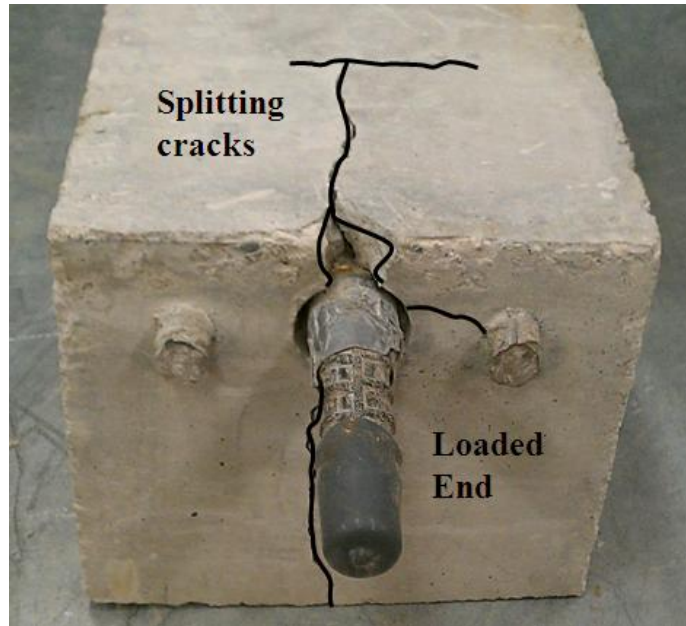


Figure 9.63 Main anchorage zone and splitting crack pattern (dissected BE-RAC3-40-125B)

By observing the main fracture plane in Figure 9.64, the fracture surface passed mainly through the RCA-3 particles indicating the aggregate strength as a significant factor influencing bond strength. Although there are some minor signs of rib crushing, the majority of the concrete rib indentations remained intact.

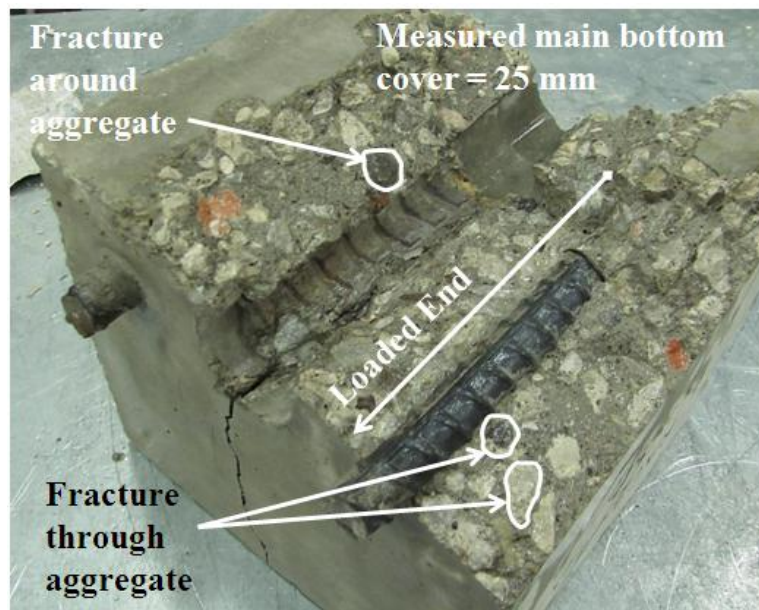


Figure 9.64 Main failure planes through concrete cover (dissected BE-RAC3-40-125B)

The actual bonded length was measured to be 125 mm and small traces of adhered concrete were observed between the ribs (refer to Figure 9.65). This observation may indicate a bond failure induced by slipping along the rib faces rather than crushing and/or shearing off of the concrete surrounding the ribs (see Figure 9.21c). Therefore, the lower pull-out force of the BE-RAC3-40-125B specimen as compared to the BE-RAC3-40-125A specimen may be explained by its shorter bonded length, smaller bottom cover and the difference in bond failure mode (i.e., rib face slipping versus crushing and/or shearing of surrounding concrete).

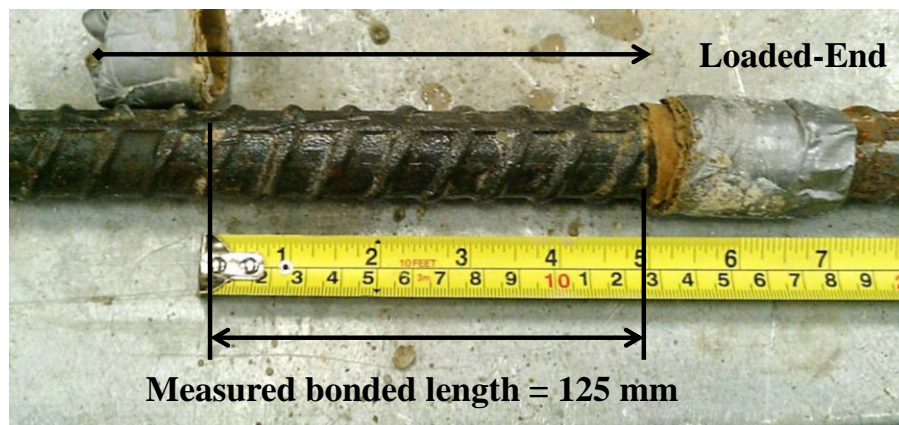


Figure 9.65 Main test bar, measured bonded length, and adhered concrete (dissected BE-RAC3-40-125B)

9.7.9.7 Summary and Conclusions from Phase 2 Dissections and Forensic Analysis

The following conclusions were based on the observations and measurements taken during the dissection of Phase 2 beam-end specimens.

- 1) Measured bonded lengths ranged between 125 and 130 mm for the shorter bonded length specimens and between 450 and 460 mm for the longer bonded length specimens. Measured cover depths varied between 25 and 30 mm. These values are believed to represent an acceptable level of variability from a construction tolerance standpoint. Note that the average bond stress values reported previously include adjustments for the actual bonded lengths measured during forensic analysis. Specifically, the average bond stress calculations for specimens BE-NAC-40-450A, BE-RAC1-40-125A and BE-RAC3-40-125A were modified to include the new, measured bonded lengths.
- 2) In most cases, differences in the pull-out bond force between duplicate specimens could be explained by differences in measured bonded length and/or measured concrete cover.

When comparing the RAC1-40-125 specimens, additional variation in construction methods and materials properties were believed to be the cause of differences in strength.

- 3) In the NA and RCA-1 concrete specimens, the bond failure mode was splitting-induced by crushing and/or shearing of the concrete adjacent to the ribs whereas for the RCA-3 concrete specimens with 125 mm bonded lengths, failure was initiated by splitting-induced by slipping at the rib faces.
- 4) Signs of slip were identified in all specimens by observing the reinforcing bar ribs displaced from the cast-in concrete rib indentations. As described in Phase 1, based on the failure mechanism of the beam-end specimens, slip of the reinforcing bar occurred due to the formation of transverse micro-cracks at the tips of the reinforcement ribs which were followed by the formation of longitudinal splitting cracks.
- 5) In all cases, the fracture planes passed mainly through the coarse aggregate particles once again highlighting the influence of aggregate strength on bond strength.

9.7.10 Conclusions from Phase 2 Bond Testing

The following conclusions can be drawn from the beam-end testing results from Phase 2 (f'_c of 40 and 60 MPa, and bonded lengths of 125 and 450 mm):

1. The NA concrete beam-end specimens had τ_b/f'_c values that were between 3 and 13% higher than the RCA concrete beam-end specimens for compressive strengths of 40 and 60 MPa and bonded lengths of 125 and 450 mm.
2. Replacing natural coarse aggregate with either RCA-1 or RCA-2 did not have a discernible effect on the general bond stress-slip response. While the maximum bond strengths for the NAC specimens were higher, the residual bond strength values were generally similar. This confirmed similar behaviour observed during the Phase 1 bond testing results.
3. Excellent correlations were found between the aggregate crushing value and the average bond strength. As coarse aggregate crushing strength decreases (ACV increases), the average bond strength decreases. This confirmed similar behaviour observed during the Phase 1 bond testing results. An analysis on the combined results of Phase 1 and 2 is

performed at the end of this chapter to confirm that the effect of ACV on bond strength is statistically significant.

4. A much stronger relationship was found between abrasion resistance increases and average bond strength for the Phase 2 specimens (R^2 values between 0.98 and 0.99, and between 0.64 and 0.74 for the 125 and 450 mm specimens, respectively) in comparison to Phase 1 results. This is most likely an indirect relationship resulting from the strong relationship that exists between ACV and micro-deval abrasion resistance.
5. A moderate relation exists between the average bond strength and hardened density of concrete for the 40 MPa specimens which had R^2 values of 0.63 and 0.64 for the 125 mm and 450 mm bonded length specimens, respectively. Within 60 MPa specimens test results, a very strong correlation between average bond strength and hardened density of concrete existed with R^2 values of 0.99 for both the 125 mm and 450 mm bonded length specimens. It was concluded that the hardened density of concrete is an indirect factor that affects bond strength; it is the aggregate strength itself that is the governing material property influencing the bond strength of reinforced RCA concrete members.
6. Phase 2 compressive strength results were also found to be in contrast to published studies in the literature for normal weight (natural aggregate) concrete as no significant relationship existed between concrete compressive strength (f'_c , $f'_c{}^{1/2}$, and $f'_c{}^{1/4}$) and the average bond strength.
7. A strong relationship between splitting tensile strength and average bond strength existed for the Phase 2 test specimens with R^2 values between 0.70 and 0.72 for the 40 MPa specimens and R^2 values between 0.91 and 0.98 for the 60 MPa specimens. This discrepancy between Phase 1 and Phase 2 most likely results from the fact that the Phase 1 splitting tensile specimens were tested 30 to 40 days after beam-end testing and their results were normalized with respect to $f'_c{}^{1/2}$, whereas the Phase 2 splitting tensile specimens were tested on the day of beam-end testing.
8. Overall, based on test results from Phase 2, it appears that the aggregate strength (i.e., ACV) is the aggregate property which has the highest influence on bond strength. Physically, the aggregate particles act as crack arrestors that intercept bond splitting cracks.

9. A strong correlation between modulus of rupture (flexural strength) of concrete and average bond strength was found for the 60 MPa specimens however, the effect of modulus of rupture on bond strength for the 40 MPa specimens was negligible. This trend is in contrast to what was found in Phase 1 where a stronger correlation between modulus of rupture and average bond strength occurred for the lower strength (30 MPa) specimens.
10. Strong correlations between fracture energy and bond strength were found for the Phase 2 specimens which were in contrast with the findings of Phase 1 however, support the theories presented in the literature.
11. After dissection and macro-level forensic analyses were performed on a select number of beam-end specimens, general beam-end structural behaviour and failure mechanism was confirmed. The NA and RCA-1 concrete dissected specimens failed by splitting-induced pull-out accompanied by crushing and/or shearing off in the concrete adjacent to the ribs. The RCA-3 concrete specimens failed by splitting-induced by slipping at the rib faces. Examination of fracture planes passing mainly through the coarse aggregate confirmed the influence of the coarse aggregate strength on bond strength.

9.8 Overall Evaluation of the Effect of Aggregate and Concrete Properties on Bond Strength

General trends and correlations have been investigated through evaluating the bond testing results of Phase 1 (natural aggregate, RCA-1, and RCA-2; 30 and 50MPa; and 125 and 375 mm bonded lengths) and Phase 2 (natural aggregate, RCA-1, and RCA-3; 40 and 60MPa; and 125 and 450 mm bonded lengths) separately. The following section analyzes and discusses the trends and relations now considering the total combined data sets (i.e., 48 beam-end specimens) of Phase 1 and 2. Based on the results of both phases, the bonded length, aggregate strength (i.e., ACV), compressive strength, splitting tensile strength, modulus of rupture (flexural strength), and fracture energy were all evaluated based on their influence on bond strength. It should be noted that the aggregate strength, splitting tensile strength, fracture energy and modulus of rupture (flexural strength) were evaluated based on their effect on the maximum experimental bond force normalized with respect to $f_c^{1/4}$ (i.e., $T_b/f_c^{1/4}$). This particular normalized value of bond force was used to allow for the comparison of the predictive experimental bond equations

developed and presented in Section 9.9 to the descriptive bond equations proposed by ACI Committee 408 (ACI 408, 2003).

9.8.1 Effect of Bonded Length on Bond Strength

Based on the combined results of Phase 1 and Phase 2, the overall effect of bonded length on the maximum bond strength is presented in Figure 9.66. Note that each value on the plot represents the maximum bond force for a single beam-end specimen (48 values in total). An excellent correlation between the bonded length and the maximum bond force was found to exist. This finding is widely acknowledged in the literature and can be explained by the fact that as the bonded length increases, the surface area over which the reinforcing bar is bonded to the concrete increases. This larger surface area reduces the average bond stress between the bar and the surrounding concrete and also reduces the average stress transferred into the surrounding concrete. Therefore, larger bar forces can be sustained before the tensile hoop stresses developed in the concrete exceed the tensile strength of the concrete causing splitting, slip and bond failure.

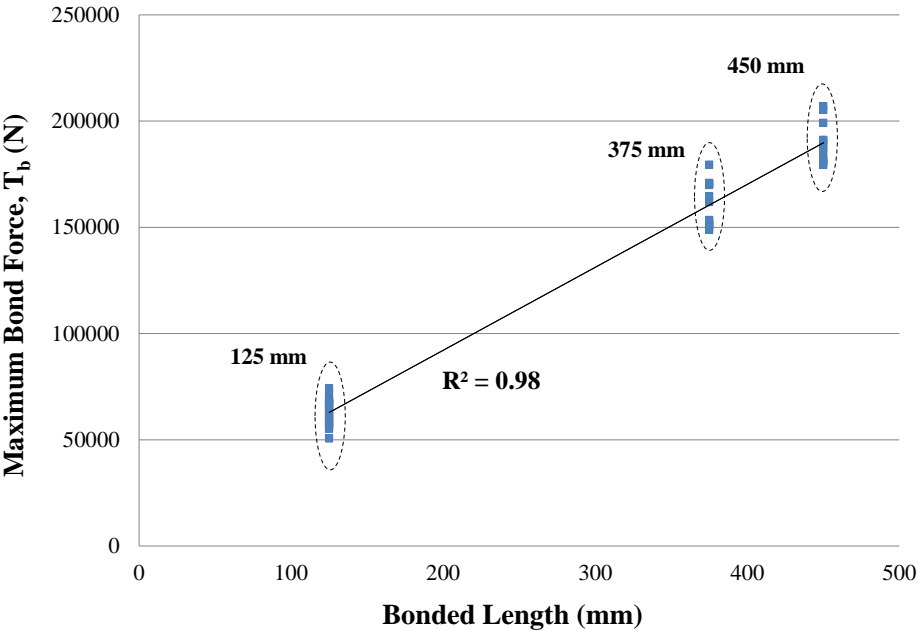


Figure 9.66 Relationship between bonded length and maximum bond force (Combined results of Phase 1 and 2)

9.8.2 Effect of Aggregate Strength on Bond Strength

Based on the results from Phases 1 and 2, it was discovered that a strong relationship exists between the bond strength and the coarse aggregate strength (measured as ACV). By combining the results of both phases, and sorting the data in terms of the three bonded lengths, the same trend found in Phases 1 and 2 is presented in Figure 9.67. Note that each data point on Figure 9.67 represents a single beam-end specimen and therefore, a total of 48 data points have been represented on this plot to confirm this trend.

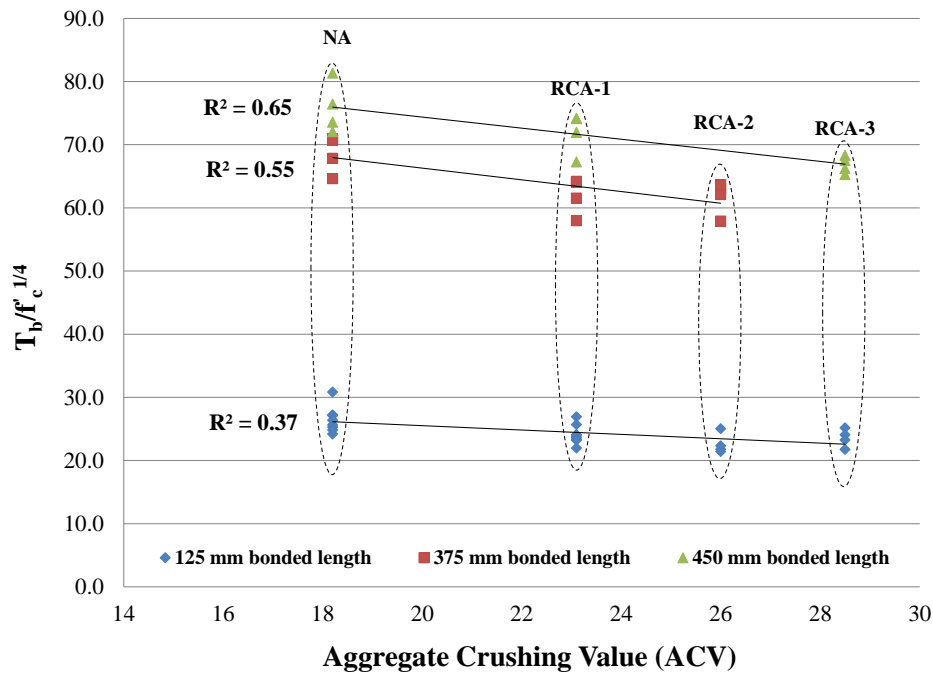


Figure 9.67 Relationship between aggregate strength (ACV) and $T_b/f_c^{1/4}$ (Combined Phase 1 and 2 results)

Although the coefficient of determination value is low for all three bonded lengths, the trend observed is significant: as aggregate strength decreases (i.e., ACV increases), the average bond strength also decreases. In addition, as the bonded length increases, the coefficient of determination also increases indicating that at longer bonded lengths, the dependence of the experimental maximum bond force normalized with respect to $f_c^{1/4}$ on the aggregate strength increases. This stronger dependence on aggregate strength at longer bonded lengths (and higher maximum bond forces) may be explained by the mechanism of splitting crack formation associated with higher bar forces. As observed in the majority of the beam-end specimens that

were dissected, bond splitting cracks occurred mainly through the coarse aggregate particles. This implies that the coarse aggregate strength (represented by ACV) was the governing factor for bond strength.

9.8.3 Effect of Compressive Strength on Bond Strength

As concluded after analyzing the bond data from Phases 1 and 2, no discernible correlation was found to exist between average bond strength and either $f'_c{}^{1/2}$ or $f'_c{}^{1/4}$. This finding has been confirmed in Figure 9.68 which presents the relationship between maximum bond force and $f'_c{}^{1/2}$ and in Figure 9.69 which presents the relationship between maximum bond force and $f'_c{}^{1/4}$. In particular, the 125 mm and 375 mm bonded length specimens had trend lines that were relatively horizontal whereas the 450 mm bonded length specimens had trend lines with negative slope. Perhaps the relationship between maximum bond force and normalized compressive strength ($f'_c{}^{1/2}$ or $f'_c{}^{1/4}$) may become more evident in specimens with longer bonded lengths. However, a larger data set with bonded lengths greater than 450 mm would need to be tested in order to verify this hypothesis. Each value on the figures represents data from a single beam-end specimen with a total 48 beam-end specimens (combined results of Phases 1 and 2).

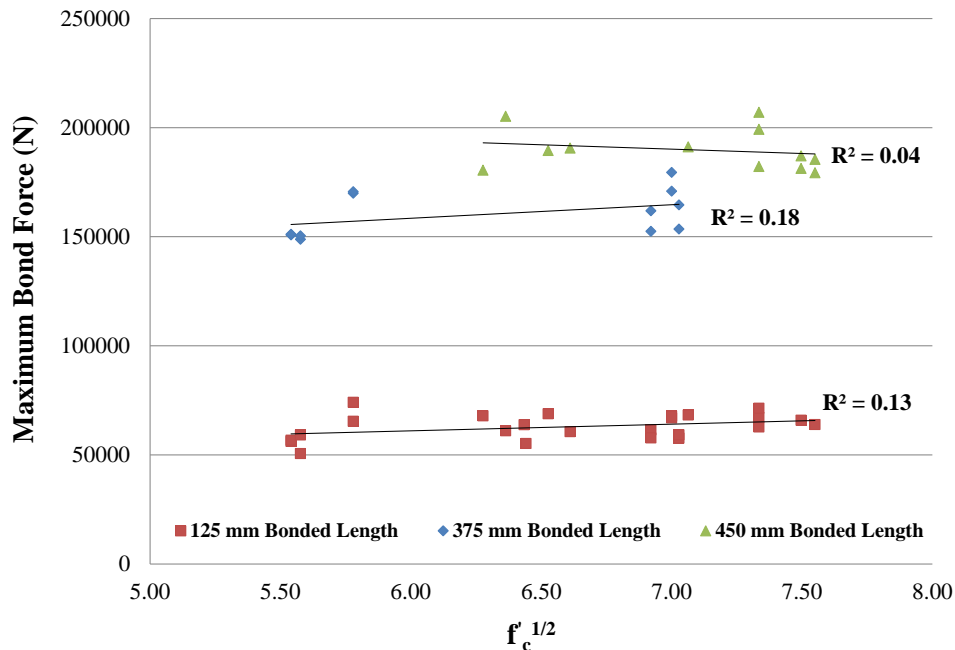


Figure 9.68 Relationship between maximum bond force and $f'_c{}^{1/2}$ (Combined results of Phase 1 and 2)

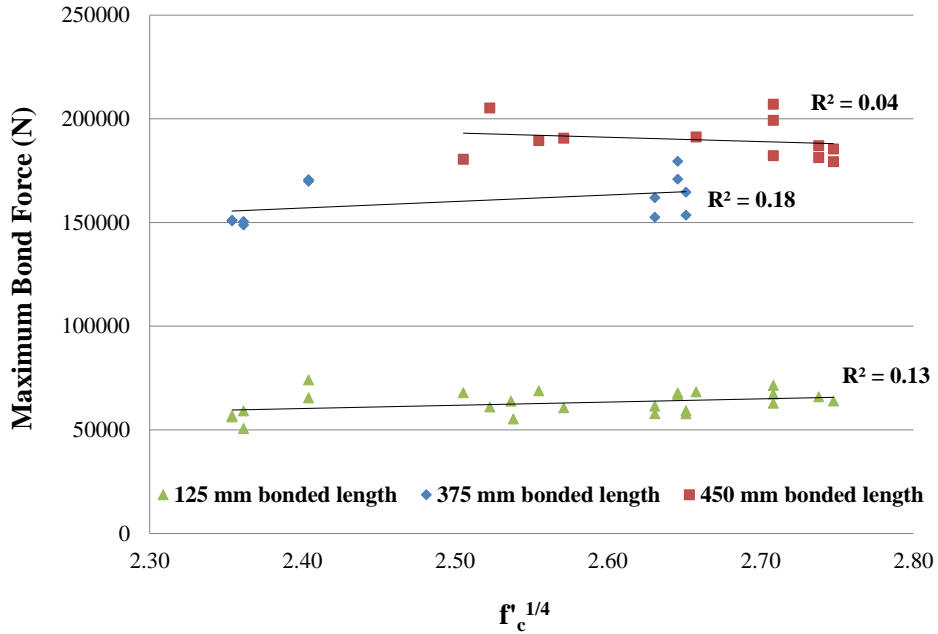


Figure 9.69 Relationship between maximum bond force and $f'_c{}^{1/4}$ (Combined results of Phase 1 and 2)

9.8.4 Effect of Splitting Tensile Strength on Bond Strength

Figure 9.70 displays the relationship between average bond strength and the normalized splitting tensile strength for the combined data set (48 values in total).

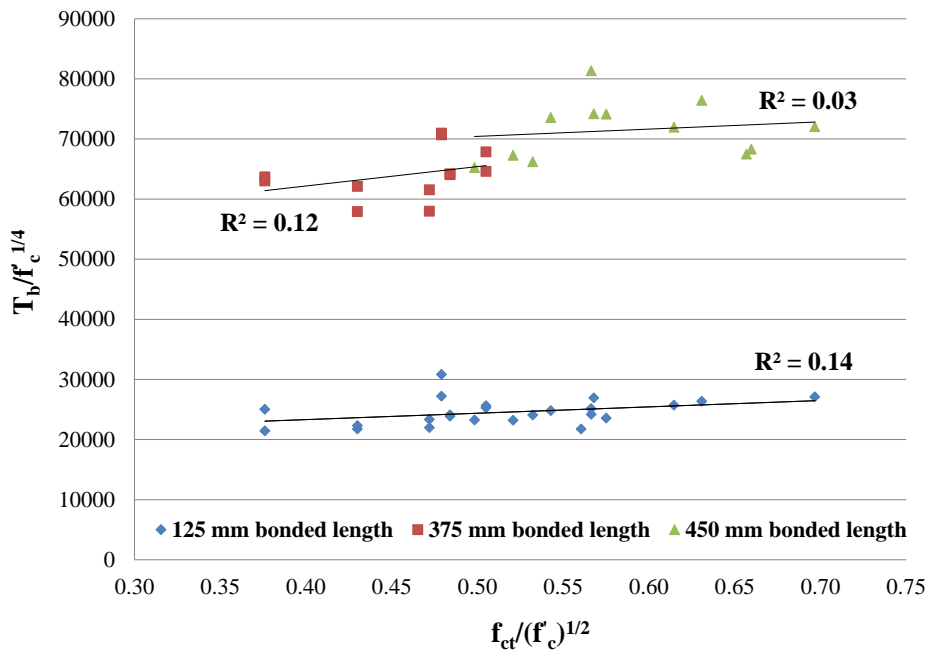


Figure 9.70 Relationship between $T_b/f'_c{}^{1/4}$ and $f_{ct}/(f'_c)^{1/2}$ (Combined results of Phase 1 and 2)

While a fairly good correlation between splitting tensile strength and bond strength existed when examining Phase 1 and 2 individually, when all data are combined (i.e., all 48 specimens), this correlation no longer exists. Although there appears to be no correlation between $T_b/f_c^{1/4}$ and $f_{ct}/f_c^{1/2}$, the trend line seems to have a positive slope indicating that as $f_{ct}/f_c^{1/2}$ increases, the average bond strength also increases. However, given the limited data set, and the inherent variability in the testing of the splitting tensile strength and the bond strength, it is difficult to validate this result.

9.8.5 Effect of Modulus of Rupture on Bond Strength

The analysis of the modulus of rupture results presented in Phase 1 and 2, was based on comparison with the average bond strength and used averaged pairs (i.e., A and B specimens) to evaluate the effect that modulus of rupture had on bond. Fairly strong correlations were found at the 30 and 60 MPa compressive strength levels however, the 40 and 50 MPa specimens showed very little relationship between modulus of rupture and bond strength.

To investigate this discrepancy in results, the results from Phase 1 and 2 were combined and an overall evaluation of the effect of modulus of rupture normalized with respect to $f_c^{1/2}$ ($f_r/f_c^{1/2}$) on maximum bond force normalized with respect to $f_c^{1/4}$ ($T_b/f_c^{1/4}$) was carried out. Figure 9.71 summarizes the relationship between $f_r/f_c^{1/2}$ and $T_b/f_c^{1/4}$ considering all 48 beam-end specimens.

Overall, no significant correlation was found between the modulus of rupture and $T_b/f_c^{1/4}$ for the 125 and 450 mm bonded length specimens. In addition, the slopes of the trend lines were relatively horizontal for the 125 and 450 mm bonded length specimens further indicating that there was no significant effect of varying $f_r/f_c^{1/2}$ on $T_b/f_c^{1/4}$. A slightly better correlation ($R^2 = 0.42$) was found to exist for the 375 mm bonded length specimens however, no general relationship between $f_r/f_c^{1/2}$ and $T_b/f_c^{1/4}$, regardless of bonded length or compressive strength, was found to exist.

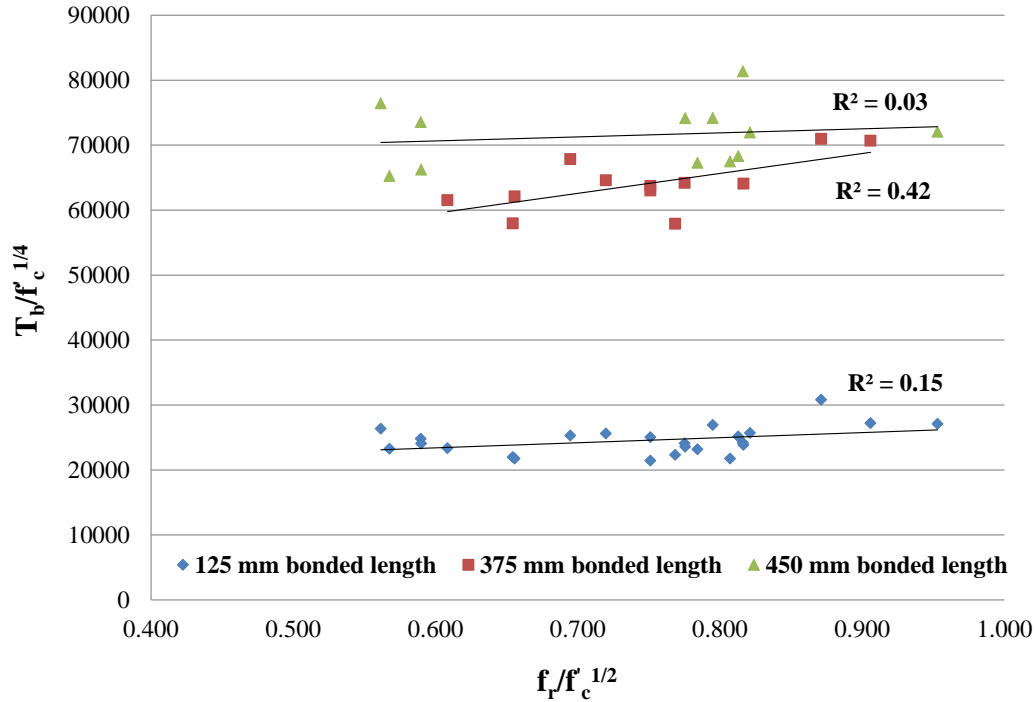


Figure 9.71 Relationship between $T_b/f_c^{1/4}$ and $f_r/f_c^{1/2}$ (Combined results of Phase 1 and 2)

9.8.6 Effect of Fracture Energy on Bond Strength

The analysis of the fracture energy results presented in Phase 1 and 2, was based on comparison with the average bond strength and used averaged pairs (i.e., A and B specimens) to evaluate the effect that fracture energy of concrete had on bond. Fairly strong correlations were found for the Phase 2 specimens however, the Phase 1 showed very little relationship between fracture energy and average bond strength. This may be a result of including a different aggregate source (i.e., RCA-3) in the Phase 2 fracture energy testing program which was less variable (i.e., did not contain significant amounts of deleterious materials) than the RCA-2 source and was able to provide information that isolated the effect of aggregate strength on fracture energy and average bond strength. To investigate this discrepancy in results, the results from Phase 1 and 2 were combined (total of 48 beam-end specimens) and presented as Figure 9.72 to allow for the overall effect of fracture energy on maximum bond force normalized with respect to $T_b/f_c^{1/4}$ to be evaluated. In general, there appears to be no significant correlation between fracture energy and $T_b/f_c^{1/4}$. In the case of the 450 mm bonded length specimens, a larger slope and slightly larger coefficient of determination value ($R^2 = 0.50$) was found to exist. Given the data available from this research it is difficult to suggest whether the effect of fracture energy on $T_b/f_c^{1/4}$ increases at

longer bonded lengths (i.e., 450 mm or larger). It should be noted that a similar lack of correlation between fracture energy and $T_b/f_c^{1/4}$ was found to exist when considering only the NA concrete beam-end specimens. Recalling the conclusions of Section 8.4.3, which noted that while replacing NA with RCA may have an effect on the fracture energy, the inherent variability in the fracture energy of NA concrete may be such that no conclusion as to whether NA or RCA has higher fracture energy can be made. In terms of the effect of fracture energy on bond strength, it may also be difficult to determine whether the relative differences in the fracture energy of NA concrete and the fracture energy of RCA concrete are significant enough to gauge their relative effect on the bond strength given the inherent variability in the measurement of fracture energy. Overall, it must be concluded that regardless of aggregate type (i.e., NA or RCA), the fracture energy still has a negligible effect on $T_b/f_c^{1/4}$ for bonded lengths of 450 mm or shorter and for compressive strengths between 30 and 60 MPa.

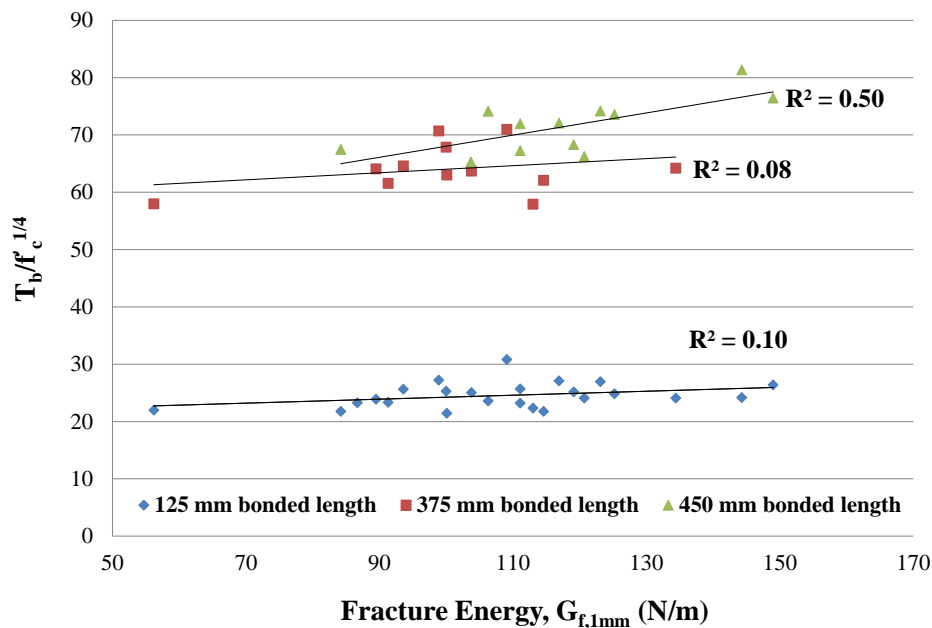


Figure 9.72 Relationship between $T_b/f_c^{1/4}$ and fracture energy, $G_{f,1mm}$ (Combined results of Phase 1 and 2)

9.8.7 Statistical Summary of Factors Affecting Bond Strength

In addition to the correlation plots presented in the previous sections, a linear regression analysis was performed to test the hypothesis on the slope of the regression line. This analysis was conducted to confirm the influence of a particular aggregate or concrete property on the bond

strength. The linear regression line takes the form of Equation 9.1.

$$Y_i = \alpha + \beta x_i + \varepsilon_i \quad \text{for } i = 1, 2, \dots, n \quad \text{Equation 9.1}$$

Where,

Y = a random variable whose distribution depends on x (i.e., the dependent variable);

x = the independent variable on which Y depends;

α = intercept of the regression line;

ε = a random variable whose value depends on possible errors in measurement of the variables other than x which may influence Y . A value of α can always be chosen such that the mean of the distribution of ε is zero; and

β = slope of the regression line.

The following assumptions and procedures were carried out for the linear regression analysis.

1. Null hypothesis: $\beta = 0$ (i.e., slope of the regression line is zero)
2. Alternative hypothesis: $\beta \neq 0$
3. Level of significance: $\alpha = 0.05$
4. Criterion: Reject the null hypothesis if $t < -t_{\text{crit}}$ or $t > t_{\text{crit}}$, where t_{crit} is the value of $t_{\alpha/2} = t_{0.025}$ for $n - 2$ degrees of freedom. In the case of the current data set a total number of 48 beam-end specimens (i.e., $n = 48$) equates to $48 - 2 = 46$ degrees of freedom and at the 5% significance level $t_{\text{crit}} = 1.960$.
5. The p-value or $\text{Prob} > |t|$, is the lowest level of significance at which the actual value of the t-statistic is significant. The evidence of non-zero slope (i.e., rejecting the null hypothesis) becomes strong when the p-value is less than the significance level (i.e., when $p < \alpha = 0.05$).
6. Microsoft Excel was used to expedite the regression analysis calculations.

In cases where the null hypothesis is not rejected (i.e., $\beta = 0$), the regression line is horizontal and the mean of the dependent variable, Y (i.e., T_b or $T_b/f_c^{1/4}$) does not depend linearly on the independent variable, X (i.e., ACV , f_c , f_{ct} , f_r , or $G_{f,1mm}$). This procedure was carried out for all

the independent variables and across all three bonded lengths (i.e., 125 mm, 375 mm, and 450 mm). A summary of the regression analysis is presented in Table 9.9.

Table 9.9 Statistical summary of aggregate and concrete properties affecting bond strength

Bonded Length (mm)	Y	X	Adjusted [‡] R ²	t-stat [†]	**Prob > t
125	$T_b/f_c'^{1/4}$	ACV	0.34	14.60*	<0.0001
	T_b	$f_c'^{1/2}$	0.09	1.80	0.086
	T_b	$f_c'^{1/4}$	0.09	1.81	0.085
	T_b	$f_{ct}/f_c'^{1/2}$	0.26	1.35	0.415
	T_b	f_r	0.02	1.22	0.237
	T_b	$G_{f,1mm}$	0.08	1.72	0.100
375	$T_b/f_c'^{1/4}$	ACV	0.51	-3.53*	0.006
	T_b	$f_c'^{1/2}$	0.09	1.47	0.174
	T_b	$f_c'^{1/4}$	0.10	1.48	0.170
	T_b	$f_{ct}/f_c'^{1/2}$	0.29	2.33*	0.042
	T_b	f_r	0.21	1.96	0.078
	T_b	$G_{f,1mm}$	0.10	0.09	0.930
450	$T_b/f_c'^{1/4}$	ACV	0.62	-4.32*	0.002
	T_b	$f_c'^{1/2}$	0.05	-0.68	0.515
	T_b	$f_c'^{1/4}$	0.05	-0.66	0.523
	T_b	$f_{ct}/f_c'^{1/2}$	0.10	0.21	0.841
	T_b	f_r	0.02	-0.89	0.393
	T_b	$G_{f,1mm}$	0.49	3.41*	0.007

[†] Note: For $n - 2 = 48 - 2 = 46$ degrees of freedom and at the 95% confidence level, $t_{\alpha/2 = 0.025} = t_{crit} = 1.960$.

* Based on the t-statistic calculated from the linear regression analysis, this independent variable was found to be statistically significant at the 95% confidence level.

** P-values lower than the level of significance (i.e., 0.05) provided strong evidence of non-zero slope (i.e., rejecting the null hypothesis) and reinforced the t-statistics' criticality.

[‡] Modification of the normal coefficient of determination that provides an adjustment considering the degrees of freedom.

Therefore, based on the relative t-statistics and associated p-values from the regression analyses presented in Table 9.9, the maximum bond force or $T_b/f_c'^{1/4}$ was found to be statistically dependent on the aggregate strength (ACV) across all bonded lengths, $f_{ct}/f_c'^{1/2}$ at the 375 mm bonded length, and on the fracture energy ($G_{f,1mm}$) at the 450 mm bonded length. This finding suggests that the aggregate crushing value may be used as an effective quality control measure for identifying RCA sources suitable for structural (reinforced) concrete applications.

9.9 Predictive Experimental Bond Equations for RCA Concrete

As established in the previous section, the effect of bonded length and coarse aggregate strength (ACV) on the maximum bond force is statistically significant for specimens of all bonded lengths (i.e., 125 mm, 375 mm, and 450 mm). The following section presents the methodology and calculations for establishing a predictive bond equation based on the experimental bond strength data presented in Phases 1 and 2. This equation will be a function of the bonded length and aggregate strength (ACV). In addition, the model will be calibrated to a normalized bond strength of $T_b/f_c^{1/4}$, to allow for comparison to other descriptive bond equations in the literature.

Based on the limited data set (i.e., 48 beam-end specimens), it was not practical to develop a design equation for predicting the maximum bond force of RCA concrete members. Instead, the model will be used to,

- Confirm and illustrate the effect that varying coarse aggregate strength (ACV) has on bond strength,
- Provide an indication of how varying aggregate strength affects the minimum bonded length required for developing the full yield strength of the reinforcing bar, and;

One of the most thoroughly developed models for bond with reinforcing steel is the equation proposed by ACI Committee 408. Based on a database of 478 development and splice beam tests of uncoated, bottom cast bars; Equation 9.2 was developed for bars not confined by transverse reinforcement (refer to Section 2.4.5 for definitions of equation variables).

$$\frac{T_b}{f_c^{1/4}} = [1.43l_d(c_{\min} + 0.5d_b) + 57.4A_b] \left(0.1 \frac{c_{\max}}{c_{\min}} + 0.90\right) \quad \text{Equation 9.2}$$

Given the configuration of the beam-end specimens and test variables that comprise this research study, Equation 9.2 can be modified to include: constant bar diameter = 25.2 mm, bar area = 500 mm² and cover dimensions ($c_{\min} = 26.6$ mm, $c_{\max} = 27.5$ mm). Thus, Equation 9.2 becomes,

$$\frac{T_b}{f_c^{1/4}} = 56.2l_b + 28797.1 \quad \text{Equation 9.3}$$

The experimental maximum bond force normalized to $f_c^{1/4}$ presented in Phase 1 and 2 were

compared to those predicted by Equation 9.3 and have been summarized in Figure 9.73.

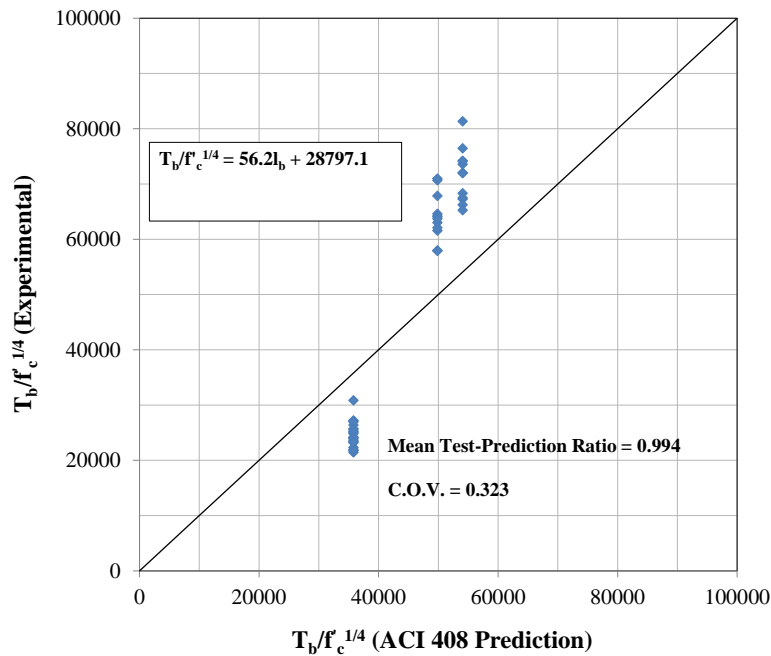


Figure 9.73 Experimental bond force, T_b normalized with respect to $f_c^{1/4}$ versus predicted normalized bond force, based on ACI 408 equation (Equation 9.2)

Based on Figure 9.73, it is clear that the ACI 408 equation (Equation 9.2) was not able to consistently predict the experimental bond strength data from the Phase 1 and 2 specimens. Overall, the ACI 408 equation over-estimated the bond strengths of the shorter 125 mm bonded length specimens and under-estimated the bond strengths of the 375 and 450 mm bonded length specimens. In addition, while the mean test-prediction ratio is fairly close to unity (0.994), the coefficient of variation is still fairly high (0.323).

Based on the experimental data, several linear regression models (Models A, B and C) were developed and their main model statistics are summarized and compared in Table 9.10. Note that Models A and B are one parameter models while Model C includes two independent parameters (X_1 and X_2). The term, β_i represent the coefficients (or slopes) of the regression line (or plane).

Table 9.10 Summary of developed regression models and their associated parameters

Main Regression Model Statistics						
Model	Y	X ₁	X ₂	† Adjusted R ²	F-stat	Prob > F
A	T _b	l _b	-	0.981	2446.7	0.00000
B	T _b /f _c ^{1/4}	l _b	-	0.972	1636.9	0.00000
C	T _b /f _c ^{1/4}	l _b	ACV	0.984	1447.7	0.00000

Parameter Estimates and Statistics							
Model	Intercept*	Parameter X ₁			Parameter X ₂		
		β ₁	t-statistic [‡]	Prob > t	β ₂	t-statistic [‡]	Prob > t
A	14088.6	390.4	49.46	< 0.0001	-	-	-
B	6182.9	148.7	40.46	< 0.0001	-	-	-
C	20781.8	149.0	53.56	< 0.0001	-641.7	-5.95	< 0.0001

* Note that all intercept values were found to be statistically significant (i.e., were required to be included in the model)

† Modification of the normal coefficient of determination that provides adjustment for the degrees of freedom.

‡ Based on the t-statistic calculated from the linear regression analysis, this independent variable was found to be statistically significant at the 95% confidence level for t_{crit} = ±1.960. In addition, the low p-value or Prob > |t| were all found to be less than the significance level 0.05 which provided strong evidence of non-zero slope (i.e., rejecting the null hypothesis) and reinforced the t-statistics' criticality.

As evidenced by the high adjusted coefficient of determination values, all models seemed to represent the experimental data fairly accurately. Model C is a two-parameter model which includes the bonded length and the aggregate crushing value. Based on their t-statistics (t_{x2} < t_{crit}) and p-values (Prob > |t| < 0.005), both the bonded length (X₁) and the ACV (X₂) were considered as significant parameters in the regression model. Equations 9.4, 9.5 and 9.6 represent the linear regression models A, B and C, respectively.

$$T_b = 390.4l_b + 14088.6 \quad \text{Equation 9.4}$$

$$\frac{T_b}{f_c^{1/4}} = 148.7l_b + 6182.9 \quad \text{Equation 9.5}$$

$$\frac{T_b}{f_c^{1/4}} = 149.0l_b - 641.7ACV + 20781.8 \quad \text{Equation 9.6}$$

To assess which regression model best predicts the experimental bond strength results, the maximum bond force predicted by the model was plotted against the maximum bond force from the experimental results. Test-prediction ratios (experimental result/predicted result) were then calculated and the mean and coefficient of variation associated with the total number of test-

prediction ratios were computed for each linear regression model. Figure 9.74, Figure 9.75, and Figure 9.76 present the test versus prediction data for the developed linear regression Models A, B and C, respectively.

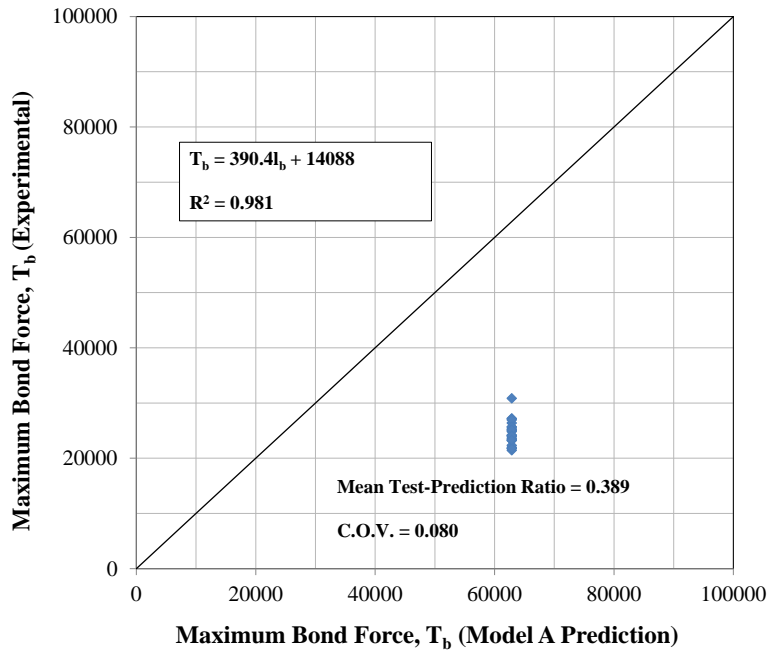


Figure 9.74 Experimental bond force, T_b versus predicted maximum bond force, based on regression Model A (Equation 9.4)

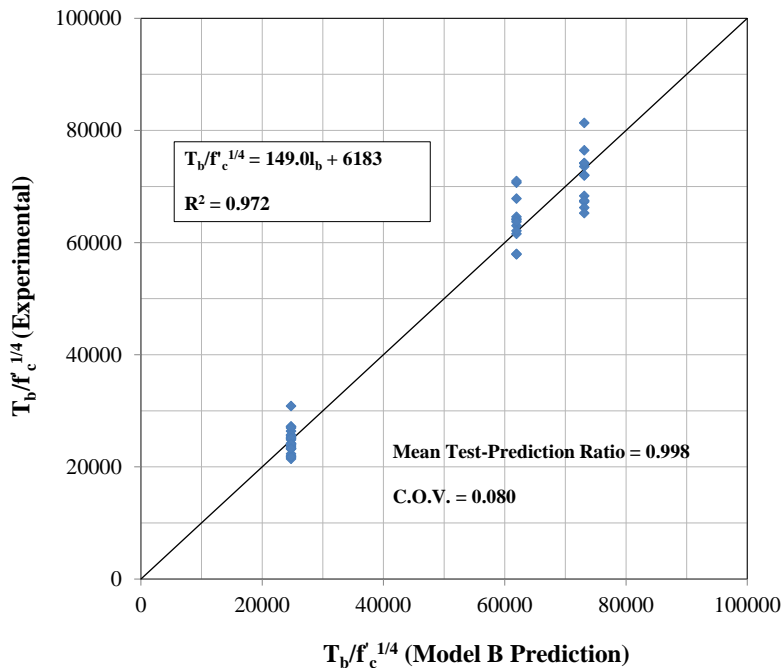


Figure 9.75 Experimental bond force, T_b normalized with respect to $f_c^{1/4}$ versus predicted normalized experimental bond force, based on regression Model B (Equation 9.5)

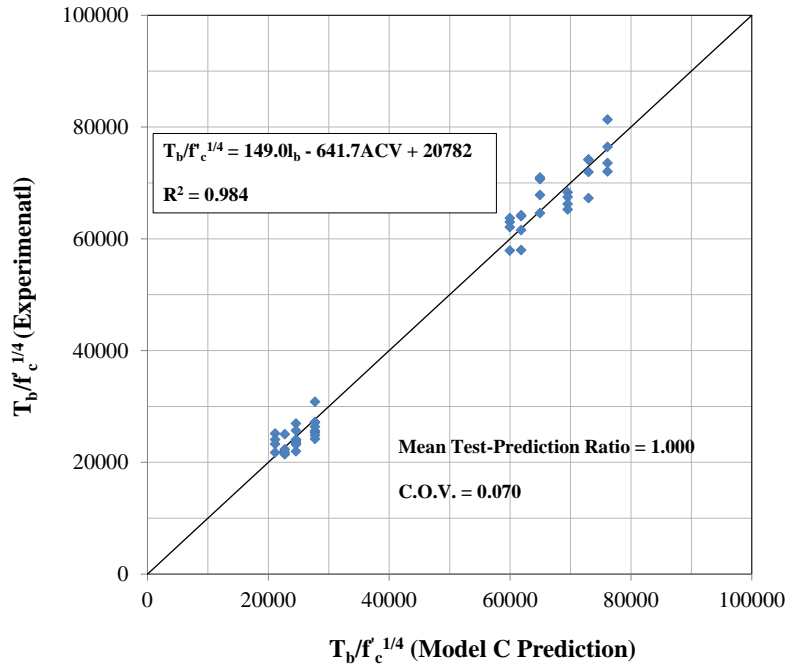


Figure 9.76 Experimental bond force, T_b normalized with respect to $f_c^{1/4}$ versus predicted normalized experimental bond force, based on regression Model C (Equation 9.6)

Based on Figure 9.74, it is apparent that while a high coefficient of determination value exists ($R^2 = 0.981$), Model A consistently under-estimates the maximum bond force (i.e., mean test-prediction ratio of 0.389). By choosing $T_b/f_c^{1/4}$ as the independent variable, Y, Model B provided a more accurate and consistent prediction of the bond strength data (i.e., mean test-prediction ratio = 0.998 and COV = 0.08). However, Model B is still only able to generate three predicted $T_b/f_c^{1/4}$ values corresponding to the 125, 375 and 450 mm bonded length specimens (see Figure 9.75).

By adding a second parameter, ACV (X_2), to the regression model as in the case of Model C, the mean test-prediction ratio and the associated COV improve slightly however, a larger range of $T_b/f_c^{1/4}$ predictions can be generated (see Figure 9.76) and the model becomes more robust. Therefore, based on the above considerations, Model C was chosen as the most accurate predictor of the experimental results.

9.9.1 Predicted Development Lengths Based on Regression Model C Developed from Experimental Results

As defined in Section 2.4.6, the development length is the shortest length of reinforcing bar embedded in concrete required to develop a bar stress equal to the yield strength (MacGregor and Bartlett, 2000). Based on the linear regression Model C (Equation 9.6) developed in the previous section, the required development length can be calculated by re-arranging Equation 9.6 and making the following substitution, $T_b = T_{s,y} = A_b f_y$. Thus, Equation 9.6 can be solved for the development length, l_d , as presented in Equation 9.7.

$$l_d = \left(\frac{f_y A_b}{f_c^{1/4}} + 641.7ACV - 20781.8 \right) / 149.0 \quad \text{Equation 9.7}$$

Based on the experimental results presented in this study, the yield strength of the test bar, f_y was 467 MPa (refer to Table 9.6) and the cross-sectional area of the 25M test bar, A_b was 500 mm². Therefore, in Equation 9.7, the term $f_y A_b = T_{s,y} = 233\,500$ N.

It is critical to note that Equation 9.7 is not appropriate for use as a design equation for RCA concrete members. Instead, it was developed to illustrate the relative effect of aggregate type (based on the crushing strength or ACV) on the required development length extrapolated from the regression Model C (Equation 9.6). Therefore, based on Equation 9.7, the effect of aggregate strength (ACV) on the development length of RCA concrete could be assessed over a range of concrete compressive strengths. Table 9.11 summarizes the results of the development length calculated based on Model C (Equation 9.6) and includes the required development length values associated with the natural aggregate, RCA-1, RCA-2 and RCA-3. The development lengths based on the code equations of CSA A23.3 and ACI 318 were also calculated to compare to the theoretically-derived lengths. In the calculation of the CSA A23.3 and ACI 318 code development lengths, the following assumptions were made: no transverse reinforcement, bars were bottom-cast, and concrete was of normal-density. Based on Table 9.11, it was observed that, depending on the compressive strength and the coarse aggregate strength (ACV), development lengths for the RCA concretes tested were between 3.5% and 8.8% longer than the length calculated for the NA concrete. Overall, the theoretical development lengths were up to 50% shorter than those calculated based on CSA A23.3 and up to 60% shorter than those calculated based on ACI 318. This result is expected as the code equations are generally

calibrated to provide additional safety that ensures an acceptably low probability of failure (ACI 408, 2003). The code equations may be even more conservative when no transverse reinforcement is included in the calculations. In addition, code equations for development length were based on simplifications of descriptive equations for bond strength with reinforcement which add additional levels of conservatism (Orangun, Jirsa and Breen, 1977).

Table 9.11 Summary of theoretical development lengths calculated based on regression model C and calculated development lengths based on CSA A23.3 and ACI 318 code equations

f'_c (MPa)	30	35	40	45	50	55	60	
CSA A23.3 l_d^* (mm)	1226	1135	1061	1001	949	905	867	
ACI 318 l_d^* (mm)	1523	1410	1319	1243	1180	1125	1077	
ACV	Theoretical Development Lengths Based on Model C (mm)[†]							
16	599	574	553	535	519	505	493	
18	608	582	561	543	527	514	501	
18.2	609	583	562	544	528	514	502	NA
20	616	591	570	552	536	522	510	
22	625	600	579	560	545	531	518	
23.1	630	604	583	565	549	536	523	RCA-1
24	634	608	587	569	553	539	527	
26.0	642	617	596	578	562	548	536	RCA-2
28	651	626	604	586	571	557	544	
28.5	653	628	607	588	573	559	546	RCA-3
30	659	634	613	595	579	565	553	
32	668	643	622	604	588	574	562	
Aggregate Type	Percent Increase from NA Concrete l_d							
RCA-1	3.5%	3.6%	3.8%	3.9%	4.0%	4.1%	4.2%	
RCA-2	5.5%	5.8%	6.0%	6.2%	6.4%	6.5%	6.7%	
RCA-3	7.3%	7.6%	7.9%	8.2%	8.4%	8.6%	8.8%	
Aggregate Type	Percent Reduction from CSA A23.3 Calculated l_d							
NA	50.3%	48.6%	47.0%	45.6%	44.3%	43.2%	42.1%	
RCA-1	48.6%	46.7%	45.1%	43.5%	42.1%	40.8%	39.6%	
RCA-2	47.6%	45.6%	43.9%	42.3%	40.8%	39.5%	38.2%	
RCA-3	46.7%	44.7%	42.9%	41.2%	39.7%	38.3%	36.9%	
Aggregate Type	Percent Reduction from ACI 318 Calculated l_d							
NA	60.0%	58.6%	57.4%	56.2%	55.2%	54.3%	53.4%	
RCA-1	58.6%	57.1%	55.8%	54.5%	53.4%	52.4%	51.4%	
RCA-2	57.8%	56.2%	54.8%	53.5%	52.4%	51.3%	50.3%	
RCA-3	57.1%	55.5%	54.0%	52.7%	51.4%	50.3%	49.3%	

* Development lengths calculated are based on calibrated code equations. They assume no transverse reinforcement and that the main test bar has a yield strength of 467 MPa.

[†] Theoretical development lengths calculated based on Model C assume steel with yield strength of 467 MPa.

Figure 9.77 illustrates the relationship between compressive strength and development length as predicted by CSA A23.3-04 and by Equation 9.7 for the NA, RCA-1, RCA-2, and RCA-3 concrete with ACVs of 18.2, 23.1, 26.0, and 28.5, respectively.

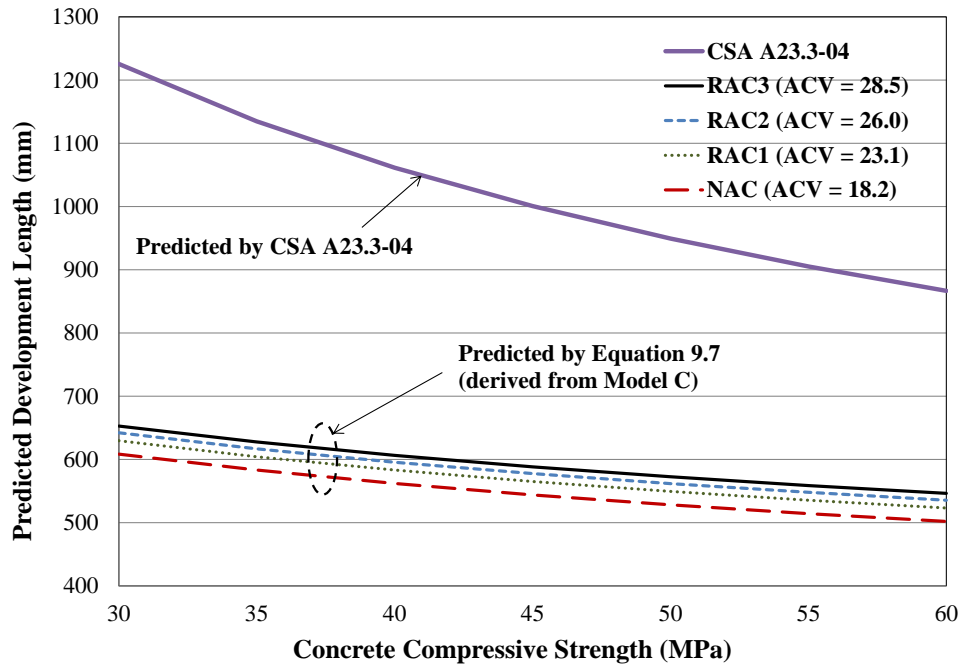


Figure 9.77 Concrete compressive strength versus development lengths predicted by CSA A23.304 code equation and equation 9.7 (Model C)

In general, the relationship between development length and compressive strength is non-linear (i.e., l_d is proportional to $f'_c{}^{1/4}$) for both the CSA A23.3-04 and the Equation 9.7 predictive equations. In comparing the Equation 9.7 predictive trend lines to the CSA A23.3-04 predictive trend lines, the latter is significantly steeper. This may be explained by the relatively small relationship between the maximum bond force and $f'_c{}^{1/4}$ found within the experimental results on which Equation 9.7 was derived (see Section 9.8.3). It is also clear from Figure 9.77 that the difference between the development lengths predicted for the RCA concretes and NA concrete is fairly small. Overall, it appears that the development lengths computed using CSA A23.3-04 (assuming no transverse reinforcement) are conservative for all concrete types considered.

By deriving the theoretical development lengths based on the developed linear regression Model C, the effect that aggregate strength (ACV) has on the development length could be assessed for the specific test results of this research study. Overall, it appears that as aggregate strength

decreases (ACV increases), the length required to develop a reinforcing bar increases non-linearly. However, the maximum percent increase in required theoretical development length for the RCA concrete compared to the NA concrete is approximately 9%.

9.10 Overall Conclusions

The following section presents the set of overall conclusions derived from the experimental results and analysis of the Phase 1 and 2 beam-end bond testing.

1. In general, replacing coarse natural aggregate with RCA while maintaining similar compressive strengths caused a decrease in bond strength with reinforcing steel. The NA concrete beam-end specimens had $\tau_b/f_c^{1/2}$ values that were between 10 and 21% higher than the RCA concrete beam-end specimens for compressive strengths of 30 and 50 MPa and bonded lengths of 125 and 375 mm. The NA concrete beam-end specimens had $\tau_b/f_c^{1/2}$ that were between 3 and 13% higher than the RCA concrete beam-end specimens for compressive strengths of 40 and 60 MPa and bonded lengths of 125 and 450 mm.
2. While the maximum bond strengths for the NA concrete specimens were higher than the bond strengths for the RCA specimens, replacing natural coarse aggregate with RCA-1, RCA-2 or RCA-3 did not have a discernible effect on the general bond stress-slip response of the beam-end specimens.
3. As coarse aggregate strength decreases (ACV increases), the average bond strength decreases. Excellent correlations were found between the ACV and the average bond strength for both Phase 1 and 2. In addition, linear regression analysis was used to confirm the dependence of bond strength on ACV.
4. After dissection and macro-level forensic analyses were performed on a select number of beam-end specimens, general beam-end structural behaviour and failure mechanism was confirmed. The NA and RCA-1 concrete dissected specimens failed by splitting-induced pull-out accompanied by crushing and/or shearing off in the concrete adjacent to the ribs. The RCA-3 concrete specimens failed by splitting-induced by slipping at the rib faces. Examination of fracture planes passing mainly through the coarse aggregate confirmed the influence of the coarse aggregate strength on bond strength. Based on the observed failure mechanism of the beam-end specimens, slip of the reinforcing bar occurred due to the

formation of transverse micro-cracks at the tips of the reinforcement ribs which were followed by the formation of longitudinal splitting cracks.

5. In contrast to published studies in the literature for normal weight (natural aggregate) concrete, no significant relationship existed between concrete compressive strength (f_c , $f_c^{1/2}$, and $f_c^{1/4}$) and the average bond strength. This was confirmed user linear regression analysis techniques that considered the bond and compressive strength results all 48 beam-end specimens.
6. In contrast to published studies in the literature for normal weight (natural aggregate) concrete, no significant correlation was found between the splitting tensile strength and the average bond strength. This was confirmed user linear regression analysis techniques that considered the bond and compressive strength results all 48 beam-end specimens.
7. Overall, no significant correlation existed between the modulus of rupture and $T_b/f_c^{1/4}$ for the 125 and 450 mm bonded length specimens. A better correlation ($R^2 = 0.86$) was found to exist for the 375 mm specimens however, no general relationship between modulus of rupture and bond strength, regardless of bonded length or compressive strength, was found to exist.
8. Strong correlations between fracture energy and bond strength were found for the Phase 2 specimens. This finding supports the theories presented in the literature but is in contrast with the findings of Phase 1. Overall, regardless of aggregate type (i.e., NA or RCA), the fracture energy was found to have a negligible effect on $T_b/f_c^{1/4}$ for bonded lengths of 450 mm or shorter and for compressive strengths between 30 and 60 MPa. In terms of using fracture energy of RCA concrete as an indicator for bond strength, given the inherent variability in the measurement of fracture energy, it may be difficult to determine whether the relative differences in the fracture energy of NA concrete and the fracture energy of RCA concrete are significant enough to gauge their relative effect on the bond strength.
9. Based on the results of the developed regression model (Model C), the theoretical development lengths for the RCA concrete beam-end specimens were 9% longer than the NA concrete specimens. This finding is in direct relation to the increase in bond strength with an increase in coarse aggregate strength (decrease in ACV). Although the regression model was able to provide a predicted set of development lengths based on ACV and concrete compressive strength, it is important to note that the data set from which it was derived is

limited and therefore, it is not appropriate for use as a design equation for RCA concrete members.

In addition to the above conclusions, through assimilation of the various trends and relationships identified in the preceding sections and chapters, a comprehensive interaction network highlighting the relationships between various aggregate, concrete, and concrete-steel bond properties was constructed and is presented as Figure 9.78.

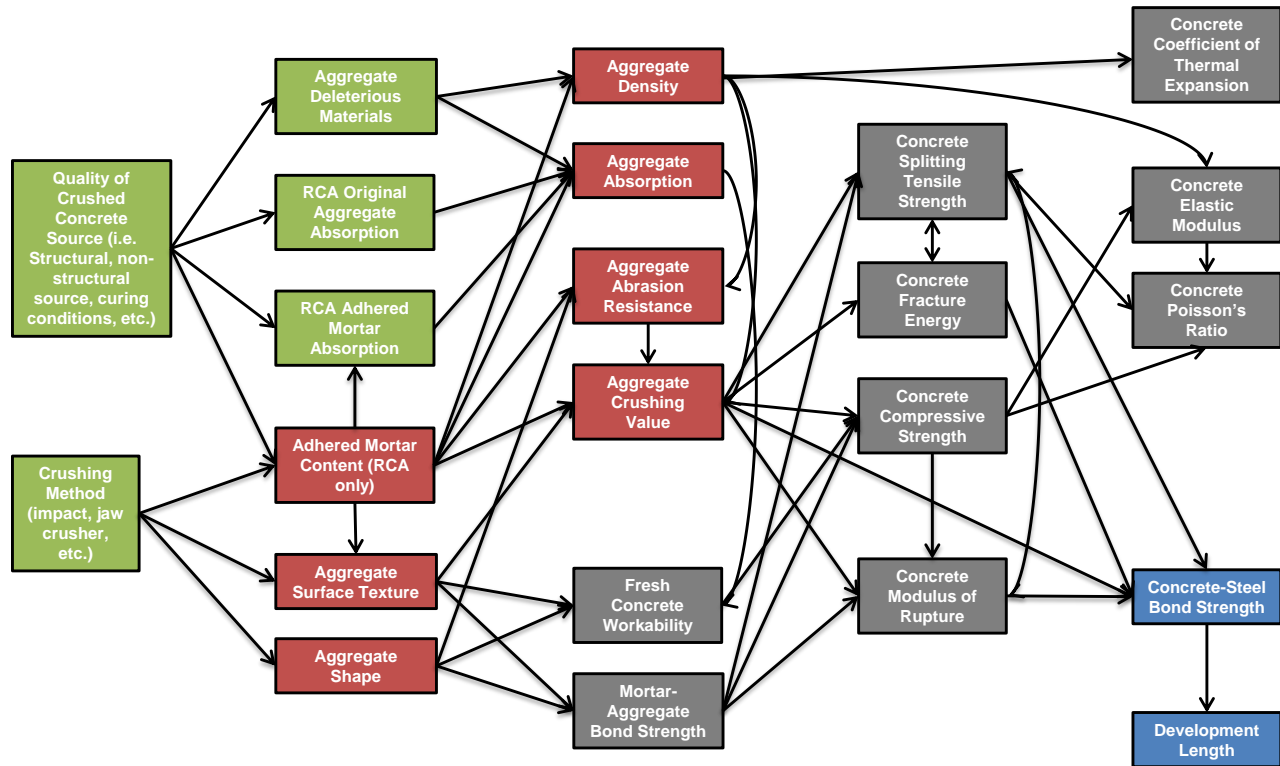


Figure 9.78 Relationship between aggregate, concrete, and concrete-steel bond properties

Chapter 10: Guidelines for Use of RCA in Structural Concrete

10.1 Overview

This chapter presents a set of guidelines for using RCA as a full or partial natural coarse aggregate replacement in new concrete (RCA concrete). Specifically, a detailed procedure has been developed that allows engineers, concrete producers, aggregate suppliers and contractors to assess whether a particular RCA source is suitable for use in reinforced concrete, plain concrete or as a fill material. Included as part of this procedure are guidelines for mixture proportioning of RCA concrete, recommended durability testing for RCA concrete and a specific reference list that provides additional information on RCA use in specialty concrete applications.

10.2 Guideline Formulation and Methodology

The guidelines have been organized in the form of a decision tree. Users of the guide will be able to proceed systematically through the decision tree and arrive at an appropriate use for their particular RCA source. Some additional information is provided on the original concrete structure being considered for demolition, material sorting considerations and crushing methods. Implementation of the procedures outlined below assumes that the RCA source being considered has come from the demolition and crushing of a concrete structure or pavements whose age and original concrete properties are unknown. Therefore, the guideline serves as a material assessment tool. In general, the guideline has been compiled based on the findings of this research however; additional references have been used where applicable. It must be noted that the guide is a recommendation of the author only and the reader is cautioned to use their own engineering judgement when interpreting the following procedures and information.

10.3 Recycled Concrete Aggregate Selection Guideline

The following guideline provides a systematic procedure for determining whether a particular crushed concrete source (i.e., an RCA source) is suitable for use in structural RCA concrete as a full or partial replacement of natural coarse aggregate. Three performance classes are proposed that classify a particular RCA source as being suitable for use in reinforced concrete, unreinforced concrete or as a fill material.

10.3.1 The Original Concrete Structure(s), Demolition, and Crushing

When concrete structures are being considered for demolition, detailed material salvage and handling plans should be established. Estimates of potentially recyclable material quantities should be well understood and taken into account in overall project costs. RCA may be derived from the crushing of a single or multiple concrete structures of varying concrete strengths and other properties.

If concrete from a single demolished structure is to be crushed and recycled, several important factors must be considered:

- 1) Ensure that the RCA source quantity is sufficient for its future application. If it is not, consider blending other natural aggregate or other higher quality RCA sources to make up the required quantities.
- 2) It is most efficient when the demolished RCA site is close to the proposed concrete structure to minimize cost.
- 3) Ideally, the demolition, crushing, screening and concrete batching would all be completed within relatively close proximity to the new concrete structure site.
- 4) If the RCA source is being considered as a replacement of natural coarse aggregate in concrete, it is necessary to ensure the RCA has been properly graded to meet the intended application.
- 5) Similar to natural aggregates, precautions should be taken to avoid contamination of the stockpiles (both prior to and after crushing and screening) with foreign materials and/or chemicals.

If concrete from multiple demolished structures of varying strength is to be crushed and recycled, several important factors must be considered:

- 1) RCA should be separated into stockpiles of similar gradation to ensure more efficient use of the material for specific applications.
- 2) Ensure that the RCA stockpile quantity is sufficient for its future application. If it is not, consider blending other natural aggregate or RCA sources to make up the required quantities.
- 3) A comprehensive quality control and testing program should be implemented which

periodically monitors the aggregate properties.

- 4) Similar to natural aggregates, precautions should be taken to avoid contamination of the stockpiles (both prior to and after crushing and screening) with foreign materials and/or chemicals.

Before considering the above factors, and if possible, it would be beneficial to obtain small samples of the crushed concrete material for preliminary testing. Following the procedures presented in the following sections will provide the developer, engineer, aggregate supplier, concrete producer or construction manager with information necessary to make better informed decisions as to the feasibility of using a particular RCA source.

10.3.2 RCA Selection Decision Tree

Once a demolished concrete structure has been crushed and stockpiled, the following general procedure is followed:

- 1) Categorize the stockpile as being composed of RCA entirely or a blend of natural aggregate and RCA.
- 2) Determine whether the particular RCA source satisfies the requirements of CSA A23.1-09 Clause 4.2.3 for normal-density natural aggregates (refer to Section 10.3.2.1).
- 3) Determine the specific performance class to which the RCA belongs (see Section 10.3.3)
- 4) Based on the performance class, determine whether the RCA source is suitable for use in reinforced concrete, unreinforced concrete, or as fill material.
- 5) Follow the recommended mixture proportioning procedures.

The detailed procedure is presented in Figure 10.1 and subsequent references within the figure are presented in Figure 10.2, Table 10.1, Table 10.2, Table 10.3, Table 10.4 and Table 10.5. Subsequent sections serve as companion documents to the procedure outlined in Figure 10.1.

10.3.2.1 CSA A23.1 Requirements for Coarse Aggregates for use in Concrete

The initial stage of assessment for an RCA source should proceed in a similar manner to the evaluation of natural aggregate. CSA A23.1 Clause 4.2.3 addresses the necessary requirements of aggregates (coarse and fine) to be used in concrete. Table 10.1 outlines the grading requirements for coarse aggregates to be used in concrete adapted from CSA A23.1 (2009).

Table 10.2 outlines the limits for deleterious substances and physical properties of coarse aggregates as defined in CSA A23.1 (2009). The deleterious substance requirements of are grouped separately from the aggregate properties requirements.

The following is an overview of the requirements under CSA A23.1 (2009) for coarse aggregates.

- Clause 4.2.3.2 Sampling and Testing
- Clause 4.2.3.4 Normal-density coarse aggregate
 1. Grading (refer to Part (a) of Table 10.1)
 2. Particle shape (refer to Part (a) of Table 10.2)
- Clause 4.2.3.5 Deleterious reactions of aggregates
 1. Alkali-aggregate reactivity
 - When potentially reactive aggregates are to be considered for use, evaluation and preventative measures shall be performed in accordance with CSA A23.2-27A (CSA A23.2, 2009)
 2. Other reactions that produce excessive expansion in concrete.
- Clause 4.1.1.2 Limits on chloride ion content for specific applications.
- Clause 4.2.3.6 Deleterious substances and physical properties (refer to Part (a) of Table 10.2)
- Clause 4.2.3.7 Petrographic examination
 - Only when required by owner.
- Clause 4.2.3.8 Aggregate acceptance
 1. Special performance requirements (i.e., scaling resistance, etc.)
 2. Historical field performance
 - This clause should be disregarded for RCA sources as they are considerably more variable materials given that they are derived from the crushing of multiple concrete structures of varying quality.

As mentioned in the above requirements, RCA sources should be evaluated for their chloride ion content. Additional research into the maximum permissible limits of chloride ions in RCA to reduce the probability of corrosion of reinforcing steel is required.

Table 10.1 Grading requirements for coarse aggregates (adapted from CSA A23.1, 2009)

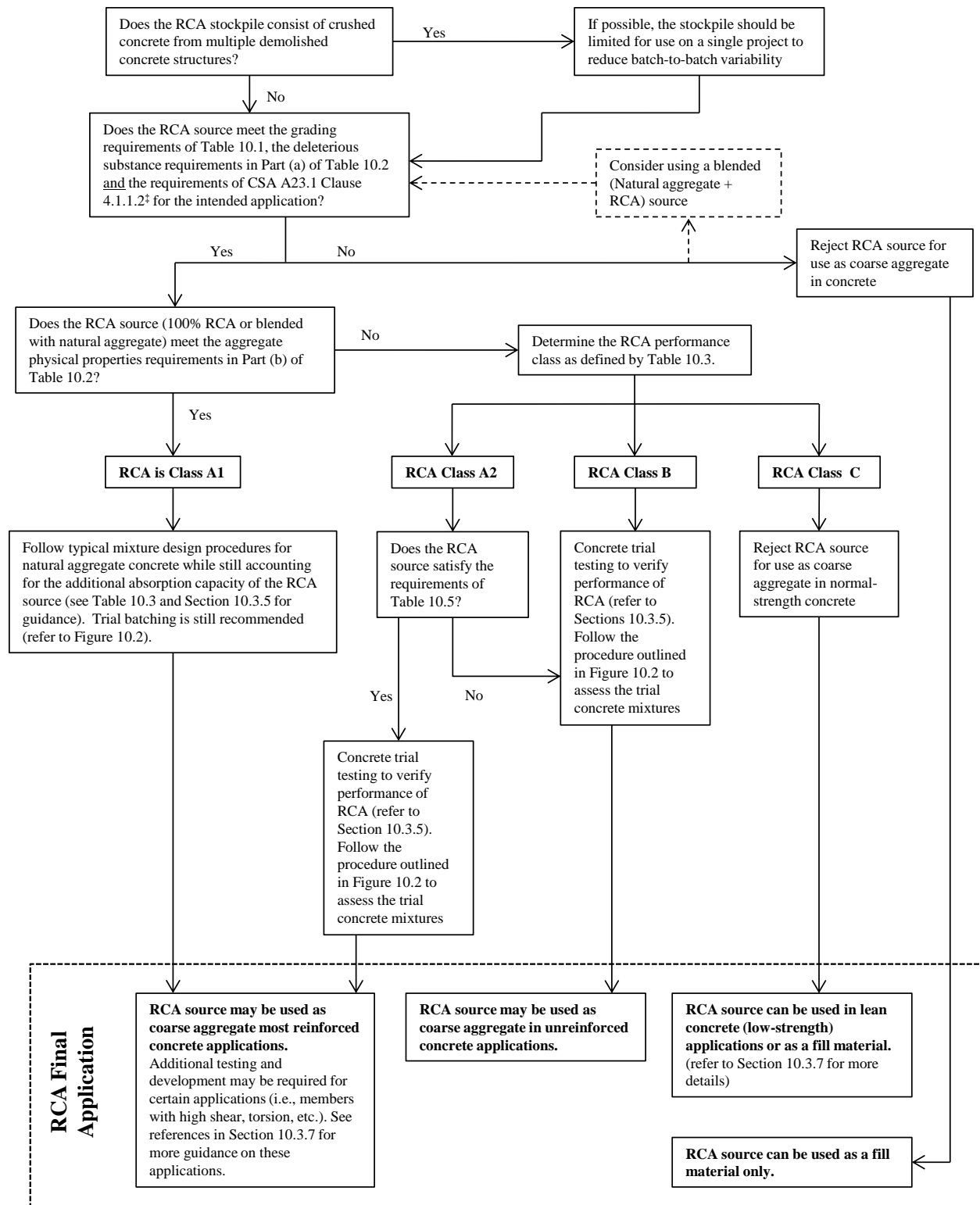
Nominal size of aggregate, mm	Total passing each sieve *, percentage by mass											
	112mm	80mm	56mm	40mm	28mm	20mm	14mm	10mm	5mm	2.5mm	1.25mm	
Group I												
40-5	-	-	100	95-100	-	35-70	-	10-30	0-5	-	-	-
28-5	-	-	-	100	95-100	-	30-65	-	0-10	0-5	-	-
20-5	-	-	-	-	100	85-100	50-90	25-60	0-10	0-5	-	-
14-5	-	-	-	-	-	100	90-100	45-75	0-15	0-5	-	-
10-2.5	-	-	-	-	-	-	100	85-100	10-30	0-10	0-5	-
Group II												
80-40	100	90-100	25-60	0-15	-	0-5	-	-	-	-	-	-
56-28	-	100	90-100	30-65	0-15	-	0-5	-	-	-	-	-
40-20	-	-	100	90-100	25-60	0-15	-	0-5	-	-	-	-
28-14	-	-	-	100	90-100	30-65	0-15	-	0-5	-	-	-
20-10	-	-	-	-	100	85-100	-	0-20	0-5	-	-	-
14-10	-	-	-	-	-	100	85-100	0-45	0-10	-	-	-
10-5	-	-	-	-	-	-	100	85-100	0-20	0-5	-	-
5-2.5	-	-	-	-	-	-	-	100	70-100	10-40	0-10	-

* Refer to CSA A23.1-09 (Table 12) for additional notes.

Table 10.2 Limits for deleterious substances* (Part a) and physical properties (Part b) of coarse aggregates (adapted from CSA, 2009)

CSA Test Method	Property	Maximum percentage by mass of total sample		
		Concrete exposed to freezing and thawing	Other exposure conditions	
A23.2-3A	Clay lumps*	0.3	0.5	(a) Deleterious substances requirements
A23.2-4A	Low-density granular materials*	0.5	1.0	
A23.2-5A	Material finer than 80 µm	1.0*	1.0*	
A23.2-13A	Flat and elongated particles			
	Procedure A, ratio 4:1; or, Procedure B	20	20	
	Flat particles	25	25	
	Elongated particles	45	45	
	Elongated particles (for pavements and HPC)	40	40	
A23.2-24A	Unconfined freeze-thaw*	6	10	
A23.2-9A	MgSO ₄ Soundness loss	12	18	
A23.2-27A	Alkali-aggregate reactivity	(Refer to CSA A23.2 Clause 4.2.3.5.1)		
A23.2-29A	Micro-Deval Abrasion Loss*	17	21	(b) Physical properties requirements
A23.2-17A	Impact and Abrasion Loss (Los Angeles test)	50	50	

* Refer to CSA A23.1-09 (Table 12) for additional notes.



‡ Note: At the engineer's discretion, if the RCA source does not meet the requirements of CSA A23.1 Cl. 4.1.1.2 (Limits on chloride ion content), it may still be considered for use in unreinforced concrete and can be assessed as either RCA Type B or C.

Figure 10.1 Process for determining whether a particular RCA source can be used as a coarse aggregate in structural concrete applications

10.3.3 Proposed RCA Performance Classes

The following RCA performance classes have been proposed based on the findings of this research. Each class has a specific set of requirements and suitable applications.

Class A1 – Consists of 100% crushed concrete or a blend of crushed concrete and natural aggregate. Satisfies the both the limits on deleterious substances and the aggregate physical properties requirements of CSA A23.1-09 Clause 4.2.3 for aggregates for use in concrete (refer to Section 10.3.3). Considered as a high quality RCA which may be used in unreinforced as well as in reinforced concrete applications.

Class A2 – Consists of 100% crushed concrete or a blend of crushed concrete and natural aggregate. Satisfies the deleterious substance limits of CSA A23.1-09 Clause 4.2.3 for aggregates for use in concrete (refer to Section 10.3.3 below). Considered as a high quality RCA which may be used in unreinforced as well as in reinforced concrete applications.

Class B – May consist of 100% crushed concrete or a blend of crushed concrete and natural aggregate. Satisfies the deleterious substance limits of CSA A23.1-09 Clause 4.2.3 for aggregates for use in concrete (refer to Section 10.3.3). This performance class of RCA is considered as a medium-grade RCA that may be used in unreinforced concrete applications of average strength.

Class C – Considered as a low-grade RCA suitable only as fill material in structural or in non-structural concrete fill applications. Satisfies the deleterious substance limits of CSA A23.1-09 Clause 4.2.3 for aggregates for use in concrete (refer to Section 10.3.3).

Based on the findings of this research, ranges of specific aggregate properties have been proposed for determining the performance class of a particular RCA source. This information has been summarized in Table 10.3.

Table 10.3 Selection chart for determining whether a particular RCA or blended RCA source is a performance class A2, B or C.

No. *	Aggregate Property	Class A1	Class A2	Class B	Class C
1	Relative Density (oven-dry)	Refer to CSA A23.1 and Table 10.1 and 10.2 for limits	2.3 and above	2.0 to 2.3	Below 2.0
2	% Adhered Mortar [†]		50% and below	Above 50%	Above 50%
3	Absorption		3% or less	3 to 6%	6% or greater
4	Abrasion Loss (Micro-Deval Method)		19 to 22%	22 to 25%	Above 25%

* To be designated as Class A2, B or C, at least three of the four aggregate properties tested must fall within the range defined by a specific class.

[†] Determined using the thermal treatment method (refer to Section 4.4.1.3) or other suitable method that ensures complete removal of adhered mortar.

When determining whether a particular RCA source falls within a specific performance class, at least three out of the four aggregate properties must fall within the range of that particular class.

For example, if an RCA source has the following properties:

Relative density (oven dry) = 2.34 (Class A2)

Adhered mortar content = 42% (Class A2)

Absorption = 4.7% (Class B)

Abrasion Resistance = 20.4% (Class A2)

According to Table 10.3, the RCA source would be designated as Class A2.

It is possible that the RCA source may be designated as a Class A1 or A2 depending on whether it is exposed to freezing and thawing. For instance, the limit for Micro-Deval abrasion loss as specified by CSA A23.1-09 (Table 12) for concrete exposed to freeze-thaw conditions is 17% whereas for concrete under other exposure conditions this limit becomes 21%. Therefore, an RCA source having a micro-deval abrasion loss of 20% would fail the CSA A23.1-09 requirements (i.e., designated as Class A2, B or C according to Table 10.3) if it is being used in concrete exposed to freezing and thawing but would satisfy the requirements (i.e., designated as Class A1) if it was being used in concrete used in other exposure conditions. In the case of the RCA sources tested as part of this research program, RCA-1 would be classified as Class A2 (or

possibly A1 depending on its impact and abrasion loss as presented in Table 10.2), RCA-2 would be Class B and RCA-3 would be Class B or C (refer to Chapter 4 for aggregate properties). In the case where an RCA source satisfies the requirements of two performance classes simultaneously (as is the case for RCA-3), the lower quality performance class governs. For example, RCA-3 met two of the requirements of Table 10.3 for to be designated as Class B and met two of the requirements to be designated as Class C. In this case, the RCA-3 source would be designated as Class C since it is the lower quality performance class.

10.3.3.1 Justification for RCA Performance Class Limits

The following section provides an explanation of how the limits were set for each of the aggregate properties outlined in Table 10.3. In general, RCAs can have variable properties and it was decided that classifying a source based on four separate properties would provide enough information on the aggregate source to confidently assign it to a particular performance class.

Relative density (oven dry)

The limits for the oven-dry relative density values were based mainly on the results of this research study. It was assumed that RCA-1, with a relative density of 2.36 would be a Class A2. Therefore, the limit for Class A2 was set as 2.30. Class B provided a fairly wide range for relative density between 2.30 and 2.00 which encompasses the majority of the RCA sources identified in the literature (refer to Section 2.2.5). Class C included RCAs that were fairly lightweight and having relative densities below 2.00.

Percent Adhered Mortar

The limits for percent adhered mortar were based mainly on this research study in which the RCA-1 would be designated as a Class A2 with an adhered mortar content of 46%. These limits were fairly basic and reflected the relatively small range of adhered mortar content of the RCAs measured for this work and those measured by other researchers (refer to Section 2.2.8). The limits designated Class A2 as being an RCA source with less than half of its mass being adhered mortar and Class B and C as being an RCA source with more than half of its weight being adhered mortar.

Absorption

The limits for absorption for Class A2 RCA were based on the Japanese Standard for high quality RCA (JIS, 2011). Limits for Class B and C were based on the results of this research study and results reported in the literature (refer to Section 2.2.4) where RCA-1 and RCA-2 would be designated as Class B and RCA-3 would be designated as Class C.

Micro-Deval Abrasion Loss

The limits for Micro-Deval abrasion loss for Class A2 RCAs were, in general, set higher than those provided by CSA A23.1 (2009) in Table 10.2. The limits for Class B and C were based on the micro-deval abrasion loss values measured for RCA-2 and RCA-3, respectively. The range was also set wide enough to reflect the range observed by other researchers (refer to Section 2.2.6).

10.3.4 RCA Concrete Mixture Proportioning Guidelines

This section outlines a set of recommended guidelines for proportioning concrete mixtures with a full or partial replacement of natural coarse aggregate by RCA. Prior to batching, all RCA types should undergo a pre-wetting process due to their high absorption capacities. Several pre-wetting procedures are presented in Table 10.4, and in general, a pre-wetting process should satisfy three requirements:

- 1) Maintain a consistent moisture content throughout the stockpile,
- 2) Be capable of being replicated over a series of various batching cycles, and
- 3) Ensure that the RCA has reached or exceeded its saturated surface dry (SSD) condition.

In general, due to their more angular shape and roughened surface texture, an RCA concrete mixture may require higher water content than an equivalent natural aggregate concrete mixture or the addition of a water-reducing admixture for equivalent workability (slump).

Table 10.4 Pre-wetting procedures for RCA prior to batching in concrete

	Procedure #1	Procedure #2
Pre-wetting procedure	Soak coarse aggregates for 24 hours prior to batching	“Pre-wet” coarse aggregates for 24 hours prior to batching
Moisture condition after pre-wetting	Ensures that aggregates have reached SSD with excess surface moisture	Does not ensure aggregates have reached SSD. Varying amounts of adhered surface moisture will be present.
Practical implications of method	Large-scale soaking 24 hours prior to batching followed by draining of coarse aggregates. This may be impractical for large-scale batching.	Large-scale pre-wetting of coarse aggregates 24 hours prior to batching requires additional effort compared to using coarse aggregate in-situ. This can be accomplished using appropriate misting or sprinkler systems.
Quality control measures	Absorption capacity and adhered surface moisture should be measured prior to batching.	Absorption capacity and adhered surface moisture should be measured at regular time intervals prior to batching. Measurements should be taken at various elevations of the stockpile.

As with the development of any new concrete mixture, several preliminary phases prior to final application are recommended:

- 1) Trial (laboratory) batching phase
- 2) Trial ready-mix batching phase
- 3) Trial field placement phase

The trial batching program should be approached systematically to assess the relation between water-binder ratio, compressive strength, workability (slump), and air content. In general, the use of water-reducing admixtures is recommended to improve workability, early-age strength and reduce cement content (by reducing water content and maintaining a constant water-cement ratio). Once all trial mixtures have been cast, select the optimum mixture proportion which satisfies all the performance requirements and still achieves satisfactory economy. See Section 10.3.5 for performance requirements of RCA concrete.

10.3.5 Performance Requirements of RCA Structural Concrete

To determine whether a particular RCA source is suitable for use in reinforced concrete, additional aggregate properties must be considered. As presented in Chapter 9, the bond strength of RCA concrete is highly influenced by the crushing strength (i.e., ACV) and the relative density of the aggregate. It is recommended that only Class A2 (or A1) RCA be used in reinforced concrete and therefore, Table 10.5 refers to Class A2 RCA sources being considered for used in reinforced concrete. The limits on aggregate strength and density proposed in Table 10.5 were set based on the results of the beam-end bond testing results of this research study. Recall that RCA-1 had the highest bond strengths as compared to the RCA-2 or RCA-3 concrete. As a result, the ACV and relative density limits in Table 10.5 were chosen as being similar to those measured in RCA-1 (i.e., RCA-1 had ACV = 23.1 and relative density = 2.36). In addition, the range of ACV values (i.e., above 24 or below 24) seems to be around the average value as those reported by other researchers (refer to Section 2.2.7). Note that the RCA source must satisfy both the ACV and relative density requirements to be used in reinforced concrete.

Table 10.5 Selection chart for determining whether a particular Class A2 RCA source may be suitable for use in reinforced concrete structures

	Reinforced Concrete*	Unreinforced Concrete
Aggregate Crushing Value (ACV)	Below 24	Above 24
Aggregate Relative Density (oven-dry)	2.30 and above	Below 2.30

* In order to be used in reinforced concrete, the RCA source must satisfy both the ACV and relative density requirements.

Whether the RCA is to be used in a reinforced or unreinforced concrete application, several concrete performance criteria must be met. As a minimum, the following concrete properties should be evaluated:

- Concrete compressive strength (early and nominal)
- Slump
- Air content (if required)
- Durability characteristics (see Section 10.3.6)
- If required, any additional concrete properties (i.e., splitting tensile strength, modulus of elasticity, etc.)

An iterative procedure has been developed to ensure that the performance requirements of a particular RCA mixture have been met. This procedure is detailed in Figure 10.2.

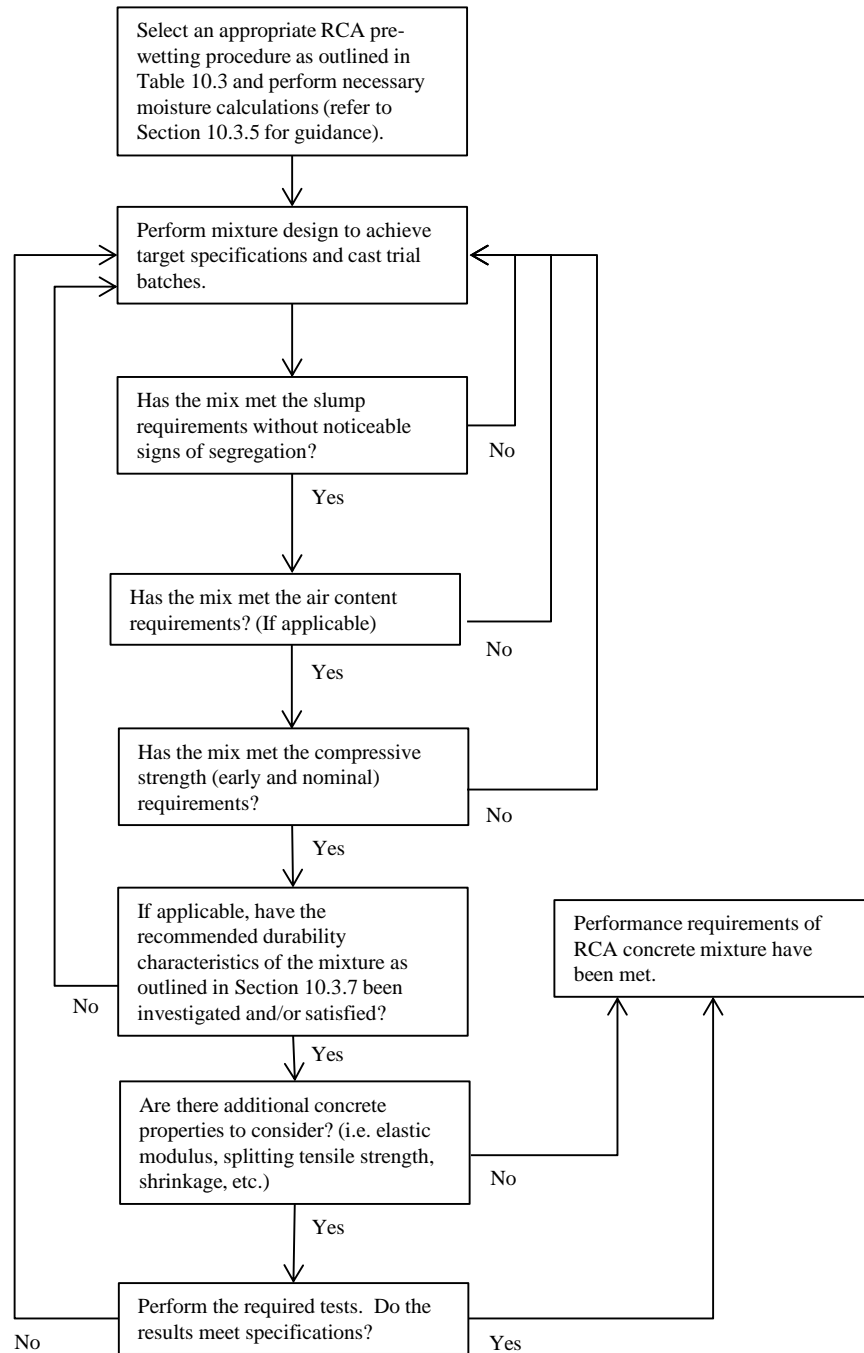


Figure 10.2 Process for assessing the performance of RCA concrete mixture proportions

10.3.6 Recommended Durability Testing for RCA Concrete

In addition to the performance requirements outlined in Section 10.3.5, an assessment of the long-term durability characteristics of an RCA concrete is also recommended. When required, the following set of durability properties should be assessed for a new RCA concrete.

- Drying Shrinkage
- Resistance to Carbonation
- Alkali-Aggregate Reactivity (should be conducted when determining whether the RCA source satisfies the requirements of CSA A23.1-09 Cl. 4.2.3)
- Sulphate Resistance
- Freeze-Thaw Resistance
- Chloride Penetration

As the durability characteristics of RCA concrete were beyond the scope of this research project, the reader is directed to Section 10.3.7 for additional references on this topic.

10.3.7 Recommended References

Table 10.6 Additional references for RCA and RCA concrete

Application	Reference
Durability of RCA Concrete	Movassaghi (2006) Shayan and Xu (2003) Sagoe-Crentsil et al. (2001) Otsuki et al. (2003)
Specialty RCA Concrete Applications	Fathifazl et al. (2011) Ajdukiewicz and Kliszczewicz (2002) Tu et al. (2006) Safiuddin et al. (2011)
Use of RCA as Fill Material	Kang et al. (2011) Park (2003)

Chapter 11: Conclusions, Contributions and Recommendations for Future Work

11.1 Overview

The following conclusions, contributions and recommendations for future work were derived based on the research presented in this thesis.

11.2 Conclusions

11.2.1 Recycled Concrete Aggregate Properties

1. The thermal treatment method is the most effective and simplest method for removing adhered mortar from RCAs.

By visual inspection, the thermal treatment method was able to remove over 95% of the adhered mortar. Adhered mortar contents of 46.4%, 55.7% and 49.6% were measured for the RCA-1, RCA-2 and RCA-3, respectively.

2. RCAs take longer to reach the saturated condition than natural aggregates due to their higher absorption capacities.

After measuring the absorption rates of each aggregate it was concluded that the natural aggregate took the least time to become fully saturated (2 hours) followed by the RCA-1 (4 hours), RCA-2 (7 hours) and the RCA-3 (8 hours). This rate of absorption was related to the amount of adhered mortar on each aggregate particle (related to the porosity of the aggregate particle). Aggregates with higher adhered mortar contents took longer to absorb water. Based on these findings, each aggregate was soaked in water for 24 hours prior concrete batching. By pre-soaking the aggregates, this would ensure that they were in a saturated condition prior to batching. This would ensure that the aggregates would not absorb any of the mixing water and increase the probability of achieving the desired water-cement ratio. Therefore, by controlling the water-cement ratio, the variability in the concrete workability and compressive strength could be reduced.

- 3. The amount of adhered surface moisture (moisture in excess of SSD) in pre-soaked aggregate could provide an indirect measure of surface texture for a range of aggregate types.**

Upon visual comparison of the shape and surface texture of the four aggregate types it was found that the RCA-1 had the most roughened surface. When the amount of free surface water present after a 24 hour soaking period was compared between each aggregate, RCA-1 had the largest amount of adhered surface moisture by weight.

- 4. The absorption of RCA particles is dependent not only on the amount of adhered mortar but also on the amount of moisture absorbed by the adhered mortar itself.**

The absorption capacity of the RCAs was not proportional to the amount of adhered mortar. This finding explained why RCA-3 which had the highest absorption (7.81%) had a smaller amount of adhered mortar than RCA-2 (49.6% versus 55.7%). The adhered mortar portion of RCA-3 accounted for 5.0% out of the 7.8% total absorption versus 2.7% out of 6.2% for the RCA-2.

- 5. As the amount of adhered mortar increases, the bulk density decreases and the absorption capacity increases.**

Due to the lower density of adhered mortar, the bulk density of the RCA particle is lower than a natural aggregate particle. Absorption capacity is related to the adhered mortar content because higher adhered mortar contents and bulk densities imply higher porosity and therefore, a larger percentage of voids in which moisture may occupy. These results confirmed similar findings reported in the literature.

- 6. A strong correlation exists between aggregate crushing value (ACV) and the Micro-Deval abrasion resistance.**

Upon examination of the aggregate crushing values and Micro-Deval abrasion resistance values for each aggregate type, a similar trend was discovered; the natural aggregate had the lowest crushing value and highest abrasion resistance followed by RCA-1, RCA-2 and RCA-3. Interaction plots with high coefficient of determination values confirmed this strong correlation between ACV and abrasion resistance. This relationship may be related to the

overall strength of the aggregate particle and its degree of brittleness when it comes in contact and is compressed against, rubbed against or collides with other aggregate particles.

11.2.2 RCA Concrete Mechanical Properties and Mixture Proportioning

- 1. Concrete produced by directly replacing natural aggregate with an equivalent volume of pre-soaked RCA while maintaining equal mixture proportions, may experience slump losses of up to 80%.**

Slump loss values were a direct result of the more roughened surface texture of the RCA particles which increased the inter-particle friction in the fresh concrete. After replacing the natural aggregate with equivalent volumes of RCA and maintaining equivalent water-cement ratios, slump values of the RCA concretes were up to 78% lower. As a result, a fairly good correlation exists between surface roughness (as determined visually and by adhered surface moisture) and slump.

- 2. A very good correlation exists between bulk density of coarse aggregate and hardened density of concrete.**

The NA concrete mixtures had the highest hardened densities followed by the RCA-1, RCA-2, and RCA-3 mixes. This was a direct result of the lower density of the adhered mortar present on the RCAs.

- 3. Concrete produced by directly replacing natural aggregate with an equivalent volume of pre-soaked RCA while maintaining equal water-cement ratios, can have higher compressive strengths than an equivalent NA concrete mixture.**

The RCA-1 concrete had compressive strengths that were up to 22% higher than the NA concrete specimens. Overall, the RCA concretes tested as part of this study had compressive strengths ranging between 81% and 122% of the compressive strength of NA concrete. In cases where fracture planes mainly passed around the aggregate particles, the increase in compressive strength of the RCA concrete is a result of the enhanced mortar-aggregate bond between the RCA and surrounding new mortar. The enhanced mortar-aggregate bond is directly related to the aggregate surface texture (as determined visually

and by adhered surface moisture). In cases where the fracture planes passed mainly through the RCA aggregate particles and both around and through the natural aggregate particles, it was inferred that the strength of the RCA is higher than the combined strength of the mortar-aggregate bond and strength of the natural aggregate.

4. The aggregate strength (as measured by the ACV) has a strong influence on the splitting tensile strength of RCA concrete.

As the ACV increases (decrease in aggregate strength), the splitting tensile strength normalized with respect to $f'_c{}^{1/2}$ decreases. In general, the majority of the fracture planes passed through the coarse aggregates in the splitting tensile strength specimens and, as a result, the strength of the aggregate (as measured by the ACV) highly influenced the splitting tensile strengths.

5. 100% replacement of natural aggregate with RCA was found to have no statistically significant effect on the linear coefficient of thermal expansion (LCTE) of concrete.

However, strong relationships were found between the LCTE, water-cement ratio and aggregate relative density. Note that only the aggregate density varies between concrete types of a certain strength level. Therefore, although differences in LCTE are not statistically significant, there is still an effect of changing coarse aggregate density on the LCTE of concrete.

6. In concrete mixtures having equivalent volumes of coarse aggregate and equivalent water-cement ratios, the modulus of elasticity normalized with respect to $f'_c{}^{1/2}$ of the NA concrete was up to 10% higher than the RCA concrete.

This is believed to be a result of the higher average secant modulus of elasticity of bulk aggregate (determined during ACV testing) of the natural aggregate as compared to the RCA.

7. A very good correlation was found between the average secant modulus of elasticity of bulk aggregate and the modulus of elasticity of concrete.

This relationship seems to agree with relations in the literature which note that for constant compressive strength, the modulus of elasticity of concrete is a function of the modulus of

elasticity of aggregate and the volumetric proportion of aggregate. Therefore, the average secant modulus of elasticity of bulk loose RCA (computed based on the ACV test) may be used to assess how replacing a natural aggregate with a particular RCA will affect the modulus of elasticity of concrete the resulting RCA concrete.

- 8. Evaluation of the fracture energy test data from this research study has provided some indication that as coarse aggregate strength increases (and ACV decreases), the fracture energy of the resulting concrete will increase.**

However, the inherent variation in fracture energy results is such that the relative differences in fracture energy between NA and RCA concrete may not be statistically significant. This is especially true when comparing RCA concrete and concrete that incorporates natural coarse aggregates of normal strength (i.e., limestone and granite).

- 9. It is feasible to produce concrete incorporating 100% RCA as coarse aggregate by adjusting only the water content, cement content and water-cement ratio to achieve compressive strengths of 30, 40, 50 and 60 MPa with slumps between 75 and 125 mm.**

However with inferior strength RCA sources (i.e., RCA-3), it may be necessary to use a high-range water reducer and/or other admixtures to achieve the desired performance requirements. While it may be possible to produce RCA concrete of higher strengths using inferior strength RCA, the high cement contents that may be required may make such mixtures economically impractical and will likely offset the environmental benefits of using RCA in concrete.

- 10. Producing concrete that replaces natural aggregate with high-quality RCA may require less cement to achieve a similar compressive strength and slump.**

Overall, RCA with a more roughened surface texture may require more water to maintain adequate workability than a concrete with equivalent mixture proportions that uses natural aggregate. This is due to the more roughened surface texture of the RCA particle that increases the inter-particle friction in the fresh concrete. However, the more roughened surface of the RCA particle may also lead to a superior mortar-aggregate bond in the resulting RCA concrete. An improvement in the mortar-aggregate bond could produce RCA concrete that requires less cement to achieve compressive strengths equivalent to that

of a NA concrete.

11.2.2 Bond Performance of RCA Concrete

- 1. Replacing natural coarse aggregate with RCA while maintaining similar compressive strengths caused a reduction in bond strength with reinforcing steel of up to 21%.**

The NA concrete beam-end specimens had $\tau_b/f_c^{1/2}$ values that were between 10 and 21% higher than the RCA concrete beam-end specimens for compressive strengths of 30 and 50 MPa and bonded lengths of 125 and 375 mm. The NA concrete beam-end specimens had $\tau_b/f_c^{1/2}$ that were between 3 and 13% higher than the RCA concrete beam-end specimens for compressive strengths of 40 and 60 MPa and bonded lengths of 125 and 450 mm. Dissections of beam-end specimens confirmed that the splitting failures occurred mainly through the aggregate particles and therefore, the aggregate strength (measured by the ACV) was a contributing factor for controlling the bond strength.

- 2. As coarse aggregate strength decreases (ACV increases), the average bond strength decreases.**

Excellent correlations were found between the ACV and the average bond strength for both Phase 1 and 2. In addition, linear regression analysis was used to confirm the dependence of bond strength on ACV. This relationship was able to explain why the NA concrete beam-end specimens had bond strengths that were higher than the equivalent RCA concrete beam-end specimens. By comparison, the ACV value of the natural aggregate was higher than those of the RCAs.

- 3. After dissection and forensic analysis of the beam-end specimens, examination of fracture planes passing mainly through the coarse aggregate confirmed the influence of the coarse aggregate strength on bond strength.**

After dissection and macro-level forensic analyses were performed on a select number of beam-end specimens, general beam-end structural behaviour and the main failure mechanism were confirmed. The NA concrete and RCA-1 concrete dissected specimens failed by splitting-induced pull-out accompanied by crushing and/or shearing off in the concrete adjacent to the ribs. The RCA-3 concrete specimens failed by splitting which was induced

by slipping at the rib faces. Splitting failures occurred mainly through the aggregate particles and this observation confirmed the strong relationship between the aggregate strength (ACV) and the bond strength.

4. Replacing natural coarse aggregate with RCA did not have a discernible effect on the general bond stress-slip response of the beam-end specimens.

While the maximum bond strengths for the NA concrete specimens were higher, the residual bond strength values and overall shape of the bond-slip curve were generally similar.

5. The experimental data (NA and RCA concretes combined) does not indicate a relationship between the normalized splitting tensile strength and bond strength, regardless of bonded length or compressive strength.

Overall, no significant correlation existed between the splitting tensile strength normalized with respect to $f'_c{}^{1/2}$ and $T_b/f'_c{}^{1/4}$ for the 125 and 450 mm bonded length specimens.

6. The experimental data (NA and RCA concretes combined) does not indicate a relationship between the modulus of rupture and bond strength, regardless of bonded length or compressive strength.

Overall, no significant correlation existed between the modulus of rupture and $T_b/f'_c{}^{1/4}$ for the 125 and 450 mm bonded length specimens.

7. Strong correlations between fracture energy and bond strength were found for the Phase 2 specimens only.

This finding supports the theories presented in the literature but is in contrast with the findings of Phase 1 where no correlation was found. Overall, when the results of Phase 1 and 2 were combined, the fracture energy was found to have a negligible effect on $T_b/f'_c{}^{1/4}$ for bonded lengths of 450 mm or shorter and for compressive strengths between 30 and 60 MPa. In terms of using fracture energy of RCA concrete as an indicator for bond strength, given the inherent variability in the measurement of fracture energy, it may be difficult to determine whether the relative differences in the fracture energy of NA concrete and the fracture energy of RCA concrete are significant enough to gauge their relative effect on the bond strength.

- 8. The theoretical development lengths for the RCA concrete beam-end specimens, as predicted by the empirically developed regression model, were up to 9% longer than the NA concrete specimens.**

This finding is in direct relation to the increase in bond strength with an increase in coarse aggregate strength (decrease in ACV). Given the limited data set from which the regression model was derived, it is not recommended that the model be used as a design equation for predicting the bond strength or development length for RCA concrete.

11.3 Contributions

The following list presents the contributions to the current state-of-the-art on RCA concrete research. They are the result of the findings and conclusions presented in this thesis.

1. Evaluation and recommendation of the thermal treatment method as being the most effective method for removal of adhered mortar on RCA particles.
2. Discovery of correlations between the following aggregate and concrete properties:
 - i. Adhered surface moisture of an aggregate particle (used as an indirect measure of surface texture/roughness) and concrete workability (slump).
 - ii. The modulus of elasticity of concrete and the average secant modulus of elasticity of bulk aggregate (determined during ACV testing).
 - iii. Fracture energy and bond strength (Phase 2 specimens only)
 - iv. Aggregate crushing value and bond strength.
3. Testing and evaluation of the most comprehensive beam-end experimental program to date for studying the effect of RCA on bond strength.
4. Development of a theoretical equation for assessing how an RCA concrete incorporating an RCA source with a particular aggregate crushing value influences the development length of reinforcement.
5. Development of an RCA classification procedure which will assist engineers, concrete producers, and aggregate suppliers characterize a particular RCA source as being suitable for use in structural or non-structural concrete applications. A detailed decision-tree approach was taken to systematically assign a performance class to an RCA source based on its measured properties.

11.4 Recommendations for Future Work

Based on the findings from this research and the current state-of-the-art of RCA concrete research, the following is a list of recommendations for future research work.

11.4.1 RCA Property Testing

1. Investigate and test additional RCA sources derived from the crushing of various concrete structures.
2. Establish a database that incorporates qualitative and quantitative data on a variety of RCA sources from around Canada. This database would enable researchers to better estimate the statistical variation in the various properties of these materials.
3. Quantify the aggregate surface texture and shape using image analysis techniques and correlate these values to the amount of adhered surface moisture.

11.4.2 RCA Concrete Mixture Proportions

1. Investigate the effect that fully or partially replacing natural sand with RCA fines (i.e. < 4.75 mm) has on the fresh and hardened properties of RCA concrete.
2. Develop commercial or ready-mix concrete mixture proportions for use in trial placement applications.

11.4.3 RCA Concrete Properties

1. Derive generalized constitutive relationships for RCA concrete that use basic RCA properties as input parameters.
2. Investigate the effect of deleterious substances (i.e., wood chips, metals, plastic, etc.) on the mechanical properties of RCA concrete. Based on this investigation, maximum limits on acceptable amounts of deleterious materials can be recommended.
3. Carry out additional studies on the effect of RCA on fracture energy of concrete.
4. Investigate the effect of RCA properties on the drying shrinkage of RCA concrete.

11.4.4 Bond Performance of RCA Concrete

1. Expand the beam-end testing program to include several other bar sizes, bonded lengths,

varied bottom and side covers and the inclusion of transverse reinforcement to study confinement effects. Develop regression models relating aggregate properties, beam end dimensions, concrete properties and bond.

2. Investigate the effect of RCA on development length using beam-splice specimens and compare results to the tested beam-end specimens.

References

- ACI Committee 211, “Standard Practice for Selecting Proportions for Normal, Heavyweight and Mass Concrete”, ACI 211.1-91, Re-approved 1997, ACI Committee 211 Report, American Concrete Institute, Farmington Hills, Michigan, 1997, 38 pages.
- ACI Committee 213, “Guide for Structural Lightweight-Aggregate Concrete”, ACI 213R-03, ACI Committee 213 Report, American Concrete Institute, Farmington Hills, Michigan, 2003, 38 pages.
- ACI Committee 214, “Guide to Evaluation of Strength Test Results of Concrete”, ACI 214R-11, ACI Committee 214 Report, American Concrete Institute, Farmington Hills, Michigan, 2011, 20 pages.
- ACI Committee 224, “Control of Cracking in Concrete Structures”, ACI 224R-01, ACI Committee 224 Report, American Concrete Institute, Farmington Hills, Michigan, 2001, 46 pages.
- ACI Committee 225, “Guide to the Selection and Use of Hydraulic Cements”, ACI 225R-99, Re-approved 2009, ACI Committee 225 Report, American Concrete Institute, Farmington Hills, Michigan, 2009, 30 pages.
- ACI Committee 318, “Building Code Requirements for Structural Concrete”, ACI 318-11, Committee 318 Report, American Concrete Institute, Farmington Hills, Michigan, 2011, 443 pages.
- ACI Committee 363, “Report on High-Strength Concrete”, ACI 363R-10, ACI Committee 363 Report, American Concrete Institute, Farmington Hills, Michigan, 2010, 69 pages.
- ACI Committee 408, “Bond and Development of Straight Reinforcing Bars in Tension”, ACI 408R-03, ACI Committee 408 Report, American Concrete Institute, Farmington Hills, Michigan, 2003, 49 pages.
- ACI Committee 408, “Opportunities in Bond Research”, ACI 408R-70, ACI Committee 408 Report, American Concrete Institute, Farmington Hills, Michigan, 1970, 11 pages.
- ACI Committee 408, “Bond Stress – The State of the Art ”, ACI 408-66, ACI Committee 408 Report, American Concrete Institute, Farmington Hills, Michigan, 1966, 30 pages.
- ACI Committee 408, “Guide for Lap Splice and Development Length of High Relative Rib Area Reinforcing Bars in Tension and Commentary”, ACI 408.3R-09, ACI Committee 408 Report, American Concrete Institute, Farmington Hills, Michigan, 2009, 12 pages.

- ACI Committee 446, “Fracture Mechanics of Concrete: Concepts, Models, and Determination of Material Properties”, ACI 446.1R-99, ACI Committee 446 Report, American Concrete Institute, Farmington Hills, Michigan, 1991 (Re-approved in 1999) , 146 pages.
- ACI Committee 555, “Removal and Reuse of Hardened Concrete”, ACI 555R-01, ACI Committee 555 Report, American Concrete Institute, Farmington Hills, Michigan, 2001, 25 pages.
- ASTM A 944-05, “Standard Test Method for Comparing Bond Strength of Steel Reinforcing Bars to Concrete Using Beam-End Specimens”, *Annual Book of ASTM Standards*, American Society for Testing and Materials, West Conshohocken, Pennsylvania, USA, 4 pgs.
- ASTM C 33 - 01, “Standard Test Method for Soundness of Aggregates by Use of Sodium Sulfate or Magnesium Sulfate”, *Annual Book of ASTM Standards*, American Society for Testing and Materials, West Conshohocken, Pennsylvania, USA.
- ASTM C 88 - 05, “Standard Test Method for Soundness of Aggregates by Use of Sodium Sulfate or Magnesium Sulfate”, *Annual Book of ASTM Standards*, American Society for Testing and Materials, West Conshohocken, Pennsylvania, USA, 5 pgs.
- ASTM C 293 - 08, “Standard Test Method for Flexural Strength of Concrete (Using Simple Beam With Center-Point Loading”, *Annual Book of ASTM Standards*, American Society for Testing and Materials, West Conshohocken, Pennsylvania, USA, 3 pgs.
- ASTM C 469 - 02, “Standard Test Method for Static Modulus of Elasticity and Poisson’s Ratio of Concrete in Compression”, *Annual Book of ASTM Standards*, American Society for Testing and Materials, West Conshohocken, Pennsylvania, USA, 5 pgs.
- ASTM C 666/C 666M - 03, “Standard Test Method for Resistance of Concrete to Rapid Freezing and Thawing”, *Annual Book of ASTM Standards*, American Society for Testing and Materials, West Conshohocken, Pennsylvania, USA, 6 pgs.
- ASTM D 3398 – 00 (Reapproved 2006), “Standard Test Method for Index of Aggregate Particle Shape and Texture”, *Annual Book of ASTM Standards*, American Society for Testing and Materials, West Conshohocken, Pennsylvania, USA, 4 pgs.
- Bazant, Z.P. and Planas, J. *Fracture and Size Effect in Concrete and Other Quasibrittle Materials*, First Edition, CRC Press LLC, United States of America, 1998, 616 pages.
- BS 812-110: 1990, “Testing Aggregates – Methods for Determination of Aggregate Crushing Value (ACV)”, *British Standards Institute*, London, England, 7 pgs.

- Abbas, A., Fathifazl, G., Isgor, O.B., Razaqpur, A.G., Fournier, B., and Foo, S., “Proposed Method for Determining the Residual Mortar Content of Recycled Concrete Aggregates”. *Journal of ASTM International*, Vol. 5, No. 1, 2008a, 12 pgs.
- Abbas, A., Fathifazl, G., Isgor, O.B., Razaqpur, A.G., Fournier, B., and Foo, S., “Durability of Recycled Aggregate Concrete Designed with Equivalent Mortar Volume (EMV) Method”, 2nd *Canadian Conference on Effective Design of Structures*, McMaster University, Hamilton, Ontario, Canada, May 20 -23, 2008b.
- Abou-Zeid, M.N., Shenouda, M.N., McCabe, S.L., and El-Tawil, F.A. “Reincarnation of Concrete”. *Concrete International*, Feb. 2005, pp. 53 – 59.
- Achtemichuk, S., Hubbard, J., Sluce, R., and Shehata, M. “Development of Controlled Low-Strength Materials Using Reclaimed Concrete Aggregates”. 2nd *Canadian Conference on Effective Design of Structures*, McMaster University, Hamilton, Ontario, Canada, May 20 -23, 2008.
- Aitcin, P.C. and Mehta, P.K. “Effect of Coarse Aggregate Characteristics on Mechanical Properties of High-Strength Concrete”. *ACI Materials Journal*, Vol. 87, No. 2, 1990, pp. 103 – 107.
- Ajdukiewicz, A. and Kliszczewicz, A. “Influence of Recycled Aggregates on Mechanical Properties of HS/HPC”. *Cement and Concrete Composites*, Vol. 24, 2002, pp. 269 – 279.
- Aydin, S., Yazici, H., Yardimci, M.Y., and Yigiter, H. “Effect of Aggregate Type on Mechanical Properties of Reactive Powder Concrete”, *ACI Materials Journal*, Vol. 107, No. 5, 2010, pp. 441 – 449.
- Bangash, M.Y.H. *Concrete and Concrete Structures: Numerical Modelling and Applications*, Elsevier Applied Science, Essex, England, 1989, 668 pgs.
- Bartlett, F.M. and MacGregor, J.G. “Statistical Analysis of the Compressive Strength of Concrete in Structures”, *ACI Materials Journal*, Vol. 93, No. 2, March – April, 1996, pp. 158 – 168.
- Bekoe, P.A., Tia, M., and Bergin, M.J. “Concrete Containing Recycled Concrete Aggregates for Use in Concrete Pavement”, *Transportation Research Record: Journal of the Transportation Research Board*, Vol. 2164, 2010, pp. 113 – 121.

- Beshr, H., Almusallam, A.A., and Maslehuddin, M. “Effect of Coarse Aggregate Quality on the Mechanical Properties of High Strength Concrete”, *Construction and Building Materials*, Vol. 17, 2003, pp. 97 – 103.
- Bordelon, A., Cervantes, V., and Roesler, J.R. “Fracture Properties of Concrete Containing Recycled Concrete Aggregates”, *Magazine of Concrete Research*, Vol. 61, No. 9, 2009, pp. 665 – 670.
- Butler, L., West, J.S., and Tighe, S.L. “Effect of RCA Properties on the Mixture Proportions of RCA Concrete Developed for Structural Applications”, *Transportation Research Record: Journal of the Transportation Research Board*, Accepted February 6, 2012.
- Butler, L., West, J.S., and Tighe, S.L. “Effect of RCA Properties on the Mixture Proportions of RCA Concrete Developed for Structural Applications”, *Annual Meeting of the Transportation Research Board Proceedings*, Washington D.C., United States, January 22 – 26, 2012.
- Butler, L., West, J.S., and Tighe, S.L. “Quantification of Recycled Concrete Aggregate (RCA) Properties for Usage in Bridges and Pavements: An Ontario Case Study”, *Annual Conference of the Transportation Association of Canada Proceedings*, Edmonton, Alberta, Canada, September 11 – 14, 2001.
- Butler, L., West, J.S., and Tighe, S.L. “The Effect of Recycled Concrete Aggregate Properties on the Bond Strength Between RCA Concrete and Steel Reinforcement”, *Cement and Concrete Research*, Vol. 41, No. 10, 2011, pp. 1037 – 1049.
- Cairns, J. and Plizzari, G.A. “Towards a Harmonised European Bond Test”, *Materials and Structures*, Vol. 36, October 2003, pp. 498 – 506.
- Canadian Urban Institute (CUI), “Between a Rock and a Hard Place: Understanding the Foundations of Ontario’s Built Future”, Report prepared by CUI for Dufferin Aggregates, Toronto, Canada, 84 pages.
- Carrasquillo, R.L, Slate, F.O. and Nilson, A.H. “Microcracking and Behaviour of High Strength Concrete under Short- and Long-Term Loadings”, *ACI Journal*, Vol. 86, No. 2, 1989, pp. 179 – 186.
- Carrasquillo, R.L, Nilson, A.H. and Slate, F.O. “Properties of High Strength Concrete Subject to Short-Term Loads”, *ACI Journal*, Vol. 78, No. 3, 1981, pp. 171 – 177.
- Casuccio, M., Torrijos, M.C., Giaccio, G., and Zerbino, R. “Failure Mechanism of Recycled Aggregate Concrete”, *Construction and Building Materials*, Vol. 22, 2008, pp. 1500 – 1506.

- CEB-FIP, “Bond of Reinforcement in Concrete”, State-of-the-art report prepared Task Group on Bond Models, Formerly Task Group 2.5, Federation Internationale du Beton, Laussane, Switzerland, 2000.
- Cement Association of Canada. “Concrete – An Important Sector of Canada’s Economy”, http://www.cement.ca/index.php/en/Economic_Contribution/Economic_Contribution.html, accessed February 2010.
- Chavez, C. and Alonso, E.E. “A Constitutive Model for Crushed Granular Aggregates which Includes Suction Effects”, *Soils and Foundations*, Vol. 43, No. 4, August 2003, pp. 215 – 227.
- Chen, H.J., Yen, T., and Chen, K.H. “Use of Building Rubbles as Recycled Aggregates”. *Cement and Concrete Research*. Vol. 33, 2003, pp. 125 – 132.
- Choi, C., Arduino, P., and Harney, M.D. “Development of a True Triaxial Apparatus for Sands and Gravels”, *Geotechnical Testing Journal*, Vol. 31, No. 1, August 2007, pp. 1 – 13.
- Choi, H.B. and Kang, K.I. “Bond Behaviour of Deformed Bars Embedded in RAC”. *Magazine of Concrete Research*. Vol. 60, No. 6, August 2008, pp. 399 – 410.
- Choi, O.C., Hadje-Ghaffari, H., Darwin, D., and McCabe, S.L. “Bond of Epoxy-Coated Reinforcement: Bar Parameters”, *ACI Materials Journal*, Vol. 88, No. 2, 1991, pp. 207 – 217.
- Choi, O.C. and Lee, W.S. “Interfacial Bond Analysis of Deformed Bars to Concrete”, *ACI Structural Journal*, Vol. 99, No. 6, 2002, pp. 750 – 756.
- Concrete Materials Recycling Association (CMRA), Case Histories – “Recycled Concrete Aggregate Ready Mix used in Structural Applications”, Accessed January 17, 2012, www.concreterecycling.org/histories.html.
- Corinaldesi, V. and Moriconi, G. “Influence of Mineral Additions on the Performance of 100% Recycled Aggregate Concrete”,
- CSA A23.1-09, “Concrete Materials and Methods of Concrete Construction”, *Canadian Standards Association*, 2009, Ottawa, Ontario, Canada.
- CSA A23.2-09, “Methods of Test and Standard Practices for Concrete”, *Canadian Standards Association*, 2009, Ottawa, Ontario, Canada.
- CSA A23.3-04, “Design of Concrete Structures”, *Canadian Standards Association*, 2004, Ottawa, Ontario, Canada.

- Darwin, D., Barham, S., Kozul, R., and Luan, S. “Fracture Energy of High-Strength Concrete”, *ACI Materials Journal*, Vol. 98, No. 5, 2001, pp. 410 – 417.
- Denis, A., Attar, A., Breysse, D., and Chauvin, J.J. “Effect of Coarse Aggregate on the Workability of Sandcrete”, *Cement and Concrete Research*, Vol. 32, 2002, pp. 701 – 706.
- DIN-4226-100 (2002), “Aggregates for mortar and concrete - Part 100: Recycled aggregates”, *Deutsches Institut für Normung (German Institute for Standardization)*, 2002, Berlin, Germany.
- Eguchi, K., Teranishi, K., Nakagome, A., Kishimoto, H., Shinozaki, K., and Narikawa, M. “Application of Recycled Coarse Aggregate by Mixture to Concrete Construction”. *Construction and Building Materials*, Vol. 21, 2007, pp. 1542 – 1551.
- Elices, M. and Rocco, C.G. “Effect of Aggregate Size on Fracture and Mechanical Properties of a Simple Concrete”, *Engineering Fracture Mechanics*, Vol. 75, 2008, pp. 3839 – 3851.
- Etkin-Johnson Group Inc., Accessed January 17, 2012, www.etkinjohnson-stapleton.com.
- Etxeberria, M. “Experimental Study on Microstructure and Structural Behaviour of Recycled Aggregate Concrete”, PhD Thesis, Universitat Politècnica de Catalunya, Barcelona, Spain, 2004, 242 pgs.
- Etxeberria, M., Vazquez, E., Mari, A., and Barra, M. “Influence of Amount of Recycled Coarse Aggregates and Production Process on Properties of Recycled Aggregate Concrete”. *Cement and Concrete Research*, Vol. 37, 2007, pp. 735 – 742.
- Fathifazl, G. “Structural Performance of Steel Reinforced Recycled Concrete Members”, PhD Thesis, Carleton University, Ottawa, Ontario, Canada, 2008, 504 pgs.
- Fathifazl, G., Razaqpur, A.G., Isgor, O.B., Abbas, A., Fournier, B., and Foo, S. “Fresh and Hardened Properties of Recycled Aggregate Concrete Proportioned by the Equivalent Mortar Volume (EMV) Method”, *2nd Canadian Conference on Effective Design of Structures*, McMaster University, Hamilton, Ontario, Canada, May 20 -23, 2008.
- Fathifazl, G., Razaqpur, A.G., Isgor, O.B., Abbas, A., Fournier, B., and Foo, S. “Flexural Performance of Reinforced Recycled Concrete Beams”, *2nd Canadian Conference on Effective Design of Structures*, McMaster University, Hamilton, Ontario, Canada, May 20 -23, 2008.

- Fathifazl, G., Razaqpur, A.G., Isgor, O.B., Abbas, A., Fournier, B., and Foo, S. “Shear Capacity Evaluation of Reinforced Recycled Concrete (RRC) Beams”, *Engineering Structures*, Vol. 33, 2011, pp. 1025 – 1033.
- Ferguson, P.M. *Reinforced Concrete Fundamentals*, Third Edition, John Wiley and Sons Inc., United States of America, 1973, 750 pages.
- Ferguson, P.M. and Thompson, J.N. “Development Length of High Strength Reinforcing Bars in Bond”, *Journal of the American Concrete Institute*, Vol. 59, No. 7, July 1962, pp. 887 – 922.
- Fernlund, J.M.R. “Image Analysis Method for Determining 3-D Shape of Coarse Aggregate”, *Cement and Concrete Research*, Vol. 35, 2005, pp. 1629 – 1637.
- Forster, S.W. “Recycled Concrete as Aggregate”, *Concrete International*, October 1986, pp. 34 – 40.
- Gokce, A., Nagataki, S., Saeki, T., and Hisada, M. “Freezing and Thawing Resistance of Air-Entrained Concrete Incorporating Recycled Coarse Aggregate: The Role of Air Content in Demolished Concrete”, *Cement and Concrete Research*, Vol. 34, 2004, pp. 799 – 806.
- Gomez-Soberon, J.M.V. “Porosity of Recycled Concrete with Substitution of Recycled Concrete Aggregate: An Experimental Study”, *Cement and Concrete Research*, Vol. 32, 2002, pp. 1301 – 1311.
- Goncalves, P. and de Brito, J. “Recycled Aggregate Concrete (RAC) – Comparative Analysis of Existing Specifications”, *Magazine of Concrete Research*, Vol. 62, No. 5, May 2010, pp. 339 – 346.
- Gonzalez-Fonteboa, B. and Martinez-Abella, F. “Shear Strength of Recycled Concrete Beams”, *Construction and Building Materials*, Vol. 21, 2007, pp. 887 – 893.
- Guinea, G.V., El-Sayed, K., Rocco, C.G., Elices, M., and Planas, J. “The Effect of the Bond Between the Matrix and the Aggregates on the Cracking Mechanism and Fracture Parameters of Concrete”, *Cement and Concrete Research*, Vol. 32, 2002, pp. 1961 – 1970.
- Hansen, T.C. “Recycled Aggregates and Recycled Aggregate Concrete Second RILEM State-of-the-Art Report Developments 1945 – 1985”, *Materials and Structures*, Vol. 19, No. 111, 1986, pp. 201 – 246.
- Hansen, T.C. and Narud, H. “Strength of Recycled Concrete Made from Crushed Concrete Coarse Aggregate”, *Concrete International*, Vol.5, No. 1, January 1983, pp. 79 – 83.

- Haralji, M.H. “Comparison of Bond Strength of Steel Bars in Normal- and High-Strength Concrete”, *Journal of Materials in Civil Engineering*, Vol. 16, No. 4, 2004, pp. 365 – 374.
- Hillerborg, A. “The Theoretical Basis of a Method to Determine the Fracture Energy G_f of Concrete”, *Materials and Structures*, Vol. 18, No. 106, 1986, pp. 291 – 296.
- Hillerborg, A., Modeer, M., and Petersson, P.E. “Analysis of Crack Formation and Crack Growth in Concrete by Means of Fracture Mechanics and Finite Elements”, *Cement and Concrete Research*, Vol. 6, 1976, pp. 773 – 782.
- Hsu, T.C. and Slate, F.O., “Tensile Bond Strength between Aggregate and Cement Paste or Mortar”, *ACI Structural Journal*, Vol. 60, No. 4, 1963, pp. 465 – 486.
- The Institution of Engineers Singapore (IES), *The Singapore Engineer*, July 2011, 52 pgs.
- International Center for Aggregates Research (ICAR), “The Effects of Aggregates Characteristics on the Performance of Portland Cement Concrete”, ICAR Research Report 104-1F, 2004, 382 pages.
- International Center for Aggregates Research (ICAR), “The Prediction of Coarse Aggregate Performance by Micro-Deval and Soundness Related Aggregate Tests”, ICAR Research Report 507-1F, 2006, 616 pages.
- Jamkar, S.S. and Rao, C.B.K. “Index of Particle Shape and Texture of Coarse Aggregate as a Parameter for Concrete Mix Proportioning”, *Cement and Concrete Research*, Vol. 34, 2004, pp. 2021 – 2027.
- JIS A 5021:2011, “Recycled Aggregate for Concrete – Class H”, *Japanese Standards Association*, 2011, Tokyo, Japan.
- JIS A 5023:2006, “Recycled Concrete Using Recycled Aggregate Class L”, *Japanese Standards Association*, 2006, Tokyo, Japan.
- Juan, M.S. and Gutierrez, P.A. “Study on the Influence of Attached Mortar Content on the Properties of Recycled Concrete Aggregate”, *Construction and Building Materials*, Vol. 23, 2009, pp. 872 – 877.
- Kang, D-H, Gupta, S.C., Ranaivoson, A.Z., Siekmeier, J. and Robersen, R. “Recycled materials as substitutes for virgin aggregates in road construction: I. Hydraulic and mechanical characteristics”, *Soil Science Society of America Journal*, Vol. 75, No. 4, July 2011, pp. 1265 – 1275.

- Katz, A., “Properties of Concrete Made with Recycled Aggregate from Partially-Hydrated Old Concrete”, *Cement and Concrete Research*, Vol. 33, 2003, pp. 703 – 711.
- Kemp, E.L. “Bond in Reinforced Concrete: Behavior and Design Criteria”, *ACI Journal*, Vol. 83, No. 1, 1986, pp. 50 – 57.
- Khatib, J.M. “Properties of Concrete Incorporating Fine Recycled Aggregate”, *Cement and Concrete Research*, Vol. 35, 2005, pp. 763 – 769.
- Kim, H. “Automation of Aggregate Characterization Using Laser Profiling and Digital Image Analysis”, PhD Thesis, The University of Texas at Austin, Austin, Texas, USA, 2002, 201 pgs.
- Kosmatka, S.H., Kerkhoff, B., Panarese, W.C., MacLeod, N.F., and McGrath, R.J. *Design and Control of Concrete Mixtures*, Seventh Edition, Cement Association of Canada, Ottawa, Ontario, Canada, 2002.
- Lam, D. and El-Lobody, E. “Behaviour of Headed Shear Stud Connectors in Composite Beam”, *ASCE Journal of Structural Engineering*, Vol. 131, No. 1, 2005, pp. 96 – 107.
- Levy, S.M. and Helene, P. “Durability of Recycled Aggregates Concrete: A Safe Way to Sustainable Development”, *Cement and Concrete Research*, Vol. 34, 2004, 1975 – 1980.
- Limbachiya, M.C. “Recycled Aggregates: Production, Properties and Value-added Sustainable Applications”, *Journal of Wuhan University of Technology – Materials Science Edition*, Vol. 21, No. 6, pp. 1011 – 1016.
- Lin, Y.H., Tyan, Y.Y., Chang, T.P., and Chang, C.Y. “An Assessment of Optimal Mixture for Concrete Made with Recycled Concrete Aggregates”, *Cement and Concrete Research*, Vol. 34, 2004, pp. 1373 – 1380.
- Liu, Q., Xiao, J., and Sun, Z. “Experimental Study on the Failure Mechanism of Recycled Concrete”, *Cement and Concrete Research*, Vol. 41, 2011, pp. 1050 – 1057.
- Luchko, I.I. “Basic Concepts of the Fracture Mechanics of Reinforced Concrete”, *Materials Science*, Vol. 31, No. 4, 1995, pp. 448 – 453.
- Lutz, L.A, and Gergely, P. “Mechanics of Bond and Slip of Deformed Bars in Concrete”, *ACI Journal*, Vol. 64, November 1967, pp. 711 – 721.
- Lydon, F.D. and Balendran, R.V. “Some Observations on Elastic Properties of Plain Concrete”, *Cement and Concrete Research*, Vol. 16, No. 3, 1986, pp. 314 – 324.

- MacGregor, J.G. and Bartlett, F.M. *Reinforced Concrete Mechanics and Design*, First Edition, Prentice Hall Canada Inc., Toronto, Ontario, Canada, 2000, 1042 pages.
- Martin, J., Stanton, J., Mitra, N., and Lowes, L.N. “Experimental Testing to Determine Concrete Fracture Energy Using Simple Laboratory Test Setup”, *ACI Materials Journal*, Vol. 104, No. 5, 2007, pp. 575 – 584.
- Masood, A., Ahmad, T., Arif, M., and Mahdi, F. “Waste Management Strategies for Concrete”, *Environmental Engineering Policy*, Vol. 3, 2002, pp. 15 – 18.
- McCabe, S.L., Darwin, D., Choi, O.C., and Hadje-Ghaffari, H. “Application of Fracture Mechanics to Steel-Concrete Bond Analysis”, *ACI Special Publication SP 134-6*, American Concrete Institute, Farmington Hills, Michigan, Sept.1, 1992, pp. 101 – 114.
- Mehta, P.K. and Monteiro, P.J.M. *Concrete Microstructure, Properties, and Materials*, McGraw-Hill Companies Inc., New York, USA, 2006.
- Meyer, C. “The Greening of the Concrete Industry”, *2nd Canadian Conference on Effective Design of Structures*, McMaster University, Hamilton, Ontario, Canada, May 20 -23, 2008.
- Miller, G. “Running Out of Gravel and Rock, But What is the True State of our Aggregates Resource?”, *Toronto Star*, January 6th, 2005, p. A22.
- Mindess, S., Young, J.F., and Darwin, D. *Concrete*, Second Edition, Prentice Hall, Upper Saddle River, New Jersey, USA, 2003, 644 pages.
- Mirza, S.A., Hatzinikolas, M. and MacGregor, J.G. “Statistical Descriptions of the Strength of Concrete”, *Proceedings ASCE, Journal of the Structural Division*, Vol. 105, No. ST6, June 1979, pp. 1021 – 1037.
- Mitchell, D.W. and Marzouk, H. “Bond Characteristics of High-Strength Lightweight Concrete”, *ACI Structural Journal*, Vol. 104, No. 1, January – February, 2007, pp.22 – 29.
- Movassaghi, R. “Durability of Reinforced Concrete Incorporating Recycled Concrete as Aggregate”, MASC Thesis, University of Waterloo, Waterloo, Ontario, Canada, 2006, 159 pgs.
- Nagataki, S., Gokce, A., Saeki, T., and Hisada, M. “Assessment of Recycling Process Induced Damage Sensitivity of Recycled Concrete Aggregates”, *Cement and Concrete Research*, Vol. 34, 2004, 965 – 971.

- Nagataki, S. and Lida, K. “Recycling of Demolished Concrete”, *Proceedings of the Fifth CANMET/ACI International Conference on Recent Advances in Concrete Technology*, ACI SP-200, V.M. Malhorta, ed. American Concrete Institute, Farmington Hills, Michigan, USA, 2001, pp. 1 – 20.
- National Cooperative Highway Research Program, “Test Methods for Characterizing Aggregate Shape, Texture, and Angularity”, *NCHRP Report 555*, 2007, 94 pages.
- Neville, A.M. *Properties of Concrete*, Fourth Edition, Prentice Hall, Essex, England, 1997, 844 pgs.
- Neville, A.M., “Aggregate Bond and Modulus of Elasticity of Concrete”, *ACI Materials Journal*, Vol. 94, No. 1, Jan. – Feb. 1997, pp. 71 – 74.
- Novokshchenov, V. and Whitcomb, W. “How to Obtain High-Strength Concrete Using Low-Density Aggregate”, *ACI Special Publication*, SP 121-33, Nov. 1, 1990, 18 pages.
- Obla, K.H. and Kim, H. “Sustainable Concrete Through Reuse of Crushed Returned Concrete”, *Transportation Research Record: Journal of the Transportation Research Board*, Vol. 2113, 2009, pp. 114 – 121.
- Oikonomou, N.D. “Recycled Concrete Aggregates”, *Cement and Concrete Composites*, Vol. 27, 2005, pp. 315 – 318.
- Oluokun, F.A. “Prediction of Concrete Tensile Strength from its Compressive Strength: Evaluation of Existing Relationships for Normal-Weight Concrete”, *ACI Materials Journal*, Vol. 88, No. 3, May – June, 1991, pp. 302 – 309.
- Ong, K.C.G. and Ravindrarajah, R.S. “Mechanical Properties and Fracture Energy of Recycled-Aggregate Concretes”, *Proceedings of the SEM/RILEM International Conference on Fracture of Concrete and Rock*, Houston, Texas, June 1987, pp. 150 – 158.
- Ontario Ministry of Natural Resources (MNR), “State of the Aggregate Resource in Ontario Study – Consolidated Report”, Feb. 2010, 34 pages.
- Ontario Ministry of Transportation (MTO). “Material Specification for Aggregates – Concrete”, OPSS 1002, 2004.
- Ontario Ministry of Transportation (MTO). “Method of Test for Freezing and Thawing of Coarse Aggregate”, MTO LS-614, 2001.
- Ontario Stone, Sand and Gravel Association (OSSGA). “The Importance of Aggregates”, Mississauga, Ontario, Canada., 5 pgs.

- Orangun, C.O., Jirsa, J.O., and Breen, J.E. “A Reevaluation of Test Data on Development Length and Splices”, *Journal of the American Concrete Institute*, Vol. 59, March 1977, pp. 114 – 122.
- Otsuki, N., Miyazato, S.I., and Yodsudjai, W. “Influence of Recycled Aggregate on Interfacial Transition Zone, Strength, Chloride Penetration and Carbonation of Concrete”, *ASCE Journal of Materials in Civil Engineering*, September/October 2003, pp. 443 – 451.
- Padmini, A.K., Ratnamurthy, K., and Mathews, M.S. “Influence of Parent Concrete on the Properties of Recycled Aggregate Concrete”, *Construction and Building Materials*, Vol. 23, 2009, pp. 829 – 836.
- Park, R. and Paulay, T. *Reinforced Concrete Structures*, John Wiley and Sons Inc., New York, United States of America, 1975.
- Park, T. “Application of Construction and Building Debris as Base and Subbase Materials in Rigid Pavements”, *ASCE Journal of Transportation Engineering*, Vol. 129, No. 5, 2003, pp. 558 – 563.
- Parkin, R.M., Calkin, D.W., and Jackson, M.R. “Roadstone Aggregate: An Intelligent Opto-Mechatronic Product Classifier for Sizing and Grading”, *Mechatronics*, Vol. 5, No. 5, 1995, pp. 461 – 467.
- Pauw, A. “Static Modulus of Elasticity of Concrete as Affected by Density”, *ACI Journal Proceedings*, Vol. 57, No. 12, Dec. 1960, pp. 679 – 687.
- Pembina Institute, “Rebalancing the Load: The Need for an Aggregates Conservation Strategy for Ontario”, January 25, 2005, 37 pages.
- Poon, C.S., Shui, Z.H., and Lam, L. “Effect of Microstructure of ITZ on Compressive Strength of Concrete Prepared with Recycled Aggregates”, *Construction and Building Materials*, Vol. 18, 2004a, pp. 461 – 468.
- Poon, C.S., Shui, Z.H., Lam, Fok, H., and Kou, S.C. “Influence of Moisture States of Natural and Recycled Aggregates on the Slump and Compressive Strength of Concrete”, *Cement and Concrete Research*, Vol. 34, 2004b, pp. 31 – 36.
- Popovics, S. “Another Look at the Relationship between Strength and Composition of Concrete”, *ACI Materials Journal*, Vol. 108, No. 2, March – April 2011, pp. 115 – 119.

- Popovics, S. and Popovics, J.S. “The Foundation of a Computer Program for the Advanced Utilization of w/c and Air Content in Concrete Proportioning”, *Concrete International*, Dec. 1994, pp. 21 – 26.
- Popovics, S. “Analysis of the Concrete Strength versus Water-Cement Ratio Relationship”, *ACI Materials Journal*, Vol. 87, No. 5, Sept. – Oct. 1990, pp. 517 – 529.
- Prasad, B.K.R., Bharatkumar, B.H., Murthy, D.S.R., Narayanan, R., and Gopalakrishnan, S. “Fracture Mechanics Model for Analysis of Plain and Reinforced High-Performance Concrete Beams”, *ASCE Journal of Engineering Mechanics*, Vol. 131, No. 8, 2005, pp. 831 – 838.
- Rahal, K. “Mechanical Properties of Concrete with Recycled Coarse Aggregate”, *Building and Environment*, Vol. 42., 2007, pp. 407 – 415.
- Rakshvir, M. and Barai, S.V. “Studies on Recycled Aggregates-Based Concrete”, *Waste Management and Research*, Vol. 24, 2006, pp. 225 – 233.
- Rao, A., Jha, K.N., and Misra, S. “Use of Aggregates from Recycled Construction and Demolition Waste in Concrete”, *Resources Conservation and Recycling*, Vol. 50, 2007, pp. 71 – 81.
- Rao, G.A. and Prasad, B.K.R. “Influence of the Roughness of Aggregate Surface on the Interface Bond Strength”, *Cement and Concrete Research*, Vol. 32, 2002, pp. 253 – 257.
- RILEM, TC 151-DRG Guidance for Demolition and Reuse of Concrete and Masonry. “Specifications for Concrete with Recycled Aggregates”, RILEM Recommendation, *Materials and Structures*, Vol. 27, 1994, pp. 557 – 559.
- RILEM, TC 148-SSC Test Methods for the Strain-Softening Response of Concrete. “Strain-Softening of Concrete in Uniaxial Compression”, RILEM Report, *Materials and Structures*, Vol. 30, May 1997, pp. 195 – 209.
- RILEM, TC 89-FMT Fracture Mechanics of Concrete – Test Methods. “Size Effect Method for Determining Fracture Energy and Process Zone Size of Concrete”, RILEM Recommendation, *Materials and Structures*, Vol. 23, 1990, pp. 461 – 465.
- RILEM, TC 50-FMC Fracture Mechanics of Concrete. “Determination of the Fracture Energy of Mortar and Concrete by Means of Three-Point Bend Tests on Notched Beams”, RILEM Recommendation, *Materials and Structures*, Vol. 18, No. 106, 1985, pp. 287 – 290.

- Robinson, G.R., Menzie, W.D., and Hyun, H. “Recycling of Construction Debris as Aggregate in the Mid-Atlantic Region, USA”, *Resources Conservation and Recycling*, Vol. 42, 2004, pp. 275 – 294.
- Safiuddin, M., Elengaram, U.J., Salam, M.A., Zumaat, M.Z., Jaafar, F.F., Saad, H.B. “Properties of High-Workability Concrete with Recycled Concrete Aggregate”, *Materials Research*, Vol. 14, No. 2, 2011, pp. 248 – 255.
- Sago-Crentsil, K.K., Brown, T., and Taylor, A.H. “Performance of Concrete Made with Commercially Produced Coarse Recycled Concrete Aggregate”, *Cement and Concrete Research*, Vol. 31, 2001, pp. 707 – 712.
- Sani, D., Moriconi, G, Fava, G., and Corinaldesi, V. “Leaching and Mechanical Behaviour of Concrete Manufactured with Recycled Aggregates”, *Waste Management*, Vol. 25, 2005, pp. 177 – 182.
- Shah, S.P., Swartz, S.E., and Ouyang, C. *Fracture Mechanics of Concrete*, John Wiley and Sons, New York, 1995, 552 pgs.
- Sharaf, H., West, J.S., Soudki, K.A., and Campbell, T.I. “Effect of Temperature on Structural Performance of Stainless Steel Reinforcement.” *Final Report - Ontario Ministry of Transportation Highway Infrastructure Innovations Funding Program*, University of Waterloo, January 2005, 82 pages.
- Shayan, A. and Xu, A. “Performance and Properties of Structural Concrete Made with Recycled Concrete Aggregate”, *ACI Materials Journal*, Vol. 100, No. 5, Sept.-Oct. 2003, pp. 371 – 380.
- Smith, J.T. “Recycled Concrete Aggregate – A Viable Aggregate Source for Concrete Pavements”, PhD Thesis, University of Waterloo, Waterloo, Ontario, Canada, 2009, 224 pgs.
- Smith, J.T. “Recycled Concrete Aggregate Coefficient of Thermal Expansion: Characterization, Variability, and Impacts on Pavement Performance”, *Transportation Research Record: Journal of the Transportation Research Board*, Vol. 2113, 2009, pp. 53 – 61.
- Swaddiwudhipong, S., Lu, H.R., and Wee, T.H. “Direct Tension Test and Tensile Strain Capacity of Concrete at Early Age”, *Cement and Concrete Research*, Vol. 33, 2003, pp. 2077 – 2084.
- Tam, V.W.Y, and Tam, C.M. “Parameters for Recycled Aggregate and their Correlation”, *Waste Management and Research*, Vol. 21, 2007, pp. 879 – 886.

- Tam, V.W.Y., Gao, X.F., Tam, C.M., and Chen, C.H. “New Approach in Measuring Water Absorption of Recycled Aggregates”, *Construction and Building Materials*, Vol. 22, 2008, pp. 364 – 369.
- Tam, V.W.Y., and Tam, C.M. “Crushed Aggregate Production from Centralized Combined and Individual Waste Sources in Hong Kong”, *Construction and Building Materials*, Vol. 21, 2007, pp. 879 – 886.
- Tang, T., Shah, S.P., and Ouyang, C. “Fracture Mechanics and Size Effect of Concrete in Tension”, *ASCE Journal of Structural Engineering*, Vol. 118, No. 11, 1992, pp. 3169 – 3185.
- Tastani, S.P. and Pantazopoulou, S.J. “Experimental Evaluation of the Direct Tension – Pullout Bond Test”, *Conference on Bond of Concrete – from Research to Standards*, Budapest, Hungary, 2002, 8 pgs.
- Topcu, I.B. and Sengel, S. “Properties of Concretes Produced with Waste Concrete Aggregate”, *Cement and Concrete Research*, Vol. 34, 2004, 1307 – 1312.
- Tavakoli, M. and Soroushian, P. “Drying Shrinkage Behaviour of Recycled Aggregate Concrete”, *Concrete International*, November 1996, pp. 58 – 61.
- Tu, T.Y., Chen, Y.Y., and Hwang, C.L. “Properties of HPC with Recycled Aggregates”, *Cement and Concrete Research*, Vol. 36, 2006, pp. 943 – 950.
- Vancura, M., Khazanovich, L, and Tompkins, D. “Reappraisal of Recycled Concrete Aggregate as Coarse Aggregate in Concretes for Rigid Pavements”, *Transportation Research Record: Journal of the Transportation Research Board*, Vol. 2113, 2009, pp. 149 – 155.
- Walpole, R.E., Myers, R.H., Myers, S.L. and Ye, K. *Probability and Statistics for Engineers and Scientists*, Eighth Edition, Prentice Hall, Upper Saddle River, United States, 2007, 816 pgs.
- Wilburn, D.R. and Goonan, T.G., “Aggregates from Natural and Recycled Sources: Economic Assessments for Construction Applications – A Materials Flow Analysis”, *United States Geological Survey Circular Report 1176*, 1998, 40 pages.
- Xiao, J. and Falkner, H. “Bond Behaviour Between Recycled Aggregate Concrete and Steel Rebars”, *Construction and Building Materials*, Vol. 21, 2007, 395 – 401.
- Xiao, J., Li, J., and Zhang, C. “Mechanical Properties of Recycled Aggregate Concrete Under Uniaxial Loading”, *Cement and Concrete Research*, Vol. 35, 2005, pp. 1187 – 1194.

- Xiao, J., Li, J., and Zhang, C. “On Relationships Between the Mechanical Properties of Recycled Aggregate Concrete: An Overview”, *Materials and Structures*, Vol. 39, 2006, pp. 655 – 664.
- Yang, D., Hao, Y. and Wang, T. “Experimental Research on Recycled Aggregate Concrete for Highway Pavement”, *International Conference of Chinese Transportation Professionals 2010*, 7 pages.
- Yamasaki, J. and Nimura, S. “A Study on the Evaluating System of Aggregate Performance Using Recycled Fine Aggregate Mortar”, *Journal of the Society of Materials Science, Japan*, Vol. 49, No. 10, pp. 1085 – 1090.
- Yiu, L.C., Tam, V.W.Y. and Kotrayothar, D. “A Simplified Testing Approach for Recycled Coarse Aggregate in Construction”, *The Hong Kong Institution of Engineers Transactions*, Vol. 16, No. 4, pp. 43 – 47.
- Zhang, W. and Ingham, J.M. “Using Recycled Concrete Aggregates in New Zealand Ready-Mix Concrete Production”, *Journal of Materials in Civil Engineering*, Vol. 22, No.5, May 2010, pp. 443 – 450.
- Zoldners, N.G., “Thermal Properties of Concrete Under Sustained Elevated Temperatures”, *ACI Materials Journal*, SP25-1, Vol. 25, 1971, 31 pgs.
- Zuo, J. and Darwin, D. “Splice Strength of Conventional and High Relative Rib Area Bars in Normal and High-Strength Concrete”, *ACI Structural Journal*, Vol. 97, No. 4, 2000, pp. 630 – 641.

Appendix A: Trial Concrete Mixture Proportions

The following sections present a total of 47 trial mixture proportions that were used in the development of the control and strength-based mixtures. Note that a total of 18 mixtures were not presented as they were rejected based on measurement and/or calculation error. Only the basic mixture proportions (i.e., water-cement ratio and water content) which were adjusted to achieve the specified strength and slump targets are presented.

A.1 NAC-30 Mixtures (Phase 1)

	Rev. 0 [†]	Rev. 1 [†]	Rev. 2 [†]	Rev. 3 [†]	Rev. 4 [‡]
Water-cement ratio*	0.51	0.60	0.60	0.60	0.60
Water (kg/m ³)*	205	190	175	160	160
Cement (kg/m ³)*	402	317	292	267	267
Slump (mm)	75	195	160	90	90
7 day f'_c (MPa)	31.2	Did not cast – high slump	Did not cast – high slump	26.1	28.1
28 day f'_c (MPa) [§]	38.5	N/A	N/A	34.4	37.1
7 d % f'_c [§]	81%	N/A	N/A	76%	76%

Note: 28 day compressive strength target = 30 MPa; initial slump target range = 75 to 125 mm.

* Water content values reported do not include adjustments for aggregate water absorption

[†] Coarse aggregates were pre-soaked 30 minutes prior to batching.

[‡] Coarse aggregates were pre-soaked for 24 hours prior to batching.

[§] No data was available.

A.2 NAC-50 Mixtures (Phase 1)

	Rev. 1 [†]	Rev. 2 [†]	Rev. 3 [†]	Rev. 4 [‡]
Water-cement ratio*	0.44	0.37	0.38	0.38
Water (kg/m ³)*	165	175	180	180
Cement (kg/m ³)*	375	473	474	474
Slump (mm)	90	60	90	85
7 day f'_c (MPa)	39.9	43.7	43.3	45.9
28 day f'_c (MPa) [§]	N/A	N/A	48.6	55.1
7 d % f'_c [§]	N/A	N/A	89%	83%

Note: 28 day compressive strength target = 50 MPa; initial slump target range = 75 to 125 mm.

* Water content values reported do not include adjustments for aggregate water absorption

[†] Coarse aggregates were pre-soaked 30 minutes prior to batching.

[‡] Coarse aggregates were pre-soaked for 24 hours prior to batching.

[§] No data was available.

A.3 RAC1-30 Mixtures (Phase 1)

	Rev. 2 [†]	Rev. 3 [‡]	Rev. 4 [‡]	Rev. 5 [‡]	Rev. 6 [‡]	Rev. 7 [‡]
Water-cement ratio*	0.60	0.65	0.66	0.70	0.69	0.72
Water (kg/m ³)*	160	170	180	184	177	175
Cement (kg/m ³)*	267	262	273	263	257	243
Slump (mm)	30	45	80	150	85	80
7 day f'_c (MPa)	31.9	27.9	29.3	Did not cast – high slump	27.8	22.7
28 day f'_c (MPa) [§]	43.5	40.4	42.0	N/A	40.0	35.3
7 d % f'_c [§]	73%	69%	70%	N/A	70%	64%

Note: 28 day compressive strength target = 30 MPa; initial slump target range = 75 to 125 mm.

* Water content values reported do not include adjustments for aggregate water absorption

[†] Coarse aggregates were pre-soaked 30 minutes prior to batching.

[‡] Coarse aggregates were pre-soaked for 24 hours prior to batching.

[§] No data was available.

A.4 RAC1-50 Mixtures (Phase 1)

	Rev. 2 [†]	Rev. 3 [‡]	Rev. 4 [‡]	Rev. 5 [‡]
Water-cement ratio*	0.38	0.42	0.45	0.47
Water (kg/m ³)*	180	195	187	190
Cement (kg/m ³)*	474	464	416	404
Slump (mm)	40	45	75	85
7 day f'_c (MPa)	53.0	47.6	45.3	43.0
28 day f'_c (MPa)	64.7	59.8	54.6	53.5
7 d % f'_c	82%	80%	83%	80%

Note: 28 day compressive strength target = 50 MPa; initial slump target range = 75 to 125 mm.

* Water content values reported do not include adjustments for aggregate water absorption

[‡] Coarse aggregates were pre-soaked for 24 hours prior to batching.

A.5 RAC2-30 Mixtures (Phase 1)

	Rev. 1 [‡]	Rev. 2 [‡]	Rev. 3 [‡]
Water-cement ratio*	0.62	0.62	0.63
Water (kg/m ³)*	175	165	165
Cement (kg/m ³)*	282	266	262
Slump (mm)	180	80	90
7 day f _c (MPa)	22.3	23.3	20.7
28 day f _c (MPa)	32.3	34.8	31.5
7 d % f _c	69%	67%	66%

Note: 28 day compressive strength target = 30 MPa; initial slump target range = 75 to 125 mm.

* Water content values reported do not include adjustments for aggregate water absorption

[‡] Coarse aggregates were pre-soaked for 24 hours prior to batching.

A.6 RAC2-50 Mixtures (Phase 1)

	Rev. 1 [‡]	Rev. 2 [‡]	Rev. 3 [‡]
Water-cement ratio*	0.38	0.38	0.38
Water (kg/m ³)*	180	183	190
Cement (kg/m ³)*	474	482	500
Slump (mm)	75	40	85
7 day f _c (MPa)	42.4	44.5	40.8
28 day f _c (MPa)	54	55.7	50.6
7 d % f _c	79%	80%	81%

Note: 28 day compressive strength target = 50 MPa; initial slump target range = 75 to 125 mm.

* Water content values reported do not include adjustments for aggregate water absorption

[†] Coarse aggregates were pre-soaked 30 minutes prior to batching.

[‡] Coarse aggregates were pre-soaked for 24 hours prior to batching.

A.7 NAC-40 Mixtures (Phase 2)

	Rev. 1 [‡]	Rev. 2 [†]
Water-cement ratio*	0.60	0.59
Water (kg/m ³)*	160	160
Cement (kg/m ³)*	267	271
Slump (mm)	50	115
7 day f _c (MPa)	29.6	25.3
28 day f _c (MPa)	41.7	38.9
7 d % f _c	71%	65%

Note: 28 day compressive strength target = 40 MPa; initial slump target range = 75 to 125 mm. Phase 1 mixture proportions were adjusted to achieve targets.

* Water content values reported do not include adjustments for aggregate water absorption

[‡] Coarse aggregates were pre-soaked for 24 hours prior to batching and used old Portland cement in mixtures.

[†] Used new Portland cement in mixtures.

A.8 NAC-60 Mixtures (Phase 2)

	Rev. 1 [‡]	Rev. 2 [‡]
Water-cement ratio*	0.38	0.37
Water (kg/m ³)*	180	180
Cement (kg/m ³)*	474	486
Slump (mm)	115	115
7 day f _c (MPa)	41.6	47.6
28 day f _c (MPa)	57.7	61.9
7 d % f _c	72%	77%

Note: 28 day compressive strength target = 60 MPa; initial slump target range = 75 to 125 mm. Phase 1 mixture proportions were adjusted to achieve targets.

* Water content values reported do not include adjustments for aggregate water absorption

[‡] Coarse aggregates were pre-soaked for 24 hours prior to batching.

A.9 RAC1-40 Mixtures (Phase 2)

	Rev. 1 [‡]	Rev. 2 [‡]
Water-cement ratio*	0.65	0.64
Water (kg/m ³)*	175	180
Cement (kg/m ³)*	269	281
Slump (mm)	75	115
7 day f _c (MPa)	25.0	26.0
28 day f _c (MPa)	37.6	38.6
7 d % f _c	66%	67%

Note: 28 day compressive strength target = 40 MPa; initial slump target range = 75 to 125 mm.

* Water content values reported do not include adjustments for aggregate water absorption

[‡] Coarse aggregates were pre-soaked for 24 hours prior to batching.

A.10 RAC1-60 Mixtures (Phase 2)

	Rev. 1 [‡]	Rev. 2 [‡]	Rev. 3 [‡]
Water-cement ratio*	0.45	0.45	0.41
Water (kg/m ³)*	190	190	190
Cement (kg/m ³)*	422	422	463
Slump (mm)	95	100	80
7 day f _c (MPa)	43.4	40.2	47.7
28 day f _c (MPa)	60.4	53.1	60.1
7 d % f _c	72%	76%	79%

Note: 28 day compressive strength target = 60 MPa; initial slump target range = 75 to 125 mm.

* Water content values reported do not include adjustments for aggregate water absorption

[‡] Coarse aggregates were pre-soaked for 24 hours prior to batching.

A.11 RAC2-40 Mixtures (Phase 2)

	Rev. 0 [‡]	Rev. 1 [‡]
Water-cement ratio*	0.59	0.59
Water (kg/m ³)*	160	165
Cement (kg/m ³)*	271	280
Slump (mm)	45	75
7 day f _c (MPa)	24.5	22.9
28 day f _c (MPa)	37.8	38.1
7 d % f _c	65%	60%

Note: 28 day compressive strength target = 40 MPa; initial slump target range = 75 to 125 mm.

* Water content values reported do not include adjustments for aggregate water absorption

[‡] Coarse aggregates were pre-soaked for 24 hours prior to batching. These mixture proportions are based on the direct replacement mixture.

A.12 RAC2-60 Mixtures (Phase 2)

	Rev. 1 [‡]	Rev. 2 [‡]	Rev. 3 [‡]
Water-cement ratio*	0.33	0.36	0.37
Water (kg/m ³)*	190	190	180
Water Reducer (mL/kg cement)	0	0	4.5
Cement (kg/m ³)*	576	528	486
Slump (mm)	40	85	105
7 day f _c (MPa)	48.9	41.1	48.1
28 day f _c (MPa)	65.9	53.3	60.2
7 d % f _c	74%	77%	80%

Note: 28 day compressive strength target = 60 MPa; initial slump target range = 75 to 125 mm.

* Water content values reported do not include adjustments for aggregate water absorption

[‡] Coarse aggregates were pre-soaked for 24 hours prior to batching.

A.13 RAC3-40 Mixtures (Phase 2)

	Rev. 1 [‡]	Rev. 2 [‡]	Rev. 3 [‡]
Water-cement ratio*	0.52	0.51	0.49
Water (kg/m ³)*	160	165	165
Cement (kg/m ³)*	308	324	337
Slump (mm)	75	90	80
7 day f _c (MPa)	24.9	26.4	31.4
28 day f _c (MPa)	38.3	37.1	42.9
7 d % f _c	65%	71%	73%

Note: 28 day compressive strength target = 40 MPa; initial slump target range = 75 to 125 mm.

* Water content values reported do not include adjustments for aggregate water absorption

[‡] Coarse aggregates were pre-soaked for 24 hours prior to batching.

A.14 RAC3-60 Mixtures (Phase 2)

	Rev. 1‡	Rev. 2‡	Rev. 3‡	Rev. 4‡	Rev. 5‡
Water-cement ratio*	0.33	0.33	0.30	0.33	0.30
Water (kg/m ³)*	180	215	225	180	180
Water Reducer (mL/kg cement)	0	0	0	4.0	7.0
Cement (kg/m ³)*	545	652	750	545	600
Slump (mm)	45	75	60	75	100
7 day f _c (MPa)	44.0	42.4	43.6	47.7	55.0
28 day f _c (MPa)	54.6	47.6	46.8	58.7	62.8
7 d % f _c	81%	89%	93%	81%	88%

Note: 28 day compressive strength target = 60 MPa; initial slump target range = 75 to 125 mm.

* Water content values reported do not include adjustments for aggregate water absorption

‡ Coarse aggregates were pre-soaked for 24 hours prior to batching.

Appendix B: Sample Statistical Calculations

B.1 Multiple Comparisons of Means using the Least Significant Difference Method

Sample Calculations:

Consider the compressive strength results for the 60 MPa direct replacement mixes (Phase 2):

f_c values in MPa	NAC	RAC1	RAC2	RAC3
#1	62.01	70.72	64.53	49.62
#2	62.40	68.19	60.85	48.69
#3	61.18	69.47	62.29	51.02
Mean	61.9	69.5	62.6	49.8

Steps in determining the 5% LSD value:

1. Choose $b = 0.05$ corresponding the 5% significance level.
2. Set $k = 4$ as the total number of concrete types (i.e. NAC, RAC1, RAC2 and RAC3)
3. Calculate $N = 12$ as the total number of compressive strength test results for all 4 concrete types.
4. Calculate $n = 3$ as the average number of compressive strength results per concrete type.
5. Calculate a value of α used for the t-test calculation as,

$$\alpha = \frac{b}{k(k-1)/2} = \frac{0.05}{4(4-1)/2} = 0.00833$$

6. Calculate the t-statistic as $t_{\alpha/2, N-k} = t_{0.00833/2, 12-4} = t_{0.005, 8} = 3.479$
7. Calculate the mean square within concrete types as the sum of squares ($SS = 200.674$) divided by the degrees of freedom with concrete types (i.e., $N - k = 8$).

Note: a one-way or single-factor ANOVA analysis was carried out using EXCEL to calculate these values:

Anova: Single Factor

SUMMARY

<i>Groups</i>	<i>Count</i>	<i>Sum</i>	<i>Average</i>	<i>Variance</i>
Column 1	3	185.59	61.86333	0.388233
Column 2	3	208.38	69.46	1.6003
Column 3	3	187.67	62.55667	3.438933
Column 4	3	149.87	49.95667	4.356033

ANOVA

<i>Source of Variation</i>	<i>SS</i>	<i>df</i>	<i>MS</i>	<i>F</i>	<i>P-value</i>	<i>F crit</i>
Between Groups	590.0661	3	196.6887	80.4165	2.58E-06	4.066181
Within Groups	19.567	8	2.445875			
Total	609.6331	11				

8. Calculate the standard error of the difference between two means as,

$$S.E. = \sqrt{\frac{2(MS)}{n}} = \sqrt{\frac{2(1.701)}{3}} = 1.065$$

9. Calculate the least significant difference (LSD) at the 5% significance level as,

$$5\% LSD = (t_{\alpha/2, N-k})(S.E.) = (3.479)(1.065) = 3.70 MPa$$

Therefore, the difference between any pairs of mean compressive strength values is significant at the 5% level if it exceeds, $LSD = 3.70 MPa$.

Appendix C: Beam-End Test Frame Design Overview

C.1 Design Concept and Parameters

Beam-end specimen dimensions were based on guidelines in ASTM A 944 – 05. These dimensions were 600 x 500 x 225.

However, in order to provide maximum flexibility in frame configuration, two separate frame arrangements were considered in design.

1. Frame arrangement(s) that would allow for larger beam-end specimens to be accommodated and would produce the largest possible design forces.
2. The actual frame arrangement to be used in the current research project.

An additional constraint was that the frame must be compatible with laboratory testing frames and load cell arrangements currently available at the University of Waterloo. For this reason, the testing frame had to be designed in a vertically-oriented position to be compatible with the 500 kN servo-hydraulically controlled load cell and actuator necessary to carry-out beam end testing.

Given the precise nature of bond strength and slip measurements the test frame was designed to ensure that any deflections of the frame were negligible compared to the slip and displacement of the test specimen. Hence, a stiffness-based rather than a strength-based design was necessary to meet these criteria.

Finally, the test frame was designed to ensure that all imposed frame displacements resulting from a maximum pull-out force of 500 kN (the maximum capacity of the load cell) satisfied the maximum deflection criteria.

As presented in Figure C.1, the testing frame design was divided into five design components:

- Component #1 – Left strut
- Component #2 – Right strut
- Component #3 – C-Channels
- Component #4 – Reaction Block
- Component #5 – Support Beam

Each component was designed based on the worst case design loads regardless of the particular

structural model used. Only static loading was considered and further design calculations are required to assess the test frame structure under dynamic (fatigue) loading.

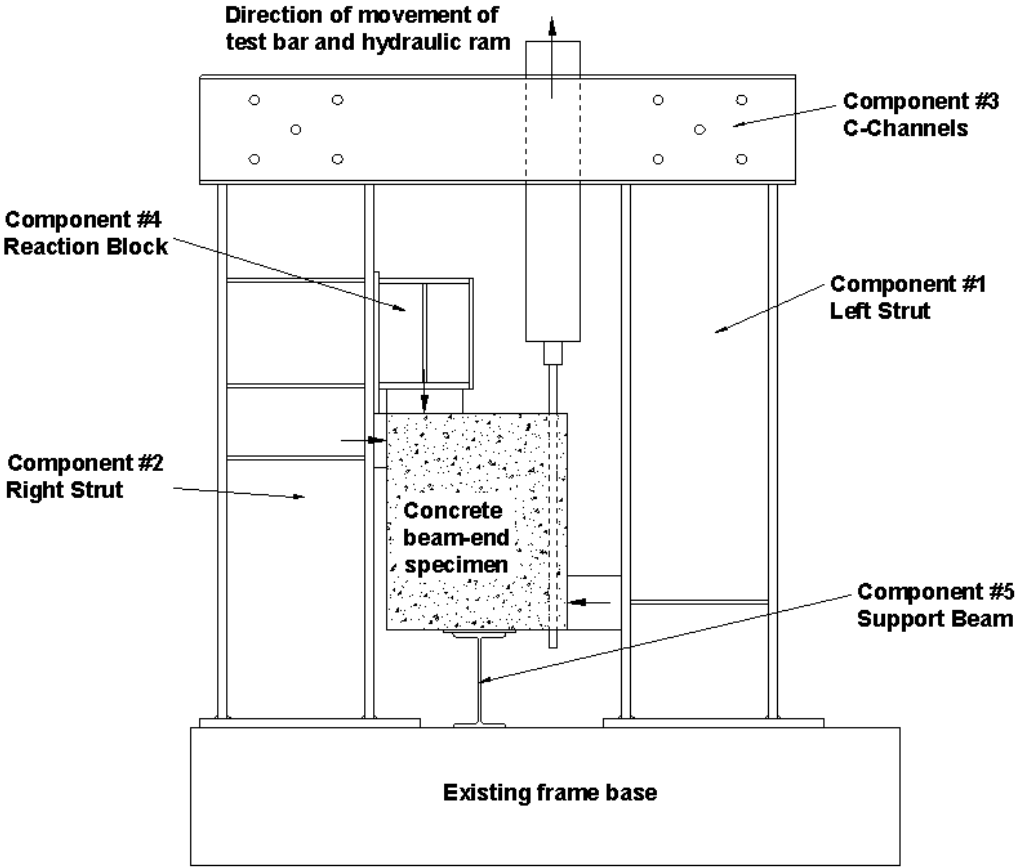


Figure C.1 Beam-end test frame schematic and component layout

C.2 Structural Models and SAP 2000 Analysis

In total, four structural models were analyzed to determine the design load cases for each structural component. Beam-end dimensions were optimized to produce the largest design forces. These calculations are summarized below.

Structural Model #1

Left and Right Strut Horizontal Forces:

Beam-end Specimen Base =	500 mm		
Beam-end Specimen Height =	500 mm		
Beam-end Specimen Thickness =	225 mm		
Bar c/c cover =	40 mm		
Top Horiz Edge Distance* =	75 mm	*Constant	Bearing Resistance Check: $f'_c = (\text{MIN } 30 \text{ MPa}) = 30 \text{ MPa}$ $\phi_c = 0.65$ $A_1 = 33750 \text{ mm}^2$ $B_r = 0.85\phi_c f'_c A_1 = 559.4 \text{ kN}$ <i>Ok for Bearing</i>
Horizontal Lever Arm =	385 mm		
T =	500 kN		
Top Moment =	192.5 kN-m		
Bottom Vert. Edge Distance =	75 mm		
Top Vert. Edge Distance =	75 mm		
Vertical Lever Arm =	350 mm		
Bottom Moment =	192.5 kN-m	Note: For equilibrium, Bottom M = Top M	
F_{horiz} =	550 kN		

Reaction Block Forces:

Total Horiz. Length of Reaction Block* =	265 mm	*Constant	
Minimum Thickness of Horiz. Spacer* =	50 mm		
Bar c/c cover =	40 mm		
Min. Bar c/c cover* =	40 mm		
Top Horiz. Edge Distance =	75 mm		
Lever Arm =	125 mm		
T =	500 kN		
Reaction Block Moment =	62.5 kN-m		

Note: The bar c/c cover dimension that produces the largest forces varies between the Left/Right Strut and the Reaction Block

Left and Right Strut Concentrated Moment:

Beam-end Specimen Base =	500 mm		
Bar c/c cover =	40 mm		
Min Bar Cover* =	40 mm		
Top Horiz Edge Distance* =	75 mm	*Constant	
Horizontal Lever Arm =	385 mm		
T =	500 kN		
Top Moment =	192.5 kN-m		
W410x149 Depth =	431 mm		
Total Horiz. Length of Reaction Block* =	265 mm	*Constant	
Minimum Thickness of Horiz. Spacer* =	40 mm		
Lever Arm to face of W410x149 =	115 mm		
Lever Arm to CL of W410x149 =	331 mm		
Concentrated Moment =	165 kN-m		

Structural Model #2															
Left and Right Strut Horizontal Forces:															
Beam-end Specimen Base =	500 mm														
Beam-end Specimen Height =	500 mm														
Beam-end Specimen Thickness =	225 mm														
Bar c/c cover =	115 mm														
Top Horiz Edge Distance* =	75 mm	*Constant	<table border="1"> <tr> <td colspan="2">Bearing Resistance Check:</td> </tr> <tr> <td>$f'_c = (\text{MIN } 30 \text{ MPa}) =$</td> <td>30 MPa</td> </tr> <tr> <td>$\phi_c =$</td> <td>0.65</td> </tr> <tr> <td>$A_1 =$</td> <td>33750 mm²</td> </tr> <tr> <td>$B_r = 0.85\phi_c f'_c A_1 =$</td> <td>559.4 kN</td> </tr> <tr> <td colspan="2" style="text-align: right;"><i>Ok for Bearing</i></td> </tr> </table>	Bearing Resistance Check:		$f'_c = (\text{MIN } 30 \text{ MPa}) =$	30 MPa	$\phi_c =$	0.65	$A_1 =$	33750 mm ²	$B_r = 0.85\phi_c f'_c A_1 =$	559.4 kN	<i>Ok for Bearing</i>	
Bearing Resistance Check:															
$f'_c = (\text{MIN } 30 \text{ MPa}) =$	30 MPa														
$\phi_c =$	0.65														
$A_1 =$	33750 mm ²														
$B_r = 0.85\phi_c f'_c A_1 =$	559.4 kN														
<i>Ok for Bearing</i>															
Horizontal Lever Arm =	310 mm														
T =	500 kN														
Top Moment =	155 kN-m														
Bottom Vert. Edge Distance =	75 mm														
Top Vert. Edge Distance =	75 mm														
Vertical Lever Arm =	350 mm														
Bottom Moment =	155 kN-m	Note: For equilibrium, Bottom M = Top M													
F_{horiz} =	443 kN														
Reaction Block Forces:															
Total Horiz. Length of Reaction Block* =	265 mm	*Constant													
Minimum Thickness of Horiz. Spacer* =	50 mm														
Bar c/c cover =	115 mm														
Min. Bar c/c cover* =	40 mm														
Top Horiz. Edge Distance =	75 mm														
Lever Arm =	200 mm														
T =	500 kN														
Reaction Block Moment =	100 kN-m														
Note: The bar c/c cover dimension that produces the largest forces varies between the Left/Right Strut and the Reaction Block															
Left and Right Strut Concentrated Moment:															
Beam-end Specimen Base =	500 mm														
Bar c/c cover =	115 mm														
Min Bar Cover* =	40 mm														
Top Horiz Edge Distance* =	75 mm	*Constant													
Horizontal Lever Arm =	310 mm														
T =	500 kN														
Top Moment =	155 kN-m														
W410x149 Depth =	431 mm														
Total Horiz. Length of Reaction Block* =	265 mm	*Constant													
Minimum Thickness of Horiz. Spacer* =	40 mm														
Lever Arm to face of W410x149 =	190 mm														
Lever Arm to CL of W410x149 =	406 mm														
Concentrated Moment =	203 kN-m														

Structural Model #3

Left and Right Strut Horizontal Forces:

Beam-end Specimen Base =	500 mm		
Beam-end Specimen Height =	900 mm		
Beam-end Specimen Thickness =	225 mm		
Bar c/c cover =	40 mm		
Top Horiz Edge Distance* =	75 mm	*Constant	Bearing Resistance Check: $f'_c = (\text{MIN } 30 \text{ MPa}) = 30 \text{ MPa}$ $\phi_c = 0.65$ $A_1 = 33750 \text{ mm}^2$ $B_r = 0.85\phi_c f'_c A_1 = 559.4 \text{ kN}$ <i>Ok for Bearing</i>
Horizontal Lever Arm =	385 mm		
T =	500 kN		
Top Moment =	192.5 kN-m		
Bottom Vert. Edge Distance =	75 mm		
Top Vert. Edge Distance =	75 mm		
Vertical Lever Arm =	750 mm		
Bottom Moment =	192.5 kN-m	Note: For equilibrium, Bottom M = Top M	
F_{horiz} =	257 kN		

Reaction Block Forces:

Total Horiz. Length of Reaction Block* =	265 mm	*Constant	
Minimum Thickness of Horiz. Spacer* =	50 mm		
Bar c/c cover =	40 mm		
Min. Bar c/c cover* =	40 mm		
Top Horiz. Edge Distance =	75 mm		
Lever Arm =	125 mm		
T =	500 kN		
Reaction Block Moment =	62.5 kN-m		

Note: The bar c/c cover dimension that produces the largest forces varies between the Left/Right Strut and the Reaction Block

Left and Right Strut Concentrated Moment:

Beam-end Specimen Base =	500 mm		
Bar c/c cover =	40 mm		
Min Bar Cover* =	40 mm		
Top Horiz Edge Distance* =	75 mm	*Constant	
Horizontal Lever Arm =	385 mm		
T =	500 kN		
Top Moment =	192.5 kN-m		
W410x149 Depth =	431 mm		
Total Horiz. Length of Reaction Block* =	265 mm	*Constant	
Minimum Thickness of Horiz. Spacer* =	40 mm		
Lever Arm to face of W410x149 =	115 mm		
Lever Arm to CL of W410x149 =	331 mm		
Concentrated Moment =	165 kN-m		

Structural Model #4

Left and Right Strut Horizontal Forces:

Beam-end Specimen Base =	500 mm		
Beam-end Specimen Height =	600 mm		
Beam-end Specimen Thickness =	225 mm		
Bar c/c cover =	50 mm		
Top Horiz Edge Distance* =	75 mm	*Constant	Bearing Resistance Check: $f'_c = (\text{MIN } 30 \text{ MPa}) = 30 \text{ MPa}$ $\phi_c = 0.65$ $A_1 = 33750 \text{ mm}^2$ $B_r = 0.85\phi_c f'_c A_1 = 559.4 \text{ kN}$ <i>Ok for Bearing</i>
Horizontal Lever Arm =	375 mm		
T =	500 kN		
Top Moment =	187.5 kN-m		
Bottom Vert. Edge Distance =	75 mm		
Top Vert. Edge Distance =	75 mm		
Vertical Lever Arm =	450 mm		
Bottom Moment =	187.5 kN-m	Note: For equilibrium, Bottom M = Top M	
F_{horiz} =	417 kN		

Reaction Block Forces:

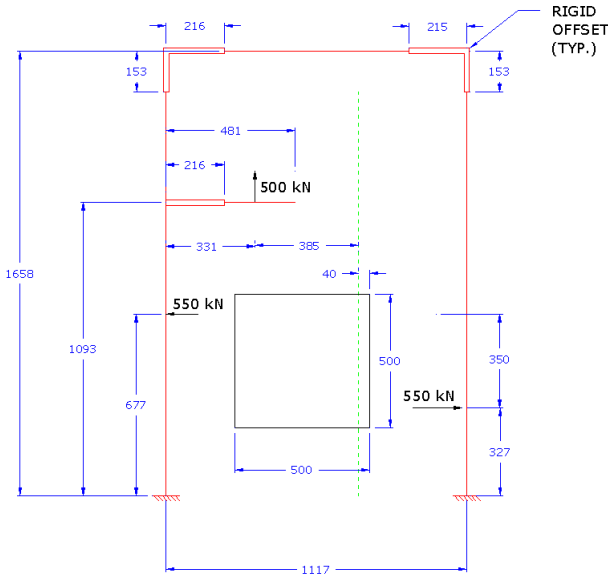
Total Horiz. Length of Reaction Block* =	265 mm	*Constant	
Minimum Thickness of Horiz. Spacer* =	50 mm		
Bar c/c cover =	40 mm		
Min. Bar c/c cover* =	40 mm		
Top Horiz. Edge Distance =	75 mm		
Lever Arm =	125 mm		
T =	500 kN		
Reaction Block Moment =	62.5 kN-m		

Note: The bar c/c cover dimension that produces the largest forces varies between the Left/Right Strut and the Reaction Block

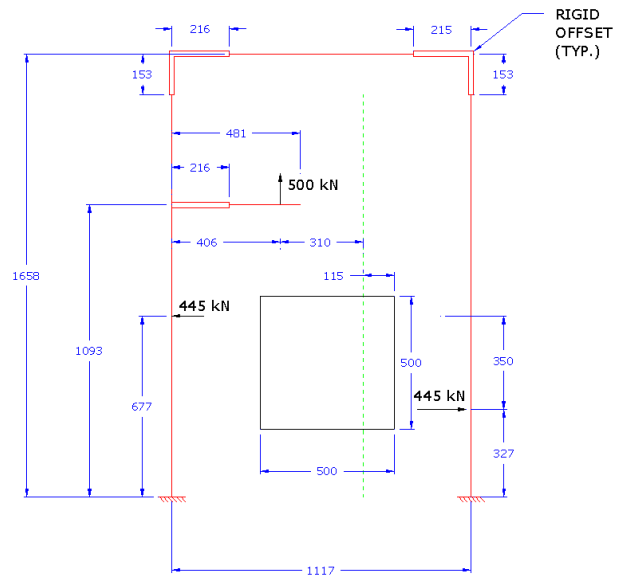
Left and Right Strut Concentrated Moment:

Beam-end Specimen Base =	500 mm		
Bar c/c cover =	40 mm		
Min Bar Cover* =	40 mm		
Top Horiz Edge Distance* =	75 mm	*Constant	
Horizontal Lever Arm =	385 mm		
T =	500 kN		
Top Moment =	192.5 kN-m		
W410x149 Depth =	431 mm		
Total Horiz. Length of Reaction Block* =	265 mm	*Constant	
Minimum Thickness of Horiz. Spacer* =	40 mm		
Lever Arm to face of W410x149 =	115 mm		
Lever Arm to CL of W410x149 =	331 mm		
Concentrated Moment =	165 kN-m		

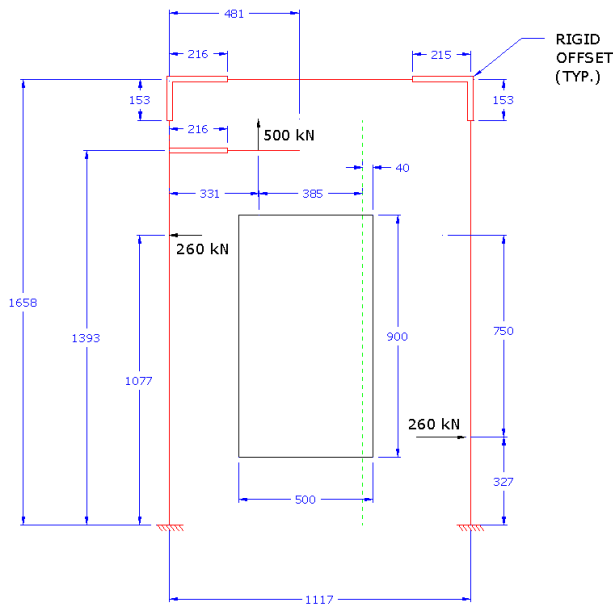
Based on the design forces calculated above, 2-D frame models were built and analyzed using SAP 2000 to determine the forces and moments produced in each structural component. These models are depicted below.



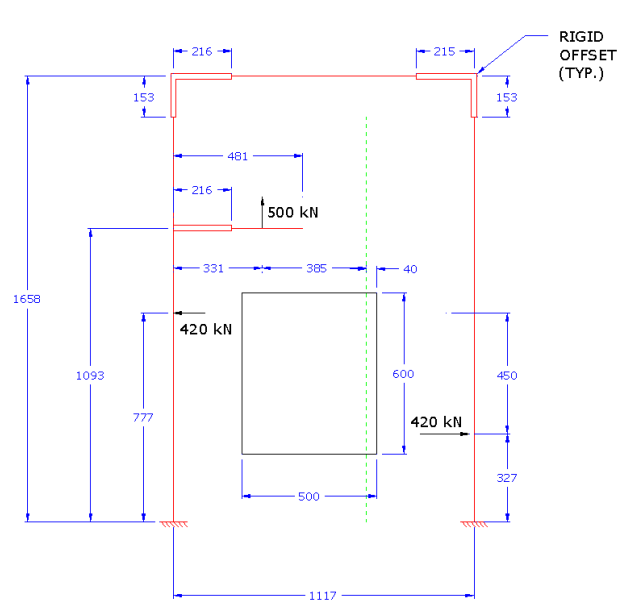
Structural Model #1



Structural Model #2



Structural Model #3



Structural Model #4

Figure C.2 SAP 2000 structural models and applied design loads

C.3 Stiffness-Based Displacement Criteria

As described above, the overall design of the frame and its components was governed by the deflection criteria. The maximum lateral deflection of the frame in all structural models occurred at the left strut to C-channel connection (i.e. the top left portion of the frame as illustrated in Figure C.1). Therefore, all design checks were based on this point having a lateral displacement of not more than 1.00 mm.

The sizing of the structural components was therefore an iterative process as after the structural model was updated with new section properties and stiffness characteristics the structural analysis was run to ensure the above displacement criteria was satisfied.

The following table summarizes the final component sizes and associated design loads based on the worst case loads from each structural model.

Table C.1 Design loads summary based on SAP 2000 analysis of structural models

	Structural Model #1	Structural Model #2	Structural Model #3	Structural Model #4 (Project Model)	Design Loads
Component #1 - Left Strut (W410X149)					
Base Moment (kN-m) =	212.3	185.1	115.4	181.1	212.3
Base Shear (kN) =	387.4	295.2	125.9	271.3	387.4
Max Span Moment (kN-m) =	147.7	155.3	143.3	148.1	155.3
Max Axial Load (kN) =	358.4	348.4	316.4	256.6	358.4
Max Horizontal Displacement (mm) =	0.731	0.710	0.700	0.758	0.758
Component #2 - Right Strut (W410X149)					
Base Moment (kN-m) =	8.7	8.0	41.5	15.1	41.5
Base Shear (kN) =	387.4	295.2	125.9	271.3	387.4
Max Span Moment (kN-m) =	117.9	104.5	95.7	103.8	117.9
Max Axial Load (kN) =	137.5	147.5	181.5	140.9	181.5
Max Horizontal Displacement (mm) =	0.673	0.656	0.652	0.682	0.682
Component #3 - C-Channels (C310X31)					
Max Moment (kN-m) =	98.5	94.9	107.8	94.1	107.8
Max Shear (kN) =	138.8	147.5	182.9	140.9	182.9
Max Axial Load (kN) =	162.6	149.8	134.1	148.7	162.6
Component #4 - Reaction Block (W310X67)					
Moment at CL of column (kN-m) =	165.4	202.9	165.4	165.4	202.9
Moment at Plate-Column Interface (kN-m) =	57.7	95.2	57.7	57.7	95.2
Base Shear (kN) =	500.0	500.0	500.0	500.0	500.0
Max Axial Load (kN) =	0.0	0.0	0.0	0.0	0.0
Upward Tip Displacement (mm) =	0.605	0.890	0.630	0.638	0.890

C.4 Component #1 Design – Left Strut

The left strut was initially sized based on the above stiffness-based analysis. A W410x149

section was chosen and verified to be adequate in both strength and serviceability. Connections to the test frame base were designed as 4-bolt extended end plate (EEP) moment connections. Bolts were 1" A490M grade bolts and 12mm fillet welds were used to secure the W410x149 section to the 1" thick end plate. The following calculations summarize the connection design. All spreadsheet design programs were checked and calculated by hand to validate their results.

4-Bolt Extended End Plate Moment Connection (Unstiffened)			
Component #1 - Left Strut			
$M_f =$	212.3 kN-m	<i>From SAP 2000 Analysis Results (Structural Model #1)</i>	
$T_f =$	523 kN		
# of Bolts in tension, n =	4 bolts		
T_f per bolt =	130.7 kN		
$d_b =$	431 mm	W410x149	
$t_b =$	25 mm		
$w_b =$	14.9 mm		
Flange Width, $w_{fb} =$	265 mm		
Choose Bolt Type:		Check Bolt Shear Capacity:	
Grade:	1.0" A490M Bolts	$V_f =$	500 kN
diameter, d =	25 mm	V_r per bolt =	190 kN Threads excluded
$d' = d + 2\text{mm} =$	27 mm	# Bolts in Shear =	6
$T_r =$	315 kN	$V_{r,tot} =$	1140 kN Ok!
Establish Plate Dimensions:		Actual Dims:	
Plate thickness, $t_p = d =$	25 mm	25	
Plate Width, $B = 10d =$	300 mm	300	
Bolt Gauge, $A = \text{MIN}(5d) =$	100 mm	100	
Bolt Pitch, $C = \text{MIN}(4d) =$	100 mm	100	
Edge Distance = $2.5d =$	62.5 mm	65	<i>* Modified to accommodate bolt hole pattern</i>
Plate Length =	556 mm	560	

Check Endplate and Bolts using Prying Equations:		
$b = (C - t_b)/2 =$	37.5 mm	<i>* Modified to accommodate bolt hole pattern</i>
$b' = b - d/2 =$	25 mm	
$a = 1.25b =$	46.875 mm	
$a' = a + d/2 =$	59.375 mm	
$a' + b' =$	84.375 mm	
$K =$	3.17	<i>No Prying Action</i>
$\delta =$	0.730	
$\alpha =$	-0.460	
Therefore, use $\alpha =$	0.000	
$\delta\alpha =$	0.000	
Amplified Bolt Force, $T_f =$	130.7 kN	<i>OK - $T_r > T_f$</i>
% Capacity =	42%	
Check Column Flange / Connection Capacity:		
<i>The end plate is bolted directly to the test frame base and thus there is no need to check the flange capacity.</i>		
Beam-Flange Weld to End Plate:		
Force/mm width of flange =	1.97 kN/mm	
Use a 12mm fillet weld around entire W-Section		

C.5 Component #2 Design – Right Strut

The right strut was initially sized based on the above stiffness-based analysis. A W410x149 section was also chosen and verified to be adequate in both strength and serviceability as well as to provide similar economy as the left strut. Connections to the test frame base were designed as 4-bolt extended end plate (EEP) moment connections. Bolts were 1” A490M grade bolts and 5 mm fillet welds were used to secure the W410x149 section to the 1” thick end plate. The following calculations summarize the connection design. Note that final as-built conditions used 12 mm fillet welds similar to the left strut arrangement. All spreadsheet design programs were checked and calculated by hand to validate their results.

4-Bolt Extended End Plate Moment Connection (Unstiffened)

Component #2 - Right Strut

$M_f =$	41.5 kN-m	<i>From SAP 2000 Analysis Results (Structural Model #3)</i>
$T_f =$	102 kN	
# of Bolts in tension, n =	4 bolts	
T_f per bolt =	25.6 kN	

$d_b =$	431 mm	W410x149
$t_b =$	25 mm	
$w_b =$	14.9 mm	
Flange Width, $w_{fb} =$	265 mm	

Choose Bolt Type:

Grade:	1.0" A490M Bolts	<i>Note: In order to accommodate a uniform bolt pattern on the test frame the same same extended endplate as the left strut will be used</i>
diameter, d =	25 mm	
$d' = d + 2\text{mm} =$	27 mm	
$T_r =$	315 kN	

Establish Plate Dimensions:

		Actual Dims:
Plate thickness, $t_p = d =$	25 mm	25
Plate Width, $B = 10d =$	290 mm	300
Bolt Gauge, $A = \text{MIN}(5d) =$	100 mm	100
Bolt Pitch, $C = \text{MIN}(4d) =$	100 mm	100
Edge Distance = $2.5d =$	62.5 mm	67
Plate Length =	556 mm	560

Check Endplate and Bolts using Prying Equations:

$b = (C - t_b)/2 =$	37.5 mm	NO PRYING ACTION
$b' = b - d/2 =$	25 mm	
$a = 1.25b =$	46.875 mm	
$a' = a + d/2 =$	59.375 mm	
$a' + b' =$	84.375 mm	
$K =$	3.17	
$\delta =$	0.730	
$\alpha =$	-1.192	
Therefore, use $\alpha =$	0.000	
$\delta\alpha =$	0.000	

Amplified Bolt Force, $T_f =$	25.6 kN	OK - $T_r > T_f$
% Capacity =	8%	

Beam-Flange Weld to End Plate:

Force/mm width of flange = 0.39 kN/mm

Use a 5mm E49XX fillet weld

C.6 Component #3 Design – C-Channels

The top C-channels were initially sized based on the above stiffness-based analysis. Two C310x31 sections were chosen to make up the top tension member. They were verified to be adequate in both strength and serviceability. Connections to the test frame right and left struts were designed as slip-critical connections. Backing plates were welded to the W-sections to provide a mechanical connection with the two C-channels. The following design checks were completed:

1. Tension member capacity (i.e. failure planes analysis, gross section yielding, shear lag considerations, etc.)
2. Backing plate material capacity
3. Slenderness and stability
4. Combined moment and shear capacity of both C-channels

Five 1” A490M grade bolts were used to secure the C310x31 sections to the 15 mm thick end plate. The end plates were welded using 5 mm thick fillet welds. In general, all design checks were met using the selected sections. All spreadsheet design programs were checked and recalculated manually to validate their results.

C.7 Component #4 Design – Reaction Block

The reaction block was initially sized based on the above stiffness-based analysis. A W310x67 section was chosen and verified to be adequate in both strength and serviceability. Connections to the test frame base were designed as 4-bolt extended end plate (EEP) moment connections. Bolts were 1” A490M grade bolts and 12mm fillet welds were used to secure the W410x149 section to the 1” thick end plate. The following calculations summarize the design. All spreadsheet design programs were checked and calculated by hand to validate their results.

4-Bolt Extended End Plate Moment Connection (Unstiffened)			
Component #4 - Reaction Block			
$M_f =$	127.5 kN-m	<i>From SAP 2000 Analysis Results (Structural Model #2 - Moment at Plate-Column Interface)</i> <i>** Also adjusted based on as-built dimensions</i>	
$T_f =$	438 kN		
# of Bolts in tension, $n =$	4 bolts		
T_f per bolt =	109 kN		
Beam Dimensions:		Column Dimensions:	
$d_b =$	306 mm	$d_c =$	431 mm
$t_b =$	14.6 mm	$t_c =$	25 mm
$w_b =$	8.5 mm	$w_c =$	14.9 mm
Flange Width, $w_{fb} =$	204 mm	Flange Width, $w_{fc} =$	265 mm
		W310x67	W410x149
Choose Bolt Type:		Check Bolt Shear Capacity:	
Grade:	M16 A490M Bolts	$V_f =$	500 kN
diameter, $d =$	19 mm	V_r per bolt =	100 kN Threads excluded
$d' = d + 2\text{mm} =$	21 mm	# Bolts in Shear =	6
$T_r =$	177 kN	$V_{r,tot} =$	600 kN Ok!
Establish Plate Dimensions:		Actual Dims:	
Plate thickness, $t_p =$	19.1 mm		19.1 mm
Plate Width, $B = 10d =$	223.1 mm		225 mm
Bolt Gauge, $A = \text{MIN}(5d) =$	100 mm		100 mm
Bolt Pitch, $C = \text{MIN}(4d) =$	100 mm		100 mm
Edge Distance = $2.5d =$	47.75 mm		45 mm
Plate Length =	415.55 mm		410 mm

Check Endplate and Bolts using Prying Equations:			
$b = (C - t_b)/2 =$	42.7 mm		
$b' = b - d/2 =$	33.15 mm		
$a = 1.25b =$	53.375 mm		
$a' = a + d/2 =$	62.875 mm		
$a' + b' =$	96.025 mm		
$K =$	4.21		
$\delta =$	0.790		
$\alpha =$	0.332	FALSE	
Therefore, use $\alpha =$	0.332		
$\delta\alpha =$	0.262		
Amplified Bolt Force, $T_f =$	121.4 kN	OK - $Tr > T_f$	
% Capacity =	69%		
Check Column Flange / Connection Capacity:			
$b = (A - w_c)/2 =$	42.55 mm		
$b' = b - d/2 =$	33.05 mm		
$a = (w_{fc} - A)/2 =$	82.5 mm		
$a' = a + d/2 =$	92 mm		
$a' + b' =$	125.05 mm		
$K =$	4.20		
$\delta =$	0.790		
$\alpha^* =$	0.176		
Therefore, use $\alpha^* =$	0.000		
Connection Capacity =	595.7 kN	OK - $Tr > T_f$	
% Capacity =	73%		
Determine Additional Tension Flange Reinforcement:			
Required Tension Flange F =	0.0 kN	None required	
Stiffener Plate t =	10 mm		
Stiffener Plate w =	50 mm		
Tension Capacity =	157.5 kN	OK!	
Check Web Crippling and Yielding (Cl. 21.3):			
*Note: Because the beam flange is bearing against the end plate and not against the column flange we can use:			
$tb = tb + 2tp =$	52.8 mm		
Determine the class of the W410x149 column compression flange:			
$F_{yc} =$	350 MPa		
$t_c =$	25 mm		
$h_c =$	431 mm		
$w_c =$	14.9 mm		
$h_c/w_c =$	28.9	$< 670/\sqrt{F_{yc}} = 35.8$	Therefore flange is Class 1
$\phi_{bi} =$	0.8		
$Br = \phi_{bi}w_c(t_b + 10t_c)F_{yc} =$	1263.3 kN	No additional column web reinforcement is required	
Beam-Flange Weld to End Plate:			
Force/mm width of flange =	2.14 kN/mm		
Use an 8mm E49XX fillet weld			

C.8 Component #5 Design – Support Beam

The support beam was not included as part of the structural analysis (i.e. in the SAP 2000 structural models) as its main function was to support the self-weight of the beam-end specimen and facilitate quick insertion and removal of the beam-end specimens via overhead crane. A simple cantilevered beam analysis was conducted to size the support beam however, geometric constraints ultimately governed the design as the height of the section was required to be 250 mm. Therefore, a W250x36 section was chosen and satisfied strength requirements.

C.9 Miscellaneous Design Items

C.9.1 Bearing resistance of concrete

To ensure that the beam-end specimen concrete did not experience a bearing failure during loading, checks for bearing resistance using CSA A23.3-04 Clause 10.8.1 were completed. A worst case concrete strength of 30 MPa was assumed during calculations. Bearing pad dimensions were adjusted accordingly to ensure bearing failure would not occur.

C.9.2 Shear resistance of beam-end specimen

To ensure that a shear failure would not occur prior to failure in bond, the shear resistance of the beam-end section was calculated using CSA A23.3-04 Clause 11.3.6. The shear resistance of the beam-end section was found to be adequate to resistance the imposed shear force for the particular beam-end specimen configuration.

C.9.3 Development length calculations

Development lengths for the test bar under various compressive strengths were calculated to ensure that the bonded lengths chosen during the research project would be short enough to ensure a bond failure.

C.9.4 Right strut and reaction block adjustable spacers/bearing pads

To facilitate the proper alignment of the beam-end specimens, the three reaction blocks had to be designed to be adjustable. Compressive strengths of the bolts and rods were checked to ensure that buckling or yielding would not occur under maximum design loads.

C.9.5 Pre-stressed Coupler Assembly

To connect the test bar to the load cell a Lenton bolt-coupler system was used to provide a mechanical connection. To ensure minimal deformation of the connector rods, the entire coupler assembly was pre-stressed. A thorough statically indeterminate analysis was performed and verified to ensure the optimal pre-stressing force that would limit significant deformation of the entire assembly.

Note: if beam-end specimen dimensions are varied in future studies the above design calculations will have to be re-done to accommodate the change in loading.

C.10 Design Drawings

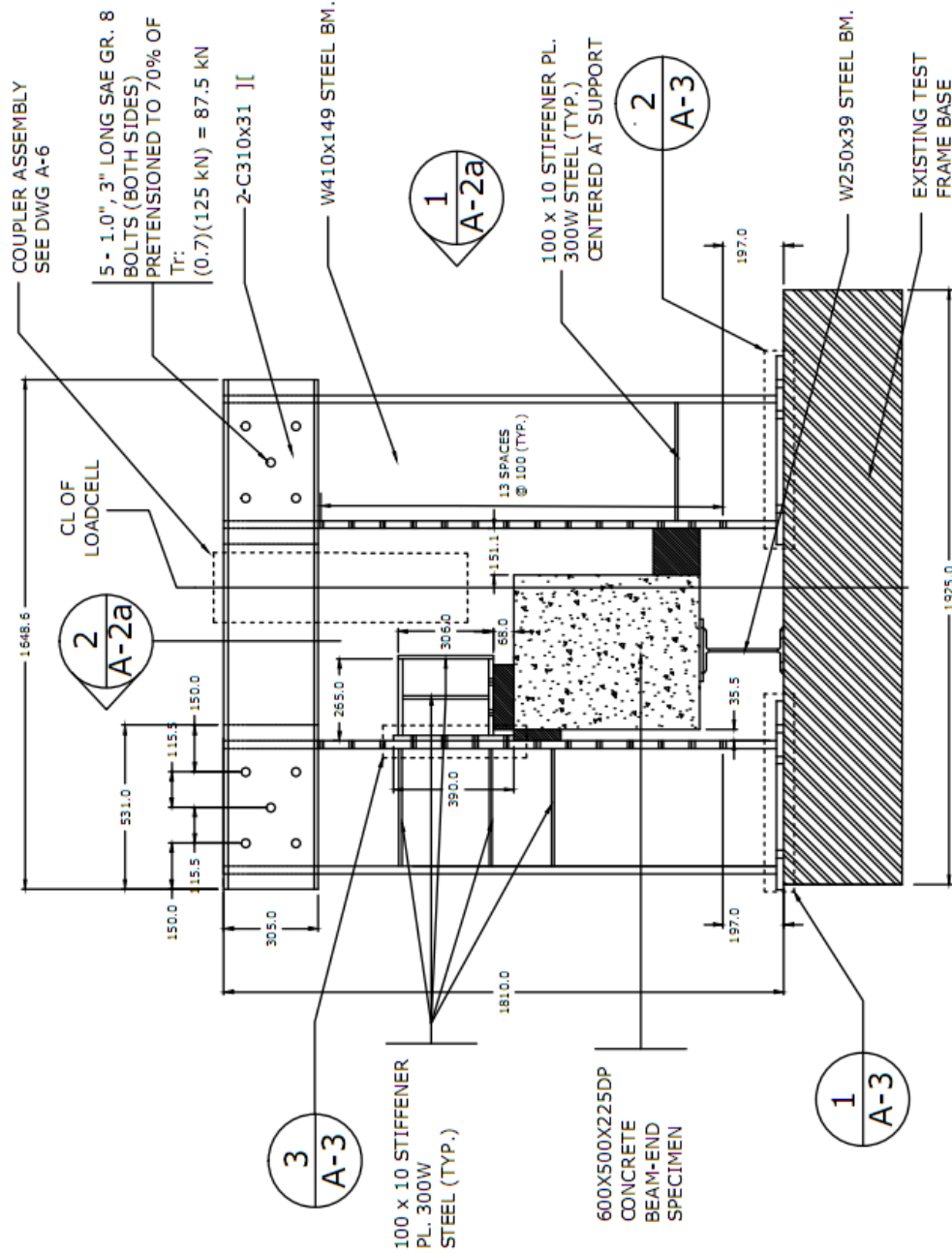
Drawing List:

A-1	Main Elevation	A-5a	Adjustable Spacers
A-2a	Sections and Elevations	A-5b	Reaction Block Adjustable Spacer
A-2b	Sections and Elevations	A-5c	Left Strut Adjustable Spacer
A-3	Extended End Plate Details	A-6	Adjustable Coupler Assembly
A-4	Proposed Bolt Hole Pattern		

Note: the following design drawings are reprints only based on original drawings produced using AutoCAD 2010.

GENERAL NOTES:

1. ALL BOLTS ON EXTENDED END PLATES CONNECTION TO BE PRE-TENSIONED
2. ALL STRUCTURAL STEEL SECTIONS TO BE G40.21 350W STEEL
3. ALL PLATE MATERIAL TO BE 300W STEEL U.N.O.
4. ALL WELD ELECTRODES TO BE E49XX (490 MPa)
5. ALL BOLTED CONNECTIONS OF CHANNELS TO W-SECTIONS TO BE SLIP-CRITICAL CONNECTIONS
6. ALL LENGTH UNITS ARE IN mm UNLESS NOTED OTHERWISE
7. ALL EXPOSED STRUCTURAL STEEL TO BE PAINTED
8. FOR SHADED BLOCKS REFER TO DWG. A-5 FOR ADJUSTABLE SPACER DETAILS



DWG NO.:

A-1

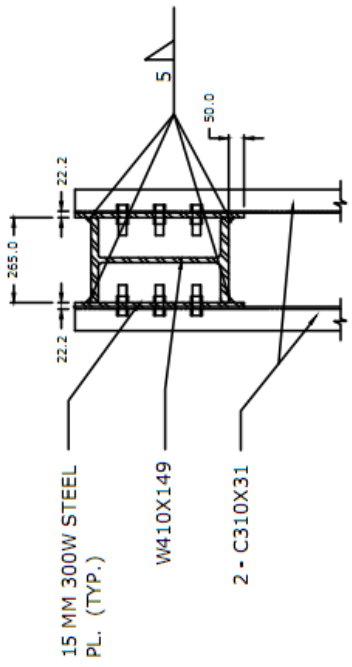
DATE: 13 MAY 09

SCALE: N.T.S.

DRAWN BY: L. BUTLER

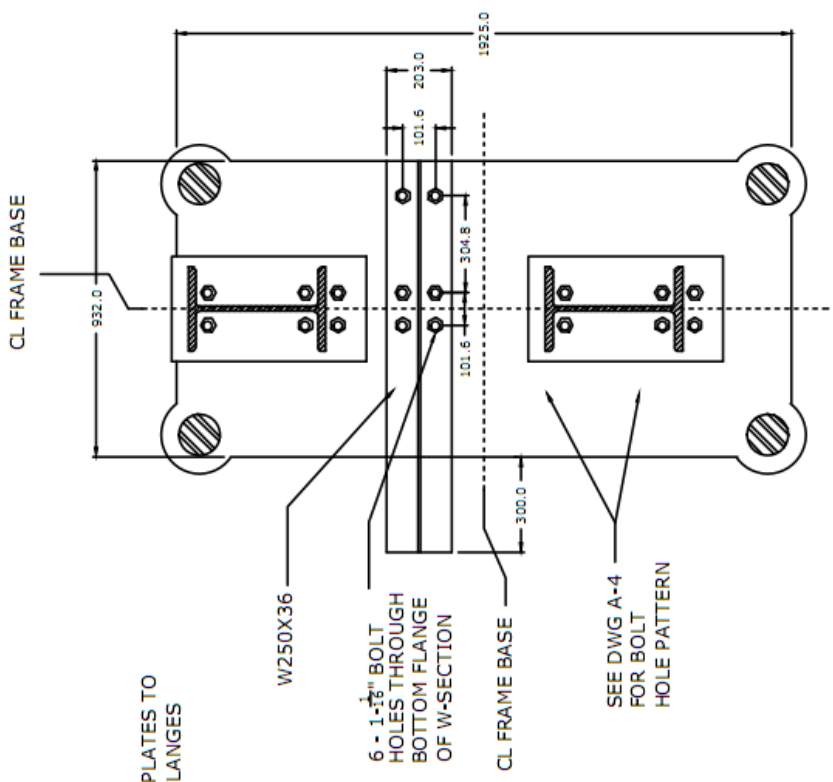
CHECKED BY: L. BUTLER

DRAWING TITLE:
**BEAM END TEST FRAME
MAIN ELEVATION**



1
A-2b

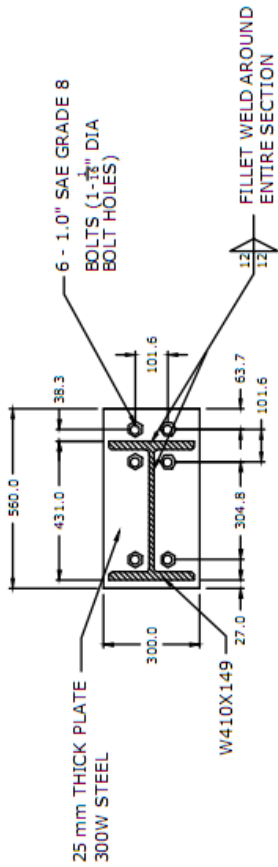
LEFT STRUT SECTION
(RIGHT STRUT SIMILAR)



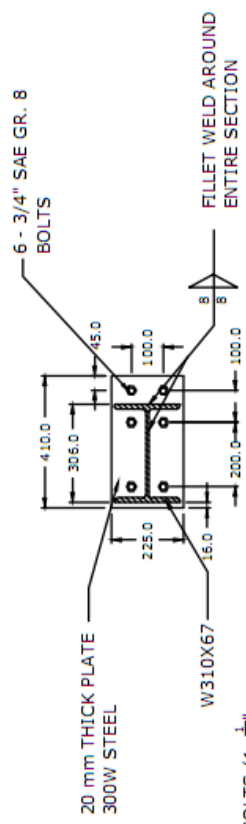
2
A-2b

PLAN SECTION - FRAME BASE

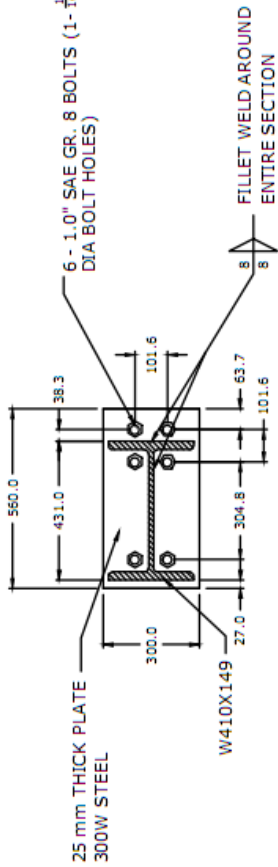
DRAWING TITLE: BEAM END TEST FRAME SECTIONS AND ELEVATIONS	DRAWN BY: L. BUTLER	DATE: 3 APR 09	DWG NO.:
	CHECKED BY: L. BUTLER	SCALE: N.T.S.	A-2b



1
A-3
LEFT STRUT EEP



3
A-3
REACTION BLOCK EEP



2
A-3
RIGHT STRUT EEP

DRAWING TITLE:

**BEAM END TEST FRAME
EXTENDED END PLATE DETAILS**

DRAWN BY:

L. BUTLER

DATE:

3 APR 09

DWG NO.:

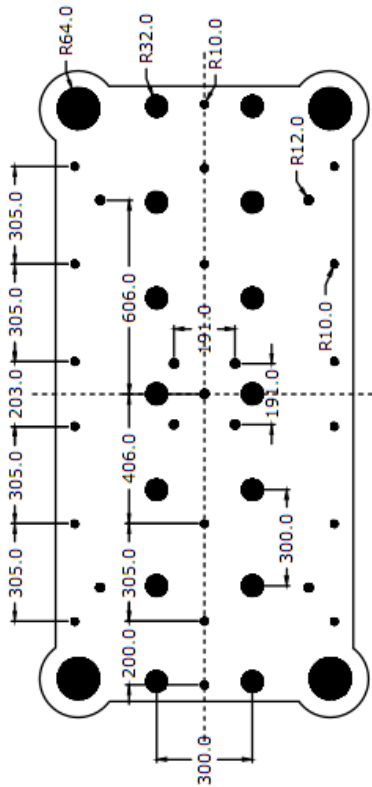
A-3

CHECKED BY:

L. BUTLER

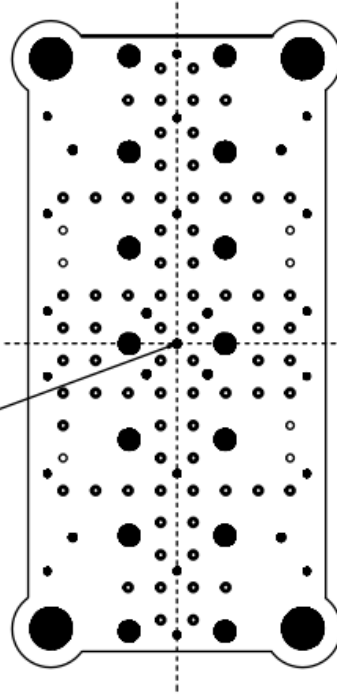
SCALE:

N.T.S.



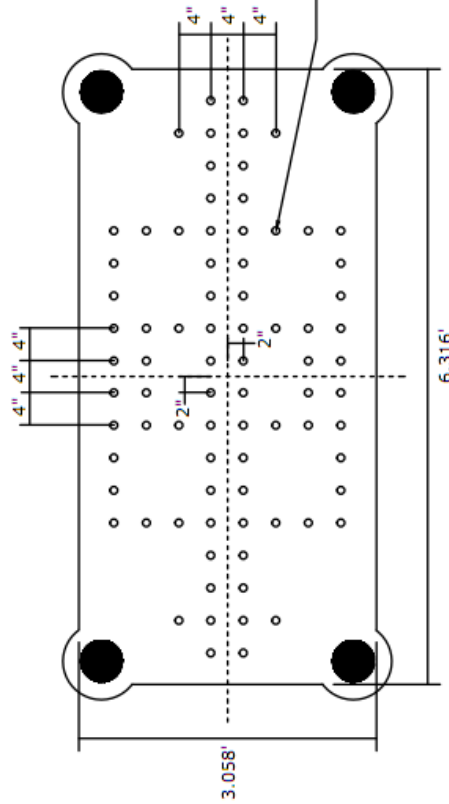
EXISTING BOLT HOLE PATTERN

SEE NOTE BELOW



OVERLAY PATTERN

1" - 8 UNC COARSE
THREADED HOLES
(80 HOLES IN TOTAL TYP.)

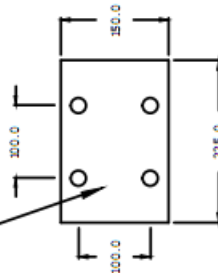


**PROPOSED BOLT HOLE PATTERN
(4" X 4" GRID w/1" UNC THREADED HOLES)**

NOTE: THE (0,0) REFERENCE COORDINATE FOR THE NEW BOLT PATTERN IS TO BE SET AT THE CENTER OF THE FRAME BASE IN LINE WITH THE CENTER OF THE EXISTING CENTER HOLE

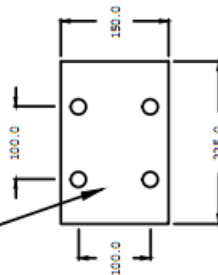
DRAWING TITLE: BEAM END TEST FRAME PROPOSED BOLT HOLE PATTERN	DRAWN BY: L. BUTLER	DATE: 23 APR 09	DWG NO.:
	CHECKED BY: L. BUTLER	SCALE: N.T.S.	A-4

2" COLD ROLLED STEEL PLATE
WITH THROUGH DRILLED AND
TAPPED $\frac{3}{4}$ " - 10 UNC THREADED
HOLES



2" PLATE ELEVATION

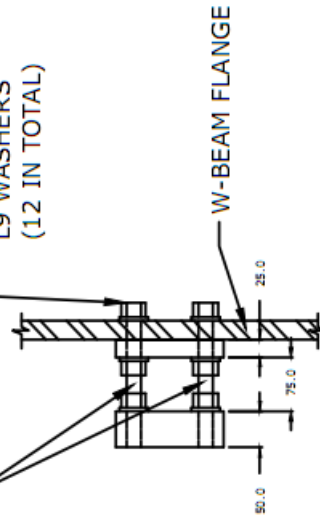
1" COLD ROLLED STEEL PLATE
WITH $\frac{3}{4}$ " THROUGH DRILLED HOLES



1" PLATE ELEVATION

FOUR $\frac{3}{4}$ " - 10 UNC SAE GR. 8
THREADED RODS 8- $\frac{1}{2}$ " LONG

$\frac{3}{4}$ " SAE GR. 8 NUTS
WITH MATCHING
L9 WASHERS
(12 IN TOTAL)



ASSEMBLY

RIGHT STRUT ADJUSTABLE SPACER

DRAWING TITLE:

BEAM END TEST FRAME
ADJUSTABLE SPACERS

DRAWN BY:

L. BUTLER

CHECKED BY:

L. BUTLER

DATE:

13 MAY 09

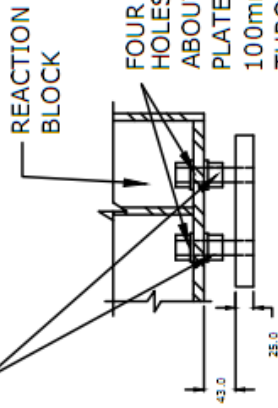
SCALE:

N.T.S.

DWG NO.:

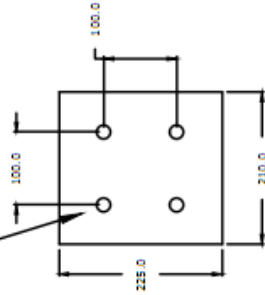
A-5a

FOUR $\frac{3}{4}$ " - 10 UNC SAE GR. 8
 THREADED RODS 4- $\frac{1}{2}$ " LONG AND
 EIGHT $\frac{3}{4}$ " SAE GR. 8 NUTS WITH
 MATCHING GR. L9 WASHERS



FOUR ADDITIONAL $\frac{3}{4}$ "
 HOLES (CENTERED
 ABOUT THE STIFFENER
 PLATE ON A 100mm X
 100mm GRID) TO BE
 THROUGH DRILLED IN
 BOTTOM OF REACTION
 BLOCK FLANGE

1" COLD ROLLED STEEL
 PLATE WITH THROUGH
 DRILLED AND TAPPED
 $\frac{3}{4}$ " - 10 UNC THREADED
 HOLES



ASSEMBLY

1" PLATE ELEVATION

REACTION BLOCK ADJUSTABLE SPACER

DRAWING TITLE:

BEAM END TEST FRAME
 ADJUSTABLE SPACERS

DRAWN BY:

L. BUTLER

DATE:

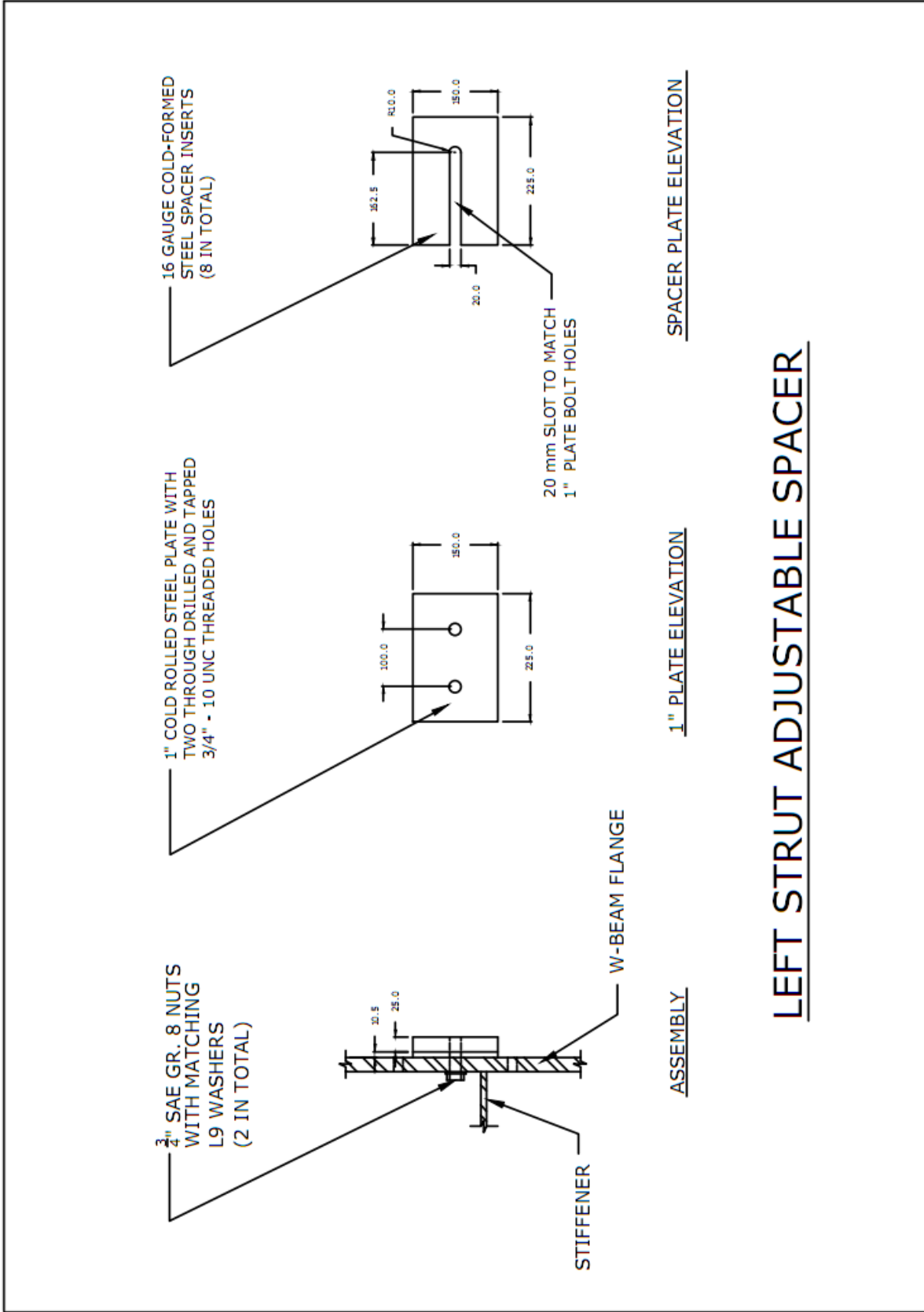
13 MAY 09

CHECKED BY:

L. BUTLER
 N.T.S.

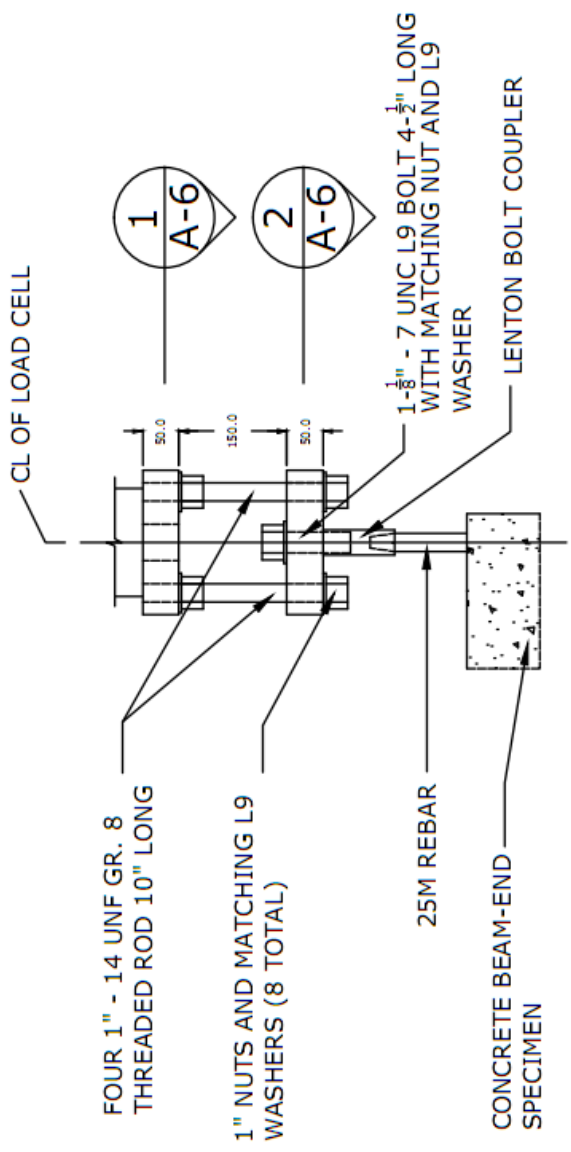
DWG NO.:

A-5b

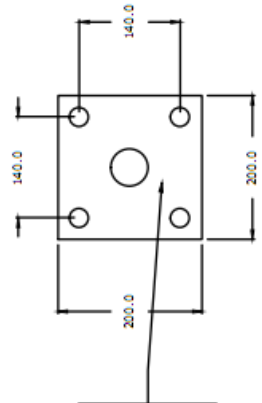


LEFT STRUT ADJUSTABLE SPACER

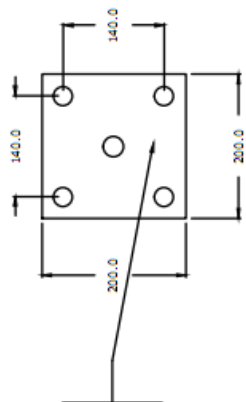
DRAWING TITLE: BEAM END TEST FRAME ADJUSTABLE SPACERS	DRAWN BY: L. BUTLER	DATE: 13 MAY 09	DWG NO.:
	CHECKED BY: L. BUTLER	SCALE: N.T.S.	A-5C



ADJUSTABLE COUPLER ASSEMBLY



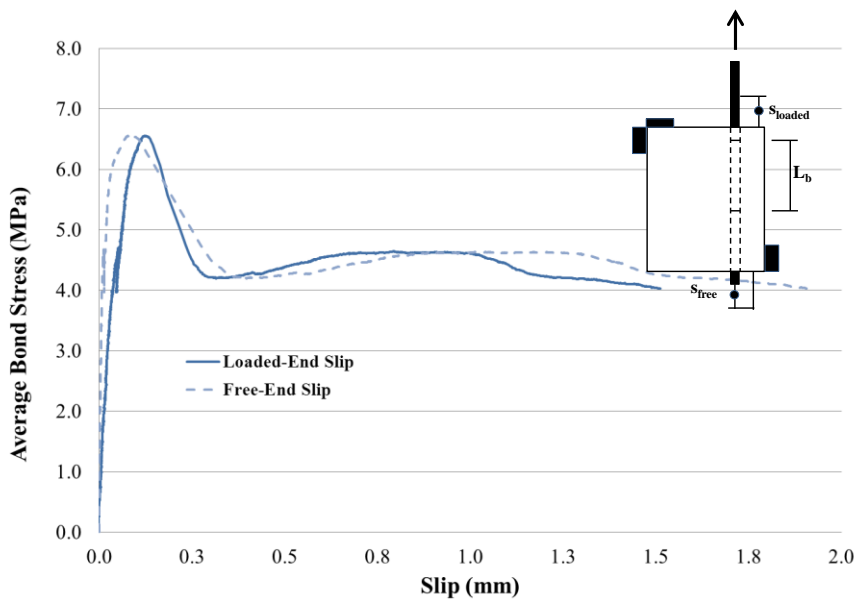
UPPER BASE PLATE 1
A-6



LOWER BASE PLATE 2
A-6

DRAWING TITLE: BEAM END TEST FRAME ADJUSTABLE COUPLER ASSEMBLY	DRAWN BY: L. BUTLER	DATE: 13 MAY 09	DWG NO.: A-6
	CHECKED BY: L. BUTLER	SCALE: N.T.S.	

Appendix D: Bond-Slip Response Curves and Crack Patterns for Beam-End Specimens

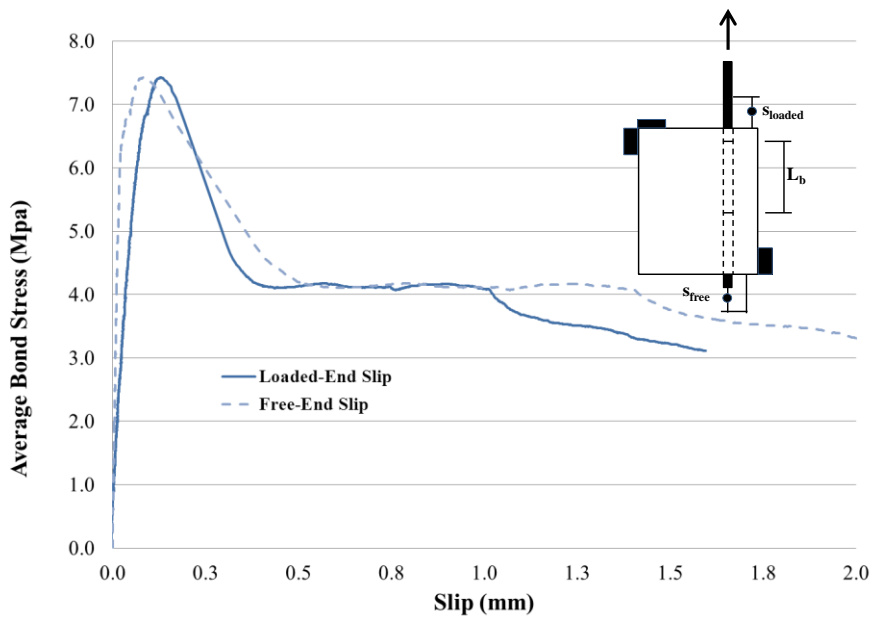


a) Bond-slip response



b) Post-failure cracking

Figure D.1 Bond-slip response and crack pattern for BE-NAC-30-125A

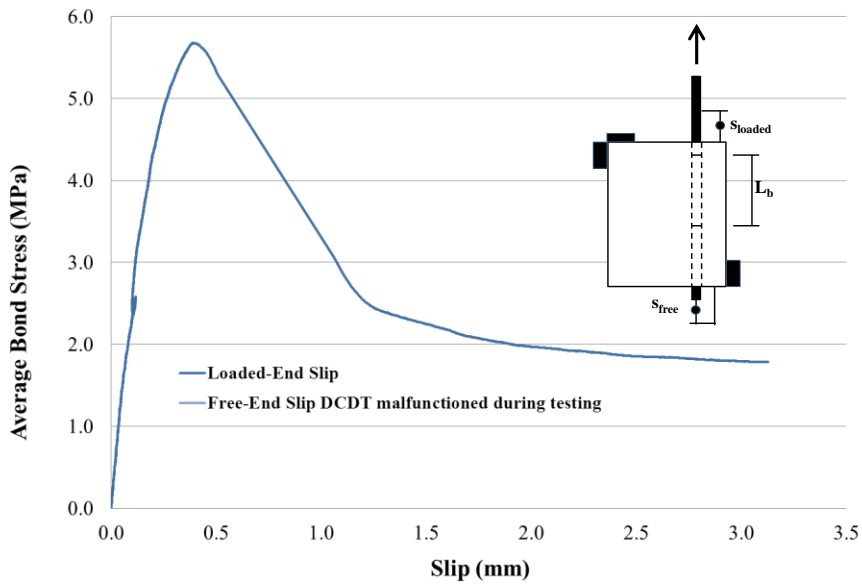


a) Bond-slip response



b) Post-failure cracking

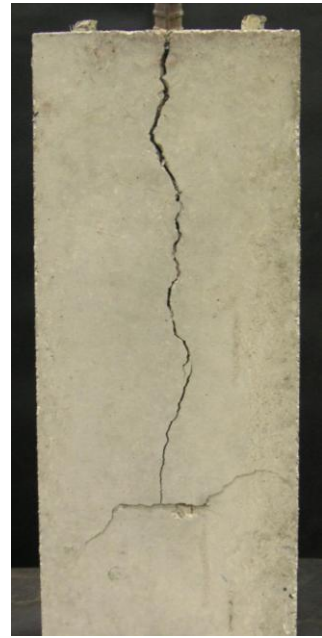
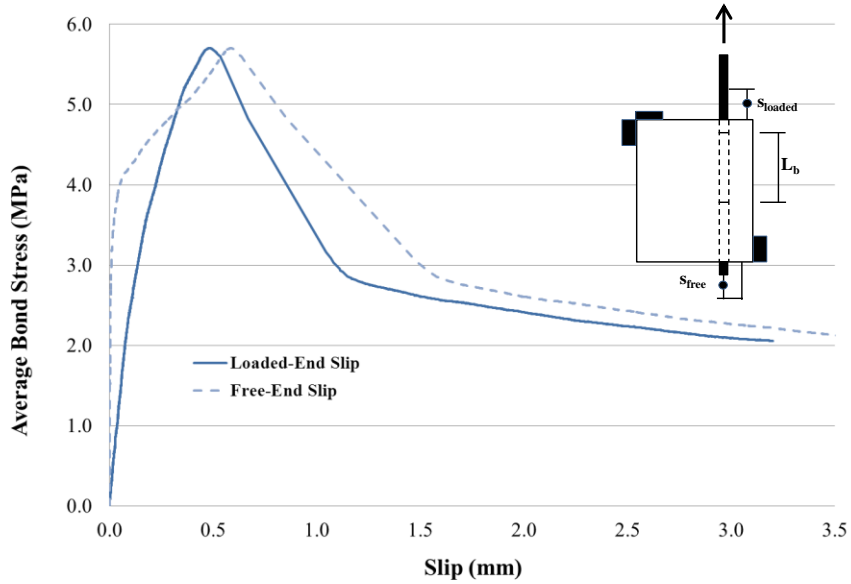
Figure D.2 Bond-slip response and crack pattern for BE-NAC-30-125B



a) Bond-slip response

b) Post-failure cracking

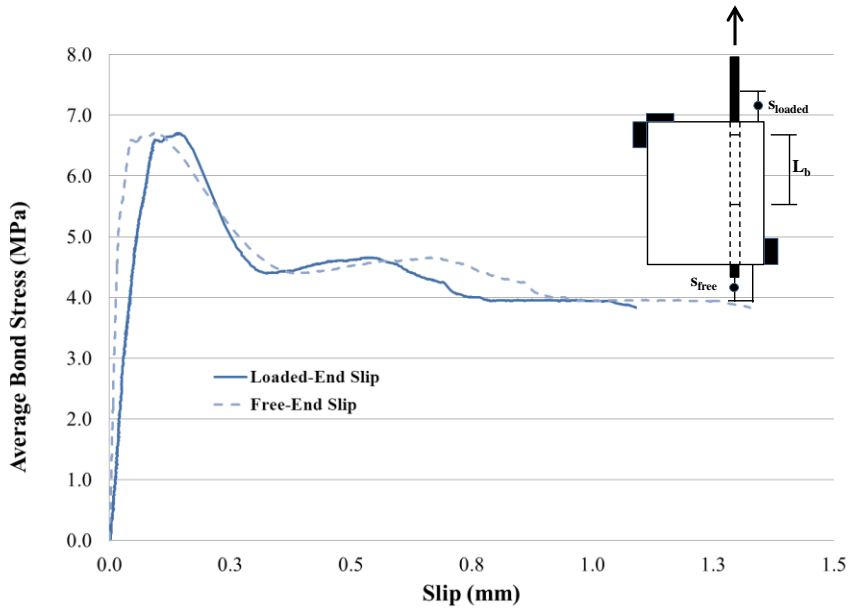
Figure D.3 Bond-slip response and crack pattern for BE-NAC-30-375A



a) Bond-slip response

b) Post-failure cracking

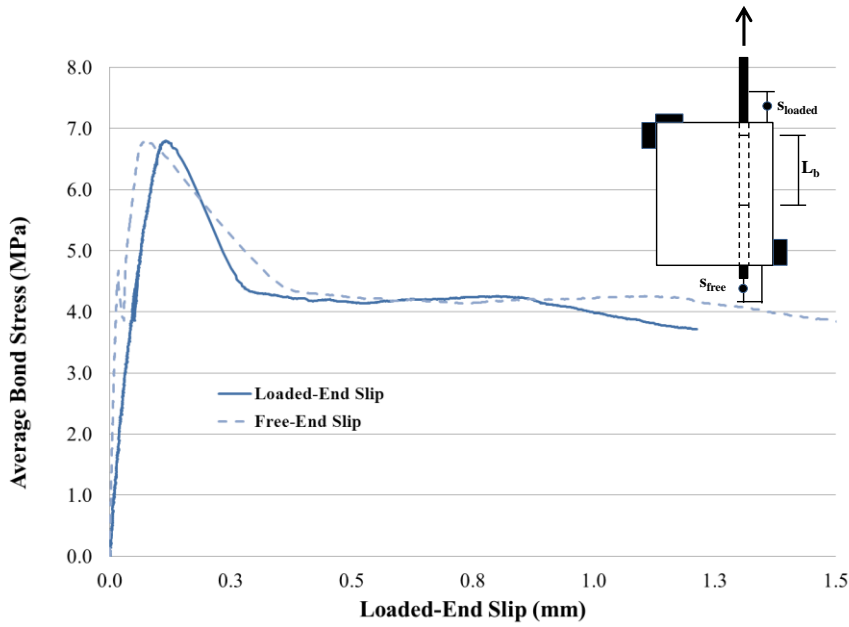
Figure D.4 Bond-slip response and crack pattern for BE-NAC-30-375B



a) Bond-slip response

b) Post-failure cracking

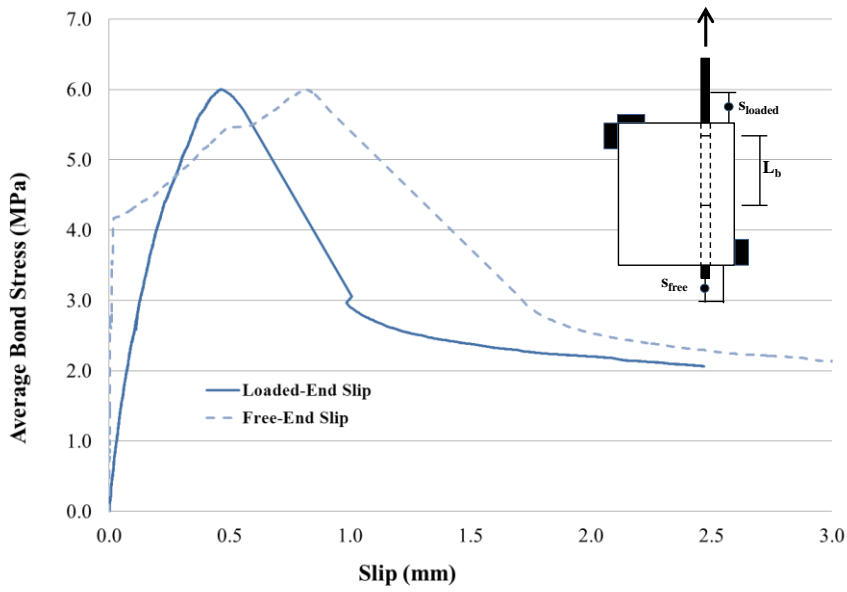
Figure D.5 Bond-slip response and crack pattern for BE-NAC-50-125A



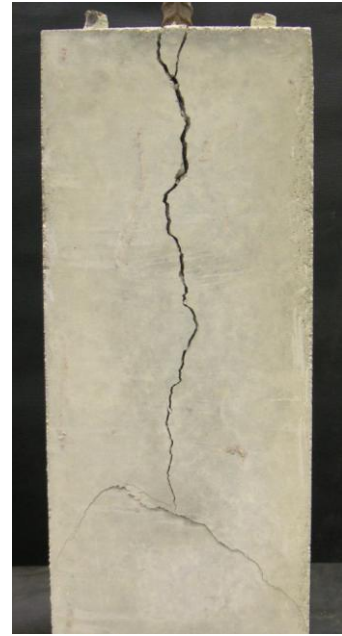
a) Bond-slip response

b) Post-failure cracking

Figure D.6 Bond-slip response and crack pattern for BE-NAC-50-125B

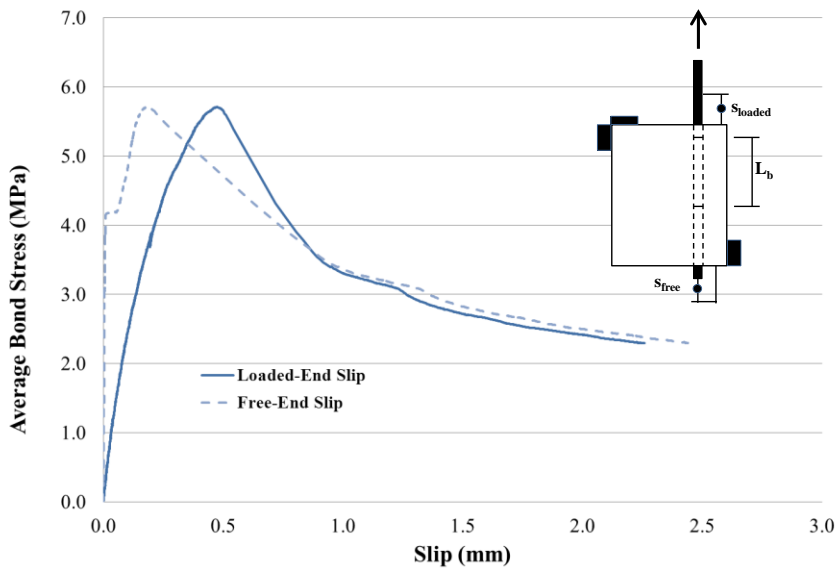


a) Bond-slip response

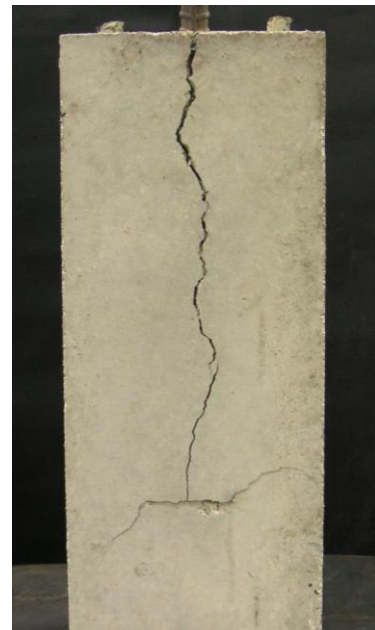


b) Post-failure cracking

Figure D.7 Bond-slip response and crack pattern for BE-NAC-50-375A

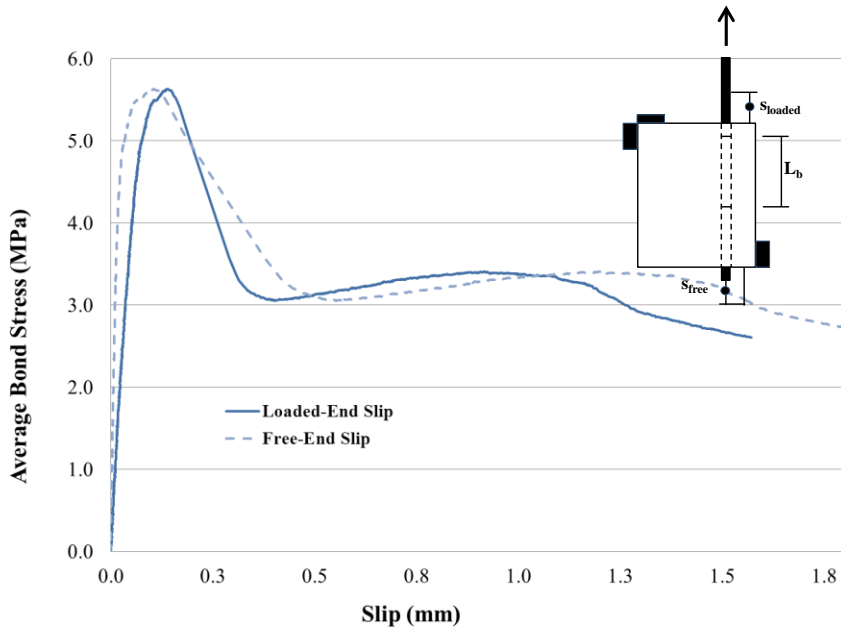


a) Bond-slip response



b) Post-failure cracking

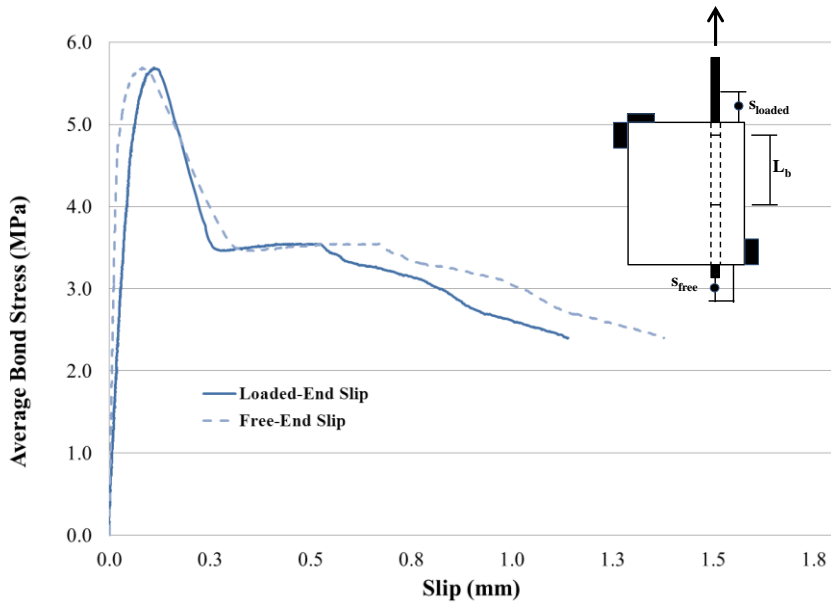
Figure D.8 Bond-slip response and crack pattern for BE-NAC-50-375B



a) Bond-slip response

b) Post-failure cracking

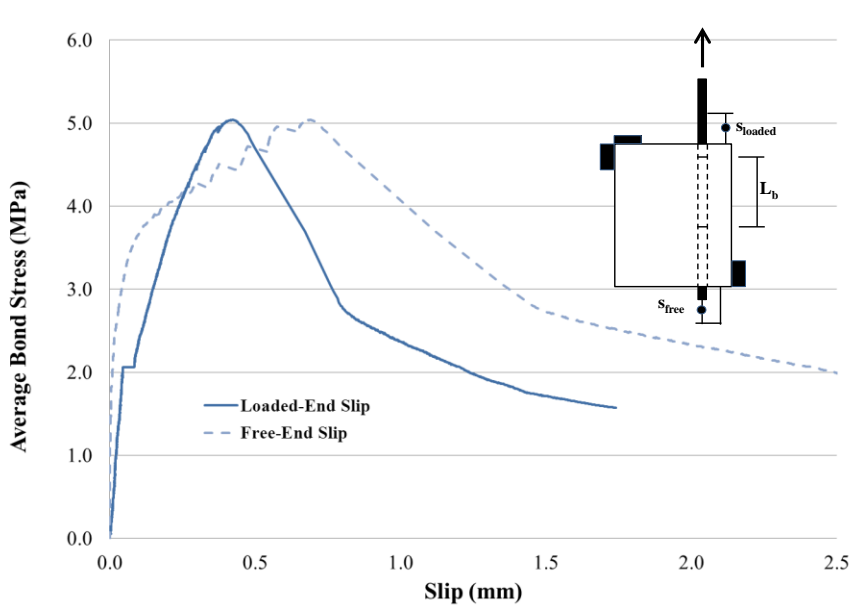
Figure D.9 Bond-slip response and crack pattern for BE-RAC1-30-125A



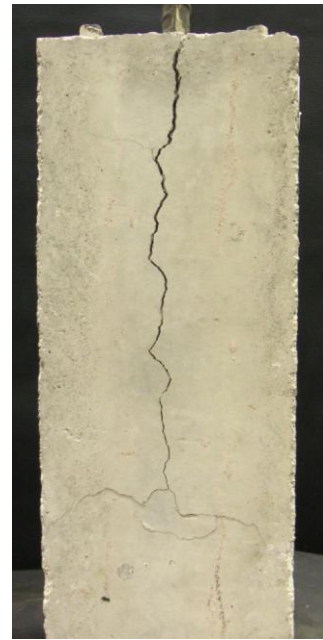
a) Bond-slip response

b) Post-failure cracking

Figure D.10 Bond-slip response and crack pattern for BE-RAC1-30-125B

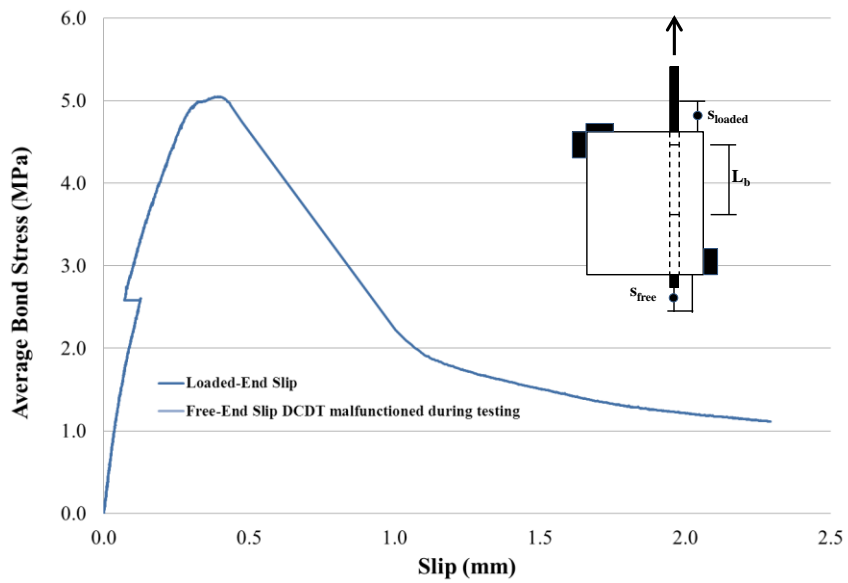


a) Bond-slip response



b) Post-failure cracking

Figure D.11 Bond-slip response and crack pattern for BE-RAC1-30-375A

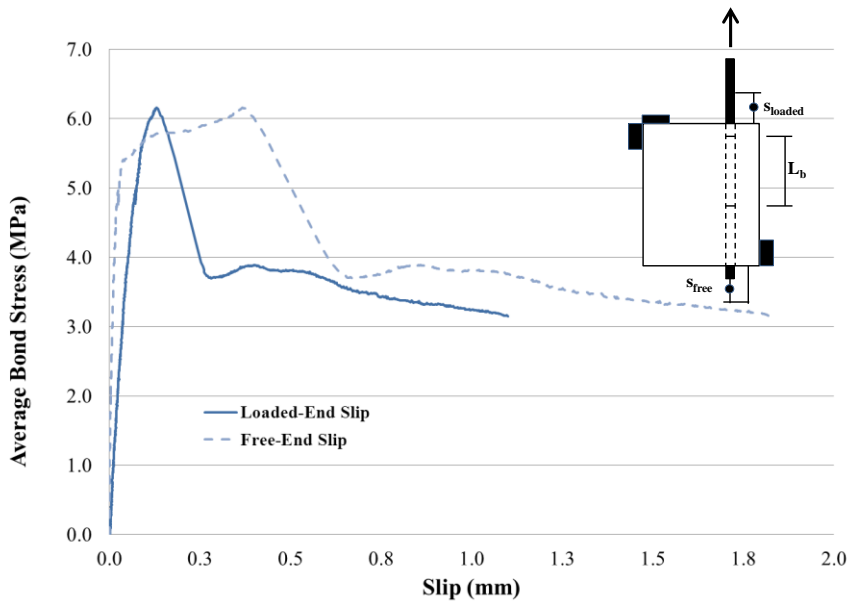


a) Bond-slip response

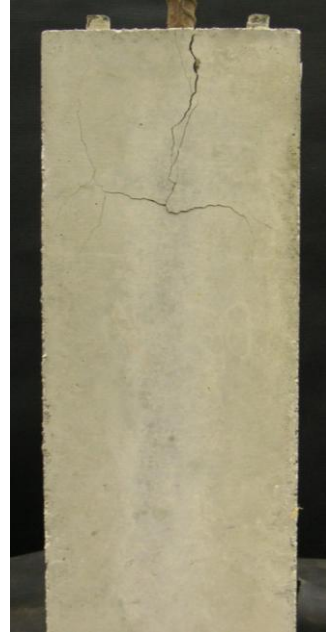


b) Post-failure cracking

Figure D.12 Bond-slip response and crack pattern for BE-RAC1-30-375B

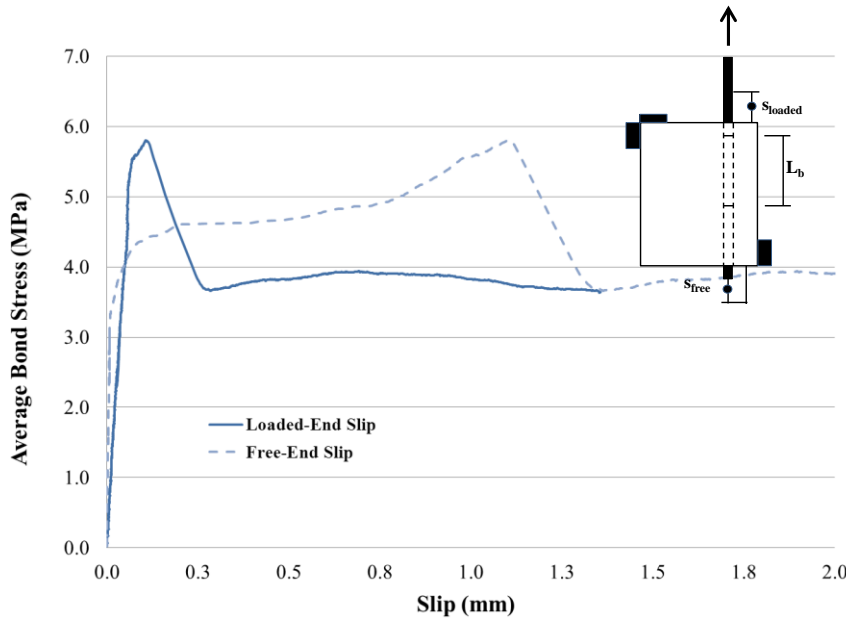


a) Bond-slip response



b) Post-failure cracking

Figure D.13 Bond-slip response and crack pattern for BE-RAC1-50-125A

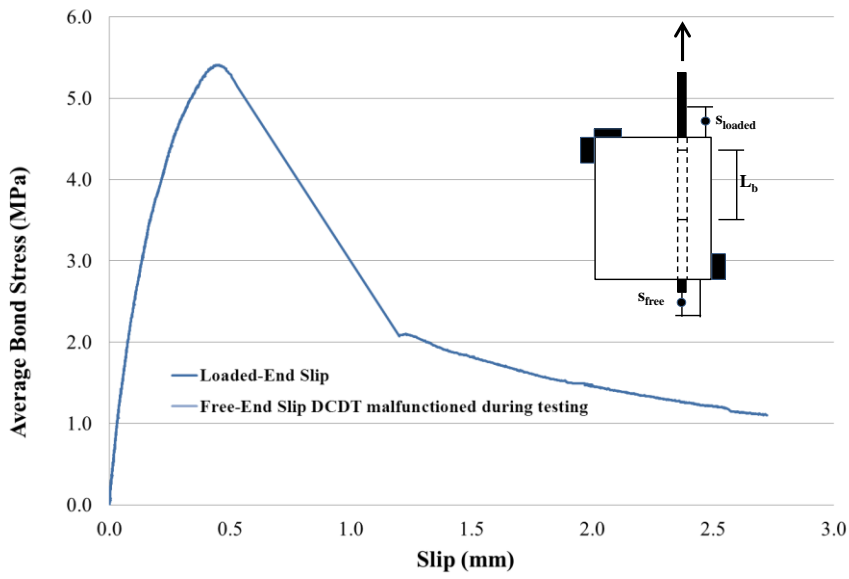


a) Bond-slip response

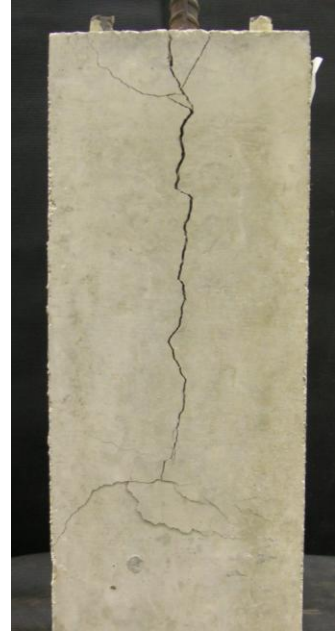


b) Post-failure cracking

Figure D.14 Bond-slip response and crack pattern for BE-RAC1-50-125B

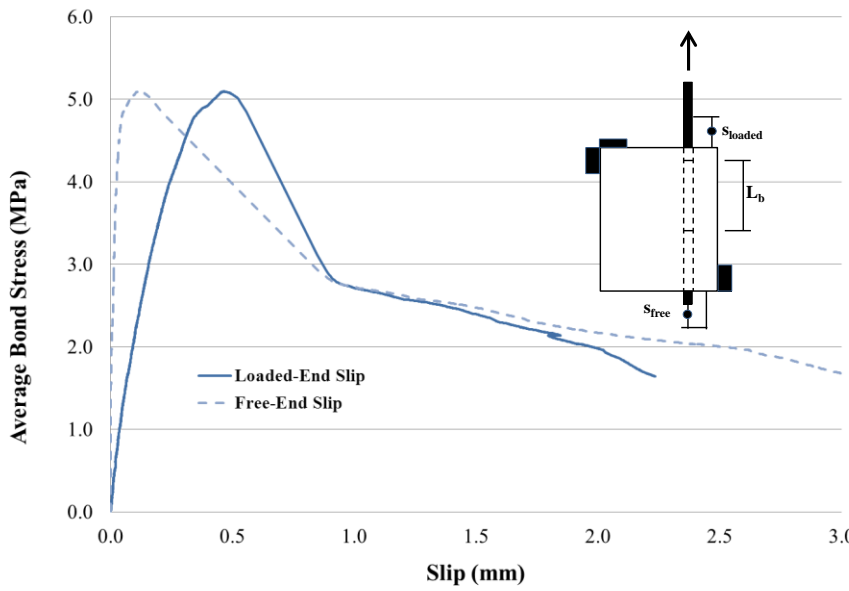


a) Bond-slip response



b) Post-failure cracking

Figure D.15 Bond-slip response and crack pattern for BE-RAC1-50-375A

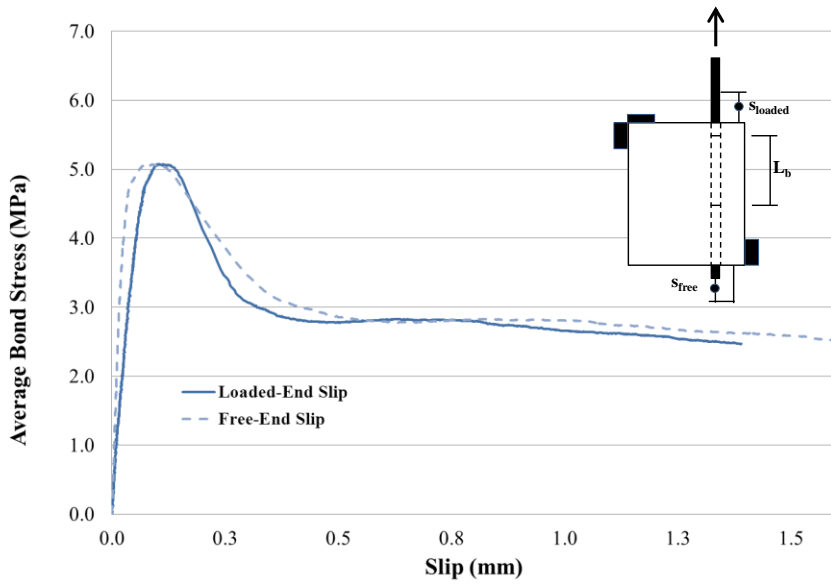


a) Bond-slip response

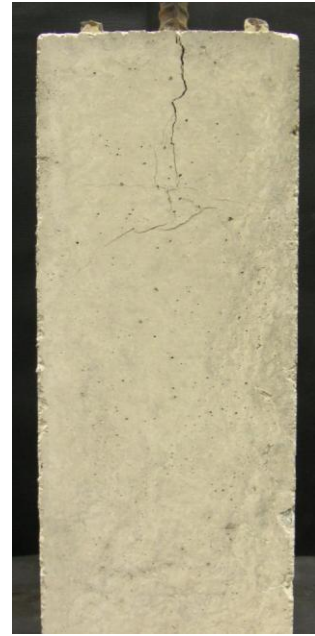


b) Post-failure cracking

Figure D.16 Bond-slip response and crack pattern for BE-RAC1-50-375B

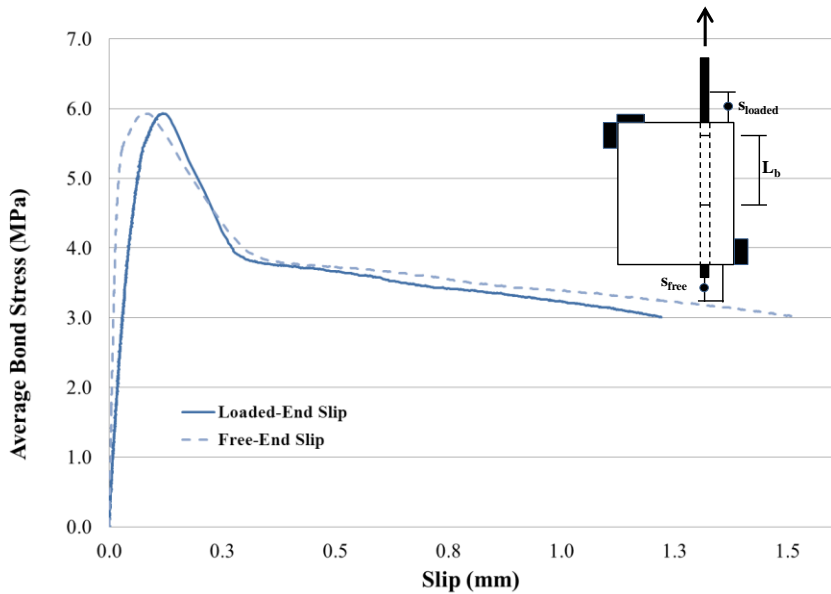


a) Bond-slip response



b) Post-failure cracking

Figure D.17 Bond-slip response and crack pattern for BE-RAC2-30-125A

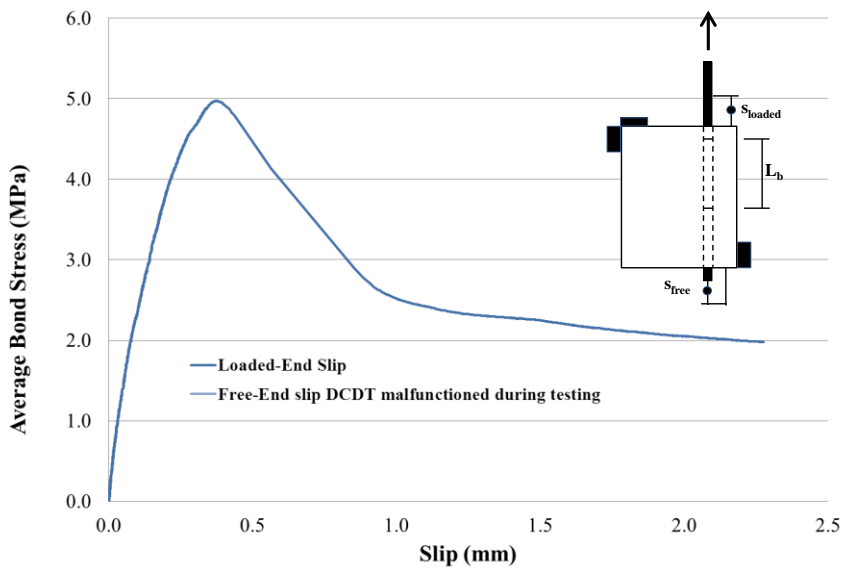


a) Bond-slip response



b) Post-failure cracking

Figure D.18 Bond-slip response and crack pattern for BE-RAC2-30-125B

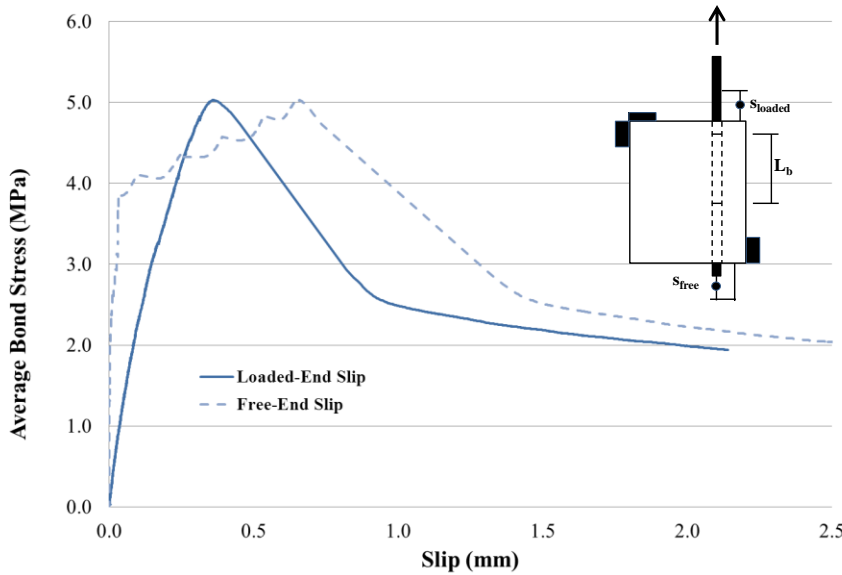


a) Bond-slip response



b) Post-failure cracking

Figure D.19 Bond-slip response and crack pattern for BE-RAC2-30-375A

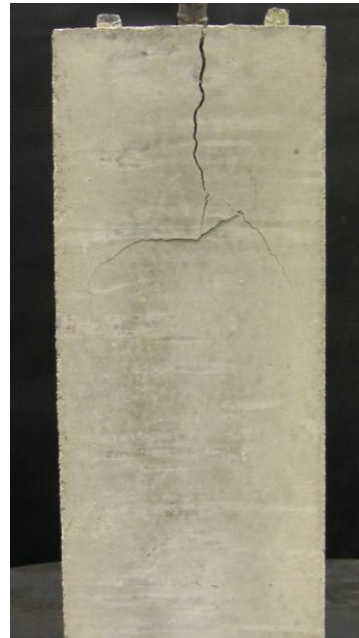
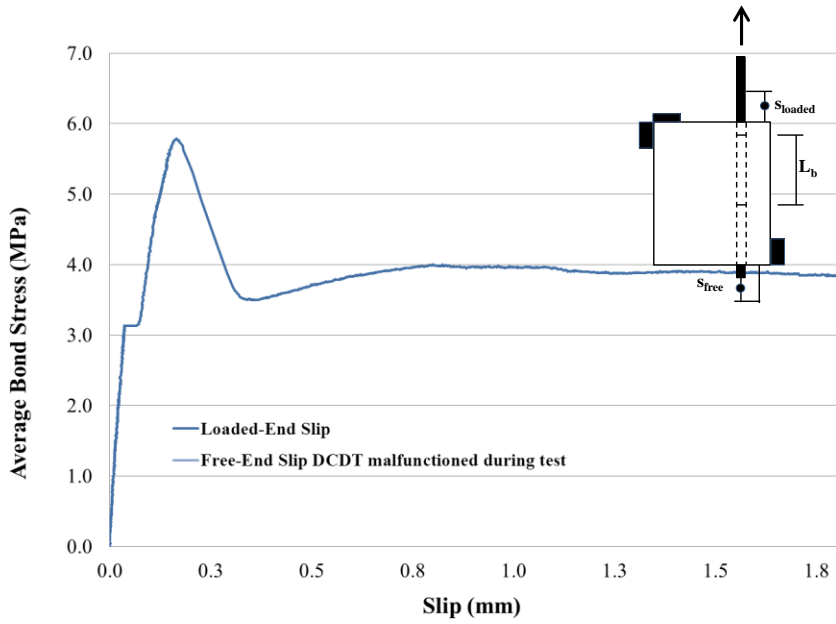


a) Bond-slip response



b) Post-failure cracking

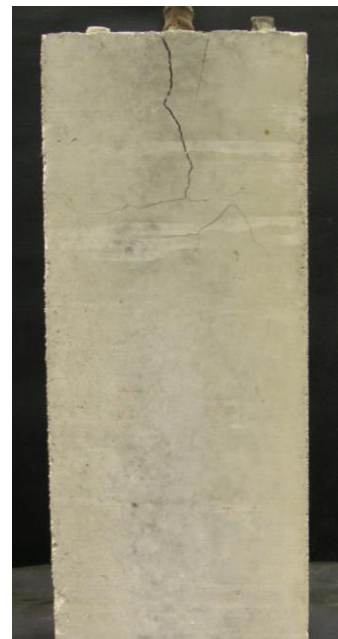
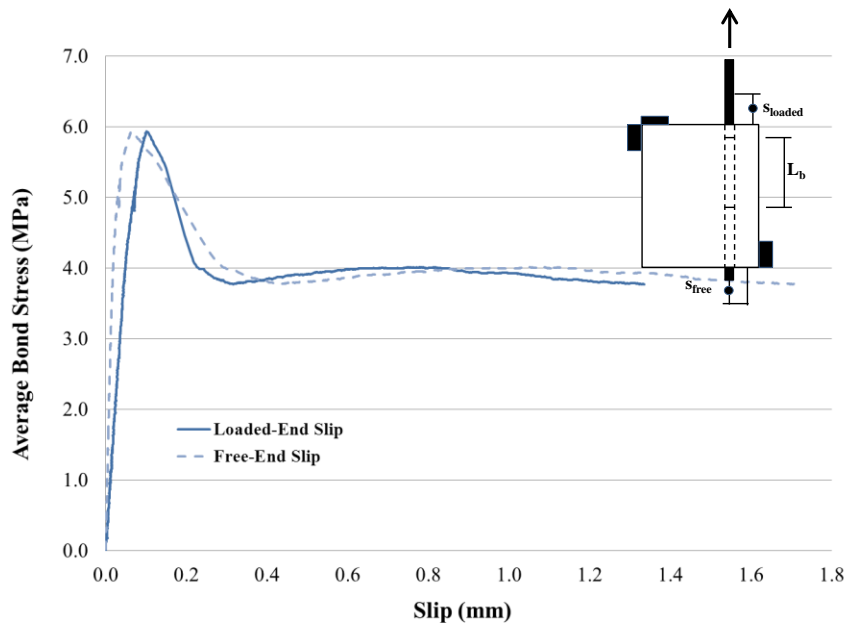
Figure D.20 Bond-slip response and crack pattern for BE-RAC2-30-375B



a) Bond-slip response

b) Post-failure cracking

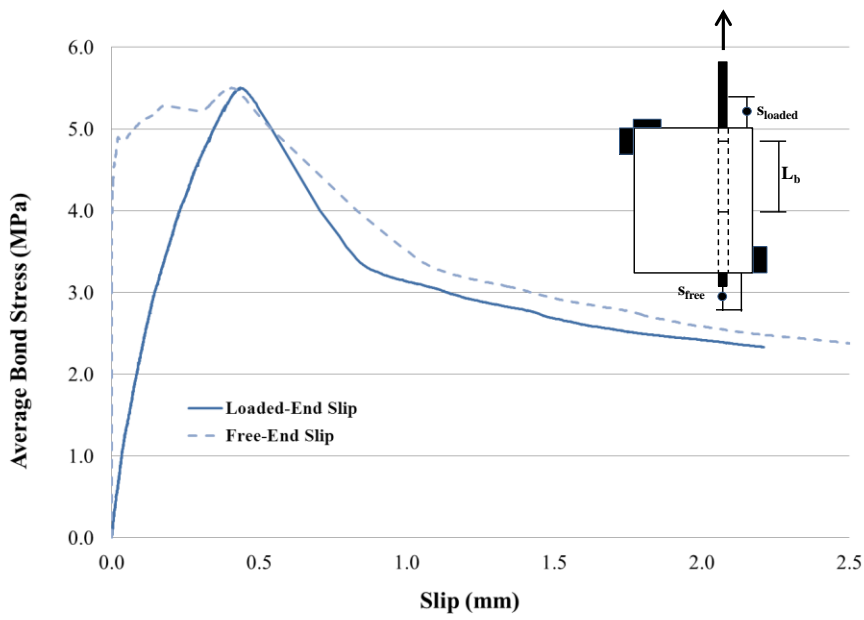
Figure D.21 Bond-slip response and crack pattern for BE-RAC2-50-125A



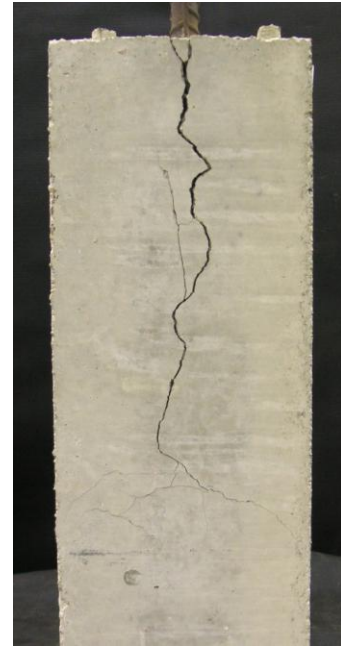
a) Bond-slip response

b) Post-failure cracking

Figure D.22 Bond-slip response and crack pattern for BE-RAC2-50-125B

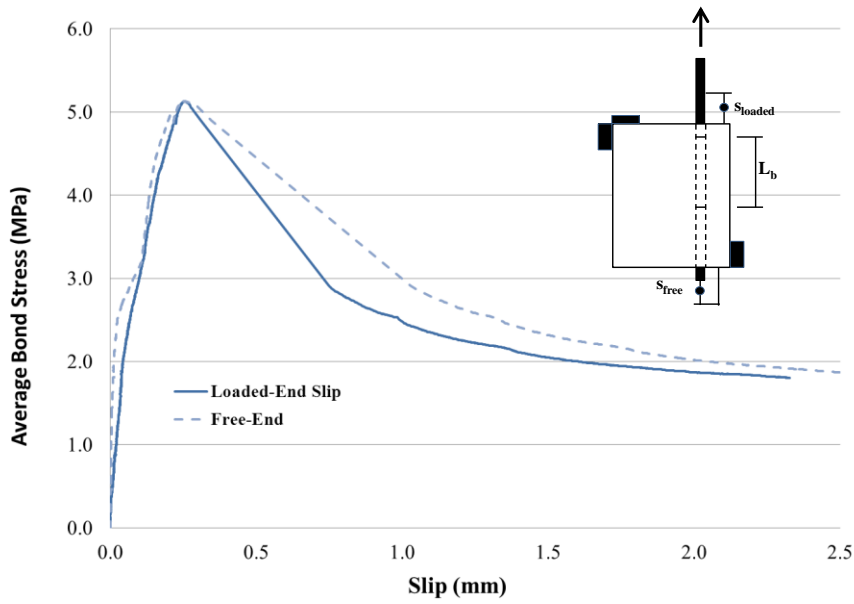


a) Bond-slip response

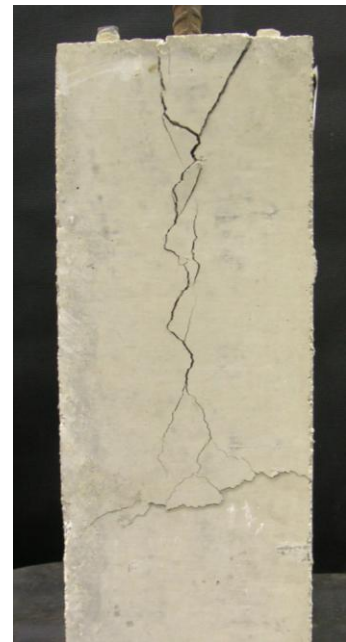


b) Post-failure cracking

Figure D.23 Bond-slip response and crack pattern for BE-RAC2-50-375A

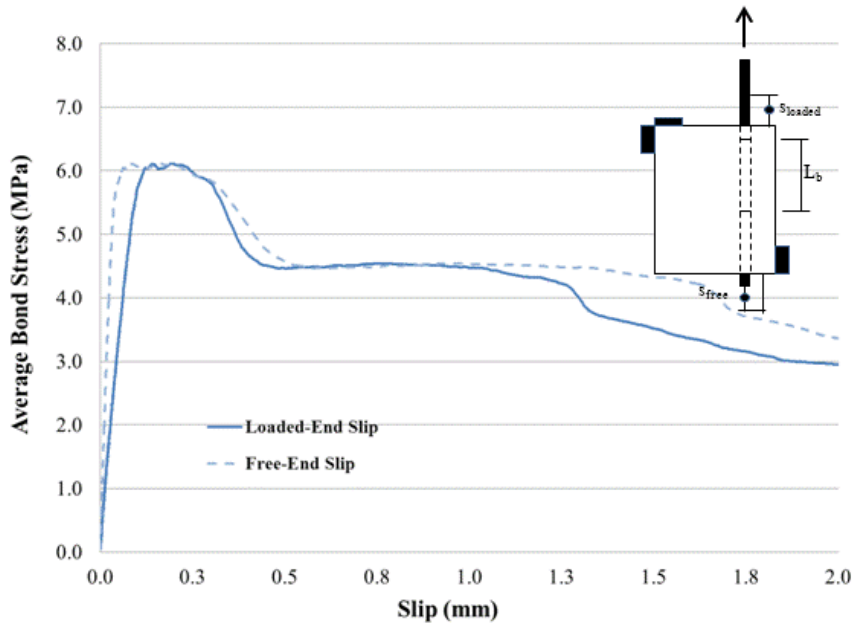


a) Bond-slip response



b) Post-failure cracking

Figure D.24 Bond-slip response and crack pattern for BE-RAC2-50-375B

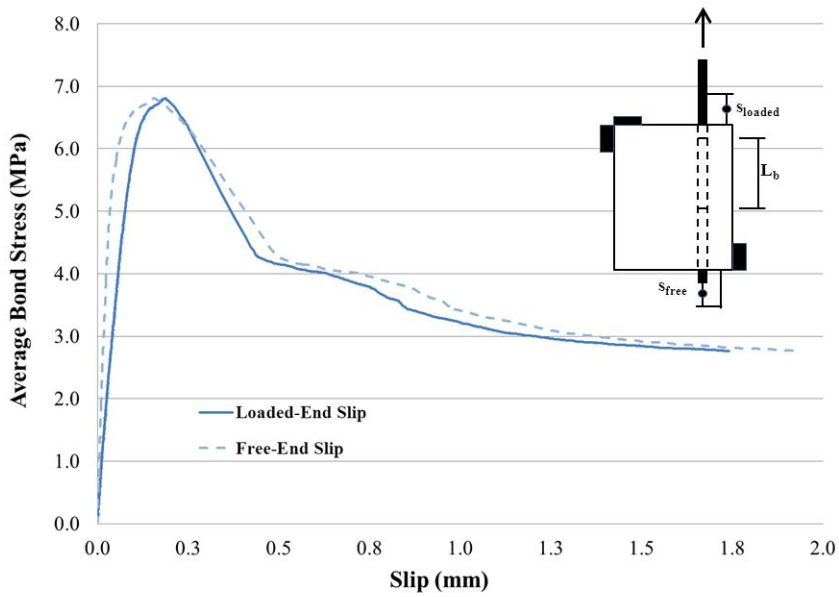


a) Bond-slip response



b) Post-failure cracking

Figure D.25 Bond-slip response and crack pattern for BE-NAC-40-125A

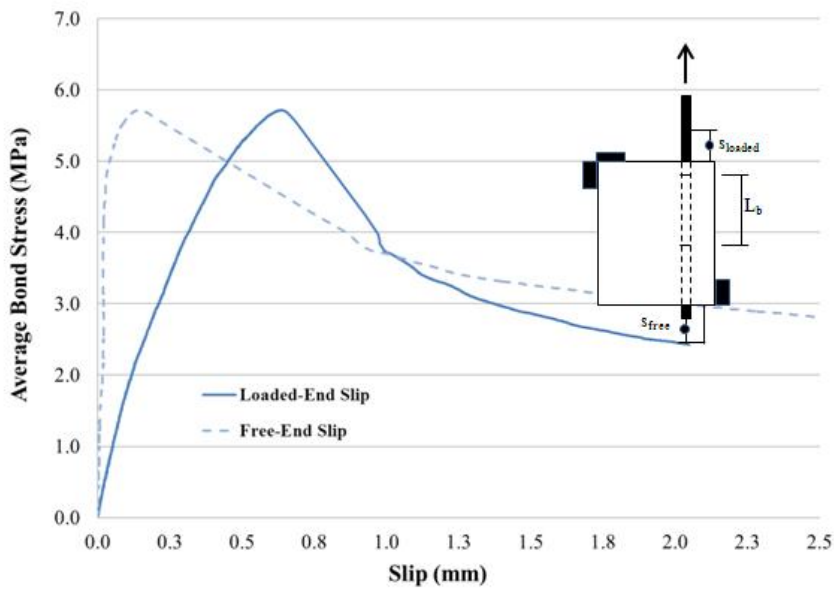


a) Bond-slip response

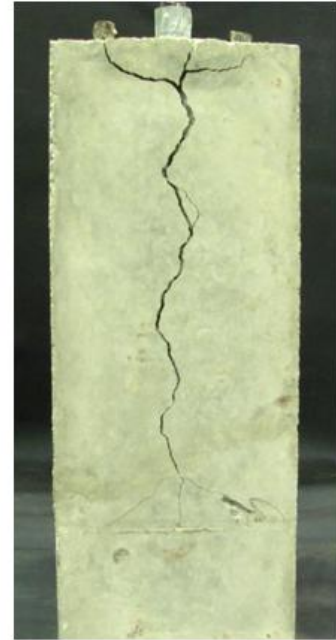


b) Post-failure cracking

Figure D.26 Bond-slip response and crack pattern for BE-NAC-40-125B

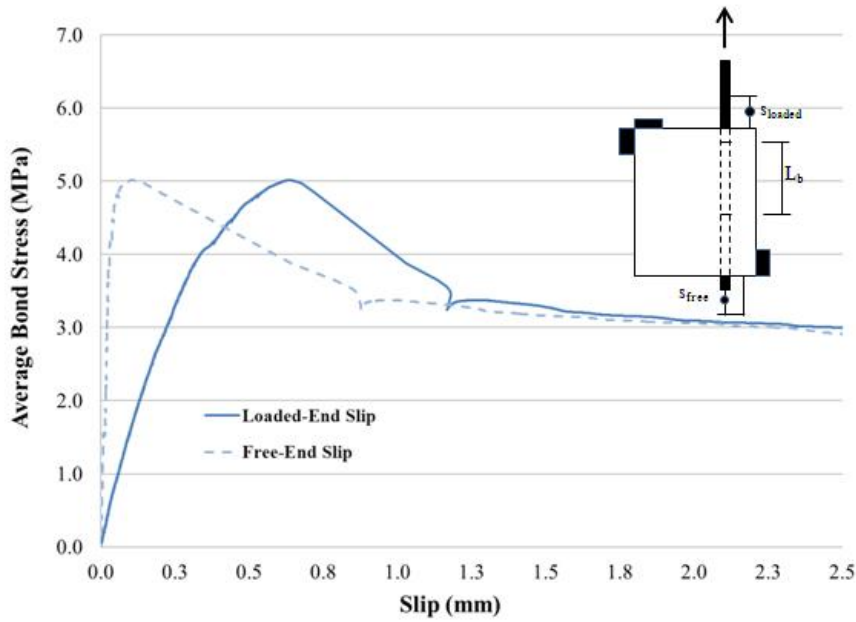


a) Bond-slip response



b) Post-failure cracking

Figure D.27 Bond-slip response and crack pattern for BE-NAC-40-450A

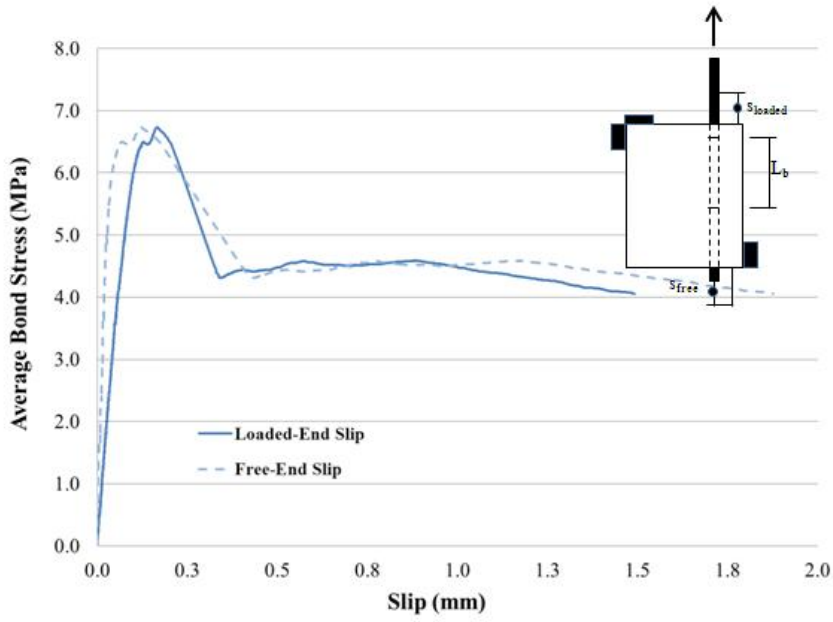


a) Bond-slip response



b) Post-failure cracking

Figure D.28 Bond-slip response and crack pattern for BE-NAC-40-450B

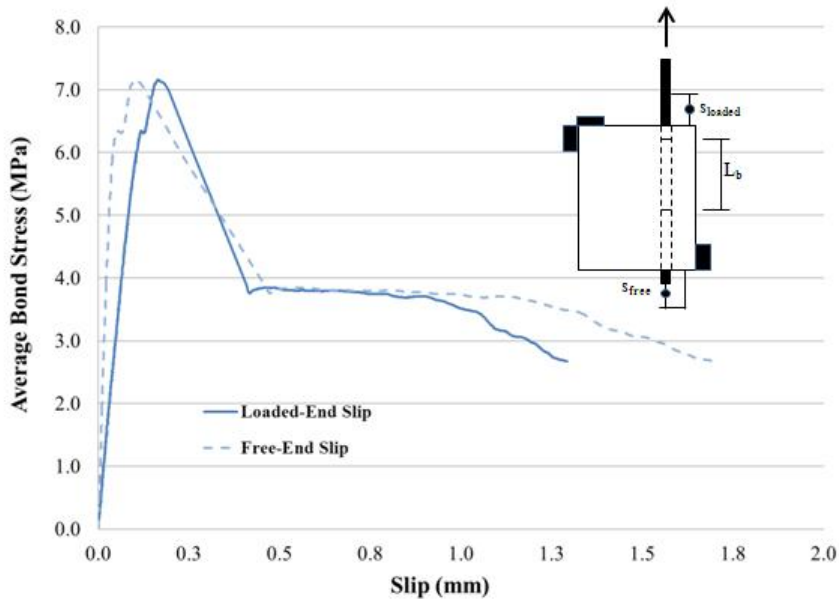


a) Bond-slip response



b) Post-failure cracking

Figure D.29 Bond-slip response and crack pattern for BE-NAC-60-125A

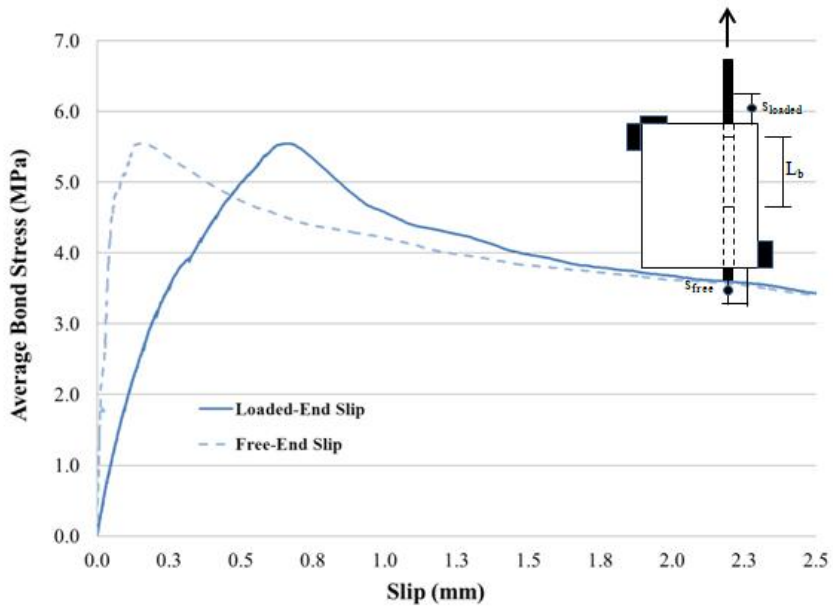


a) Bond-slip response



b) Post-failure cracking

Figure D.30 Bond-slip response and crack pattern for BE-NAC-60-125B

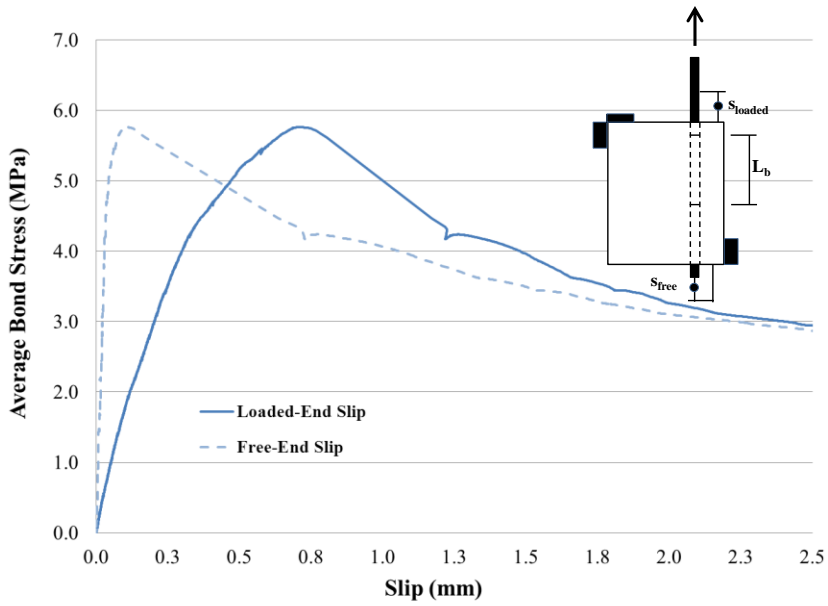


a) Bond-slip response



b) Post-failure cracking

Figure D.31 Bond-slip response and crack pattern for BE-NAC-60-450A

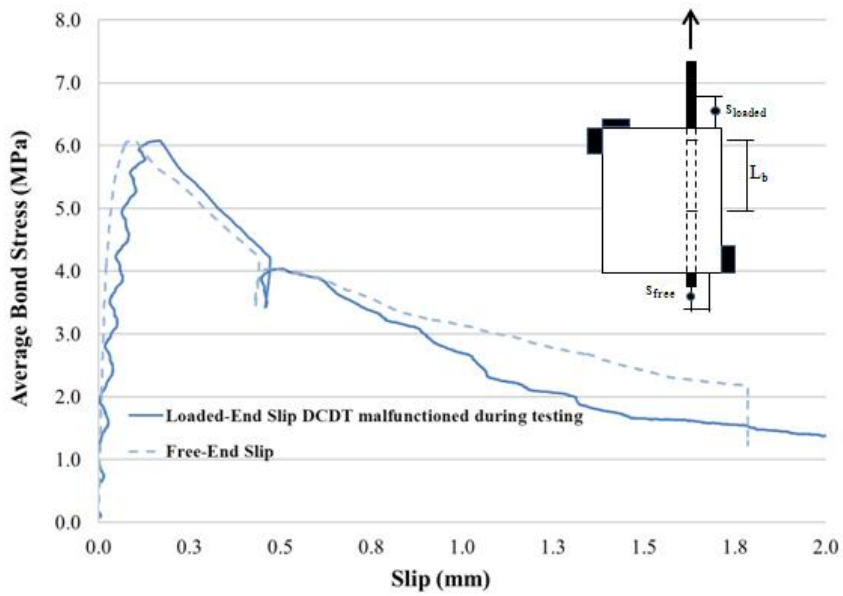


a) Bond-slip response



b) Post-failure cracking

Figure D.32 Bond-slip response and crack pattern for BE-NAC-60-450B

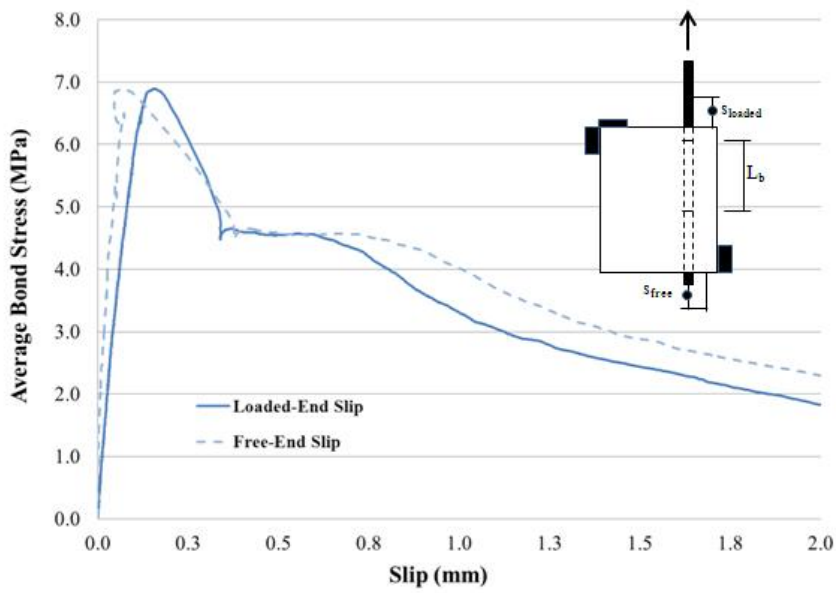


a) Bond-slip response



b) Post-failure cracking

Figure D.33 Bond-slip response and crack pattern for BE-RAC1-40-125A

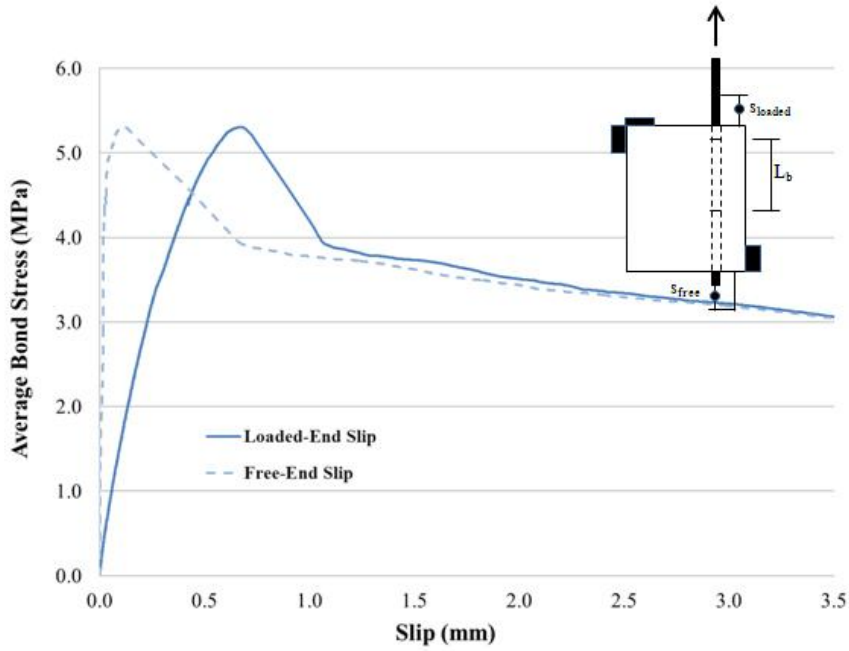


a) Bond-slip response



b) Post-failure cracking

Figure D.34 Bond-slip response and crack pattern for BE-RAC1-40-125B

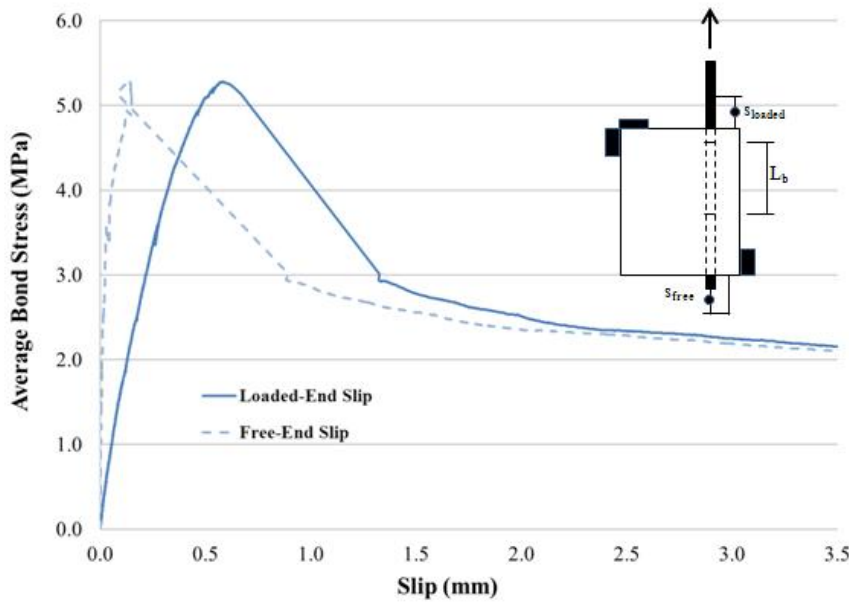


a) Bond-slip response



b) Post-failure cracking

Figure D.35 Bond-slip response and crack pattern for BE-RAC1-40-450A

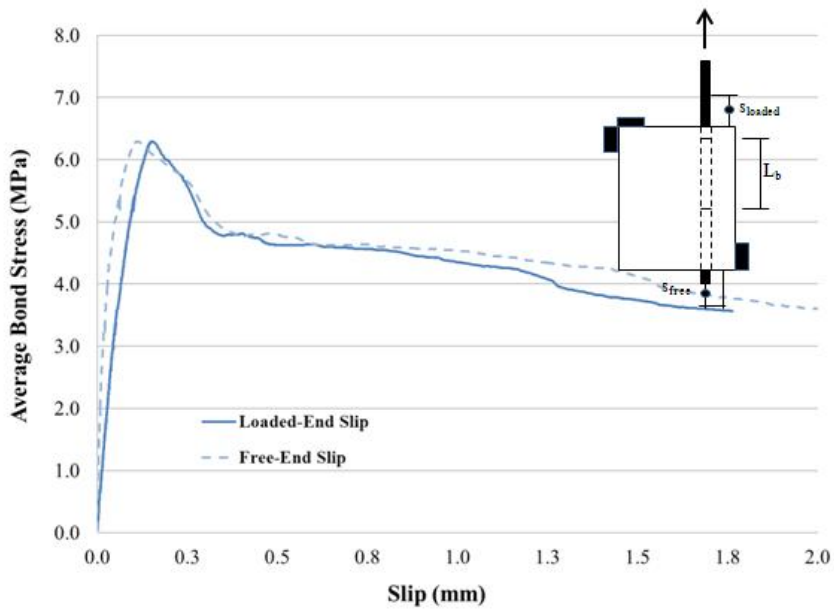


a) Bond-slip response



b) Post-failure cracking

Figure D.36 Bond-slip response and crack pattern for BE-RAC1-40-450B

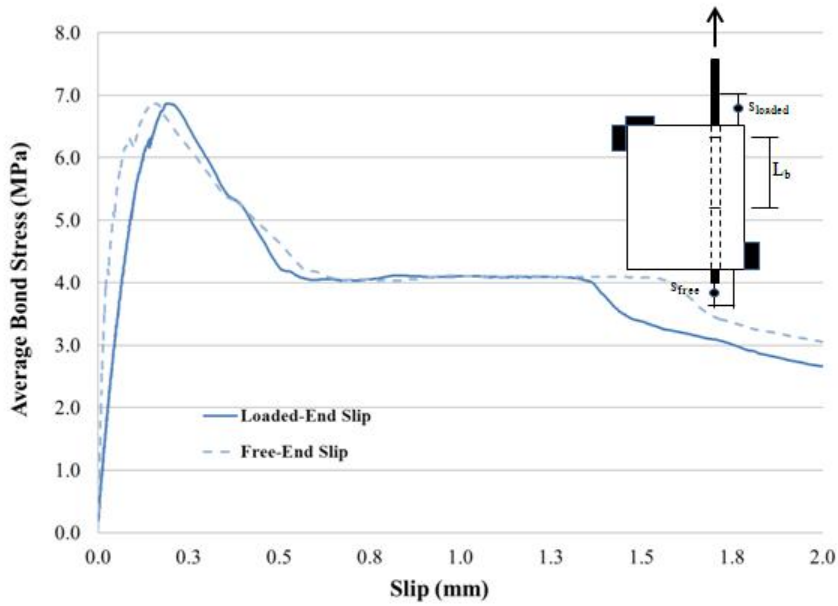


a) Bond-slip response



b) Post-failure cracking

Figure D.37 Bond-slip response and crack pattern for BE-RAC1-60-125A

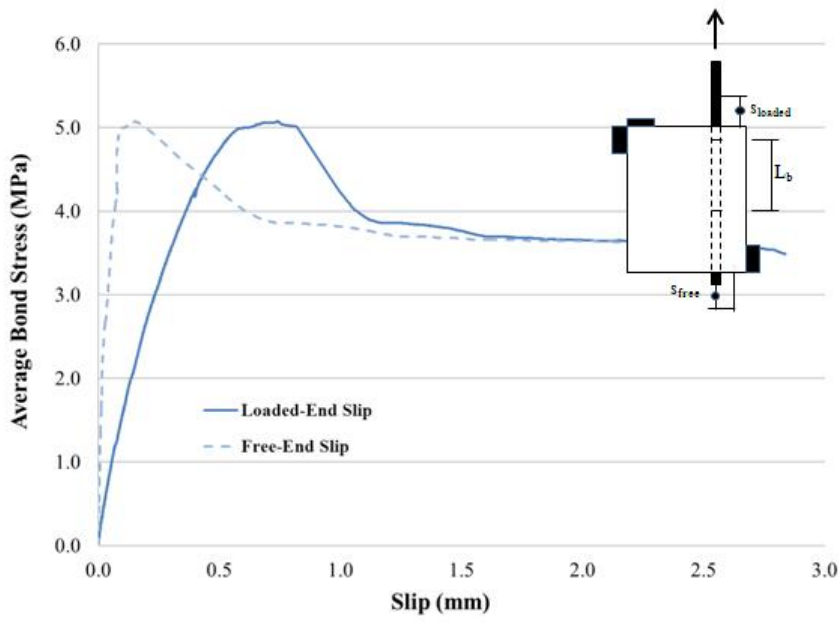


a) Bond-slip response



b) Post-failure cracking

Figure D.38 Bond-slip response and crack pattern for BE-RAC1-60-125B

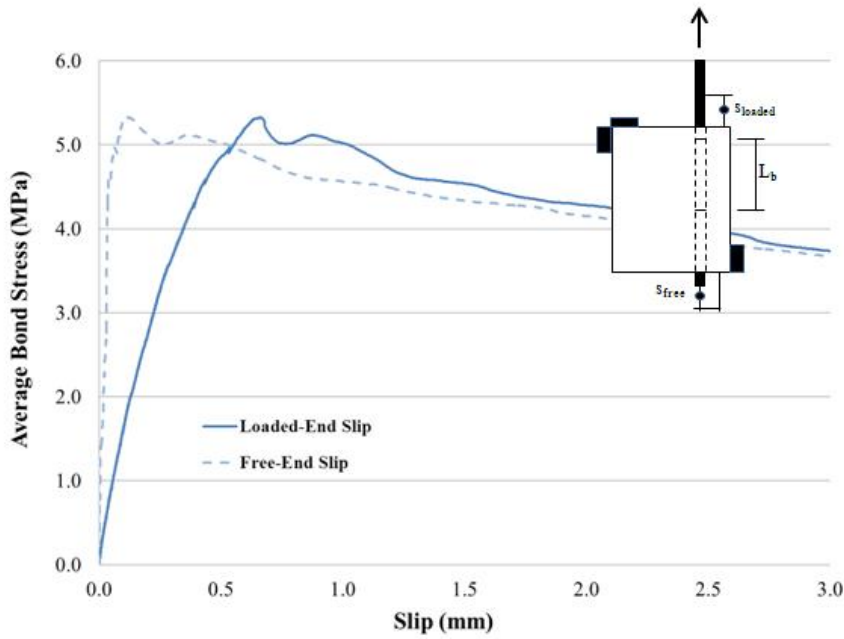


a) Bond-slip response



b) Post-failure cracking

Figure D.39 Bond-slip response and crack pattern for BE-RAC1-60-450A

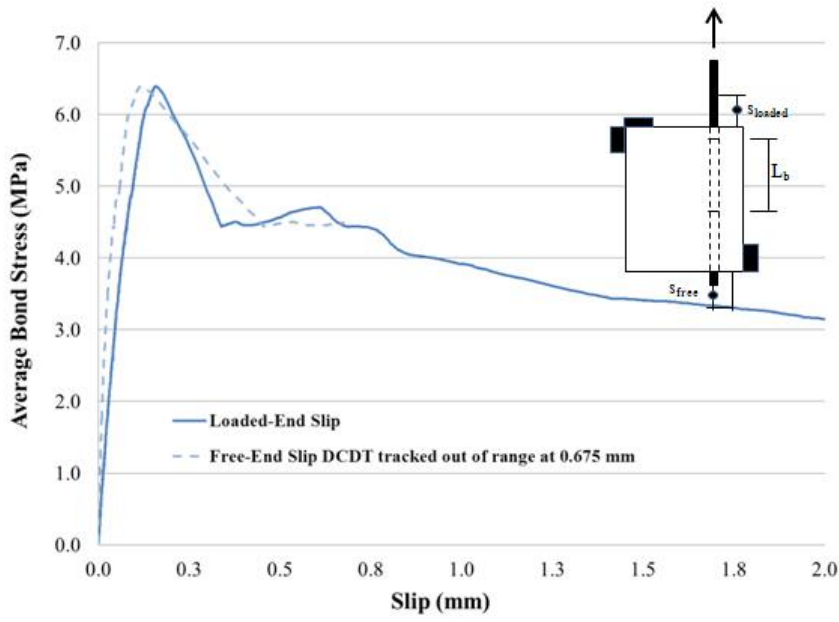


a) Bond-slip response



b) Post-failure cracking

Figure D.40 Bond-slip response and crack pattern for BE-RAC1-60-450B

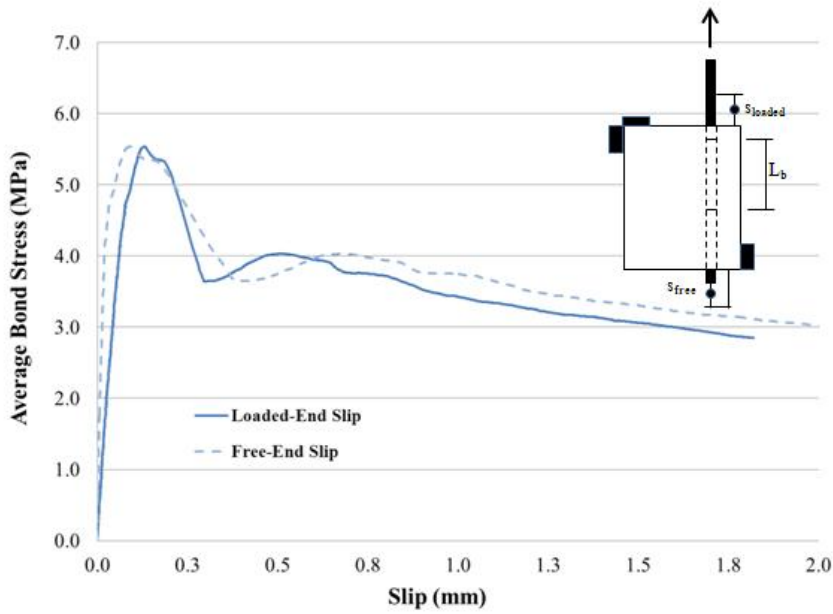


a) Bond-slip response



b) Post-failure cracking

Figure D.41 Bond-slip response and crack pattern for BE-RAC3-40-125A

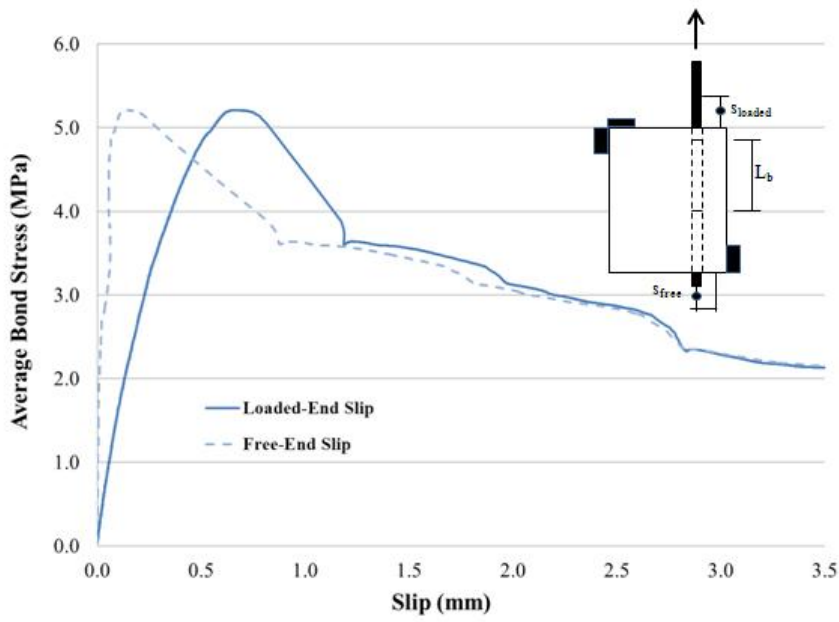


a) Bond-slip response



b) Post-failure cracking

Figure D.42 Bond-slip response and crack pattern for BE-RAC3-40-125B

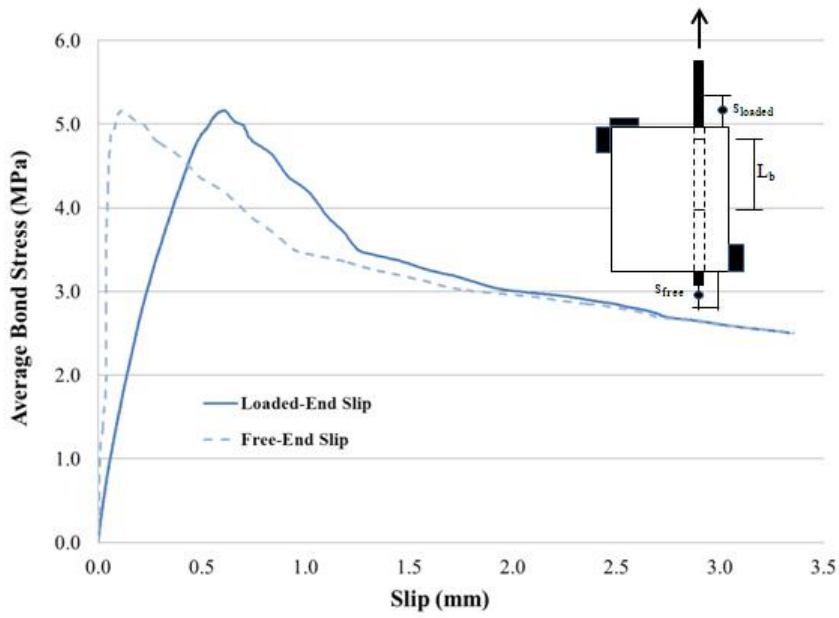


a) Bond-slip response



b) Post-failure cracking

Figure D.43 Bond-slip response and crack pattern for BE-RAC3-40-450A

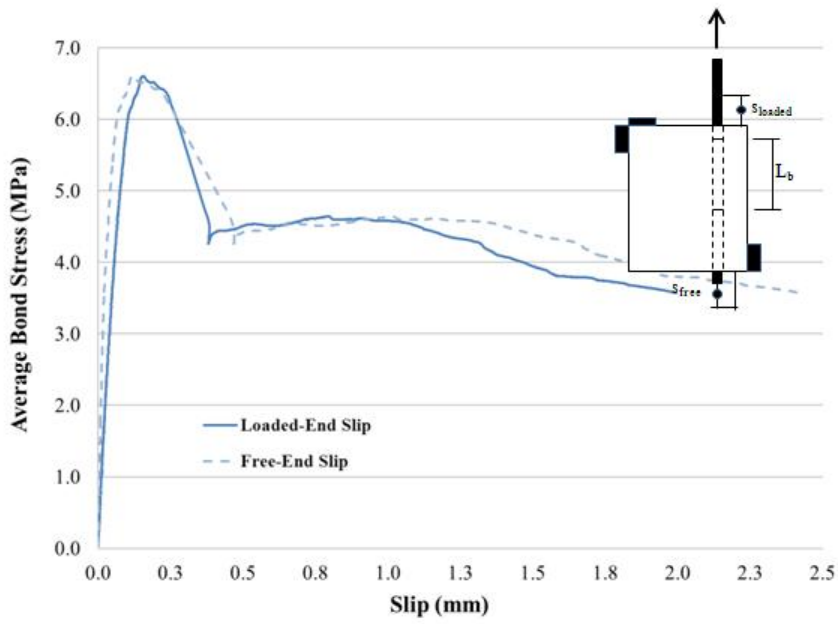


a) Bond-slip response



b) Post-failure cracking

Figure D.44 Bond-slip response and crack pattern for BE-RAC3-40-450B

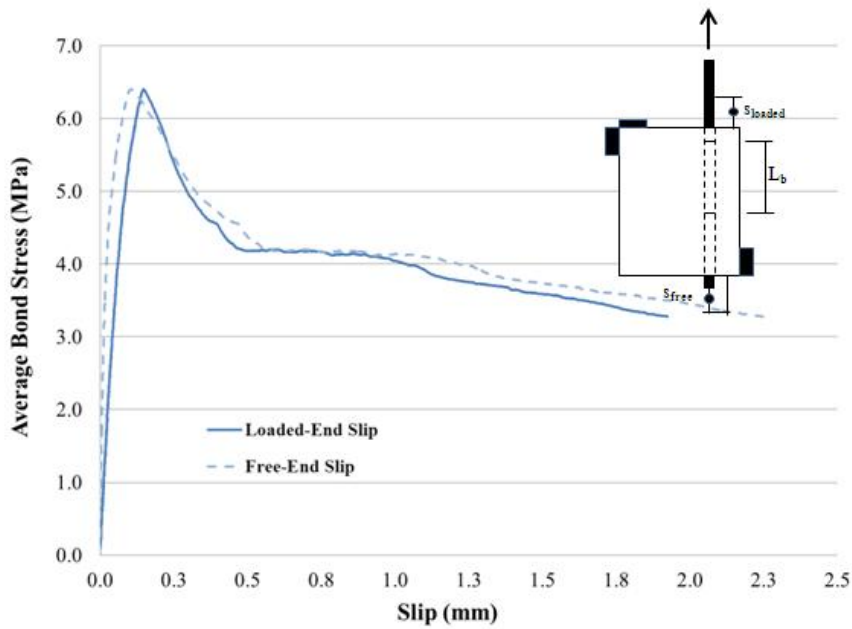


a) Bond-slip response



b) Post-failure cracking

Figure D.45 Bond-slip response and crack pattern for BE-RAC3-60-125A

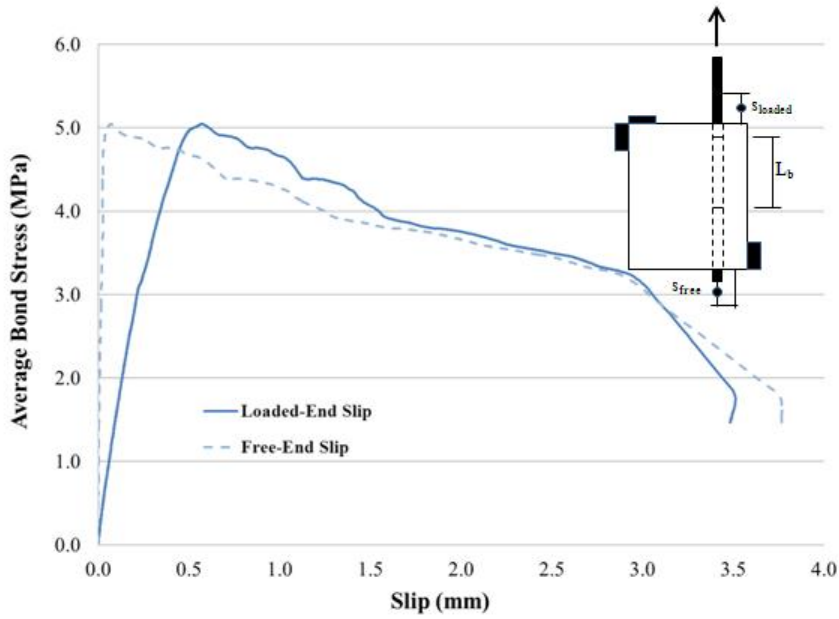


a) Bond-slip response



b) Post-failure cracking

Figure D.46 Bond-slip response and crack pattern for BE-RAC3-60-125B

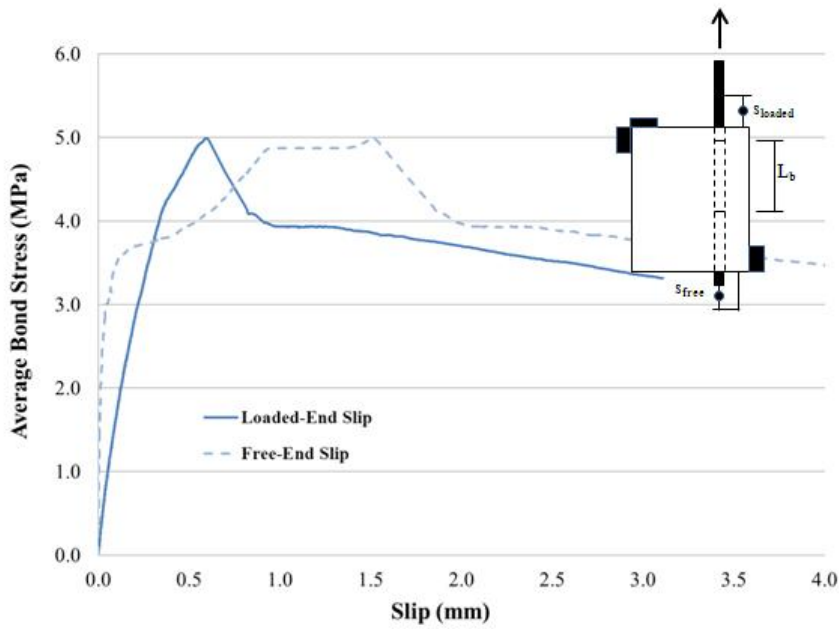


a) Bond-slip response

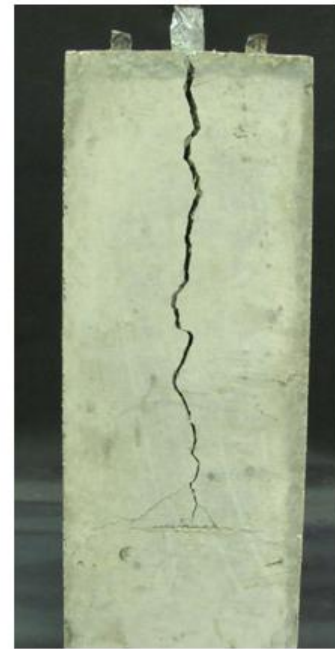


b) Post-failure cracking

Figure D.47 Bond-slip response and crack pattern for BE-RAC3-60-450A



a) Bond-slip response



b) Post-failure cracking

Figure D.48 Bond-slip response and crack pattern for BE-RAC3-60-450B